University of Florida
Civil and Coastal Engineering

UF

University of Florida
Civil and Coastal Engineering

G A T O R
Engineering
University of Florida
Civil and Coastal Engineering

Final Report   June 2013

Bridge Girder Drag Coefficients and Wind-Related Bracing Recommendations

Principal investigators:
Gary R. Consolazio, Ph.D.
Kurtis R. Gurley, Ph.D.

Graduate research assistant:
Zachary S. Harper

Department of Civil and Coastal Engineering
University of Florida
P.O. Box 116580
Gainesville, Florida 32611

DISCLAIMER

The opinions, findings, and conclusions expressed in this publication are those of the authors and not necessarily those of the State of Florida Department of Transportation.

SI (MODERN METRIC) CONVERSION FACTORS

APPROXIMATE CONVERSIONS *TO* SI UNITS

SYMBOL	WHEN YOU KNOW	MULTIPLY BY	TO FIND	SYMBOL
LENGTH				
in	inches	25.4	millimeters	mm
ft	feet	0.305	meters	m
yd	yards	0.914	meters	m
mi	miles	1.61	kilometers	km
AREA				
in^2	square inches	645.2	square millimeters	mm^2
ft^2	square feet	0.093	square meters	m^2
yd^2	square yard	0.836	square meters	m^2
ac	acres	0.405	hectares	ha
mi^2	square miles	2.59	square kilometers	km^2
VOLUME				
fl oz	fluid ounces	29.57	milliliters	mL
gal	gallons	3.785	liters	L
ft^3	cubic feet	0.028	cubic meters	m^3
yd^3	cubic yards	0.765	cubic meters	m^3
NOTE: volumes greater than 1000 L shall be shown in m^3				
MASS				
oz	ounces	28.35	grams	g
lb	pounds	0.454	kilograms	kg
T	short tons (2000 lb)	0.907	Megagrams	Mg (or "t")
TEMPERATURE (exact degrees)				
^{o}F	Fahrenheit	5(F-32)/9 or (F-32)/1.8	Celsius	^{o}C
ILLUMINATION				
fc	foot-candles	10.76	lux	lx
fl	foot-Lamberts	3.426	candela/m^2	cd/m^2
FORCE and PRESSURE or STRESS				
kip	1000 pounds force	4.45	kilonewtons	kN
lbf	pounds force	4.45	newtons	N
lbf/in^2	pounds force per square inch	6.89	kilopascals	kPa
psf	pounds force per square foot	47.88	pascals	Pa

1. Report No.	2. Government Accession No.	3. Recipient's Catalog No.

4. Title and Subtitle	5. Report Date
Bridge Girder Drag Coefficients and Wind-Related Bracing Recommendations	June 2013
	6. Performing Organization Code
7. Author's	8. Performing Organization Report No.
Gary R. Consolazio, Kurtis R. Gurley, Zachary S. Harper	2013/87322

9. Performing Organization Name and Address	10. Work Unit No. (TRAIS)
University of Florida Department of Civil and Coastal Engineering 365 Weil Hall, P.O. Box 116580 Gainesville, FL 32611-6580	
	11. Contract or Grant No.
	BDK75 977-33
12. Sponsoring Agency Name and Address	13. Type of Report and Period Covered
Florida Department of Transportation Research Management Center 605 Suwannee Street, MS 30 Tallahassee, FL 32399-0450	Final Report May 2010 – June 2013
	14. Sponsoring Agency Code

15. Supplementary Notes

16. Abstract

A key objective of this study was to experimentally quantify wind load coefficients (drag, torque, and lift) for common bridge girder shapes, and to quantify shielding effects arising from aerodynamic interference between adjacent girders. Wind tunnel tests were performed on reduced-scale models of Florida-I Beam (FIB), plate girder, and box girder cross-sectional shapes to measure the aerodynamic properties of individual girders as well as systems of multiple girders. The focus of this study was on construction-stage structural assessment under wind loading conditions, therefore, the multiple girder systems that were considered did not have a bridge deck in place (and therefore air flow between adjacent girders was permitted). Results from the wind tunnel tests were synthesized into simplified models of wind loading for single and multiple girder systems, and conservative equations suitable for use in bridge design were developed. Separate wind load cases were developed for assessing overall system stability and required brace strength.

Also included in this study was the development of procedures for assessing temporary bracing requirements to resist wind load during bridge construction. Numerical finite element models and analysis techniques were developed for evaluating the stability of precast concrete girders (Florida-I Beams), both individually and in systems of multiple girders braced together. A sub-component of this effort resulted in the development of a new calculation procedure for estimating bearing pad roll stiffness, which is known to affect girder stability during construction. After integrating the improved estimates of wind loads and bearing pad stiffnesses into finite element models of individual and multiple girder braced systems, several large-scale parametric studies were performed (in total, more than 50,000 separate stability analyses were conducted). The parametric studies included consideration of different Florida-I Beam cross-sections, span lengths, wind loads, skew angles, anchor stiffnesses, and brace stiffnesses. Regression analyses were performed on the parametric study results to develop girder capacity prediction equations suitable for use in the design of temporary bracing for Florida-I Beams during construction.

17. Key Words	18. Distribution Statement
Bridge construction, wind loading, drag coefficient, wind tunnel testing, girder, stability, bearing pad, buckling capacity	No restrictions.

19. Security Classif. (of this report)	20. Security Classif. (of this page)	21. No. of Pages	22. Price
Unclassified	Unclassified	383	

Form DOT F 1700.7 (8-72). Reproduction of completed page authorized

ACKNOWLEDGEMENTS

EXECUTIVE SUMMARY

A key objective of this study was to experimentally quantify wind load coefficients (drag, torque, and lift) for common bridge girder shapes, and to quantify shielding effects arising from aerodynamic interference between adjacent girders. Wind tunnel tests were performed on reduced-scale models of Florida-I Beam (FIB), plate girder, and box girder cross-sectional shapes to measure the aerodynamic properties of individual girders as well as systems of multiple girders. The focus of this study was on construction-stage structural assessment under wind loading conditions, therefore, the multiple girder systems that were considered did not have a bridge deck in place (and therefore air flow between adjacent girders was permitted). Results from the wind tunnel tests were synthesized into simplified models of wind loading for single and multiple girder systems, and conservative equations suitable for use in bridge design were developed. Separate wind load cases were developed for assessing overall system stability and required brace strength.

Also included in this study was the development of procedures for assessing temporary bracing requirements to resist wind load during bridge construction. Numerical finite element models and analysis techniques were developed for evaluating the stability of precast concrete girders (Florida-I Beams), both individually and in systems of multiple girders braced together. A sub-component of this effort resulted in the development of a new calculation procedure for estimating bearing pad roll stiffness, which is known to affect girder stability during construction. After integrating the improved estimates of wind loads and bearing pad stiffnesses into finite element models of individual and multiple girder braced systems, several large-scale parametric studies were performed (in total, more than 50,000 separate stability analyses were conducted). The parametric studies included consideration of different Florida-I Beam cross-sections, span lengths, wind loads, skew angles, anchor stiffnesses, and brace stiffnesses. Regression analyses were performed on the parametric study results to develop girder capacity prediction equations suitable for use in the design of temporary bracing for Florida-I Beams during construction.

TABLE OF CONTENTS

LIST OF FIGURES

xiii

LIST OF TABLES

CHAPTER 1
INTRODUCTION

1.1 Introduction

Prestressed concrete girders are commonly used in bridge construction because they are an economical choice for supporting very long spans. For example, the 96-inch-deep Florida-I Beam (FIB), one of the standard girder designs employed by the Florida Department of Transportation (FDOT), is able to support spans of 200 ft or more. However, as such girders increase in span length, they become more susceptible to issues of lateral instability.

The most critical phase of construction, with regard to stability, is after girder placement (prior to the casting of the deck), when girders are supported only by flexible bearing pads and can be subject to high lateral wind loads. In many bridge designs, girders may be positioned (laterally spaced) near enough to one another that a single unstable girder can knock over adjacent girders, initiating a progressive collapse that can result in severe economic damage and risk to human life. To prevent such a scenario, it is typical for girders to be temporarily braced together (Fig. 1.1) to form a more stable structural unit.

Figure 1.1 Prestressed concrete girders braced together for stability

During the construction phase, wind loads tend to control the design of temporary bracing, so it is important that such loads be known as accurately as possible. Lateral wind loads are generally calculated using a *drag coefficient*, a dimensionless quantity that relates the wind pressure on an object to its size and wind speed. However, the drag coefficients of most common bridge girder cross-sectional shapes have not been adequately addressed in the literature.

Furthermore, once multiple adjacent girders have been placed, the leading girder acts as a windbreak and disrupts the airflow over subsequent girders, resulting in a phenomenon referred to as *aerodynamic interference* (or *shielding*). At common girder spacings, the alteration to the wind stream will reduce or even reverse the direction of wind pressure on leeward girders. A thorough understanding of this shielding effect is necessary to develop appropriately conservative bracing design forces. However, this area has also received little attention in the literature.

1

1.2 Objectives

The primary objective of this research was to experimentally quantify drag coefficients for common bridge girder shapes as well as shielding effects arising from the aerodynamic interference between adjacent girders, and to synthesize the results into a set of conservative design parameters that can be used to compute lateral wind loads for design and construction calculations. A secondary objective was to use analytical models of braced girder systems to develop recommendations for temporary bracing of prestressed concrete girders (FIBs) subjected to the new design wind loads.

1.3 Scope of work

- Experimental testing: Wind tunnel tests were performed to measure the aerodynamic coefficients (drag, lift, and torque) of five (5) bridge girder cross-sectional shapes [two (2) plate girder; two (2) FIB; and one open-top box], chosen to be representative of a wide range modern Florida bridges. In addition to measuring the aerodynamic coefficients of the individual girders, tests were performed on groups of adjacent girders in a variety of common configurations in order to quantify the shielding effects caused by aerodynamic interference.

- Design wind loads: Measurements from the wind tunnel tests were analyzed to identify common trends and to develop a conservative set of simplified wind load parameters that are suitable for use in design.

- Analysis method for bearing pad stiffnesses: Experimental bearing pad stiffness measurements from a previous FDOT research project (BDK75 977-03, Consolazio et al. 2012) were used to develop and validate a new analytical method for estimating the girder support stiffnesses provided by steel-reinforced elastomeric bearing pads.

- System-level analytical models: Analytical models were developed that were capable of evaluating the lateral stability of Florida-I Beams (FIBs). The models incorporated the estimated support stiffnesses provided by standard FDOT bearing pads and were capable of capturing system-level behavior of multiple girders braced together with any of several common brace types.

- Wind load capacity of individual FIBs: An analytical parametric study was conducted to determine a simplified equation for estimating the maximum wind pressure that an individual (unbraced) FIB can resist without becoming unstable.

- Recommendations for temporary bracing: Analytical parametric studies were conducted using the system-level models and the design wind loads to evaluate temporary bracing requirements for FIB systems in a variety of configurations. In addition to general recommendations for temporary bracing design, the results of the parametric study were used to develop simplified equations for estimating the capacity of braced systems of FIBs.

CHAPTER 2
PHYSICAL DESCRIPTION OF BRIDGES DURING CONSTRUCTION

2.1 Introduction

This study is concerned with the stability of long-span prestressed concrete girders during the construction process. Specifically, the girders under investigation are Florida-I Beams (FIBs), a family of standard cross-sectional shapes of varying depths that are commonly employed in bridge designs in Florida. These beams are typically cast offsite, transported to the construction site by truck, then lifted into position one-at-a-time by crane, where they are placed on elastomeric bearing pads and braced together for stability. It is this stage of construction, prior to the casting of the deck that is primarily of interest. In this chapter, a physical description of the construction-stage bridge structures under consideration in this study will be provided along with the definition of relevant terminology.
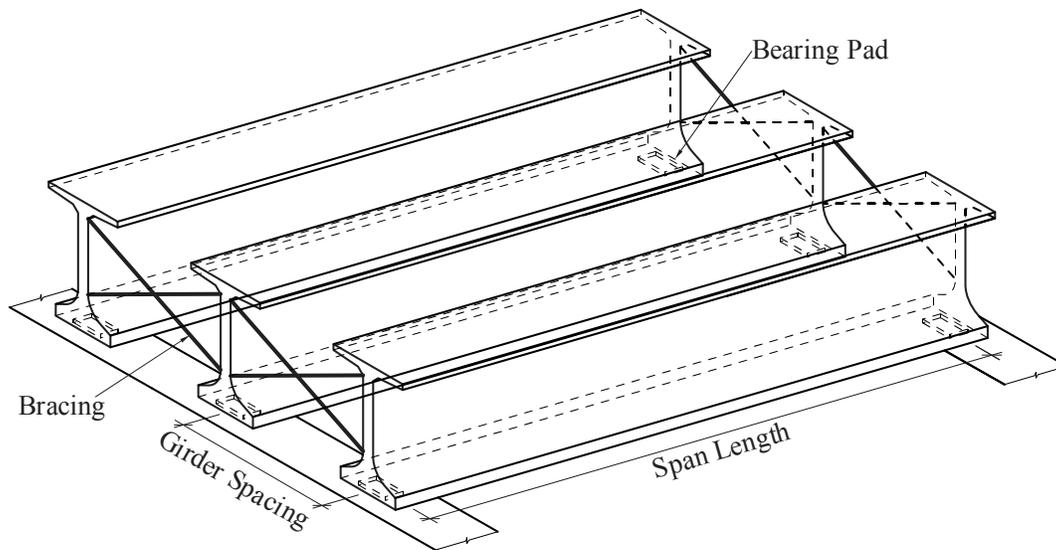
Figure 2.1 Girder system

2.2 Geometric parameters

The term *girder system* will be used to refer to a group of one or more FIBs braced together in an evenly spaced row (Figure 2.1). In addition to span length and spacing, there are several geometric parameters that define the shape and placement of the girders within a system. They are:

- Grade: Longitudinal incline of the girders, typically expressed as a percentage of rise per unit of horizontal length (Figure 2.2).
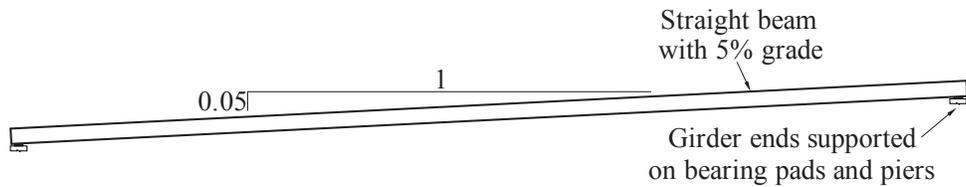
Figure 2.2 Definition of grade (side view)

- Cross-slope: The transverse incline (slope) of the deck, expressed as a percentage, which results in girders that are staggered vertically (Figure 2.3).
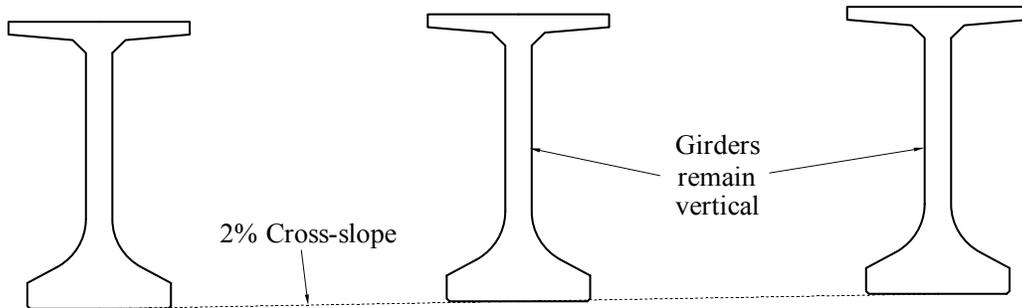
Figure 2.3 Definition of cross-slope (section view)

- Skew angle: Longitudinal staggering of girders, due to pier caps that are not perpendicular to the girder axes (Figure 2.4).
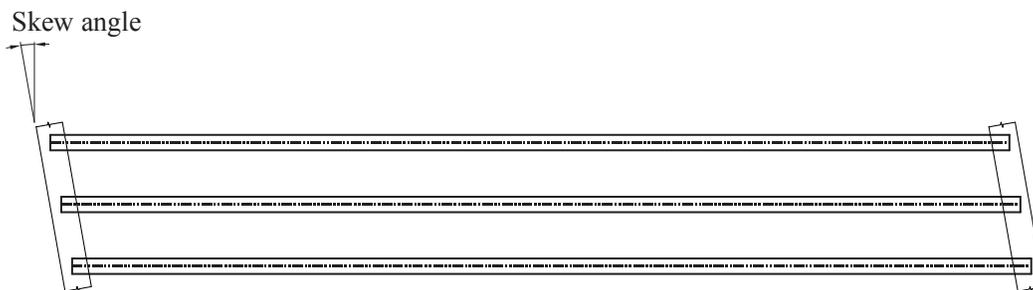
Figure 2.4 Definition of skew (top view)

- Camber: Vertical bowing of the girder (Figure 2.5) due to prestressing in the bottom flange expressed as the maximum vertical deviation from a perfectly straight line connecting one end of the girder to the other. Note that the total amount of vertical camber immediately following girder placement is larger than the camber in the completed bridge structure because the weight of the deck is not yet present.
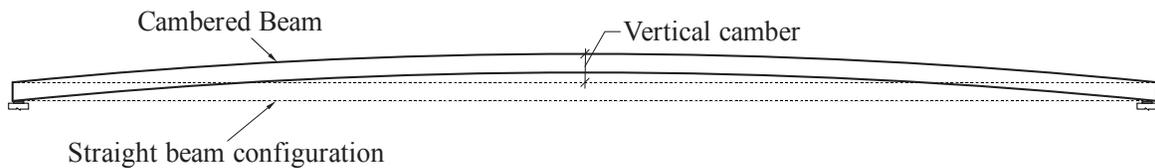
Figure 2.5 Definition of camber (elevation view)

- <u>Sweep</u>: Lateral bowing of the girder (Figure 2.6) due to manufacturing imperfections, expressed as the maximum horizontal deviation from a perfectly straight line connecting one end of the girder to the other.
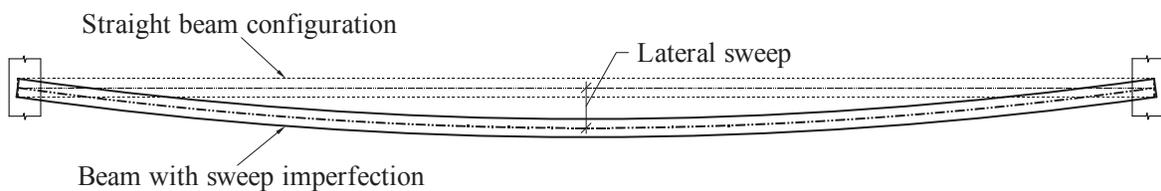
Figure 2.6 Definition of sweep (plan view)

2.3 Bearing pads

Bridge girders rest directly on steel-reinforced neoprene bearing pads which are the only points of contact between the girder and the substructure. There is generally sufficient friction between the pad and other structural components so that any movement of a girder relative to the substructure (with the exception of vertical uplift) must also move the top surface of the pad relative to the bottom surface. As a result, the girder support conditions in all six degrees of freedom can be represented as finite stiffnesses that correspond to the equivalent deformation modes of the pad. These deformation modes fall into four categories: shear, compression (axial), rotation (e.g., roll), and torsion. Calculation of these stiffnesses is addressed in Chapter 6.

2.4 Sources of lateral instability

Girder instability arises when the structural deformations caused by application of a load act to increase the moment arm of that load to such an extent that equilibrium cannot be achieved. The additional moment (often called the *secondary effects*) causes the structure to deform further, which increases the moment arm even more. In a stable system, this process continues until the structure converges on a deformed state in which static equilibrium is achieved. However, if the load exceeds some critical value (i.e., the buckling load), the system becomes unstable, in which case the process diverges and the structural deformations increase without bound (i.e., the structure collapses). Long-span bridge girders are susceptible to two primary modes of instability: *girder rollover* and *lateral-torsional buckling*.

Girder rollover refers to the rigid-body rotation of a girder with sweep imperfections resting on end supports (i.e., bearing pads) that have a finite roll stiffness. Sweep imperfections cause the force resultant of the girder self-weight (F) to be offset a small distance (Δ) from the

centerline of the supports (Figure 2.7). The eccentric vertical load imparts an overturning moment that causes the rigid girder to rotate until an equivalent restoring moment is generated at the supports. However, during rotation, the eccentricity of the load is increased, creating the potential for instability. If the weight of the girder is high enough and/or the bearing pad roll stiffness is low enough, the process will continue until the girder rolls off the pad.
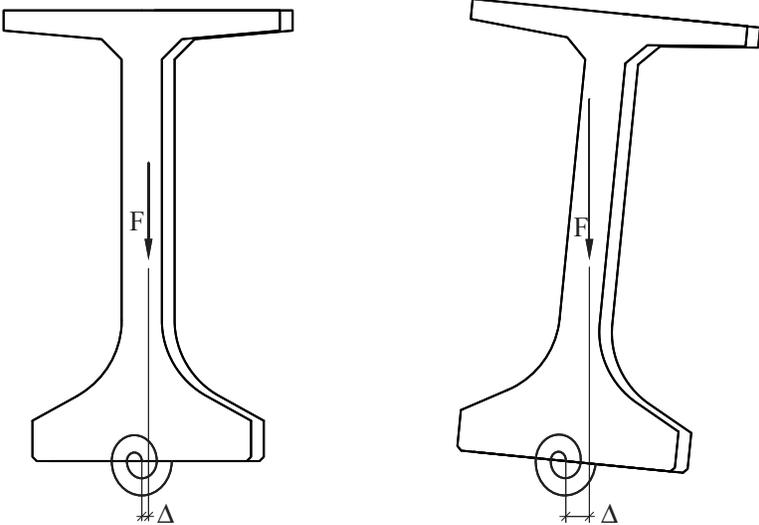
Figure 2.7 Rollover instability of girder

Lateral-torsional buckling is a similar phenomenon that occurs in flexible girders, even if the supports are rotationally rigid. In this case, the eccentric load induces lateral-torsional deformations in the girder that increase the load eccentricity (Figure 2.8). If the load is high enough to generate instability, the girder continues to deform until material failure (e.g., cracking) and, ultimately, structural collapse.
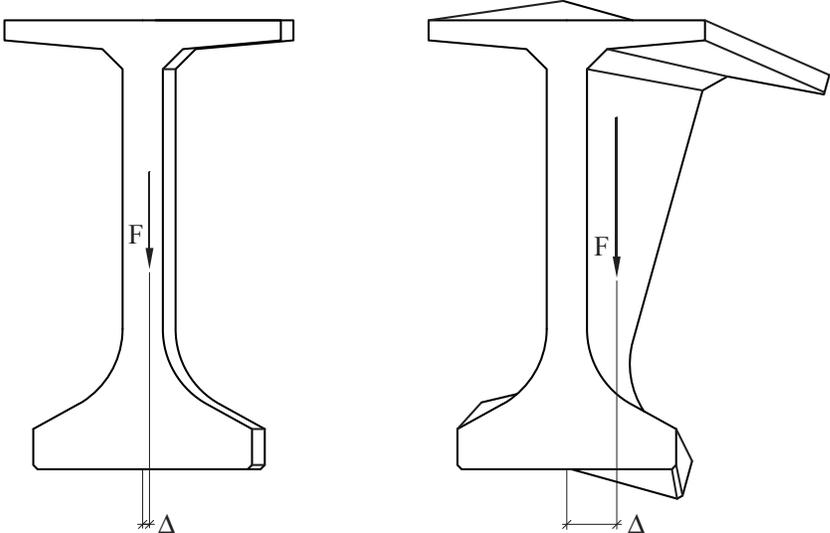
Figure 2.8 Lateral-torsional instability of girder

Both girder rollover and lateral-torsional buckling have been studied thoroughly in isolation. However, in real girders, the instability modes are *coupled*: any additional load eccentricities caused by girder rollover will induce additional lateral-torsional buckling, and vice versa. It is not sufficient to perform separate analyses of each mode and superpose the results.

Deviations from ideal straightness tend to increase the potential for girder instability. This is most intuitive in the case of sweep: a higher initial eccentricity induces more overturning moment. However, increasing vertical camber can also make a beam less stable by elevating the center of gravity of the girder. A higher load application point will displace farther laterally under the same amount of initial deformation (Figure 2.9) increasing the magnitude of the secondary effects. Effectively, two equal loads that are applied at different elevations will force a girder to roll/deform different amounts before reaching equilibrium. For a long-span girder, this difference can mean the difference between stable equilibrium being achieved, or buckling instability occurring.
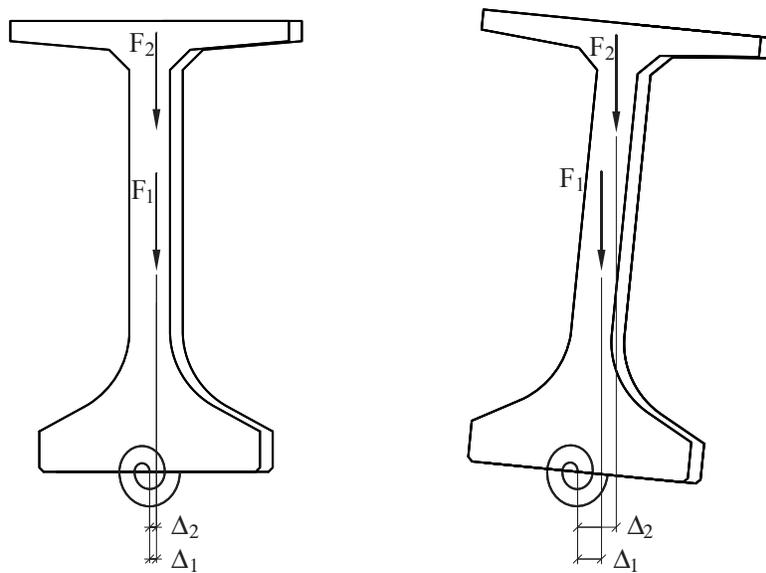
Figure 2.9 Increase in secondary effects due to higher application of vertical load

2.5 Lateral wind loads

In addition to gravity induced self-weight, girder systems are also subjected to intermittent lateral wind loads of varying intensity throughout the construction process. Wind loads are generally modeled as uniform pressure loads applied to girders in the lateral (transverse) direction. These types of loads can have a severely destabilizing effect on girder systems. Because the force resultant at the center of pressure (W) is offset from the bearing pad supports, large overturning moments can be generated that contribute directly to girder rollover. Furthermore, the wind force causes the girders to bend laterally (about their weak axes). This can increase the eccentricity of the self-weight, increasing the potential for instability (Figure 2.10).
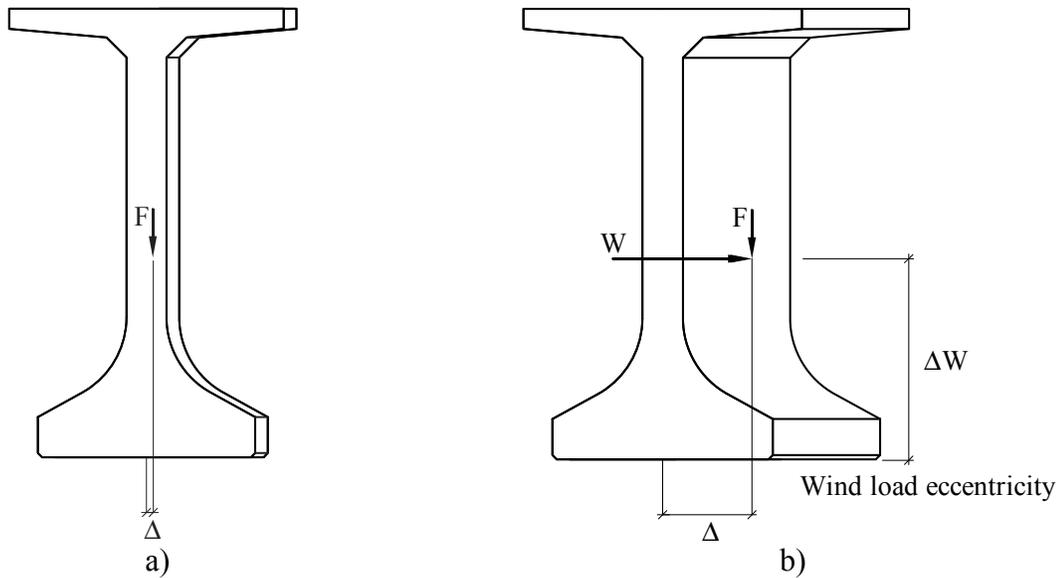
Figure 2.10 Effects of wind on stability of girder:
a) Girder without wind load; b) Girder with wind load

2.6 Temporary bracing

During construction, girders are often braced to prevent lateral instability from arising. Usually, these braces are temporary and are removed after the deck is cast. Bracing is divided into two basic types: anchor bracing and girder-to-girder bracing.

2.6.1 Anchor bracing

Because the first girder in the erection sequence has no adjacent girders to brace against, *anchors* are used to brace the ends of the girder to the pier. Anchors can take the form of inclined structural members such as telescoping steel rods (Figure 2.11a) or tension-only members such as cables (Figure 2.11b) or chains (Figure 2.11c). In addition to their lateral incline, it is common for anchors to also be inclined inward (towards the center of the span) so that they can reuse the same precast connections that are used to stabilize girders during transportation (Figure 2.12).

Anchors are generally not as effective as girder-to-girder bracing; because they can only restrain the girders at the ends, they can prevent girder rollover but not lateral-torsional buckling. For this reason, anchors are generally only used on the first girder to be erected and are not used on subsequent girders.
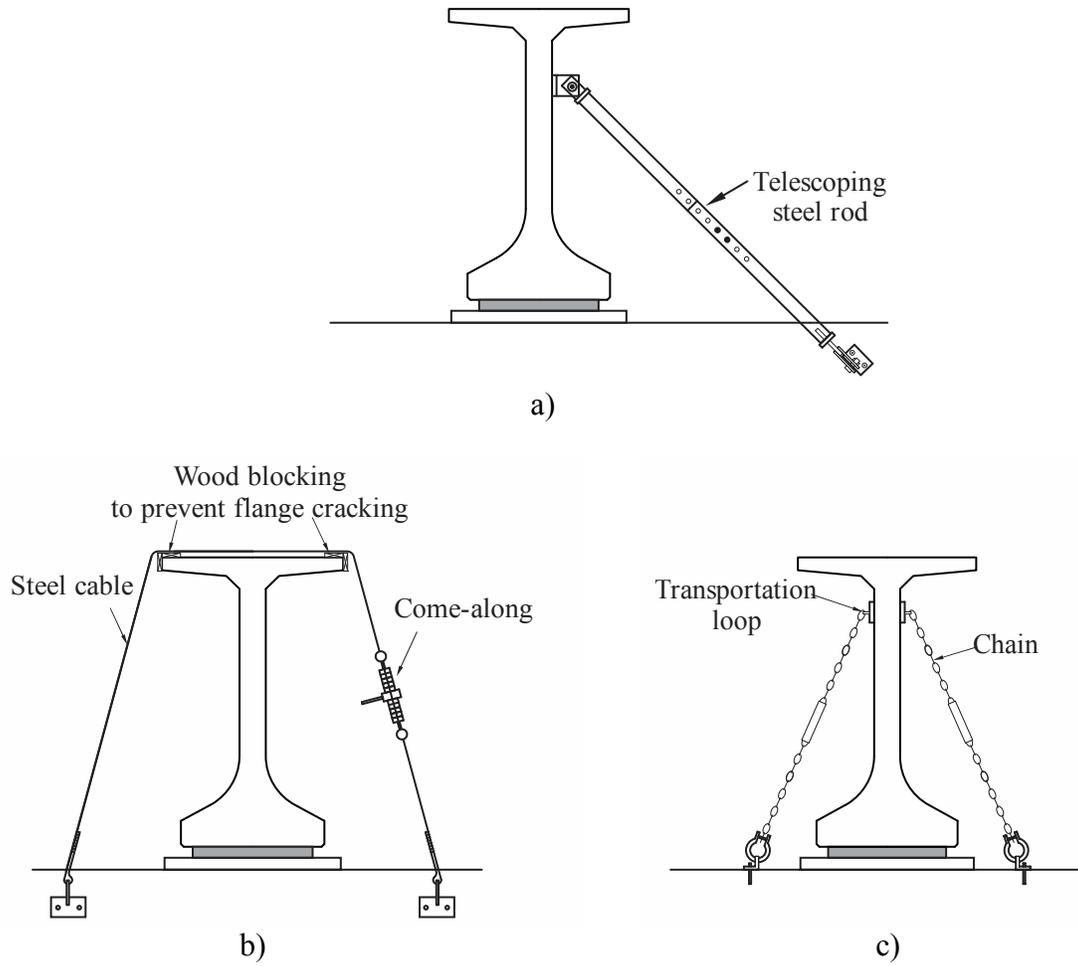
Figure 2.11 Common anchor types: a) Structural member; b) Cable; c) Chain

Figure 2.12 Chain braces on Florida Bulb-Tee during transportation

2.6.2 Girder-to-girder bracing

As adjacent girders are erected, girder-to-girder braces (henceforth known simply as *braces*) are used to connect the girders together into a single structural unit. Because the braces can be installed at interior points (i.e., away from the girder ends), they are capable of providing resistance to both lateral-torsional and rollover instabilities. Typically, interior braces are spaced at unit fractions of the girder length. For example, *third-point bracing* divides the girder into three equal unbraced lengths. Brace point locations are offset somewhat in skewed bridges because *Design Standard No. 20005: Prestressed I-Beam Temporary Bracing* (FDOT, 2012a) requires that all braces be placed perpendicular to the girders (Fig. 2.13).
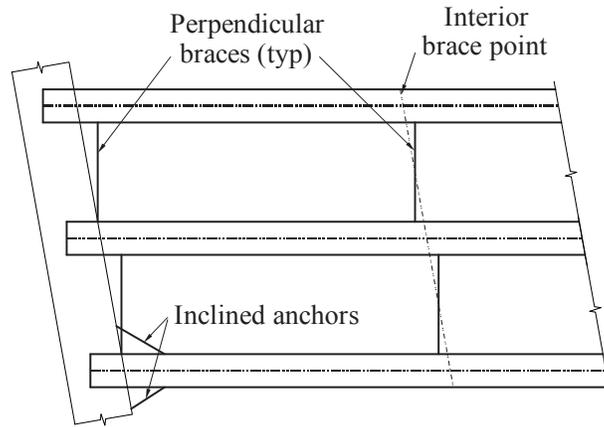
Figure 2.13 Perpendicular brace placement on skewed bridge

Braces are typically constructed from timber or rolled-steel members, but individual brace designs are left to the discretion of the contractor, so a wide variety of bracing configurations are used in practice. Common types of brace include X-braces (Figure 2.14a), K-braces (Figure 2.14b), and simple compression struts (Fig 2.14c). Braces are attached to the girders via bolted connections, welded to cast-in steel plates, or simply wedged tightly in place between the girders. In the latter case, an adjustable tension tie, such as a threaded bar (Figure 2.14d), is normally included to prevent the girders from separating far enough for the braces to become dislodged.
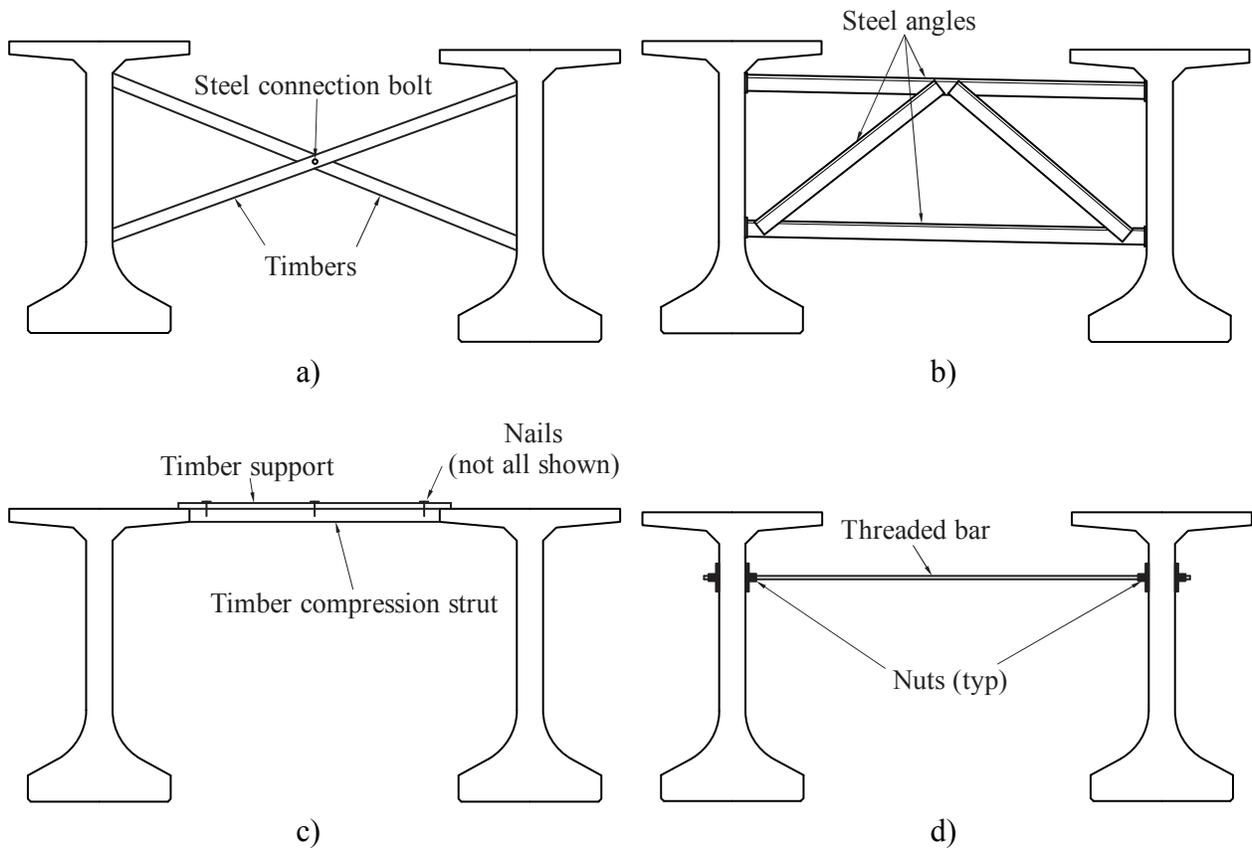
Figure 2.14 Common brace types:
a) X-brace; b) K-brace; c) Compression strut; d) Tension tie

CHAPTER 3
BACKGROUND ON DRAG COEFFICIENTS

3.1 Introduction

In order to calculate the wind load on a bridge girder, it is necessary to know the drag coefficient for the girder cross-sectional shape. The drag coefficient is a type of *aerodynamic coefficient*: a dimensionless factor that relates the magnitude of the fluid force on a particular geometric shape to the approaching wind speed. Drag coefficients are typically a function of the relative orientation of the object with the direction of the impinging wind.

3.2 Dimensionless aerodynamic coefficients

Fluid forces arise when a solid body is submerged in a moving fluid. As the fluid flow is diverted around the body, a combination of inertial and frictional effects generates a net force on the body. It is observed that this force—called aerodynamic force (*F*) when the fluid under consideration is air—is directly proportional the dynamic pressure (*q*) of the fluid:

$$q = \frac{1}{2}\rho V^2 \tag{3.1}$$

where ρ is the mass density of the fluid and *V* is the flow velocity (Çengel and Cimbala, 2006). Dynamic pressure can be considered as the *kinetic energy density* of the fluid. This offers an intuitive explanation for its proportional relationship to aerodynamic force, which is, at the most fundamental level, the cumulative effect of innumerable microscopic collisions with individual fluid particles. Similarly, if the dimensions of the body are scaled up, it is observed that the aerodynamic force increases quadratically, reflecting the fact that the increased surface area results in a greater total number of collisions.

These proportional relationships can be combined and expressed as:

$$F = C_F q L_0 L_1 \tag{3.2}$$

where L_0 and L_1 are arbitrary reference lengths and C_F is a combined proportionality factor, called a *force coefficient*. The selection of L_0 and L_1 does not affect the validity of Equation 3.2 as long as they both scale with the structure. However, it is important to be consistent; force coefficients that use different reference lengths are not directly comparable, and a coefficient for which the reference lengths are not explicitly known is useless for predicting aerodynamic forces. In structural applications, it is common for the product $L_0 L_1$ to be expressed in the form of a reference area, *A*, which is typically taken as the *projected area* of the structure in the direction of wind.

By an analogous process, it is possible to derive a *moment coefficient* (C_M), which normalizes aerodynamic moment load in the same way that the force coefficient normalizes aerodynamic force. The only difference is that aerodynamic moment grows cubically with body size rather than quadratically (because the moment arms of the individual collisions grow along with the surface area). Therefore, the moment proportionality expression is:

$$M = C_M q L_0 L_1 L_2 \tag{3.3}$$

As with the force coefficient, the reference lengths must be known in order to properly interpret the C_M. However, with moment coefficients, it is equally important to know the center of rotation about which the normalized moment acts. Together, C_F and C_M are called *aerodynamic coefficients*, and they can be used to fully describe the three-dimensional state of aerodynamic load on a structure (for a particular wind direction).

When working with bridge girders, or other straight, slender members, it is often convenient to assume that the length of the girder is effectively infinite. This simplifies engineering calculations by reducing the girder to a two-dimensional cross-section subjected to in-plane aerodynamic line-loads (Figure 3.1). Depending on the direction of wind, out-of-plane forces and moments may exist, but they generally do not contribute to the load cases that control design and can therefore be considered negligible. In two dimensions, the proportionality expressions for the aerodynamic coefficients become:

$$F' = C_F q L_1 \tag{3.4}$$

$$M' = C_M q L_1 L_2 \tag{3.5}$$

where F' is a distributed force (force per unit length) and M' is a distributed torque (moment per unit length). Note that two-dimensional aerodynamic coefficients can be used interchangeably in the three-dimensional formulation if one reference length (L_0) is taken to be the out-of-plane length of the girder. All further discussions of aerodynamic coefficients in this report will use the two-dimensional formulation unless stated otherwise. The remaining reference lengths (L_1 and L_2) will always be taken as the girder depth, D, so that the force and moment coefficients are defined as:

$$C_F = \frac{F'}{\frac{1}{2}\rho V^2 D} \tag{3.6}$$

$$C_M = \frac{M'}{\frac{1}{2}\rho V^2 D^2} \tag{3.7}$$
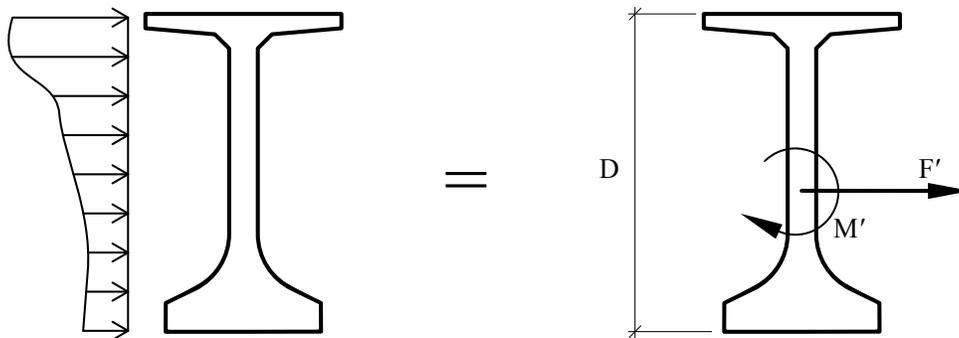
Figure 3.1 Two-dimensional bridge girder cross-section with in-plane line loads

13

Aerodynamic coefficients are sometimes called *shape factors* because they represent the contribution of the geometry of an object (i.e., the way airflow is diverted around it), independent of the scale of the object or the intensity of the flow. Because of the complexity of the differential equations governing fluid flow, the aerodynamic coefficients of a structure are not calculated from first principles but can, instead, be measured directly in a wind tunnel using reduced-scale models.

3.3 Terminology related to aerodynamic coefficients

Aerodynamic force on a body is typically resolved into two orthogonal components, drag and lift. These components have corresponding force coefficients: the *drag coefficient* (C_D) and *lift coefficient* (C_L). In this report, drag is defined as the lateral component of force and lift is defined as the vertical component of force, regardless of the angle of the applied wind.

In several subfields of fluid dynamics, it is more conventional to define drag as the component of force along the direction of the wind stream and lift as the component perpendicular to the wind stream. However, this is inconvenient when evaluating wind loads on stationary structures (e.g., bridge girders) because the angle of the wind stream can change over time. Where necessary in this report, the names *stream drag* (C_{SD}) and *stream lift* (C_{SL}) (Figure 3.2) will be used to refer to the force components that are aligned with, and perpendicular to, the wind stream.
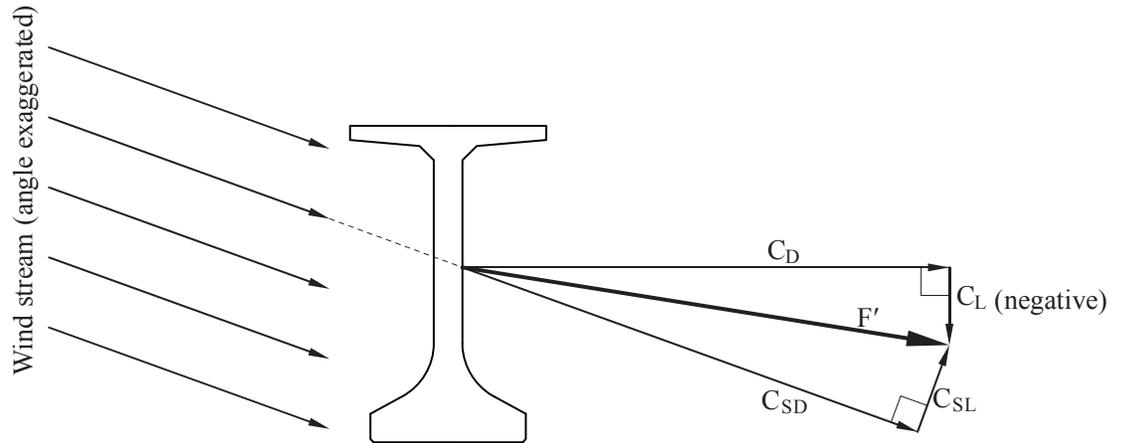
Figure 3.2 Definition of C_D, C_L, C_{SD}, and C_{SL}
(shown in positive direction except when noted)

Finally, the term *pressure coefficient* (C_P), is an alternative name for C_D, and is often used in design codes to indicate that it is to be used to calculate a wind *pressure* load (P) rather than a total force, as in:

$$P = C_P \frac{1}{2} \rho V^2 \tag{3.8}$$

This is advantageous because it obviates the need to explicitly specify the characteristic dimensions that were used to normalize the coefficient. Instead, denormalization occurs

implicitly when the pressure load is applied over the projected surface area of the structure. Unfortunately, this approach breaks down when working with drag and lift coefficients together. If drag and lift are both represented as pressure loads, then the areas used to normalize the coefficients will differ (unless by chance the depth and width of the structure are equal). As a result, the magnitudes of the coefficients are not directly comparable—that is, equal coefficients will not produce loads of equal magnitude—and they cannot be treated mathematically as components of a single force vector, which complicates coordinate transformations and other operations. For this reason, the term pressure coefficient is not used in this report, except when in reference to design codes that use the term.

In this report, the term *torque coefficient* (C_T) refers to the in-plane moment that acts about the centroid of the cross-section. This is a convenient choice of axis because it coincides with the axes of beam elements in most structural analysis software. Loads calculated from C_D, C_L, and C_T can be applied directly to beam nodes (located at the centroid of the cross-section) to correctly model the two-dimensional state of aerodynamic load. However, most design codes represent wind load as a uniform pressure load that produces a resultant force acting at a location called the *center of pressure* (Figure 3.3), which is typically assumed to correspond to the mid-height of the cross-section. For reasons that are explained fully in Chapter 5, it is occasionally more convenient to work with a torque coefficient that acts about that center of pressure. In such circumstances, the term *pressure torque coefficient* (C_{PT}) will be used to differentiate it from the C_T, which always acts about the centroid (Figure 3.4).
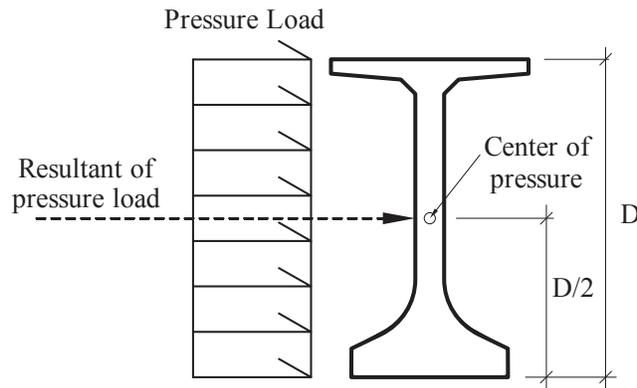
Figure 3.3 Center of pressure of a bridge girder

Torque acting about
the centroid +

Torque acting about the
center of pressure ○
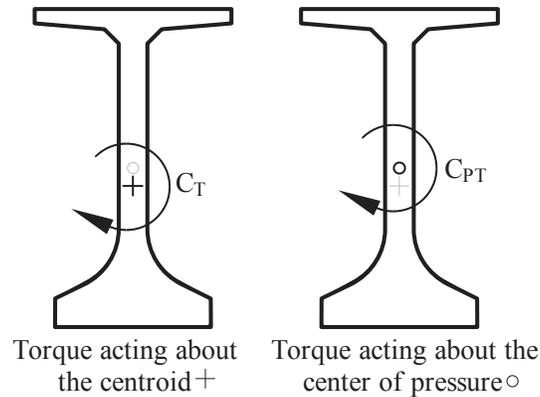
Figure 3.4 Definition of C_T and C_{PT} (shown in positive direction)

A summary of the different types of aerodynamic coefficient used in this report is presented in Table 3.1.

Table 3.1 Summary of aerodynamic coefficients

	Coefficient name	Description
C_D	Drag	Component of force in horizontal (lateral) direction
C_L	Lift	Component of force in vertical direction
C_{SD}	Stream Drag	Component of force parallel to wind stream
C_{SL}	Stream Lift	Component of force perpendicular to wind stream
C_P	Pressure	Alternative name for C_D
C_T	Torque	Torque measured about centroid
C_{PT}	Pressure Torque	Torque measured about center of pressure

3.4 Current wind design practice in Florida

Bridge structures in Florida are designed in accordance with the provisions of the *Structures Design Guidelines* (SDG; FDOT, 2012e). As with most modern design codes, the wind load provisions in the SDG are based on Equation 3.8, with additional scale factors included to adjust the intensity of the wind load according to the individual circumstances of the bridge. Specifically, Section 2.4 of the SDG gives the equation:

$$P_Z = 2.56 \times 10^{-6} K_Z V^2 G C_P \tag{3.9}$$

where P_Z is the design wind pressure (ksf), K_Z is the velocity pressure exposure coefficient, V is the basic wind speed (mph), and G is the gust effect factor. The constant term, 2.56×10^{-6}, represents the quantity $\frac{1}{2}\rho$ from equation 3.8 expressed in derived units of $(\text{ksf})/(\text{mph})^2$.

Each county in Florida is assigned a basic wind speed, V, adapted from wind maps published by the American Society of Civil Engineers (ASCE 2006), which are based on statistical analyses of historical wind speed records compiled by the National Weather Service. Statistically, V represents the peak 3-second gust wind speed for a 50-year recurrence interval. In other words, if the average wind speeds during every 3-second time interval were recorded over

16

a period of 50 years, V is the expected value of the maximum speed that would be recorded. It is important to note that this does *not* mean that Florida bridges are only designed to resist 50-year wind loads. Different load combinations use load factors for wind that effectively adjust the recurrence interval up or down. For example, the Strength III limit state, as stipulated by the SDG, includes a wind load factor of 1.4, which increases the recurrence interval to approximately 850 years (FDOT 2009). Load combinations for scenarios that do not include extreme wind speeds stipulate that the wind load be calculated using a basic wind speed of 70 mph, regardless of the location of the structure.

Basic wind speeds published by ASCE are based on measurements taken at an elevation of 33 ft and are not directly applicable to structures at other elevations. Wind that is closer to ground level is slowed by the effect of surface friction, resulting in a vertical wind gradient called the atmospheric boundary layer (Holmes, 2007). The purpose of the velocity pressure exposure coefficient, K_Z, is to modify the wind pressure load to account for differences in elevation. Because surface roughness of the terrain is known to reduce the steepness of the gradient, ASCE divides terrains into three exposure categories, B, C, and D, and provides equations for each category. However, for simplicity, the SDG conservatively assumes that all Florida structures are in the Exposure C category. As a result, the equation for K_Z in Florida is:

$$K_Z = 2.01 \left(\frac{z}{900} \right)^{0.2105} \geq 0.85 \tag{3.10}$$

where z is the elevation above ground (ft). Note that K_Z is equal to unity at an elevation of 33 ft (corresponding to the wind speed measurements) and that wind speed is assumed to be constant for elevations of 15 ft or less (Figure 3.5).
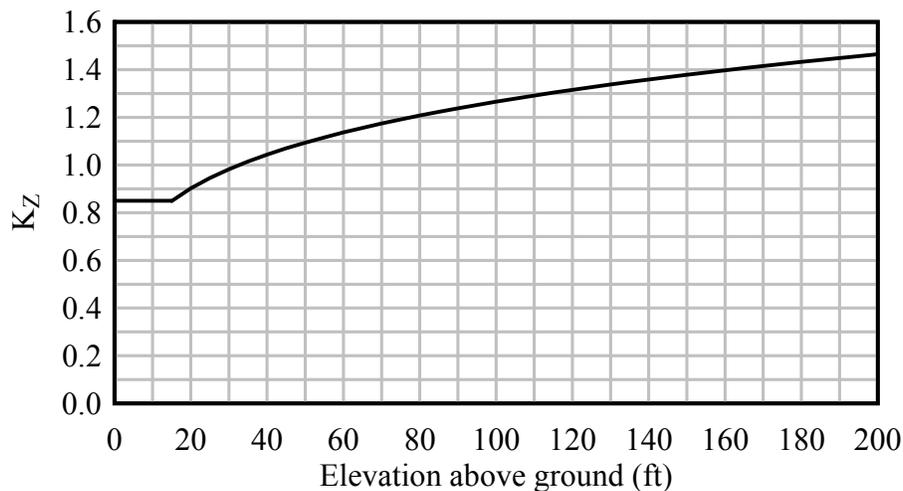
Figure 3.5 Velocity pressure exposure coefficient used by FDOT

Wind is characteristically gusty and turbulent, producing dynamic structural loads that can fluctuate significantly over short periods of time. However, it is simpler and more efficient to design structures to resist static loads. Furthermore, wind tunnel measurements of static force coefficients are typically performed in steady flow (with a major exception being site-specific

wind tunnel testing, which models a proposed structure along with its surrounding terrain for the express purpose of capturing turbulent loads). The gust effect factor, G, modifies the static design wind pressure so as to envelope the effects of wind gustiness and dynamic structural response on peak structural demand. For aerodynamically rigid bridge structures, defined as those with spans less than 250 ft and elevations less than 75 ft, the SDG prescribes a gust effect factor of 0.85. By this definition, the vast majority of precast prestressed concrete girder bridges in Florida are aerodynamically rigid. It is noted that G actually *reduces* the design wind pressure on rigid bridges, reflecting the fact that peak gust pressures are unlikely to occur over the entire surface area of such structures simultaneously (Solari and Kareem, 1998).

The SDG further provides specific guidance on the calculation of wind loads during the bridge *construction* stage (as opposed to the calculation of wind loads on the completed bridge structure). If the exposure period of the construction stage is less than one year, a reduction factor of 0.6 on the basic wind speed is allowed by the SDG. During active construction, the basic wind speed can be further reduced to a base level of 20 mph. Temporary bracing must be designed for three load cases: Girder Placement (construction active), Braced Girder (construction inactive), and Deck Placement (construction active).

Calculation of wind pressure using Equation 3.9 requires that an appropriate pressure coefficient (C_P) be determined for the structure under consideration. Pressure coefficients are provided by the SDG for several broad categories of bridge component as indicated in Table 3.2. In the Girder Placement and Braced Girder load cases noted above, pressure coefficients are needed for girders *without* deck forms or a completed deck in place. As Table 3.2 indicates, the SDG provides two such values of C_P depending on the shape of the girder cross-section: $C_P =$ 2.2 for I-shaped girders (Figure 3.6), and $C_P = 1.5$ for box or U-shaped girders (Figure 3.7).

Table 3.2 Pressure coefficients in *Structures Design Guidelines* (FDOT, 2012e)

Bridge component	C_P
Substructure	1.6
Girders with deck forms	1.1
Completed superstructure	1.1
I-shaped bridge girders	2.2
Box and U-shaped girders	1.5
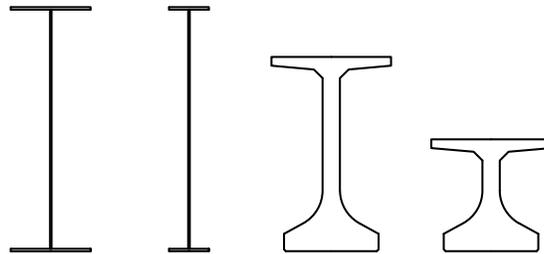
Figure 3.6 Examples of I-shaped girders (steel plate girders and Florida-I Beams) for which $C_P = 2.2$ (per FDOT, 2012e)

Figure 3.7 Example open-top box girder cross-section for which $C_P = 1.5$ (per FDOT, 2012e)

3.5 Literature review: drag coefficients for bridge girders

The wind load provisions in the SDG are, for the most part, well supported by research. The main exception is the pressure coefficients (drag coefficients) prescribed for girders in partially-erected bridges without deck forms or a completed deck in place. While experimentally measured drag coefficients have been published for simple geometric shapes, truss members, buildings, and complete bridge superstructures, there has been little investigation of the aerodynamic properties of individual bridge girder shapes in the literature, and none specifically addressing the Florida FIB shapes. In lieu of more specific information, the SDG pressure coefficients (noted in Table 3.2) are based on the assumption that the drag (or pressure) coefficient (C_D) of a girder can be approximated by the C_D of a rectangle with the same width-to-depth ratio. Drag coefficients for rectangles with various width-to-depth ratios, taken from Holmes (2007) and other sources, are shown in Figure 3.8. It is clear that there is significant variation of C_D as the width-to-depth (W/D) ratio changes. Also shown in the figure are W/D ranges for typical girder types common to the state of Florida. Finally, W/D values for the specific girder cross-sectional shapes tested (in a wind tunnel) in this study are also indicated (additional details regarding these shapes will be provided in Chapter 4).
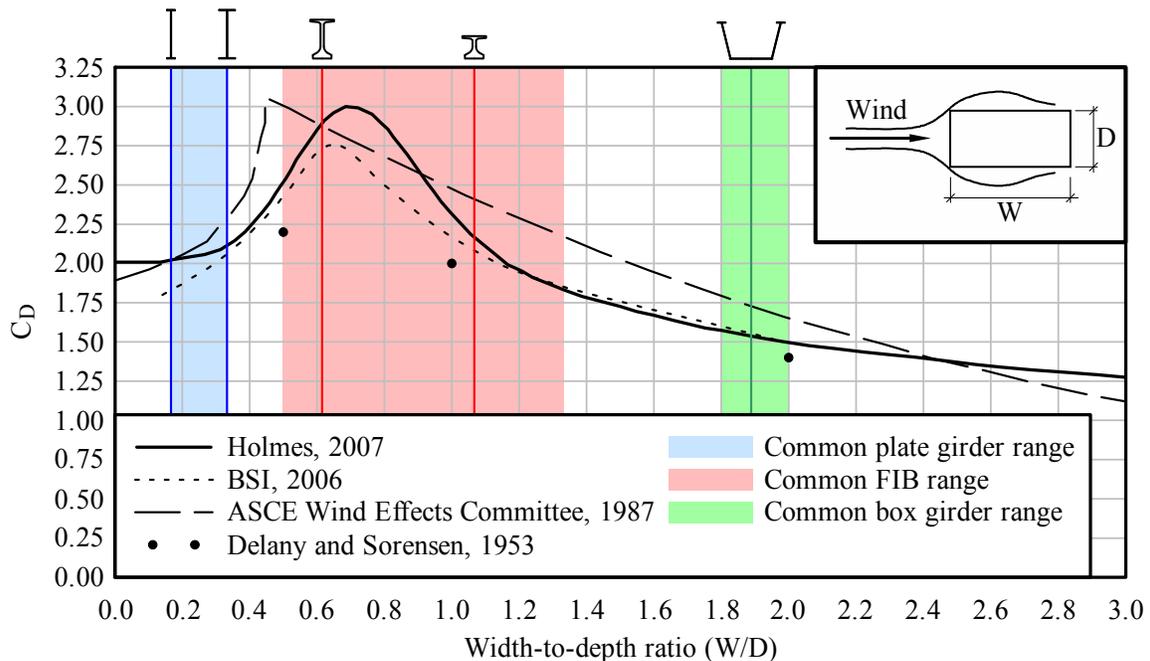
Figure 3.8 Drag coefficients for rectangular sections with various width-to-depth ratios

While drag coefficients for typical concrete bridge girder I-shapes could not be located in the literature, there have been some published studies of thin-walled I-shapes characteristic of rolled steel members (Table 3.3).

Table 3.3 Drag coefficients (C_D) of thin-walled I-shapes

	Width-to-depth ratio (W/D)				
Data source	0.48	0.50	0.64	1.00	1.23
Maher and Wittig (1980)	-	-	-	-	1.90
Grant and Barnes (1981)	-	-	2.20	-	-
Simiu and Miyata (2006)	-	1.87	-	1.78	-
SIA *Normen 160* (1956)	2.05	-	-	1.60	-
AIJ (2004)	-	2.10	-	-	-
ESDU (1982)	-	1.94	-	1.62	-

Maher and Wittig (1980) measured C_{SD}, C_{SL}, and C_T for a truss bridge member with a width-to-depth ratio of 1.23. In head-on wind (0° angle of attack), the C_D was reported as 1.9. Similarly, Grant and Barnes (1981) performed wind tunnel tests on several structural members, including an I-shape with a width-to-depth ratio of approximately 0.64 (exact dimensions were not given) which had a C_D of 2.2. In a general reference text, Simiu and Miyata (2006) provided several plots of drag coefficients for a wide range of shapes. These plots included two data points for I-shapes with ratios of 0.50 ($C_D = 1.87$) and 1.00 ($C_D = 1.78$).

Some of the most widely published coefficients for I-shapes were originally produced by the Swiss Society of Engineers and Architects (SIA) for *Normen ["Standard"] 160: On Load Assumptions, Acceptance and Supervision of Buildings* (1956, English translation reproduced in Davenport, 1960). Normen 160 contained pressure coefficient specifications for a wide variety of structures and structural components that, at the time, were considered the most refined and comprehensive treatment of the subject (Davenport, 1960). Tables of drag and lift coefficients from Normen 160—including I-shapes with width-to-depth ratios of 0.48 ($C_D = 2.05$) and 1.00 ($C_D = 1.6$)—have since been reproduced in multiple sources, including the Commentary of the National Building Code (NBC) of Canada (NRC, 2005; Sachs, 1978; Scruton and Newberry, 1963). The exact origins of the coefficients are unknown, but the NBC commentary states that they were based on "wind-tunnel experiments".

Other jurisdictions provide varying levels of guidance regarding drag coefficients for I-shapes. In Japan, the de facto design code (AIJ, 2004) includes a C_D of 2.1 for an I-shape with a width-to-depth ratio of 0.50. The AIJ commentary cites an unobtainable Japanese-language paper as the source of this value. Great Britain, like the FDOT, assumes that the girder cross-sections are aerodynamically similar to rectangles, and provides a plot (reproduced in Figure 3.8) for selecting the coefficient based on the width-to-depth ratio of the cross-section (BSI, 2006). The European Union simply recommends a blanket value of 2.0 for all "sharp-edged structural sections" (CEN 2004).

ESDU, a non-governmental organization that produces engineering reference materials, has performed its own literature review of drag coefficients for structural members, and it has published a reference (ESDU, 1982) that synthesizes data from multiple sources, including several of those discussed above and several foreign language sources. Drag coefficients are

provided for I-shapes with width-to-depth ratios of 0.50 ($C_D = 1.94$) and 1.00 ($C_D = 1.62$), with an estimated uncertainty of approximately ±15%. Interpolation between the two data points is encouraged.

All of the I-shapes investigated in the literature are for basic truss or building members and did not include any width-to-depth ratios less than approximately 1/2. However, most steel I-shapes used in long-span bridge girders have width-to-depth ratios that range roughly from 1/6 to 1/3. Because C_D tends to vary with width-to-depth ratio, there is no reason to believe that the results of these studies are directly applicable to steel bridge girders. Furthermore, when the data are plotted (Figure 3.9), it becomes clear that the equivalent rectangle is a poor (albeit conservative) predictor of aerodynamic properties.
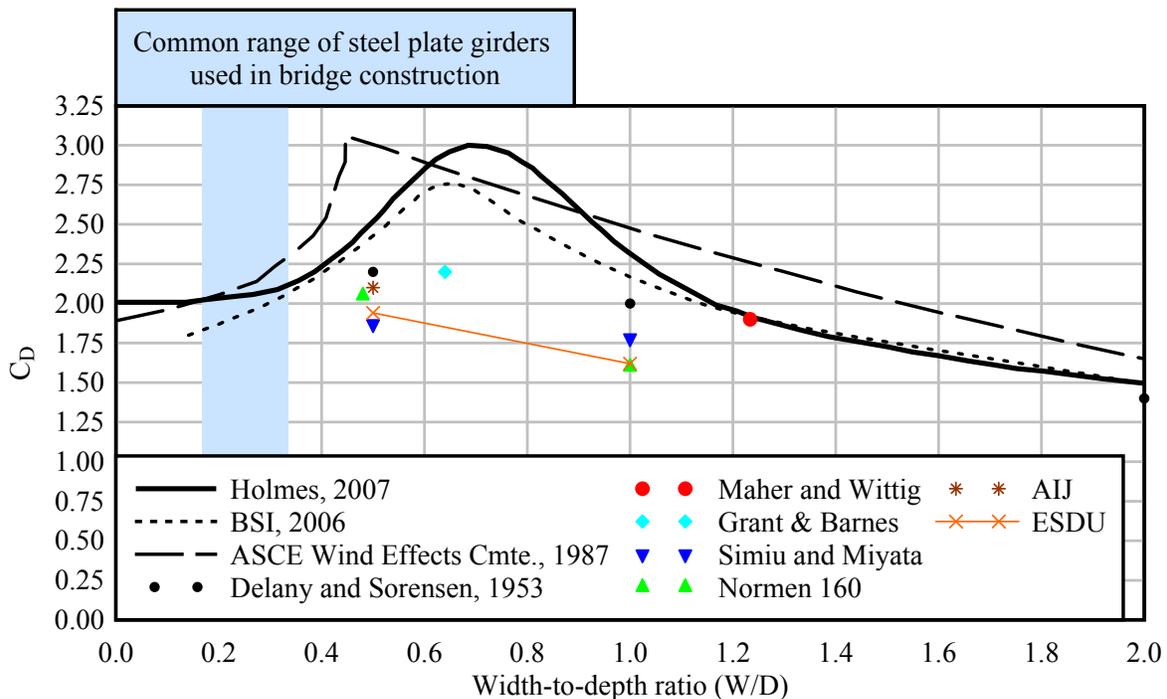
Figure 3.9 Drag coefficients for plate girder shapes and rectangles
with various width-to-depth ratios

Regarding box girders, the SDG provides a value of 1.5, which is a common choice for box-shaped bridge decks. However, before the deck is cast, the top of the girder is open. A search of the literature found only one source that discusses the aerodynamic properties of open-top box girders. Myers and Ghalib (n.d.) used a two-dimensional computational fluid dynamics analysis to calculate the drag on a pair of such girders. While coefficients for the individual girders were not provided, they concluded that drag coefficients can be significantly higher on a girder with an open top.

CHAPTER 4
WIND TUNNEL TESTING

4.1 Introduction

A key goal of this research was the characterization of temporary bracing requirements for long-span prestressed concrete girders, prior to the casting of the deck. Wind tunnel tests were an important component of this investigation because lateral wind loads tend to control bracing designs. However, the aerodynamic properties of most common bridge girder shapes have not been widely studied, so additional goals of this research were to use wind tunnel testing to quantify aerodynamic properties (e.g., drag coefficients) and to develop a simplified loading procedure that can be applied to wide variety of common girder shapes.

Because nearly all bridge structures are made up of multiple girders positioned side by side, it was necessary to investigate the effect of shielding (i.e., aerodynamic interference), in which the windward girder acts as a wind break and reduces the total force on subsequent girders. Wind tunnel tests were therefore performed on groups of identical girders positioned in several different testing configurations.

4.2 Testing configurations

Five different girder cross-sectional shapes (Figure 4.1) were selected as being representative of a wide range of modern Florida bridges:

- 78-inch-deep Florida-I Beam (*78″ FIB*): Of the most commonly used FIB shapes, the 78″ FIB is the deepest and is most susceptible to instability.

- 45-inch-deep Florida-I Beam (*45″ FIB*): All FIB shapes have identical flanges, with the differences in girder depth arising from differences in the height of the web. The 45″ FIB was included in the study to quantify the effect of changing the FIB depth, and to ensure that the resulting design loads would be applicable to a range of FIB shapes.

- Wide-flange plate girder (*WF Plate*): Drag coefficients of I-shaped girders have been studied for width-to-depth ratios ranging from 1:1 to 2:1 (see Chapter 2). However, built-up steel plate girders commonly used to support bridge decks tend to be much deeper than they are wide. The WF Plate girder considered in this study has an 8-ft deep web and 2′-8″ wide flanges, resulting in a width-to-depth ratio of 3:1, representing the approximate lower bound for bridge girders.

- Narrow-flange plate girder (*NF Plate*): The NF Plate girder is identical to the WF Plate, but with flanges that are only one-half as wide. This gives it an upper bound width-to-depth ratio of 6:1.

- Open-top box girder (*Box*): The aerodynamic properties of box girder bridges have been studied, but experimental studies have not been performed on box girders with an open top (without the deck in place). A survey of existing box girder bridges was used to develop a representative 6-ft deep cross-section.

These sections were tested individually, as well as in groups of 2, 5, and 10 (Fig. 4.2). Fully dimensioned drawings of these girder cross-sections and each test configuration are included in Appendix A.
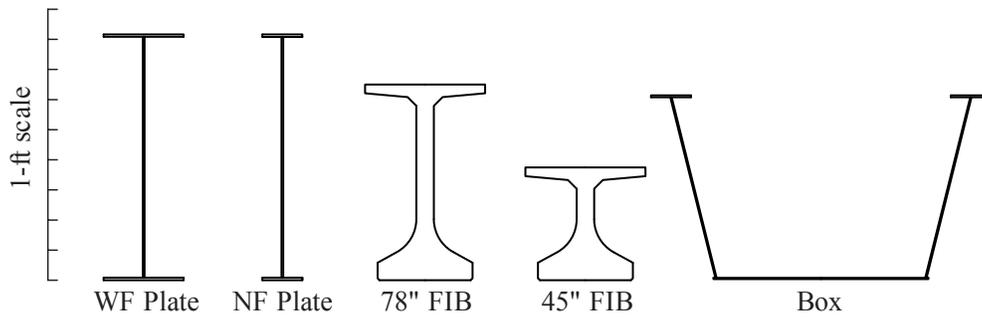
Figure 4.1 Girder cross-sections used in study (drawn to scale)
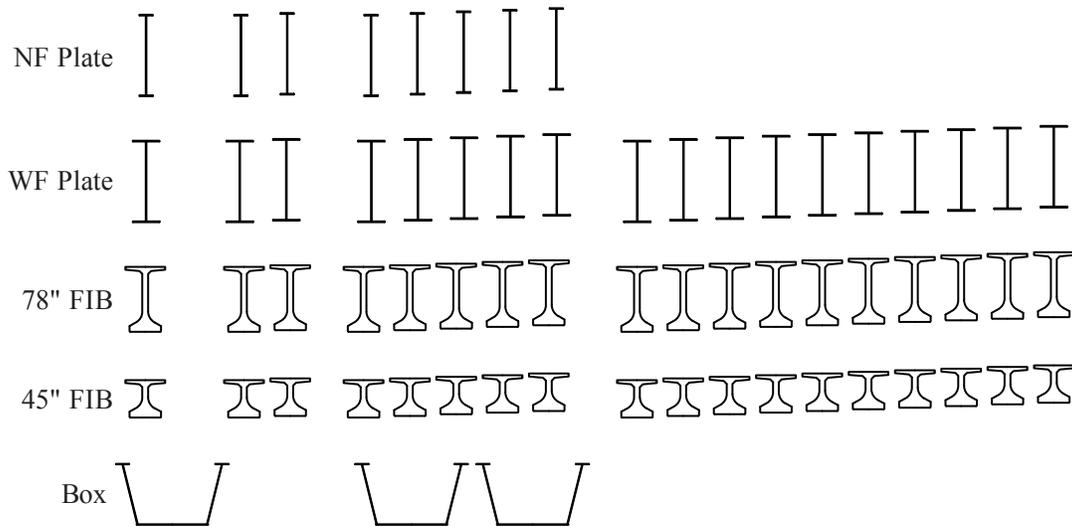
Figure 4.2 Girder groupings investigated in study
(girder-to-girder spacing not drawn to scale; cross-slopes vary)

The full set of test configurations is available in Table 4.1. Each testing configuration can be described by a unique combination of spacing, cross-slope, and number of girders (Fig 4.3):

G1   G2   G3   G4   G5

Girders remain veritcal

Cross-slope

Spacing

Windward Girder

Shielded girders
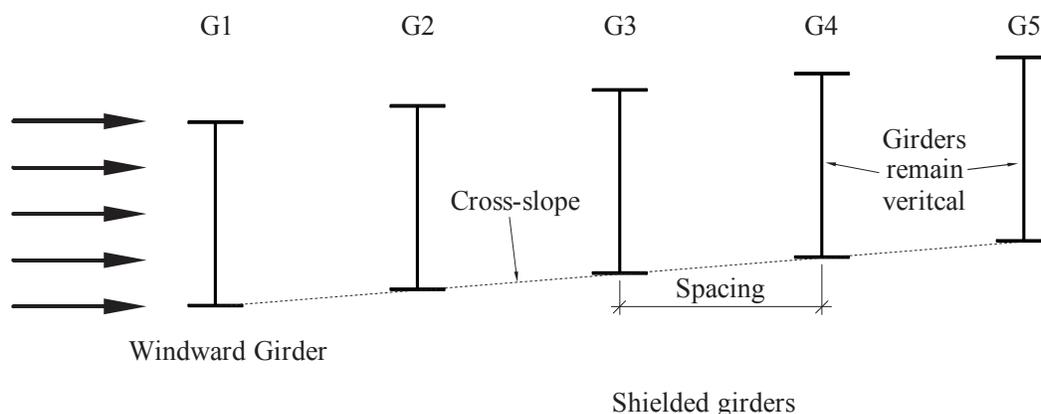
Figure 4.3 Parameters definitions for each testing configuration

Table 4.1 Testing configurations

	Min spacing	Max spacing	Tested wind angles (deg)
WF Plate	10 ft	14 ft	−5, −2.5, 0, +2.5, +5
NF Plate	10 ft	14 ft	−5, −2.5, 0, +2.5, +5
78″ FIB	10 ft	13 ft	−5, −2.5, 0, +2.5, +5
45″ FIB	10 ft	13 ft	−5, −2.5, 0, +2.5, +5
Box	20 ft	22 ft	−10, −5, 0, +5, +10

	2-girder models			5-girder models			10-girder-models	
	Min sp.	Max sp.	Inst.	Min sp.	Max sp.	Inst.	Max sp.	Inst.
WF Plate	2%, 8%	2%, 8%	All	2%, 8%	2%, 8%	All	8%	All
NF Plate	2%	2%	All	2%	2%	G1–G3	-	-
78″ FIB	2%	2%	All	2%	2%	G1–G3	+2%, −2%	All
45″ FIB	2%	2%	All	2%	2%	G1–G3	+2%, −2%	All
Box	0%	0%	All	-	-	-	-	-

4.2.1 Number of girders

In addition to tests of individual girders, wind tunnel tests were performed on 2-girder, 5-girder, and 10-girder configurations. Each girder in a given test configuration was referred to by a sequential number starting with the windward girder, G1. In most configurations, individual force measurements were recorded for each girder. The only exceptions were the 5-girder configurations of the NF Plate, 78″ FIB, and 45″ FIB where measurements were only recorded for girders G1–G3.

4.2.2 Spacing

Spacing refers to the horizontal center-to-center distance between girders. Characteristic maximum and minimum spacings were determined for each girder type (Table 4.1) based on a survey of existing bridge designs and consultations with the FDOT. Each testing configuration for a given girder type uses either the maximum or minimum spacing.

4.2.3 Cross-slope

Most bridge decks are designed with a cross-slope of 2% or greater, and the girders are usually aligned vertically along that slope so that they can evenly support the deck. Therefore, all of the FIBs and plate girders were tested at +2% cross-slope. Steel bridges can have a greater amount of horizontal curvature, so higher cross-slopes are often included to improve vehicle handling. To account for this, the WF Plate girders were also tested in configurations with +8% cross-slope. Additionally, because the top and bottom flanges of the FIB cross-sections differ in width and shape, the exposed portions of the shielded girders have a different shape if the cross-slope is negative (or, equivalently, if the wind blows from the opposite direction). To account for this, the FIB sections were also tested in configurations with a −2% cross-slope.

In contrast to I-shaped girders, box girders are not aligned vertically when supporting a cross-sloped deck. Instead, the girders are inclined to follow the cross-slope (see Figure 4.5). As a result, the box girders were only tested in 0% (unsloped) configuration but the range of tested wind angles was increased, as described below.

4.2.4 Wind angle

In practical bridge construction situations, the direction of wind flow will not always be perfectly horizontal. To account for the natural variation in wind angle (and at the recommendation of a commercial wind tunnel test facility) each bridge configuration was tested at five (5) different wind angles ranging from −5° to +5° in increments of 2.5° (Fig. 4.4). In the case of the box girder, such a change in wind angle is geometrically equivalent to the way the girders are rotated to support a cross-sloped deck (Figure 4.5). As a result, the box girder was measured at −10°, −5°, 0°, +5°, and +10° angles, in order to include the combined effects of 5° of wind angle and 5° (8.7%) of cross-slope.

+5° Wind   −5° Wind
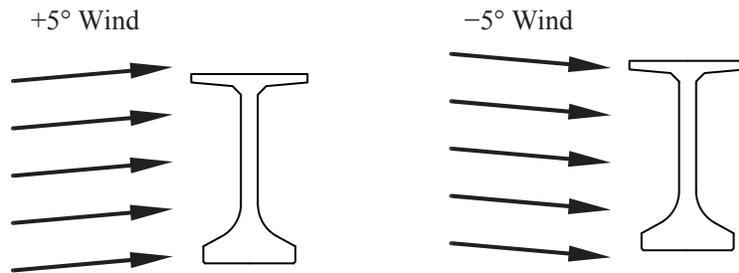
Figure 4.4 Wind angle sign convention

5° Wind

−5° Cross-slope

Field conditions

10° Wind

0° Cross-slope

Equivalent test configuration
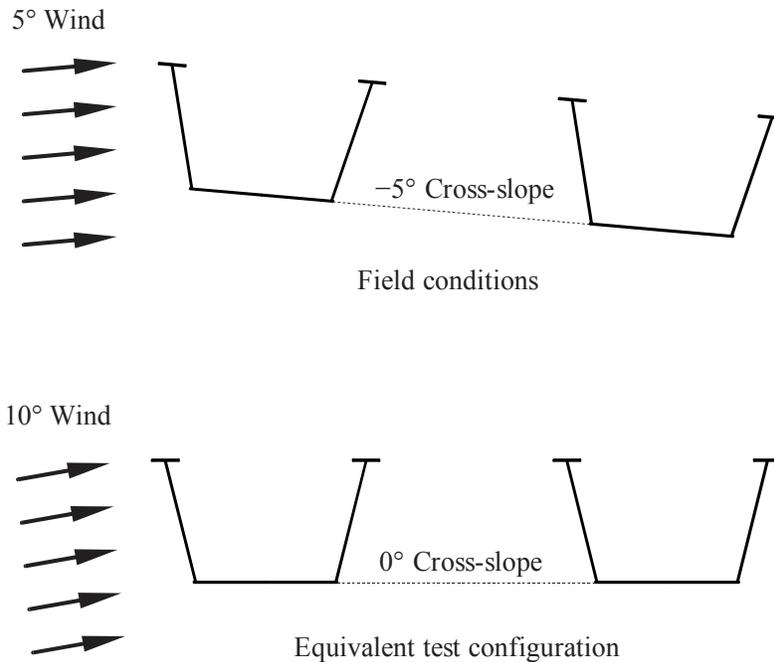
Figure 4.5 Equivalence between wind angle and cross-slope for box girders

4.3 Testing procedure

The Boundary Layer Wind Tunnel Laboratory at the University of Western Ontario (UWO) was contracted to fabricate the test specimens and to perform all wind tunnel measurements. Based on the size of the UWO wind tunnel, the girder models were constructed at reduced scale, with air flow properties similarly adjusted so that the resulting forces would be applicable at full-scale. All testing was performed in smooth flow, with turbulence intensities less than 0.5%. Because the tested cross-sections were sharp-edged, it was expected that the measured wind forces would not be sensitive to Reynolds number. The specific Reynolds numbers at which the tests were performed, and results reported, are shown in Table 4.2. Further, the assertion that wind forces would not be sensitive to Reynolds number was verified by UWO by additionally performing selected tests at lower Reynolds numbers (approximately 33% smaller than those shown in Table 4.2). Results from these additional tests did not reveal any obvious Reynolds number sensitivities.

Table 4.2 Wind tunnel test scaling

	Model scale	Reynolds number
WF Plate	1:25	77000
NF Plate	1:25	77000
78″ FIB	1:28	56000
45″ FIB	1:28	33000
Box	1:25	59000

The scaled girder models were all 7-ft long (equivalent to 175-ft and 196-ft girders at full scale) and were constructed to be fully rigid, without exhibiting any aeroelastic effects. An

adjustable frame was used to keep the girders properly oriented relative to each other in each test configuration. To measure wind-induced girder forces at varying wind angles of attack, the entire bridge cross-sectional assembly was rotated in-place relative to the wind stream.

Wind forces on the girders in each test configuration were measured individually with a high-precision load balance that recorded the time-averaged horizontal load (drag), vertical load (lift), and torque (overturning moment). These loads were then normalized to produce the aerodynamic coefficients for drag (C_D), lift (C_L), and torque (C_T). Finally, the torque coefficient was adjusted so that it represented the torque about the centroid of the section, rather than the torque about the point of measurement (which was at mid-height for the I-shaped girders and at an arbitrary point for the box girders). For additional details regarding the wind tunnel test procedures, please see Appendix I.

CHAPTER 5
WIND TUNNEL RESULTS AND ANALYSIS

5.1 Introduction

Wind tunnel tests were performed on the bridge girder test configurations described in Chapter 4. In addition to aerodynamic coefficients for individual girders, groups of laterally spaced girders were tested to quantify shielding effects, identify trends, and assess the importance of girder spacing, girder cross-slope and wind angle. From analysis of the results, a set of simplified design loads was developed for assessing the stability of a single girder or a system of braced girders. Additionally, a separate loading procedure was identified for conservatively predicting internal forces in brace members and a reduction factor on global drag was developed for use in strength design calculations. The complete set of wind tunnel test data is available in Appendix B.

5.2 Aerodynamic coefficients for individual girders

Of the wind tunnel tests that were performed, the most fundamental and broadly applicable results were the aerodynamic coefficients measured for the individual cross-sectional shapes (Table 5.1). In addition to being measured in level (0°) wind, the aerodynamic coefficients were measured in a range of angles of attack in order to determine how the coefficients were affected by variation in wind angle.

Table 5.1 Aerodynamic coefficients of bridge girder cross-sectional shapes

	0° wind			Minimum value			Maximum value			SDG
	C_D	C_L	C_T	C_D	C_L	C_T	C_D	C_L	C_T	C_D
WF Plate	2.12	−0.01	0.03	2.12	−0.02	0.03	2.13	0.00	0.03	2.2
NF Plate	2.12	−0.04	0.00	2.12	−0.05	0.00	2.13	−0.04	0.01	2.2
78″ FIB	1.89	0.15	0.11	1.89	0.13	0.10	1.91	0.18	0.12	2.2
45″ FIB	1.85	0.37	0.04	1.81	0.24	0.01	1.85	0.48	0.08	2.2
Box	1.81	1.22	0.73	1.68	0.71	0.69	1.93	1.62	0.85	1.5

With regard to girder stability, the drag coefficient (Figure 5.1) is the most critical aerodynamic coefficient. Of the five (5) cross-sectional shapes that were tested, the plate girder sections had the highest drag coefficients and were the least sensitive to wind angle, with both the wide-flange and narrow-flange varieties having coefficients that ranged from 2.12 to 2.13. The FIB sections had comparatively lower drag, with the 78″ FIB ranging from 1.89 to 1.91 and the 45″ FIB ranging from 1.81 to 1.85. Because of its more complex shape, the box girder section had by far the most sensitivity to wind angle, ranging from 1.68 to 1.93, with a median value of 1.81 in level (0°) wind. It is worth noting that the FDOT SDG currently overpredicts the C_D of plate girders and FIBs, but *under*predicts the C_D of box girders with an open top.
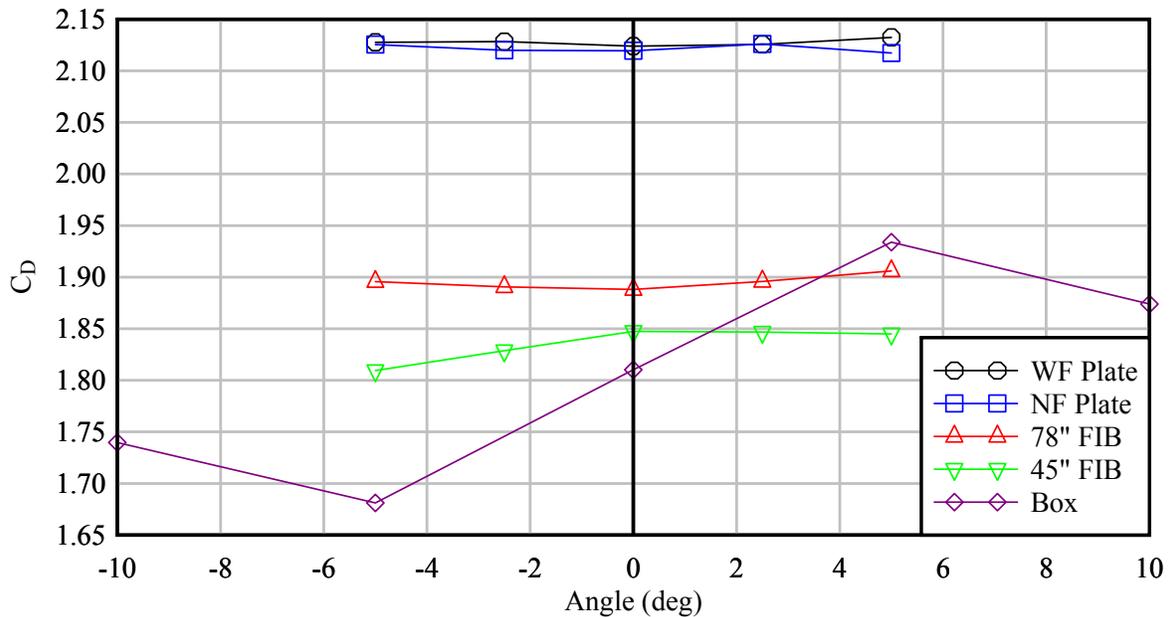
Figure 5.1 Effect of wind angle on individual girder drag coefficients (C_D)

Lift coefficients (C_L) for the five cross-sectional shapes are plotted in Figure 5.2. Because of their vertical symmetry, the plate girder sections generate negligible lift, with no coefficient exceeding a magnitude of 0.05. In contrast, the unsymmetrical FIB sections (with differently shaped flanges on top and bottom) generate significant uplift. For both FIBs, lift is sensitive to wind angle, tending to decrease as the wind angle increases. However, while the 78″ FIB lift coefficient ranges only from 0.13 to 0.18, the 45″ FIB is much more sensitive, ranging from 0.24 to 0.48. Finally, because of its angled webs, the box girder generates far more uplift than the other sections, with C_L ranging from 0.71 to 1.62. In −5° wind, the box girder generates nearly as much lift ($C_L = 1.62$) as it does drag ($C_D = 1.68$).
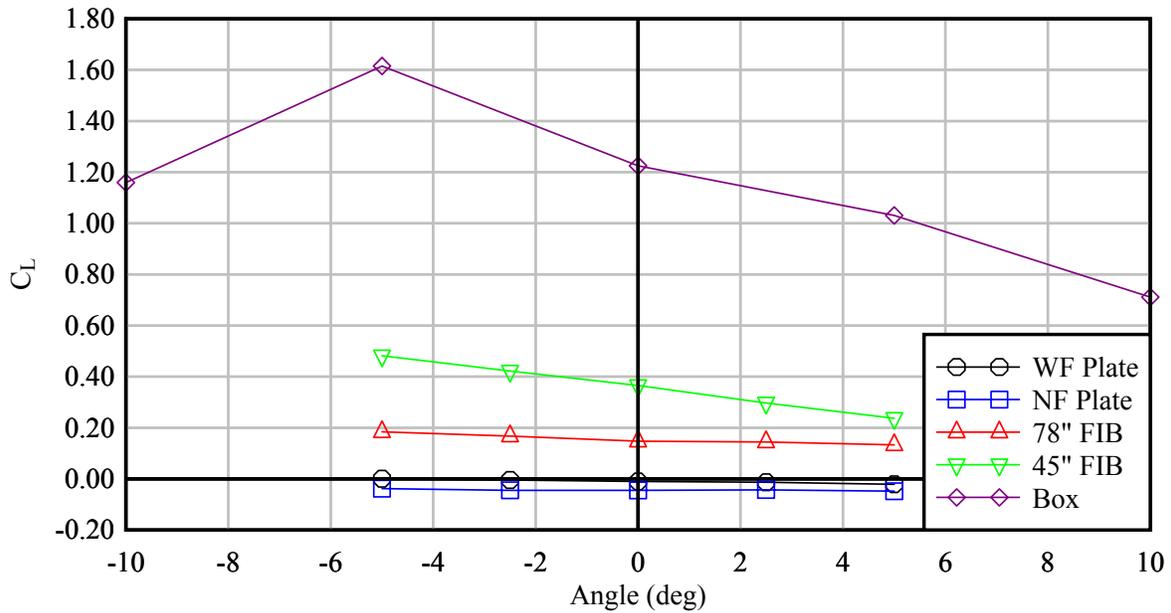
Figure 5.2 Effect of wind angle on individual girder lift coefficients (C_L)

Torque coefficients (C_T) for the five cross-sectional shapes are plotted in Figure 5.3. Qualitatively, the torque data are broadly similar to the lift data in that the symmetrical plate girder sections generate negligible torque, the FIB sections generate a small amount, and the box girder generates a much larger amount. Contrary to lift, the 78″ FIB generates more torque than the 45″ FIB (although the 45″ FIB remains more sensitive to wind angle than the 78″ FIB). Another difference in coefficient trends is that for the box girder, in terms of relative magnitude, C_T (ranging from 0.69 to 0.85) is less sensitive to wind angle than C_L (ranging from 0.71 to 1.62). (Recall from Chapter 3 that, while the magnitudes of the force coefficients, C_D and C_L, can be directly compared, C_T, a moment coefficient, is normalized differently, so absolute comparisons between the numeric values of C_T and the values of C_D and C_L are meaningless.)
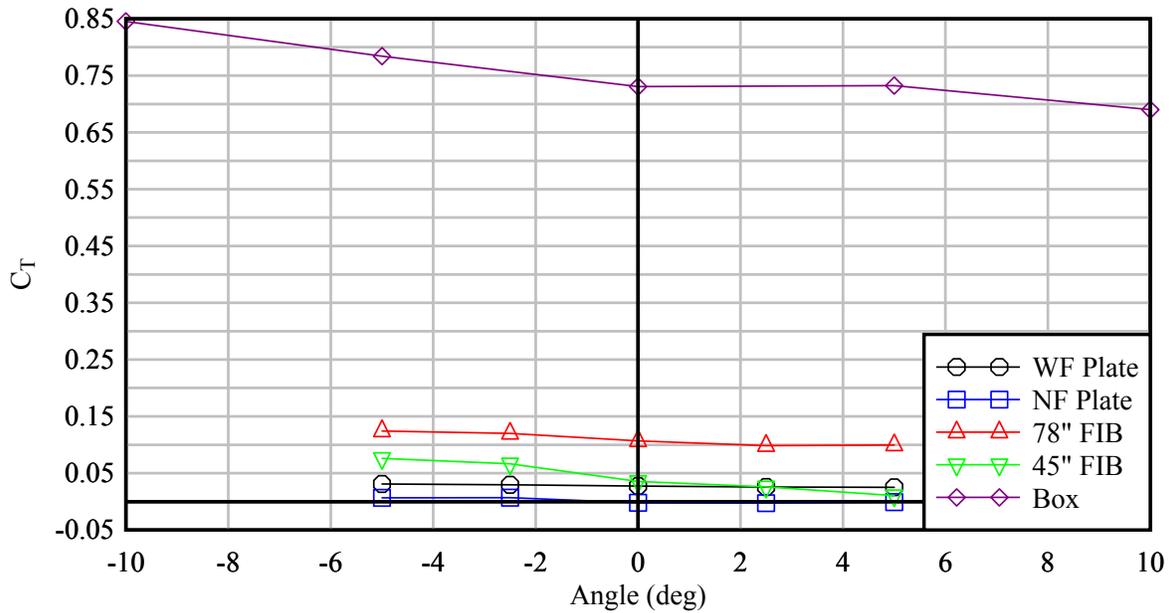
Figure 5.3 Effect of wind angle on individual torque coefficients (C_T)

5.3 Examination of shielding trends

Groups of multiple girders were tested in several different configurations (see Chapter 4) to quantify shielding effects. Because the largest variety of tests was performed using WF plate girders, data from those tests will be used for demonstration when discussing most shielding trends.

In the case of I-shaped girders (plate girders and FIBs), the most fundamental shielding trend that was observed was a basic *down-then-up* pattern (Figure 5.4). While the windward girder (G1) experiences the highest drag force in the system, there is a sharp and immediate reduction in drag so that the drag coefficient of the first shielded girder (G2) becomes negative (indicating that the drag force acts in the opposite direction, against the wind stream). In some cases, such as the one shown in Figure 5.4, drag sometimes continues to decrease, so that the girder with the most negative drag force is either G2 or G3. Upon reaching the most negative value, drag then slowly increases for subsequent girders, with the drag coefficient gradually becoming less negative and then increasingly positive. The first shielded girder with a positive drag coefficient is generally G3, G4 or G5. As can be seen in Figure 5.4, girder spacing and, to a lesser extent, cross-slope can affect the shielding pattern, but not enough to disrupt the overall trend. In general, a larger spacing decreases the total amount of shielding, but, as will be discussed, the effect of cross-slope is dependent on the wind angle of attack.
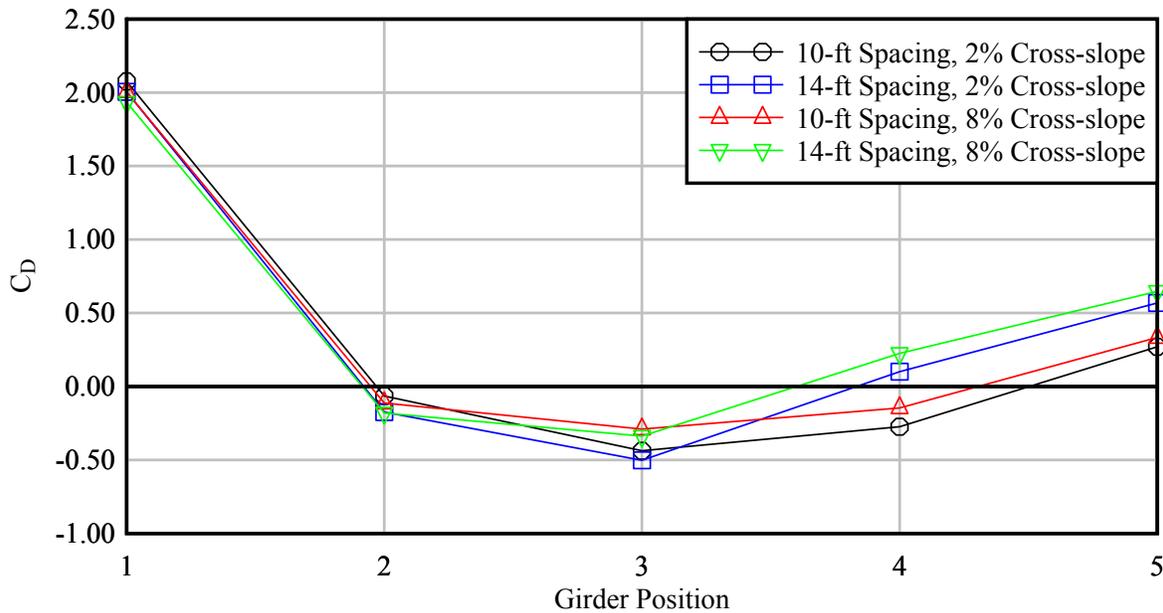
Figure 5.4 Drag coefficients of WF Plate girders in 5-girder configurations (0° Wind)

In addition to shielding effects, which propagate down-stream, the presence of shielded girders can modify the drag on girders that are farther up-stream (Figure 5.5). In the case of a two girder system, the presence of the shielded girder (G2) increases the total drag on the windward girder (G1). However, as additional shielded girders are added, they tend to reduce the drag on up-stream girders. As a result, the largest drag force drag on the windward girder (G1) and the most negative drag on the first shielded girder (G2) usually both occur in the two-girder configuration.

Figure 5.5 Effect of adding additional girders
(WF Plate, 14-ft spacing, 8% cross-slope, 0° Wind)

All of the previously discussed examples have been in perfectly level wind (0°). However, changing the wind angle can alter the shielding pattern. The effect of wind angle tends to be strongest on the more leeward (down-stream) girders (Figure 5.6). Note that in this example (with 8% cross-slope), a wind angle of +5° provides the most total shielding (i.e., the most overall reduction in drag) and a wind angle of −5° provides the least total shielding.
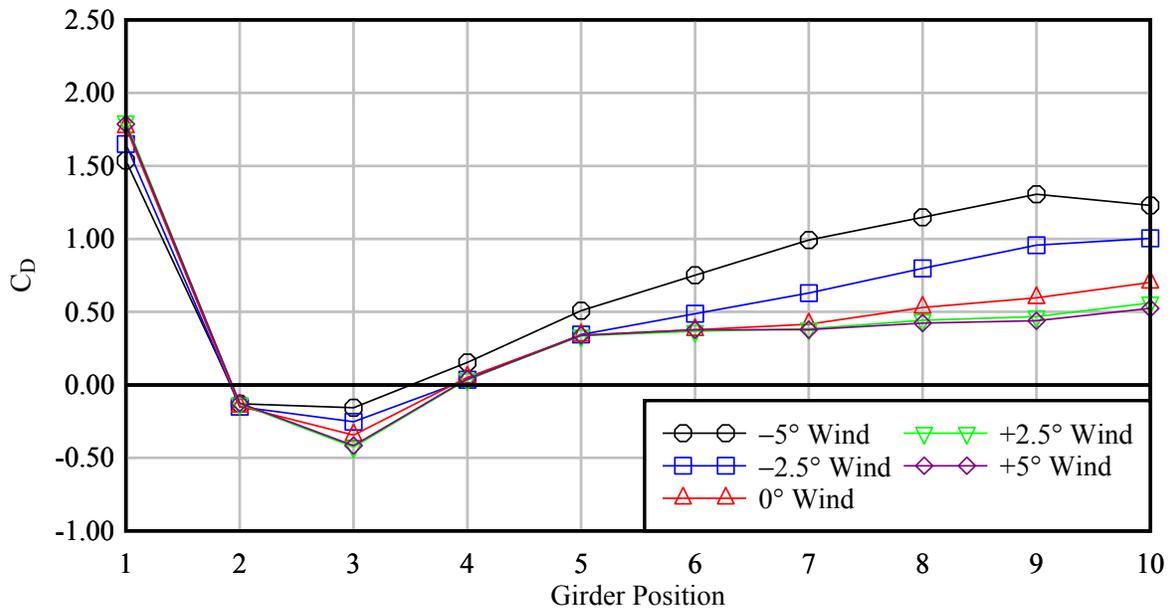
Figure 5.6 Effect of wind angle on C_D (WF Plate girder, 14-ft spacing, 8% cross-slope)

Whether a change in wind angle will increase or decrease the total shielding in a particular testing configuration depends on the cross-slope of the system (Figure 5.7). Maximum shielding is achieved when the wind angle is equal to the angle of the cross-slope, so that as much of the shielded girder as possible is blocked along the direction of the wind stream. As the difference between the cross-slope and wind angle increases, larger portions of the shielded girders are exposed and the total amount of shielding decreases. This also explains the previously-noted trend that increasing girder spacing reduces shielding, as this exposes more of the girder for a given angle. However, while changing girder spacing can amplify or attenuate the shielding effect, it does not alter the sign of the C_D values for shielded girders. From knowledge of the cross-slope, it is possible to determine best- and worst-case wind angles (Table 5.2).
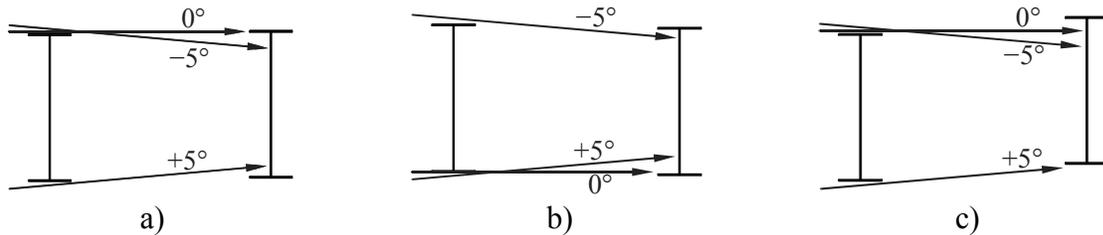
Figure 5.7 Interaction between wind angle and cross-slope
a) +2% cross-slope; b) −2% cross-slope c) 8% cross-slope

Table 5.2 Extreme combinations of tested wind angle and cross-slope

	Ideal shielding angle	Best tested case	Worst tested case
+2% cross-slope	+1.15°	0°	−5°
−2% cross-slope	−1.15°	0°	+5°
+8% cross-slope	+4.57°	+5°	−5°

When the shielding is close to maximum, the drag on leeward girders tends to plateau (Figure 5.8), even if the plateau value is initially exceeded, as with the 45″ FIB in this example. In the tested cases where the wind angle was most different from the cross-slope (Figure 5.9), the drag continued to increase on each subsequent girder, until reaching either a plateau or a change in direction at approximately G9. Note that the WF Plate girder almost reaches the same amount of drag on G9 as it does on G1.
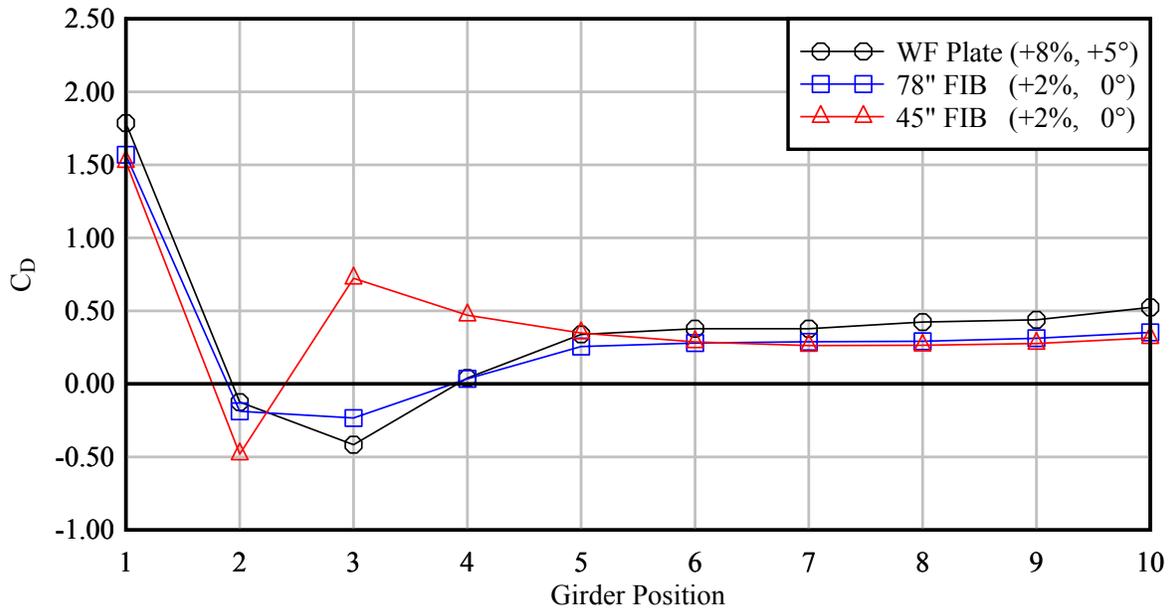
Figure 5.8 Ten (10) girder models tested at wind angles producing maximum shielding
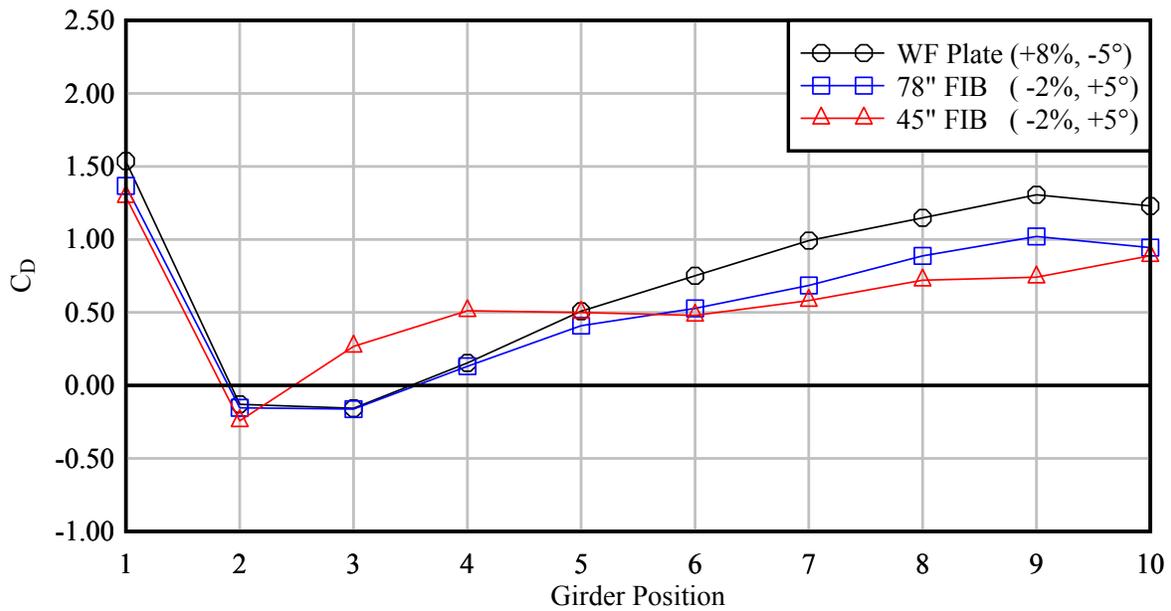
Figure 5.9 Ten (10) girder models tested at wind angles producing minimum shielding

Box girders were only tested in groups of two (2), with girders spaced at 20 ft and 22 ft (Figure 5.10). Girder spacing was found to have almost no effect on the drag force on either the windward girder (G1) or the shielded girder (G2). By comparison, the wind angle was a much stronger influence. In the most sensitive case, a change in wind angle from 0° to −5° on the 22 ft spaced group resulted in the C_D of G2 changing sign and increasing from −0.34 to +0.45.
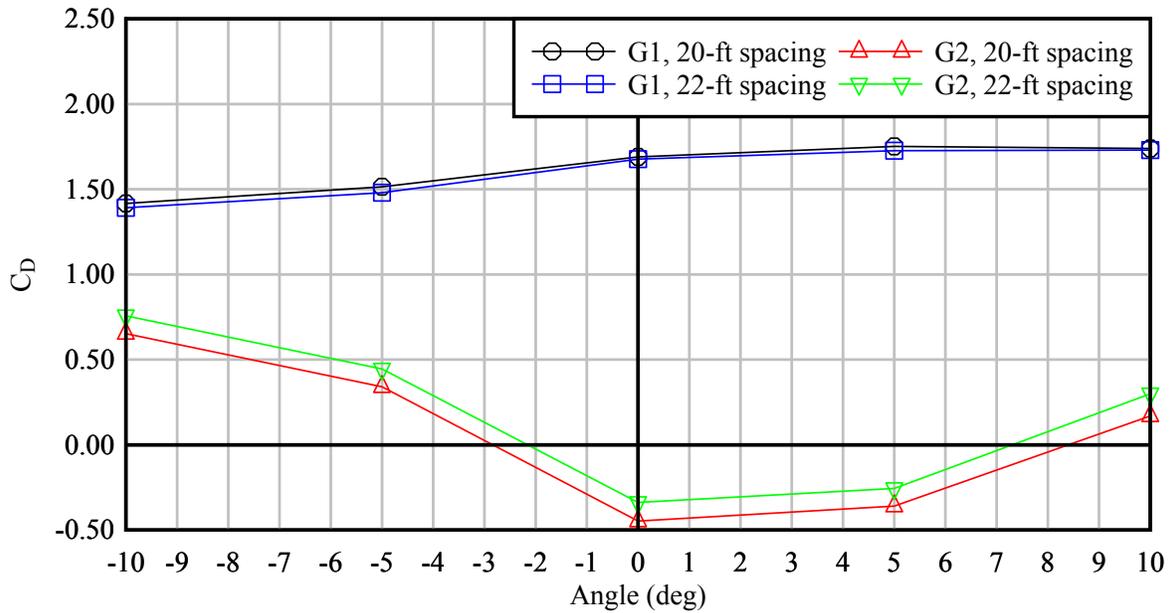
Figure 5.10 Effect of wind angle on two (2) Box girder system drag coefficients (C_D).

5.4 Effective drag coefficient

As discussed in Chapter 3, the *Structures Design Guidelines* (SDG; FDOT, 2012e), along with most design codes, assumes that horizontal wind can be approximated as a uniform pressure load. This is convenient because a single coefficient (C_D) is all that is necessary to characterize the aerodynamic properties of a structure. However, the results of the wind tunnel tests have shown that aerodynamic loads on bridge girders can include lift forces and torques that are too large to be considered negligible. Lift coefficients for I-shaped girders (FIBs and plate girders) can be as large as ±0.5 (Figure 5.11) and torque coefficients can range from −0.10 to 0.21 (Figure 5.12). The additional structural demand contributed by lift and torque should therefore be included when evaluating girder stability. As will be presently shown, it is possible to define an *effective drag coefficient* ($C_{D,eff}$) that conservatively combines the effects of both drag and torque into a single coefficient that can be used in design codes as if it were a standard drag coefficient. (It is not possible to incorporate lift in the same manner, but the effect of lift will be accounted for in the proposed girder capacity equations presented later in this report.)
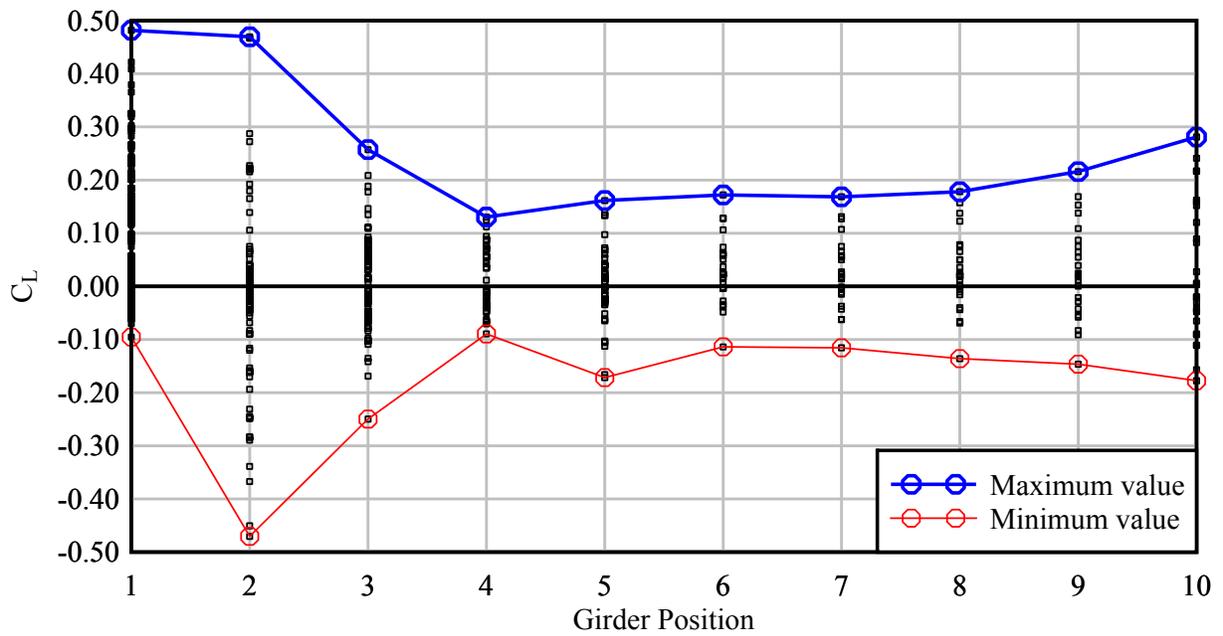
Figure 5.11 Lift coefficients on all I-shaped girder test configurations (plate girders and FIBs)
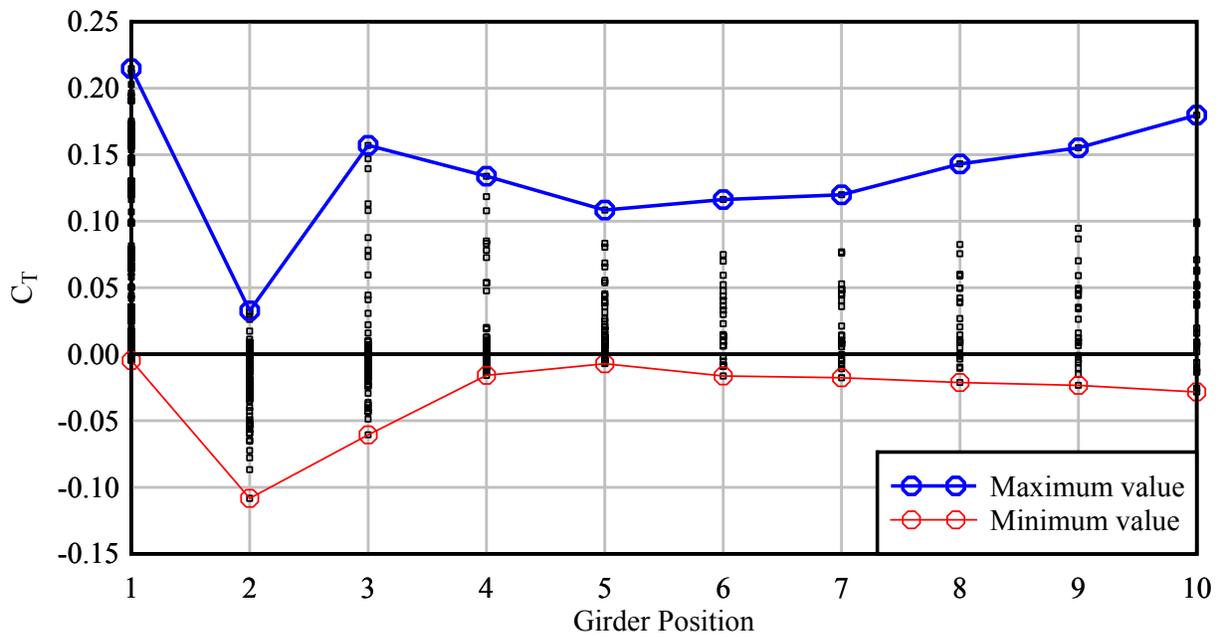
Figure 5.12 Torque coefficients on all I-shaped girder test configurations (plate girders and FIBs)

C_T represents aerodynamic torque measured about the centroid of the section. However, in the SDG, wind load computed from C_D is applied at the center of pressure which is assumed to be at mid-height of the girder. In the case of asymmetric girder shapes such as FIBs, the center

of pressure is separated from the centroid by a vertical distance, δ (Figure 5.13a). For consistency, before C_T can be incorporated into $C_{D,eff}$, it must be transformed into the *pressure torque coefficient* (C_{PT}), which represents the torque about the center of pressure (rather than about the centroid). An equation for calculating C_{PT} in terms of C_D and C_T can be derived in closed-form.

As discussed in Chapter 3, C_D and C_T represent a force and moment, F' and M' applied at the centroid (Figure 5.13b). From principles of statics, this state of load is equivalent to a single force applied at some height, Δ, above the centroid (Figure 5.13c), where:

$$\Delta = \frac{M'}{F'} \tag{5.1}$$

When the same state of load is considered from the center of pressure (Figure 5.13d), the moment that is generated (M_P') is equal to:

$$M_P' = F'\left(\Delta - \delta\right) \tag{5.2}$$

which can be combined with Equation 5.1 to create the expression:

$$M_P' = M' - F'\delta \tag{5.3}$$

Based on concepts presented in Chapter 3, these forces are related to their corresponding aerodynamic coefficients as:

$$
\begin{aligned}
F' &= C_D q D \\
M' &= C_T q D^2 \\
M_P' &= C_{PT} q D^2
\end{aligned}
\tag{5.4}
$$

where D is the depth of the girder cross-section. After substituting the expressions above into Equation 5.3 and solving for C_{PT}, the final equation for the transformation is:

$$C_{PT} = C_T - C_D \frac{\delta}{D} \tag{5.5}$$
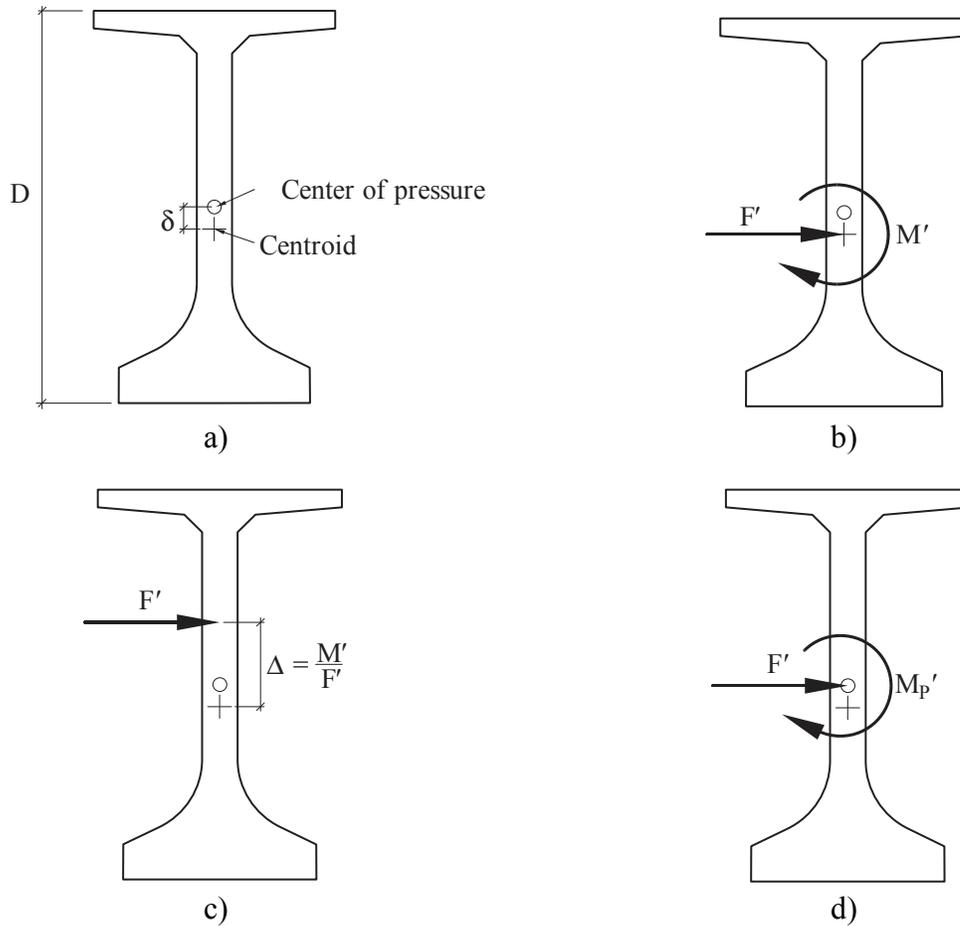
Figure 5.13 Transformation of C_T to C_{PT}

Once the value of C_{PT} has been determined, it is necessary to represent it in the form of a drag coefficient so that it can be added to C_D to form $C_{D,eff}$. In other words, the moment load, M_P', (Figure 5.14a) must be replaced by a drag force, F_M', that produces an equivalent amount of moment. After normalizing that force in the manner of a drag coefficient, it can be directly added to C_D:

$$C_{D,eff} = C_D + \frac{F_M'}{qD}$$
(5.6)

In the field, drag force generates an equal but opposite reaction force at the support (Figure 5.14b), producing a force couple with an arm equal to half of the girder depth, D. As a result, the force necessary to generate M_P' is:

$$F_M' = M_P'\left(\frac{2}{D}\right)$$
(5.7)

Substituting the expression for M_P' from Equation 5.4 into the equation above yields:

$$F'_M = C_{PT} q D^2 \left(\frac{2}{D}\right) = 2 C_{PT} q D \tag{5.8}$$

which can be substituted into Equation 5.6, resulting in:

$$C_{D,eff} = C_D + 2 C_{PT} \tag{5.9}$$

In this expression, the term $2C_{PT}$ can be thought of as a correction factor that ensures equivalence of moment by giving up equivalence of lateral force. In the majority of cases, the resulting value of $C_{D,eff}$ is greater than C_D, meaning that $C_{D,eff}$ conservatively overpredicts the amount of lateral force in the system. However, in some cases (e.g., when C_D is positive and C_{PT} is negative), the $C_{D,eff}$ expression given in Equation 5.9 underpredicts the amount of lateral force in order to achieve equivalence of moment. In these cases, the basic (rather than effective) C_D coefficient is the conservative choice because it overpredicts moment but correctly predicts lateral force. Ensuring that neither lateral force nor moment are underpredicted can be achieved by redefining $C_{D,eff}$ as:

$$C_{D,eff} = \max(C_D, C_D + 2 C_{PT}) \tag{5.10}$$

The definition of $C_{D,eff}$ given in Equation 5.10 was therefore used to develop the proposed design loads in this study.
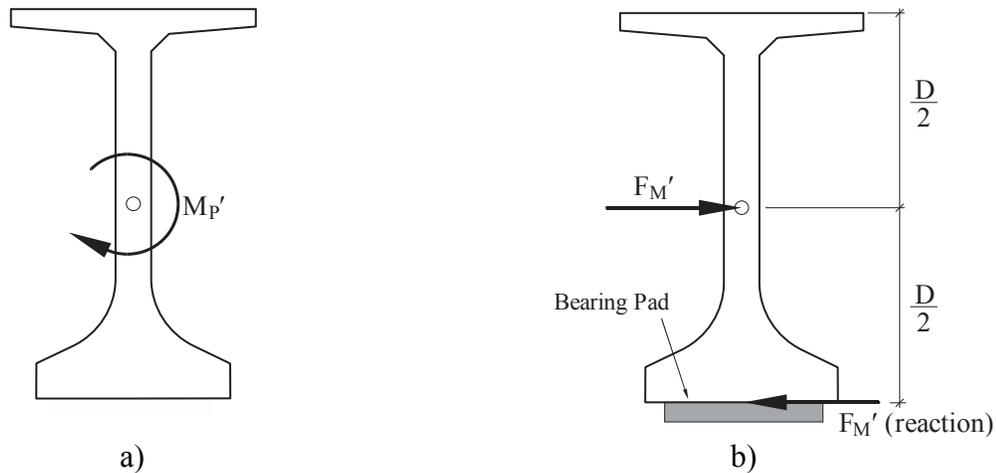
Figure 5.14 Moment load expressed as equivalent drag force.

It is important to note that Equations 5.5 and 5.9 are only valid for aerodynamic coefficients that are normalized by girder depth. This is true of all coefficients presented in this report, but these equations cannot be applied to coefficients from other sources that are normalized by different reference lengths.

40

5.5 Proposed wind loads for design

After calculating effective drag coefficients for every wind tunnel test conducted in this study, the results were synthesized into simplified loads suitable for use in the design of girder bracing. Potential design loads were evaluated according to three criteria:

- Conservatism: Design loads must be conservative or they are useless. However, overly conservative design loads are also undesirable. Part of the motivation for studying shielding was to allow for reduced (i.e., less conservative) wind loads on shielded girders.

- Generality: To maximize utility, design loads must be applicable to as wide a range of designs as possible, including cross-sections, spacings, or cross-slopes that were not directly tested. Consequently, attempting to develop design loads that recreated the tested load measurements as closely as possible was considered counterproductive.

- Simplicity: Simplicity in design codes is advantageous, but it must be balanced against the drawbacks of overconservatism. In general, the addition of significant mathematical or procedural complexity in exchange for a slight reduction in conservatism was considered undesirable.

When designing girder bracing for lateral stability, the worst-case distribution of wind load is when the total drag force (i.e., the sum of the force on each girder in the system) is as large as possible. Negative drag on any girder is transferred through the braces to the rest of the system and acts to resist collapse. (A separate load case that maximizes the internal forces of individual brace members is described in the next section.) Therefore, design loads for stability should be based on configurations where girder drag is the largest (or least negative). Additionally, it is worth noting that because the highest-drag cases tend not to coincide with high-torque cases, the use of $C_{D,eff}$ instead of C_D does not significantly increase total structural demand or conservatism (Figure 5.15).

41
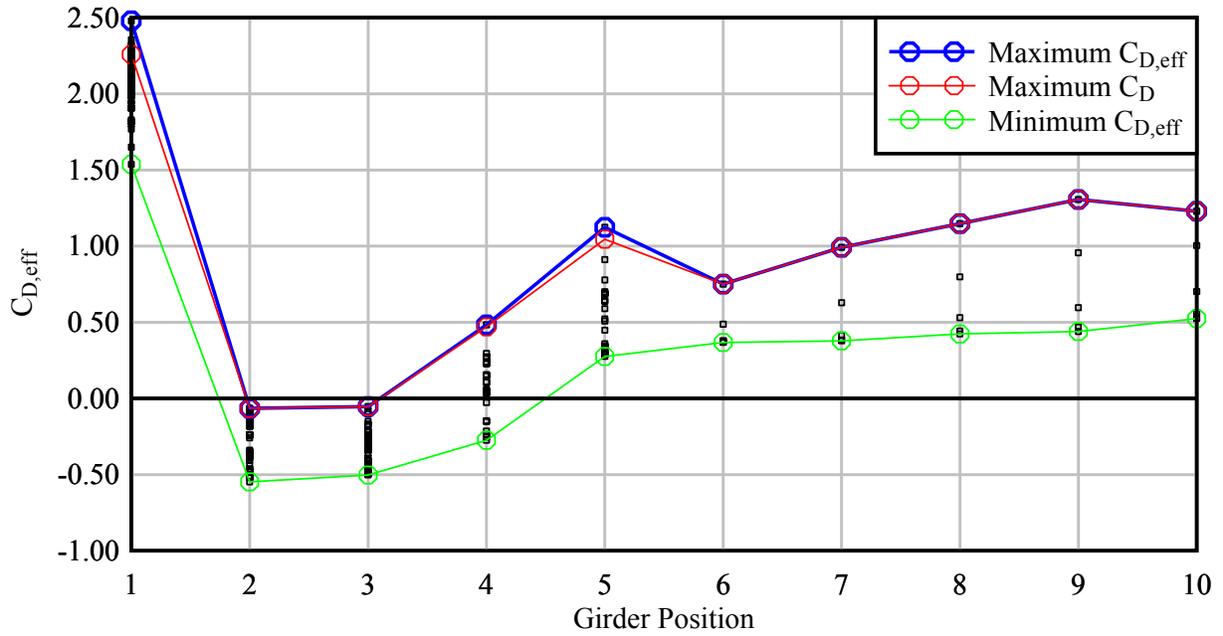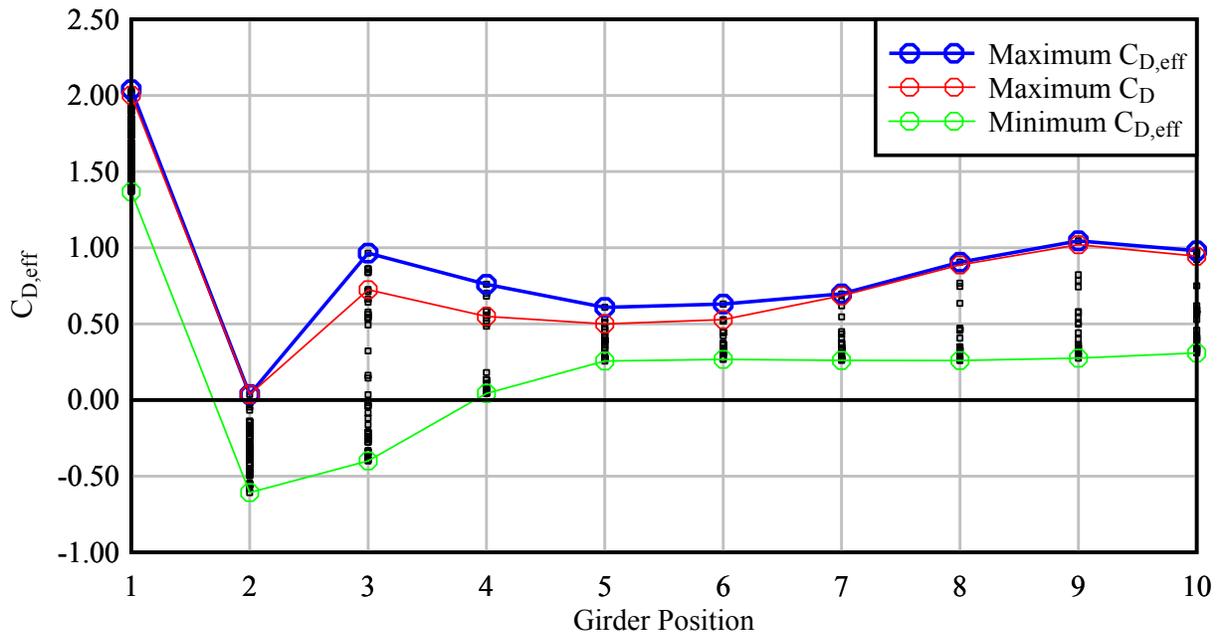
Figure 5.15 Comparison between maximum C_D and maximum $C_{D,eff}$ for:
a) all plate girder sections; b) all FIB sections

Girder spacing and cross-slope were rejected as possible input parameters—meaning that, for example, two otherwise identical bridge designs with different girder spacings would have

the same design loads—because of the relatively small effect they have in isolation (recall Figure 5.4) and the complexity of their interactions with other parameters (such as wind angle). Additionally, because (for budgetary reasons) the 10-girder groups were only tested at the maximum spacing and cross-slope, including spacing and cross-slope as parameters would have required extrapolation of their effect on the 5 most-leeward girders (G6–G10). Instead, it was considered more conservative to envelope the $C_{D,eff}$ values for every combination of spacing and cross-slope that was tested in order to identify the worst case.

Similarly, the width-to-depth ratio of the cross-section was rejected as an input parameter because of the small differences observed between the WF Plate and NF Plate girders and between the 45″ FIB and 78″ FIB, and because data were not collected for intermediate shapes. Instead, only the type of section—plate girder or Florida-I Beam—was considered significant enough to modify the design loads.

Finally, the number of girders in the system was considered as an input parameter. While it was observed that adding additional downwind girders tended to reduce wind force on up-stream girders (recall Figure 5.5), the fact that data are only available for 2-, 5-, and 10-girder groups makes the effect impossible to predict with any certainty. For example, because the drag on the windward girder (G1) increases in a 2-girder group and decreases in a 5-girder group, it is unclear whether it would increase or decrease for a 3-girder group. For this reason, it was decided to assign a single design load to each girder that would envelope all cases.

Also evident from Figure 5.5 is the fact that the drag coefficients in a 5-girder model tend to 'rebound' from the negative range at a higher rate than the 10-girder models, with the result that the drag force on the final girders is approximately equal. It is conceivable that this pattern holds true for 3-girder models as well. Indeed, in the case of the 45″ FIB (which is much shorter, relative to the girder spacing, than the other sections), G3 sometimes sustains the maximum drag out of all the shielded girders (recall Figure 5.8). Therefore, it was assumed that girders G3–G10 are all potentially capable of being exposed to the maximum shielded drag.

The final proposed design loads (Figure 5.16) are based on the basic down-then-up trend that was observed in all tested configurations. An initial pressure coefficient (C_P) (i.e., $C_{D,eff}$) is assigned to G1 based on the type of girder section: 2.5 for plate girders (Figure 5.17) and 2.0 for FIBs (Figure 5.18). Girder G2 is assigned a C_P of 0 (i.e., no load) while G3 and all subsequent girders are assigned a C_P equal to half of the load on the windward girder.
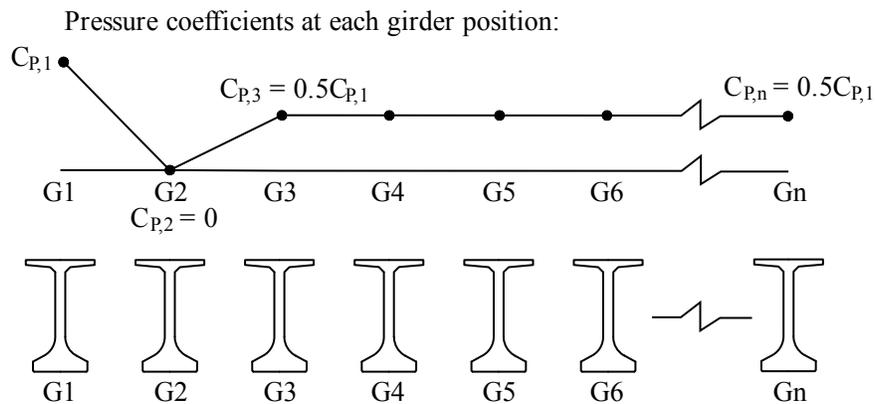
Figure 5.16 Proposed wind load shielding model for stability evaluation
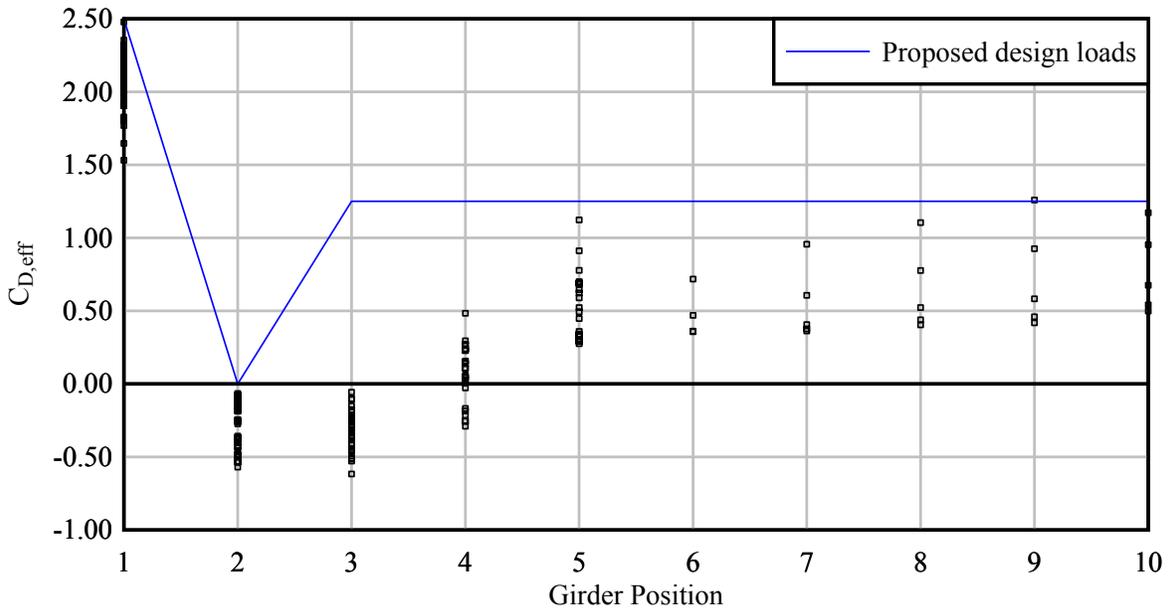
Figure 5.17 Proposed design loads for plate girders
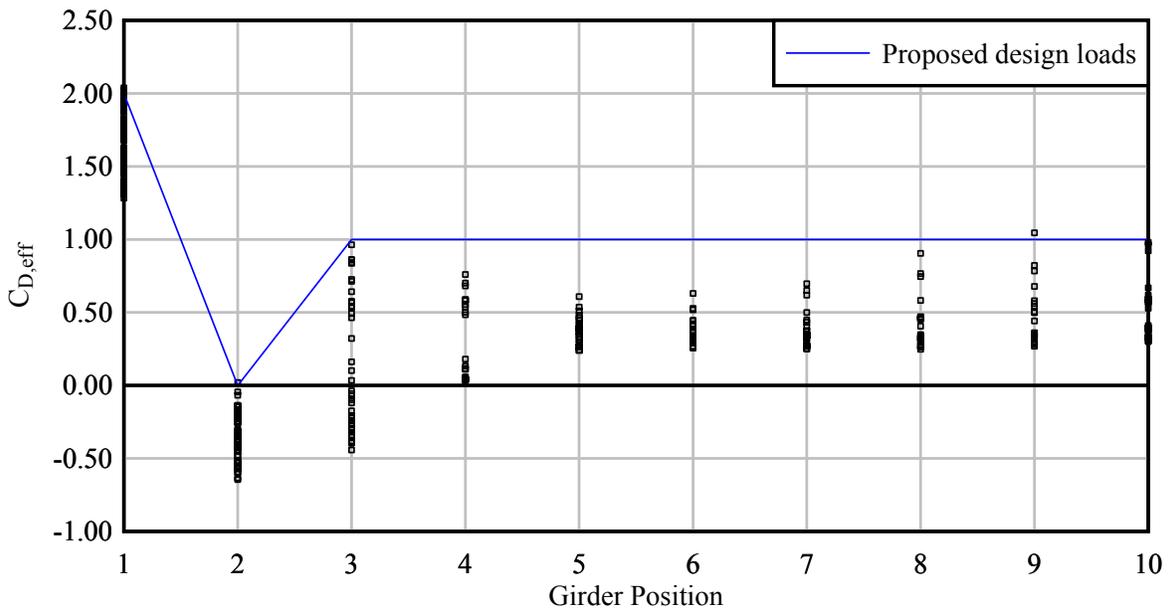
Figure 5.18 Proposed design loads for FIBs

5.6 Proposed procedure for calculation of brace forces

As previously discussed, system-level stability is most critical when the total unidirectional wind load on the system is as high as possible. Brace designs must provide sufficient stiffness to keep the system stable under such loading conditions. However, to reach a stable equilibrium position, it is equally important that the strengths of the individual brace

44

members not be exceeded, because an individual brace failure can initiate a progressive collapse. Individual brace forces (as opposed to overall system lateral loads) are maximized when differential wind forces on adjacent girders act to maximize compression of the braces that connect the girders together. Because the design loads proposed in the previous section are intended to maximize overall system loads, and not individual brace compression forces, a separate load case is required for evaluating brace strength in compression.

Wind force differentials are always highest between the windward girder (G1) and the first shielded girder (G2), with the positive drag on G1 and the negative drag on G2 combining to produce a total compressive brace load (Figure 5.19) that consistently exceeds that of any other pair of adjacent girders. Recall from Figure 5.5 that the 2-girder configuration (with no additional down-stream girders) has both the most positive drag on G1 and the most negative drag on G2. Because typical erection sequences always include a two-girder phase (even if only briefly), the wind load on such systems was selected as the controlling load case for brace force determination. Upon checking every tested 2-girder configuration, the worst-case compression load for plate girders was a system with a $C_{D,eff}$ of 2.48 for G1 and −0.40 for G2 (Figure 5.20). Similarly, for FIBs, the worst case had a $C_{D,eff}$ of 2.04 for G1 and −0.56 for G2 (Figure 5.21). The combined effect of $C_{D,eff}$ for G1 and G2 is then equivalent to using a single combined coefficient of 2.88 for plate girders and 2.60 for FIBs. To ensure that that brace force calculations remain conservative for untested girder configurations, it is recommended that these values be rounded up to 3.0 for plate girders and 2.75 for FIBs.

$(C_{D,eff} = 2.48)$ $(C_{D,eff} = −0.40)$

a)

$(C_{D,eff} = 2.88)$

b)
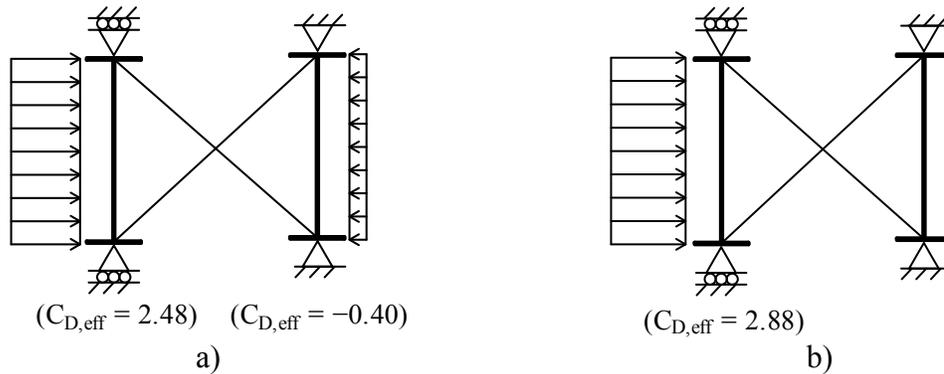
Figure 5.19 Representation of positive and negative drag loads as a combined compression load
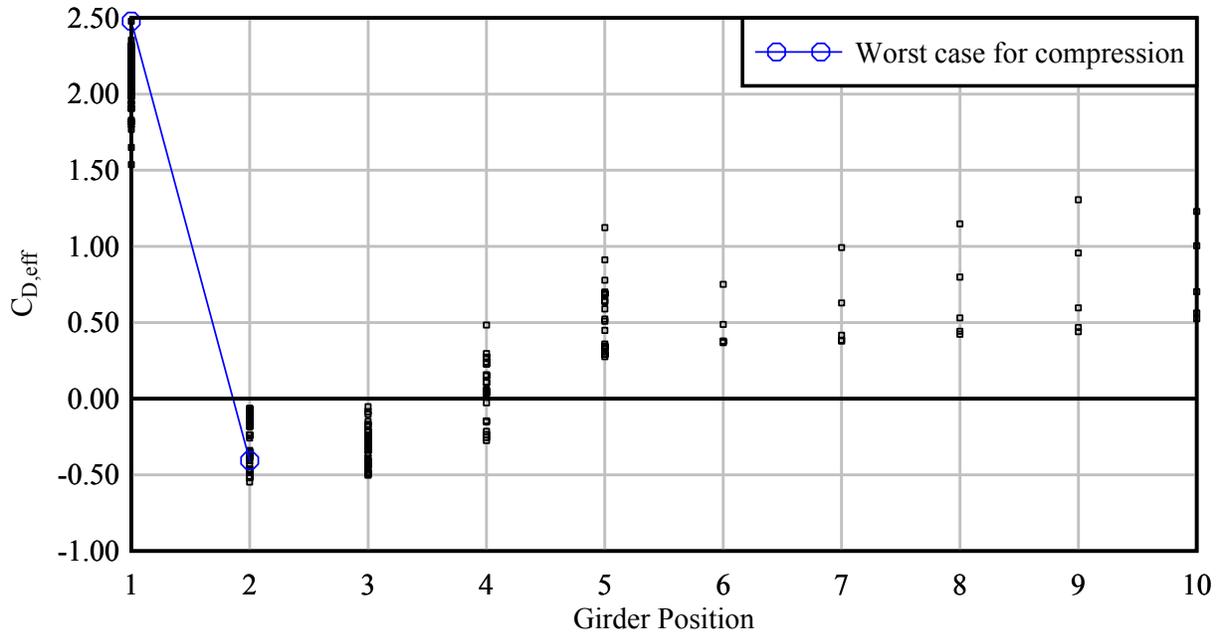
Figure 5.20 Proposed brace force design loads for plate girders
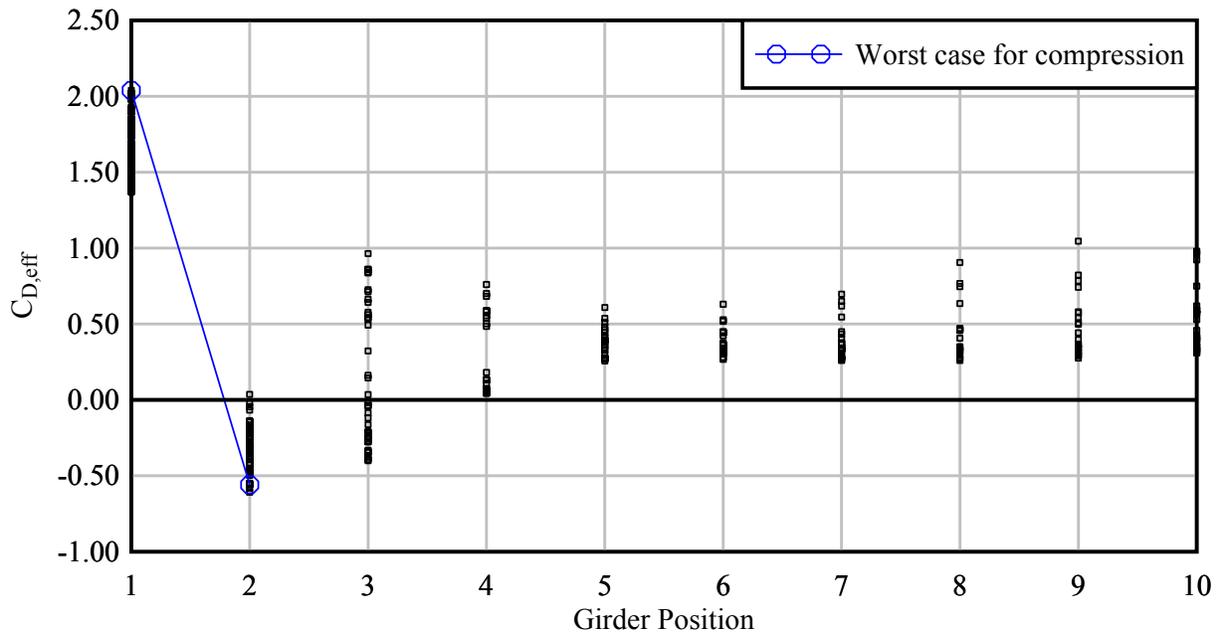
Figure 5.21 Proposed brace force design loads for FIBs

Even with well-defined wind loads, a pair of braced girders is a three-dimensional structural system with several sources of variability. A simplified structural model (Figure 5.22) is therefore proposed for conservative determination of brace forces using the loads described above. This approach is not restricted to any particular brace configuration: the core of the approach is a structural model of the brace, the configuration and implementation of which is left

to the judgment of the Engineer of Record. Fixed boundary conditions are applied at every node where the brace connects to G2, while rigid links are used to link all of the G1 connection nodes to a pin located at the base of G1. An additional rigid link connects the base pin to the center of pressure where the total tributary wind load is applied as a single horizontal force.

a)

b)
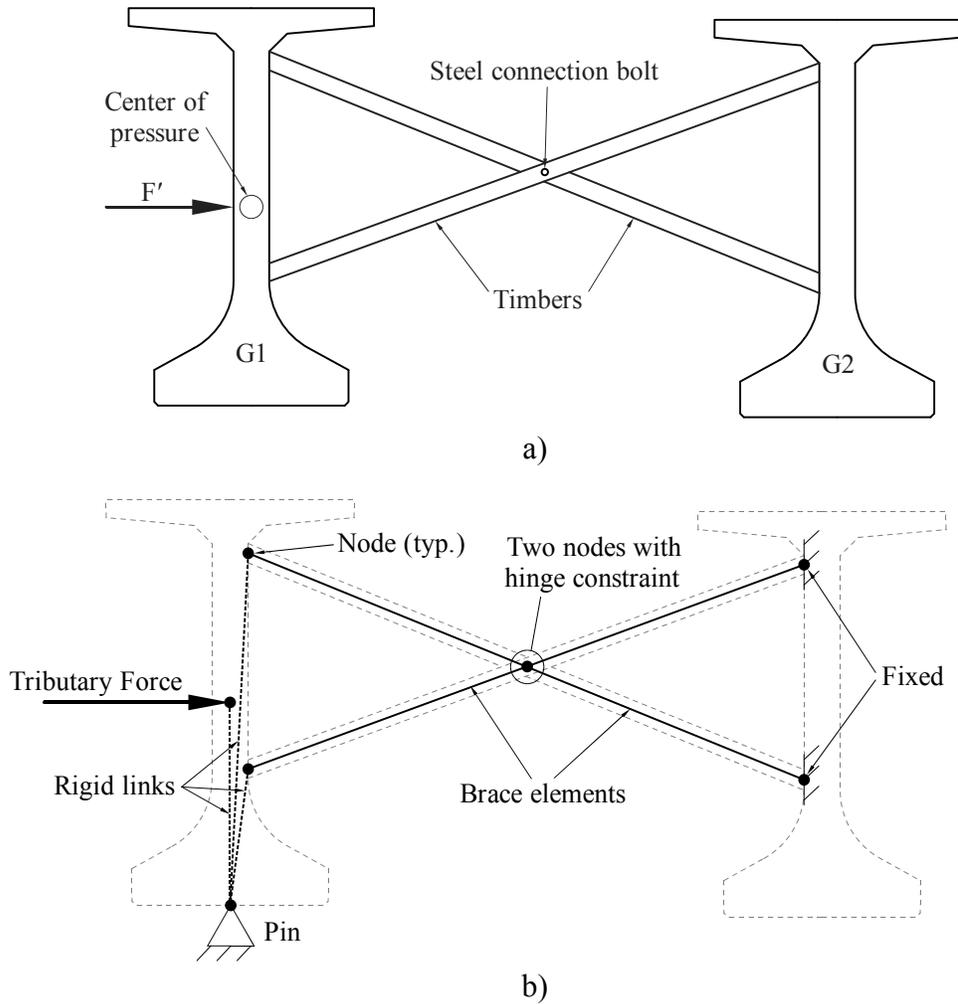
Figure 5.22 Simplified brace force analysis:
a) Example X-brace; b) equivalent structural model for brace force determination

In the field, the connections between the brace elements and the girders are likely to be neither perfectly fixed nor perfectly pinned, but rather achieve some intermediate level of moment transfer. If desired and appropriate, brace elements may include partial end-releases at the girder connection points. This can lessen the resulting brace forces somewhat. However, it is important not to underpredict the amount of fixity in the connections or unconservative results may be obtained. Given the significant amount of uncertainty that is generally involved in such determinations, it is recommended that full fixity be provided in the model unless reliable partially-restrained connection information is available.

5.7 Proposed reduction factor for global strength design

The shielding model and associated load cases described in previous sections are appropriate for stability limit states, which must be satisfied at the component level. However, because the shielding model for stability assigns a conservative load to each component (i.e., girder), the *total* predicted drag force on the system can be excessively conservative in comparison to measured wind tunnel data, which show that the most conservative component loads are rarely, if ever, encountered simultaneously. As a result, the *global pressure coefficient*—defined as the sum of the pressure coefficients of each girder in the system—that is predicted by the shielding model used for stability evaluation (Figure 5.16) is too conservative for global strength limit state evaluation (e.g., determination of wind load reactions on the substructure during construction). To reduce the global system loads to a more reasonable level for strength calculations, a reduction factor (α) is applied to the summation of the predicted pressure coefficients, as follows:

$$C_{P,global\text{-}strength} = \alpha \sum_{i=1}^{n} (C_P)_i \qquad (5.11)$$

where $(C_P)_i$ is the pressure coefficient for the girder at position i according to the shielding model (Figure 5.16) and n is the number of girders in the system. Note that α shall only be employed when considering the *global* wind loads and shall not be applied to the loads on individual girders when conducting stability evaluation or brace force determination.

Recall from Figure 5.7 that magnitudes of the wind loads on shielded girders are highly dependent on the interaction between the system cross-slope angle ($\theta_{cross\text{-}slope}$) and the wind angle ($\theta_{wind}$). As the absolute difference between those angles increases, a greater portion of the shielded girders are exposed to direct wind flow, resulting in a roughly proportional increase in girder load. Consequently, a strong predictor of total wind load on a girder system is the *projected area* of the system (i.e., the total unshielded area). To appropriately capture this trend, α must be a function of the *projected depth* ($D_{projected}$).

Because the projected depth is a function of θ_{wind}, which fluctuates randomly over time, engineering judgment must be used in selecting a design value of θ_{wind} such that it represents the maximum expected angle during the exposure period. For conservatism, the sign of θ_{wind} must be chosen to be in opposition to that of $\theta_{cross\text{-}slope}$, so that the maximum angle difference (θ_{max}) is computed as:

$$\theta_{max} = |\theta_{wind}| + |\theta_{cross\text{-}slope}| \qquad (5.12)$$

θ_{max} can then be used to calculate the *projected depth*, $D_{projected}$, of the girder system, as:

$$D_{projected} = D + (n-1)(S)(\tan(\theta_{max})) \qquad (5.13)$$

where n is the number of girders in the system, D is the girder depth, and S is the girder spacing (Figure 5.23). In this formulation, wind streamlines are assumed to be straight and the shielding effects of girder flanges are ignored as they are not expected to significantly shield leeward girders.
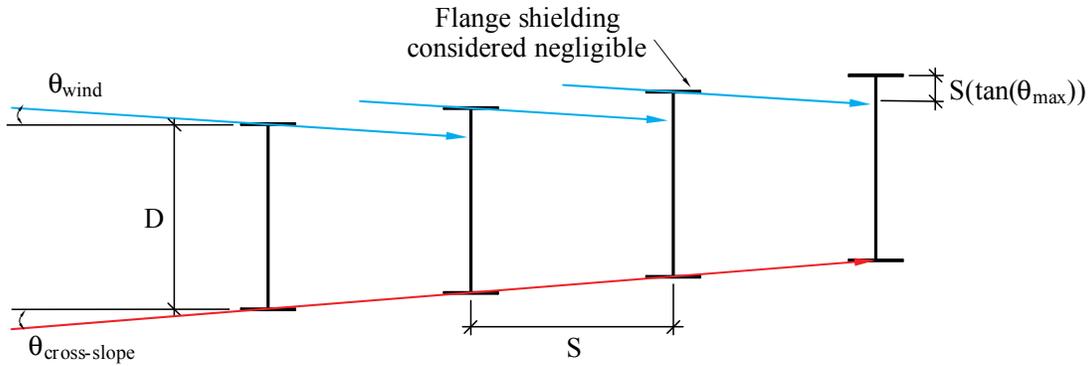
Figure 5.23 Influence of cross-slope and wind angle on projected depth

5.7.1 Development of a reduction factor for systems with five (5) or more girders

Most of the experimental wind tunnel data measured in this study were for 5-girder and 10-girder models, and because the observed shielding patterns were broadly similar, it was concluded that the data set could reasonably be used to characterize the behavior of systems with five (5) or more girders. (Systems with less than five (5) girders are discussed in the next section.) Measurements of 5-girder models in which the not all of the girders were instrumented were excluded from development of the reduction factor α because the global drag coefficient could not be exactly computed for these cases. As a result, the WF Plate models were the only 5-girder models used in development of the reduction factor, whereas for 10-girder cases, both plate girder and FIB data were available and used in reduction factor development.

For each fully instrumented wind tunnel test with five (5) or more girders, the experimental global coefficient was computed by summing the effective drag coefficients ($C_{D,eff}$) for each girder. This experimentally-determined global coefficient was then divided by the global C_P (predicted by the stability shielding model, Figure 5.16), to yield an 'ideal' reduction factor (i.e., the factor required bring the shielding-model-predicted value into agreement with the wind-tunnel-measured value).

For each wind tunnel test, the computed ideal reduction factor was found to be linearly correlated to the projected depth normalized by the girder depth (i.e., the dimensionless quantity $D_{projected}/D$). Therefore, linear regression was used to develop an expression for the reduction factor in terms of the normalized projected depth. To ensure that conservatism was achieved, the parameters of the best fit line (slope and intercept) were determined as a function of the desired confidence interval, thus forming an upper bound line. When this process was employed using a 99% upper bound confidence interval the following reduction factor equation (Figure 5.24) was obtained:

$$\alpha_{\geq 5\,girders} = 0.240 + 0.136 \left(\frac{D_{projected}}{D} \right) \tag{5.14}$$

When this definition of α is used with Equation 5.11 to calculate global pressure coefficients for strength limit states, an appropriate level of conservatism (Figure 5.25) is displayed relative to the wind tunnel measurements. In Figure 5.25, values greater than unity are conservative.
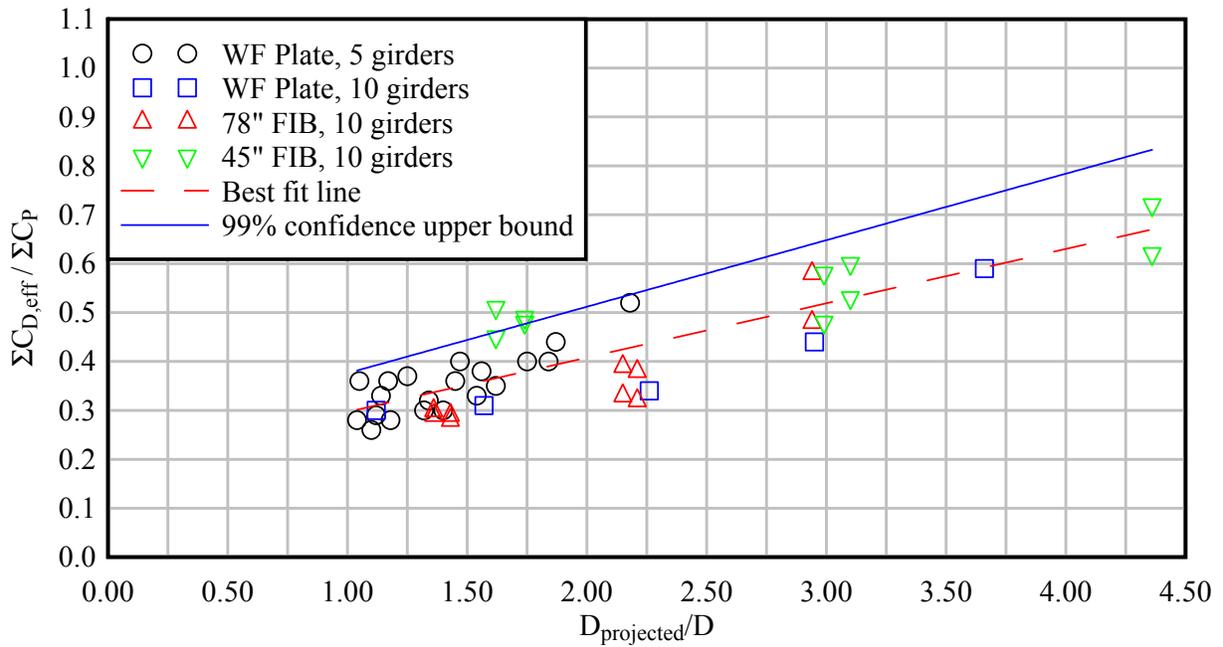
Figure 5.24 Global pressure coefficient reduction factor (α)
for systems with five (5) or more girders
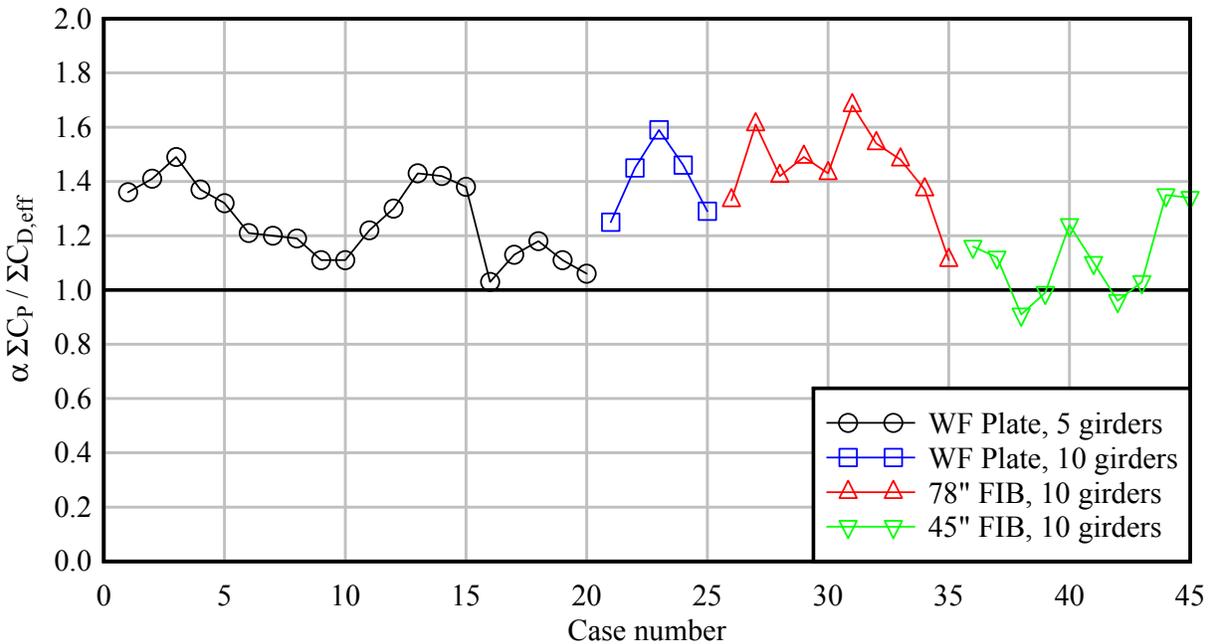
Figure 5.25 Normalized level of conservatism for models with five (5) or more girders

5.7.2 Development of a reduction factor for systems with less than five (5) girders

While direct wind tunnel measurements were performed for individual girders and for 2-girder systems, it was necessary to estimate effective drag coefficients (i.e. $C_{D,eff}$) for 3-girder and 4-girder systems for the purpose of developing a reduction factor for systems with less than five (5) girders. Such data estimation necessitated a separate approach than that described in the previous section. Effective drag coefficients for 3-girder and 4-girder systems were estimated using available wind tunnel data, which included:

- 5-girder WF Plate girder models: All positions (G1–G5) instrumented.

- 5-girder 45″ FIB, 78″ FIB, and NF Plate girder models: Three positions (G1–G3) instrumented.

- 10-girder 45″ FIB, 78″ FIB, and WF Plate girder models: All positions (G1–G10) instrumented.

The following estimation process was then utilized to estimate drag coefficients for 3- and 4-girder systems:

- WF Plate girders (3- and 4-girder systems): 5-girder measurements were truncated to produce estimates for both 3- and 4-girder systems.

- NF Plate girder (3-girder systems): 5-girder measurements with only G1–G3 instrumented were used as estimates for 3-girder systems. Because no measurements were performed for position G4 in any NF plate model, 4-girder systems were not estimated.

- FIBs (3-girder systems): 5-girder measurements with only G1–G3 instrumented were used as estimates for 3-girder systems.

- FIBs (4-girder systems): 5-girder measurements with only G1–G3 instrumented were used as estimates for positions G1–G3. Position G4 was estimated by using the ratio between positions G4 and G3 in the 10-girder models, as follows:

$$C_{D4,\ four\ girders} = C_{D3,\ five\ girders}\left(\frac{C_{D4,\ ten\ girders}}{C_{D3,\ ten\ girders}}\right) \tag{5.15}$$

Note that the 5-girder, 45″ FIB systems tend to have a lower $C_{D,eff}$ at position G3 in comparison to 10-girder systems (Figure 5.26). Additionally, a majority of 10-girder models have decreasing $C_{D,eff}$ between positions G3 to G4. Therefore, the 4-girder system estimates also decreased from position G3 to G4 by the same proportionality as the corresponding 10-girder measurements.
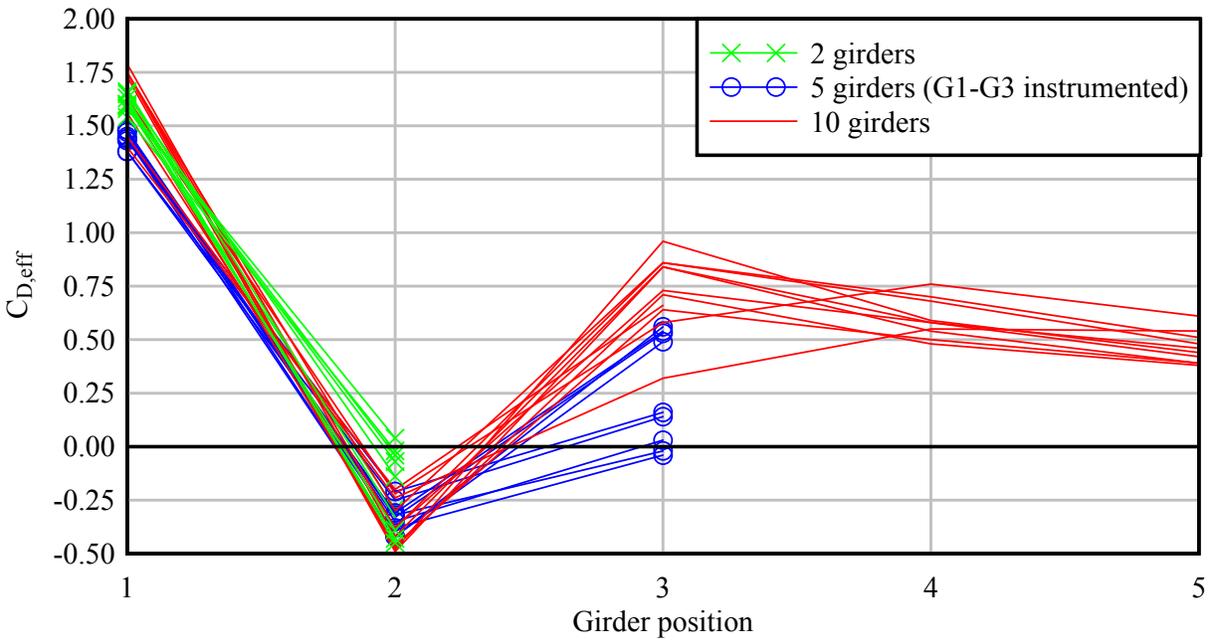
Figure 5.26 Effective drag coefficients ($C_{D,eff}$) measured for all 45″ FIB models

The following reduction factors (to be applied the shielding model in Figure 5.16) were found to be conservative for measured 1-girder and 2-girder wind tunnel results and estimated 3-girder and 4-girder $C_{D,eff}$ values:

$$\alpha_{<5\,girders} = \begin{cases} 1 & n=1 \\ 1 & n=2 \\ 2/3 & n=3 \\ 1/2 & n=4 \end{cases} \tag{5.16}$$

It should be noted that applying these reduction factors in conjunction with the stability shielding model for $1 \leq n \leq 4$ produces a global pressure coefficient that is equal to the pressure coefficient of the leading girder (i.e. 2.0 for FIBs and 2.5 for plate girders). The level of conservatism produced by these reduction factors (relative to estimates, in most cases) is illustrated in Figure 5.27. Out of 140 total cases, only two (2) of the 45″ FIB cases were underpredicted, both of which involved maximum tested wind angles (−5° and +5°).
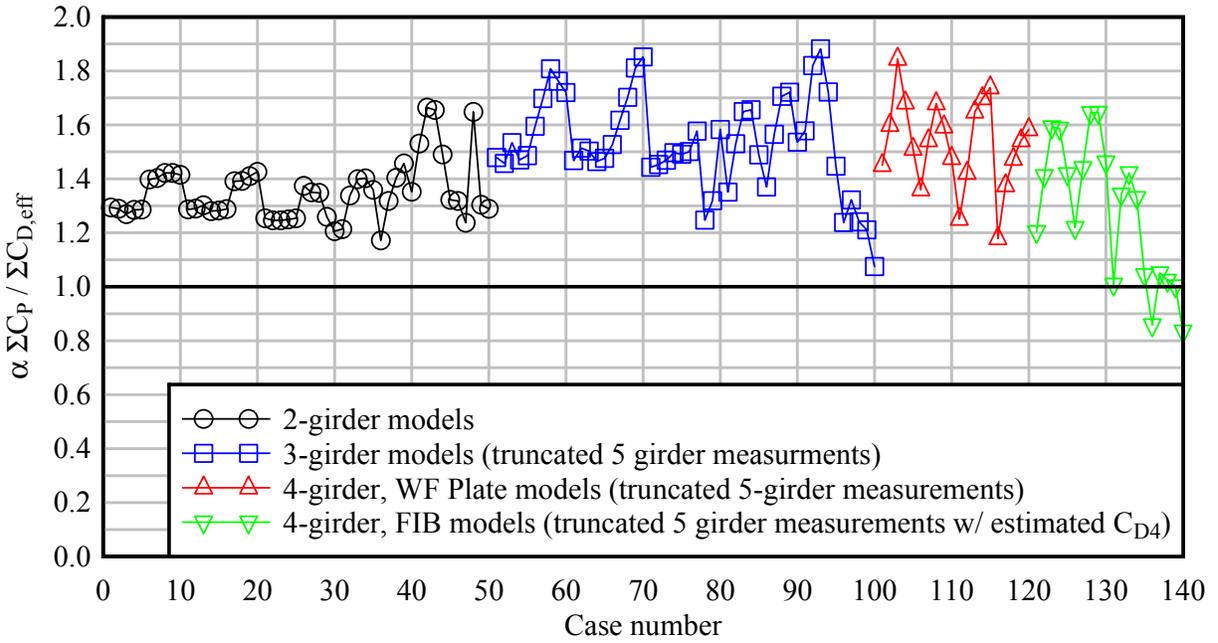
Figure 5.27 Normalized level of conservatism for models with less than five (5) girders

5.7.3 Global pressure coefficients for strength design

As described in the previous sections, *global pressure coefficients for strength design* can be calculated using a reduction factor applied to the summation of design loads given in Figure 5.16. Hence, repeating Equation 5.11 for convenience:

$$C_{P,global\text{-}strength} = \alpha \sum_{i=1}^{n} (C_P)_i \tag{5.17}$$

The reduction factor for five or more girders (Equation 5.14) can be combined with the reduction factor for less than 5 girders (Equation 5.16) to produce a reduction factor for any number of girders (n):

$$\alpha = \begin{cases} 1 & n=1 \\ 1 & n=2 \\ 2/3 & n=3 \\ 1/2 & n=4 \\ 0.240 + 0.136\left(\dfrac{D_{projected}}{D}\right) & n \geq 5 \end{cases} \tag{5.18}$$

where the projected depth, $D_{projected}$, is defined as:

$$D_{projected} = D + (n-1)(S)(\tan(\theta_{max})) \tag{5.19}$$

53

and the angle θ_{max} is defined as:

$$\theta_{max} = \left|\theta_{wind}\right| + \left|\theta_{cross\text{-}slope}\right| \tag{5.20}$$

An example calculation of the global pressure coefficient with reduction factor is presented in Appendix F.

CHAPTER 6
BEARING PADS

6.1 Introduction

When analyzing the stability of girder systems, it is important to consider the support conditions of the girders. In order to determine the support stiffness in each degree of freedom, it is necessary to calculate bearing pad stiffness in each of four pad deformation modes: shear, torsion, compression (axial) and rotation. While relatively simple methods are available for the calculation of shear and torsional stiffnesses, the calculation of axial and rotational stiffnesses requires more advanced calculation methods.

Empirical equations for calculating the compressive stiffness of a pad are available in the literature (Gent, 2001; Stanton et al., 2008; Podolny and Muller, 1982), but they frequently produce results that differ significantly from each other. One proven reliable method for quantifying compressive pad stiffness is the finite element method, but most bridge engineers have limited experience in modeling incompressible materials such as elastomer.

In addition to axial deformations, bearing pads are susceptible to roll rotations about two orthogonal axes; roll about the transverse centerline (*bending roll*) is typically the result of the end rotations of the girder as it bends about its major axis, while rotation about the longitudinal centerline (*overturning roll*) corresponds to overturning rotations of the girder at the supports. Estimation of these stiffnesses is often required for construction and design calculations, but methods for calculating such stiffnesses are not comprehensively addressed in the literature. For example, overturning roll stiffness at the supports is of particular importance during the construction (prior to casting of the deck) of long-span prestressed concrete girder bridges, as it can have a significant influence on the lateral stability of an unbraced girder, and is sometimes the only source of structural resistance to overturning moments generated by lateral loads (e.g., wind) or eccentric gravity loads. Recent experimental measurements of bearing pad roll stiffness (Consolazio et al., 2012), which extended into the nonlinear range, have provided an opportunity to develop an empirical calculation method capable of approximating roll stiffness while preserving nonlinear effects.

6.1.1 Physical description of pads

The types of bearing pads under consideration in this study consist of rectangular steel plates separated by layers of neoprene rubber (Figure 6.1). An external neoprene cover layer, typically thinner than the internal layers, surrounds the pad on all sides, sealing the steel reinforcement against corrosive agents in the environment. During the vulcanization process, the neoprene becomes fully bonded to the steel. Because the elastic modulus of the steel is so much greater than that of the neoprene, it can be considered to be effectively rigid.
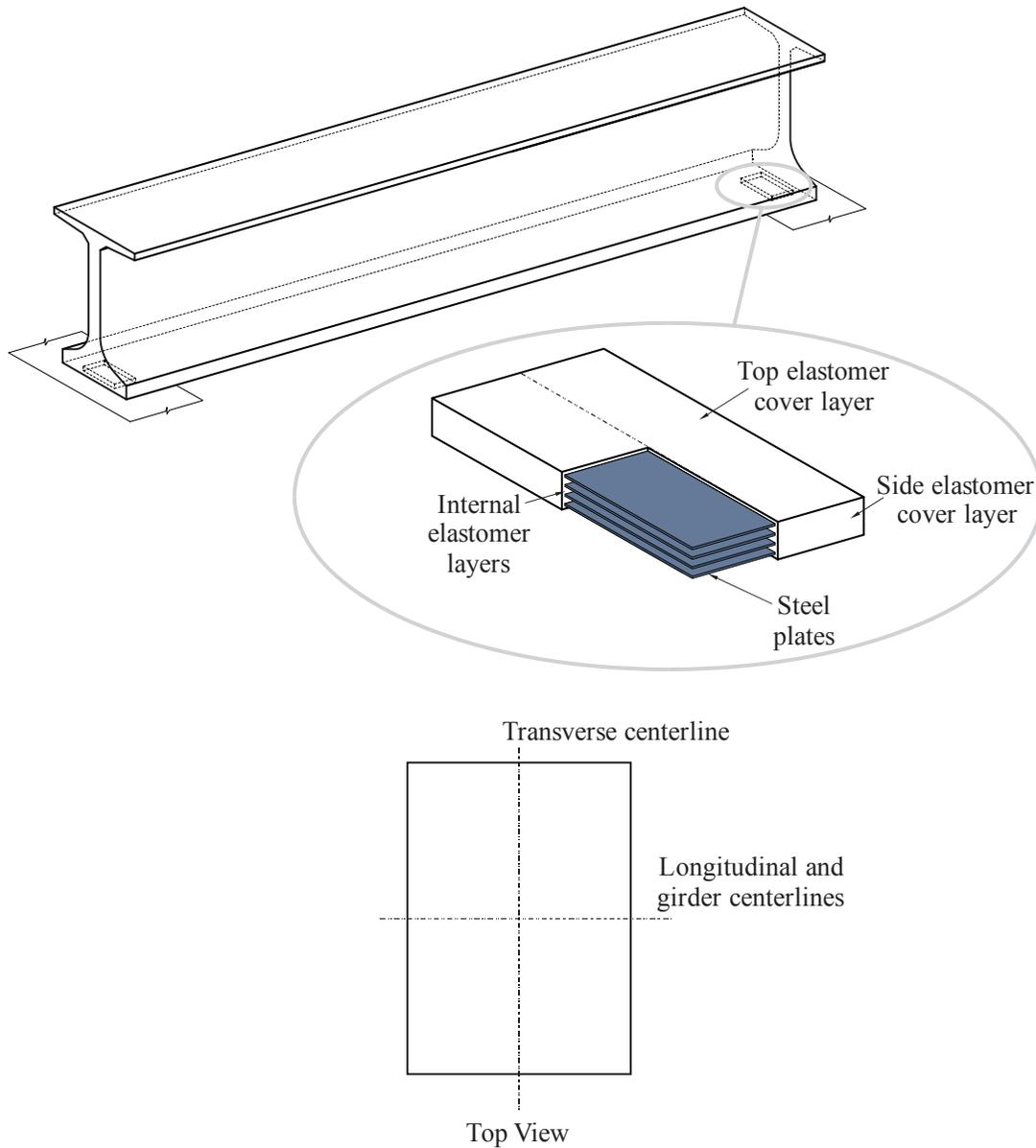
Figure 6.1 Location and structure of neoprene bearing pads

6.2 Behavior of pads in compression

Elastomeric rubbers, such as neoprene, are almost completely incompressible (i.e., with a Poisson's ratio $v > 0.49$), and when subjected to a uniaxial compressive force, they tend to expand laterally to preserve their volume. However, in a steel-reinforced bearing pad, the steel plates are stiff enough to effectively restrain all movement of the neoprene at the steel–neoprene interfaces. As a result, when a pad is compressed, the neoprene layers respond by bulging outward at the edges (Figure 6.2). Restraint of this expansion by the steel plates makes the pad much stiffer in compression than an unreinforced pad with equivalent thickness and volume of elastomer. At extreme levels of compression, the stiffness becomes nonlinear as the bulging displaces a significant portion of elastomer outside of the primary load path, reducing the

56

effective layer thickness and stiffening the pad. However, if the pad has been properly sized according to the provisions of AASHTO (2010) or similar, then determining just the initial linear stiffness is sufficient for most relevant bridge engineering calculations.

a)
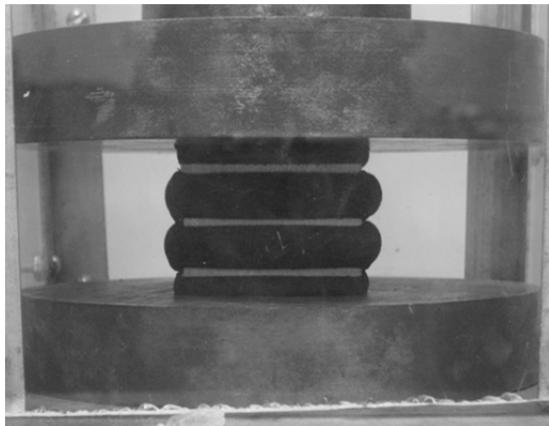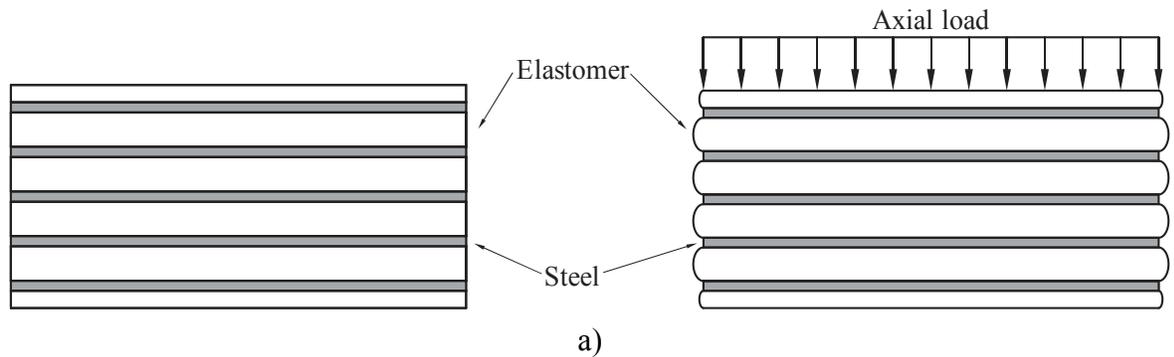
b)

c)

Figure 6.2 Bulging of neoprene layers under compression:
a) Illustration of bulging; b) 2-in. x 2-in. pad in compression; c) 12-in. x 23-in. pad in compression

One consequence of the characteristic bulge response is an uneven distribution of compressive stiffness throughout the pad such that local compressive stiffness at any point is a function of the distance from the center of the pad. Near the center, there is a large amount of surrounding rubber that must be displaced laterally in order for the neoprene layers to bulge at the edges. In contrast, near the edges of the pad, the rubber is less confined and comparatively little force is required for the rubber to bulge. This confinement effect can be demonstrated by prescribing a uniform downward displacement on the top surface of a finite element model of a layer of neoprene and plotting the distribution of the reaction forces (Figure 6.3). Because every point on the pad is compressed (deformed) vertically the same amount, the reaction force distribution is proportional to the distribution of local stiffness.
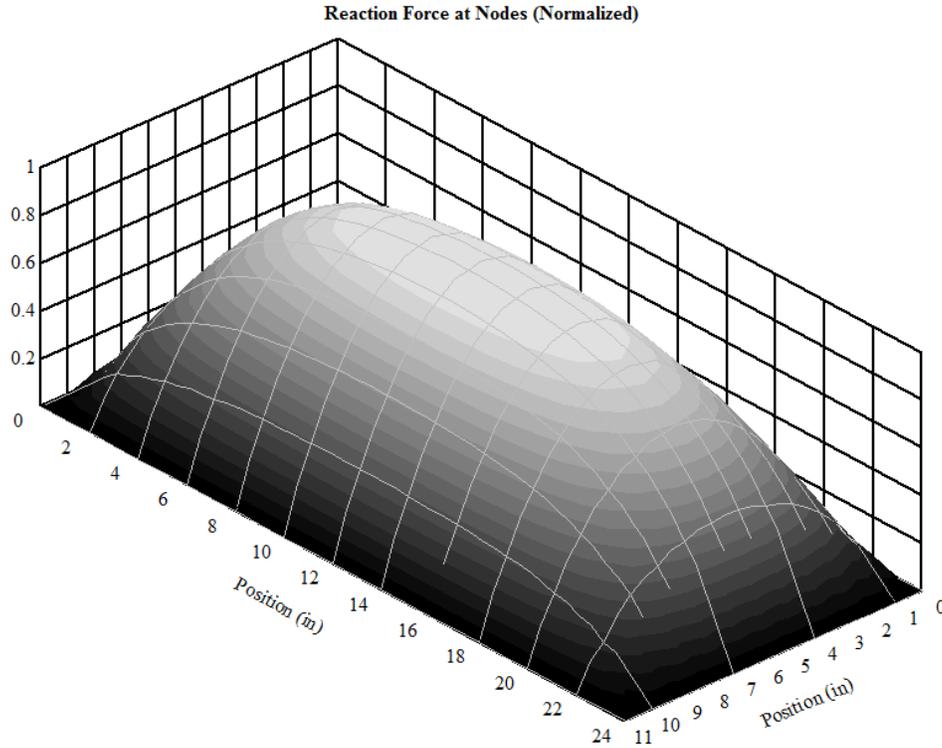
Figure 6.3 Distribution of reaction force under bearing pad subjected to uniform axial load (FEA results)

Gent (2001) and others have published correlations between the axial stiffness of a bearing pad and the *shape factor, S*, of the internal elastomer layers of the pad. The shape factor is a dimensionless ratio between the *load area* (i.e., plan-view area of the pad) and the *bulge area* (i.e., the perimeter area). Most shape factor–based methods use the same basic functional form:

$$E_c = E\left(1 + B_a S^2\right)$$ (6.1)

(where B_a is an empirically-determined constant) to calculate an effective elastic modulus for compression, E_c, that incorporates the additional restraint provided by the steel reinforcement. Stanton et al. (2008) have refined this approach, providing a method for determining B_a that takes into account the bulk compressibility of the elastomer. In contrast, Podolny and Muller (1982) have provided an empirical formula:

$$k_{axial} = \frac{GAa^2}{Ct^3}$$ (6.2)

that does not incorporate the shape factor, but does include a constant, C, that changes depending on the aspect ratio of the pad.

58

6.3 Behavior of pads in roll rotation

As a girder rolls, the top surface of the pad becomes angled relative to the bottom surface, lifting upward from one side of the pad and depressing the opposite side. Because the pad is already compressed by the weight of the girder it supports, the entire width of the pad initially remains in contact with the girder and the initial roll stiffness of the pad is linear. However, if the roll angle becomes large enough, the girder will begin to lift off the pad, and the roll stiffness will become nonlinear (Figure 6.4). The critical roll angle at which this occurs is dependent on the initial compression load. As more of the pad becomes disengaged, the roll stiffness softens until the moment vs. rotation (angle) curve becomes horizontal (*plateaus*) and the girder rolls off of the pad.
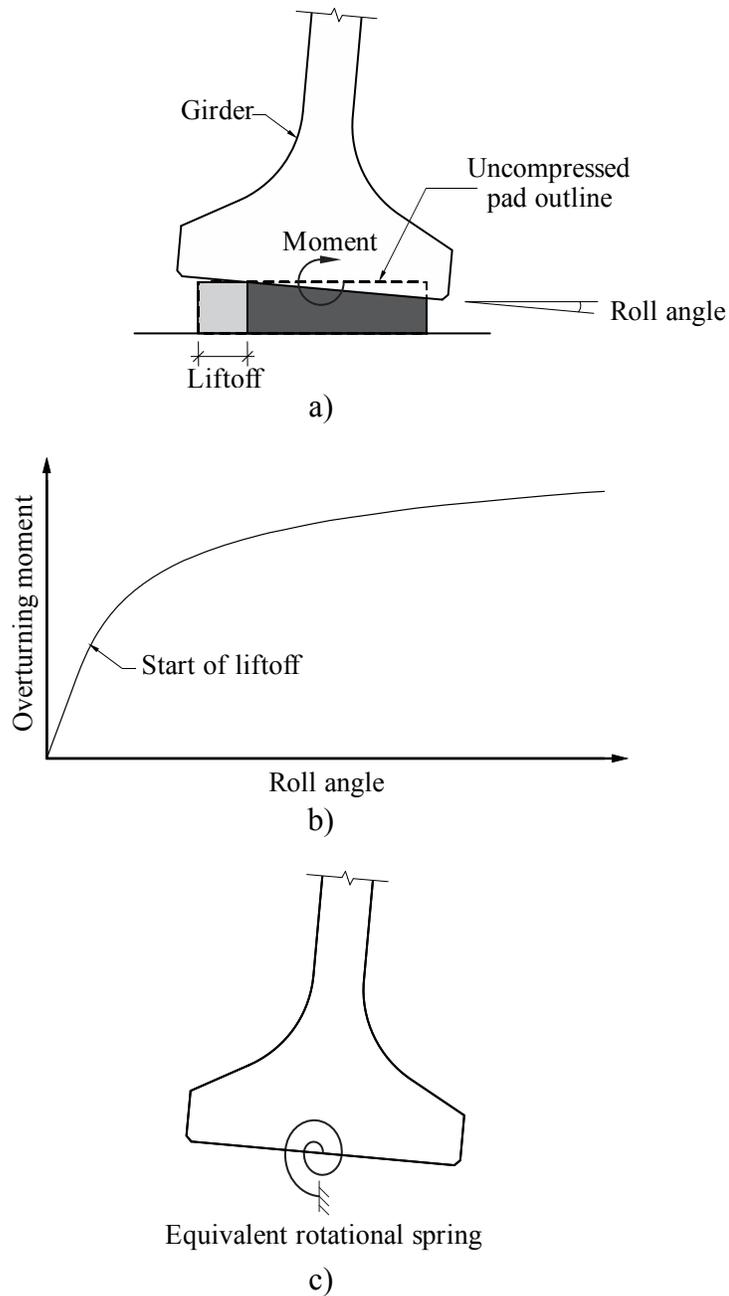
Figure 6.4 Behavior of bearing pads during girder rollover:
a) Girder liftoff from pad; b) Nonlinear roll stiffness curve; c) Equivalent conceptual model

In 2012, an experimental study (Consolazio et al., 2012) demonstrated that an increase in the initial compression load results in an approximately proportional increase in the plateau value (while the initial roll stiffness remains essentially unaffected). Also demonstrated in the study were the effects of the geometric orientation of the girder centerline relative to the longitudinal centerline of the pad. Specifically, the two types of orientation angle considered were *slope* (divergence of the centerlines in elevation view) and *skew* (divergence in plan view). It was found that overturning roll stiffness was significantly reduced when skew was present, and that

this effect was exacerbated by the simultaneous inclusion of a non-zero slope angle. These experimental findings confirmed results from an earlier study (Consolazio et al., 2007) in which the interaction between skew and slope was examined analytically. The effect of slope alone (with no skew) was less conclusive in the experimental study due to scatter in the experimental data, but the majority of the test specimens exhibited at least some reduction in roll stiffness associated with an increase in slope angle.

From the experimental study, it was concluded that bearing pad skew has the potential to drastically reduce girder stability during construction and should be avoided. Data from the study were used to support implementation of a departmental (FDOT) design policy change requiring that bearing pads be aligned with bridge girders thus eliminating skew between girder and pad. For this reason, the effects of bearing pad skew have been ignored in the present study and report.

6.4 Calculation of shear and torsion stiffness

Because shear and torsional deformation modes involve shear, but not compression of the elastomer, the pad can be treated as a linear-elastic shear deformable material. Only the basic dimensions of the pad (Figure 6.5) and the shear modulus, G, are then required to calculate the shear and torsional stiffnesses from basic principles of mechanics as follows:

$$k_{shear} = \frac{LWG}{T} \tag{6.3}$$

$$k_{torsion} = \frac{J_{pad}G}{T} \tag{6.4}$$

The torsional constant, J, for a rectangular pad can be calculated from a formula provided by Roark (Young and Budynas, 2002):

$$J_{pad} = \left(\frac{WL^3}{16}\right)\left(\frac{16}{3} - 3.36\left(\frac{L}{W}\right)\left(1 - \frac{L^4}{12W^4}\right)\right) \quad \text{where } W \geq L \tag{6.5}$$
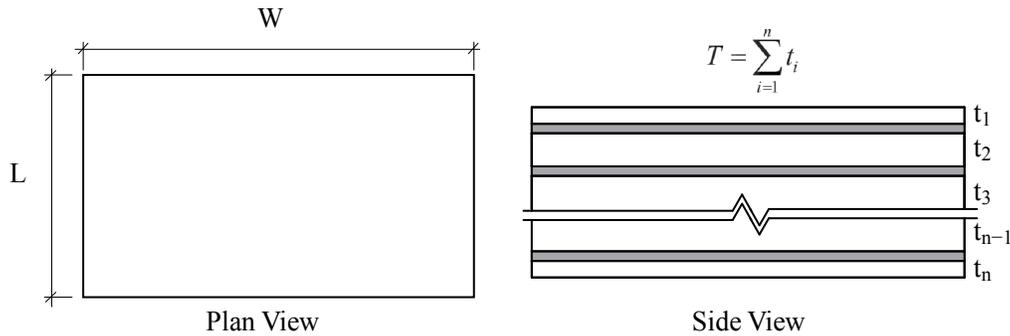
Figure 6.5 Dimensions of a bearing pad.

6.5 Calculation of axial stiffness

Finite element analysis can be used to determine the axial stiffness of a bearing pad but most bridge engineers have limited experience modeling rubber with three-dimensional solid elements. The following describes a simple, accurate, numerically stable, and computationally efficient modeling approach for quantifying axial stiffness, without the need for specialized material testing.

6.5.1 Stiffness of neoprene layers

As previously mentioned, steel reinforcing plates are stiff enough, relative to neoprene, that they can be treated as effectively rigid. As a result, the overall axial stiffness of a pad is equivalent to the individual stiffnesses of the neoprene layers (including the top and bottom cover layers) combined in series (Figure 6.6). It is only necessary to model the individual neoprene layers and then combine the results to determine the axial stiffness of the pad. Because all internal layers typically have the same thickness, generally it will only be necessary to create two finite element layer models—an internal layer model and a cover layer model.
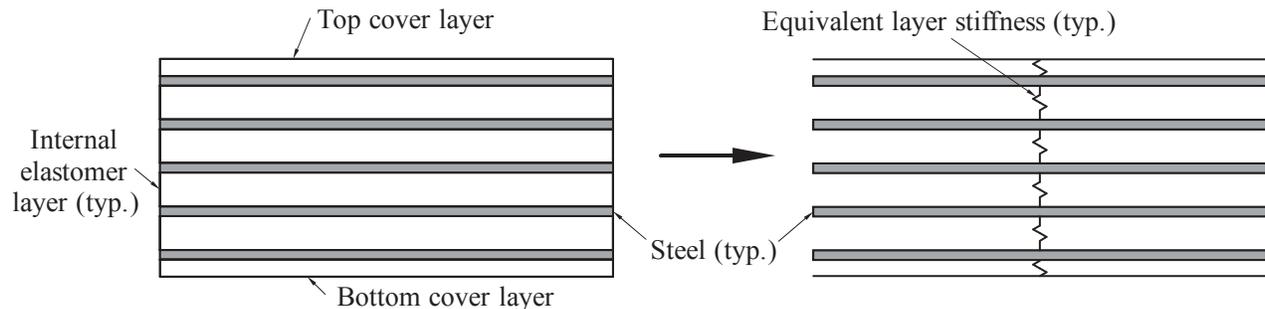
Figure 6.6 Axial stiffness of pad as individual layer stiffnesses combined in series

6.5.2 Model dimensions and meshing

While it is important to include the cover layers at the top and bottom of the pad, the side layer that surrounds the perimeter of the pad does not contribute significantly to pad stiffness and does not need to be included in the finite element models. Instead, both layer models (internal and cover) should have the same plan-view dimensions as the steel reinforcing plates, differing only in thickness.

The use of tri-quadratic solid elements (e.g., 20-node or 27-node) is highly recommended to avoid shear locking, as the higher-order shape functions employed by such elements more naturally approximate the curvature of the elastomeric bulge. A much smaller quantity of solid elements is then required, significantly reducing the computational burden. A mesh convergence study has demonstrated that if 27-node solid elements are used, a layer model need only be two elements thick, and the plan-view dimensions of the elements can be as large as 1 in. on either side (as long as the model has a minimum subdivision of eight elements in both directions) (Figure 6.7).
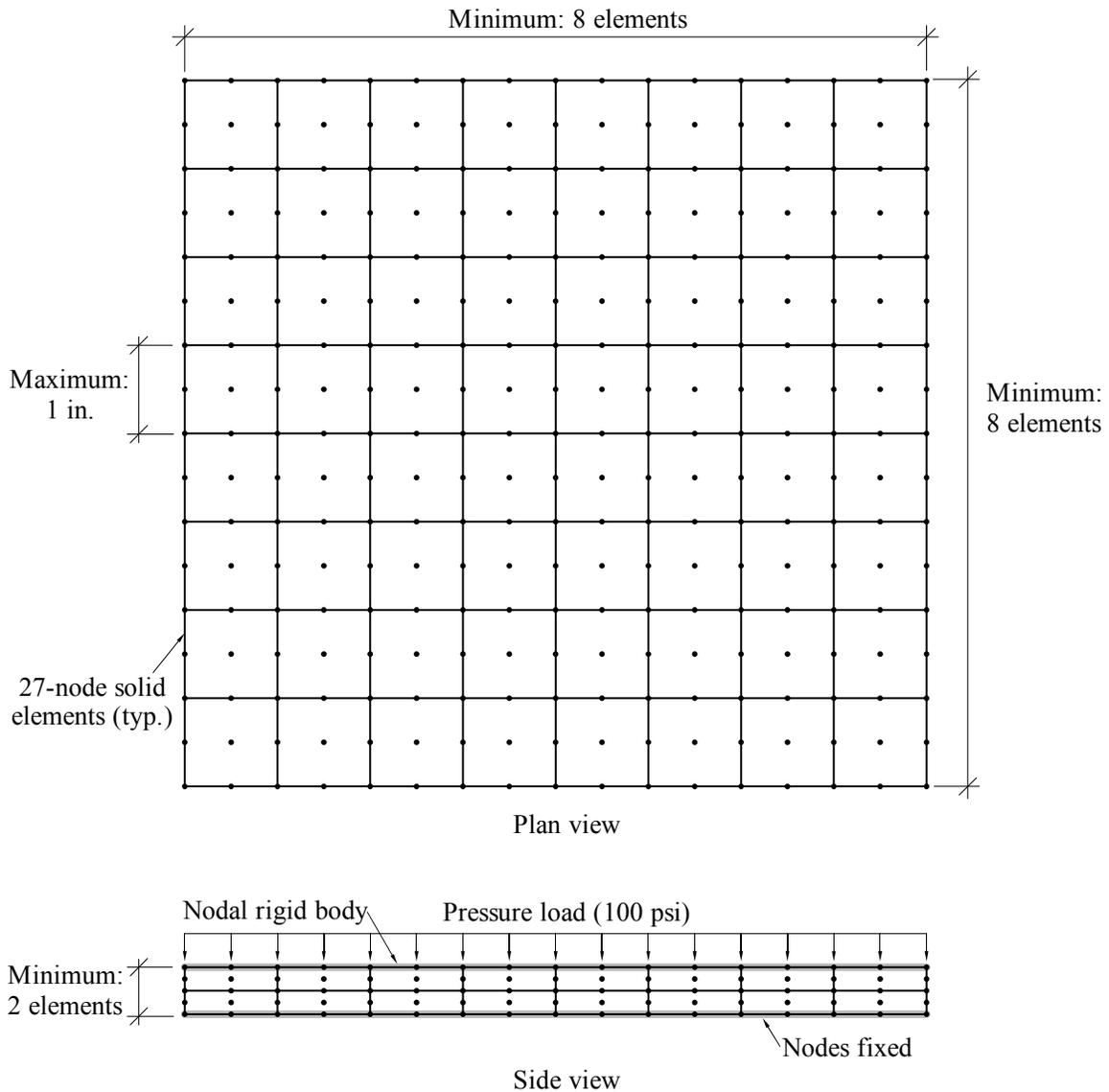
Figure 6.7 Finite element model of elastomer layer

6.5.3 Loading and boundary conditions

All of the nodes on the bottom surface of each elastomer layer model should be fixed in place, while the nodes on the top surface are constrained together into a nodal rigid body, representing the restraint provided by the steel reinforcement (or by friction between the pad and the girder or substructure). Application of a uniform axial pressure load of 100–200 psi is sufficient to characterize the initial axial stiffness of typical pads.

6.5.4 Material model

Rubbers and other incompressible materials are generally modeled as hyperelastic materials, meaning that the mechanical properties are defined by a strain energy density function, $W(\lambda_1, \lambda_2, \lambda_3)$, which relates the total strain energy per unit volume to the deformed state of the

63

material. Each hyperelastic model uses a different form of W, which is nearly always written in terms of the principal stretch ratios, λ_1, λ_2, and λ_3, which represent the material deformation. Stretch is defined as the ratio of deformed length to undeformed length, so the principal stretches can be related to the principal strains as:

$$\lambda_i = \frac{L_i + \Delta L_i}{L_i} = 1 + \varepsilon_i \qquad (6.6)$$

In most hyperelastic materials, the functional form of W is selected empirically, and requires two or more material parameters which must be determined from experimental testing of specially-prepared material specimens. Material testing is often not feasible for bridge design and, in most circumstances, the only available material data for the neoprene in a bearing pad is the shear modulus, G. In some cases, only a durometer hardness value may be available, which can be converted into an approximate shear modulus empirically (Podolny and Muller, 1982; AASHTO, 2010).

In contrast, a neo-Hookean hyperelastic model (Haslach and Armstrong, 2004) employs a strain energy density function that is not empirical, but is based on a statistical-mechanical analysis of linked polymer chains. This results in a relatively simple strain energy density function:

$$W(\lambda_1,\lambda_2,\lambda_3) = C_1\left(\lambda_1^2 + \lambda_2^2 + \lambda_3^2 - 3\right) \qquad \text{where } C_1 = \frac{G}{2} \qquad (6.7)$$

with only one material parameter, C_1. It can be demonstrated (Treloar, 1975) that for consistency with linear elasticity, C_1 is equal to half of the shear modulus, so no material testing is required as long as the shear modulus is known. The neo-Hookean model is only accurate for small strains, but this range is sufficient for capturing the initial axial stiffness of a neoprene layer.

It is noted that many finite element software packages do not explicitly offer a neo-Hookean material option because it is a degenerate form of the more general Mooney–Rivlin model:

$$W(\lambda_1,\lambda_2,\lambda_3) = C_1\left(\lambda_1^2 + \lambda_2^2 + \lambda_3^2 - 3\right) + C_2\left(\lambda_1^2\lambda_2^2 + \lambda_2^2\lambda_3^2 + \lambda_3^2\lambda_1^2 - 3\right)$$
$$\text{where } C_1 + C_2 = \frac{G}{2} \qquad (6.8)$$

Standard neo-Hookean behavior can be achieved by selecting a Mooney–Rivlin material model and setting C_2 equal to zero (Bathe, 1996).

Both the neo-Hookean and Mooney–Rivlin material formulations assume fully incompressible behavior, which is a reasonable assumption for elastomeric layer models. However, it is also common for finite element packages to include compressible behavior by adding a volumetric strain term to the strain energy density function. This requires that the user supply a finite value for the bulk modulus, K (or another property, such as the Poisson's ratio, which can be used together with G to calculate K). Layer models are not highly sensitive to changes in K as long as a reasonably high value of K is used. A default value of 200 ksi is recommended by Gent (2001) for situations where the actual value of K is unknown. Alternatively, the AASHTO LRFD (AASHTO, 2010) suggests a value of 450 ksi, and others,

such as Bradley and Chang (1998), have reported measurements as high as 470 ksi for individual pad rubber specimens.

6.5.5 Experimental validation

In order to validate the finite element analysis approach, experimental axial compression tests were performed on two standard types of Florida bridge bearing pads to measure stiffness. Two pads of each type were tested (i.e., four pads total) with each pad loaded to a maximum pressure of 1 ksi over three complete load cycles. It was found that the average measured axial stiffness for each pad type was within 2% of the stiffness predicted by the corresponding finite element models when using Gent's suggested bulk modulus of 200 ksi (Figure 6.8). When K is doubled to 400 ksi, the calculated pad stiffnesses only increases by about 15%. These findings support the use of Gent's value in most situations, but higher accuracy can be achieved if the value of K is more precisely known.
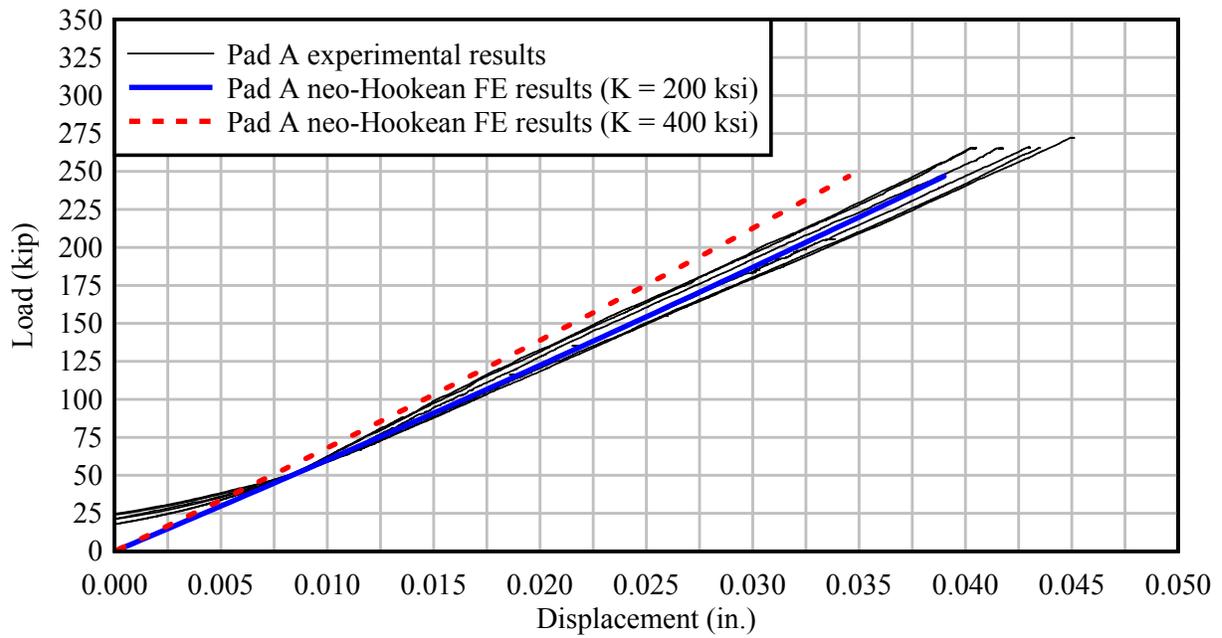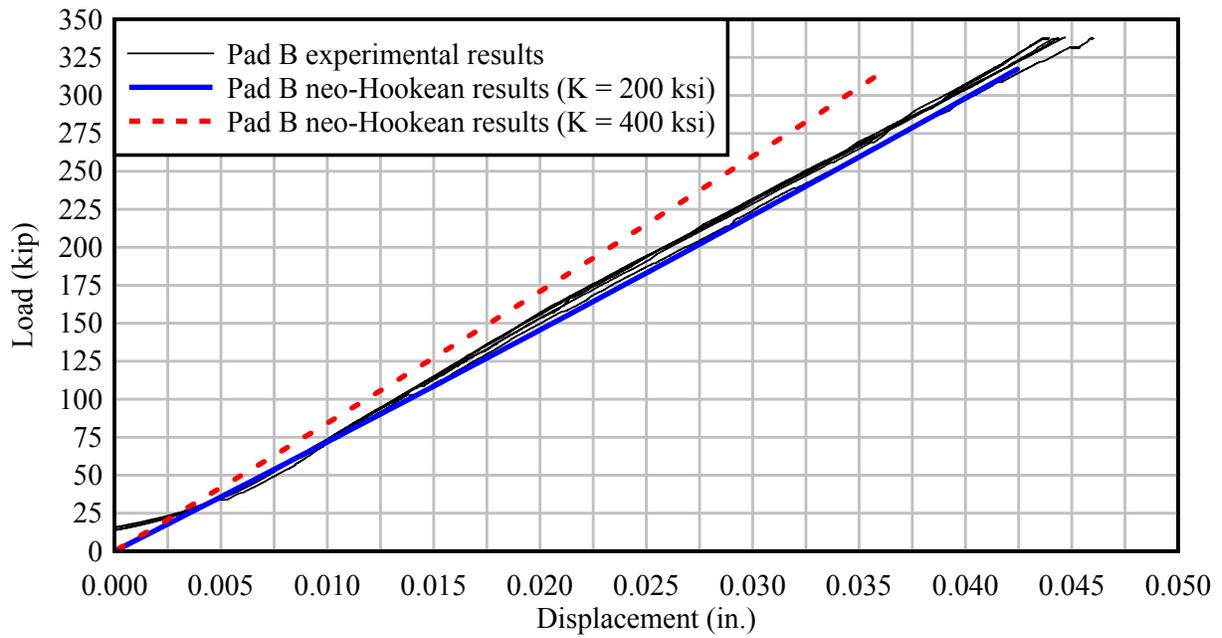
Figure 6.8 Validation of neo-Hookean material model: a) Pad A; b) Pad B

6.6 Calculation of nonlinear roll stiffness curves

In roll, different areas of the pad are compressed by different amounts, so when computing the equilibrium position of the girder, it is necessary to consider the non-uniform distributions of deformation and axial stiffness across the pad. It is also necessary to include the softening effect of liftoff.

6.6.1 Grillage model

Estimation of the roll stiffness of a bearing pad can be accomplished using a simplified *grillage model*, which divides the pad into discrete rectangular regions and models each region with a spring representing the stiffness contribution of that region. Compression-only springs are used to allow the girder to liftoff from the pad. The upper nodes of the springs are linked together into a rigid body which represents the top surface of the pad (i.e., the surface in contact with the girder), while the bottom nodes are fixed in place.

The grillage model must first be compressed by a uniform axial load, representing the weight of the girder. Then an overturning moment can be applied to the top surface and a structural analysis can be used to determine the resulting roll angle (Figure 6.9). If the overturning moment is increased incrementally, a complete stiffness curve can be generated.
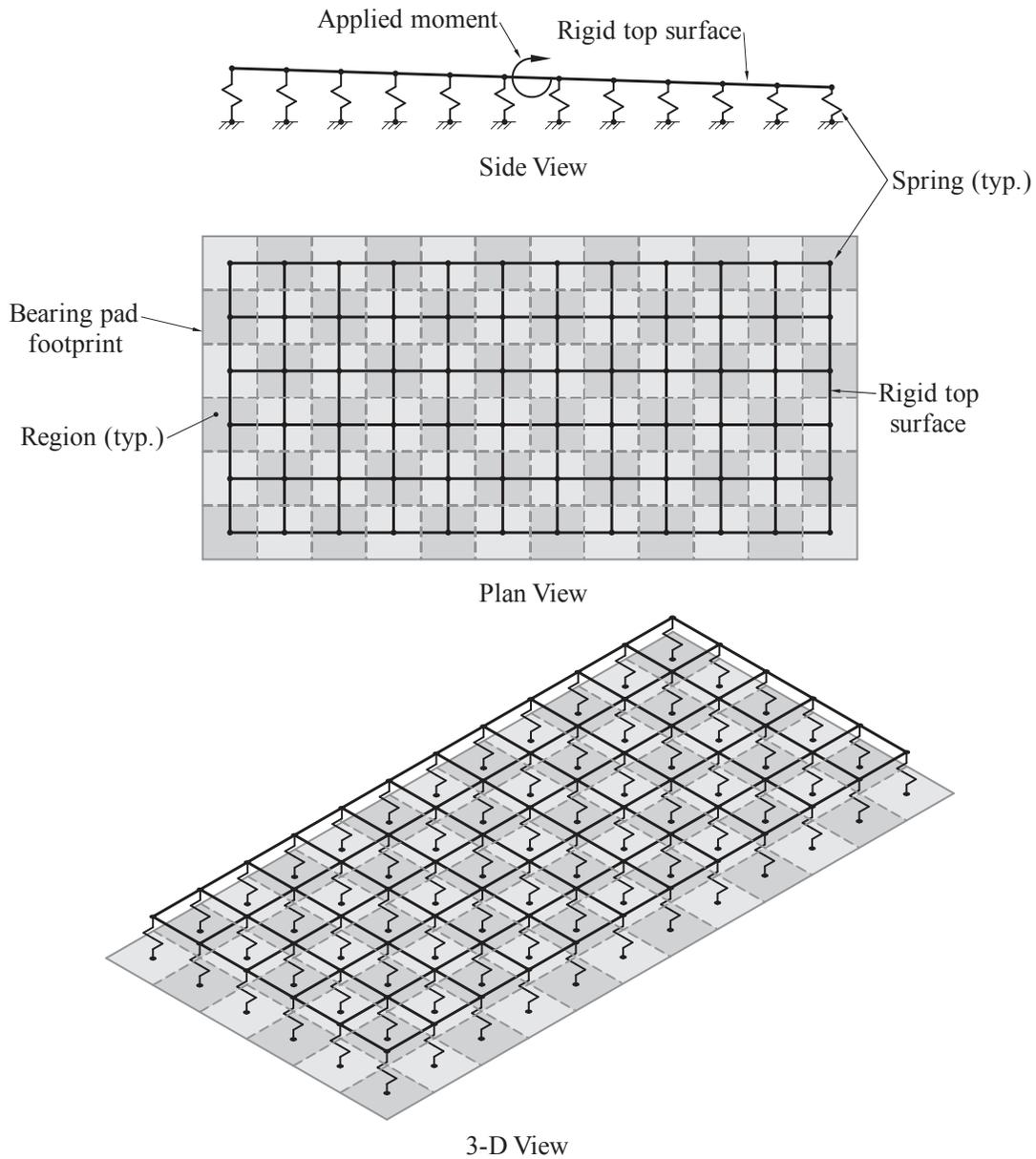
Figure 6.9 Simplified grillage model of a bearing pad

6.6.2 Spring stiffness distribution in grillage model

Several methods of distributing stiffness values to the springs in the grillage model were considered and the resulting stiffness curves were compared to experimental roll stiffness measurements (Consolazio et al., 2012) that were obtained for three standard FDOT pad types (Figure 6.10), designated A, B, and C. Empirically, the best approach was found to involve the use of a parabolic bubble function (Figure 6.11) to assign stiffnesses to the grillage springs. This function approximates the shape (but not the magnitude) of the true axial stiffness distribution within the pad (recall Figure 6.3).

The bubble function must be scaled so that its maximum value (at the center of the pad) is equal to the full axial stiffness of the pad normalized by the pad area and multiplied by the

68

tributary area of a single region. The full axial stiffness of the pad can be obtained using the finite element procedure outlined in the previous section. Note that while the value of the bubble function is zero at the pad edges, the outermost grillage springs are sampled at the center of their respective tributary regions, so they will have small non-zero stiffnesses.

Typical section: Bearing pad type A

Typical section: Bearing pad types B & C

Plan view
Bearing pad types A, B & C
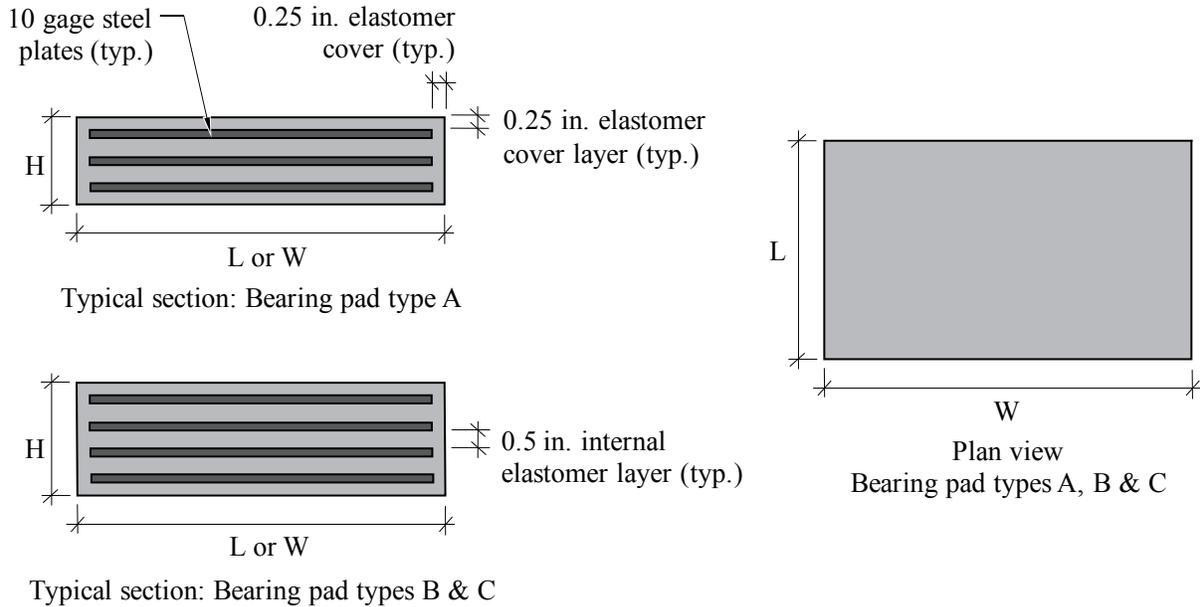
	Bearing pad type		
	A	B	C
Bearing pad length, L (in.)	11	14	12
Bearing pad width, W (in.)	24	24	23
Bearing pad height, H (in.)	1-29/32	2-9/16	2-9/16
Number of internal plates	3	4	4

Figure 6.10 Standard FDOT bearing pads used for experimental verification.

Spring locations

Bearing pad footprint

Region (typ.)

a)
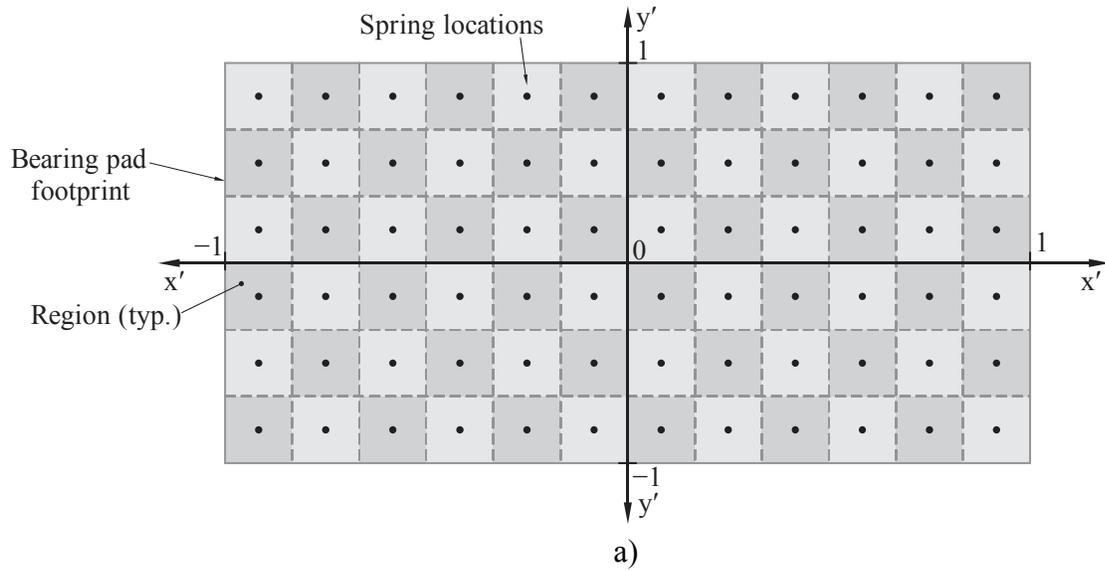
$$k_{spring}(x',y') = A_{region}\left(\frac{k_{axial}}{A_{pad}}\right)\left(1-(x')^2\right)\left(1-(y')^2\right)$$

b)
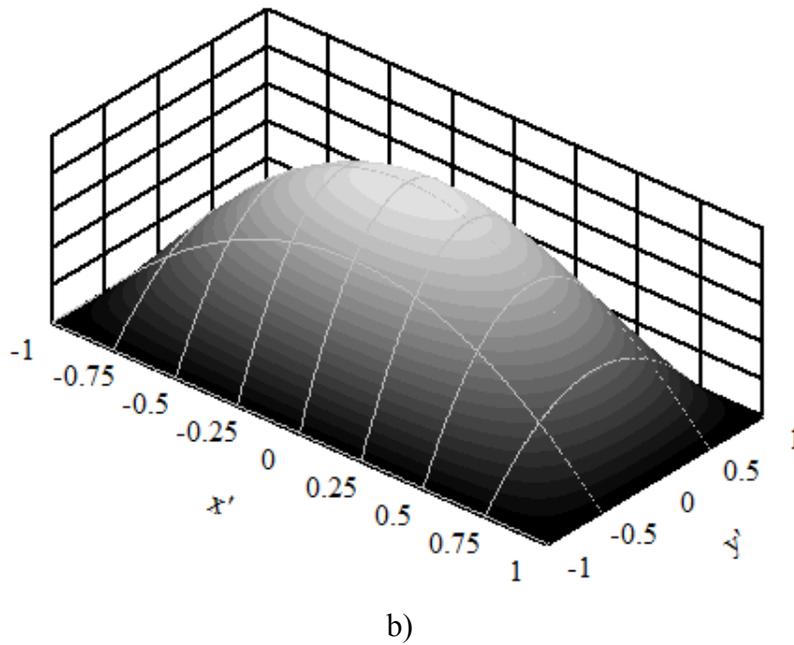
Figure 6.11 Distribution of stiffness to grillage springs:
a) Normalized coordinate system; b) Scaled bubble function

The roll stiffness curves obtained from the grillage approach show close agreement to experimentally measured curves (Figure 6.12) that were obtained for a variety of pad dimensions and axial load levels. Also, the grillage approach correctly exhibits the proportional relationship between initial axial load and roll stiffness plateau value (Consolazio et al., 2012). A mesh

convergence study has demonstrated that a grillage of 1 in. x 1 in. square regions provides sufficient discretization to fully capture the nonlinear roll stiffness of pad sizes that are typical of bridge construction. Because the method is not highly sensitive to small changes in axial stiffness, the choice of bulk modulus (K) has minimal effect on the resulting roll stiffness curves.
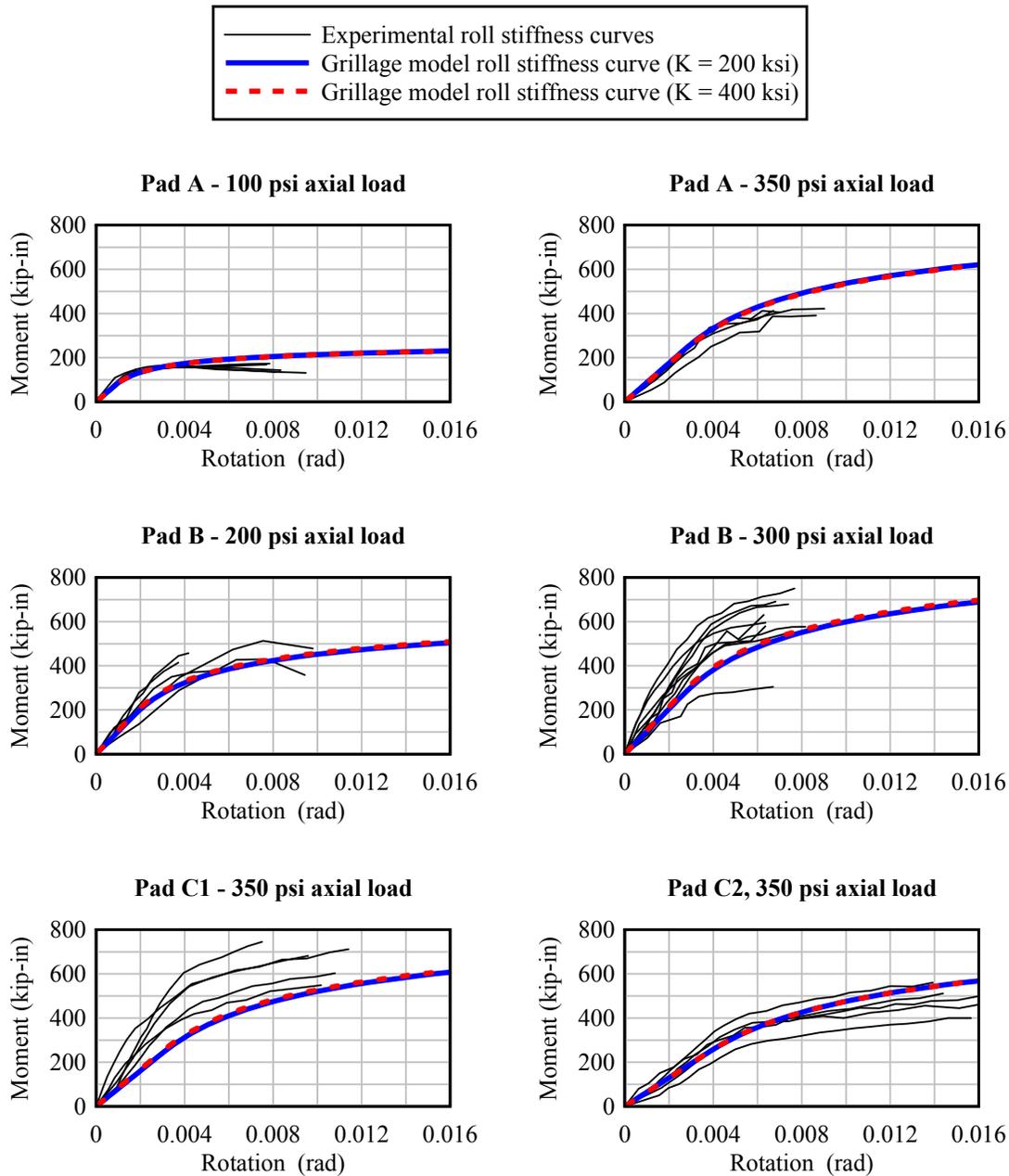
Figure 6.12 Comparison of experimentally measured bearing pad roll stiffnesses and roll stiffnesses predicted by the proposed computation method.

6.6.3 Incorporating girder slope

During bridge construction, the stage at which prestressed concrete girders are most susceptible to lateral instability is immediately after girder placement and before the casting of the deck. Girder stability at this stage is dependent on the overturning roll stiffness of the bearing pads, especially if the girders are unbraced (Mast, 1993). However, because the weight of the deck is not yet present, and therefore is not available to counteract vertical camber of the girder, significant slopes (Figure 6.13a) can be induced at the girder ends. (These slopes will be reduced or eliminated later, after the deck has been cast.) If the weight of the girder does not compress the pad sufficiently, an edge region of the pad may not be in contact with the girder and therefore will be unable to contribute to the overall roll stiffness. Because sloped contact on a bearing pad has been shown to have a detrimental effect on girder stability (Consolazio et al., 2012), the effect of slope should be considered when estimating the roll stiffness of the supports for use in lateral stability calculations.

Slope can be incorporated into the grillage model as an angular deformation that is imposed about the transverse centerline of the grillage (Figure 6.13b). The angular deformation and initial axial load must be applied to the top surface prior to applying the overturning moment about the longitudinal centerline. If the slope angle is large enough (or the initial axial load is small enough), the grillage may include an initial 'liftoff' region— corresponding approximately to the region of the pad not in contact with the girder—in which the compression-only springs generate no force. As roll angle increases, the superposition of roll angle and slope angle will cause the liftoff region to change shape. The resulting roll stiffnesses curves do not match experimental measurements (Figure 6.14) as closely as in the unsloped cases, however they are found to be conservatively low. In each case, the initial stiffness predicted by the grillage approach consistently remains within 40% of the lowest measured stiffness for that case.
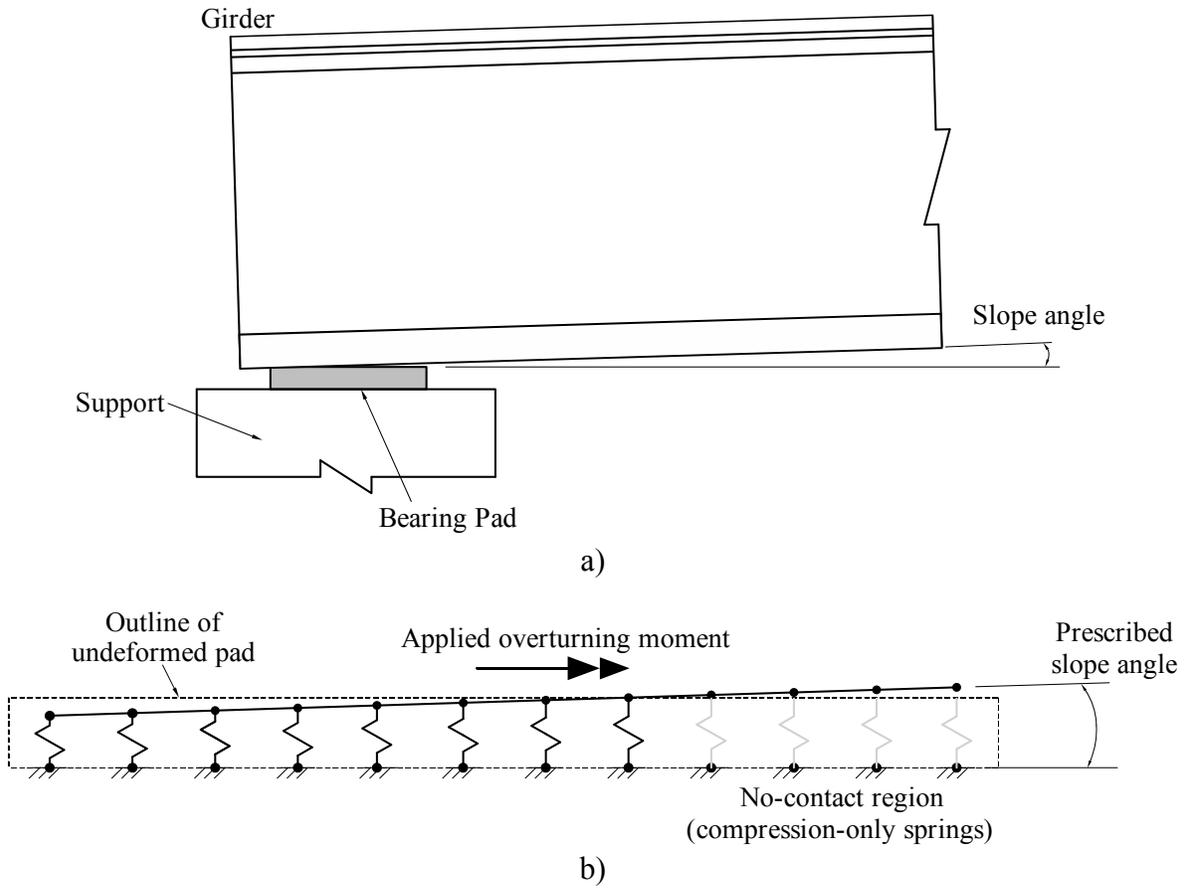
Figure 6.13 Bearing pad slope:
a) Sloped girder in partial contact with pad; b) Grillage model incorporating slope
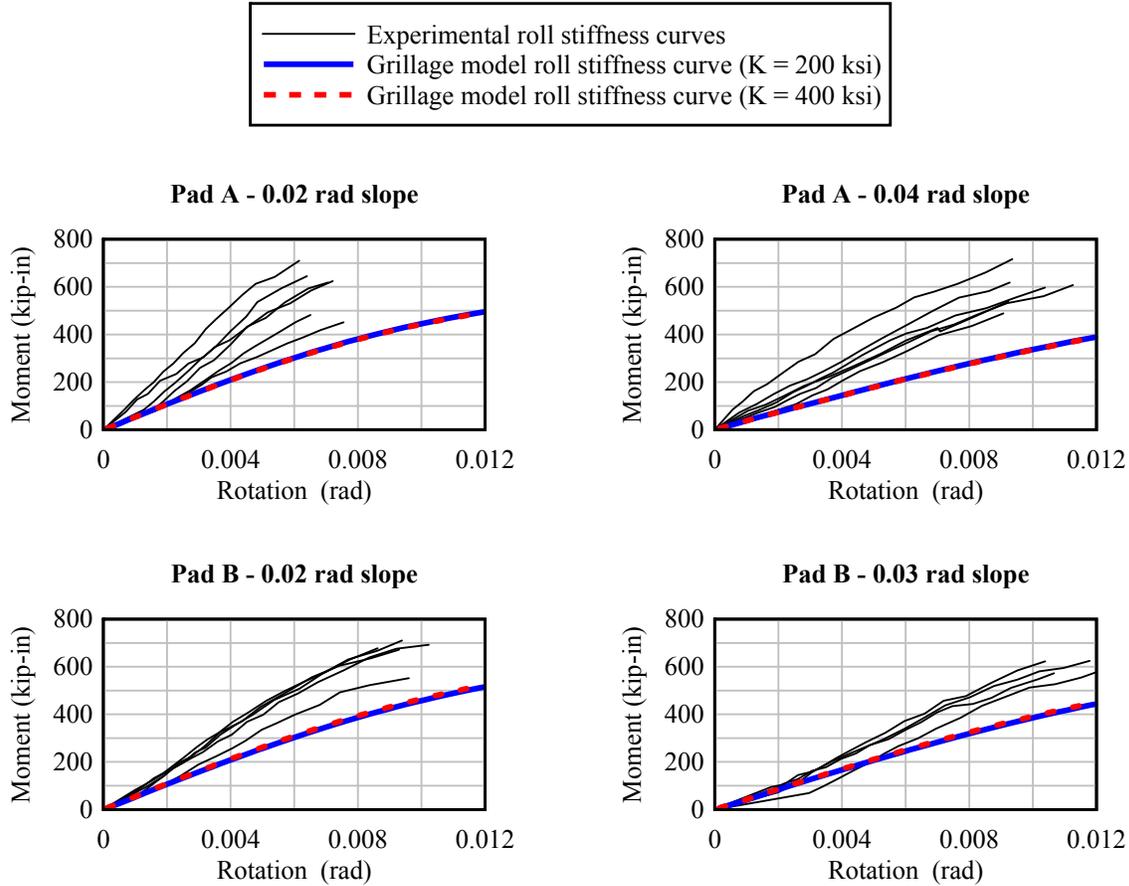
Figure 6.14 Comparison of experimentally measured bearing pad roll stiffnesses and roll stiffnesses predicted by the proposed computation method with non-zero slope

6.7 Simplified method for calculating axial stiffness and instantaneous roll stiffnesses

The calculation methods described in the previous sections produce accurate results, but require the use of finite element software (to compute k_{axial}) and structural analysis software (to compute k_{roll}). For bridge designers, the use of such software may be time consuming and impractical, particularly if the analyses have to be repeated several times during an iterative design process. While the grillage method is capable of producing complete nonlinear roll stiffness curves, some applications require only knowledge of the initial (instantaneous) roll stiffness. For such cases, it is possible to derive an expression for the initial roll stiffness of the grillage in closed form, obviating the need to construct and analyze a structural model. This is accomplished by considering a *continuous grillage*: a grillage discretized into an infinite number of springs, each representing an infinitesimal *differential area* of the pad, dA. Such a grillage can be treated mathematically as a continuum, and properties (such as roll stiffness) arising from the aggregated actions of individual springs can be determined in closed-form by integrating over the area of the pad.

In the sections below, simplified methods for computing axial pad stiffness, k_{axial}, and instantaneous pad roll stiffness, k_{roll}, are described.

6.7.1 Axial stiffness

In the finite element approach described earlier, individual finite element models are constructed for each elastomer layer in a bearing pad, and the resulting stiffnesses (k_{layer}) are combined in series to produce an overall axial stiffness for the pad (k_{axial}). A simplified method proposed by Stanton et al. (2008) can be used in lieu of the finite element models to compute the stiffnesses of individual elastomer layers in closed form, in terms of the layer dimensions and elastomeric material properties. Stanton's simplified equations produce k_{layer} values that are consistently within 2% of the equivalent finite element model results. As noted in the discussion of the finite element approach, the plan view dimensions of the steel reinforcing plates (L_s and W_s) should be used in place of the nominal pad dimensions (L and W) because the side cover layer of rubber does not contribute significantly to the axial resistance of the pad. However, the stiffnesses of the top and bottom cover layers should be included in the final calculation of k_{axial}.

Like many empirical expressions for layer axial stiffness available in the literature, such as that provided by Gent (2001), the method suggested by Stanton calculates an effective compression modulus, E_c, (Equation 6.1) in terms of the dimensionless *shape factor* (S) which can be calculated for a layer with thickness, t, as follows:

$$S = \frac{L_s W_s}{2t\left(L_s + W_s\right)} \tag{6.9}$$

The effective compression modulus E_c can be interpreted as the hypothetical elastic modulus that would be required for an equivalent unreinforced elastomeric layer (with the same dimensions as the reinforced layer) to exhibit the same axial stiffness as the reinforced layer when loaded in pure compression. By definition, the axial stiffness of the layer is:

$$k_{layer} = \frac{A}{t}E_c = \frac{L_s W_s}{t}E\left(1 + B_a S^2\right) \tag{6.10}$$

where B_a is a fitting parameter. This can also be expressed in terms of the shear modulus (G) as:

$$k_{layer} = \frac{L_s W_s}{t}3G\left(1 + B_a S^2\right) \tag{6.11}$$

due to the near-incompressibility of the elastomer.

Stanton's refinement of this approach involved the development of a method by which B_a is selected. B_a is shown to depend, in part, on the *bulk compressibility* of the elastomer layer, as measured by the *compressibility index*, λ, defined as:

$$\lambda = S\sqrt{\frac{3G}{K}} \tag{6.12}$$

and Stanton develops an empirical equation for B_a in terms of λ and the layer dimensions, as follows:

$$B_a = (2.31 - 1.86\lambda) + (-0.90 + 0.96\lambda)\left(1 - \min\left(\frac{L_s}{W_s}, \frac{W_s}{L_s}\right)\right)^2 \qquad (6.13)$$

Using Equations 6.11, 6.12, and 6.13, k_{layer} can be computed for every elastomer layer in the pad, and the total axial stiffness can be computed as:

$$k_{axial} = \left(\sum \frac{1}{k_{layer}}\right)^{-1} \qquad (6.14)$$

In most cases, only two unique values of k_{layer} will need to be computed: one for the internal elastomer layers and one for the top and bottom cover layers (which typically differ in thickness from the internal layers and therefore have a different value of S). Note that in this scenario, separate values of B_a must be calculated for each layer group because λ is a function of S. In general, B_a must be recalculated for any change in layer dimensions (including thickness) or elastomeric material properties.

6.7.2 Basic derivation of instantaneous roll stiffness of a continuous grillage

The following derivations employ a principal coordinate system (x,y) in which the y-axis coincides with the girder centerline (i.e., the longitudinal axis of the girder). In these coordinates, the pad (and, therefore, the grillage) extends $\pm0.5W$ in the x-direction and $\pm0.5L$ in the y-direction (Figure 6.15). All derivations will assume that roll occurs about the y-axis (corresponding to overturning roll). Stiffness of roll about the x-axis (i.e., bending roll) can then be obtained from symmetry by simply transposing the values of W and L.
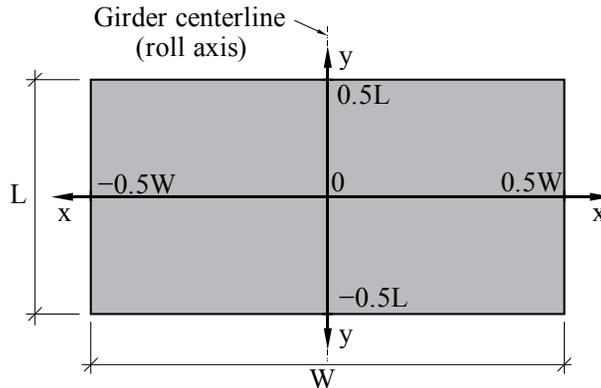
Figure 6.15 Coordinate system of continuous grillage (plan view)

Instantaneous roll stiffness of a continuous grillage is determined by imposing a differential angular displacement in the direction of roll $(d\theta)$ and computing the total restoring moment (dM) generated by the resulting spring forces. Recall from Figure 6.11 that the stiffness of each spring varies depending on its location within the grillage according to a scaled bubble function expressed in normalized coordinates. In principal coordinates, the stiffness at every point (x,y), is:

$$k_{spring}(x,y) = dA\left(\frac{k_{axial}}{A_{pad}}\right)\left(1-\left(\frac{x}{0.5W}\right)^2\right)\left(1-\left(\frac{y}{0.5L}\right)^2\right)$$ (6.15)

When a differential roll angle ($d\theta$) is imposed about the y-axis, an axial displacement field is produced, so that every spring displaces a vertical distance of:

$$\Delta z(x,y) = xd\theta$$ (6.16)

depending on its distance from the roll axis. At every point (x,y), the total axial restoring force is therefore the product of $k_{spring}(x,y)$ and $\Delta z(x,y)$. Because each spring has a moment arm of x (the distance from the y-axis), the total restoring moment exerted by the deformed grillage of springs can be computed with the following integral:

$$dM = \int_A x\left[\Delta z(x,y)\right]\left[k_{spring}(x,y)\right]$$ (6.17)
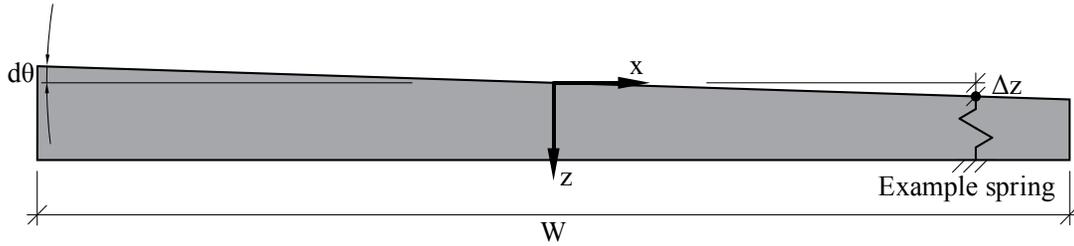
Figure 6.16 Continuous grillage with imposed differential angle
(Example spring shown, all others omitted for clarity)

Substituting Equations 6.15 and 6.16 into Equation 6.17, rewriting A_{pad} as the product LW, and dividing through by $d\theta$ results in an integral expression for the instantaneous roll stiffness of the grillage:

$$\frac{dM}{d\theta} = k_{roll} = \int_A x^2\left[\left(\frac{k_{axial}}{LW}\right)\left(1-\left(\frac{x}{0.5W}\right)^2\right)\left(1-\left(\frac{y}{0.5L}\right)^2\right)\right]dA$$ (6.18)

in terms of L, W, k_{axial}, and the coordinate variables x and y. To evaluate the surface integral in closed-form, it is necessary to reformulate it as a double integral in x and y, evaluated over the plan-view dimensions of the pad:

$$k_{roll} = \frac{k_{axial}}{LW}\int_{-0.5L}^{0.5L}\int_{-0.5W}^{0.5W} x^2\left(1-\left(\frac{x}{0.5W}\right)^2\right)\left(1-\left(\frac{y}{0.5L}\right)^2\right)dxdy$$ (6.19)

which reduces to a simple closed-form expression:

$$k_{roll} = \frac{k_{axial}W^2}{45}$$ (6.20)

in terms of only the total axial stiffness of the pad (k_{axial}) and the width of the pad in the direction perpendicular to the roll axis (W).

6.7.3 Incorporating girder slope

By integrating over the entire plan-view area of the bearing pad (i.e., the grillage), the preceding derivation assumes that the entire surface of the pad is in contact with the girder. This assumption may not hold if there is a non-zero slope angle (ϕ), as the total axial load exerted on the pad by the girder may not be sufficient to compress the pad far enough to achieve full contact (recall Figure 6.13). Such a condition reduces the effective area of the pad that contributes to roll stiffness. This phenomenon can be accounted for in the calculation by altering the limits of integration to include only the region of the bearing pad grillage that is in initial contact with the girder, as follows:

$$k_{roll} = \frac{k_{axial}}{LW} \int_{-0.5L}^{-0.5L+pL} \int_{-0.5W}^{0.5W} x^2 \left(1 - \left(\frac{x}{0.5W}\right)^2\right)\left(1 - \left(\frac{y}{0.5L}\right)^2\right) dxdy \qquad (6.21)$$

where p is the proportion of the pad area that is in contact ($0 \le p \le 1$). Closed-form evaluation of the modified integral produces the expression:

$$k_{roll} = p^2 (3 - 2p) \frac{k_{axial}W^2}{45} \qquad (6.22)$$

which reduces to Equation 6.20 when $p = 1$.

For a given configuration, the value of p depends on the total distance that the grillage is initially compressed, which is a function of both ϕ and the initial axial load resulting from girder self-weight (F_{axial}). When F_{axial} is applied, the sloped upper surface of the grillage deforms downward (increasing the contact area) until the total restoring force in the compressed springs achieves equilibrium with F_{axial}. From statics, the force equilibrium equation for the continuous grillage is:

$$F_{axial} = \int_{A} \left[\Delta z(x,y)\right]\left[k_{spring}(x,y)\right] dA \qquad (6.23)$$

where $\Delta z(x,y)$ is the displacement field imposed on the bearing pad grillage by the sloped surface of the girder. Slope-induced displacements, $\Delta z(x,y)$, do not vary in the x-direction, and can therefore be expressed as a line in the y-z plane, with slope ϕ and y-intercept p, as follows:

$$\Delta z(x,y) = \phi\left[y - (-0.5L + pL)\right] \qquad (6.24)$$

where ($-0.5L + pL$) is the y-coordinate of p in principal coordinates. Substituting Equations 6.24 and 6.15 into Equation 6.23 and reformulating it as a double integral (which must also include p in the limits of integration), results in the following equation:

$$F_{axial} = \phi \frac{k_{axial}}{LW} \int_{-0.5L}^{-0.5L+pL} \int_{-0.5W}^{0.5W} \left[y - (-0.5L + pL)\right]\left(1 - \left(\frac{x}{0.5W}\right)^2\right)\left(1 - \left(\frac{y}{0.5L}\right)^2\right) dxdy \qquad (6.25)$$

$$F_{axial} = \frac{2}{9} L\phi k_{axial} p^3 (2-p) \qquad (6.26)$$

in which p is the only unknown. Rearranging the terms of Equation 6.26 yields:

$$p^4 - 2p^3 + \eta = 0 \quad \text{where} \quad \eta = \frac{9F_{axial}}{2L\phi k_{axial}} \qquad (6.27)$$

revealing p to be the root of a quartic equation.

For polynomials of degree < 5, general solutions for the roots can be expressed as closed-form equations in terms of the polynomial coefficients. In the case of Equation 6.27, there are four roots and four corresponding equations (omitted here for brevity). Recall that the quantity p is only meaningful over the interval $0 \leq p \leq 1$, and note that if $p = 0$, η must also be 0; if $p = 1$, η must also be 1; and within that interval, η increases monotonically with p. Consequently, solutions for p need only be defined over the interval, $0 \leq \eta \leq 1$. Upon substituting the polynomial coefficients from Equation 6.27 (quartic in p: 1; cubic in p: −2; quadratic in p: 0; linear in p: 0; and constant: η) into the four root equations, the only one that results in a positive real root within the intended range for $0 \leq \eta \leq 1$ reduces to:

$$p(\eta) = \frac{1}{2} + B - \frac{\sqrt{B + 3B^2 - 4B^4}}{2B}$$

$$\text{where} \quad B = \sqrt{\frac{A}{2} + \frac{\eta}{6A} + \frac{1}{4}} \quad \text{and} \quad A = \sqrt[3]{\frac{\eta}{4} + \sqrt{\left(\frac{\eta}{4}\right)^2 - \left(\frac{\eta}{3}\right)^3}} \qquad (6.28)$$

Equation 6.28, which is exact but somewhat cumbersome, can be closely and conservatively approximated as the much simpler $\sqrt{\eta}$ (Figure 6.17). In practice, given the empirical approximations introduced by the grillage representation of a bearing pad and the inherent variability in pad construction and behavior, the error introduced by using $\sqrt{\eta}$ in place of Equation 6.28 is insignificant. Substituting in the definition of η from Equation 6.27, the final expression for the approximate instantaneous overturning roll stiffness of a rectangular bearing pad is:

$$k_{roll,overturning} = p^2 (3-2p) \frac{k_{axial} W^2}{45} \quad \text{where} \quad p = \begin{cases} 1.0 & \text{if } \phi = 0 \\ \sqrt{\dfrac{9F_{axial}}{2L\phi k_{axial}}} \leq 1.0 & \text{if } \phi > 0 \end{cases} \qquad (6.29)$$

where k_{axial} is the total axial stiffness of the pad, F_{axial} is the initial axial load (i.e., the reaction on the pad due to girder weight), ϕ is the girder slope angle, and W and L are the plan-view dimensions of the pad (perpendicular to and parallel to the girder axis, respectively). An analogous expression for the bending roll stiffness can be obtained by transposing the pad dimensions W and L in the equation above, and recognizing that no slope angle is present in bending roll (i.e., $\phi = 0$). These changes lead to:

$$k_{roll,bending} = \frac{k_{axial}L^2}{45} \qquad (6.30)$$

where L is the plan-view dimension of the pad parallel to the girder axis. Example calculations, demonstrating the use of these methods compute bearing pad stiffnesses in all deformation modes, are presented in Appendix G.
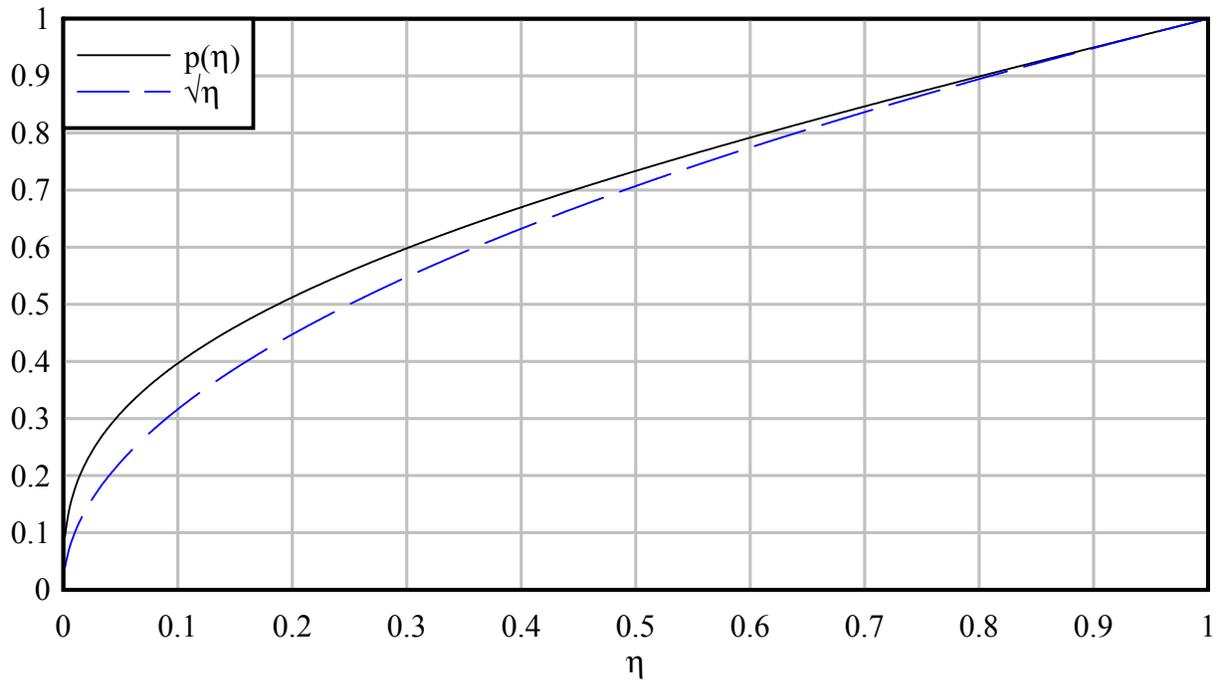
Figure 6.17 Comparison between Equation 6.28 and the square root approximation

CHAPTER 7
MODEL DEVELOPMENT

7.1 Introduction

In addition to proposing design wind loading drag coefficients, a secondary goal of this research was to investigate temporary bracing requirements for Florida-I Beams (FIBs) subjected to wind loads. To that end, finite element models (Figure 7.1) were developed for evaluating the lateral stability of braced systems of FIBs, using the ADINA finite element code. The models incorporated bearing pad support stiffnesses (as discussed in the previous chapter), and were capable of capturing system-level buckling behavior of braced FIBs, while remaining computationally efficient enough that thousands of parametric analyses could be performed. In the global coordinate system of the models, X corresponded to the transverse direction, Y to the longitudinal direction, and Z to the vertical direction. A local girder coordinate system (u,v,w) was also used corresponding to the same directions, with the origin at one end of the girder at the centroid of the cross-section.

Buckling capacities were determined using large-displacement analyses, in which static loads were applied to the models in incremental steps, taking into account the deformed state of the structure at each step. Instability was initiated by the presence of girder fabrication imperfections (i.e., sweep) in the models, so that every load step caused the models to deform further in the direction of the final buckled shape. By tracking the displacement history at each step, it was possible, using a modified version of a method originally proposed by Southwell (1932), to determine when the displacements began to grow asymptotically, indicating a collapse.
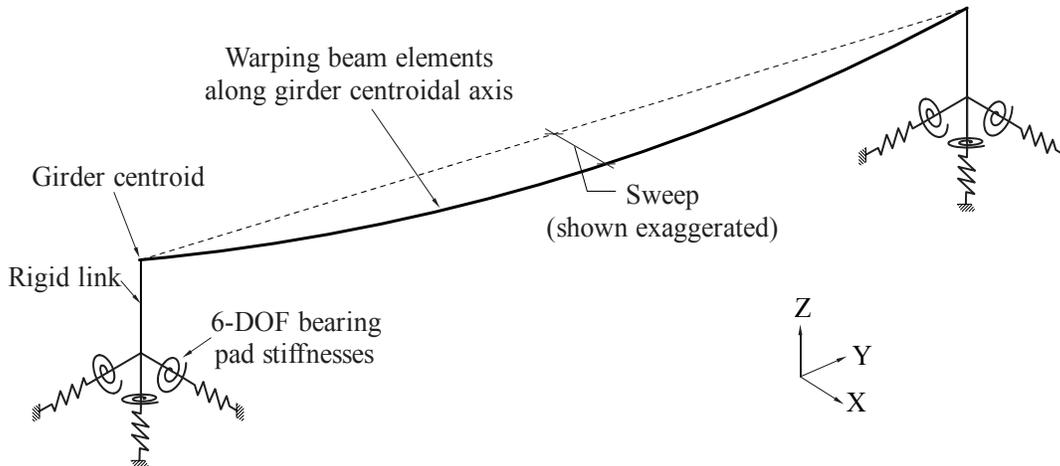
Figure 7.1 Finite element model of a single FIB (isometric view)

7.2 Modeling of bridge girders

Bridge girders were modeled using *warping beams*, an advanced beam element formulation provided by ADINA that possesses a 7th degree of freedom in each end node, representing the torsionally-induced out-of-plane warping of the cross-section (ADINA, 2012). Warping beams are primarily intended for modeling thin-walled sections for which warping effects can significantly affect structural response, but they also have several additional

refinements that make them superior to standard Hermitian beam elements in buckling applications. For example, offsets between the shear center and the centroid of asymmetric cross-sections are accounted for automatically, and the kinematic formulation of the element includes coupling between bending and torsional deformation modes.

Warping beam cross-sections require the calculation of a comprehensive set of cross-sectional properties, several of which require knowledge of the *warping function*, which cannot be calculated in closed-form and must be solved for numerically. Details relating to the section properties that were calculated in this study for the FIB cross-sectional shapes are provided in Appendix C. Material properties assumed for the prestressed concrete FIBs were $f_c' = 6.5$ ksi, unit weight = 150 pcf, and Poisson's ratio = 0.2. Using these values and the PCI Design Handbook (PCI, 2010), the concrete elastic modulus was computed to be E = 4887 ksi.

Construction tolerances for FIBs are specified in the *Standard Specifications for Road and Bridge Construction* (FDOT, 2010), which limits girder sweep to ⅛ in. for every 10 ft of girder length, but not to exceed 1.5 in. To ensure conservative buckling capacity results, all FIBs were modeled with the maximum allowable sweep (u_{max}) for their length. Geometrically, sweep was implemented using a sinusoidal function (Figure 7.2) with the maximum allowable sweep at midspan, so that the lateral deviation, *u*, at every point along the girder length, *v*, was:

$$u(v) = u_{max} \sin\left(\frac{\pi v}{L}\right) \tag{7.1}$$
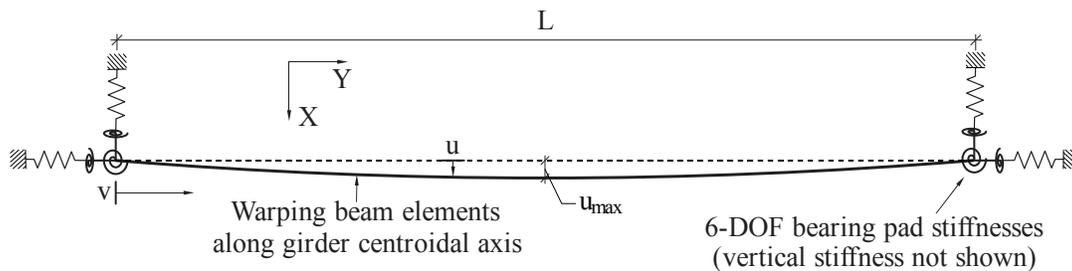
Figure 7.2 Representation of sweep in FIB model (plan view)

During early phases of bridge construction, the bridge deck is not present and hence the weight of the deck is not yet present. Consequently, the girders will have more camber at this stage than they will have in the completed configuration of the bridge (when deck self-weight is active). In this study, it was important to represent the 'deck-free' girder camber in the models, because the additional elevation of the girder center of gravity reduces buckling capacity by a small amount. (recall Figure 2.9). To establish maximum probable girder camber for use in model development, trial beam designs were produced for all eight (8) FIB cross-sections with the goal of maximizing camber. This was accomplished by placing all prestressing tendons as low as possible in the bottom flange and finding the span length at which camber was maximized. For the purposes of these designs, long-term creep effects were ignored and it was assumed that no cracking occurred. From these designs, it was determined that 3.25 in. was a reasonable upper bound for FIB camber during construction.

It is important to recognize that the measured camber of a bridge girder in the field is a superposition of two independent deflections: an upward deflection caused by prestress forces and a downward deflection caused by the self-weight of the girder. The initial (undeformed)

geometry of a finite element model should represent its free-body state, prior to the application of any external loads, including gravity loads. Therefore, it was necessary to add additional camber to the models to offset the expected self-weight deflection. In other words, the geometric camber included in the finite elements models represented *only the upward deflection caused by prestressing* so that after self-weight was applied to the model, the total deflection would match the camber that would be measured in the field. As a result, each girder model was assigned a maximum geometric camber (w_{max}) of:

$$w_{max} = 3.25 \text{ in.} + \frac{5A\gamma L^4}{384EI} \tag{7.2}$$

where A is the girder cross-sectional area, γ is the unit weight of the concrete, L is the span length, E is the elastic modulus, and I is the major-axis moment of inertia.

Because the geometric camber in the models represented upward deflections caused by straight prestressing tendons (which generate a constant internal moment throughout the length of the beam), the girder camber was implemented with a parabolic shape (Figure 7.3) so that the vertical deviation, w, at every point along the girder length, v, was:

$$w(v) = 4w_{max}\left[\left(\frac{v}{L}\right) - \left(\frac{v}{L}\right)^2\right] \tag{7.3}$$
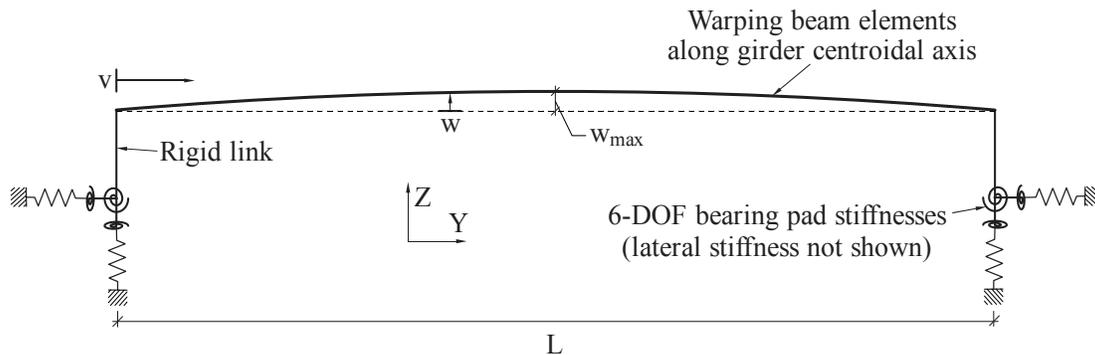
Figure 7.3 Representation of camber in FIB model (elevation view)

7.3 Modeling of end supports

Girder support stiffnesses were modeled with six (6) geometrically linear springs to represent the stiffness of the bearing pad in each degree of freedom, with each spring corresponding to one of the four (4) main deformation modes of the pad: shear, axial, torsion, and roll (Figure 7.4). These stiffnesses were obtained using the calculation methods discussed in Chapter 6. The roll stiffness springs (in both the overturning and bending directions) were assigned nonlinear moment-rotation curves that captured the softening effects of partial girder liftoff from the pad. The remaining pad stiffnesses were treated as linear.

7.3.1 Pad selection

Seven (7) standard types of elastomeric bearing pad are provided in *Design Standard No. 20510: Composite Elastomeric Bearing Pads – Prestressed Florida-I Beams* (FDOT, 2012c) for use with FIBs. During design, selection of the type of pad that will be used in a particular bridge is based on thermal expansion and live load deflection limit states of the completed bridge, neither of which can be predicted based solely on girder dimensions (cross-sectional and span length). As such, it is not appropriate to assume that for each FIB type, there is a specific corresponding type of bearing pad that would be utilized. Hence, in this study, it was conservatively assumed that the pad type with the lowest roll stiffness (which will produce the lowest buckling capacity) would be used in conjunction with all FIB types. After calculating the roll stiffness of every standard FDOT FIB pad type (see Appendix D for details), using the grillage method that was discussed in Chapter 6, the Type J bearing pad was selected for use in this study.
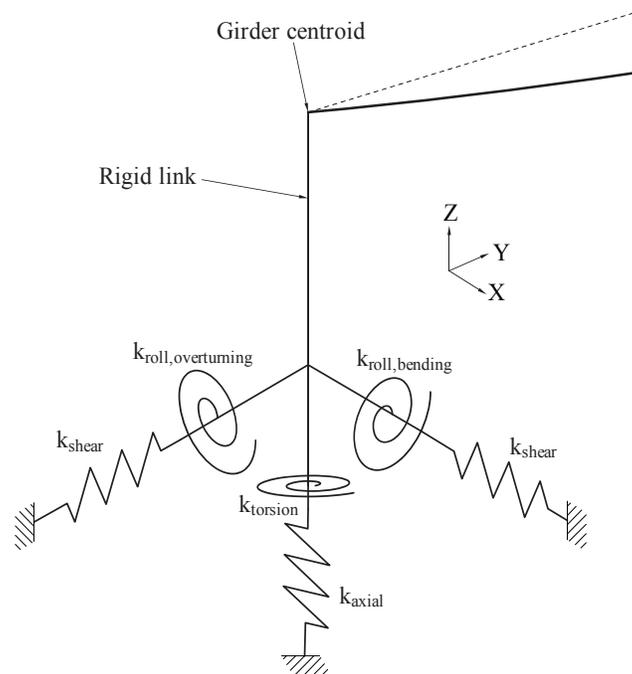
Figure 7.4 Bearing pad stiffness springs in FIB model (isometric view)

7.3.2 Axial load selection

In Chapter 6, it was noted that the amount of axial load applied to a pad does not change the initial linear portion of the roll stiffness curve, but it does affect the moment required to initiate girder roll-off from the pad. Reducing the compressive axial load on a pad reduces the moment that is required to cause girder roll-off. Additionally, reducing girder span length reduces girder self-weight which, in turn, reduces the axial loads on the bearing pads. Therefore, to be conservative in this study, the minimum length ranges for each FIB shape were determined from design aids in *Instructions for Design Standard No. 20010: Prestressed Florida-I Beams* (IDS 20010; FDOT, 2012b) and the minimum expected axial pad load was calculated for each FIB shape. (These calculations assumed that the girders were simply supported. Additionally, the

effects of wind uplift forces were conservatively ignored.) Using this process, a single worst-case (minimized) roll stiffness curve was calculated for each type of FIB, resulting in a total of seven (7) bearing pad moment-rotation curves.

7.3.3 Girder slope selection

In Chapter 6, it was also noted that overturning roll stiffness is reduced by the presence of girder slope, which can arise from a combination of girder camber and bridge grade. According to *Instructions for Design Standard No. 20510: Composite Elastomeric Bearing Pads – Prestressed Florida-I Beams* (IDS 20510; FDOT, 2012d), the maximum expected slope angle in the *completed bridge* is 0.0125 rad, because if this angle is exceeded, beveled bearing plates must be installed to eliminate slope. Therefore, the maximum expected camber *prior to the casting of the deck* is the sum of 0.0125 rad and any camber-induced slope that is negated by the downward deflection under the weight of the deck and other superimposed dead loads (SDL). After a series of trial beam design calculations was performed, it was determined that a reasonable upper limit for the SDL-negated slope was 0.01 rad. Additionally, AASHTO LRFD (2010) recommends an "allowance for uncertainties" of 0.005 rad with regard to bearing pad slope angle. The maximum completed slope of 0.0125 rad, the SDL-negated slope of 0.01 rad, and the slope uncertainty of 0.005 rad combined for a total maximum slope angle of 0.0275 rad. This was conservatively rounded up to a slope angle of 0.03 rad, which was used to compute the bearing pad overturning roll stiffness curves.

7.4 Modeling of braces and anchors

Because the design of bracing has historically been left to the discretion of the contractor, a wide variety of bracing configurations are used in practice. Consequently, in this study, it was not possible for every potential brace configuration to be represented in the parametric studies. After conducting a survey of bracing designs used in the construction of bridges throughout Florida, four (4) representative brace configurations were identified:

- Top strut (Figure 7.5a): a horizontal timber compression strut situated between the edges of the top flanges. The top strut is typically nailed to the underside of a slightly longer timber member, creating 'lips' that rest on the top of the flanges.

- Parallel strut (Figure 7.5b): Two (or more) horizontal timber compression struts wedged in place between the girder webs.

- X-brace (Figure 7.5c): Two diagonal timber members wedged between the webs that cross in the middle to form an 'X' shape. A steel bolt typically passes through both members at the crossing point to create a hinge.

- K-brace (Figure 7.5d): Steel members (typically steel angles) welded together into a 'K'-shaped frame and welded or bolted to steel plates cast into the webs.

The majority of brace designs that were encountered were variations of one of these four basic configurations.

For analysis purposes, braces were modeled primarily with beam elements, with each brace member represented by a single element. At the girder connection points, rigid links were used to connect the braces to the girder elements (i.e., warping beams located at the girder centroids). It was assumed that the brace–girder connections were ideal pins, which was

conservative with regard to girder stability. Pins and hinges were modeled with beam end-releases and nodal constraints, respectively.

During the survey of bracing designs, the vast majority of timber braces that were encountered were composed of 4x4 Southern Pine sawn lumber. According to the *National Design Specification for Wood Construction* (AF&PA, 2005), 4x4 Southern Pine has a 3.5″ x 3.5″ square cross-section and an elastic modulus of E = 495 ksi (based on an E_{min} of 550 ksi for 4-inch-wide "Construction-grade" lumber and a Wet Service Factor of 0.9). These properties were used to model all timber brace members including the top strut, parallel strut, and X-brace. Based on a typical bridge bracing design that was acquired during the survey, K-brace members were modeled as 4″ x 4″ x ⅜″ steel angles, with an elastic modulus of E = 29000 ksi.
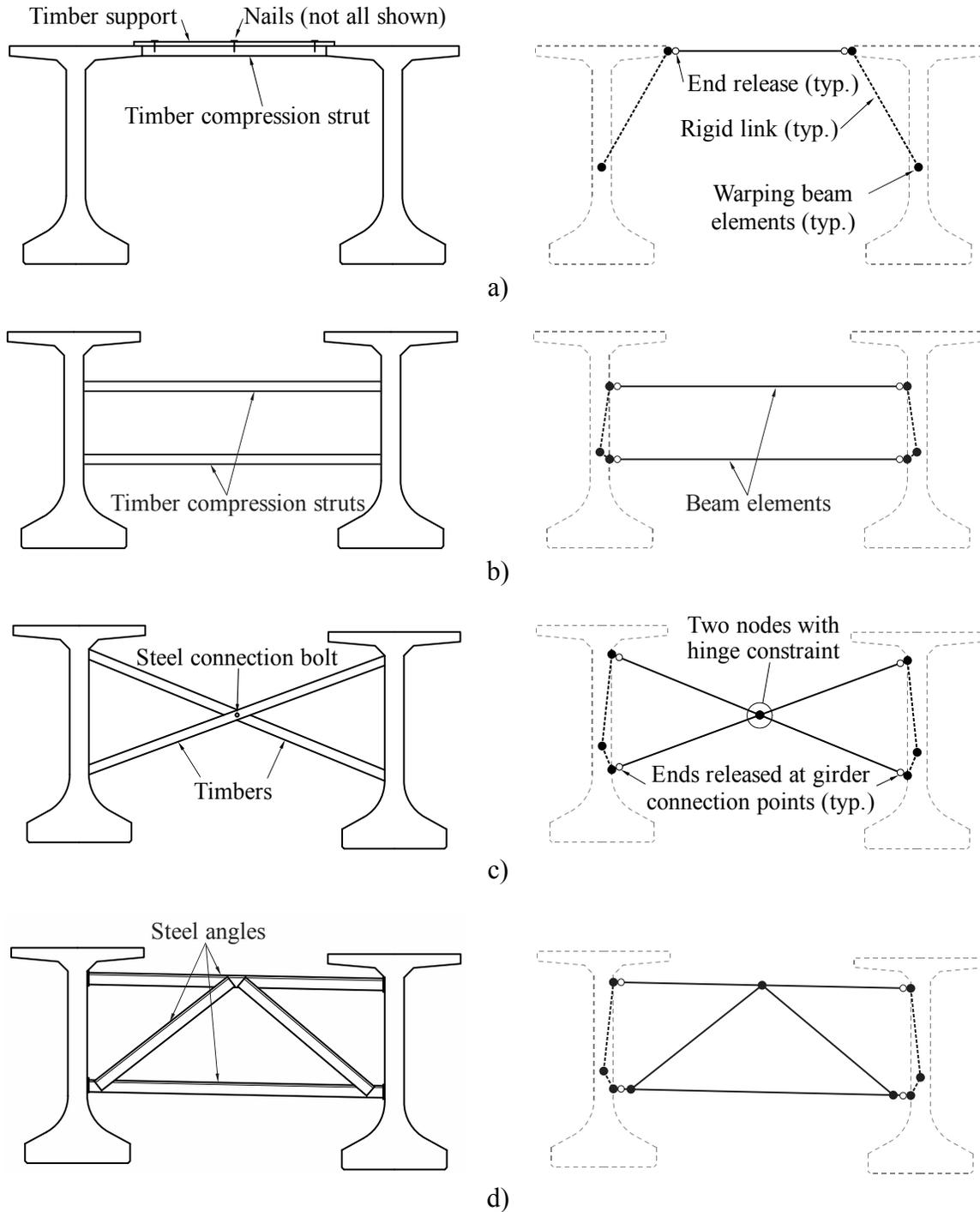
Figure 7.5 Representation of brace configurations in FIB system models:
a) Top strut brace; b) Parallel strut brace; c) X-brace; d) K-brace

In contrast to braces, girder anchors were not modeled with structural elements. Instead, the additional roll stiffness provided by the anchors ($k_{roll,anchor}$) was quantified directly and added to the bearing pad support stiffness ($k_{roll,overturning}$). It was assumed that only one FIB in

each bridge cross-section was anchored and that anchors at each end of the girder were of equal stiffness.

Anchor roll stiffness is a function of the axial stiffness of the anchor (k_{anchor}), the radial distance from the center of rotation to the anchor connection point (R), and the angle between the anchor member and the tangential force exerted by the girder (θ) (Figure 7.6), and can be calculated as follows:

$$k_{roll,anchor} = k_{anchor} \left(\cos(\theta)\right)^2 R^2$$ (7.4)

It is important to note that θ may become a three-dimensional angle if the anchor is inclined longitudinally (away from the girder ends) with the result that the roll stiffness provided by the anchor may be reduced. In the presence of girder skew, this practice can also cause paired tension-only anchors (i.e., chains or cables) to be of different lengths (Figure 7.7), in which case the average length is used to compute k_{anchor}.
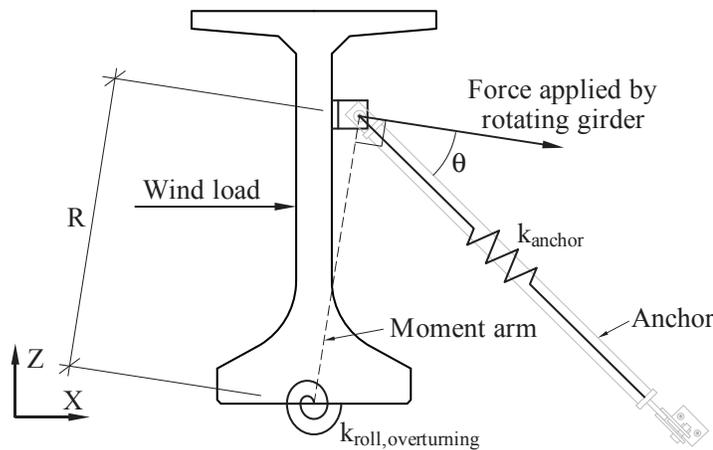
Figure 7.6 Calculation of rotational stiffness of anchor
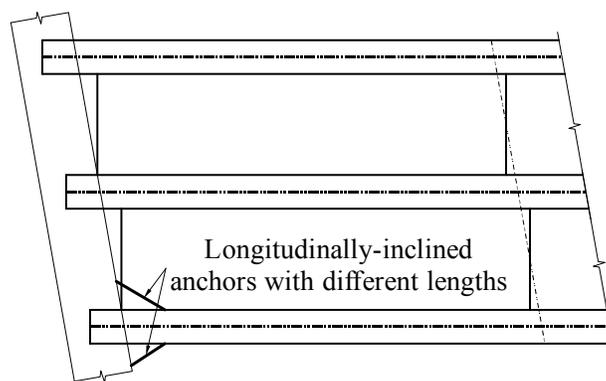
Figure 7.7 Longitudinally-inclined anchors on skewed bridges.

7.5 Loads

Two types of structural load were included in the models: wind loads and gravity load. Lateral wind loads were calculated for each girder in the system using the design drag coefficients proposed earlier for FIBs (recall Figure 5.18) and were applied to the girder elements as tributary nodal loads (Figure 7.8a). Small overturning moments were also applied at each node to compensate for the eccentricity between the centroid of the cross-section (where the nodes and elements were located) and the center of pressure (where the lateral load was assumed to act on the girder) (Figure 7.8b). Wind loads were always applied in the direction of increasing girder sweep.
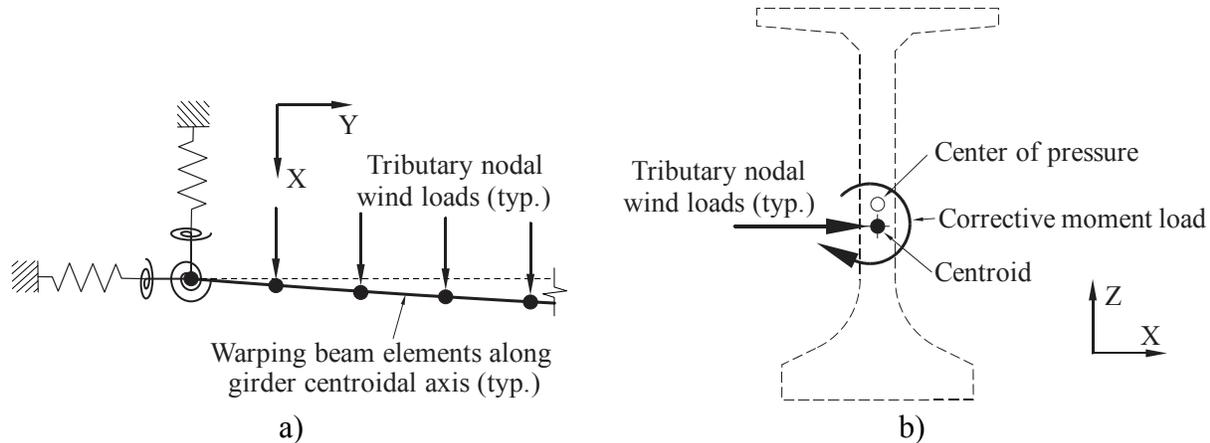
Figure 7.8 Representation of wind load in structural models:
a) Lateral nodal loads (top view); b) Overturning moments (section view)

Gravity was applied as a vertical 'acceleration' load (mass-proportional body force) in units of g, the acceleration due to gravity, so that a load of 1 g represented the self-weight of the model. In field conditions, girders are always subjected to a constant gravity load of 1 g. In the structural models analyzed in this study, however, gravity loading was used to initiate instability. After wind loads were applied, gravity load was linearly ramped up—beyond 1 g if possible—until girder instability occurred. Subsequently, the capacity of the system was expressed as a gravity load (in g), which can also be thought of as capacity-to-demand ratio. For example, if the system became unstable at a gravity load of 1.5 g, then the ratio of capacity (1.5 g) to demand (1 g) would 1.5.

7.6 Modified Southwell buckling analysis

To assess system stability from the results of the large-displacement analyses, it was necessary to define the *system capacity* in terms of displacement–load results data. In typical buckling problems, as the displacements increase, the applied load approaches an asymptote called the *critical buckling load* (where the displacements are considered to be infinite). In this study, the location of the asymptote was determined using a method originally proposed by Southwell (1932) for use with axially-loaded columns.

Southwell was able to demonstrate mathematically (using the governing differential equation of an axially-loaded column with a non-zero sweep) that that expected shape of the

displacement–load curve (using the lateral displacement of the beam at midspan) is a rectangular hyperbola (Figure 7.9a) of the form:

$$y = \frac{\beta x}{x + \alpha} \tag{7.5}$$

where β is the horizontal asymptote (and therefore the critical buckling load). The value of β can be determined using a *Southwell Plot* (Figure 7.9b), in which the midspan displacement (*x*) is plotted as a function of the ratio of displacement to load (*x/y*). By rearranging Equation 7.5, it becomes evident that the resulting relationship is linear:

$$\left(\frac{x}{y} \right) = \frac{1}{\beta} x + \frac{\alpha}{\beta} \tag{7.6}$$

with the critical buckling load being equal to the inverse slope of the line (Figure 7.9b). The critical buckling load can therefore be determined by applying linear least-squares regression to the transformed analysis results (i.e., pairs of x and $^x/_y$ values). Using this technique, reliable determination of the critical load can be obtained from displacement–load data, even if only a portion of the overall displacement–load plot is available. (This aspect of the method is particularly useful for physical testing, as specimens do not need to be loaded all the way to failure in order for the buckling capacity to be quantified.)

Theoretically, the mathematical foundation for the Southwell method is only valid for axial column buckling. For this reason, several authors (Massey, 1963; Trahair, 1969; Meck, 1977) have published alternative methods mathematically formulated for lateral stability problems (based on the governing differential equation for lateral-torsional buckling of a beam). However, despite these developments, studies involving experimental test programs have frequently demonstrated that the Southwell method works well for lateral-torsional buckling (Mandal and Calladine, 2002), and at least one survey of the different methods on the same set of experimental data (Kalkan, 2010), found the Southwell method to be superior to the supposedly more refined alternatives. Mandal and Calladine (2002) have published a discussion of this apparent contradiction which provides a mathematical explanation for why the Southwell method produces excellent results even in lateral-torsional buckling applications.

The large-displacement structural analyses performed in this study did not exhibit pure lateral-torsional buckling, but included several additional components (e.g., flexible bearing-pad support conditions, lateral wind loads) that significantly complicate the governing differential equations. Consequently, there was no mathematical justification for using any particular method. However, when the methods (those of Southwell, Massey, Trahair, and Meck) were evaluated using displacement–load data from the structural analyses, it was found that the Southwell method produced excellent results, while the alternative methods produced unusable results. This was attributed to the fact that the alternative methods were more dependent upon the underlying assumptions (e.g., pinned but torsionally rigid beam support conditions) and were less tolerant of small deviations from the ideal shape of the displacement–load curve. It was concluded that the Southwell method for determining critical buckling load was an acceptable choice for any stability problem exhibiting asymptotic behavior because fitting a hyperbola to the data is a robust way of approximating the location of the asymptote, even if the data are not strictly hyperbolic (Figure 7.10). As a result, in this study, the Southwell method was used to determine the critical buckling loads from lateral girder displacement data computed at midspan.

For models with multiple girders, a Southwell analysis was performed on displacement data for each girder, and the smallest resulting buckling load was used.
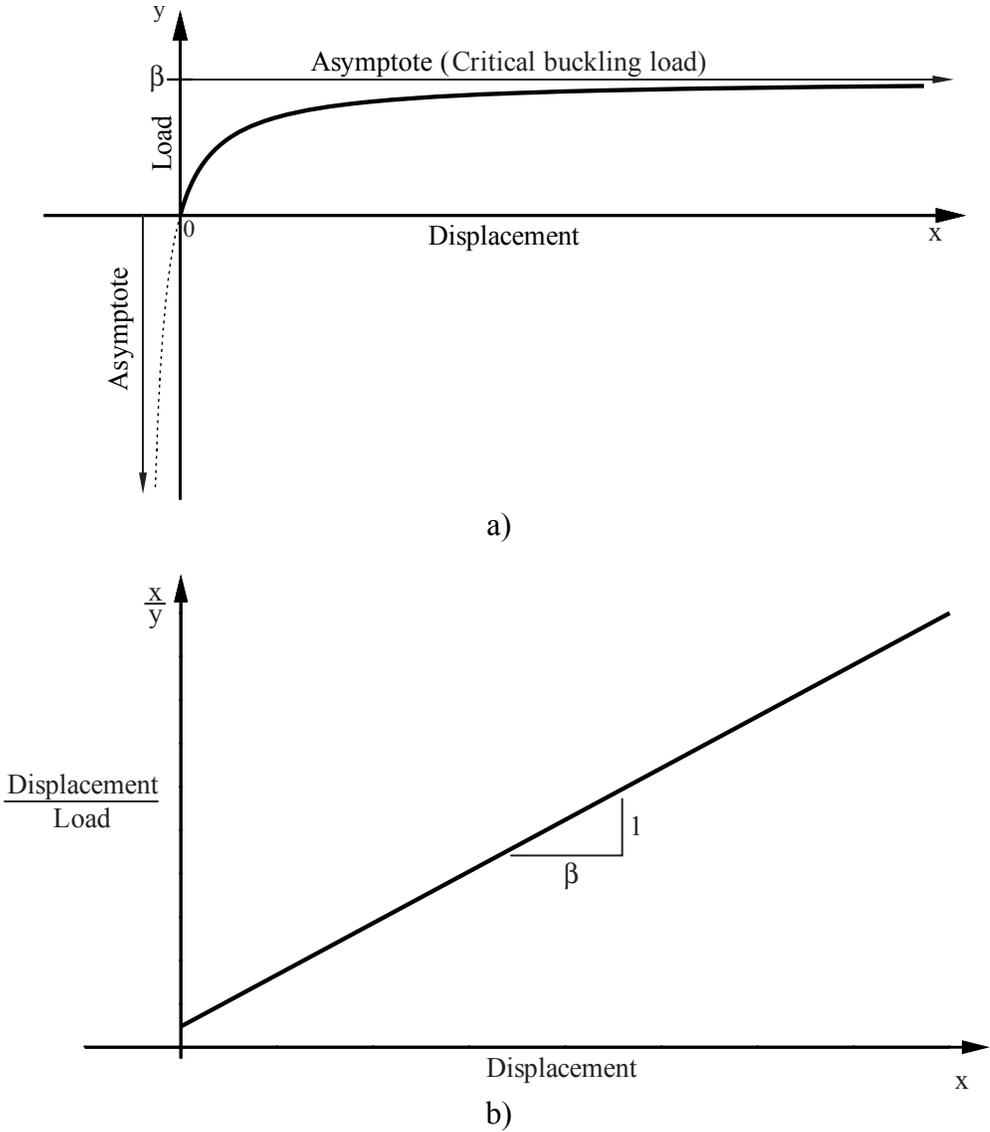
Figure 7.9 Southwell method for determining critical buckling load (β):
a) Displacement–load curve (rectangular hyperbola); b) Southwell plot
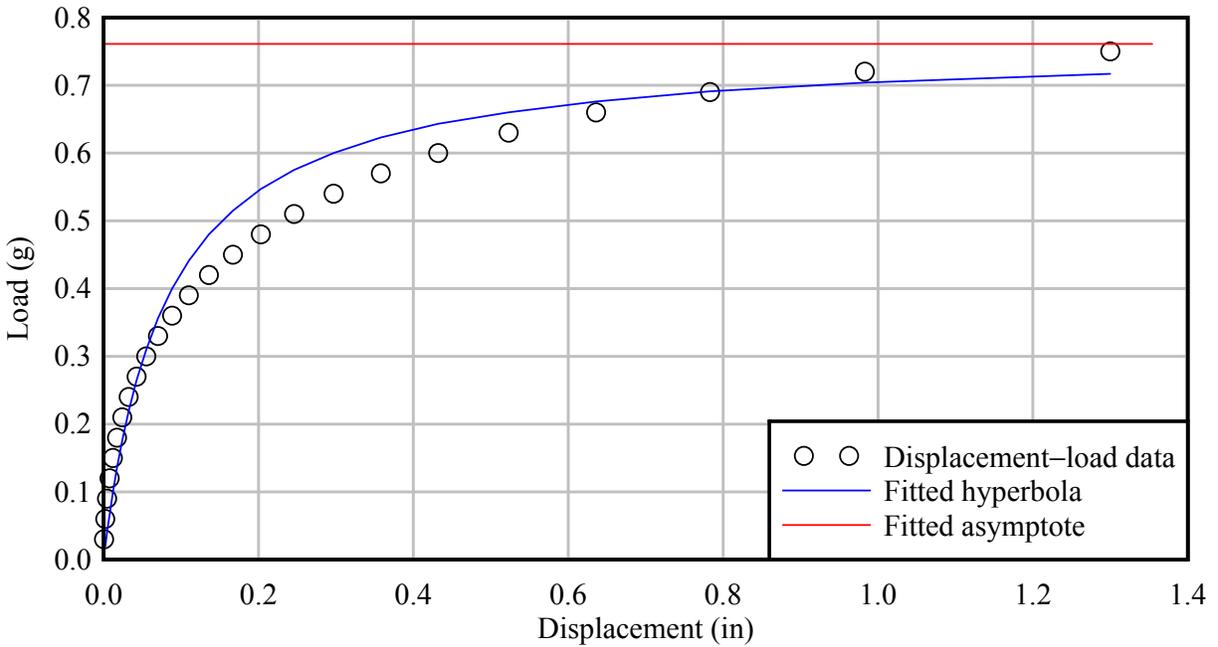
Figure 7.10 Southwell analysis of non-hyperbolic displacement–load data
obtained from a large-displacement structural analysis

In a physical bridge system, girders are not capable of sustaining arbitrarily high levels of lateral displacement, as is implied by using the critical buckling load (the asymptote) as the definition of system capacity. Therefore, a modified version of the Southwell method, developed for use in a previous study (BDK75 977-03, Consolazio et al., 2012) and referred to as the "10% rule", was used instead. In the modified method, system capacity is defined as the point on the load versus midspan displacement curve (Figure 7.11) at which the tangent slope of the fitted hyperbola drops below 10% of the initial slope (at the origin). It can be demonstrated that this procedure is mathematically equivalent to multiplying the value of the asymptotically-quantified critical buckling load by a scale factor of 0.684.
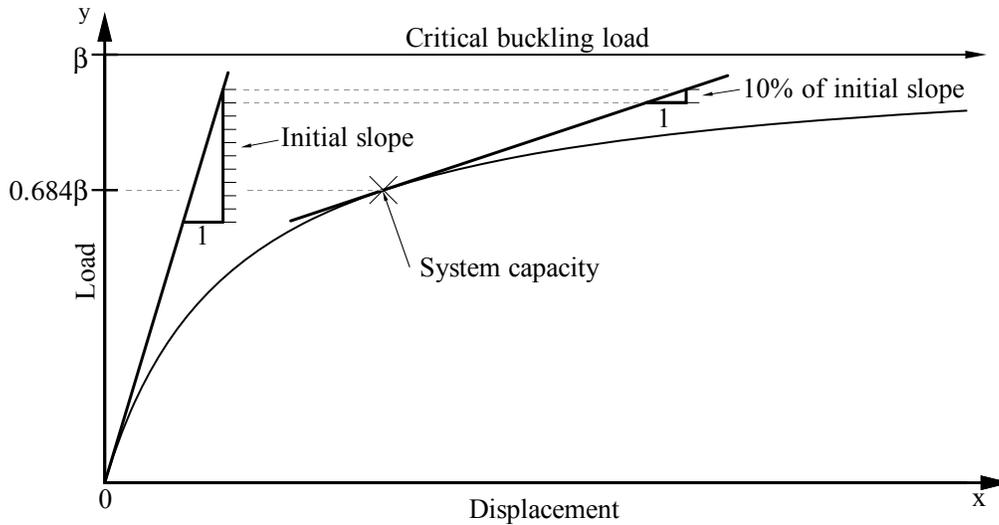
Figure 7.11 Determination of buckling capacity using modified Southwell approach
(Adapted from Consolazio et al. 2012)

Hence, the complete procedure used in the present study for quantifying system capacity was as follows:

- Wind loads (if any) were applied to the model.

- Gravity load was linearly and incrementally increased until the model failed to converge (i.e., until a system instability occurred).

- Displacement vs. load curves were produced for each girder in the system, using the lateral displacement of the girders at midspan.

- Southwell analyses were performed to locate the asymptotes (critical buckling loads) of the displacement–load curves.

- The minimum critical buckling load from among all girders in the model was selected and multiplied by 0.684 (to apply the 10% rule) to calculate the system capacity.

CHAPTER 8
PARAMETRIC STUDY OF INDIVIDUAL BRIDGE GIRDERS

8.1 Introduction

During the bridge construction process, the stage at which wind loading is often most critical is when the first girder is erected. At this stage there are no other girders to brace against, hence the initial girder cannot be braced at interior points, and can only be anchored to the pier at the ends. For bridge designs in which girder stability is a primary concern, girder erection can sometimes be scheduled to minimize the exposure period for the initial girder, so that it is statistically unlikely that peak wind forces will occur. However, meeting such a schedule is not always feasible. For example, strong afternoon thunderstorms can form rapidly in Florida during the summer months. In such situations, it is important to be able to assess, in advance, whether anchor bracing will be needed to prevent girder collapse under the effects of thunderstorm-force winds.

To investigate this scenario, a parametric study was performed, using finite element models of single Florida-I Beams (FIBs) over a range of span lengths, both with and without anchor bracing in place. For each model, the system capacity was evaluated several times at different wind pressures, iterating until the capacity was within 1% of 1 g (i.e., the capacity-to-demand ratio was approximately unity). For each such case, the resulting wind pressure was termed the *wind capacity* of that girder, representing the maximum wind load that can be sustained by the girder without collapsing. Using the results of the parametric study, equations were developed for predicting the wind capacity of a single FIB.

8.2 Selection of parameters

The girder parameters that were varied in the parametric study were as follows:

- FIB cross-section depth (in)

- Span length (ft)

- Rotational stiffness of anchor bracing (kip-ft/rad)

All eight (8) standard FIB cross-sections were included in the study, with depths ranging from 36 in. to 96 in. For each FIB, wind capacity analyses were performed for every combination of span length and anchor stiffness, sampled from the values listed in Table 8.1. Bridge grade was also considered as a potential parameter, but was rejected after preliminary analyses showed that it had a negligible effect on wind capacity. Therefore, all analyses were performed on girder models with a level (0%) grade.

Table 8.1 Parameter values used in parametric study for each FIB cross-section

Span length, *L* (ft)

36″ FIB	45″ FIB	54″ FIB	63″ FIB	72″ FIB	78″ FIB	84″ FIB	96″ FIB
75	95	110	120	135	145	155	170
80	100	115	125	140	150	160	175
85	105	120	130	145	155	165	180
90	110	125	135	150	160	170	185
95	115	130	140	155	165	175	190
100	120	135	145	160	170	180	195
105	125	140	150	165	175	185	200
110	130	145	155	170	180	190	205
-	-	-	160	175	185	195	210
-	-	-	-	180	-	-	215

Anchor rotational stiffness, $k_{roll,anchor}$ (kip-ft/rad)

36″ FIB	45″ FIB	54″ FIB	63″ FIB	72″ FIB	78″ FIB	84″ FIB	96″ FIB
0	0	0	0	0	0	0	0
15	30	50	75	125	160	210	410
30	60	100	150	250	320	420	820
45	90	150	225	375	480	630	1230
60	120	200	300	500	640	840	1640
75	150	250	375	625	800	1050	2050
90	180	300	450	750	960	1260	2460
105	210	350	525	875	1120	1470	2870
120	240	400	600	1000	1280	1680	3280
135	270	450	675	1125	1440	1890	3690
150	300	500	750	1250	1600	2100	4100

Maximum and minimum span lengths used in the parametric study were based on design aids included in *Instructions for Design Standard No. 20010: Prestressed Florida-I Beams* (IDS 20010; FDOT, 2012b), which provides estimated span lengths (Table 8.2) for FIBs with different lateral spacings, based on representative bridge design calculations. Maximum lengths were based on a spacing of 6 ft and an environment classified as "Moderately Aggressive", while minimum lengths assumed a 12-ft spacing and an "Extremely Aggressive" environment. To ensure that the considered length ranges included all reasonable beam designs, the basic ranges taken from IDS 20010 were extended by 3 ft on each end, and then extended further so that range limits were even multiples of 5 ft. The parametric study included span lengths chosen at 5-ft intervals over the final ranges.

Table 8.2 Range of allowable span lengths for FIBs

| | Values from IDS 20010 | | |
	Min length (ft)	Max length (ft)	Final tested range
36″ FIB	80	105	75–110
45″ FIB	98	126	95–130
54″ FIB	113	142	110–145
63″ FIB	124	155	120–160
72″ FIB	142	173	135–180
78″ FIB	151	182	145–185
84″ FIB	159	191	155–195
96″ FIB	175	208	170–215
Spacing	12 ft	6 ft	
Environment	Extremely aggressive	Moderately aggressive	

A survey of bracing designs used in girder bridges constructed in Florida revealed anchors with equivalent rotational stiffnesses ranging from 500 to 50,000 kip-ft/rad. However, it was found that when large anchor stiffnesses were included in girder models, particularly for shorter span, shallower girders less prone to instability, the models no longer exhibited a normal buckling response. In moderate cases, this caused the computed wind capacity to be artificially inflated, and, in the most extreme cases, the wind capacity could not be computed at all (i.e., the wind pressures required to initiate girder instability under self-weight were so large—well beyond material strength limits—that the displacement–load results ceased to be characteristically asymptotic and the modified Southwell analysis method was no longer applicable). Therefore, a maximum practical anchor stiffness (at which a wind capacity could be computed) was established for each FIB through trial and error, and the parametric study included ten (10) evenly-distributed stiffness values up to and including that maximum (in addition to the unanchored case, with zero anchor stiffness).

In practice, the maximum practical anchor stiffness was smaller for FIBs with shorter span lengths, but it was not feasible to determine a different maximum stiffness for every FIB at every span length. Instead, a maximum anchor stiffness was established based on the maximum span length for each FIB, and the parametric study was carried out with the understanding that not every combination of parameters would result in a computable wind capacity. At the minimum span length, it was common to obtain results for only the lowest 4 or 5 stiffness values. There were also two cases (the 215-ft, 96″ FIB with anchor stiffnesses of 0 and 410 kip-ft/rad) for which a meaningful wind capacity did not exist because the girder was inherently unstable, collapsing under less than 1 g in the absence of any wind. In total, 781 wind capacity analyses were attempted in the parametric study, of which 471 produced results. (The 471 computed wind capacities included the some of the artificially-inflated values described above. Identification and rejection of those data points is discussed in more detail later in the chapter.)

8.3 Results

Wind capacities computed from the parametric study are summarized in Figure 8.1. Visually, the data are divided into eight (8) major groups, each of which corresponds to one of

the tested FIB cross-sections, ranging from the 36″ FIB (cases 1–48) to the 96″ FIB (cases 405–471). Each group contains several subgroups—visually identifiable as diagonal lines of consecutive data points—that represent the wind capacities computed for a single span length (at several different anchor stiffnesses). The 'cloud' of outlier points, located well above the subgroups, consists of the artificially-inflated wind-capacities that occurred at higher anchor stiffnesses.
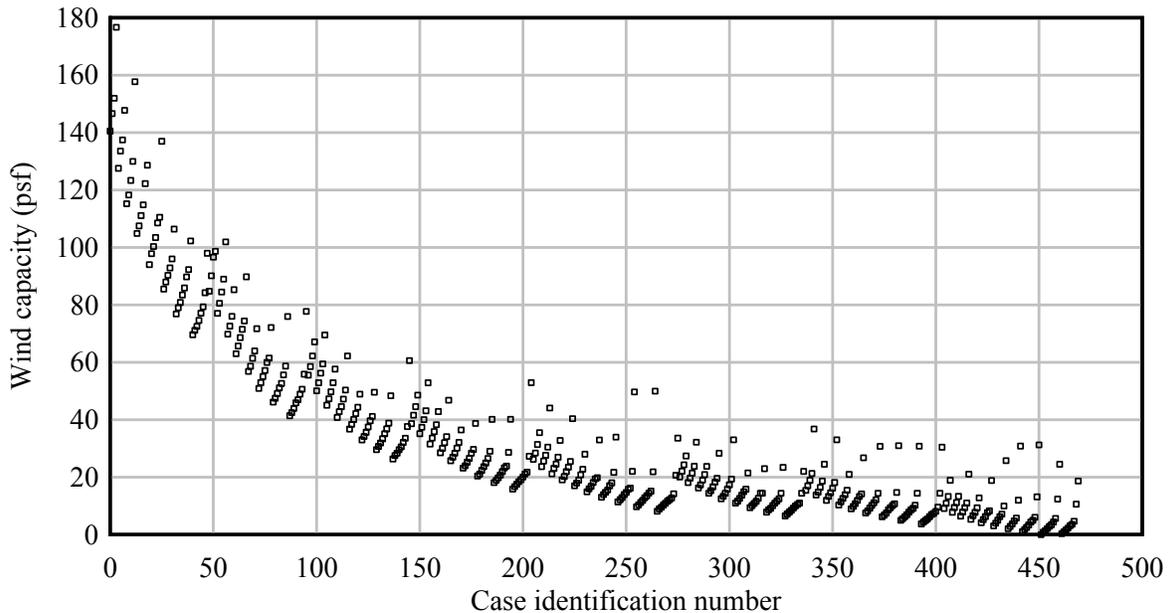
Figure 8.1. Summary of single-girder wind-load parametric study results

The results of the parametric study were used to develop an equation for estimating the wind capacity (P_{max}) of any FIB. This was accomplished by first developing an equation for the wind capacity of an unanchored FIB ($P_{max,0}$), in terms of the section depth (D) and span length (L) and then determining a linear correction factor that incorporated the effect of the anchor stiffness (k).

8.3.1 Wind capacity of a single unanchored girder

The relationship between wind capacity and span length for unanchored FIBs is plotted in Figure 8.2. It is evident from the plot that span length is the strongest predictor of wind capacity, which declines sharply as span length increases. Wind capacity is also reduced when the girder depth increases, which can be attributed to the larger sail area (projected area) over which the wind pressure is applied. There is no data for the 215-ft 96″ FIB because, as noted earlier, its capacity-to-demand ratio was less than 1 prior to the application of wind. In the final equation, this situation will be indicated by producing a negative wind capacity value.

97
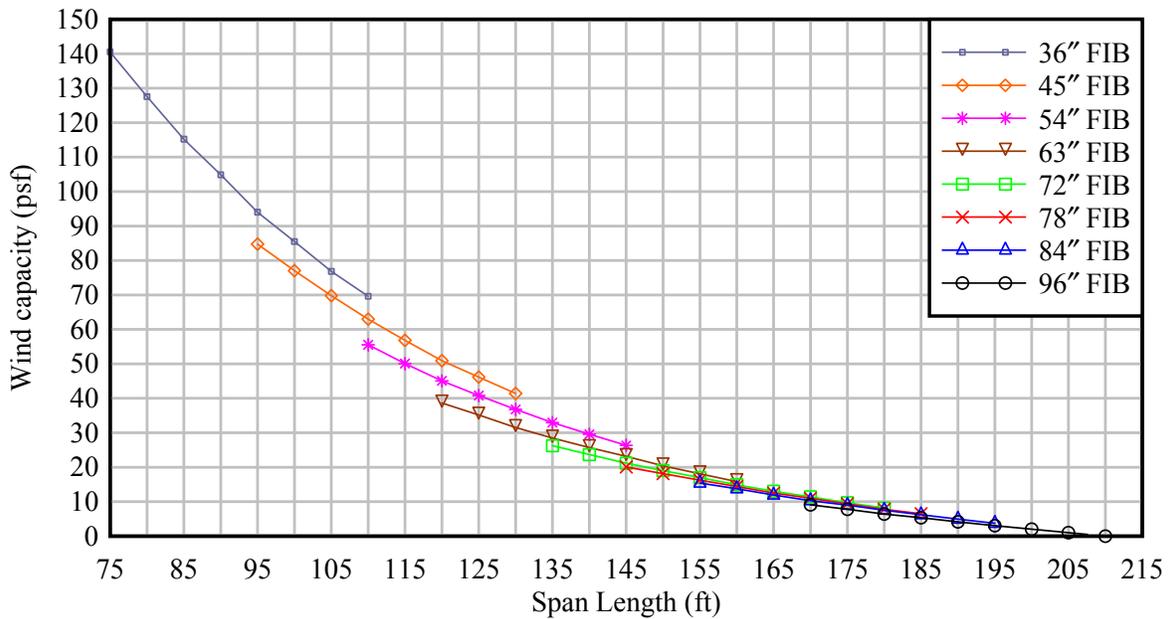
Figure 8.2 Wind capacities of unanchored FIBs at various span lengths

The functional form found to be the closest fit to each of the FIB curves was an exponential relationship:

$$y = ae^{-bx} + c \tag{8.1}$$

where *a*, *b*, and *c* are fitting parameters. For each FIB, a separate exponential curve-fit was performed to relate wind capacity to span length, *L*. It was found that the value of b in these curve-fits was approximately constant, while the variance in the *a* and *c* terms had a similar exponential relationship with FIB depth, *D*. Substituting curve fits for *a* and *c* into the original exponential fit resulted in a final equation for wind capacity of an unanchored girder:

$$P_{max,0} = 123e^{\frac{-L}{100}}\left(1 + 15e^{\frac{-D}{22}}\right) - 750e^{\frac{-D}{16}} - 16 \tag{8.2}$$

where $P_{max,0}$ is in psf, *L* is the span length in ft, and *D* is the FIB cross-section depth in inches. Equation 8.2 predicts conservative wind capacities for every case analyzed in the parametric study (Figure 8.3).
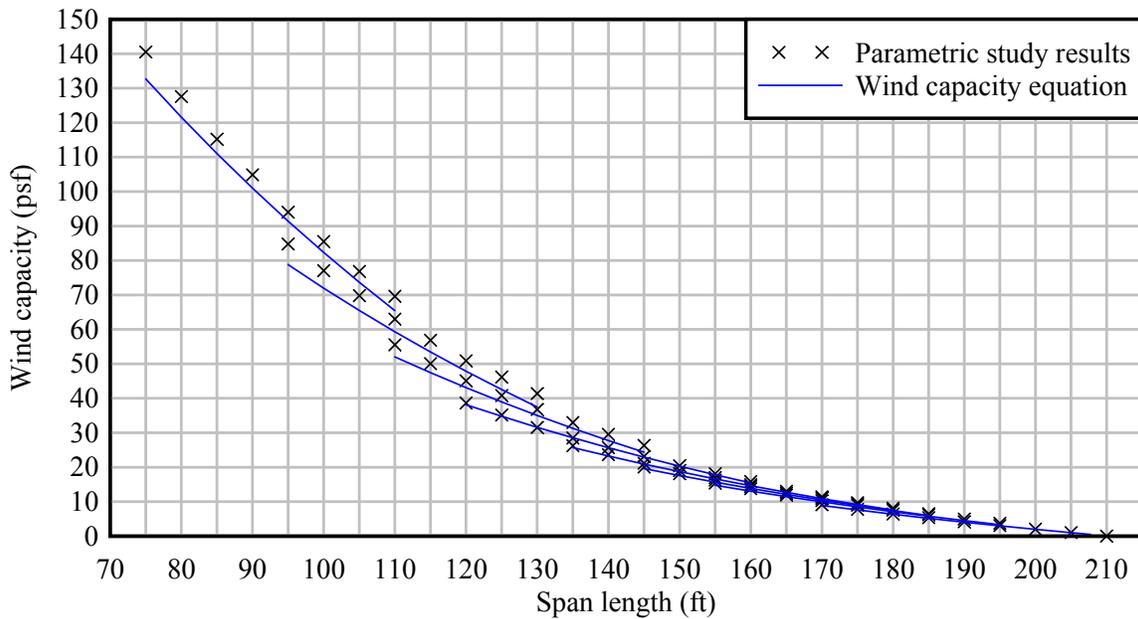
Figure 8.3 Wind capacity of an unanchored girder as predicted by Equation 8.2

Due to the complexity of Equation 8.2, an alternative, *simplified equation* was also produced that took the form of a basic exponential function that enveloped all of the data points (Figure 8.4). The simplified equation is a function of span length only:

$$P_{max,0} = 1000e^{\frac{-L}{38}} - 4 \tag{8.3}$$

where $P_{max,0}$ is in psf, L is the span length in ft. The simplified Equation 8.3 is easier to use, but, as shown in Figure 8.5, produces more conservative results. In practice, either Equation 8.2 or 8.3 can be used to compute conservative estimates of unanchored girder wind load capacity.

99
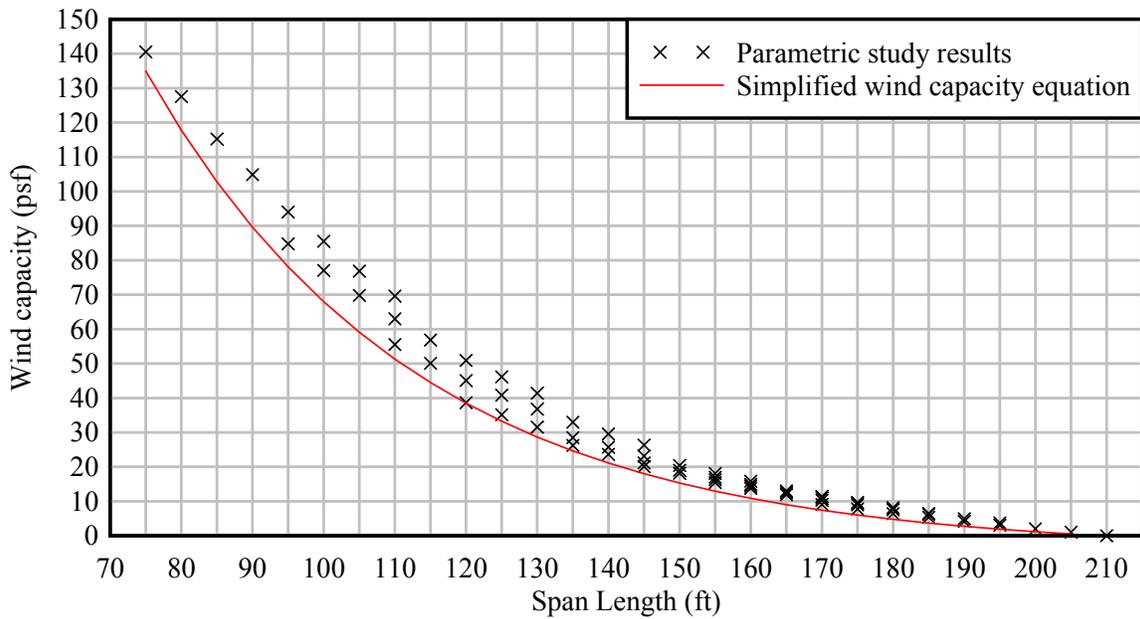
Figure 8.4 Wind capacity of an unanchored girder as predicted by simplified Equation 8.3
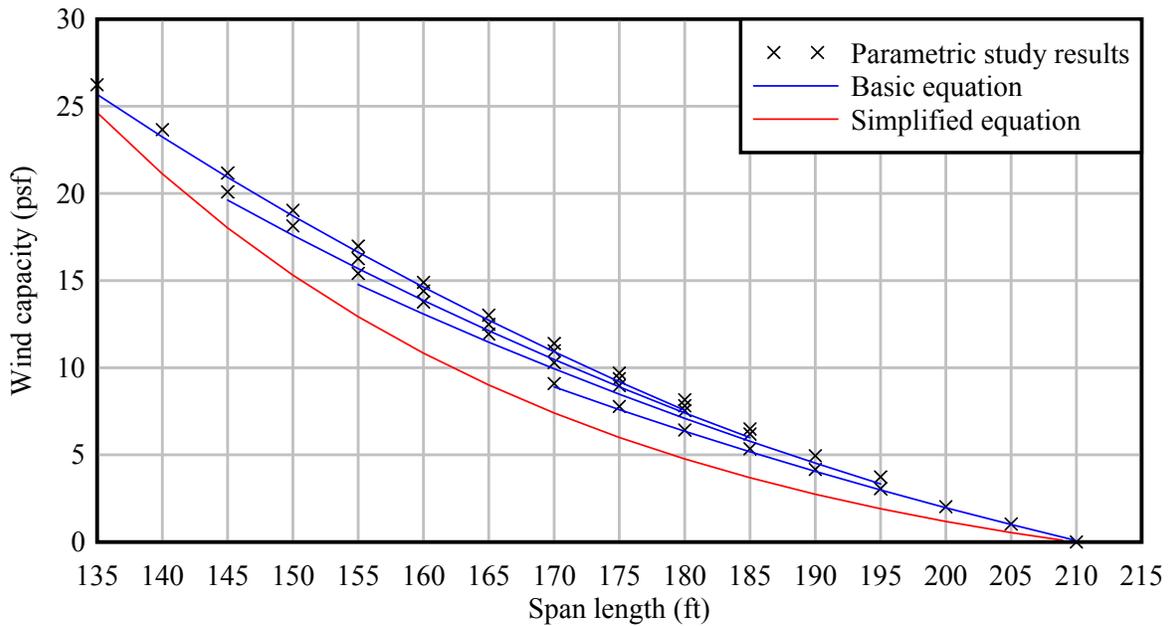
Figure 8.5 Comparison of basic and simplified unanchored girder
wind capacity equations, Equations 8.2 and 8.3, respectively
(Only data for FIBs with depths 72 in. or greater shown)

8.3.2 Wind capacity of a single anchored girder

The relationship between wind capacity and anchor rotational stiffness ($k_{roll,anchor}$) for the 84″ FIB is plotted in Figure 8.6 with separate curves for each tested span length. (Data for the other FIB sections are qualitatively similar.) As expected, the stability provided by the anchor stiffness—which adds to the roll stiffness of the bearing pad—tends to increase wind capacity monotonically relative to the unanchored case (i.e., the case where $k_{roll,anchor} = 0$). For each curve, the relationship between wind capacity and anchor stiffness follows the same basic pattern: a steady linear increase followed by a much sharper increase in the last 1–3 data points. As previously described, the sudden increase is artificial—a moderate form of the same numerical problems noted earlier—and the inflated data points must be discarded.
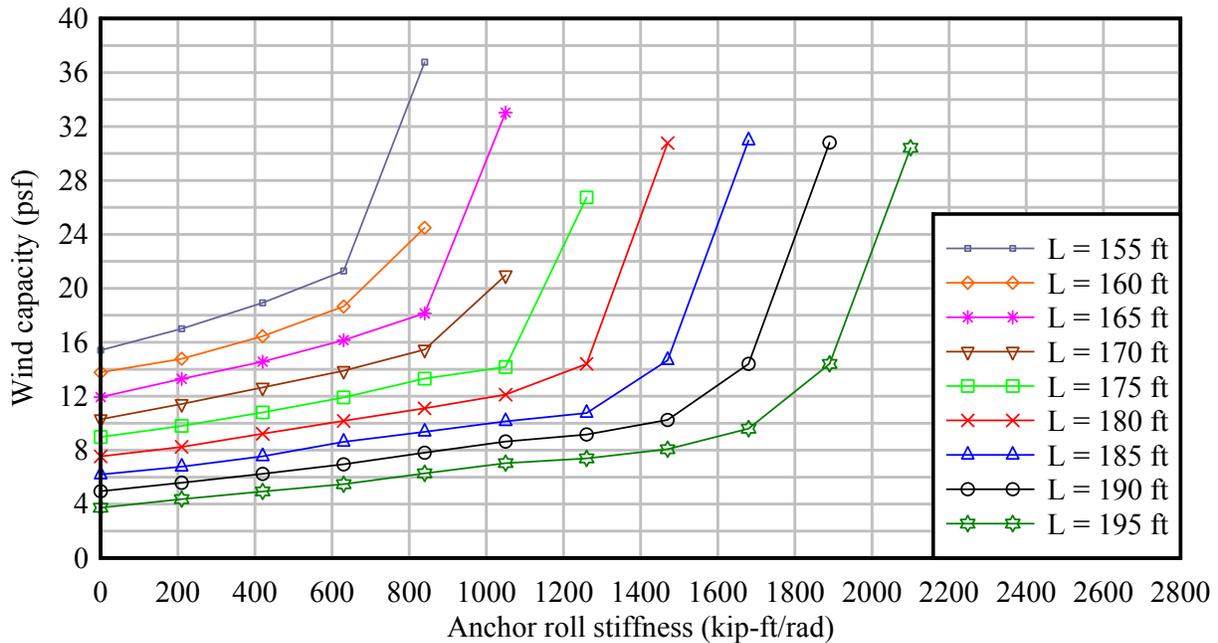
Figure 8.6 Effect of anchor rotational stiffness on wind capacity for 84″ FIB

Based on an examination of system characteristics (span length, etc.) and the analysis results, it was determined that meaningful results data were restricted to the linear portion of each curve and that points contained within the nonlinear portions should be rejected. Hence, starting with the first three (3) points in each curve, a linear least-squares regression was performed and the resulting line was extrapolated to predict the wind capacity of the next point. If the predicted wind capacity was within 5% of the computed value then the point was accepted, the regression line was recomputed (to include the new point). The process was then repeated on the next point in the curve. If a point failed the test, it was considered to be outside the linear range of the curve, and all remaining points were rejected (Figure 8.7).
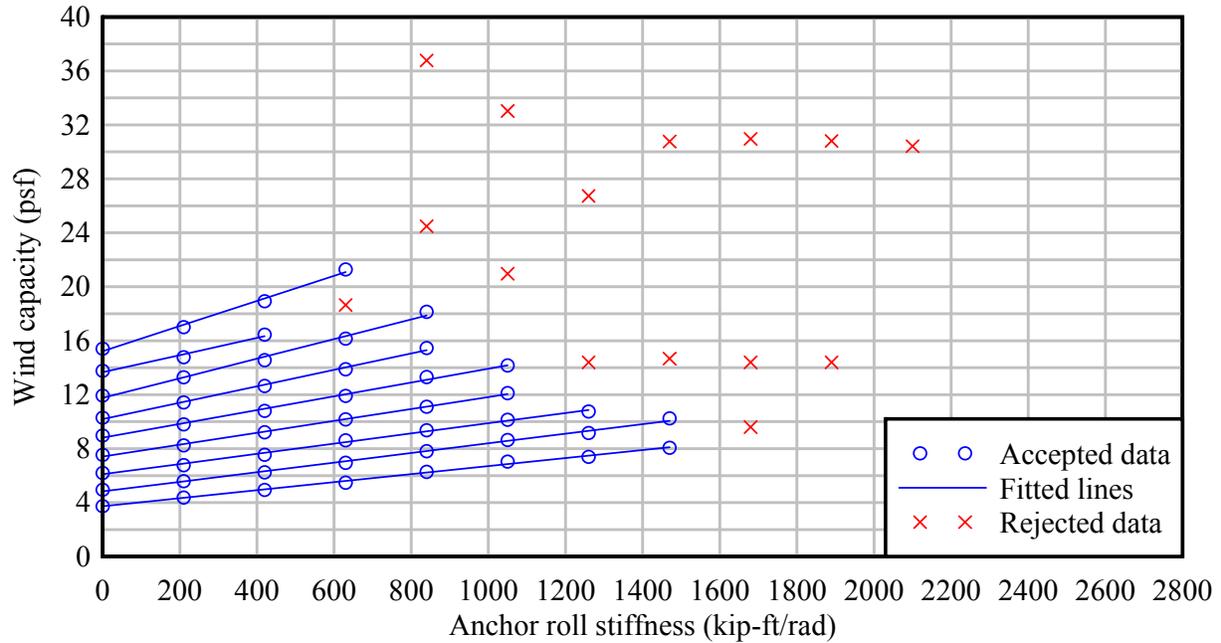
Figure 8.7 Rejection of artificially-inflated wind capacity data points (84″ FIB)

Because the y-intercept of each curve in Figure 8.7 is equal to the unanchored wind capacity ($P_{max,0}$), the slope (m) of each regression line can be thought of as an *anchor stiffness coefficient* such that the total wind capacity (P_{max}) of the anchored girder is calculated as follows:

$$P_{max} = P_{max,0} + m\left(k_{roll,anchor}\right) \tag{8.4}$$

After computing m for every tested combination of girder cross-section and span length, it was found to be primarily correlated with span length (Figure 8.8). An exponential least-squares curve fit was performed, resulting in an equation for m as a function of span length:

$$m = 11e^{\frac{-L}{22}} \tag{8.5}$$

where m has units of psf/(kip-ft/rad), and L is the span length in ft.

Equation 8.5 conservatively underpredicts nearly all computed values of m. In the few cases where m is slightly over predicted, the amount of unconservatism is either negligibly small or is compensated for by conservatism in the determination of $P_{max,0}$. As a result, the wind capacity of a single anchored girder can be predicted as follows:

$$P_{max} = P_{max,0} + 11e^{\frac{-L}{22}}\left(k_{roll,anchor}\right) \tag{8.6}$$

where $k_{roll,anchor}$ is in kip-ft/rad, L is the span length in ft, and $P_{max,0}$ is in psf and is calculated using either Equation 8.2 or 8.3. When Equation 8.2 is used, the majority of wind capacities

102

predicted by Equation 8.6 fall within 10% (see Figure 8.6) of the corresponding values computed in the parametric study. Example calculations, demonstrating the application of the wind capacity equation developed in this chapter, are presented in Appendix H.
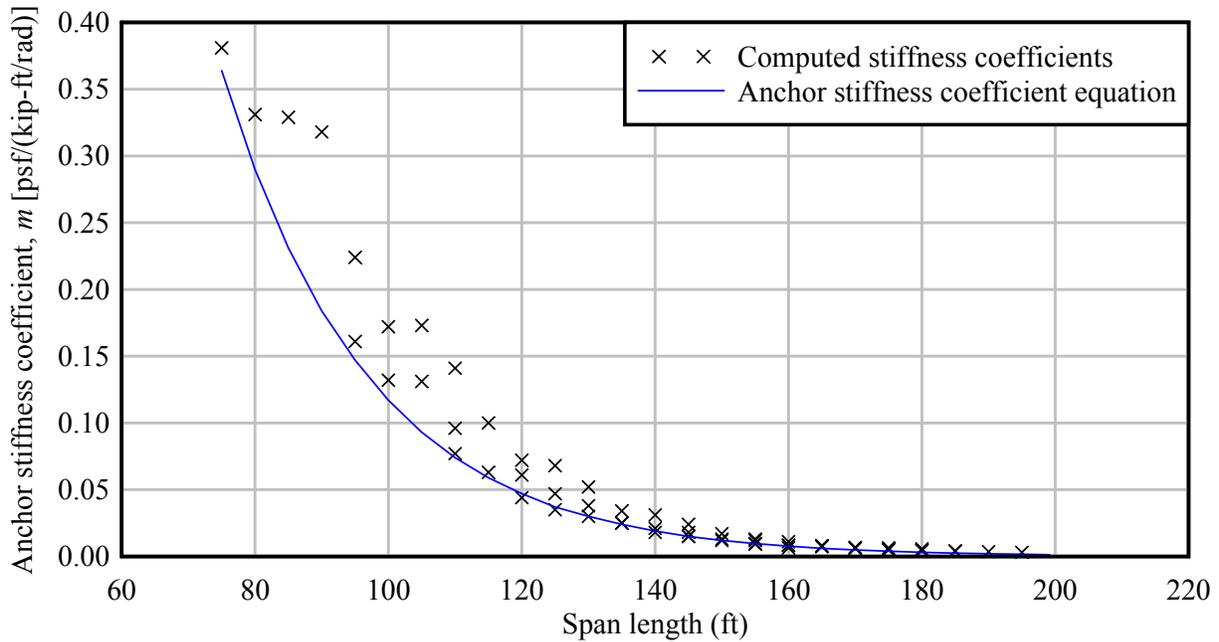
Figure 8.8 Anchor stiffness coefficient Equation 8.5 compared to parametric study results
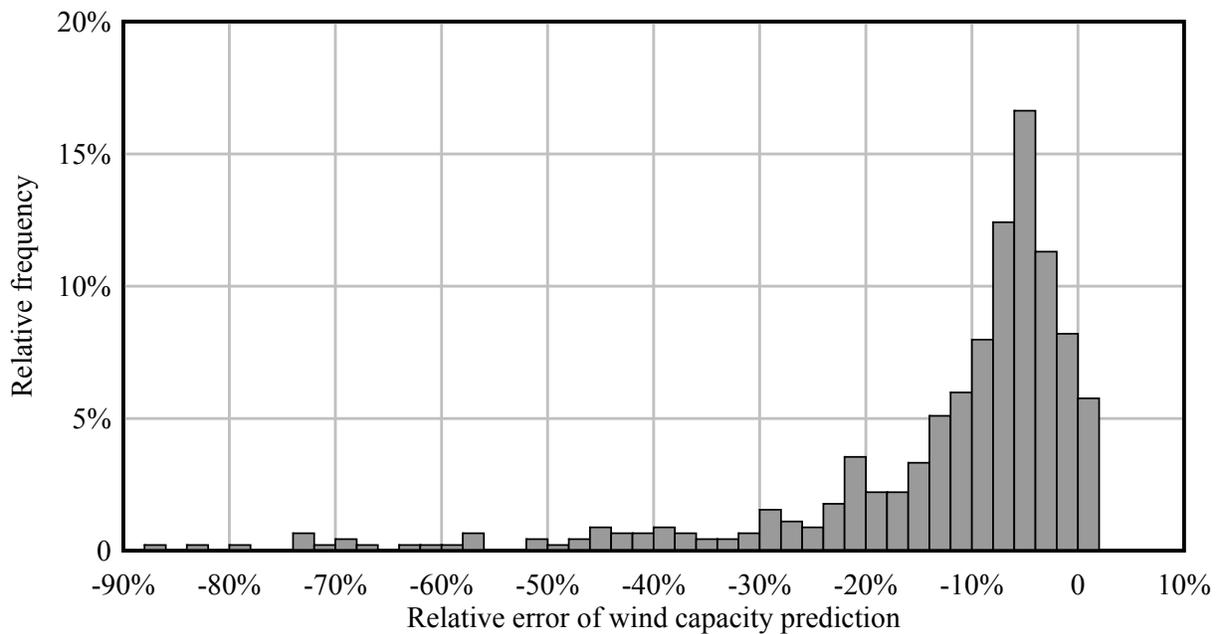
Figure 8.9 Comparison of wind capacity results computed using the combination of Equations 8.2 and 8.6 versus corresponding parametric study results
(Note: negative relative error indicates that the combination of Equations 8.2 and 8.6 is conservative relative to the parametric study data)

CHAPTER 9
PARAMETRIC STUDY OF BRACED MULTI-GIRDER SYSTEMS

9.1 Preliminary sensitivity studies

Fully characterizing a braced multi-girder system requires a large number of geometric parameters. Consequently, conducting parametric studies in which all possible combinations of these parameters are considered (even if only a few discrete values are selected per parameter) would require hundreds of thousands of analyses to be performed. To avoid such a situation, several limited-scope preliminary sensitivity studies were performed to help guide the design of efficient final parametric studies. As a result of these preliminary investigations—the details of which will be omitted here for brevity—several system parameters were identified as having negligible influence on system capacity. Consequently, these parameters were not varied in the final parametric studies. The parameters were:

- Bridge grade: All analyses were performed on girder models with level (0%) grade.

- Cross-slope: Multi-girder models had a default −2% cross-slope.

- Location of anchored girder in bridge cross-section: In cases where anchors were included, they were always attached to the most leeward (downwind) girder.

The preliminary studies also revealed that braces were naturally divided into two categories that had very different effects on system behavior: *strut braces* and *moment-resisting braces*. As a result, separate parametric studies were performed for each brace category.

9.1.1 Strut braces

Top struts and parallel struts (Figure 9.1) are both examples of strut braces, which include (but are not limited to) all brace designs consisting solely of horizontal compression members. Somewhat surprisingly, it was found that all strut brace designs are essentially interchangeable with regard to lateral stability. That is, a girder system braced with top struts has the same capacity as an otherwise identical system braced instead with parallel struts (or any other type of strut brace). As a result, the capacity of a strut-braced system is also insensitive to girder spacing (which only affects the length—and thus the axial stiffness—of the strut members). Additionally, there is no measurable gain in system capacity that results from the installation of struts at interior brace points. End bracing alone is sufficient to mobilize all of the girder buckling capacity that can be provided by strut braces. It is also worth noting that the capacity of a strut-braced system decreases as additional girders are added.
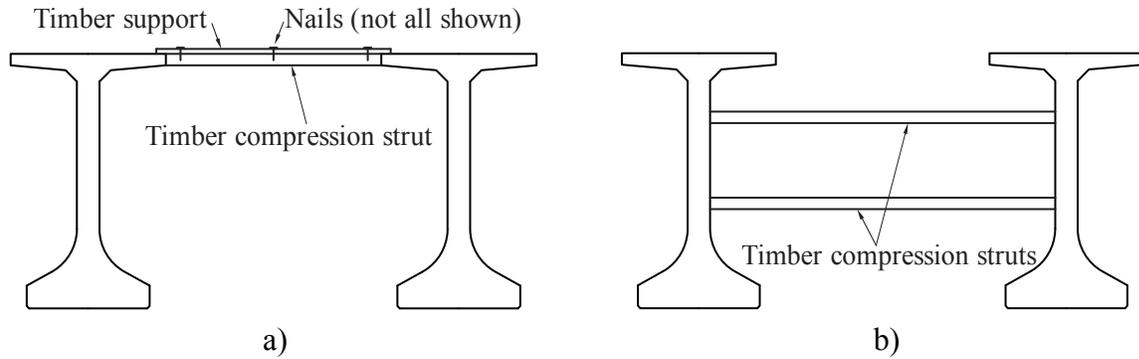
Figure 9.1 Examples of strut bracing: a) top strut; b) parallel struts

Strut braces can be defined (or identified) by their lack of resistance to girder overturning. In a small-displacement (geometrically linear) analysis of a system with zero bearing pad rotational stiffness, a strut with ideal pin connections forms a collapse mechanism (Figure 9.2) that allows the connected girders to rotate freely in unison. Therefore, struts can only provide stability by coupling the girders together, and resistance to collapse is primarily provided by the roll stiffness of the anchors and, to a lesser extent, the roll stiffness of the bearing pad supports. This behavior is also the reason that adding girders to a system reduces stability: each new girder adds additional wind load (and additional bearing pad stiffness) while the number of anchors remains constant.
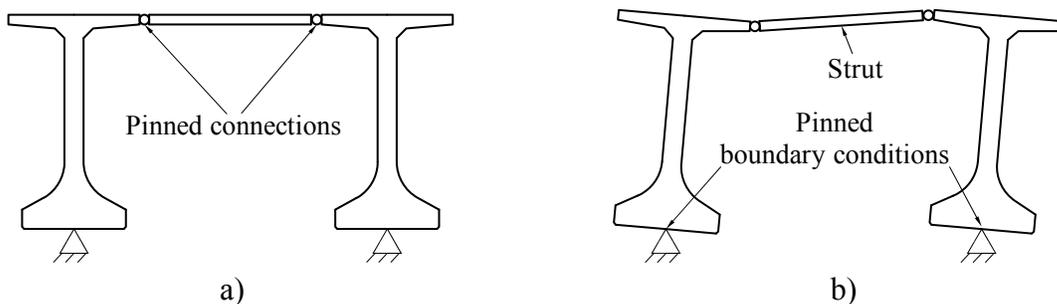
Figure 9.2 Collapse mechanism possible with strut bracing:
a) Undeformed configuration; b) Collapse mechanism

9.1.2 Moment-resisting braces

X-braces and K-braces (Figure 9.3) are both examples of moment-resisting braces, which are capable of resisting girder overturning. Unlike struts, the system capacity provided by different moment-resisting brace designs varies significantly, and capacity can be increased by the installation of braces at interior brace points. Systems with moment-resisting braces become more stable as additional girders are added; hence a two-girder system is nearly always the most unstable bridge cross-section possible. In the presence of moment-resisting bracing, the additional roll stiffness and stability provided by anchors is typically negligible.
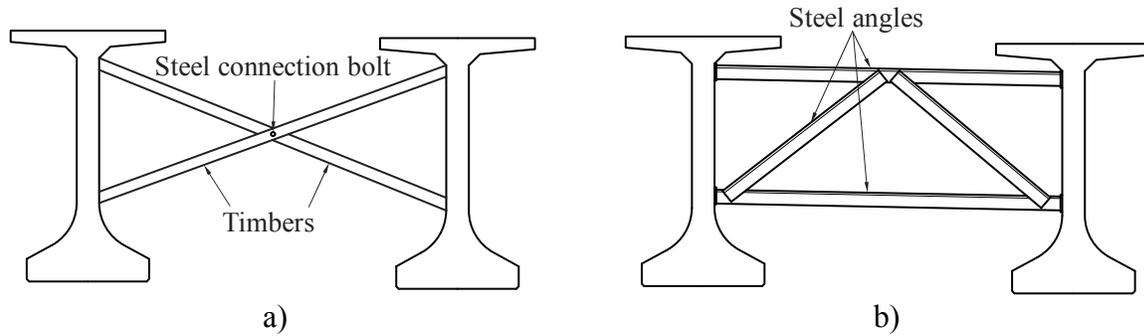
Figure 9.3 Examples of moment-resisting braces: a) X-brace; b) K-brace

9.2 Modeling of bridge skew and wind load

In a braced system of girders, the introduction of bridge skew causes the girders to become staggered longitudinally. This affects system capacity in two ways (Figure 9.4):

- Brace placement: Because girders are installed perpendicular to the girder axes (per *Design Standard No. 20005: Prestressed I-Beam Temporary Bracing*, FDOT, 2012a), the region within which braces can be placed is smaller (shorter) than the span length of the girders. As a result, girder stability can increase due to the reduced distance between brace points.

- Incomplete shielding: In a skewed system, none of the girders are completely shielded with respect to wind load. Rather, an end portion of each girder is exposed to full (unshielded) wind pressure. The aerodynamic properties of the exposed end region have not been measured in a wind tunnel, so specific 'edge effects' that may result from the presence of upwind girders are unknown.

The magnitude of both of these effects is a function of the girder offset length (L_{offset}), (Figure 9.4) which is dependent on both skew angle and girder spacing.
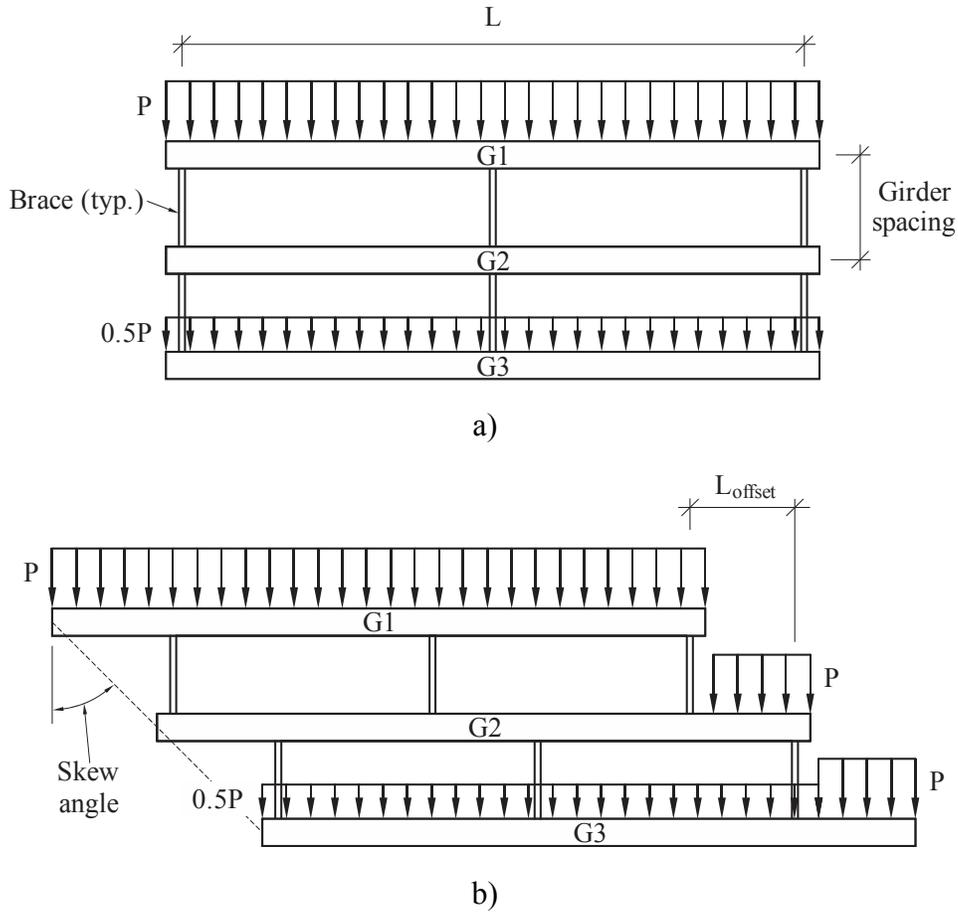
Figure 9.4. Effect of bridge skew on wind loading of braced 3-girder system (plan view): a) Unskewed system; b) Skewed system

Conducting wind tunnel testing to experimentally quantify the effects of skew on girder-end shielding was outside the scope of this study. Consequently, the non-uniform wind pressure distribution shown for leeward girders in Figure 9.4b is an approximation based on engineering judgment. Lacking wind tunnel confirmation of this approximation, it was deemed unwarranted to model this distribution in detail in the parametric studies. Instead, a simplified, but statically similar, representation was used in which the wind load on each girder was modeled as a single, weighted-average uniform pressure along the entire length of the girder. The uniform wind load applied to each partially-shielded girder (P) was computed as a weighted average of the shielded and unshielded wind loads, as follows:

$$P = P_U \frac{L_{offset}}{L} + P_S \frac{L - L_{offset}}{L}$$ (9.1)

where P_U is the unshielded wind load (on the windward girder), P_S is the shielded wind load, L is the girder length, and L_{offset} is the length of girder offset produced by skew.

9.3 Selection of parameters for strut brace parametric study

System parameters that were varied in the strut brace parametric study were as follows:

- FIB cross-section depth (in)
- Span length (ft)
- Number of girders
- Rotational stiffness of anchor bracing (kip-ft/rad)
- Wind pressure (psf)
- Skew angle (deg)

All eight (8) standard FIB cross-sections were included in the study, with depths ranging from 36 in. to 96 in. For each FIB, capacity analyses were performed for every combination of span length, anchor stiffness, wind pressure, skew angle, and number of girders, sampled from the values listed in Table 9.1, for a total of 37,800 analyses.

Table 9.1 Parameter values used in strut brace parametric study

Span length, L (ft)

36″ FIB	45″ FIB	54″ FIB	63″ FIB	72″ FIB	78″ FIB	84″ FIB	96″ FIB
75	95	110	120	135	145	155	170
85	105	120	130	145	155	165	180
95	115	130	140	155	165	175	190
105	125	140	150	165	175	185	200
115	135	150	160	175	185	195	205
-	-	-	-	185	-	-	220

Anchor rotational stiffness, $k_{anchor,roll}$ (kip-ft/rad)

36″ FIB	45″ FIB	54″ FIB	63″ FIB	72″ FIB	78″ FIB	84″ FIB	96″ FIB
0	0	0	0	0	0	0	0
30	60	100	150	250	320	420	820
60	120	200	300	500	640	840	1640
90	180	300	450	750	960	1260	2460
120	240	400	600	1000	1280	1680	3280
150	300	500	750	1250	1600	2100	4100

Unshielded wind pressure, P_U (psf)	Number of girders, n	Skew angle
0	2	0°
40	3	2°
80	5	5°
120	7	10°
160	9	25°
		50°

Maximum and minimum span lengths were based on the same span length ranges used for the single girder study (see Chapter 8). However, to reduce the number of analyses to a feasible level, the study used lengths chosen at 10-ft intervals instead of 5-ft intervals. When necessary, the upper limit of the range was increased by 5 ft so that the total range was evenly divisible into 10-ft intervals. Similarly, the maximum anchor stiffnesses were the same that were used for the single-girder study, but five (5) evenly distributed values were used instead of ten (10).

As noted earlier, preliminary analyses demonstrated that the capacity of a strut-braced system continues to decrease as more girders are added. A practical upper bound of nine (9) girders was selected to be representative of wide bridge cross-sections while simultaneously limiting the finite element models to a manageable size (number of nodes, elements, and degrees of freedom).

Wind pressure loads were applied to the girders using the shielding pattern proposed in Chapter 5, and using the wind pressures listed in Table 9.1. Wind pressures specified in the table refer to the unshielded pressure load applied to the windward girder (G1). Hence, in accordance with the model proposed in Chapter 5, the first shielded girder (G2) received no wind load and

all subsequent girders (G3, G4, etc.), if any, received half of the listed pressure load. The maximum wind pressure of 160 psf was determined using the *Structures Design Guidelines* (FDOT, 2012e) by assuming a pressure coefficient of $C_P = 2.0$, a basic wind speed of $V = 150$ mph, a bridge elevation of $z = 75$ ft, a gust effect factor of $G = 0.85$ and a load multiplier of $\gamma_{ws} = 1.4$ (corresponding to the Strength III limit state).

During preliminary sensitivity studies, the effect of girder spacing (and therefore, axial strut stiffness) was found to be small enough so as to have no practical effect on the determination of system capacity. There was, however, a very slight (< 1%) reduction in capacity for a system spaced at 6 ft on center relative to an otherwise equivalent system spaced at 14 ft (an 80% difference in strut length). Therefore, for conservatism, all systems in the parametric study were spaced at 6 ft on center. However, skew effects, which are a function of the girder offset length (L_{offset}), are minimized when the smallest girder spacing is selected. Therefore, to maintain conservatism in the system models, the girders were offset longitudinally as if they were spaced at 14 ft (Table 9.2). Essentially, the effective skew angle in each model was greater than the nominal bridge skew, so that a conservative girder offset was produced. In this way, brace placement and wind loads were modeled conservatively while maintaining a 6-ft spacing.

Table 9.2 Girder offset lengths in model for each skew angle

Nominal skew angle	Offset length
2°	0′-6″
5°	1′-3″
10°	2′-6″
25°	6′-6″
50°	16′-8″

9.4 Results of strut brace parametric study

The results of the strut brace parametric study are summarized in Figure 9.5. Recall from Chapter 7 that the system capacity computed for each case represents the total gravity load (in g) that can be resisted by the system without failing due to lateral instability (primarily a buckling phenomenon in systems where an anchor is present). Five (5) main groups are visible in the summary of results, each of which corresponds to a different wind pressure value (in increasing order from 0 to 160 psf). Each group contains eight (8) subgroups—corresponding to the tested FIB cross-sections—each of which is composed of five (5) or six (6) adjacent groups of data points arranged in a steep diagonal line—corresponding to the tested span lengths. Variation within the data groups reflects the relatively small effects of anchor stiffness and the number of girders in the system.
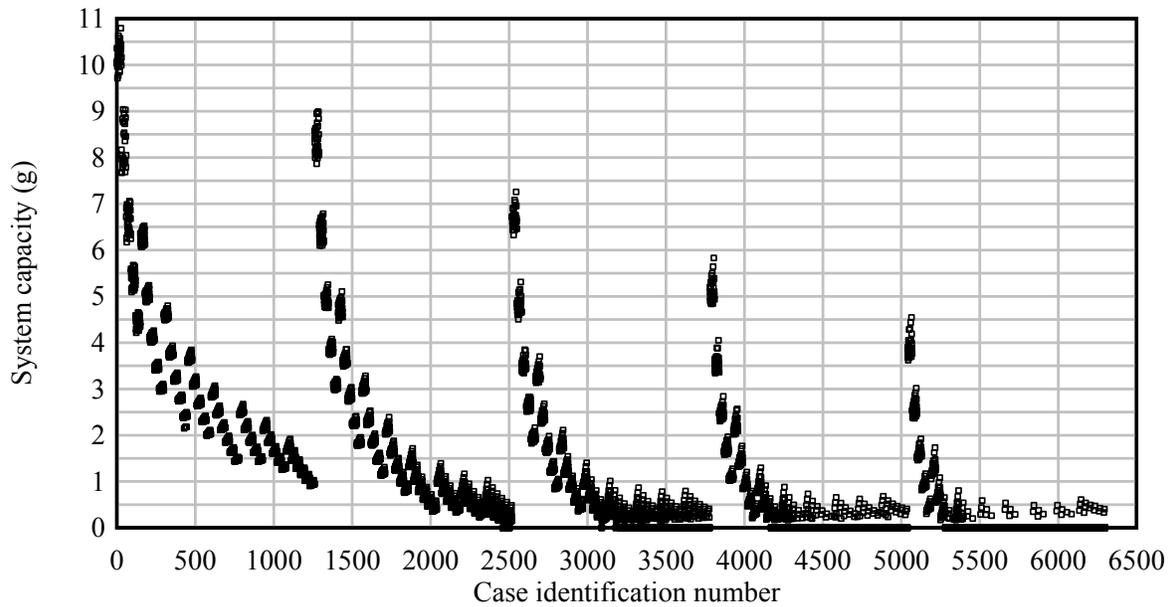
Figure 9.5. Summary of strut brace parametric study results

The results were used to develop an equation for capacity (C) of a strut-braced system of FIBs. This was accomplished by first determining the baseline capacity of an unanchored system of two girders in zero wind conditions (C_0), and then developing correction factors to adjust the system capacity upward in response to anchor stiffness and downward in response to wind load and the erection of additional girders. A wide range of FIB system capacities (up to 10 g) were present in the parametric study results, but under heavy wind, a large number of systems also had a capacity of 0, which the capacity equations indicate by computing a negative capacity value.

Two techniques were used to simplify interpretation of the parametric study results. The large number of interacting parameters and the wide range of the capacity values made it impractical to produce equations with a uniform level of conservatism throughout the data set. Therefore, capacity prediction equations were considered satisfactory if they conservatively enveloped 95% of the data points, and as long as none of the unconservative cases were more than 5% in error with regard to computed capacity. Also, while it was important that the equations be accurate and not overly conservative for systems where stability was likely to control design, the same characteristics are less important for extremely stable systems. Therefore, when appropriate, to simplify the data interpretation process systems with capacities greater than 3.0 g were excluded from curve fits or other trend determinations, so long as the resulting equations met the conservatism requirements over the full range of data.

9.4.1 System capacity of unanchored two-girder system in zero wind

The baseline system capacity results for strut-braced systems of two (2) FIBs with no anchor and no wind are plotted in Figure 9.6. With the exception of the 36″ FIB, it is clear that the FIB depth (D) has almost no effect on capacity, which is correlated primarily with span length (L). Therefore, an equation for C_0 in terms of L was produced using an exponential curve fit:

111

$$C_0 = 39e^{\frac{-L}{48}} + 0.5 \qquad\qquad (9.2)$$

where C_0 is in g and L is the span length in ft. Equation 9.2 conservatively envelopes 95% of the available data points (Figure 9.7).
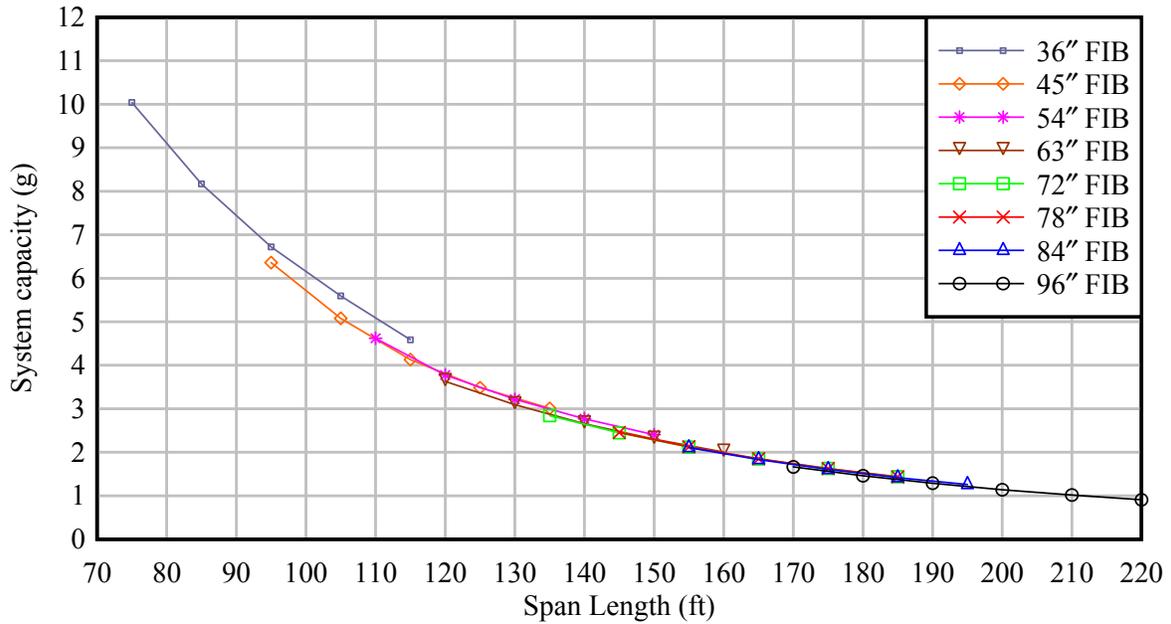
Figure 9.6. System capacities of unanchored two-girder strut-braced systems in zero wind at various span lengths
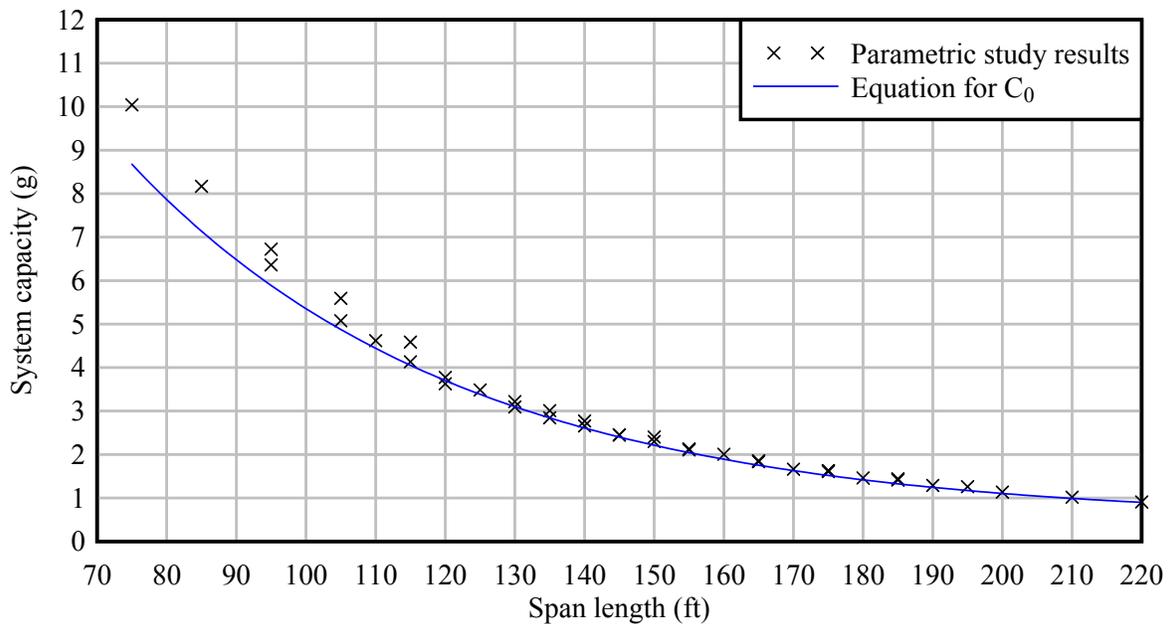
Figure 9.7. System capacity of an unanchored strut-braced two-girder system
in zero wind as predicted by Equation 9.2

9.4.2 System capacity increase from inclusion of anchor

The inclusion of an anchor tends to increase the capacity of the system linearly with the roll stiffness of the anchor, as shown in Figure 9.8 for the 96″ FIB. Data for other FIB cross-sections are qualitatively similar, though the linearity is noisier for shallower FIB sections. The linear relationship between buckling capacity and anchor stiffness is similar to the effect of anchor stiffness on wind capacity (discussed in Chapter 8) and, as with wind capacity, anchor stiffness coefficients were determined by using linear regressions to calculate the slope (m_a) of the anchor stiffness curves.

113
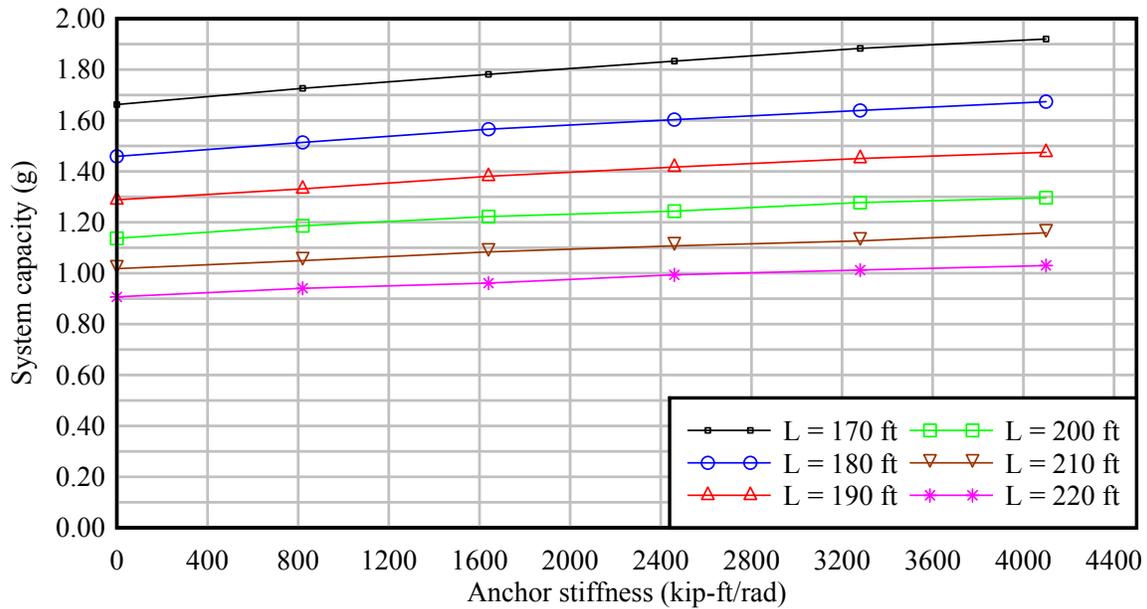
Figure 9.8. Effect of anchor stiffness on capacity of 96″ FIB system

Anchor stiffness coefficients (m_a) were calculated for every curve, each corresponding to a unique combination of span length and FIB depth. However, to facilitate interpretation of the data, the m_a values for curves within which every capacity value was greater than 3.0 were rejected. This prevented the data obtained from such highly stable systems from obscuring overall trends that were pertinent to systems of primary interest in this study. The remaining (i.e., non-rejected) values of m_a were found to be most strongly correlated to D, therefore regression was used to construct a best-fit linear relationship between m_a and D. This relationship (Figure 9.9, dashed line) overpredicted m_a in roughly half of the observed cases (which is consistent with the concept of a best-fit line). Because overprediction of m_a sometimes (but not always) resulted in unconservative capacity predictions, the fit parameters were adjusted (Figure 9.9, solid line) such that when the equation was later incorporated into the system capacity equation, all of the system capacity values in the data set (except those that exceeded 3.0 g) were conservatively predicted (Figure 9.10). The resulting equation for m_a was:

$$m_a = \frac{100 - D}{250,000} \tag{9.3}$$

where m_a has units of g/(kip-ft/rad), and D is the FIB cross-section depth in inches.

114
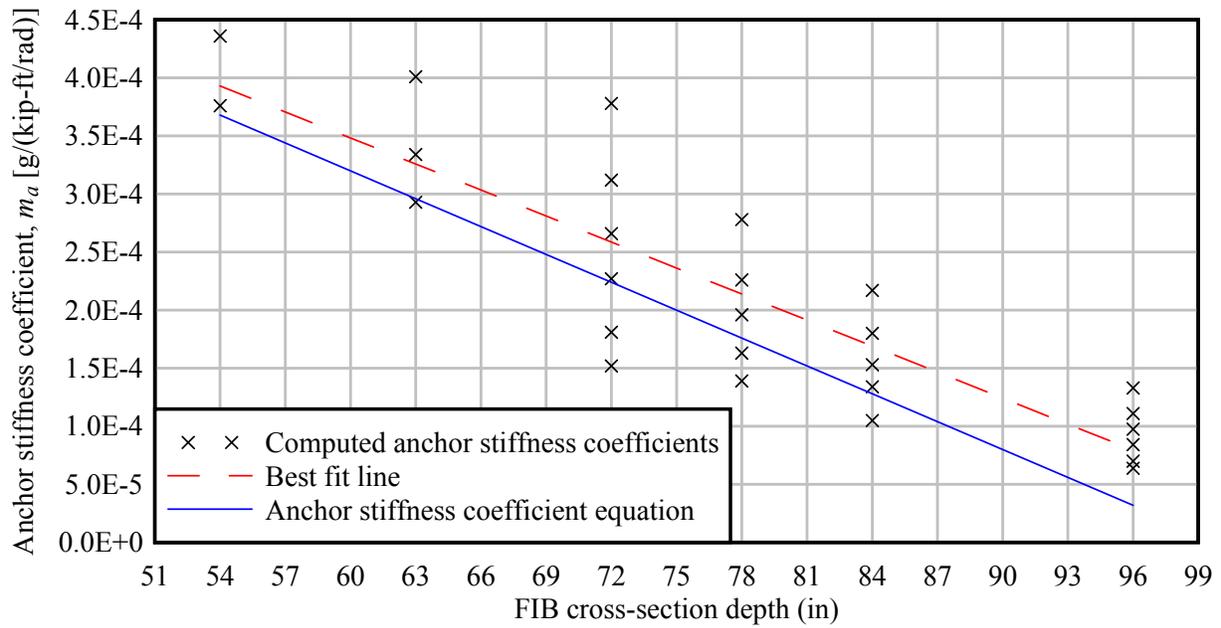
Figure 9.9. Anchor stiffness coefficient Equation 9.3 compared to parametric study results

Equation 9.3 was incorporated into the system capacity equation as follows:

$$C = C_0 + k_{roll,anchor} \frac{100 - D}{250,000} \tag{9.4}$$

where C is the buckling capacity in g, $k_{roll,anchor}$ is the anchor rotational stiffness in kip-ft/rad, D is the FIB cross-section depth in in., and C_0 is calculated using Equation 9.2 and is in g.
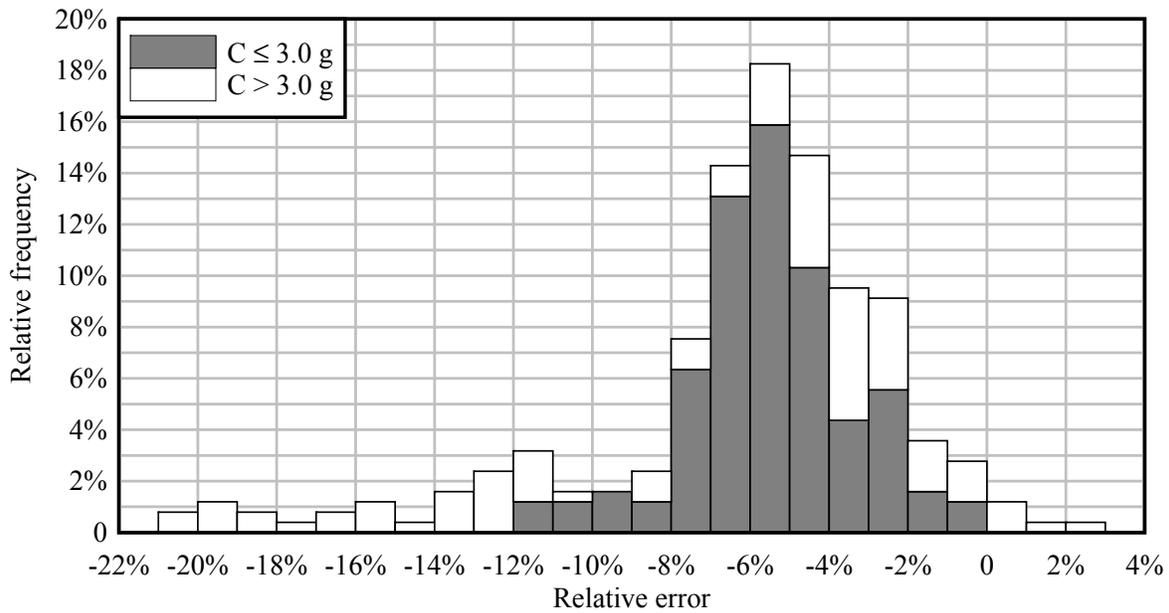
Figure 9.10. Relative error of system capacity values predicted by Equation 9.4
(Note: negative relative error indicates conservative prediction of capacity)

9.4.3 System capacity reduction from erection of additional girders

As noted earlier in Section 9.1.1, the erection of additional girders causes a reduction in system capacity because the resistance provided by the anchor is shared by multiple girders. Therefore, it was hypothesized that the effect could be accounted for by restating Equation 9.4 in terms of the average anchor stiffness:

$$\overline{k}_{roll,anchor} = \frac{k_{roll,anchor}}{n} \tag{9.5}$$

where n is the number of girders in the system. Because Equation 9.4 was fitted to data where $n = 2$, the stiffness values that were used in that fit were equivalent to the quantity $2\overline{k}_{roll,anchor}$. Substituting this into Equation 9.4 resulted in a new expression:

$$C = C_0 + \overline{k}_{roll,anchor} \frac{100 - D}{250,000} \tag{9.6}$$

When the data set was expanded to include systems with between two (2) and nine (9) girders, Equation 9.6 was found to predict the system capacities with approximately the same degree of accuracy (Figure 9.11) that Equation 9.4 achieved for the data set restricted to two-girder systems only, with conservative capacity predictions in 94.3% of cases.

116
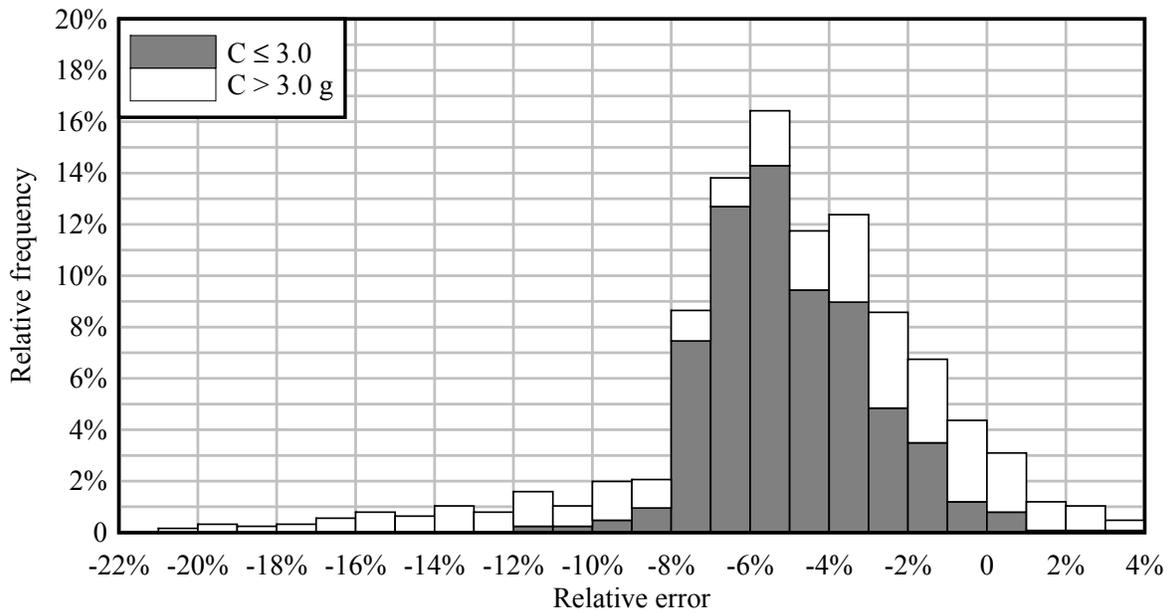
Figure 9.11. Relative error of system capacity values predicted by Equation 9.6
(Note: negative relative error indicates conservative prediction of capacity)

9.4.4 System capacity reduction from inclusion of wind load

The process of evaluating and predicting the effects of wind pressure on system capacity employed a concept similar to the average anchor stiffness concept introduced in the previous section; the use of an average wind pressure per girder, $\bar{P}$:

$$\bar{P} = \frac{\sum P}{n}$$

(9.7)

where n is the number of girders in the bridge and $\sum P$ is the sum of the individual wind pressures on all girders. Due to the nature of the shielding pattern that was employed, the average wind pressure ($\bar{P}$) for *unskewed* systems was always equal to one half of the unshielded wind pressure (P_U, listed previously in Tables 9.1 and listed later in Table 9.3), regardless of the number of girders in the system. In contrast, $\bar{P}$ for *skewed* systems is larger due to the fact that a portion of each girder remains unshielded.

As shown in the example cases presented in Figure 9.12, the decrease in system capacity produced by wind pressure is not linear. However, it was found to be approximately linear with respect to the square root of the wind pressure in most cases (Figure 9.13). This fact made it possible to define the wind pressure coefficient, m_w as the slope obtained from linear regression of system capacities expressed as a function of $\sqrt{\bar{P}}$. This linear regression process was carried out to obtain a value of m_w for every unique combination of D, L, and $\bar{k}_{roll,anchor}$.

117
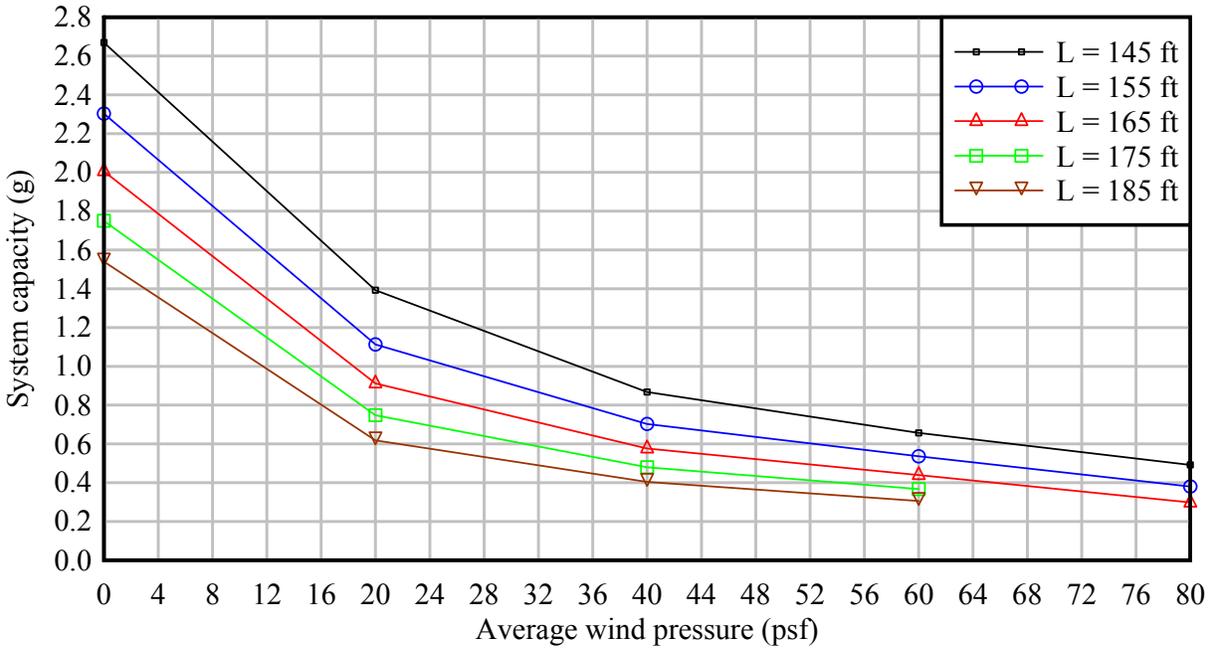
Figure 9.12. Effect of average wind pressure on system capacity of 78″ 2-FIB system with anchor stiffness of 1600 kip-ft/rad
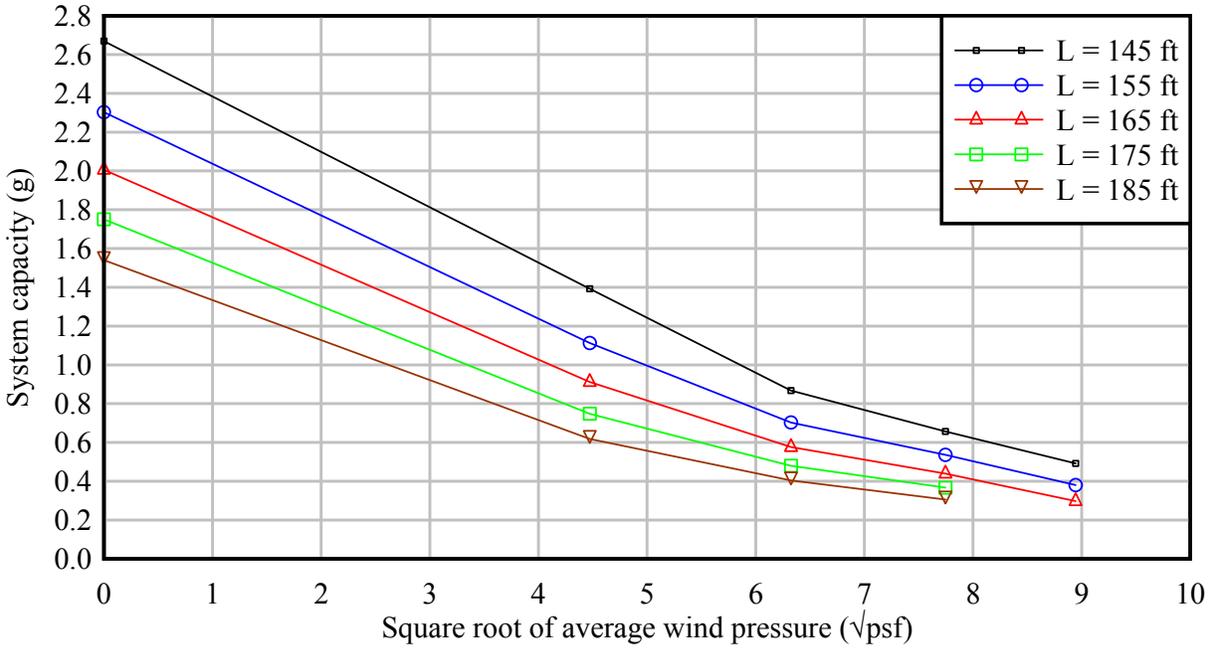
Figure 9.13. Approximate linear relationship between system capacity and square root of average wind pressure (shown for 78″ 2-FIB system with anchor stiffness of 1600 kip-ft/rad)

The wind pressure coefficients, m_w, thus computed, were found to be nonlinearly correlated with both span length and average anchor stiffness. Therefore, an expression for the

wind pressure coefficient was fitted to both variables simultaneously as a quadratic surface of the form:

$$m_w = a(L)^2 + b(\bar{k}_{roll,anchor})^2 + c(L)(\bar{k}_{roll,anchor}) + d(L) + e(\bar{k}_{roll,anchor}) + f \qquad (9.8)$$

where a, b, c, d, e, and f are fitting parameters. When multivariate least squares regression was performed, the parameters b and e were found to be negligibly small and so those terms were omitted and the remaining terms were adjusted such that more than 95% of the results were conservatively predicted by the final surface fit (Figure 9.14), which was:

$$m_w = \frac{\left(-L^2 + 0.01L\bar{k}_{roll,anchor} + 405L - 50,000\right)}{37,000} \qquad (9.9)$$

where m_w is in g/($\sqrt{\text{psf}}$), L is the span length in ft, and $\bar{k}_{roll,anchor}$ is the anchor roll stiffness in kip-ft/rad. Incorporating Equations 9.9 and 9.7 into Equation 9.6 yields the system buckling capacity equation:

$$C = C_0 + \bar{k}_{roll,anchor}\frac{100 - D}{125,000} - \frac{\sqrt{\bar{P}}}{37,000}\left(L^2 - 405L - 0.01L\bar{k}_{roll,anchor} + 50,000\right) \qquad (9.10)$$

where C is in g, L is the span length in ft, D is the FIB cross-section depth in in., $\bar{P}$ is the average wind load per girder in psf, $\bar{k}_{roll,anchor}$ is the average anchor roll stiffness per girder in kip-ft/rad and C_0 is calculated using Equation 9.2 and is in g.

119
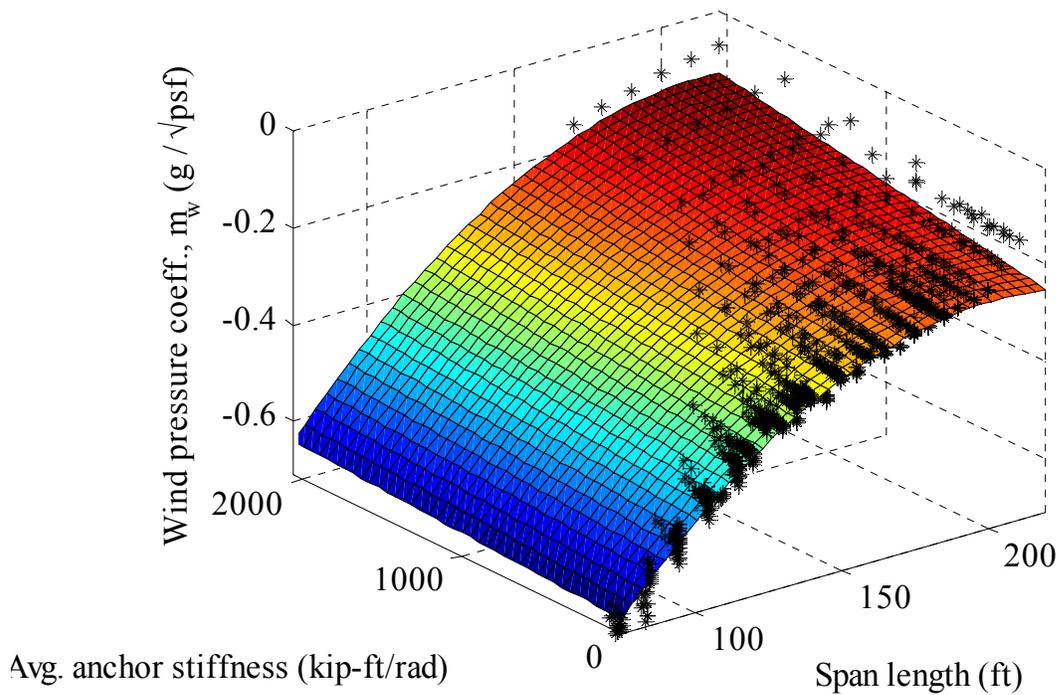
Figure 9.14. Quadratic surface (Equation 9.9) fitted to wind pressure coefficient values

Once the parametric study data set was expanded to include cases with non-zero wind, relative error ceased to be a useful metric for evaluating the accuracy of the system capacity prediction equation. This is because a large number of the cases had buckling capacity values at or near 0, where relative error is ill-defined. However, the distribution of absolute error in predicted buckling capacity (Figure 9.15) shows that Equation 9.10 conservatively predicts the system capacity in more than 95% of cases. Plots illustrating the conservatism of Equation 9.10 relative to the parametric study results for selected cases are available in Appendix E.
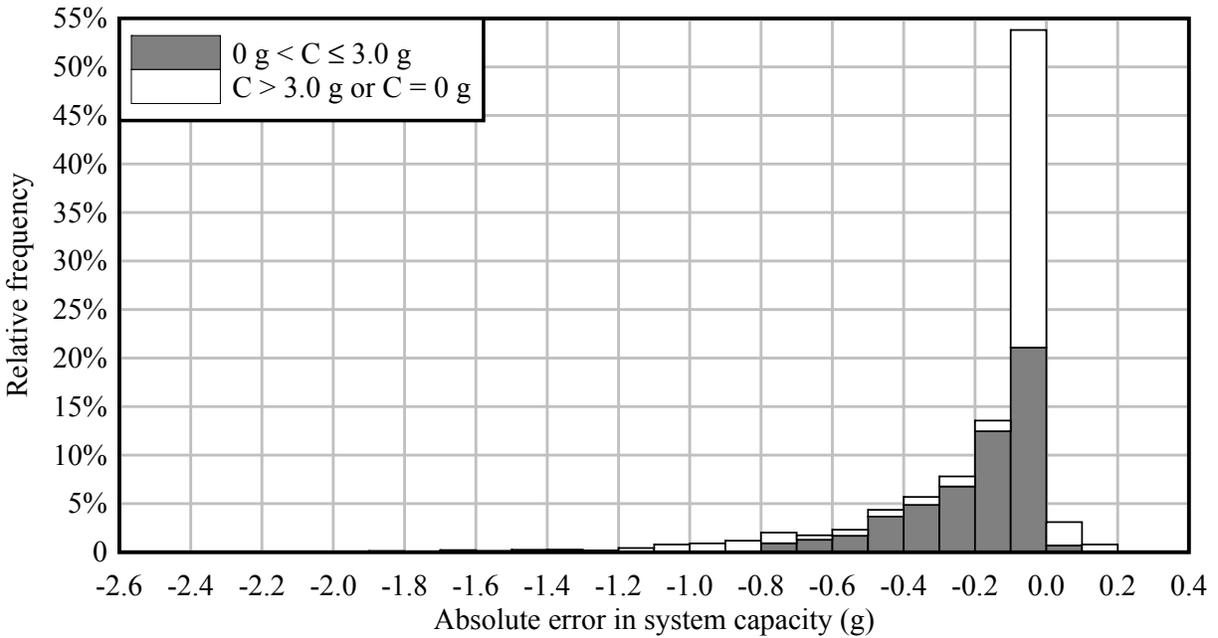
Figure 9.15. Absolute error of system capacity values predicted by Equation 9.10

9.4.5 Consideration of skew

Inclusion of skew effects was found to reduce computed system capacities by as much as 30–40% for large skew angles. However, it was also determined that, as long as the average wind pressure per girder, $\bar{P}$, calculated using Equation 9.7, was based on skew-modified wind loads calculated using Equation 9.1, the error distribution for Equation 9.10 was not significantly altered by inclusion of skew (Figure 9.16). Approximately 8% of all predictions, including cases with severe skew angles (those approaching 50°), were unconservative. An unconservative prediction rate of 8%, which was larger than the previously targeted 5% criterion, was considered acceptable in this situation given that the distribution of bridge skew angles is biased toward smaller, rather than larger, skew angles. For this reason, and for the sake of simplicity no further modifications were made to Equation 9.10 to account for the effects of bridge skew.
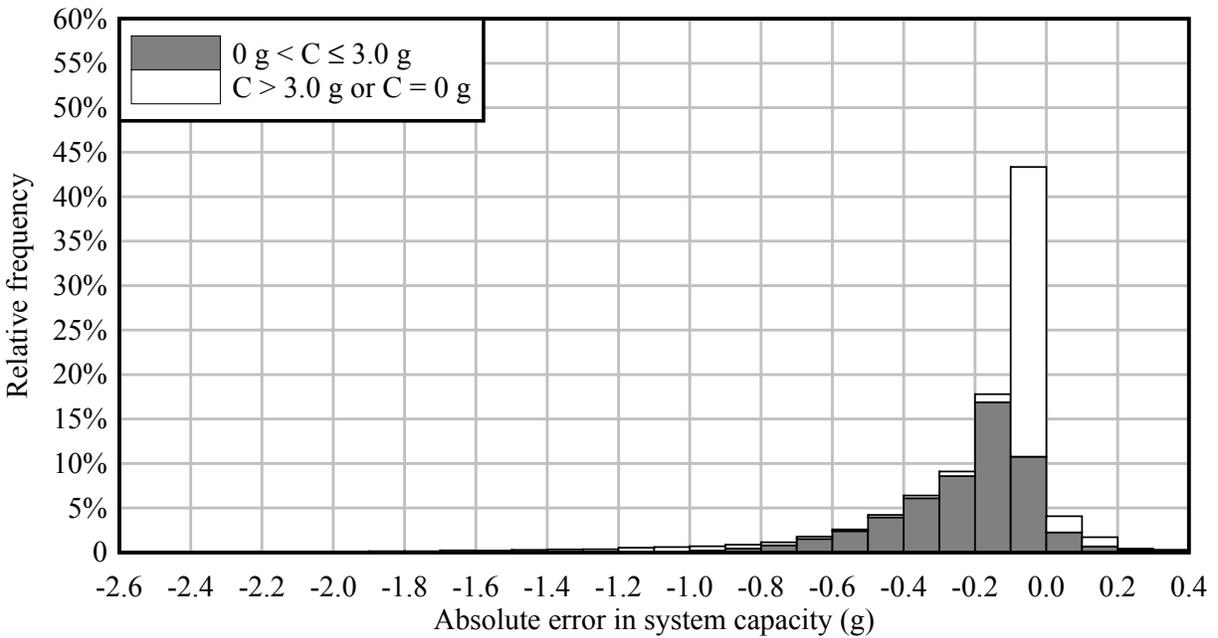
Figure 9.16. Absolute error of system capacity values predicted by Equation 9.10 for strut-braced systems, including systems with non-zero skew angles

9.5 Stiffness of moment-resisting braces

In order for the results of the parametric studies to be as widely applicable as possible, it was necessary to define an effective brace stiffness (k_{eff}): a single numerical value describing the stability contribution of a moment-resisting brace that can be computed for any brace configuration. Ideally, all braces configurations with the same k_{eff} would be interchangeable (like strut braces). Unfortunately, in practice, the best that could be achieved was a strong correlation between k_{eff} and system capacity. To evaluate potential brace stiffness definitions, an inventory of brace configurations was developed from fifteen (15) different X- and K-brace designs (Figure 9.17). Each design was implemented at three (3) different FIB depths (54, 78 and 96 in.) and at three (3) different girder spacings (6, 10, and 14 ft) for a total of 135 unique brace configurations in the inventory.

122
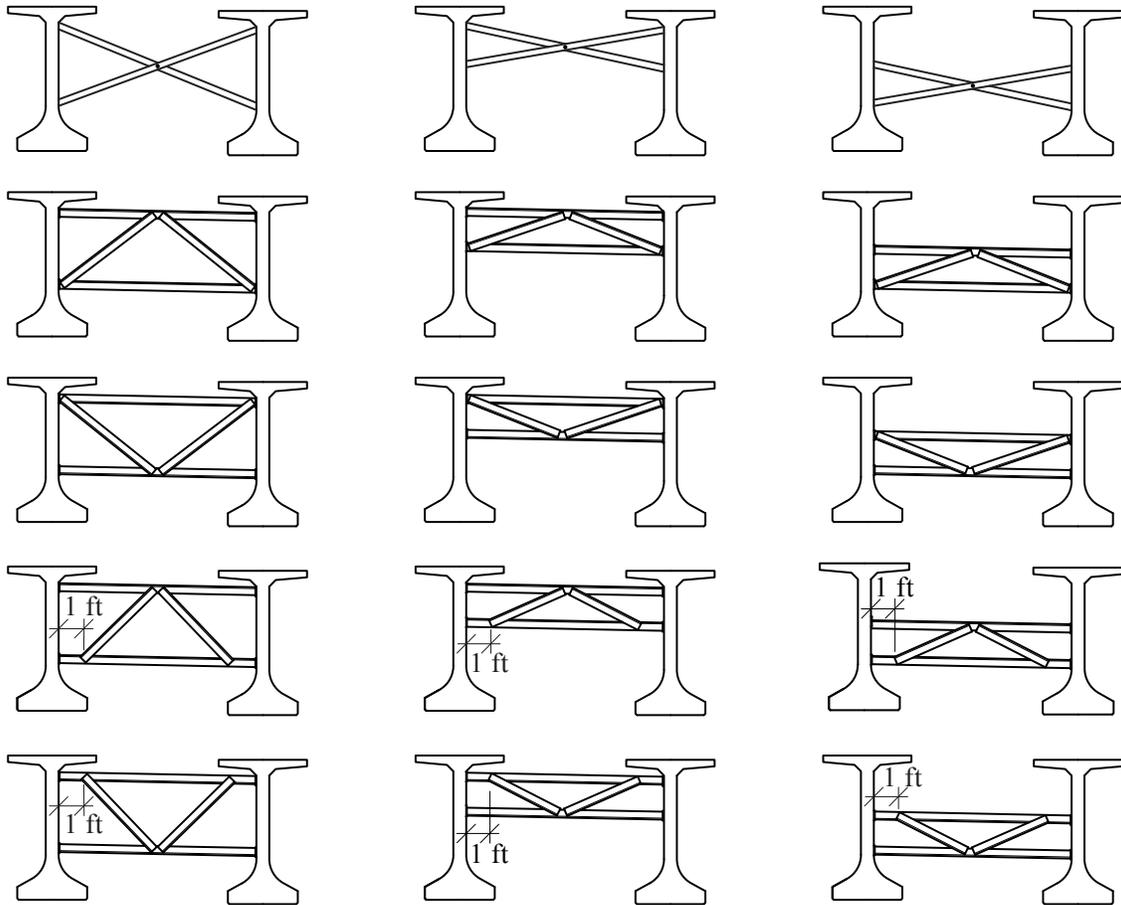
Figure 9.17 Brace designs in brace inventory (each implemented at three different spacings and three different FIB depths)

The effectiveness of each potential definition of k_{eff} was tested by adjusting the elastic moduli of all brace configurations in the inventory such that the braces all had the same computed k_{eff}. A limited-scope parametric study was then performed for each brace configuration and the resulting capacity values were compared to determine how close to equal they were. After testing several potential definitions of k_{eff} in this manner, the best correlation between k_{eff} and system capacity was obtained from the use of a rotational stiffness computed using a simplified brace model (Figure 9.18). The simplified model is similar to that which was proposed for evaluating brace forces (recall Chapter 5), but with ideal pins at the girder connection points and with a unit torque load applied at the girder center of rotation.
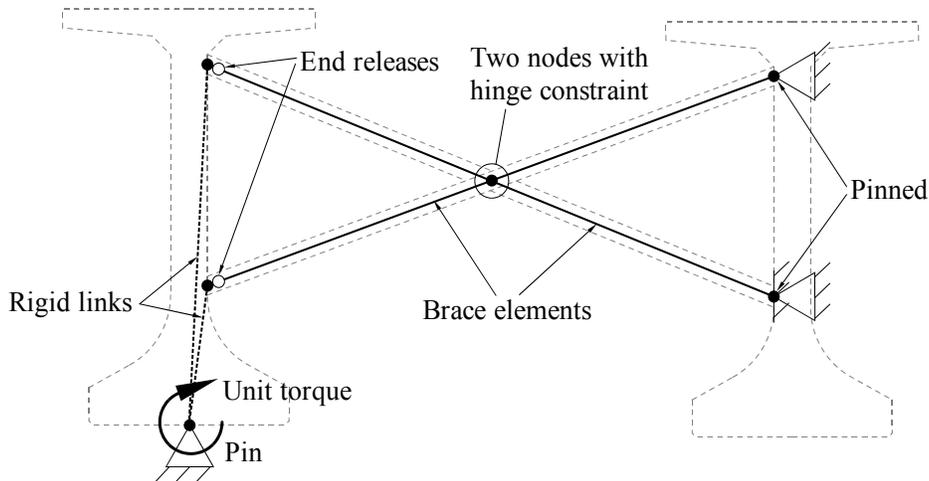
Figure 9.18 Model used to compute effective stiffness of brace configurations
(X-brace shown)

In the parametric study for systems with moment-resisting braces (discussed later in this chapter), k_{brace} was the only parameter related to the structural configuration of the braces that was varied. As a result, k_{brace} was the only such parameter included in the proposed system capacity prediction equation that was developed using the results of that study. It is intended that practicing engineers will create a structural model of the type shown in Figure 9.18 to evaluate k_{brace} for a potential brace design, and then use the resulting k_{brace} in the capacity prediction equation to evaluate the stability of the system. However, because k_{brace} is not a perfect predictor of system capacity, it is probable that different brace configurations having the same value of k_{brace} might result in structural systems that have somewhat differing capacities, even though the proposed equation would predict identical capacities. These differences in capacity (termed *ancillary effects*) are attributed to the involvement of brace deformation modes that are not perfectly represented by the simplified brace model (used to compute k_{brace}), and to changes in brace geometry that occur as the system deforms. (Note that both of these phenomena were included in the large-displacement numerical analyses of system capacity that were performed in the parametric studies).

To separate the ancillary effects from effects attributable to k_{brace}, a single structural configuration of brace was sought for use throughout the moment-resisting brace parametric study, with different values of k_{brace} achieved by altering the elastic modulus of the brace members. This *reference brace* configuration was chosen from the brace inventory using the results of the *limited-scope* bracing parametric study. Every brace in the limited-scope bracing study was adjusted (by calibration of material properties) to have the same value of k_{brace}, so that differences in capacity between otherwise identical systems were a reflection only of the ancillary effects. Relative differences in capacity were then evaluated for every combination of brace design (Figure 9.17) and girder spacing. The combination that produced the lowest capacity on average, which turned out to be a K-brace at 6-ft girder spacing (Figure 9.19), was then selected as the reference brace. Consequently, an arbitrary brace configuration designed by a practicing engineer is likely to have ancillary effects that only *increase* the capacity of the system relative to the reference brace used in this study, and the capacity of the system predicted

by the equations developed in this study is therefore likely to be conservatively low. In all subsequent parametric studies discussed in this chapter, different values of k_{brace} were achieved by altering the elastic modulus of the brace members in the reference brace shown in Figure 9.19.
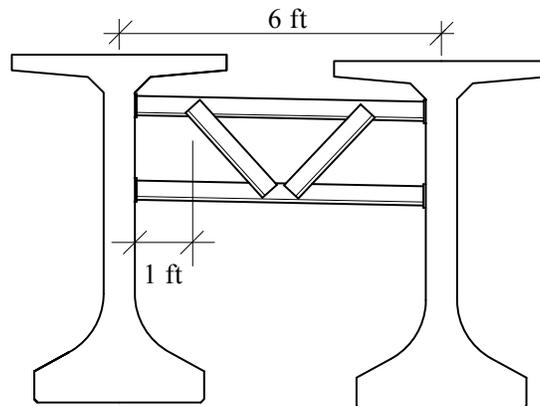
Figure 9.19. Reference brace configuration used in parametric studies

9.6 Selection of parameters for moment-resisting brace parametric study

System parameters that were varied in the moment-resisting brace parametric study were as follows:

- FIB cross-section depth (in)
- Span length (ft)
- Wind pressure (psf)
- Effective brace stiffness (kip-ft/rad)
- Number of interior brace points
- Skew angle (deg)

Seven (7) of the eight (8) standard FIB cross-sections were included in the study. (The 36″ FIB was excluded because the cross-section (Figure 9.20) is so shallow that usage of moment-resisting braces is unwarranted and unfeasible.) For each FIB, capacity analyses were performed for every combination of span length, wind pressure, effective brace stiffnesses, and number of interior brace points sampled from the values listed in Table 9.3, for a total of 17,760 analyses. This study only considered two-girder systems because it was determined from sensitivity studies that when moment-resisting braces are used, the two-girder system is always the least stable phase of construction.
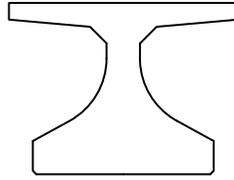
Figure 9.20. Cross-section of 36″ FIB

Table 9.3 Parameter values used in moment-resisting brace parametric study

Span length, *L* (ft)						
45″ FIB	54″ FIB	63″ FIB	72″ FIB	78″ FIB	84″ FIB	96″ FIB
95	110	120	135	145	155	170
105	120	130	145	155	165	180
115	130	140	155	165	175	190
125	140	150	165	175	185	200
135	150	160	175	185	195	205
-	-	-	185	-	-	220

Unshielded wind pressure, P_U (psf)	Eff. brace stiffness, k_{brace} (kip-ft/rad)	Int. brace points, n_i	Skew angle
0	15,000	0	0°
40	200,000	1	2°
80	400,000	2	5°
120	600,000	3	10°
160			25°
			50°

Span lengths, skew angles, and wind pressure values were identical to those used in the strut brace parametric study, while the number of interior brace points varied from 0 (end bracing only) to 3 (end bracing with quarter-point interior bracing). As in the strut brace study, the girders in each system model were spaced at 6 ft on center (because the reference brace configuration was 6 ft wide). For systems with moment-resisting braces, changes in girder spacing produce changes in the geometric configuration of the brace members, thus changing the effective stiffness of the braces. Such changes can significantly affect system capacity and must be considered. In the moment-resisting brace parametric study, the effects of changing girder spacing were accounted for by varying the effective brace stiffness parameter, even though the physical length of the reference brace remained a constant 6 ft.

Effective brace stiffness values were selected using the brace inventory. Effective stiffness was computed for each brace (Figure 9.21) using the unadjusted material properties of timber and steel and stiffness values of 200,000, 400,000, and 600,000 kip-ft/rad were selected to cover the range of representative values. However, the spread of values in Figure 9.21 corresponds primarily to the K-braces, with all but one of the X-brace stiffnesses confined to the leftmost column. When examining the distribution of k_{eff} for X-braces alone (Figure 9.22), it is clear that they are clustered at a much lower stiffness range. Therefore, to ensure adequate

126

coverage for X-braces, an additional representative value of 15,000 kip-ft/rad was chosen as the fourth value.
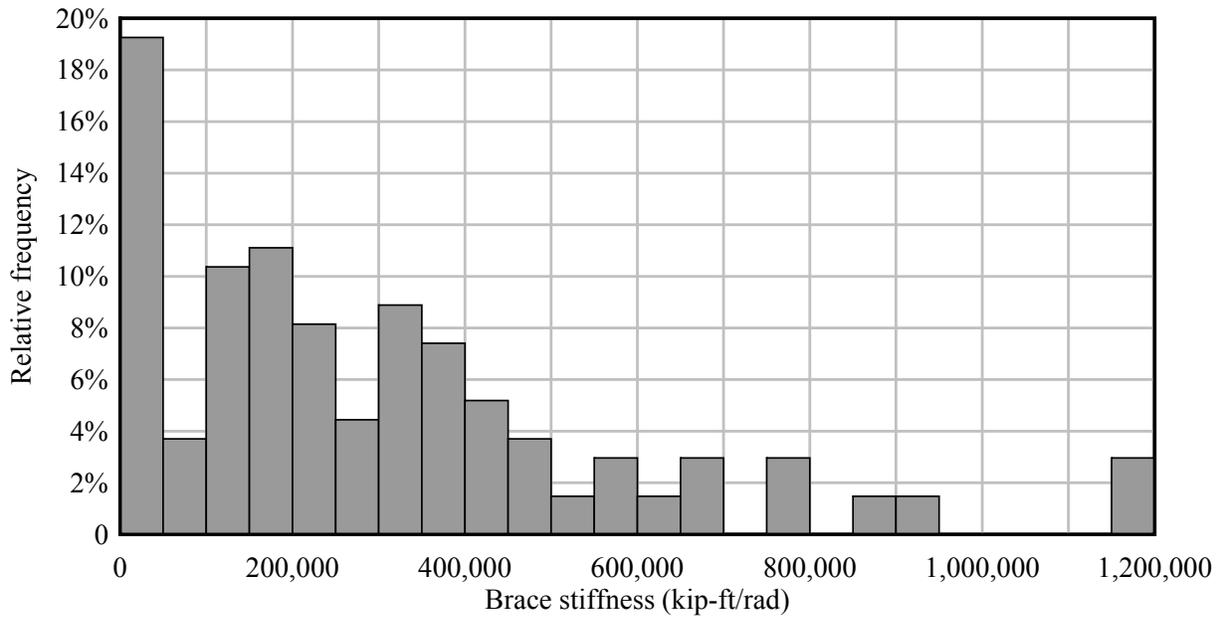
Figure 9.21 Stiffness of every brace in brace inventory
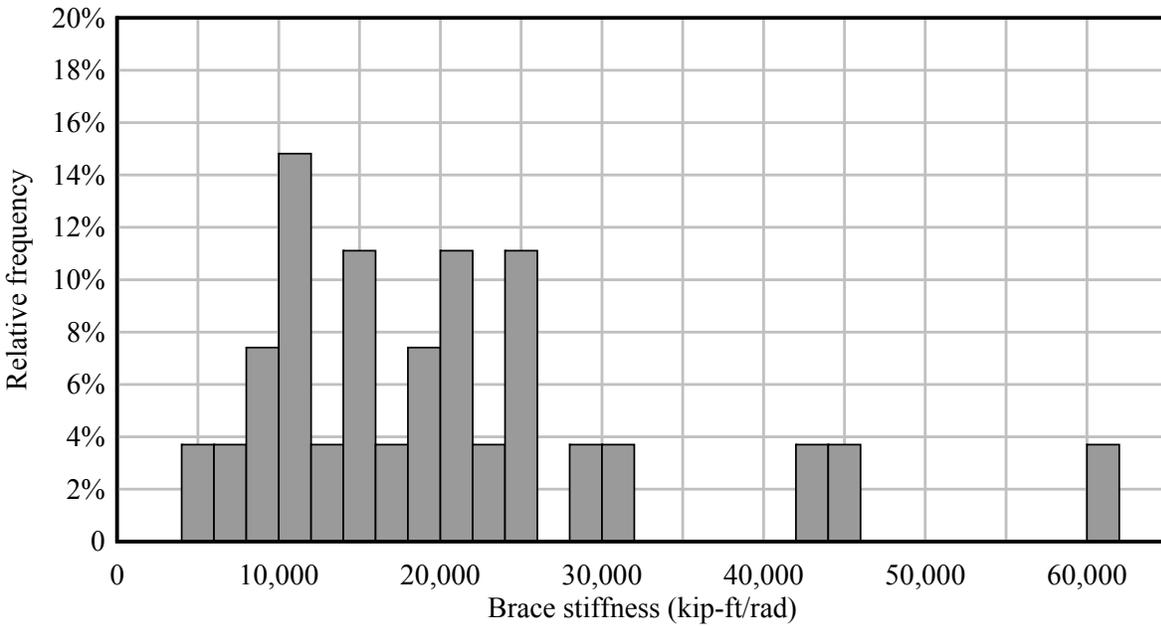
Figure 9.22 Stiffness of every X-brace in brace inventory

9.7 Results of moment-resisting brace parametric study

Results from the moment-resisting brace parametric study are summarized in Figure 9.23. As with the earlier summary of strut brace parametric study results (Figure 9.5), the results shown in Figure 9.23 are divided into five (5) main groups representing the different wind pressures, then subgroups for the different cross-sections and span lengths. The subgroups are less visually distinctive in Figure 9.23 than in Figure 9.5 because in moment-resisting brace cases, the effective brace stiffness has a much greater influence on the system capacity than does the anchor stiffness or the number of girders.

128
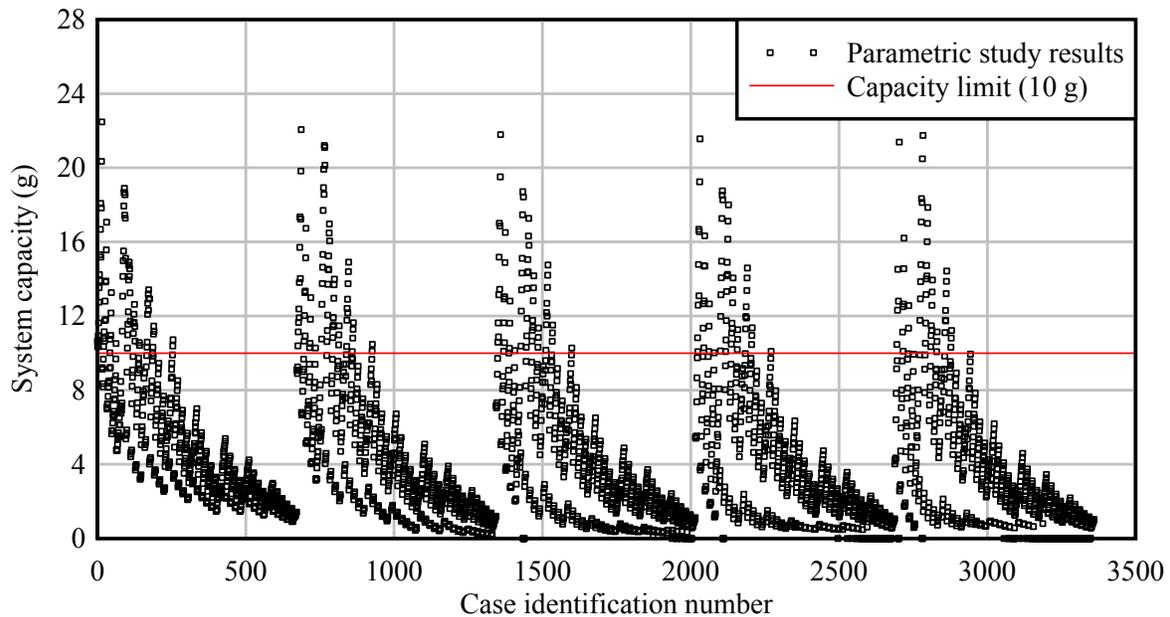
Figure 9.23. Summary of moment-resisting brace parametric study results

In order to develop a capacity prediction equation for moment-resisting braced systems, it was useful to establish a baseline capacity (C_0) to which correction factors could be added to account for the effects of bracing stiffness and wind pressure. However, it would have been illogical to include systems with zero (0) effective brace stiffness in the study, because this would have been equivalent to simultaneously analyzing two individual (structurally independent) girders. Instead, a system with zero effective brace stiffness was defined as being strut-braced, so that the girders were structurally connected but no moment resistance was provided. Therefore, data points from Figure 9.6 were included in the interpretation of the moment-resisting brace study results, and Equation 9.2 was used as the baseline of the capacity prediction equation.

All cases for which the capacity exceeded 10 g were excluded from consideration because the behavior of such systems did not exhibit meaningful lateral instability. Aside from this change, the same criteria were used in developing the capacity prediction equation as were used for the strut-braced study: conservative capacity predictions in 95% of cases, with the unconservative cases not in error by more than 5%.

9.7.1 System capacity increase from inclusion of moment-resisting end braces

Inclusion of moment-resisting braces at the girder ends increases the capacity of the system, however, as the effective stiffness of the end braces increases, the additional stability produced diminishes in magnitude, resulting in capacity vs. effective brace stiffness curves that tend to plateau (Figure 9.24). It was determined that the functional form that was the closest fit to this behavior was a rectangular hyperbola:

$$y = \frac{\beta x}{\alpha + x} \tag{9.11}$$

where α and β are fitting parameters. To represent the *increase* in capacity from the baseline value (C_0), each effective brace stiffness curve (corresponding to a unique combination of FIB depth and span length), was translated vertically so that it passed through the origin. A rectangular hyperbola was then fitted (using regression) to each translated curve, producing an α and a β value.
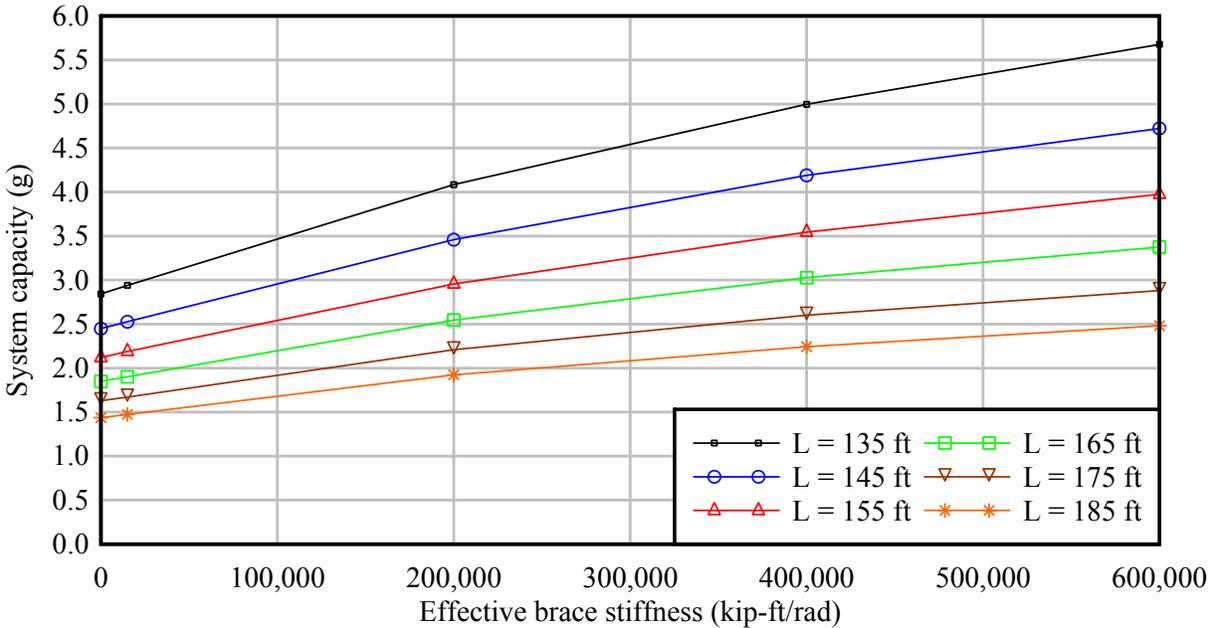
Figure 9.24. Effect of effective brace stiffness on capacity of 96″ 2-FIB system

The distribution of α values in the data set exhibited no particular trends, so a constant value of 1,000,000 (the mean value of α, rounded off) was selected. However, the β term showed a clear dependence on span length, so an exponential regression fit (Figure 9.25) was performed, resulting in the expression:

$$\beta = 620e^{\frac{-L}{30}} \qquad (9.12)$$

where L is the span length in ft. The constant value of 1,000,000 for α and Equations 9.12 and 9.11 were incorporated together to form the capacity prediction equation:

$$C = C_0 + \frac{620k_{brace}e^{\frac{-L}{30}}}{k_{brace} + 1,000,000} \qquad (9.13)$$

where C is in g, k_{brace} is the effective moment-resisting brace stiffness in kip-ft/rad, C_0 is calculated using Equation 9.2 and is in g, and L is in ft. Equation 9.13 meets the 95% criterion for conservative capacity prediction.
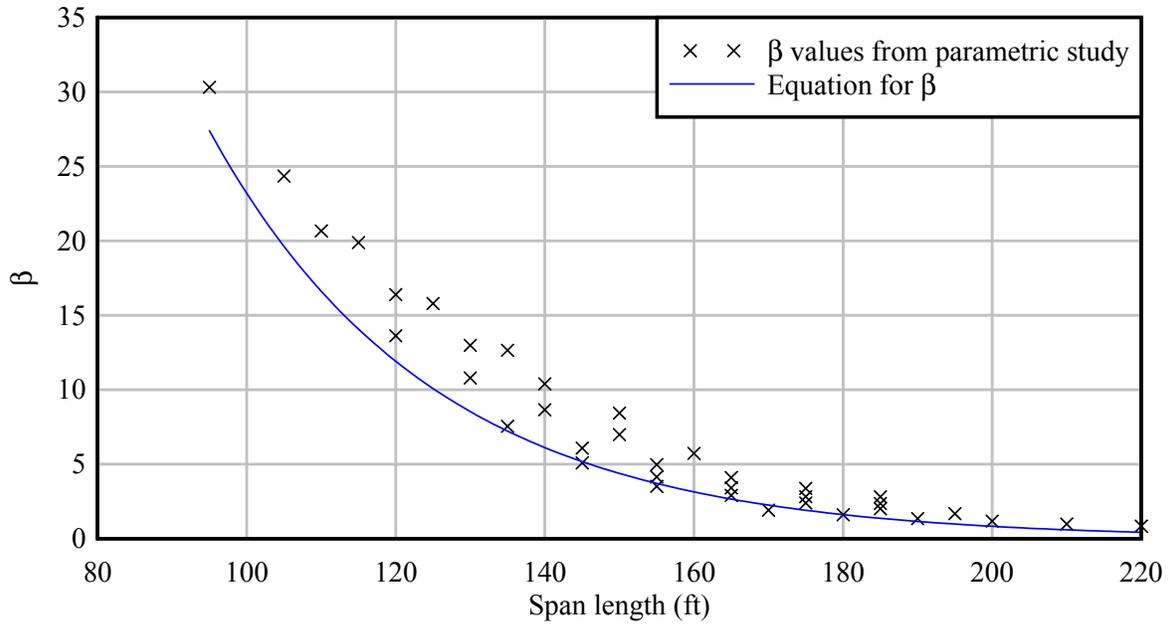
Figure 9.25. Equation 9.12 (β) compared to parametric study results
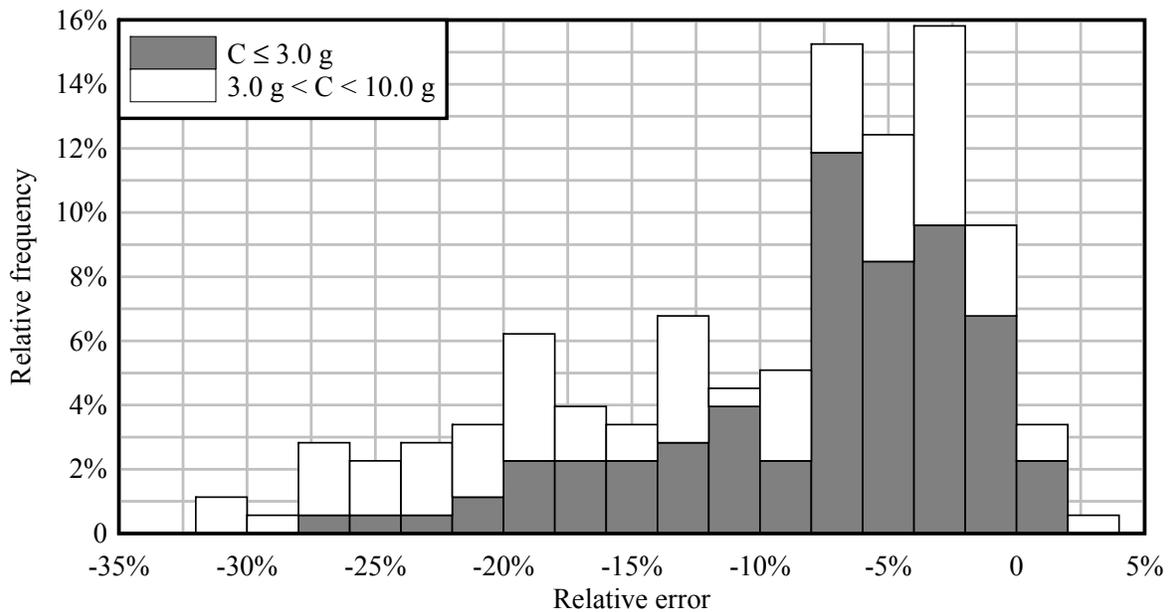
Figure 9.26. Relative error of system capacity values predicted by Equation 9.13
(Note: negative relative error indicates conservative prediction of capacity)

9.7.2 System capacity increase from installation of braces at interior points

If braces are installed at interior points (in addition to braces at the girder ends), the additional brace stiffness increases the overall system capacity. However, the *incremental* increase in system capacity that is achieved by the addition of each new interior brace diminishes. For example, the additional stability provided by a midpoint brace is greater than the

additional stability provided by replacing the midpoint brace with two (2) third-point braces (all else being equal). However, there were no clearly observable trends between the number of interior brace points (denoted n_i) and the system capacity that could be quantitatively related to the geometric parameters the system. Therefore the effect of interior braces was accounted for by introducing an empirically-determined scale factor, ω, into the brace stiffness term in the capacity prediction equation:

$$C = C_0 + \omega \frac{620 k_{brace} e^{\frac{-L}{30}}}{k_{brace} + 1,000,000} \tag{9.14}$$

where C and C_0 are in g, L is the span length in ft, k_{brace} is the effective brace stiffness in kip-ft/rad, and ω is a dimensionless scale factor that is equal to 1 when n_i is 0.

To determine appropriate values of ω for $n_i > 0$, three subsets of the parametric study results data were produced, corresponding to the non-zero values of n_i (1, 2, and 3). The subsets were restricted to cases where $C < 3.0$ g, to ensure that each subset was representative of the types of systems pertinent to this study. For each subset, a maximum value of ω was determined (through trial and error), such that more than 95% the capacity values predicted by Equation 9.14 were conservative. Those values of ω were then reduced by approximately the same proportion until 95% conservatism was achieved over the *full* data set (Figure 9.27), including those cases where $C \geq 3.0$ g. Final ω values for use in the capacity prediction equation are listed in Table 9.4.

Table 9.4 Empirically-determined values of ω for different numbers of interior braces

n_i	Brace locations	ω
0	End bracing	1.0
1	Midpoint bracing	1.4
2	Third-point bracing	1.6
3	Quarter-point bracing	1.7
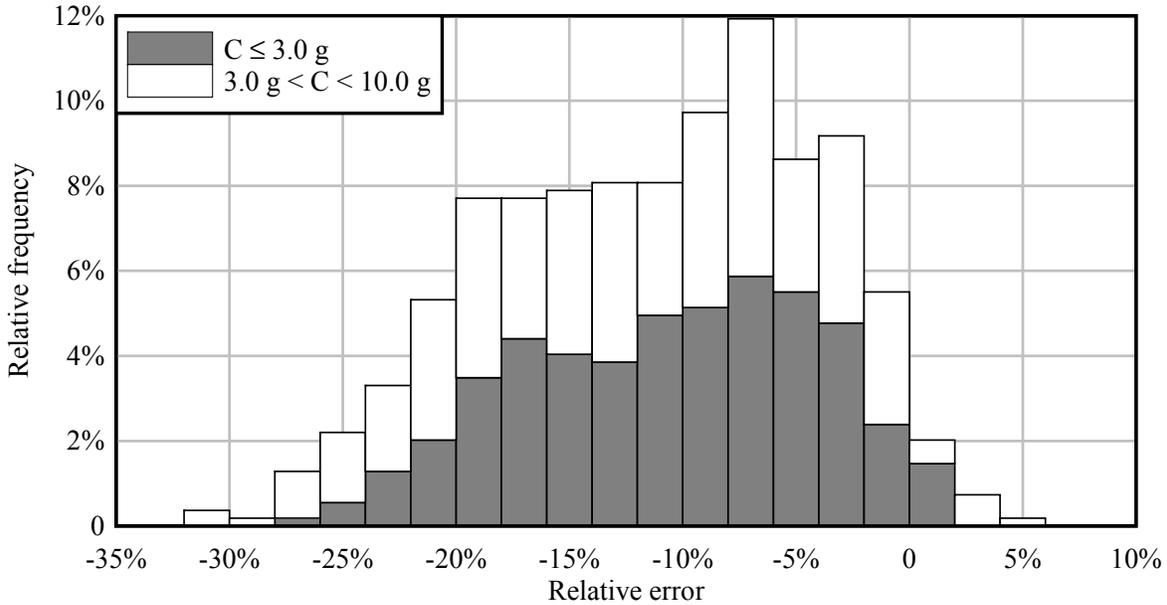
Figure 9.27. Relative error of system capacity values predicted by Equation 9.14

9.7.3 System capacity reduction from inclusion of wind load

The process by which the effect of average wind pressure, $\bar{P}$, on system capacity, C, was interpreted and predicted for moment-resisting braced systems was very similar to that used for the strut-braced systems (recall Section 9.4.4). As in the case of strut-braced systems, a linear relationship (Figure 9.28) was observed for moment-resisting braced systems between the square root of average wind pressure ($\sqrt{\bar{P}}$) and system capacity, and the corresponding slope was defined as the wind pressure coefficient (m_w). For moment-resisting braced systems in which the effective brace stiffness was small, the relationship between C and $\bar{P}$ was not as linear as it was in strut-braced systems, but for the sake of consistency, the assumption of linearity was considered an acceptable approximation.

133
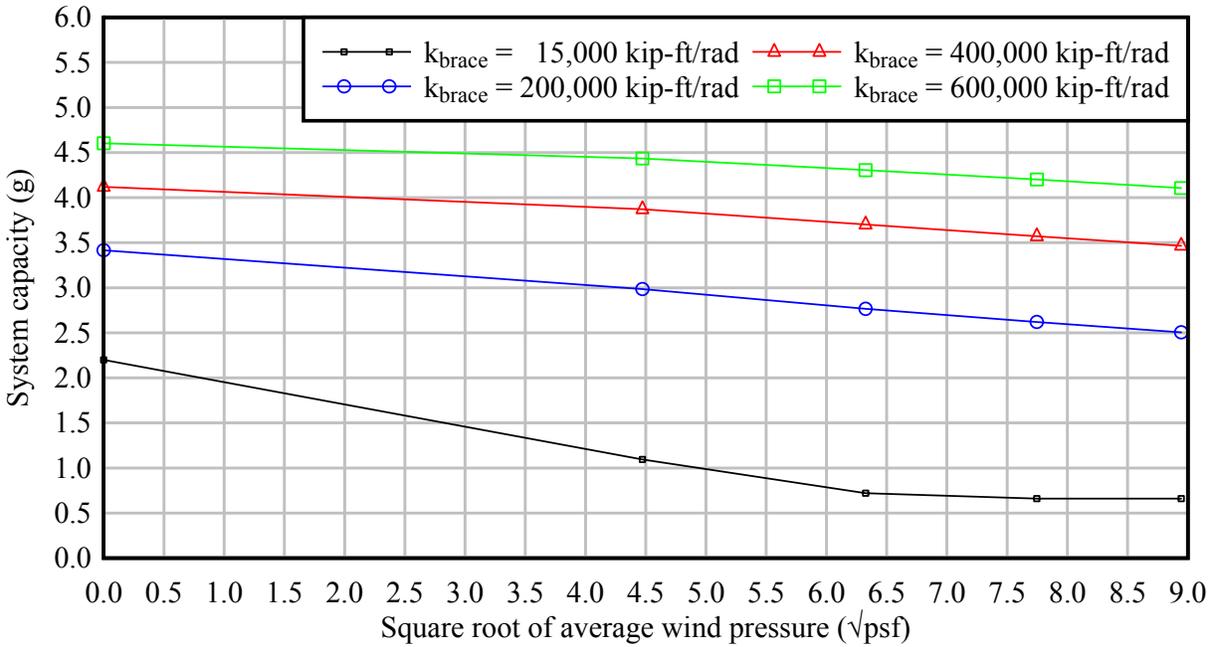
Figure 9.28. Approximate linear relationship between system capacity and square root of average wind pressure (Data shown are for 160-ft, 63″ 2-FIB systems with third-point bracing)

Linear regressions were performed to determine values of m_w for every unique combination of FIB depth, span length, effective brace stiffness, and number of interior brace points (n_i). The resulting values of m_w were observed to vary nonlinearly with both span length and effective brace stiffness, so a quadratic surface was fitted to both variables simultaneously, in the form:

$$m_w = a(L)^2 + b(k_{brace})^2 + c(L)(k_{brace}) + d(L) + e(k_{brace}) + f \qquad (9.15)$$

where a, b, c, d, e, and f are fitting parameters. In the resulting equation, the b parameter was found to be negligibly small, so it was discarded and the remaining parameters were adjusted such that system capacities were predicted conservatively in 95% of cases. The final curve fit (Figure 9.29) was:

$$m_w = \frac{\left(-8L^2 + 0.004Lk_{brace} + 5100L + k_{brace} - 900,000\right)}{1,000,000} \qquad (9.16)$$

where m_w is in g/($\sqrt{\text{psf}}$), L is the span length in ft, and k_{brace} is the effective brace stiffness in kip-ft/rad.

134
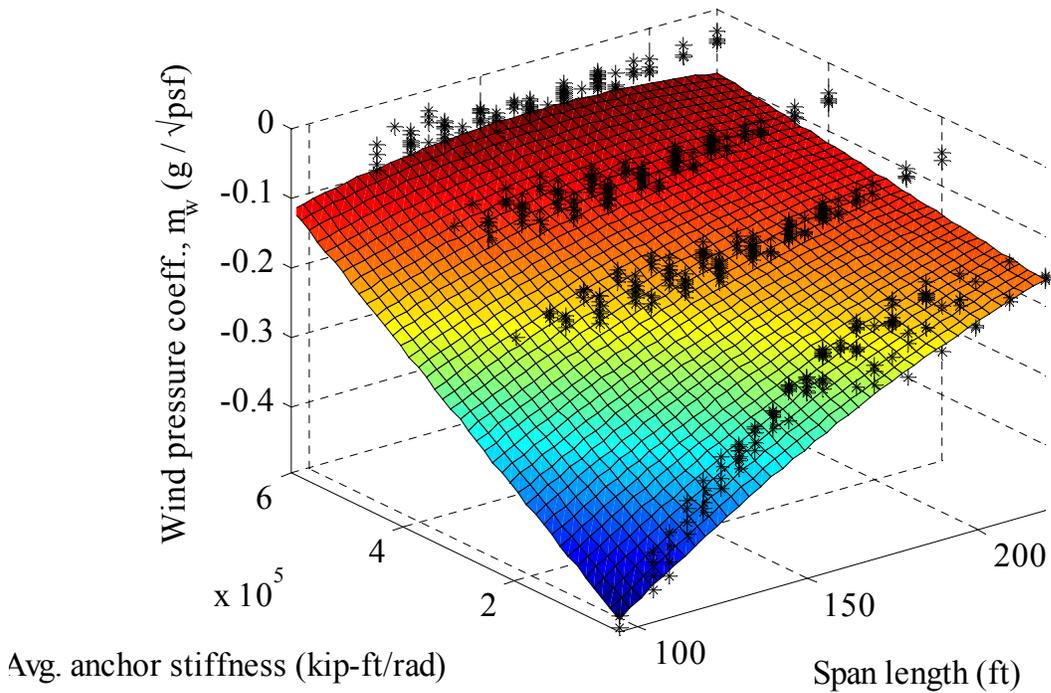
Figure 9.29. Quadratic surface (Equation 9.16) fitted to wind pressure coefficient values and adjusted to produce conservative results in 95% of cases

Equation 9.16 was incorporated into Equation 9.14 to produce the final capacity prediction equation for moment-resisting braced systems:

$$C = C_0 + \omega \frac{620 k_{brace} e^{\frac{-L}{30}}}{k_{brace} + 1,000,000} - \frac{\sqrt{\bar{P}}}{1,000,000} \left(8L^2 + 0.004 L k_{brace} - 5100L - k_{brace} + 900,000 \right) \tag{9.17}$$

where C is the system capacity in g, L is the span length in ft, D is the FIB cross-section depth in in., $\bar{P}$ is the average wind load per girder (calculated using Equation 9.7) in psf, k_{brace} is the is the the effective brace stiffness in kip-ft/rad, ω is determined from Table 9.4, and C_0 (calculated using Equation 9.2) is in g. As shown in the distribution of absolute prediction error (Figure 9.30), Equation 9.17 conservatively predicts the system capacity of a moment-resisting braced system in over 95% of cases. Plots illustrating the conservatism of Equation 9.17 relative to the parametric study results for selected cases are available in Appendix E.
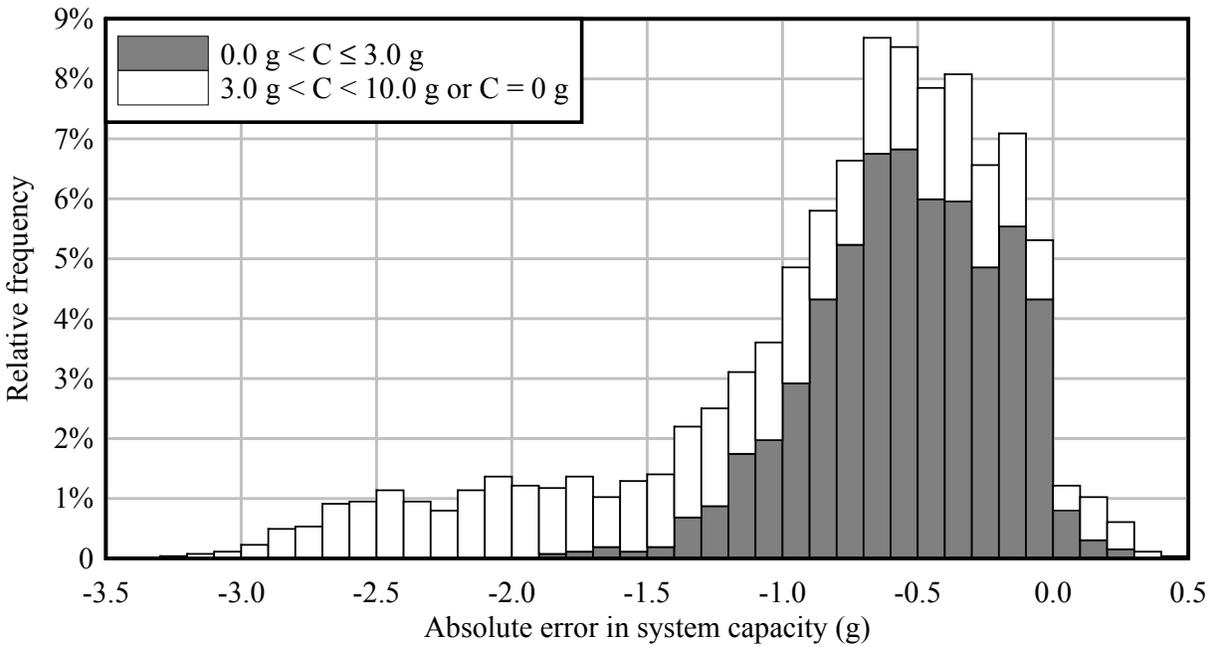
Figure 9.30. Absolute error of system capacity values predicted by Equation 9.17 for moment-resisting braced systems

9.7.4 Consideration of skew

For moment-resisting braced systems, it was found that Equation 9.17 predicted the capacity of skewed systems with approximately the same accuracy as was achieved for unskewed systems (Figure 9.31). Conservative capacity predictions were obtained in approximately 92% of cases (i.e., approximately 8% of cases were unconservative). Therefore, for the same reasons that were described in earlier in Section 9.4.5 (for strut-braced systems), no further modifications were made to Equation 9.17 to account for the effects of bridge skew.
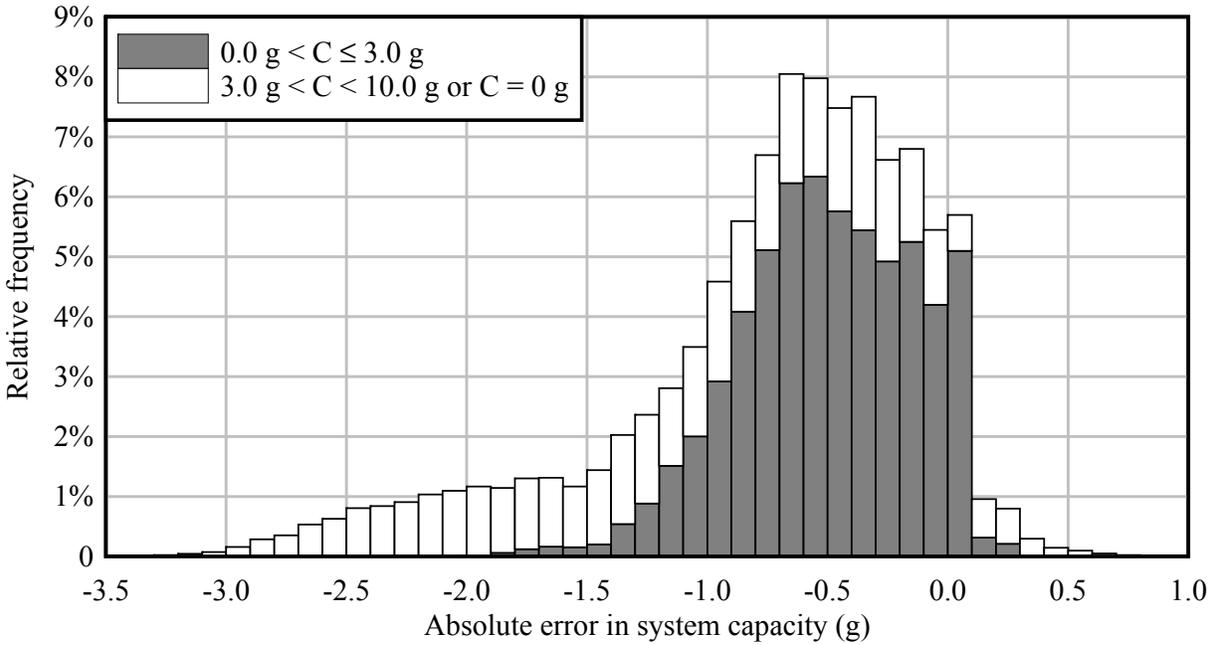
Figure 9.31. Absolute error of system capacity values predicted by Equation 9.17 for moment-resisting braced systems, including systems with non-zero skew angles

9.8 Incorporation of aerodynamic lift

In addition to horizontal wind pressure (drag), FIBs subjected to wind flow can also experience vertical lift forces and torques. As discussed in Chapter 5, the drag coefficient (C_D) can be modified to include the structural demand associated with aerodynamic torque to form an effective drag coefficient ($C_{D,eff}$) that represents both drag and torque. However, lift cannot be accommodated in the same manner and must be accounted for separately. Because lift acts along the same vertical axis as gravity, it directly affects system capacity by either cancelling out (offsetting) a portion of the girder self-weight (positive lift; increased system capacity), or by adding to the total downward load on the girders (negative lift; decreased system capacity). If lift force is expressed as an equivalent load acting on the girder (in units of g), in can be either directly added to or subtracted from the system capacity.

Recall from Figure 5.11 that FIBs can have lift coefficients (C_L) as large as ±0.5. For conservatism, it was deemed necessary to assume that every girder in the system might have a C_L of −0.5 (i.e., a force acting in the downward direction, reducing the system capacity). Recalling concepts introduced in Chapter 3, the force coefficient Equation (3.6) can be rearranged and applied both to drag force (F'_D) and lift force (F'_L) as:

$$F_L' = C_L qD$$
$$F_D' = C_D qD$$

(9.18)

137

where $q = \left(\frac{1}{2}\right)\rho V^2$ [as was defined in Equation 3.1], and both F'_D and F'_L are proportional to their respective coefficients (C_L and C_D) by the same proportionality factor (qD). It follows therefore that:

$$F'_L = \frac{C_L}{C_D} F'_D \qquad (9.19)$$

The drag force, F'_D, can be expressed in terms of the system parameters as:

$$F'_D = \frac{D}{12} P_U \qquad (9.20)$$

where F'_D is in lbf/ft (force per unit length of beam), D is in inches, P_U is the unshielded wind pressure in psf, and 12 is a unit conversion factor. Substituting Equation 9.20 into Equation 9.19, employing a C_L of −0.5 (for reasons of conservatism, as noted above), and adopting a drag coefficient of $C_D = 2.0$ (based on the proposed design loads from Chapter 5), an expression for F'_L in terms of the system parameters is obtained:

$$F'_L = \left(\frac{-0.5}{2.0}\right)\frac{D}{12} P_U = -\frac{D}{48} P_U \qquad (9.21)$$

where F'_L is in lbf/ft. Note that by expressing F'_L in terms of the design wind load, any additional design factors (e.g., gust effect factor) are automatically incorporated.

F'_L can be converted into units of g by dividing it by the girder self-weight (w_{sw}) in lbf/ft. Values of w_{sw} are provided by the *Structures Design Guidelines* (FDOT, 2012e) for each of the eight FIB cross-sections (Table 9.5). Therefore, the final system capacity equation for strut-braced systems is:

$$C = C_0 + \bar{k}_{roll,anchor}\frac{100 - D}{125,000} - $$
$$\frac{\sqrt{\bar{P}}}{37,000}\left(L^2 - 405L - 0.01L\bar{k}_{roll,anchor} + 50,000\right) - \frac{D}{48}\frac{P_U}{w_{sw}} \qquad (9.22)$$

and the final system capacity equation for moment-resisting-braced systems is:

$$C = C_0 + \omega\frac{620k_{brace}e^{\frac{-L}{30}}}{k_{brace} + 1,000,000} - $$
$$\frac{\sqrt{\bar{P}}}{1,000,000}\left(8L^2 + 0.004Lk_{brace} - 5100L - k_{brace} + 900,000\right) - \frac{D}{48}\frac{P_U}{w_{sw}} \qquad (9.23)$$

where C is the system capacity in g, L is the span length in ft, D is the FIB cross-section depth in in., P_U is the unshielded wind load in psf, $\bar{P}$ is the average wind load per girder (calculated using Equation 9.7) in psf, $\bar{k}_{roll,anchor}$ is the average anchor roll stiffness per girder (calculated using

138

Equation 9.5) in kip-ft/rad, k_{brace} is the is the effective brace stiffness in kip-ft/rad, ω is determined from Table 9.4, w_{sw} is the girder self-weight in lbf/ft (from Table 9.5), and C_0 (calculated using Equation 9.2) is in g. Example calculations, demonstrating the application of the system capacity equations developed in this chapter, are presented in Appendix H.

Table 9.5 Self-weight (w_{sw}) of each FIB cross-sectional shape (from FDOT, 2012e)

Cross-section	w_{sw} (lbf/ft)
36″ FIB	840
48″ FIB	906
54″ FIB	971
63″ FIB	1037
72″ FIB	1103
78″ FIB	1146
84″ FIB	1190
96″ FIB	1278

CHAPTER 10
CONCLUSIONS AND RECOMMENDATIONS

10.1 Introduction

In this study, design issues related to wind loading and the stability of long-span braced bridge girders were investigated. Wind tunnel tests were performed to measure the aerodynamic properties (drag coefficients, lift coefficients, torque coefficients, and shielding effects) of several common cross-sectional shapes used for bridge girders. Additionally, numerical models were employed to evaluate the stability of braced systems of Florida-I Beams (FIBs) subjected to wind loads. Based on the results of these investigations, conclusions and recommendations are discussed in the sections that follow.

10.2 Drag coefficients

Drag coefficients (C_D) were measured using wind tunnel testing for five (5) different girder cross-sectional shapes (Figure 10.1) that are typical of bridge construction in the state of Florida. Considering wind angles ranging from −5° to +5°, tested drag coefficients of FIBs did not exceed 1.95, and the drag coefficients of built-up steel plate girders did not exceed 2.15. In both cases, the *Structures Design Guidelines* (SDG; FDOT, 2012e) currently conservatively overpredicts the drag coefficient by prescribing a value of 2.2. In contrast, for the open-top box girder shape, where wind angles ranging from −10° to +10° were tested, the drag coefficient did not exceed 1.95, but this value exceeds the value of 1.5 currently prescribed by the SDG.

FDOT SDG C_D = 2.2 (I-Shapes)   FDOT SDG C_D = 1.5 (Box)

Plate Girders   Florida-I Beams (FIBs)   Box Girder
$C_D \leq 2.15$ $C_D \leq 1.95$ $C_D \leq 1.95$
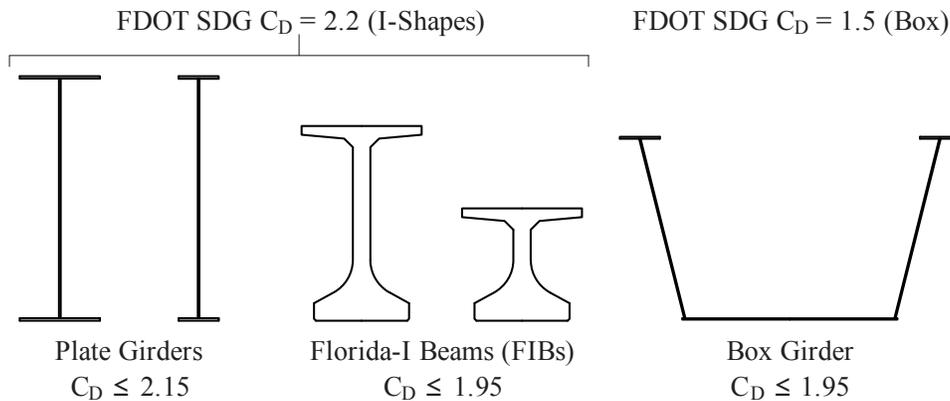
Figure 10.1 Girder cross-sectional shapes tested in the wind tunnel

Wind tunnel test results also indicated significant shielding effects when multiple adjacent girders were subjected to lateral wind. In general, the windward girder (G1) acted as a windbreak, causing the drag force on subsequent girders to be reduced sharply enough that the drag coefficient of the first shielded girder (G2) was typically negative (indicating that the drag force acted in the opposite direction, i.e., against the wind). Drag forces on shielded girders (G2, G3, etc.) tended to follow a *down-then-up* pattern: drag coefficients dropped to their most negative value at girder G2 or G3, then gradually grew more positive until a positive plateau value was reached farther down-stream. Based on the wind tunnel test results, shielding patterns

for specific bridge cross-sectional configurations could not be predicted with certainty, but were influenced by the interaction of cross-slope, wind angle, section depth, and girder spacing.

In addition to drag (horizontal) forces, it was observed that bridge girders subjected to lateral wind can also be subjected to both lift (vertical) forces and torques that are too large to be considered negligible. To address this issue, the concept of an *effective drag coefficient* ($C_{D,eff}$) was developed to envelope the combined effects of both drag and torque. The effective drag coefficient can be used in design calculations in the same manner that a standard drag coefficient is used. Unless project-specific wind tunnel test results are available, the following pressure coefficients (C_P) are recommended for systems of adjacent girders (Figure 10.2):

- Assign the windward girder (G1) an initial C_P, depending on the type of section ($C_P =$ 2.0 for FIBs, $C_P = 2.5$ for plate girders).

- Assign the first shielded girder (G2) no wind load ($C_P = 0$).

- Assign all subsequent shielded girders (G3 and greater) a C_P equal to one-half of the initial C_P that was assigned to the windward girder (G1).

These design loads are intended for use in system stability analyses, and incorporate the structural demand associated with both aerodynamic drag and aerodynamic torque.
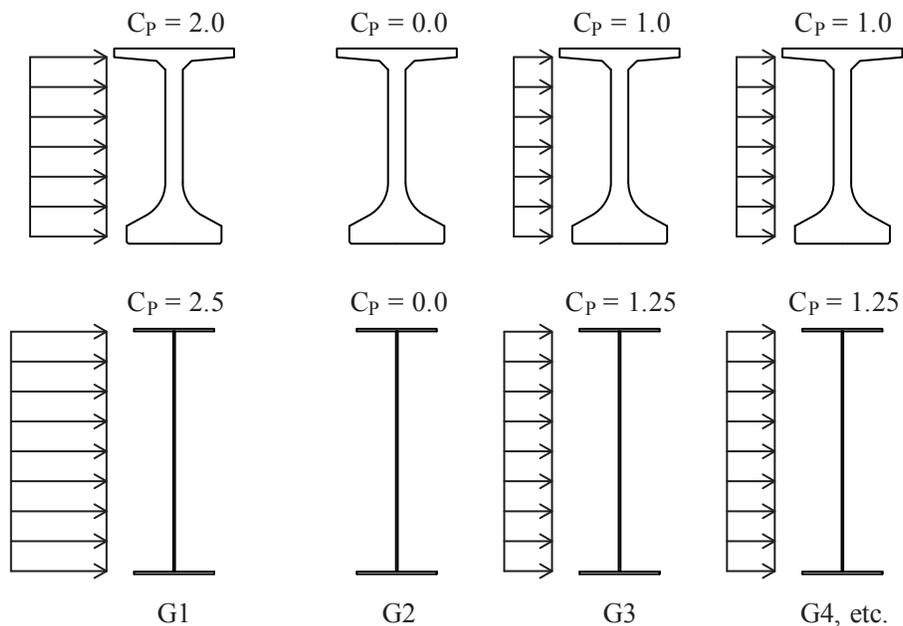
Figure 10.2 Recommended design wind loads for systems of adjacent girders

It is important to note that the wind loads that produce the greatest potential for lateral instability in a braced girder system are *not* generally the loads that produce the largest individual brace forces. Therefore, two separate wind load cases are required when designing braces to withstand both limit states. Individual brace forces are maximized when wind forces on adjacent girders act in *opposite* directions (thus compressing elements of the brace). In contrast, lateral instability is maximized when girder wind loads act together in the *same* direction to maximize the total lateral force exerted on the braced girder system.

When evaluating brace forces (as opposed to system stability), it is recommended that a C_P of 2.75 be used for FIBs and a C_P of 3.0 be used for plate girders. These coefficients approximate the maximum total compressive brace load that arises from the combination of a large positive load on the windward girder (G1) and a smaller, negative load on the first shielded girder (G2). To ensure conservative determination of brace forces, it is recommended that a structural analysis be performed on a girder and brace sub-assembly model (Figure 10.3). Required characteristics of the model include a pinned support at the base of G1, a fixed boundary conditions in place of G2, and full moment transfer (i.e., no pins or end-releases) at the brace–girder connection points. For global strength limit state evaluation, it is permissible that a reduction factor (Equation 5.18) be used in conjunction with the design loads indicated in Figure 10.2.

10.3 Individual unbraced Florida-I Beams

An investigation into the stability of individual unbraced girders supported by bearing pads, both with and without anchors in place, was a key component of this study. Numerical analysis techniques were developed to compute the *wind capacity* of such girders: i.e., the critical wind load at which a girder collapses under its own self-weight. A parametric study was performed in which the wind capacity was computed for all eight (8) FIB cross-sections at a variety of span lengths, both unanchored and with anchors of varying stiffnesses.

From the results of the parametric study, regression techniques were used to develop an empirical equation for computing the wind capacity of an unanchored girder (Chapter 8, Equation 8.2). Parametric study results were similarly used to develop a capacity modification (correction) factor to account the increase in wind capacity that is produced by the presence of an anchor of specified stiffness. Combining the unanchored girder capacity equation with the correction factor produced a generalized wind capacity prediction equation (Chapter 8, Equation 8.6) that is recommended for use in assessing the stability of individual (anchored or unanchored) Florida-I Beams (FIBs) subjected to wind loading.

10.4 Braced systems of multiple Florida-I Beams

For a collection of girders braced together into a single structural system, numerical analysis techniques were developed to compute the *system capacity* in units of g (the acceleration due to gravity), representing the total gravity load that can be applied before the system becomes unstable (collapses). Sensitivity studies were performed to evaluate the influence of a number of geometric parameters on the system capacity. From the results of the sensitivity studies, it was concluded that girder braces can be divided into two basic categories: strut braces, which merely connect the girders together with axial stiffness but without providing any overturning resistance, and moment-resisting braces, which resist girder overturning. The two categories of brace have very different effects on the capacity of a girder system.
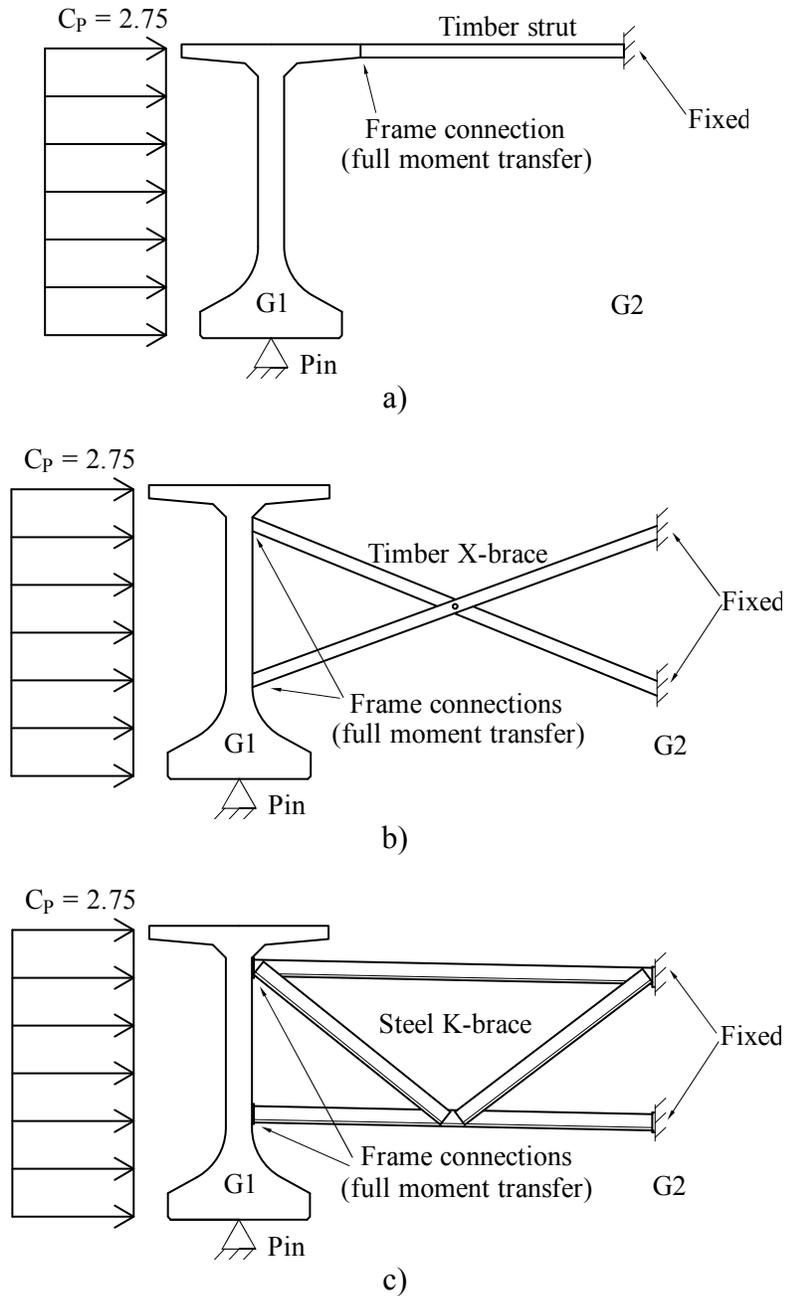
Figure 10.3 Recommended structural analysis model for use in determining brace forces:
a) Strut brace; b) X-brace; c) K-Brace

For strut-braced systems, it was determined that varying the properties of the brace members had essentially no effect on system capacity. It was also found that no significant increase in system capacity was achieved by installing braces at interior brace points in addition to the girder end points. That is, a strut-braced system with both end braces and interior braces has nearly the same capacity as a system with end braces only.

In contrast, with moment-resisting braces, the properties and geometric configuration of the brace members were found to have a very significant effect on system capacity, as was the

presence of additional moment-resisting braces at interior brace points. In order to predict the effect that a particular moment-resisting brace design would have on system capacity, an *effective brace stiffness* was defined, the value of which is computed using a simplified structural model.

Two large-scale parametric studies were performed: one for strut-braced systems and one for systems with moment-resisting braces. Structural parameters that were varied included the FIB cross-section type, span length, skew angle, anchor stiffness (for strut-braced systems), and both effective brace stiffness and number of interior brace points (for systems with moment-resisting braces). Wind loads associated with lateral drag force, torque, and vertical uplift were all taken into account. From the results of these parametric studies, system capacity prediction equations were developed and recommended for use in assessing the stability of multi-girder systems with strut braces (Chapter 9, Equation 9.22) and moment-resisting braces (Chapter 9, Equation 9.23).

10.5 Future research

Wind tunnel testing performed in the present study focused on individual girders and groups of unconnected girders without any additional components present. No consideration was given to the changes in aerodynamic properties that might occur when stay-in-place deck forms or overhangs are present. Additionally, it was not within the scope of the wind tunnel testing conducted in this study to quantify changes in drag force that might occur when an otherwise shielded girder is partially exposed due to bridge skew. Hence, it may be appropriate to address these issues with future wind tunnel testing. Alternatively, it may be possible to use a computational fluid dynamics (CFD) analysis approach to investigate one or both of these situations. Such an approach could potentially be validated using the wind tunnel measurements obtained during the present study.

REFERENCES

AASHTO (American Association of State Highway and Transportation Officials) (2010). *LRFD Bridge Design Specifications: 5th Edition*, AASHTO, Washington, D.C.

ADINA (2012). *Theory and Modeling Guide, Volume 1: ADINA Solids & Structures*, ADINA R&D, Inc, Watertown, MA.

AF&PA (American Forest & Paper Association) (2005). *National Design Specification for Wood Construction and Supplement*, AF&PA, Washington, D.C.

AIJ (Architectural Institute of Japan) (2004). *AIJ Recommendations for Loads on Buildings*, AIJ, Tokyo.

ASCE (American Society of Civil Engineers) (2006). *ASCE 7–05: Minimum Design Loads for Buildings and Other Structures*, ASCE, New York, NY.

ASCE Wind Effects Committee (1987). *Wind Loading and Wind-Induced Structural Response*, American Society of Civil Engineers, New York, NY.

Bathe, K. (1996). *Finite Element Procedures*, Prentice Hall, Englewood Cliffs, NJ.

Bradley, G. and Chang, P. (1998). *Determination of the Ultimate Capacity of Elastomeric Bearings Under Axial Load, NISTIR 6121*, Building and Fire Research Laboratory, Gaithersburg, MD.

BSI (British Standards Institution) (2006). *BS 5400: Steel concrete and composite bridges: Part 2: Specification for loads*, BSI, London.

CEN (European Committee for Standardization) (2004). *Eurocode 1: Actions on Structures – Part 1–4: General Actions – Wind Actions (prEN 1991–1–4:2004)*. CEN, Brussels.

Çengel, Y. and Cimbala, J. (2006). *Fluid Mechanics: Fundamentals and Applications*, McGraw–Hill Higher Education, Boston, MA.

Consolazio, G., Hamilton, H., and Berry, M. (2012). *Experimental Validation Of Bracing Recommendations For Long-Span Concrete Girders*, Structures Research Report No. 2012/72909–74040, University of Florida, Gainesville, FL.

Consolazio, G., Hamilton, H., Bui, L., and Chung, J. (2007). *Lateral Bracing of Long-Span Florida Bulb-Tee Girders*, Structures Research Report No. 2007/52290, University of Florida, Gainesville, FL.

Davenport, A. (1960). *Wind Loads on Structures*, Technical Paper No. 88, Division of Building Research, Ottawa, Canada.

Delany, N. and Sorensen, N. (1953). *Low Speed Drag of Cylinders of Various Shapes*, Technical Note 3038, National Advisory Committee for Aeronautics, Washington, D.C.

ESDU (1982). *ESDU 82007: Structural Members: Mean Fluid Forces on Members of Various Cross Sections*, ESDU, London.

FDOT (Florida Department of Transportation) (2009). *Temporary Design Bulletin C09–07*, FDOT, Tallahassee, FL.

FDOT (Florida Department of Transportation) (2010). *Standard Specifications for Road and Bridge Construction*, FDOT, Tallahassee, FL.

FDOT (Florida Department of Transportation) (2012a). *Design Standard No. 20005: Prestressed I-Beam Temporary Bracing*, FDOT, Tallahassee, FL.

FDOT (Florida Department of Transportation) (2012b). *Instructions for Design Standard No. 20010: Prestressed Florida-I Beams*, FDOT, Tallahassee, FL.

FDOT (Florida Department of Transportation) (2012c). *Design Standard No. 20510: Composite Elastomeric Bearing Pads – Prestressed Florida-I Beams*, FDOT, Tallahassee, FL.

FDOT (Florida Department of Transportation) (2012d). *Instructions for Design Standard No. 20510: Composite Elastomeric Bearing Pads – Prestressed Florida-I Beams*, FDOT, Tallahassee, FL.

FDOT (Florida Department of Transportation) (2012e). *Structures Manual Volume I: Structures Design Guidelines*, FDOT, Tallahassee, FL.

Gent, A. (2001). *Engineering with Rubber: How to Design Rubber Components 2nd Edition*, HanserGardner Publications Inc., Cincinnati, OH.

Grant, I. and Barnes, F. (1981). "The Vortex Shedding and Drag Associated with Structural Elements", *Journal of Wind Engineering and Industrial Aerodynamics*, Vol. 8, pp. 115–122.

Haslach, H. and Armstrong, R. (2004). *Deformable Bodies and their Material Behavior*, John Wiley & Sons, New York, NY.

Holmes, J. (2007). *Wind Loading of Structures: 2nd Edition*, Taylor & Francis, New York, NY.

Kalkan, İ. (2010). "Application of Southwell Method on the Analysis of Lateral Torsional Buckling Tests on Reinforced Concrete Beams", *International Journal of Engineering Research & Development*, Vol. 2, No. 1, pp. 58–66.

Mast, R. (1993). "Lateral Stability of Long Prestressed Concrete Beams – Part 2", *PCI Journal*, Vol. 38, No. 1, January–February 1993, pp. 70–88.

Maher, F. and Wittig, L. (1980). "Aerodynamic Response of Long H-Section", *Journal of the Structural Division*, ASCE, Vol. 106, No. ST1, pp. 183–198.

Mandal, P. and Calladine, C. (2002). "Lateral–Torsional Buckling of Beams and the Southwell Plot", *International Journal of Mechanical Sciences*, Vol 44, No. 12, pp. 2557–2571.

Massey, C. (1963). "Elastic and Inelastic Lateral Instability of I-Beams", *The Engineer*, Vol. 216, No. 5622, pp. 672–674.

Meck, H. (1977). "Experimental Evaluation of Buckling Loads", *Journal of the Engineering Mechanics Division*, ASCE, Vol. 103, No. 2, pp. 331–337.

Myers, G. and Ghalib, A. (n.d.). "Wind Loads on Steel Box Girders During Construction Using Computational Fluid Dynamic Analysis", *Atkins Technical Journal*, Vol 7, No. 110, pp. 83–92.

NRC (National Research Council) (2005). *User's Guide – NBC 2005, Structural Commentaries*, NRC, Ottawa, Canada.

PCI (2010). *PCI Design Handbook: 7th Edition*, Precast/Prestressed Concrete Institute, Chicago, IL.

Podolny, W. and Muller, J. (1982). *Construction and Design of Prestressed Concrete Segmental Bridges*, John Wiley & Sons, New York, NY.

Sachs, P. (1978). *Wind Forces in Engineering: 2nd Edition*, Pergamon Press, Oxford.

Scruton, C. and Newberry, C. (1963). "On the Estimation of Wind Loads for Building and Structural Design", *ICE Proceedings*, Vol. 25, No. 2, June 1963, pp. 97–126.

Simiu, E. and Miyata, T. (2006). *Design of Buildings and Bridges for Wind: A Practical Guide for ASCE-7 Standard Users and Designers of Special Structures*, John Wiley & Sons, New York, NY.

Solari G. and Kareem A. (1998). "On the Formulation of ASCE 7–95 Gust Effect Factor", *Journal of Wind Engineering and Industrial Aerodynamics*, Vol. 77, pp. 673–684.

Southwell, R. (1932). "On the Analysis of Experimental Observations in Problems of Elastic Stability", *Proceedings of the Royal Society of London*, Vol. 135, No. 828, pp. 601–616.

Stanton, J., Roeder, C., Mackenzie-Helnwein, P., White, C., Kuester, C., and Craig, B. (2008). *Rotation Limits for Elastomeric Bearings: Appendix F*, NCHRP Report 596, Transporation Research Board, National Research Council, Washington D.C.

Trahair, N. (1969). "Deformations of Geometrically Imperfect Beams", *Journal of the Structural Division*, ASCE, Vol. 95, No. ST7, pp. 1475–1496.

Treloar, L. (1975). *The Physics of Rubber Elasticity: 3rd Edition*, Clarendon Press, Oxford.

Young, W. C. and Budynas, R. G. (2002). *Roark's Formulas for Stress and Strain: 7th Edition*, McGraw–Hill, New York, NY.

APPENDIX A
DIMENSIONED DRAWINGS OF WIND TUNNEL TEST CONFIGURATIONS

This appendix includes dimensioned drawings of every girder configuration that was subjected to wind tunnel testing.

Configuration A2 (2% cross-slope)
─10'-0"─
2.4"

Configuration B2 (2% Cross-slope)
─14'-0"─
3.36"

Configuration C2 (8% Cross-slope)
─10'-0"─
9.6"

Configuration D2 (8% Cross-slope)
─14'-0"─
13.44"

Wide-Flange Plate Girder

2'-8"
1'-4"
℞ 1"
8'-0"
℞ 3/4"
Direction of Wind
1'-4"
℞ 1"
2'-8"

REVISIONS

149

5 sp. @ 3.36"

5 sp. @ 14'-0"

Configuration B5 (2% Cross-slope)

5 sp. @ 13.44"

5 sp. @ 14'-0"

Configuration D5 (8% Cross-slope)

5 sp. @ 2.4"

5 sp. @ 10'-0"

Configuration A5 (2% Cross-slope)

5 sp. @ 9.6"

5 sp. @ 10'-0"

Configuration C5 (8% Cross-slope)

Direction of Wind

10 sp. @ 13.44"

10 sp. @ 14'-0"

Configuration D10 (8% Cross-slope)

REVISIONS		Bridge Girder Drag Coefficients and Wind-Related Bracing Recommendations	
		University of Florida	Wide-Flange Plate Girder Test Configurations	Sheet 2 of 8
Revision 1: 2010-11-08			
Revision 2: 2011-02-14			

Configuration E2 (2% Cross-slope)

10'-0" 2.4"

Configuration F2 (2% Cross-slope)

14'-0" 3.36"

Configuration E5 (2% Cross-slope)

5 sp. @ 10'-0" 2.4"

Configuration F5 (2% Cross-slope)

5 sp. @ 14'-0" 3.36"

Narrow-Flange Plate Girder

8'-0"

1'-4" 8"

ℓ 1"

ℓ ¾"

Direction of Wind

ℓ 1"

1'-4" 8"

78" Florida-I Beam

Configuration G2 (2% cross-slope)
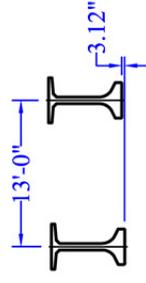
Configuration H2 (2% cross-slope)

Bridge Girder Drag Coefficients and Wind-Related Bracing Recommendations

REVISIONS			University of Florida	78" Florida-I Beam Test Configurations	Sheet 4 of 8
Revision 1: 2010-11-08					
Revision 2: 2012-02-14					

Direction of Wind

5 sp. @ 10'-0" 5 sp. @ 2.4"

Configuration G5 (2% Cross-slope)

5 sp. @ 13'-0" 5 sp. @ 3.12"

Configuration H5 (2% Cross-slope)

10 sp. @ 13'-0" 10 sp. @ 3.12"

Configuration H10 (2% cross-slope)

10 sp. @ 13'-0" 10 sp. @ 3.12"

Configuration I10 (-2% cross-slope)

REVISIONS

Revision 1: 2010-11-08

Revision 2: 2012-02-14

Bridge Girder Drag Coefficients and Wind-Related Bracing Recommendations		
University of Florida	78" Florida-I Beam Test Configurations	Sheet 5 of 8

Configuration J2 (2% cross-slope)

—2.4"—

—10'-0"—
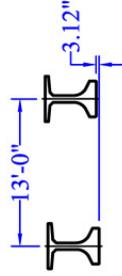
Configuration K2 (2% cross-slope)

—3.12"—

—13'-0"—

45" Florida-I Beam

5"

8½"

2'-0"

R1'-3"

Symm. about ₵

7"

3½"

1'-5"

Direction of Wind

¾" Chamfer

1'-7"

7"

3½"

1'-3½"

3'-9"

REVISIONS

Revision 1: 2010-11-08

Revision 2: 2011-02-14

Bridge Girder Drag Coefficients and Wind-Related Bracing Recommendations

University of Florida

45" Florida-I Beam
Test Configurations

Sheet 6 of 8

5 sp. @ 10'-0"
5 sp. @ 2.4"

Configuration J5 (2% Cross-slope)

5 sp. @ 13'-0"
5 sp. @ 3.12"

Configuration K5 (2% Cross-slope)

Direction of Wind

10 sp. @ 13'-0"
10 sp. @ 3.12"

Configuration K10 (2% Cross-slope)

10 sp. @ 13'-0"
10 sp. @ 3.12"

Configuration L10 (-2% Cross-slope)

Open-Top Box Girder

5'-0"

6'-0"

R⅝"

R½"

1"

3'-6"

Symm. about ₵

R¾"

1'-4"

8"

4

1

Direction of Wind

Configuration M2 (0% Cross-slope)

Configuration N2 (0% Cross-slope)

20'-0"

22'-0"

APPENDIX B
TABULATED RESULTS FROM WIND TUNNEL TESTS

This appendix contains results from all of the wind tunnel tests that were performed, including drag, lift, and torque coefficients, as well as *effective drag coefficients* (discussed in Chapter 5) that combine the structural demand of both drag and torque. Results for each test configuration are given an ID code consisting of a letter and 2 numbers. The letter describes the geometric arrangement of the girders (Table B.1), the first number is the number of girders and the second number is the girder being measured. For example, the designation *B5–3* refers to the third (3) WF Plate girder in a group of five (5) with a spacing of 14 ft and a cross-slope of 2%.

Table B.1 Meaning of letters in configuration IDs

Configuration ID letter	Section	Cross-slope	Spacing (ft)
A	WF Plate	2%	10
B	WF Plate	2%	14
C	WF Plate	8%	10
D	WF Plate	8%	14
E	NF Plate	2%	10
F	NF Plate	2%	14
G	78″ FIB	2%	10
H	78″ FIB	2%	13
I	78″ FIB	–2%	13
J	45″ FIB	2%	10
K	45″ FIB	2%	13
L	45″ FIB	–2%	13
M	Box	0%	20
N	Box	0%	22

Testing Configuration A
Cross-section: WF Plate
Spacing: 10 ft
Cross-slope: +2%
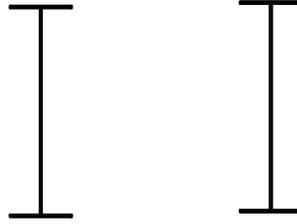
Drag coefficient (C_D)

Wind Angle	Indv.	A2–1	A2–2	A5–1	A5–2	A5–3	A5–4	A5–5
−5.0°	2.13	2.23	−0.36	1.99	−0.11	−0.24	0.03	0.34
−2.5°	2.13	2.25	−0.37	2.05	−0.09	−0.29	−0.15	0.29
0°	2.12	2.26	−0.35	2.08	−0.07	−0.44	−0.27	0.27
2.5°	2.13	2.25	−0.36	2.06	−0.08	−0.34	−0.24	0.29
5.0°	2.13	2.24	−0.35	2.00	−0.11	−0.26	−0.06	0.31

Lift coefficient (C_L)

Wind Angle	Indv.	A2–1	A2–2	A5–1	A5–2	A5–3	A5–4	A5–5
−5.0°	0.00	0.02	−0.04	0.05	−0.01	−0.05	−0.03	−0.17
−2.5°	0.00	0.01	−0.02	0.03	−0.01	−0.04	−0.07	−0.11
0°	−0.01	−0.01	0.00	−0.01	0.00	−0.01	−0.02	−0.03
2.5°	−0.01	−0.02	0.01	−0.05	−0.01	0.03	0.06	0.07
5.0°	−0.02	−0.03	0.03	−0.07	0.01	0.05	0.06	0.14

Torque coefficient (C_T)

Wind Angle	Indv.	A2–1	A2–2	A5–1	A5–2	A5–3	A5–4	A5–5
−5.0°	0.03	0.03	0.00	0.03	0.00	0.00	−0.01	0.00
−2.5°	0.03	0.03	0.00	0.03	0.00	0.00	−0.02	0.00
0°	0.03	0.03	−0.01	0.03	0.00	−0.01	−0.01	0.00
2.5°	0.03	0.03	−0.01	0.03	0.00	−0.01	0.01	0.01
5.0°	0.03	0.03	−0.01	0.03	0.00	−0.01	0.02	0.01

Effective drag coefficient ($C_{D,eff}$)

Wind Angle	Indv.	A2–1	A2–2	A5–1	A5–2	A5–3	A5–4	A5–5
−5.0°	2.19	2.30	−0.36	2.04	−0.11	−0.24	0.03	0.34
−2.5°	2.19	2.31	−0.37	2.10	−0.09	−0.29	−0.15	0.29
0°	2.18	2.32	−0.35	2.13	−0.07	−0.44	−0.27	0.28
2.5°	2.18	2.31	−0.36	2.12	−0.08	−0.34	−0.21	0.31
5.0°	2.18	2.30	−0.35	2.06	−0.11	−0.26	−0.03	0.34

Testing Configuration B
Cross-section: WF Plate
Spacing: 14 ft
Cross-slope: +2%

Drag coefficient (C_D)

Wind Angle	Indv.	B2–1	B2–2	B5–1	B5–2	B5–3	B5–4	B5–5
−5.0°	2.13	2.19	−0.46	1.89	−0.17	−0.22	0.26	0.64
−2.5°	2.13	2.20	−0.48	1.97	−0.16	−0.39	0.15	0.64
0°	2.12	2.22	−0.52	2.01	−0.17	−0.50	0.10	0.57
2.5°	2.13	2.21	−0.51	1.98	−0.16	−0.46	0.14	0.65
5.0°	2.13	2.19	−0.48	1.90	−0.17	−0.32	0.23	0.71

Lift coefficient (C_L)

Wind Angle	Indv.	B2–1	B2–2	B5–1	B5–2	B5–3	B5–4	B5–5
−5.0°	0.00	0.02	−0.12	0.04	−0.03	−0.07	−0.07	0.03
−2.5°	0.00	0.01	−0.07	0.03	−0.01	−0.08	−0.07	0.02
0°	−0.01	−0.01	−0.02	−0.01	0.00	−0.03	−0.01	−0.01
2.5°	−0.01	−0.02	0.03	−0.04	0.01	0.05	0.07	−0.03
5.0°	−0.02	−0.04	0.08	−0.06	0.02	0.07	0.08	−0.02

Torque coefficient (C_T)

Wind Angle	Indv.	B2–1	B2–2	B5–1	B5–2	B5–3	B5–4	B5–5
−5.0°	0.03	0.03	−0.01	0.03	0.00	−0.01	0.00	−0.01
−2.5°	0.03	0.03	−0.01	0.03	0.00	−0.01	−0.01	0.00
0°	0.03	0.03	−0.01	0.03	0.00	−0.01	0.00	0.01
2.5°	0.03	0.03	−0.01	0.03	0.00	0.00	0.01	0.02
5.0°	0.03	0.03	−0.01	0.02	−0.01	0.00	0.01	0.03

Effective drag coefficient ($C_{D,eff}$)

Wind Angle	Indv.	B2–1	B2–2	B5–1	B5–2	B5–3	B5–4	B5–5
−5.0°	2.19	2.25	−0.46	1.95	−0.17	−0.22	0.27	0.64
−2.5°	2.19	2.26	−0.48	2.03	−0.16	−0.39	0.15	0.64
0°	2.18	2.27	−0.52	2.06	−0.17	−0.50	0.11	0.59
2.5°	2.18	2.27	−0.51	2.03	−0.16	−0.46	0.15	0.68
5.0°	2.18	2.24	−0.48	1.94	−0.17	−0.31	0.24	0.78

Testing Configuration C
Cross-section: WF Plate
Spacing: 10 ft
Cross-slope: +8%
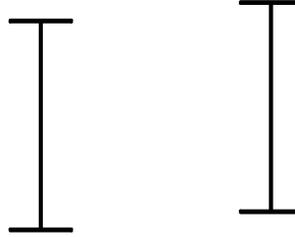
Drag coefficient (C_D)

Wind Angle	Indv.	C2–1	C2–2	C5–1	C5–2	C5–3	C5–4	C5–5
−5.0°	2.13	2.24	−0.36	1.86	−0.11	−0.10	0.27	0.49
−2.5°	2.13	2.24	−0.36	1.94	−0.12	−0.22	0.10	0.40
0°	2.12	2.26	−0.39	2.00	−0.11	−0.29	−0.15	0.33
2.5°	2.13	2.26	−0.36	2.05	−0.08	−0.32	−0.24	0.27
5.0°	2.13	2.26	−0.36	2.05	−0.08	−0.32	−0.26	0.28

Lift coefficient (C_L)

Wind Angle	Indv.	C2–1	C2–2	C5–1	C5–2	C5–3	C5–4	C5–5
−5.0°	0.00	0.03	−0.09	0.06	−0.02	−0.03	−0.01	−0.17
−2.5°	0.00	0.02	−0.05	0.06	−0.02	−0.06	−0.02	−0.11
0°	−0.01	0.01	−0.03	0.04	−0.01	−0.06	−0.05	−0.07
2.5°	−0.01	−0.01	−0.01	0.01	0.00	−0.03	−0.04	−0.03
5.0°	−0.02	−0.02	0.00	−0.04	−0.01	0.01	0.03	0.07

Torque coefficient (C_T)

Wind Angle	Indv.	C2–1	C2–2	C5–1	C5–2	C5–3	C5–4	C5–5
−5.0°	0.03	0.03	0.00	0.03	0.00	0.00	0.01	0.02
−2.5°	0.03	0.03	0.00	0.03	0.00	0.00	0.00	0.02
0°	0.03	0.03	0.00	0.03	0.00	0.00	−0.01	0.01
2.5°	0.03	0.03	−0.01	0.03	0.00	0.00	−0.01	0.01
5.0°	0.03	0.03	−0.01	0.03	0.00	−0.01	0.00	0.01

Effective drag coefficient ($C_{D,eff}$)

Wind Angle	Indv.	C2–1	C2–2	C5–1	C5–2	C5–3	C5–4	C5–5
−5.0°	2.19	2.30	−0.36	1.91	−0.10	−0.10	0.30	0.52
−2.5°	2.19	2.30	−0.36	1.99	−0.12	−0.22	0.11	0.45
0°	2.18	2.31	−0.39	2.07	−0.11	−0.29	−0.15	0.36
2.5°	2.18	2.31	−0.36	2.11	−0.08	−0.32	−0.24	0.29
5.0°	2.18	2.31	−0.36	2.10	−0.08	−0.32	−0.25	0.29

Testing Configuration D
Cross-section: WF Plate
Spacing: 14 ft
Cross-slope: +8%

Drag coefficient (C_D)

Wind Angle	Indv.	D2–1	D2–2	D5–1	D5–2	D5–3	D5–4	D5–5
−5.0°	2.13	2.22	−0.34	1.77	−0.14	−0.05	0.47	1.05
−2.5°	2.13	2.21	−0.47	1.85	−0.18	−0.18	0.27	0.84
0°	2.12	2.22	−0.48	1.93	−0.18	−0.34	0.22	0.65
2.5°	2.13	2.24	−0.52	1.99	−0.18	−0.48	0.24	0.65
5.0°	2.13	2.25	−0.55	1.97	−0.17	−0.49	0.19	0.67

Lift coefficient (C_L)

Wind Angle	Indv.	D2–1	D2–2	D5–1	D5–2	D5–3	D5–4	D5–5
−5.0°	0.00	0.04	−0.23	0.04	−0.03	−0.05	−0.03	−0.02
−2.5°	0.00	0.03	−0.15	0.04	−0.04	−0.06	−0.04	−0.03
0°	−0.01	0.01	−0.08	0.03	−0.02	−0.08	−0.05	−0.03
2.5°	−0.01	−0.01	−0.04	−0.01	−0.01	−0.05	−0.01	0.00
5.0°	−0.02	−0.02	0.02	−0.04	0.00	0.03	0.06	0.07

Torque coefficient (C_T)

Wind Angle	Indv.	D2–1	D2–2	D5–1	D5–2	D5–3	D5–4	D5–5
−5.0°	0.03	0.03	−0.02	0.03	0.00	0.00	0.01	0.04
−2.5°	0.03	0.03	−0.01	0.03	0.00	−0.01	0.00	0.04
0°	0.03	0.03	−0.01	0.03	0.00	−0.01	0.00	0.03
2.5°	0.03	0.03	−0.01	0.03	0.00	−0.02	0.00	0.02
5.0°	0.03	0.03	−0.01	0.03	0.00	−0.01	0.02	0.01

Effective drag coefficient ($C_{D,eff}$)

Wind Angle	Indv.	D2–1	D2–2	D5–1	D5–2	D5–3	D5–4	D5–5
−5.0°	2.19	2.28	−0.34	1.83	−0.14	−0.05	0.48	1.12
−2.5°	2.19	2.27	−0.47	1.91	−0.18	−0.18	0.27	0.91
0°	2.18	2.27	−0.48	1.99	−0.18	−0.34	0.23	0.70
2.5°	2.18	2.29	−0.52	2.04	−0.18	−0.48	0.24	0.69
5.0°	2.18	2.30	−0.55	2.02	−0.17	−0.49	0.23	0.69

Testing Configuration D
Cross-section: WF Plate
Spacing: 14 ft
Cross-slope: +8%
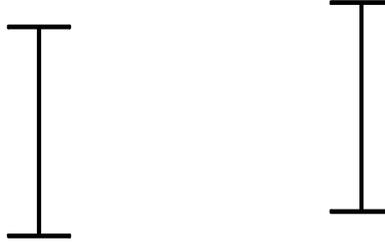
Drag coefficient (C_D)

Wind Angle	D10–1	D10–2	D10–3	D10–4	D10–5	D10–6	D10–7	D10–8	D10–9	D10–10
−5.0°	1.54	−0.13	−0.16	0.15	0.51	0.75	0.99	1.15	1.31	1.23
−2.5°	1.65	−0.15	−0.25	0.04	0.35	0.49	0.63	0.80	0.96	1.00
0°	1.77	−0.15	−0.34	0.05	0.34	0.38	0.42	0.53	0.60	0.70
2.5°	1.80	−0.13	−0.43	0.04	0.34	0.37	0.38	0.44	0.47	0.56
5.0°	1.79	−0.12	−0.42	0.04	0.34	0.38	0.38	0.42	0.44	0.52

Lift coefficient (C_L)

Wind Angle	D10–1	D10–2	D10–3	D10–4	D10–5	D10–6	D10–7	D10–8	D10–9	D10–10
−5.0°	0.00	−0.02	−0.05	−0.01	0.04	0.06	0.06	0.04	0.01	−0.02
−2.5°	−0.01	−0.02	−0.06	−0.03	0.02	0.05	0.05	0.05	0.02	−0.03
0°	−0.02	−0.01	−0.06	−0.03	0.01	0.02	0.02	0.03	0.02	−0.04
2.5°	−0.06	0.00	−0.03	−0.02	0.00	0.00	0.00	0.00	0.00	−0.02
5.0°	−0.10	0.00	0.04	0.04	0.03	0.03	0.03	0.02	0.02	0.03

Torque coefficient (C_T)

Wind Angle	D10–1	D10–2	D10–3	D10–4	D10–5	D10–6	D10–7	D10–8	D10–9	D10–10
−5.0°	0.00	0.00	0.00	0.00	−0.01	−0.02	−0.02	−0.02	−0.02	−0.03
−2.5°	0.00	0.00	0.01	0.01	0.00	−0.01	−0.01	−0.01	−0.02	−0.03
0°	0.00	0.00	0.00	0.00	0.00	−0.01	−0.01	0.00	−0.01	−0.01
2.5°	0.01	0.00	0.01	0.00	0.00	−0.01	0.00	0.00	0.00	−0.01
5.0°	0.01	0.00	0.01	−0.01	−0.01	−0.01	−0.01	−0.01	−0.01	−0.01

Effective drag coefficient ($C_{D,eff}$)

Wind Angle	D10–1	D10–2	D10–3	D10–4	D10–5	D10–6	D10–7	D10–8	D10–9	D10–10
−5.0°	1.54	−0.13	−0.15	0.16	0.51	0.75	0.99	1.15	1.31	1.23
−2.5°	1.65	−0.15	−0.24	0.05	0.35	0.49	0.63	0.80	0.96	1.00
0°	1.77	−0.15	−0.33	0.06	0.34	0.38	0.42	0.53	0.60	0.70
2.5°	1.82	−0.13	−0.41	0.04	0.34	0.37	0.38	0.44	0.47	0.56
5.0°	1.80	−0.12	−0.41	0.04	0.34	0.38	0.38	0.42	0.44	0.52

Testing Configuration E
Cross-section: NF Plate
Spacing: 10 ft
Cross-slope: +2%
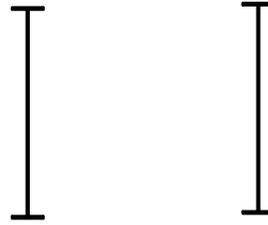
Drag coefficient (C_D)

Wind Angle	Indv.	E2–1	E2–2	E5–1	E5–2	E5–3	E5–4	E5–5
−5.0°	2.13	2.22	−0.24	2.01	−0.08	−0.21	-	-
−2.5°	2.12	2.23	−0.24	2.06	−0.07	−0.28	-	-
0°	2.12	2.25	−0.26	2.09	−0.07	−0.34	-	-
2.5°	2.13	2.24	−0.24	2.07	−0.07	−0.33	-	-
5.0°	2.12	2.23	−0.24	2.02	−0.07	−0.27	-	-

Lift coefficient (C_L)

Wind Angle	Indv.	E2–1	E2–2	E5–1	E5–2	E5–3	E5–4	E5–5
−5.0°	−0.04	−0.03	−0.01	−0.02	−0.01	−0.03	-	-
−2.5°	−0.04	−0.04	0.00	−0.02	0.00	−0.02	-	-
0°	−0.04	−0.04	0.00	−0.04	0.00	−0.01	-	-
2.5°	−0.04	−0.05	0.00	−0.05	0.00	0.01	-	-
5.0°	−0.05	−0.05	0.00	−0.06	0.00	0.02	-	-

Torque coefficient (C_T)

Wind Angle	Indv.	E2–1	E2–2	E5–1	E5–2	E5–3	E5–4	E5–5
−5.0°	0.01	0.01	0.00	0.01	0.00	−0.01	-	-
−2.5°	0.01	0.01	0.00	0.01	0.00	0.00	-	-
0°	0.00	0.01	−0.01	0.01	−0.01	−0.01	-	-
2.5°	0.00	0.00	−0.01	0.00	−0.01	−0.01	-	-
5.0°	0.00	0.00	−0.01	0.00	−0.01	−0.01	-	-

Effective drag coefficient ($C_{D,eff}$)

Wind Angle	Indv.	E2–1	E2–2	E5–1	E5–2	E5–3	E5–4	E5–5
−5.0°	2.14	2.23	−0.24	2.03	−0.08	−0.21	-	-
−2.5°	2.13	2.24	−0.24	2.07	−0.07	−0.28	-	-
0°	2.12	2.26	−0.26	2.11	−0.07	−0.34	-	-
2.5°	2.13	2.24	−0.24	2.07	−0.07	−0.33	-	-
5.0°	2.12	2.23	−0.24	2.02	−0.07	−0.27	-	-

Testing Configuration F
Cross-section: NF Plate
Spacing: 14 ft
Cross-slope: +2%

Drag coefficient (C_D)

Wind Angle	Indv.	F2–1	F2–2	F5–1	F5–2	F5–3	F5–4	F5–5
−5.0°	2.13	2.22	−0.44	1.90	−0.13	−0.36	-	-
−2.5°	2.12	2.20	−0.38	1.96	−0.14	−0.50	-	-
0°	2.12	2.20	−0.36	1.99	−0.16	−0.09	-	-
2.5°	2.13	2.21	−0.37	1.95	−0.14	−0.17	-	-
5.0°	2.12	2.22	−0.41	1.90	−0.13	−0.43	-	-

Lift coefficient (C_L)

Wind Angle	Indv.	F2–1	F2–2	F5–1	F5–2	F5–3	F5–4	F5–5
−5.0°	−0.04	−0.03	−0.06	−0.01	−0.01	−0.06	-	-
−2.5°	−0.04	−0.03	−0.02	−0.02	0.00	−0.05	-	-
0°	−0.04	−0.04	0.00	−0.03	0.00	−0.01	-	-
2.5°	−0.04	−0.05	0.01	−0.05	0.00	0.04	-	-
5.0°	−0.05	−0.05	0.03	−0.05	0.01	0.06	-	-

Torque coefficient (C_T)

Wind Angle	Indv.	F2–1	F2–2	F5–1	F5–2	F5–3	F5–4	F5–5
−5.0°	0.01	0.02	−0.03	0.13	−0.01	−0.05	-	-
−2.5°	0.01	0.02	−0.03	0.13	−0.01	−0.06	-	-
0°	0.00	0.01	−0.02	0.13	−0.01	−0.01	-	-
2.5°	0.00	0.07	−0.03	0.13	−0.01	0.00	-	-
5.0°	0.00	0.13	−0.03	0.12	−0.01	−0.01	-	-

Effective drag coefficient ($C_{D,eff}$)

Wind Angle	Indv.	F2–1	F2–2	F5–1	F5–2	F5–3	F5–4	F5–5
−5.0°	2.14	2.26	−0.44	2.16	−0.13	−0.36	-	-
−2.5°	2.13	2.23	−0.38	2.22	−0.14	−0.50	-	-
0°	2.12	2.22	−0.36	2.25	−0.16	−0.09	-	-
2.5°	2.13	2.35	−0.37	2.20	−0.14	−0.17	-	-
5.0°	2.12	2.48	−0.41	2.14	−0.13	−0.43	-	-

Testing Configuration G
Cross-section: 78″ FIB
Spacing: 10 ft
Cross-slope: +2%
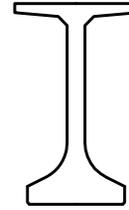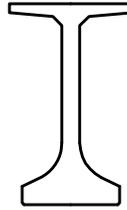
Drag coefficient (C_D)

Wind Angle	Indv.	G2–1	G2–2	G5–1	G5–2	G5–3	G5–4	G5–5
−5.0°	1.90	1.95	−0.37	1.57	−0.17	−0.08	-	-
−2.5°	1.89	1.97	−0.50	1.65	−0.22	−0.27	-	-
0°	1.89	1.97	−0.55	1.71	−0.30	−0.33	-	-
2.5°	1.90	1.98	−0.56	1.70	−0.28	−0.35	-	-
5.0°	1.91	2.00	−0.55	1.66	−0.20	−0.26	-	-

Lift coefficient (C_L)

Wind Angle	Indv.	G2–1	G2–2	G5–1	G5–2	G5–3	G5–4	G5–5
−5.0°	0.18	0.24	−0.25	0.24	−0.02	−0.05	-	-
−2.5°	0.17	0.20	−0.16	0.22	−0.03	−0.10	-	-
0°	0.15	0.16	−0.03	0.15	−0.01	−0.05	-	-
2.5°	0.14	0.13	0.07	0.09	0.02	0.06	-	-
5.0°	0.13	0.09	0.18	0.04	0.03	0.07	-	-

Torque coefficient (C_T)

Wind Angle	Indv.	G2–1	G2–2	G5–1	G5–2	G5–3	G5–4	G5–5
−5.0°	0.12	0.14	−0.05	0.17	−0.01	−0.01	-	-
−2.5°	0.12	0.12	−0.05	0.17	−0.01	−0.04	-	-
0°	0.11	0.12	−0.05	0.16	−0.03	−0.04	-	-
2.5°	0.10	0.10	−0.05	0.16	−0.03	−0.02	-	-
5.0°	0.10	0.12	−0.04	0.15	−0.02	0.00	-	-

Effective drag coefficient ($C_{D,eff}$)

Wind Angle	Indv.	G2–1	G2–2	G5–1	G5–2	G5–3	G5–4	G5–5
−5.0°	1.93	2.01	−0.37	1.74	−0.17	−0.08	-	-
−2.5°	1.92	1.99	−0.50	1.80	−0.22	−0.27	-	-
0°	1.89	1.98	−0.55	1.85	−0.30	−0.33	-	-
2.5°	1.90	1.98	−0.56	1.82	−0.28	−0.34	-	-
5.0°	1.91	2.02	−0.55	1.78	−0.20	−0.24	-	-

Testing Configuration H
Cross-section: 78″ FIB
Spacing: 13 ft
Cross-slope: +2%
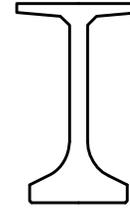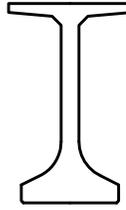
Drag coefficient (C_D)

Wind Angle	Indv.	H2–1	H2–2	H5–1	H5–2	H5–3	H5–4	H5–5
−5.0°	1.90	1.87	−0.30	1.54	−0.19	−0.04	-	-
−2.5°	1.89	1.88	−0.49	1.61	−0.23	−0.24	-	-
0°	1.89	1.90	−0.58	1.65	−0.21	−0.40	-	-
2.5°	1.90	1.90	−0.61	1.64	−0.20	−0.39	-	-
5.0°	1.91	1.91	−0.56	1.58	−0.18	−0.24	-	-

Lift coefficient (C_L)

Wind Angle	Indv.	H2–1	H2–2	H5–1	H5–2	H5–3	H5–4	H5–5
−5.0°	0.18	0.24	−0.34	0.21	−0.04	−0.14	-	-
−2.5°	0.17	0.20	−0.24	0.19	−0.05	−0.14	-	-
0°	0.15	0.17	−0.09	0.14	−0.01	−0.05	-	-
2.5°	0.14	0.14	0.07	0.09	0.02	0.07	-	-
5.0°	0.13	0.10	0.22	0.05	0.03	0.09	-	-

Torque coefficient (C_T)

Wind Angle	Indv.	H2–1	H2–2	H5–1	H5–2	H5–3	H5–4	H5–5
−5.0°	0.12	0.18	−0.05	0.16	−0.01	−0.02	-	-
−2.5°	0.12	0.17	−0.06	0.16	−0.02	−0.04	-	-
0°	0.11	0.16	−0.06	0.16	−0.02	−0.04	-	-
2.5°	0.10	0.15	−0.05	0.15	−0.02	−0.02	-	-
5.0°	0.10	0.17	−0.03	0.14	−0.02	0.00	-	-

Effective drag coefficient ($C_{D,eff}$)

Wind Angle	Indv.	H2–1	H2–2	H5–1	H5–2	H5–3	H5–4	H5–5
−5.0°	1.93	2.01	−0.30	1.69	−0.19	−0.04	-	-
−2.5°	1.92	2.00	−0.49	1.75	−0.23	−0.24	-	-
0°	1.89	2.01	−0.58	1.78	−0.21	−0.40	-	-
2.5°	1.90	1.98	−0.61	1.75	−0.20	−0.39	-	-
5.0°	1.91	2.04	−0.56	1.69	−0.18	−0.21	-	-

Testing Configuration H
Cross-section: 78″ FIB
Spacing: 13 ft
Cross-slope: +2%
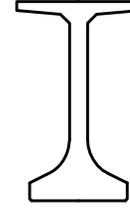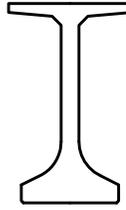
Drag coefficient (C_D)

Wind Angle	H10–1	H10–2	H10–3	H10–4	H10–5	H10–6	H10–7	H10–8	H10–9	H10–10
−5.0°	1.41	−0.19	−0.14	0.18	0.39	0.45	0.55	0.63	0.74	0.75
−2.5°	1.52	−0.20	−0.27	0.10	0.27	0.31	0.33	0.35	0.40	0.46
0°	1.57	−0.19	−0.23	0.04	0.26	0.28	0.29	0.29	0.31	0.35
2.5°	1.56	−0.17	−0.26	0.05	0.35	0.27	0.26	0.26	0.27	0.31
5.0°	1.48	−0.16	−0.25	0.07	0.33	0.31	0.36	0.47	0.57	0.58

Lift coefficient (C_L)

Wind Angle	H10–1	H10–2	H10–3	H10–4	H10–5	H10–6	H10–7	H10–8	H10–9	H10–10
−5.0°	0.16	−0.03	−0.07	−0.05	0.01	0.02	0.02	0.00	−0.04	−0.11
−2.5°	0.15	−0.03	−0.10	−0.06	−0.02	0.00	−0.01	−0.01	−0.03	−0.09
0°	0.10	0.00	−0.02	−0.01	0.02	0.02	0.02	0.02	0.02	0.00
2.5°	0.05	0.02	0.09	0.07	0.04	0.07	0.08	0.08	0.09	0.12
5.0°	0.02	0.03	0.09	0.09	0.05	0.06	0.06	0.07	0.11	0.22

Torque coefficient (C_T)

Wind Angle	H10–1	H10–2	H10–3	H10–4	H10–5	H10–6	H10–7	H10–8	H10–9	H10–10
−5.0°	0.06	−0.01	0.00	0.01	0.01	0.01	0.01	0.01	0.01	0.00
−2.5°	0.07	−0.01	0.00	0.01	0.00	0.00	0.00	0.00	0.00	−0.01
0°	0.08	−0.01	−0.01	0.01	0.01	0.01	0.01	0.01	0.01	0.01
2.5°	0.08	−0.01	−0.04	0.00	0.01	0.01	0.01	0.01	0.01	0.02
5.0°	0.08	0.00	−0.02	−0.01	0.01	0.01	0.01	0.02	0.03	0.04

Effective drag coefficient ($C_{D,eff}$)

Wind Angle	H10–1	H10–2	H10–3	H10–4	H10–5	H10–6	H10–7	H10–8	H10–9	H10–10
−5.0°	1.41	−0.19	−0.12	0.18	0.39	0.45	0.55	0.63	0.74	0.75
−2.5°	1.52	−0.20	−0.24	0.11	0.27	0.31	0.33	0.35	0.40	0.46
0°	1.57	−0.19	−0.22	0.04	0.26	0.28	0.29	0.29	0.31	0.35
2.5°	1.56	−0.17	−0.26	0.05	0.35	0.27	0.26	0.26	0.27	0.31
5.0°	1.48	−0.14	−0.25	0.07	0.33	0.31	0.36	0.47	0.57	0.59

Testing Configuration I
Cross-section: 78″ FIB
Spacing: 13 ft
Cross-slope: −2%
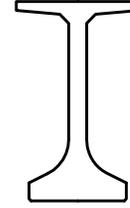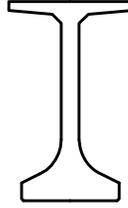
Drag coefficient (C_D)

Wind Angle	I10–1	I10–2	I10–3	I10–4	I10–5	I10–6	I10–7	I10–8	I10–9	I10–10
−5.0°	1.52	−0.21	−0.24	0.13	0.28	0.32	0.29	0.32	0.36	0.42
−2.5°	1.57	−0.20	−0.36	0.05	0.27	0.31	0.27	0.27	0.29	0.32
0°	1.55	−0.18	−0.38	0.05	0.30	0.33	0.28	0.28	0.30	0.33
2.5°	1.46	−0.17	−0.28	0.07	0.36	0.37	0.38	0.47	0.57	0.60
5.0°	1.37	−0.15	−0.16	0.13	0.41	0.53	0.68	0.89	1.02	0.94

Lift coefficient (C_L)

Wind Angle	I10–1	I10–2	I10–3	I10–4	I10–5	I10–6	I10–7	I10–8	I10–9	I10–10
−5.0°	0.14	−0.02	−0.11	−0.09	−0.05	−0.03	−0.06	−0.07	−0.09	−0.16
−2.5°	0.09	0.00	−0.05	−0.04	−0.01	0.01	−0.01	−0.02	−0.02	−0.05
0°	0.04	0.03	0.06	0.05	0.04	0.04	0.05	0.05	0.05	0.08
2.5°	0.01	0.04	0.09	0.07	0.01	0.02	0.02	0.01	0.04	0.16
5.0°	−0.01	0.04	0.08	0.04	0.01	0.00	−0.01	0.02	0.06	0.15

Torque coefficient (C_T)

Wind Angle	I10–1	I10–2	I10–3	I10–4	I10–5	I10–6	I10–7	I10–8	I10–9	I10–10
−5.0°	0.06	−0.02	0.00	0.01	0.01	0.01	0.01	0.01	0.01	0.01
−2.5°	0.07	−0.01	−0.01	0.00	0.01	0.01	0.01	0.01	0.01	0.01
0°	0.08	0.00	−0.03	0.00	0.01	0.01	0.01	0.01	0.02	0.02
2.5°	0.08	0.00	−0.02	−0.01	0.01	0.02	0.02	0.03	0.04	0.04
5.0°	0.07	0.00	−0.01	0.00	0.02	0.03	0.04	0.06	0.07	0.07

Effective drag coefficient ($C_{D,eff}$)

Wind Angle	I10–1	I10–2	I10–3	I10–4	I10–5	I10–6	I10–7	I10–8	I10–9	I10–10
−5.0°	1.52	−0.21	−0.21	0.13	0.28	0.32	0.29	0.32	0.36	0.42
−2.5°	1.57	−0.19	−0.35	0.06	0.27	0.31	0.27	0.27	0.29	0.32
0°	1.55	−0.17	−0.38	0.05	0.30	0.33	0.28	0.28	0.30	0.33
2.5°	1.46	−0.15	−0.28	0.07	0.36	0.37	0.38	0.47	0.58	0.62
5.0°	1.37	−0.14	−0.16	0.13	0.41	0.53	0.70	0.91	1.05	0.98

Testing Configuration J
Cross-section: 45″ FIB
Spacing: 10 ft
Cross-slope: +2%
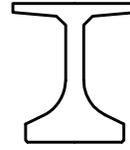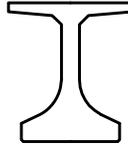
Drag coefficient (C_D)

Wind Angle	Indv.	J2–1	J2–2	J5–1	J5–2	J5–3	J5–4	J5–5
−5.0°	1.81	1.59	−0.29	1.38	−0.29	0.14	-	-
−2.5°	1.83	1.63	−0.44	1.44	−0.37	−0.02	-	-
0°	1.85	1.66	−0.52	1.48	−0.42	−0.06	-	-
2.5°	1.85	1.67	−0.42	1.48	−0.41	−0.01	-	-
5.0°	1.84	1.65	−0.22	1.43	−0.26	0.16	-	-

Lift coefficient (C_L)

Wind Angle	Indv.	J2–1	J2–2	J5–1	J5–2	J5–3	J5–4	J5–5
−5.0°	0.48	0.41	−0.47	0.32	−0.16	−0.25	-	-
−2.5°	0.42	0.38	−0.25	0.30	−0.09	−0.17	-	-
0°	0.37	0.32	0.04	0.26	0.06	0.02	-	-
2.5°	0.30	0.23	0.29	0.17	0.19	0.19	-	-
5.0°	0.24	0.15	0.47	0.09	0.17	0.26	-	-

Torque coefficient (C_T)

Wind Angle	Indv.	J2–1	J2–2	J5–1	J5–2	J5–3	J5–4	J5–5
−5.0°	0.08	0.07	−0.06	0.07	0.01	−0.01	-	-
−2.5°	0.07	0.07	−0.02	0.05	0.01	−0.02	-	-
0°	0.04	0.07	0.01	0.04	0.00	0.01	-	-
2.5°	0.03	0.04	0.03	0.03	0.01	0.02	-	-
5.0°	0.01	0.02	0.03	0.01	0.01	0.01	-	-

Effective drag coefficient ($C_{D,eff}$)

Wind Angle	Indv.	J2–1	J2–2	J5–1	J5–2	J5–3	J5–4	J5–5
−5.0°	1.81	1.59	−0.29	1.38	−0.25	0.14	-	-
−2.5°	1.83	1.63	−0.43	1.44	−0.32	−0.02	-	-
0°	1.85	1.66	−0.45	1.48	−0.38	−0.04	-	-
2.5°	1.85	1.67	−0.33	1.48	−0.35	0.03	-	-
5.0°	1.84	1.65	−0.14	1.43	−0.21	0.16	-	-

Testing Configuration K
Cross-section: 45″ FIB
Spacing: 13 ft
Cross-slope: +2%
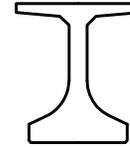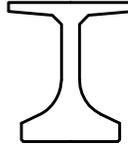
Drag coefficient (C_D)

Wind Angle	Indv.	K2–1	K2–2	K5–1	K5–2	K5–3	K5–4	K5–5
−5.0°	1.81	1.54	−0.02	1.38	−0.33	0.51	-	-
−2.5°	1.83	1.58	0.04	1.44	−0.44	0.48	-	-
0°	1.85	1.60	−0.41	1.47	−0.49	0.56	-	-
2.5°	1.85	1.60	−0.14	1.45	−0.41	0.53	-	-
5.0°	1.84	1.60	−0.12	1.40	−0.25	0.66	-	-

Lift coefficient (C_L)

Wind Angle	Indv.	K2–1	K2–2	K5–1	K5–2	K5–3	K5–4	K5–5
−5.0°	0.48	0.33	−0.45	0.28	−0.28	−0.10	-	-
−2.5°	0.42	0.30	−0.16	0.27	−0.17	−0.01	-	-
0°	0.37	0.27	−0.02	0.24	0.05	0.09	-	-
2.5°	0.30	0.21	0.22	0.17	0.22	0.11	-	-
5.0°	0.24	0.16	0.47	0.12	0.27	0.11	-	-

Torque coefficient (C_T)

Wind Angle	Indv.	K2–1	K2–2	K5–1	K5–2	K5–3	K5–4	K5–5
−5.0°	0.08	0.07	−0.06	0.06	−0.01	0.04	-	-
−2.5°	0.07	0.07	−0.01	0.05	−0.01	0.03	-	-
0°	0.04	0.04	−0.01	0.04	0.01	0.02	-	-
2.5°	0.03	0.02	0.03	0.01	0.02	−0.01	-	-
5.0°	0.01	0.02	0.03	0.01	0.01	−0.01	-	-

Effective drag coefficient ($C_{D,eff}$)

Wind Angle	Indv.	K2–1	K2–2	K5–1	K5–2	K5–3	K5–4	K5–5
−5.0°	1.81	1.54	−0.02	1.38	−0.31	0.54	-	-
−2.5°	1.83	1.58	0.04	1.44	−0.42	0.49	-	-
0°	1.85	1.60	−0.39	1.47	−0.42	0.56	-	-
2.5°	1.85	1.60	−0.07	1.45	−0.33	0.53	-	-
5.0°	1.84	1.60	−0.04	1.40	−0.20	0.66	-	-

Testing Configuration K
Cross-section: 45″ FIB
Spacing: 13 ft
Cross-slope: +2%
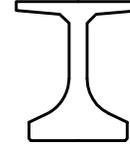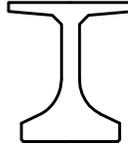
Drag coefficient (C_D)

Wind Angle	K10–1	K10–2	K10–3	K10–4	K10–5	K10–6	K10–7	K10–8	K10–9	K10–10
−5.0°	1.38	−0.22	0.48	0.55	0.44	0.44	0.46	0.51	0.57	0.67
−2.5°	1.49	−0.38	0.63	0.52	0.36	0.33	0.31	0.33	0.36	0.41
0°	1.52	−0.48	0.72	0.47	0.35	0.29	0.26	0.26	0.28	0.32
2.5°	1.51	−0.49	0.69	0.44	0.32	0.27	0.27	0.28	0.29	0.33
5.0°	1.38	−0.38	0.61	0.46	0.36	0.34	0.34	0.38	0.45	0.52

Lift coefficient (C_L)

Wind Angle	K10–1	K10–2	K10–3	K10–4	K10–5	K10–6	K10–7	K10–8	K10–9	K10–10
−5.0°	0.26	−0.29	−0.03	0.04	−0.06	−0.05	−0.06	−0.07	−0.08	−0.11
−2.5°	0.23	−0.28	0.15	0.11	−0.03	−0.04	−0.04	−0.04	−0.06	−0.09
0°	0.18	−0.12	0.18	0.09	0.04	0.02	0.01	0.02	0.02	0.01
2.5°	0.12	0.11	0.08	0.09	0.10	0.11	0.11	0.12	0.14	0.16
5.0°	0.08	0.22	0.06	0.13	0.16	0.17	0.17	0.18	0.22	0.28

Torque coefficient (C_T)

Wind Angle	K10–1	K10–2	K10–3	K10–4	K10–5	K10–6	K10–7	K10–8	K10–9	K10–10
−5.0°	0.20	−0.11	0.07	0.13	0.11	0.12	0.12	0.14	0.16	0.18
−2.5°	0.20	−0.07	0.15	0.11	0.08	0.07	0.08	0.08	0.09	0.10
0°	0.19	−0.07	0.16	0.08	0.07	0.05	0.05	0.05	0.04	0.06
2.5°	0.19	−0.04	0.11	0.07	0.06	0.05	0.05	0.05	0.05	0.05
5.0°	0.16	−0.03	0.09	0.09	0.07	0.06	0.05	0.06	0.05	0.05

Effective drag coefficient ($C_{D,eff}$)

Wind Angle	K10–1	K10–2	K10–3	K10–4	K10–5	K10–6	K10–7	K10–8	K10–9	K10–10
−5.0°	1.63	−0.22	0.58	0.76	0.61	0.63	0.65	0.75	0.82	0.96
−2.5°	1.75	−0.38	0.86	0.68	0.48	0.44	0.43	0.46	0.50	0.57
0°	1.75	−0.48	0.96	0.59	0.44	0.36	0.34	0.34	0.34	0.41
2.5°	1.73	−0.49	0.84	0.54	0.39	0.34	0.33	0.35	0.36	0.40
5.0°	1.56	−0.38	0.73	0.58	0.46	0.42	0.40	0.46	0.51	0.57

Testing Configuration L
Cross-section: 45″ FIB
Spacing: 13 ft
Cross-slope: −2%
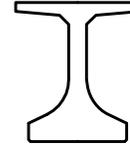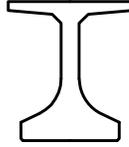
Drag coefficient (C_D)

Wind Angle	L10–1	L10–2	L10–3	L10–4	L10–5	L10–6	L10–7	L10–8	L10–9	L10–10
−5.0°	1.47	−0.30	0.65	0.52	0.38	0.34	0.33	0.35	0.39	0.43
−2.5°	1.53	−0.42	0.69	0.48	0.35	0.28	0.27	0.27	0.28	0.31
0°	1.52	−0.47	0.62	0.42	0.32	0.27	0.27	0.27	0.28	0.30
2.5°	1.42	−0.46	0.58	0.44	0.34	0.32	0.33	0.37	0.39	0.49
5.0°	1.29	−0.24	0.27	0.51	0.50	0.48	0.58	0.72	0.74	0.89

Lift coefficient (C_L)

Wind Angle	L10–1	L10–2	L10–3	L10–4	L10–5	L10–6	L10–7	L10–8	L10–9	L10–10
−5.0°	0.29	−0.37	0.08	0.01	−0.10	−0.11	−0.12	−0.14	−0.15	−0.18
−2.5°	0.24	−0.19	0.13	0.05	−0.02	−0.03	−0.04	−0.04	−0.05	−0.07
0°	0.18	0.00	0.05	0.05	0.06	0.06	0.07	0.08	0.08	0.09
2.5°	0.12	0.23	0.04	0.09	0.13	0.13	0.13	0.14	0.15	0.22
5.0°	0.08	0.14	0.21	0.12	0.13	0.13	0.13	0.16	0.17	0.24

Torque coefficient (C_T)

Wind Angle	L10–1	L10–2	L10–3	L10–4	L10–5	L10–6	L10–7	L10–8	L10–9	L10–10
−5.0°	0.21	−0.09	0.14	0.12	0.08	0.07	0.08	0.08	0.09	0.10
−2.5°	0.21	−0.08	0.11	0.08	0.05	0.04	0.05	0.04	0.05	0.05
0°	0.19	−0.05	0.08	0.05	0.05	0.03	0.04	0.04	0.03	0.04
2.5°	0.17	−0.04	0.06	0.05	0.04	0.04	0.04	0.04	0.05	0.04
5.0°	0.15	−0.02	0.04	0.05	0.04	0.04	0.05	0.06	0.06	0.06

Effective drag coefficient ($C_{D,eff}$)

Wind Angle	L10–1	L10–2	L10–3	L10–4	L10–5	L10–6	L10–7	L10–8	L10–9	L10–10
−5.0°	1.75	−0.30	0.86	0.70	0.51	0.45	0.45	0.47	0.54	0.59
−2.5°	1.79	−0.42	0.84	0.58	0.42	0.33	0.34	0.33	0.35	0.38
0°	1.75	−0.47	0.71	0.48	0.38	0.31	0.32	0.32	0.32	0.35
2.5°	1.61	−0.46	0.64	0.50	0.39	0.36	0.37	0.41	0.44	0.53
5.0°	1.45	−0.24	0.32	0.55	0.54	0.52	0.62	0.77	0.78	0.92

Testing Configuration M
Cross-section: Box
Spacing: 20 ft
Cross-slope: 0%

Drag coefficient (C_D)

Wind Angle	Indv.	M2–1	M2–2
−10.0°	1.74	1.42	0.65
−5.0°	1.68	1.51	0.34
0°	1.81	1.69	−0.45
5.0°	1.93	1.75	−0.36
10.0°	1.87	1.74	0.17

Lift coefficient (C_L)

Wind Angle	Indv.	M2–1	M2–2
−10.0°	1.16	1.32	−1.07
−5.0°	1.62	1.63	−1.09
0°	1.22	0.87	−0.39
5.0°	1.03	0.59	0.67
10.0°	0.71	0.26	0.94

Torque coefficient (C_T)

Wind Angle	Indv.	M2–1	M2–2
−10.0°	0.85	0.72	0.02
−5.0°	0.78	0.73	−0.17
0°	0.73	0.67	−0.14
5.0°	0.73	0.66	−0.01
10.0°	0.69	0.61	0.10

Effective drag coefficient ($C_{D,eff}$)

Wind Angle	Indv.	M2–1	M2–2
−5.0°	3.20	2.67	0.65
−2.5°	3.03	2.78	0.34
0°	3.04	2.81	−0.45
2.5°	3.15	2.84	−0.34
5.0°	3.01	2.74	0.35

Testing Configuration N
Cross-section: Box
Spacing: 22 ft
Cross-slope: 0%

Drag coefficient (C_D)

Wind Angle	Indv.	N2–1	N2–2
−10.0°	1.74	1.39	0.76
−5.0°	1.68	1.48	0.45
0°	1.81	1.68	−0.34
5.0°	1.93	1.73	−0.26
10.0°	1.87	1.73	0.30

Lift coefficient (C_L)

Wind Angle	Indv.	N2–1	N2–2
−10.0°	1.16	1.37	−0.98
−5.0°	1.62	1.65	−1.04
0°	1.22	0.85	−0.54
5.0°	1.03	0.61	0.72
10.0°	0.71	0.22	1.01

Torque coefficient (C_T)

Wind Angle	Indv.	N2–1	N2–2
−10.0°	0.85	0.71	0.10
−5.0°	0.78	0.71	−0.09
0°	0.73	0.65	−0.18
5.0°	0.73	0.64	0.03
10.0°	0.69	0.61	0.14

Effective drag coefficient ($C_{D,eff}$)

Wind Angle	Indv.	N2–1	N2–2
−10.0°	3.20	2.64	0.86
−5.0°	3.03	2.71	0.45
0°	3.04	2.76	−0.34
5.0°	3.15	2.77	−0.16
10.0°	3.01	2.73	0.54

APPENDIX C
CROSS-SECTIONAL PROPERTIES OF FLORIDA-I BEAMS

In this study, finite element models were analyzed to evaluate the lateral stability of Florida-I Beams (FIBs). In each model, the FIBs were modeled using *warping beams*, specialized beam elements available in the ADINA finite element code, which require the calculation of a comprehensive set of cross-sectional properties. This appendix provides mathematical definitions of all such properties and corresponding numeric values that were calculated for each FIB cross-sectional shape.

Definitions of the cross-sectional properties that are required to use the warping beam element in ADINA are listed in Table C.1. Each property requires the evaluation of an integral over the area of the cross-section, in which the integrands are written in terms of coordinates x and y, referenced to the geometric centroid of the section (Figure C.1). Some properties also require knowledge of the *warping function, $\psi(x,y)$*, which represents the torsionally-induced out-of-plane warping displacements per rate of twist at every point on the cross-section. (The units of ψ are therefore in/(rad/in) or in^2.)

Table C.1 Definitions of cross-sectional properties required for use of a warping beam element

Property	Integral form	Units	Description
A	$\int_A dA$	in^2	Cross-sectional area
I$_{yy}$	$\int_A y^2 dA$	in^4	Strong-axis moment of inertia
I$_{xx}$	$\int_A x^2 dA$	in^4	Weak-axis moment of inertia
I$_{xy}$	$\int_A x^2 dA$	in^4	Product of inertia
x$_s$	$-\dfrac{1}{I_{yy}}\int_A (y\psi_c) dA$	in	X-coordinate of shear center
y$_s$	$\dfrac{1}{I_{xx}}\int_A (x\psi_c) dA$	in	Y-coordinate of shear center
J	$\int_A \left(x^2 + y^2 + x\dfrac{d\psi}{dy} - y\dfrac{d\psi}{dx} \right) dA$	in^4	St. Venant torsional constant
C$_\omega$	$\int_A \psi^2 dA$	in^6	Warping constant
I$_{xr}$	$\int_A x(x^2 + y^2) dA$	in^5	Twist/strong-axis bending coupling term
I$_{yr}$	$\int_A y(x^2 + y^2) dA$	in^5	Twist/weak-axis bending coupling term
I$_{\omega r}$	$\int_A \psi(x^2 + y^2) dA$	in^6	Twist/warping coupling term
I$_{rr}$	$\int_A (x^2 + y^2)^2 dA$	in^6	Wagner constant
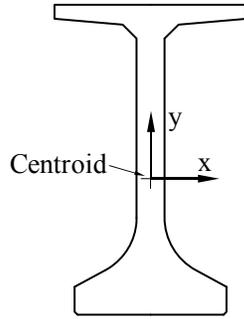
Figure C.1 Coordinate system used in the calculation of cross-sectional properties

For general cross-sectional shapes (e.g., an FIB), analytical (closed-form) solutions for $\psi(x,y)$ do not exist; instead the warping field $\psi(x,y)$ must be solved numerically. In this study, the calculation of $\psi(x,y)$ for each FIB shape was accomplished by discretizing the cross-sectional shape into a high-resolution mesh of thousands of two-dimensional triangular elements, and then employing a finite element approach to solve the governing differential equation.

In general, solutions for $\psi(x,y)$ change depending on the assumed location of the center of twist. In the literature, the term 'warping function' typically refers to a particular solution (ψ in Table C.1) corresponding to a state of *pure torsion*, i.e., torsion about the shear center. As a result, prior knowledge of the location of the shear center is required to compute several of the warping beam properties. However, it is possible to calculate the coordinates of the shear center, x_S and y_S (Table C.1), using an alternative solution to the warping function (ψ_c), where the center of twist is assumed to be located at the centroid of the section. Therefore, two different warping functions were computed for each FIB section: first the section centroid was used to compute ψ_c and then the location of the shear center, obtained from ψ_c, was used to compute ψ as well as the remaining cross-sectional properties.

Because all FIB cross-sections are symmetric about the y-axis, I_{xy}, x_S, I_{xr}, and $I_{\omega r}$ have a value of zero (0) by definition. The remaining cross-sectional properties calculated for each FIB shape are summarized in Table C.2.

Table C.2. Cross-sectional properties of Florida-I Beams

Section	A (in^2)	I_{yy} (in^4)	I_{xx} (in^4)	y_s (in)	J (in^4)	C_ω (in^6)	I_{yr} (in^5)	I_{rr} (in^6)
36″ FIB	807	127,700	81283	3.00	30,864	11,577,000	703,250	86,224,000
45″ FIB	870	226,810	81540	3.46	31,885	21,835,000	1,521,200	167,760,000
54″ FIB	933	360,270	81798	3.81	32,939	35,370,000	2,760,500	315,370,000
63″ FIB	996	530,790	82055	4.07	33,973	52,203,000	4,471,300	562,480,000
72″ FIB	1059	741,060	82314	4.27	35,041	72,337,000	6,693,800	951,390,000
78″ FIB	1101	904,610	82484	4.38	35,693	87,610,000	8,473,400	1,314,600,000
84″ FIB	1143	1,087,800	82657	4.46	36,421	104,350,000	10,504,000	1,781,400,000
96″ FIB	1227	1,516,200	83,002	4.56	37,859	142,280,000	15,336,000	3,107,900,000

APPENDIX D
PROPERTIES OF FLORIDA BEARING PADS

This appendix includes computed stiffnesses (Table D.1) for several standard types of FDOT bearing pad, produced using the calculation methods discussed in Chapter 6. Pad types D, E, F, G, H, J, and K are current designs intended for use with Florida-I Beams (FIBs), while pad types A, B, and C were formerly provided for use with Florida Bulb-Tees (FBTs). While Florida Bulb-Tee girders are no longer used in new bridge designs, they are still in service in existing bridges throughout Florida, thus stiffness data for pad types A, B, and C are included here for completeness. Each pad type is defined by four design parameters (Figure D.1): the plan-view length and width (L and W), elastomer shear modulus (G), and the number of internal elastomer layers (n).

Linear stiffnesses corresponding to bearing pad shear, torsion, axial compression, overturning roll (about the y-axis) for the *zero-slope* condition, and bending roll (about the x-axis) are presented in Table D.1. Unlike bending roll, overturning roll stiffness varies depending on the total axial load (i.e., girder weight) when the slope angle is non-zero. Consequently, nonlinear overturning roll stiffness curves for several combinations slope angle and axial load are provided on the following pages.

Table D.1. Bearing pad dimensions and computed stiffnesses

	Pad Type	L (in)	W (in)	G (psi)	n	K_{shear} (kip/ft)	K_{axial} (kip/ft)	$k_{torsion}$ (kip-ft/rad)	$k_{roll,overturning}$ *(for zero slope)* (kip-ft/rad)	$k_{roll,bending}$ (kip-ft/rad)
FBTs	A	11	24	110	2	232	71000	46.4	6330	1330
	B	14	24	110	3	222	85300	64.0	7600	2590
	C	12	23	150	3	248	72200	55.8	5900	1610
FIBs	D	8	32	110	2	225	45900	28.1	7270	458
	E	10	32	110	2	282	81400	52.4	12900	1260
	F	10	32	110	3	211	57300	39.3	9080	890
	G	10	32	150	3	288	72700	53.6	11500	1130
	H	10	32	150	4	230	56300	42.8	8910	870
	J	10	32	150	5	192	45900	35.7	7260	712
	K	12	32	150	5	230	70200	58.7	11100	1560
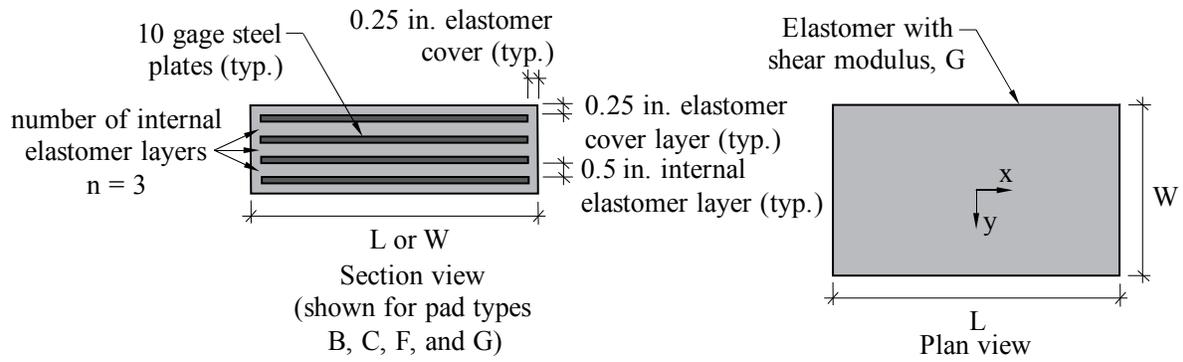
Figure D.1 Bearing pad dimensions and variables

On the pages that follow, each curve corresponds to a unique combination of pad type, slope angle, and axial load (the quantities noted in kips). On each curve, K_r is the initial overturning roll stiffness in kip-ft/rad.

Pad Type A

Pad Type B

180

Pad Type C

181

Pad Type D

Top-left chart:

120 kip (K_r = 12900)
100 kip (K_r = 12900)
80 kip (K_r = 12900)
60 kip (K_r = 12900)
40 kip (K_r = 12900)
20 kip (K_r = 12900)

Overturning moment (kip-ft)
120 110 100 90 80 70 60 50 40 30 20 10 0
0   0.01   0.02   0.03   0.04   0.05
Roll angle (rad)
Slope angle = 0.00 rad

Top-right chart:

120 kip (K_r = 12500)
100 kip (K_r = 12000)
80 kip (K_r = 10900)
60 kip (K_r = 9350)
40 kip (K_r = 7480)
20 kip (K_r = 5410)

Overturning moment (kip-ft)
120 110 100 90 80 70 60 50 40 30 20 10 0
0   0.01   0.02   0.03   0.04   0.05
Roll angle (rad)
Slope angle = 0.01 rad

Bottom-left chart:

120 kip (K_r = 9260)
100 kip (K_r = 8480)
80 kip (K_r = 7410)
60 kip (K_r = 6450)
40 kip (K_r = 5480)
20 kip (K_r = 3630)

Overturning moment (kip-ft)
120 110 100 90 80 70 60 50 40 30 20 10 0
0   0.01   0.02   0.03   0.04   0.05
Roll angle (rad)
Slope angle = 0.02 rad

Bottom-right chart:

120 kip (K_r = 7410)
100 kip (K_r = 7410)
80 kip (K_r = 6450)
60 kip (K_r = 5480)
40 kip (K_r = 4380)
20 kip (K_r = 2790)

Overturning moment (kip-ft)
120 110 100 90 80 70 60 50 40 30 20 10 0
0   0.01   0.02   0.03   0.04   0.05
Roll angle (rad)
Slope angle = 0.03 rad

Pad Type E

183

Pad Type F

Pad Type G

185

Pad Type H

186

Pad Type J

Pad Type K

APPENDIX E
PLOTS OF CAPACITY PREDICTION EQUATIONS

This appendix contains plots of subsets of the parametric study results along with the corresponding capacity prediction equations, as reported in Chapter 9. The intent of the plots is to illustrate the level of conservatism of the capacity prediction equations relative to the data, as well as the sensitivity of select system parameters. Figures E.1–E.5 illustrate the effect that changes in wind load have on the capacity of strut-braced girder systems. For girder systems with moment-resisting braces, Figures E.6–E.9 show the effect of changes in the effective brace stiffness (k_{brace}), Figures E.10–E.13 show the effect of changes in the number of interior brace points, and Figures E.14–E.18 show the effect of changes in wind load.
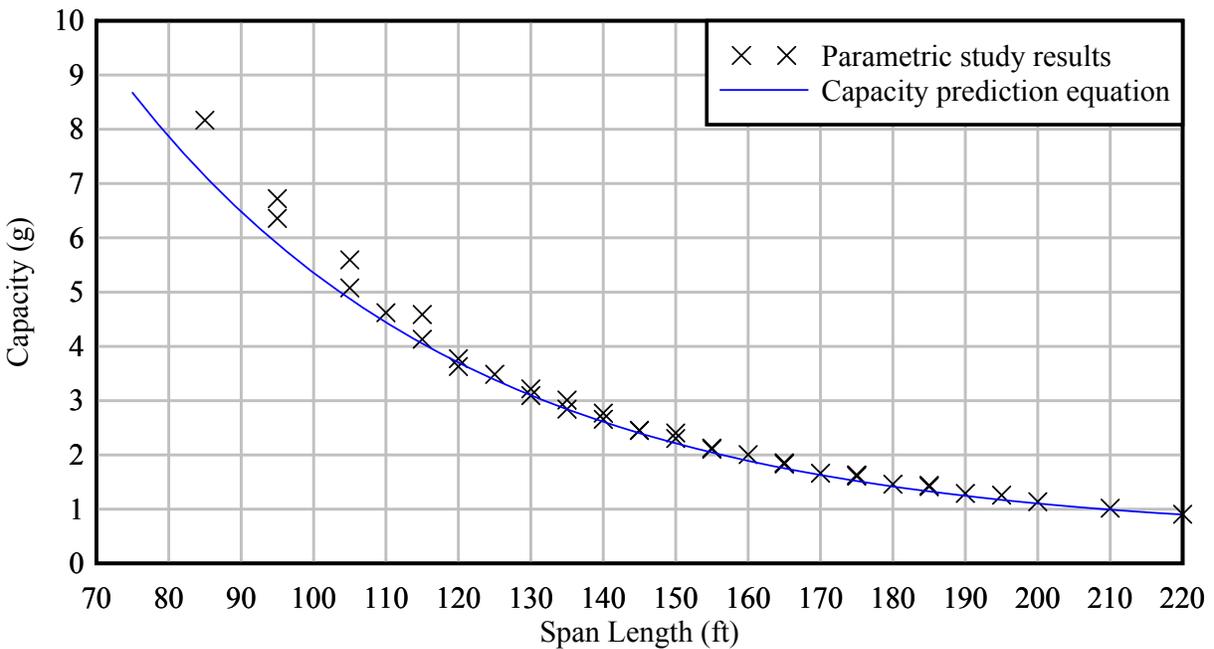
Figure E.1. Prediction of system capacity for 2-girder, unanchored strut-braced systems in 0-psf wind (Equation 9.10)
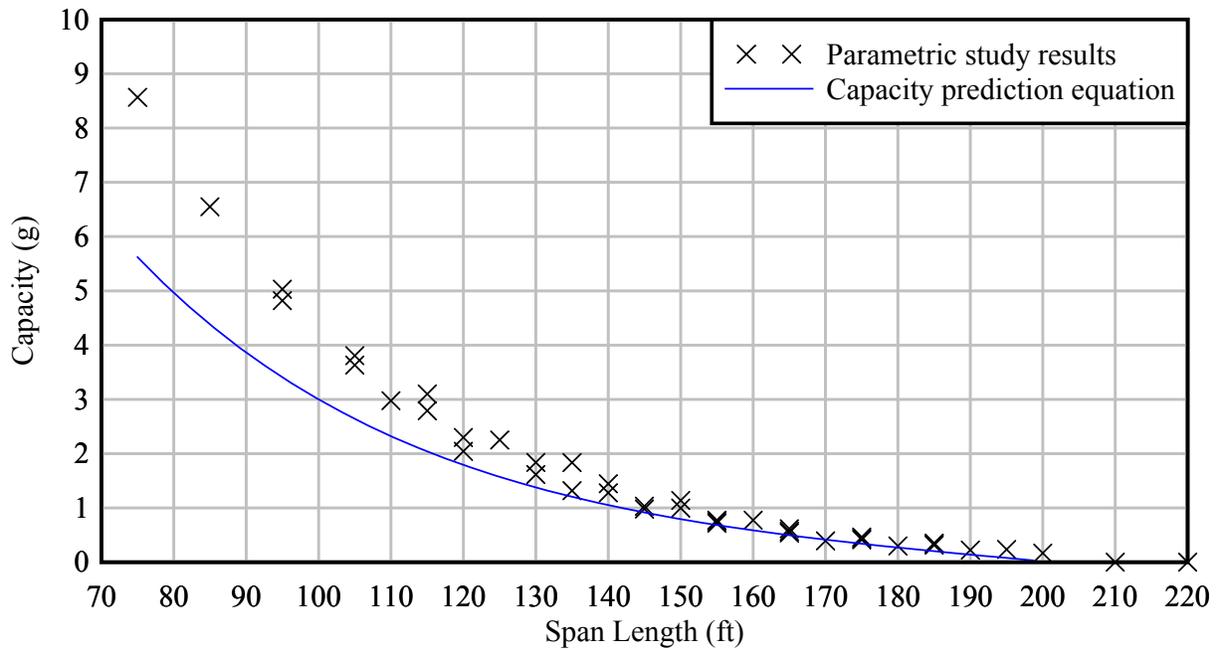
Figure E.2. Prediction of system capacity for 2-girder, unanchored strut-braced systems in 40-psf wind (Equation 9.10)
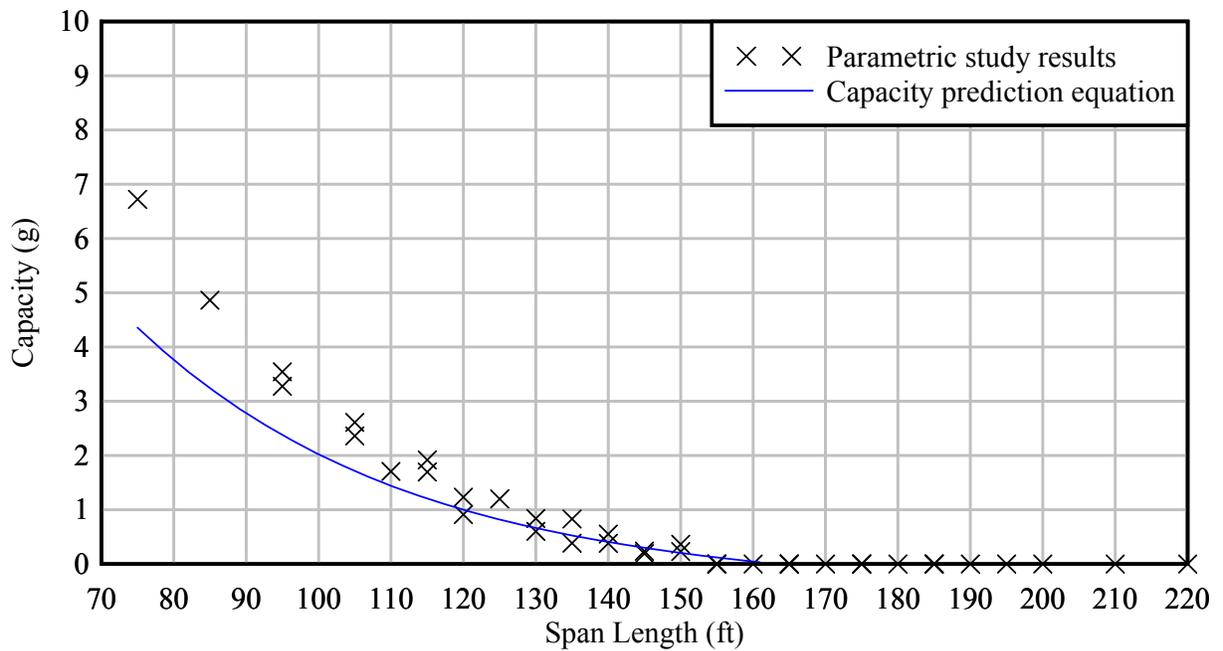
Figure E.3. Prediction of system capacity for 2-girder, unanchored strut-braced systems in 80-psf wind (Equation 9.10)

190
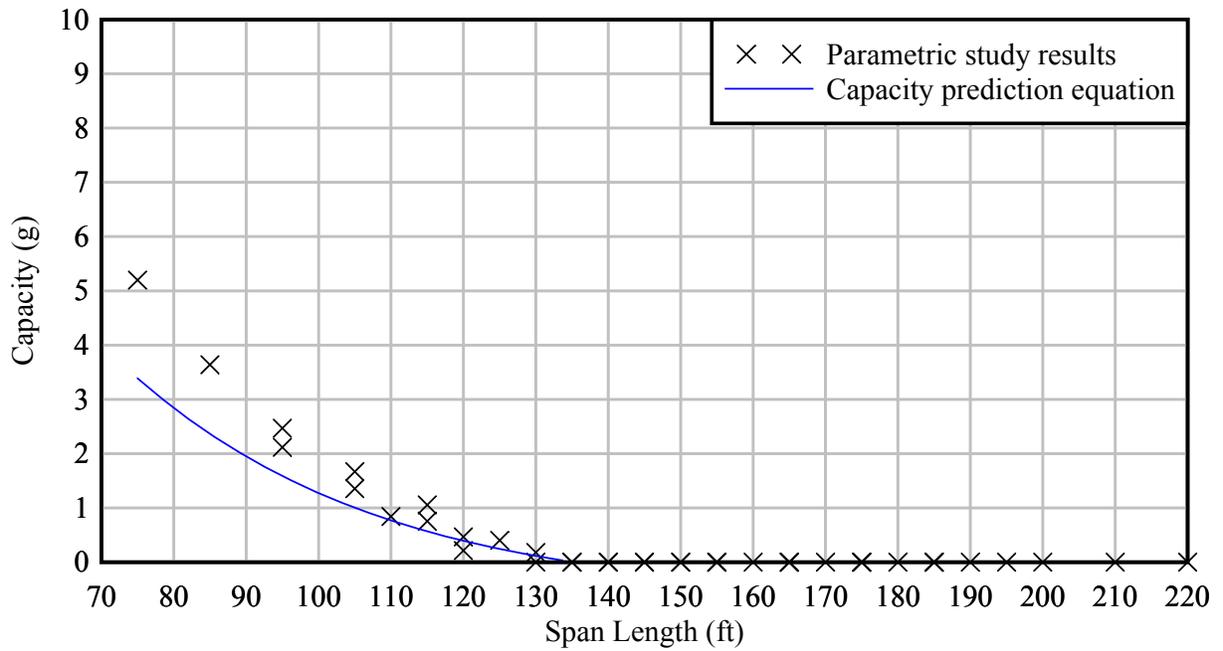
Figure E.4. Prediction of system capacity for 2-girder, unanchored strut-braced systems in 120-psf wind (Equation 9.10)
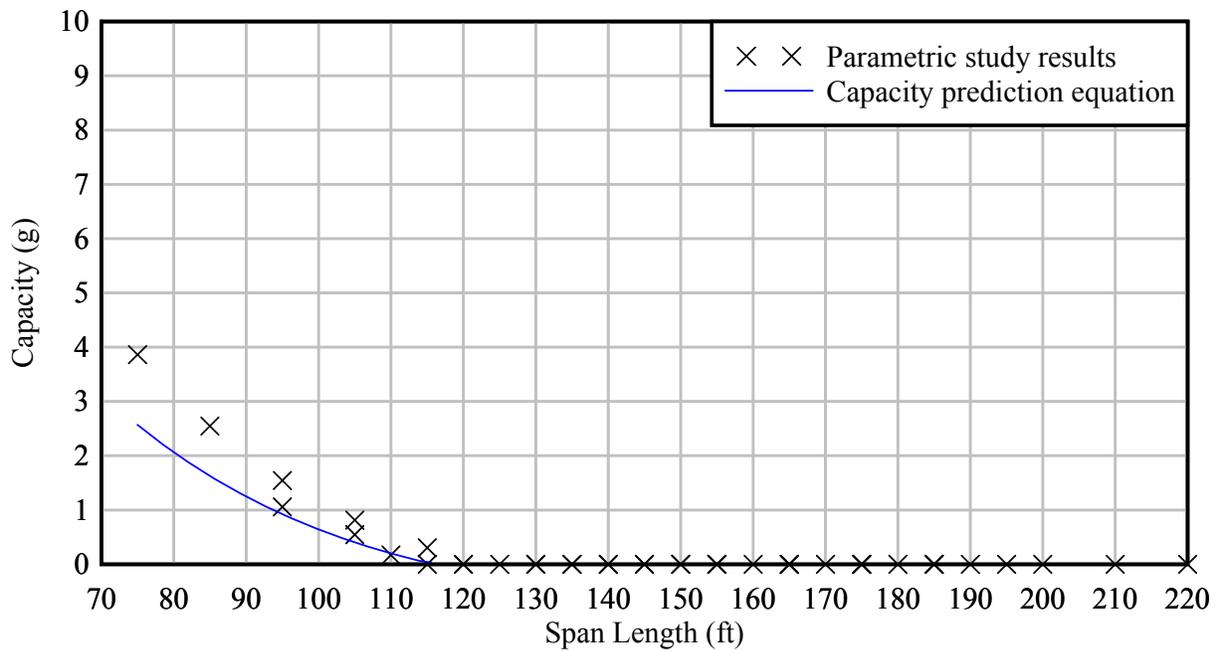
Figure E.5. Prediction of system capacity for 2-girder, unanchored strut-braced systems in 160-psf wind (Equation 9.10)

191
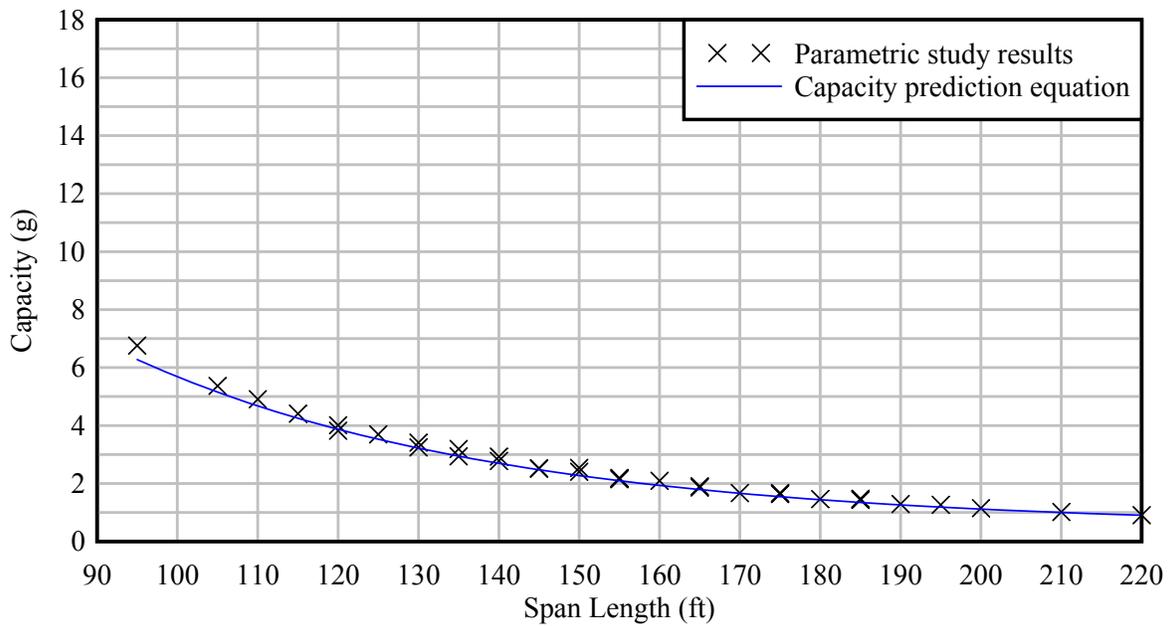
Figure E.6. Prediction of system capacity for end-braced systems in 0-psf wind with moment-resisting braces with k_{brace} = 15,000 kip-ft/rad (Equation 9.17)
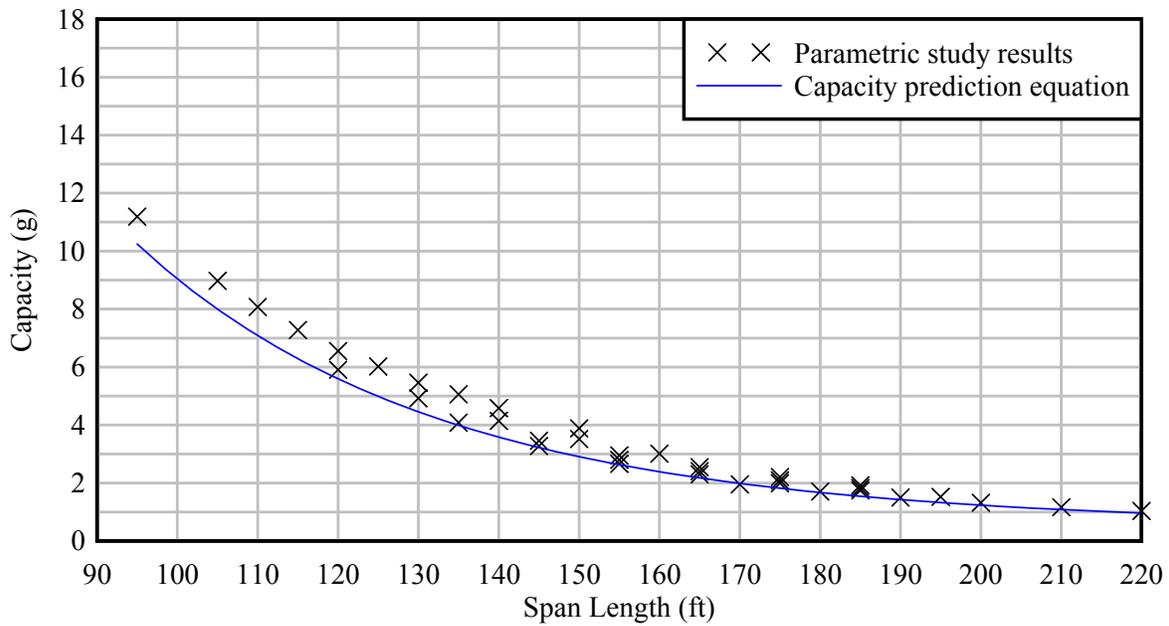
Figure E.7. Prediction of system capacity for end-braced systems in 0-psf wind with moment-resisting braces with k_{brace} = 200,000 kip-ft/rad (Equation 9.17)
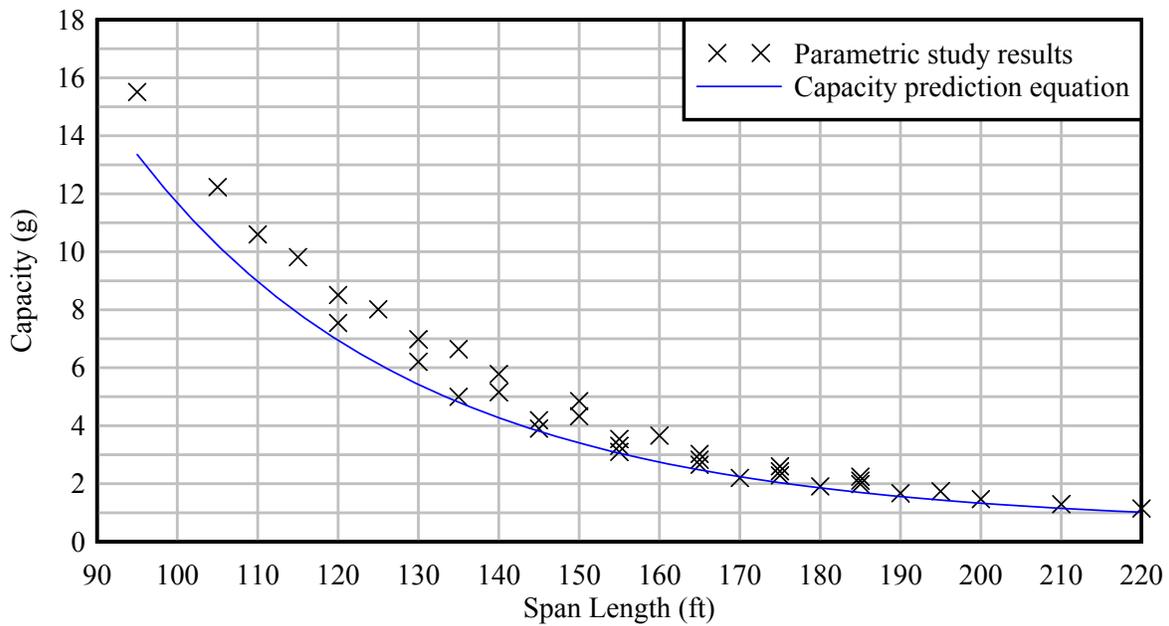
Figure E.8. Prediction of system capacity for end-braced systems in 0-psf wind with moment-resisting braces with k_{brace} = 400,000 kip-ft/rad (Equation 9.17)
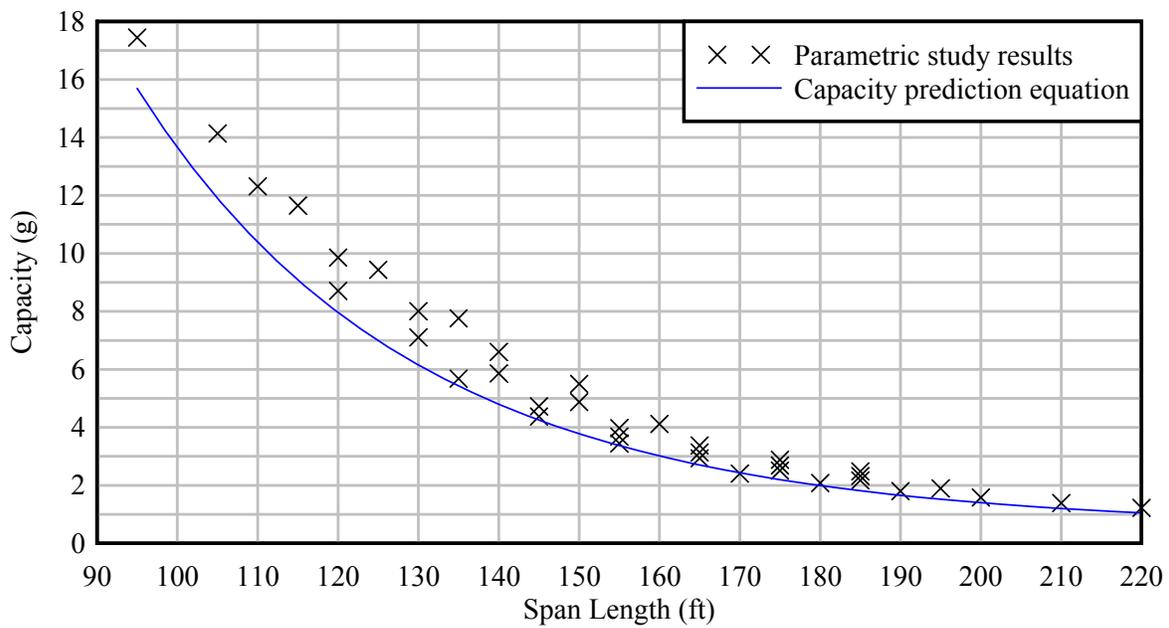
Figure E.9. Prediction of system capacity for end-braced systems in 0-psf wind with moment-resisting braces with k_{brace} = 600,000 kip-ft/rad (Equation 9.17)

193
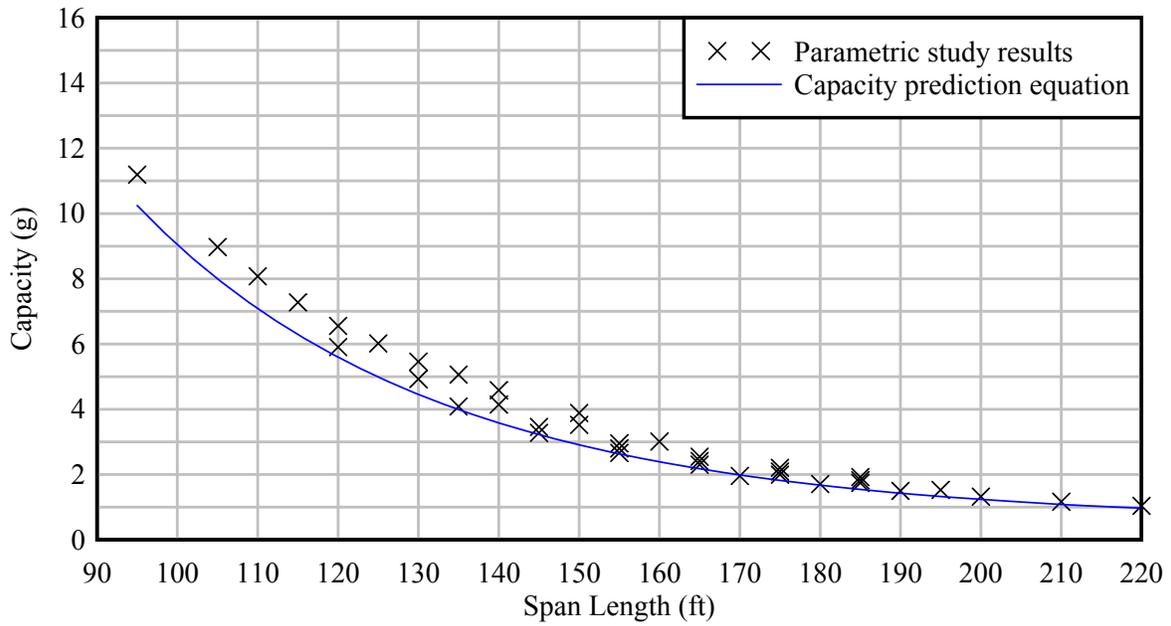
Figure E.10. Prediction of system capacity for systems in 0-psf wind with moment-resisting braces (k_{brace} = 200,000 kip-ft/rad) with no interior brace points (Equation 9.17)
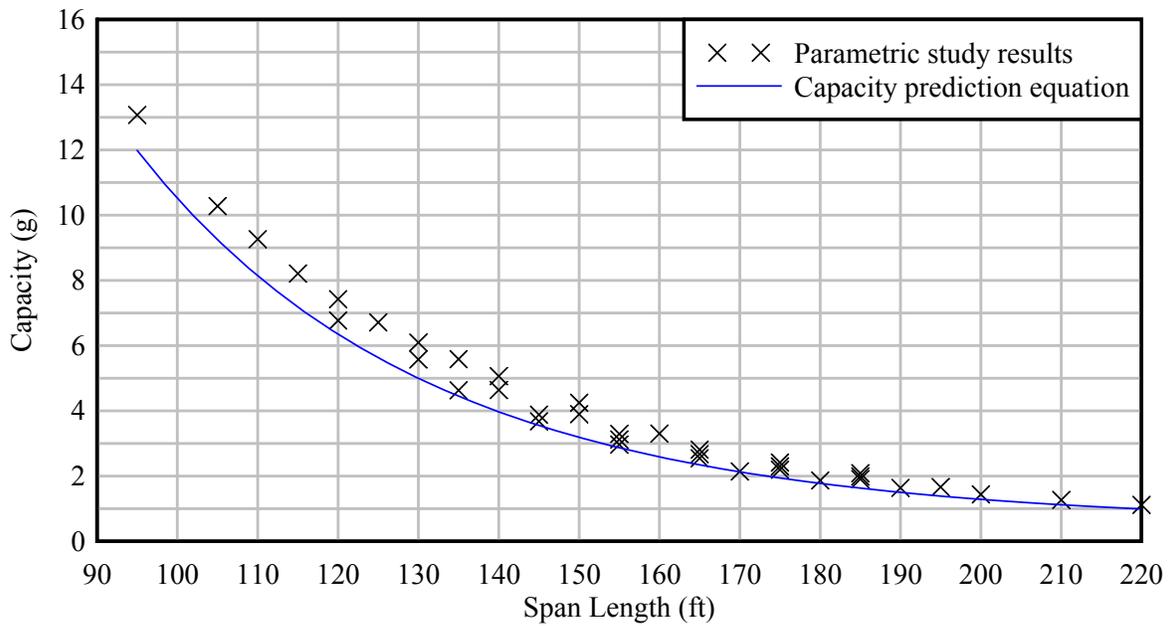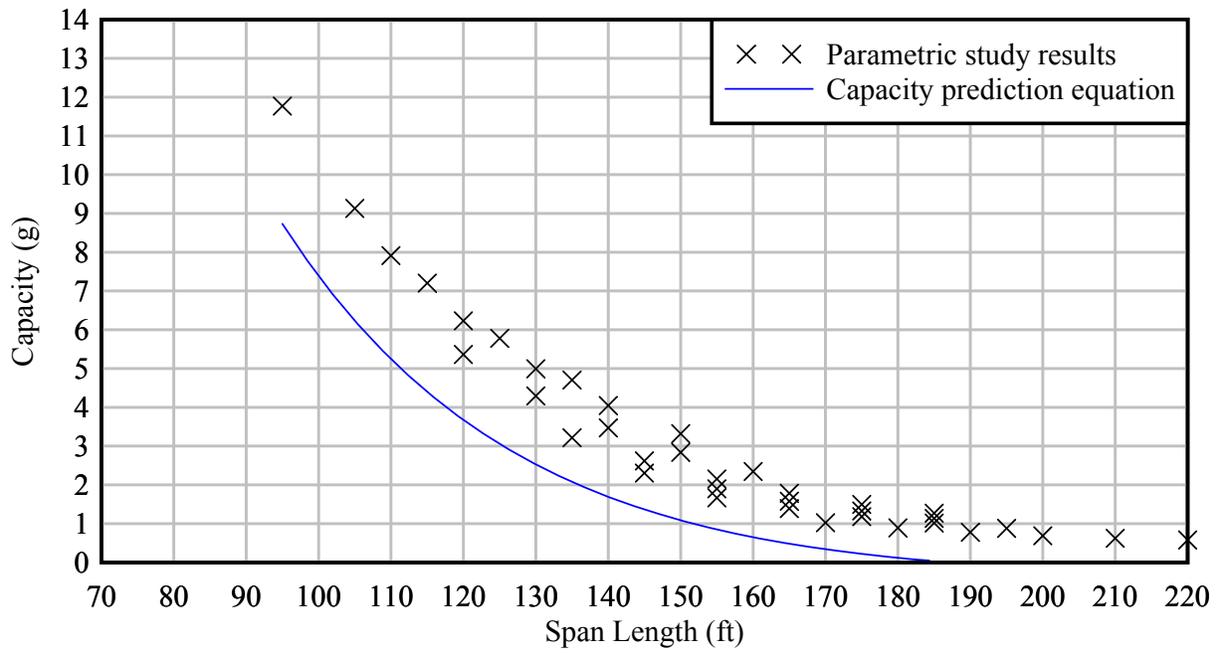

Figure E.11. Prediction of system capacity for systems in 0-psf wind with moment-resisting braces (k_{brace} = 200,000 kip-ft/rad) with 1 interior brace point (Equation 9.17)
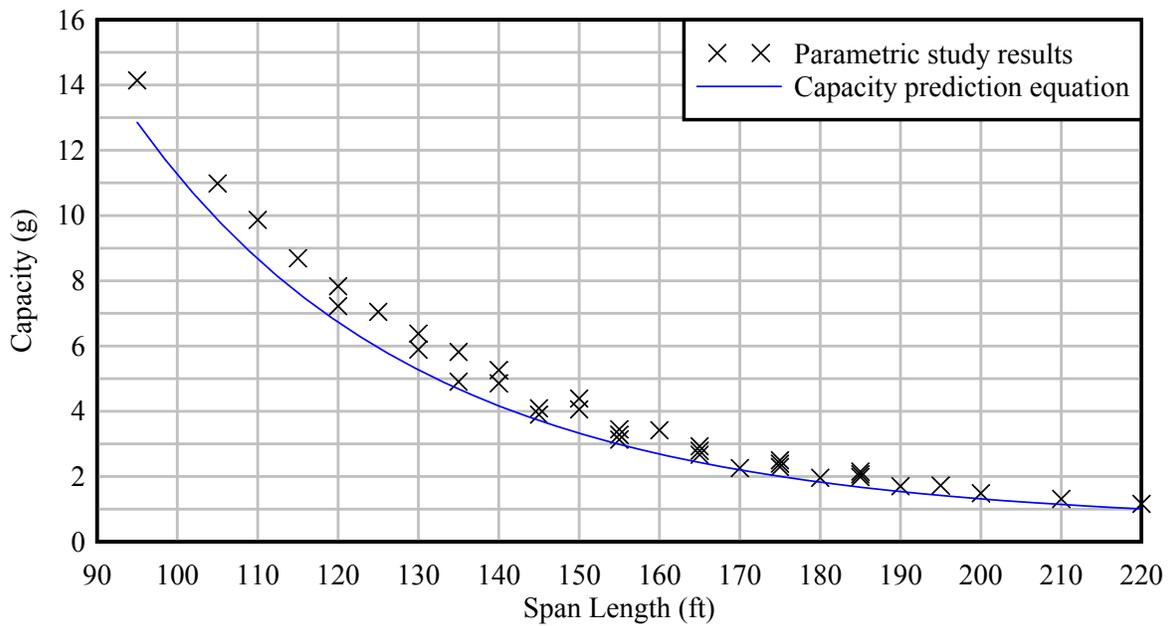
Figure E.12. Prediction of system capacity for systems in 0-psf wind with moment-resisting braces (k_{brace} = 200,000 kip-ft/rad) with 2 interior brace points (Equation 9.17)
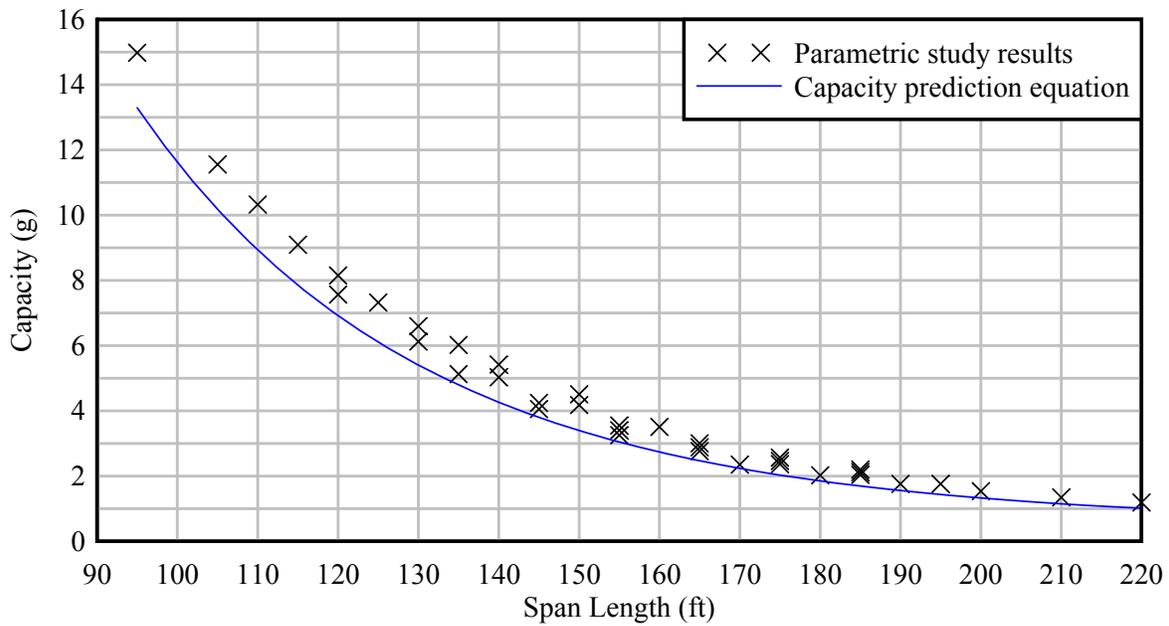
Figure E.13. Prediction of system capacity for systems in 0-psf wind with moment-resisting braces (k_{brace} = 200,000 kip-ft/rad) with 3 interior brace points (Equation 9.17)
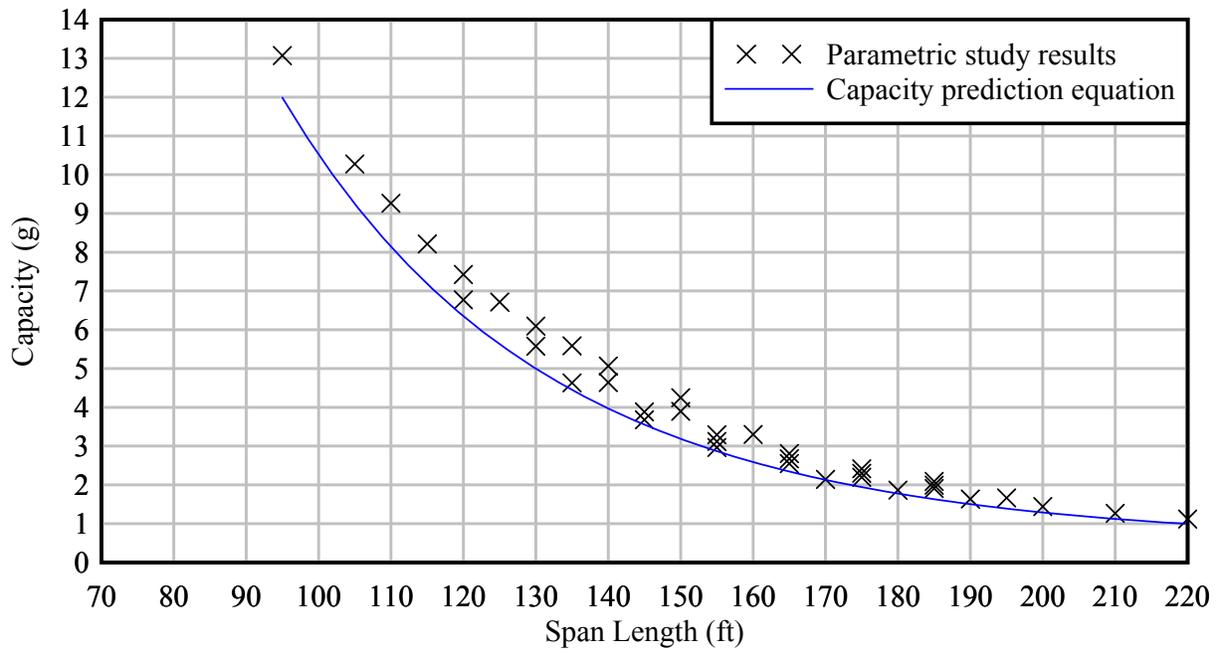
Figure E.14. Prediction of system capacity for systems with moment-resisting braces (k_{brace} = 200,000 kip-ft/rad) with 1 interior brace point in 0-psf wind (Equation 9.17)
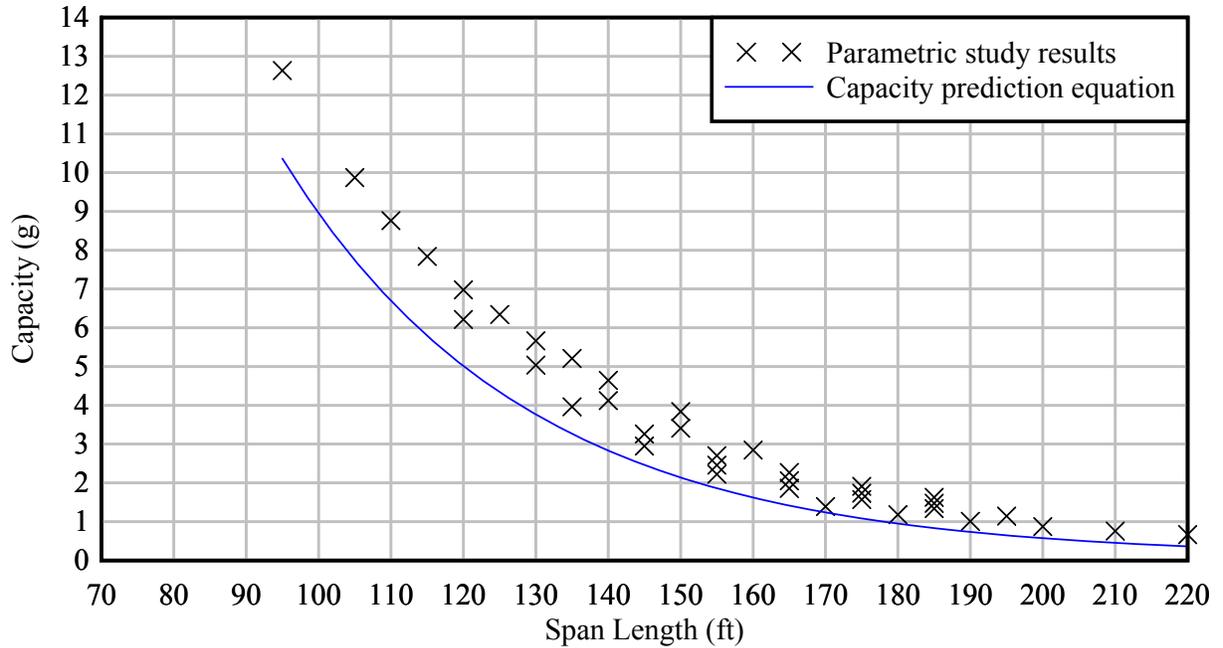
Figure E.15. Prediction of system capacity for systems with moment-resisting braces (k_{brace} = 200,000 kip-ft/rad) with 1 interior brace point in 40-psf wind (Equation 9.17)
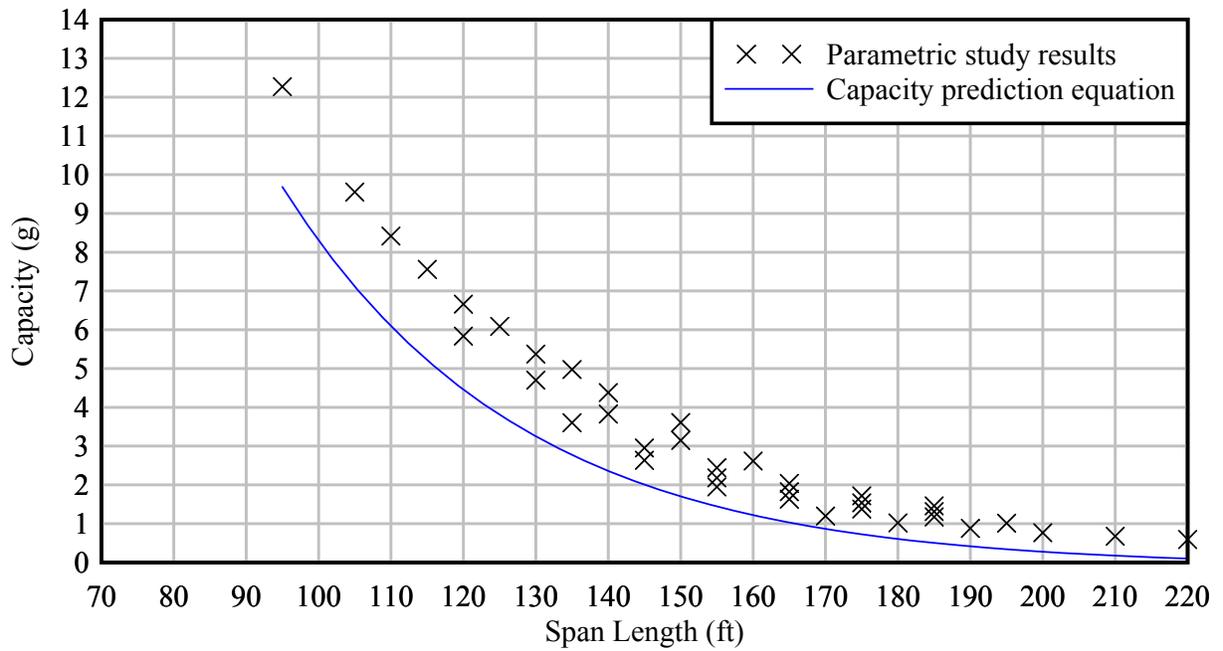
Figure E.16. Prediction of system capacity for systems with moment-resisting braces (k_{brace} = 200,000 kip-ft/rad) with 1 interior brace point in 80-psf wind (Equation 9.17)
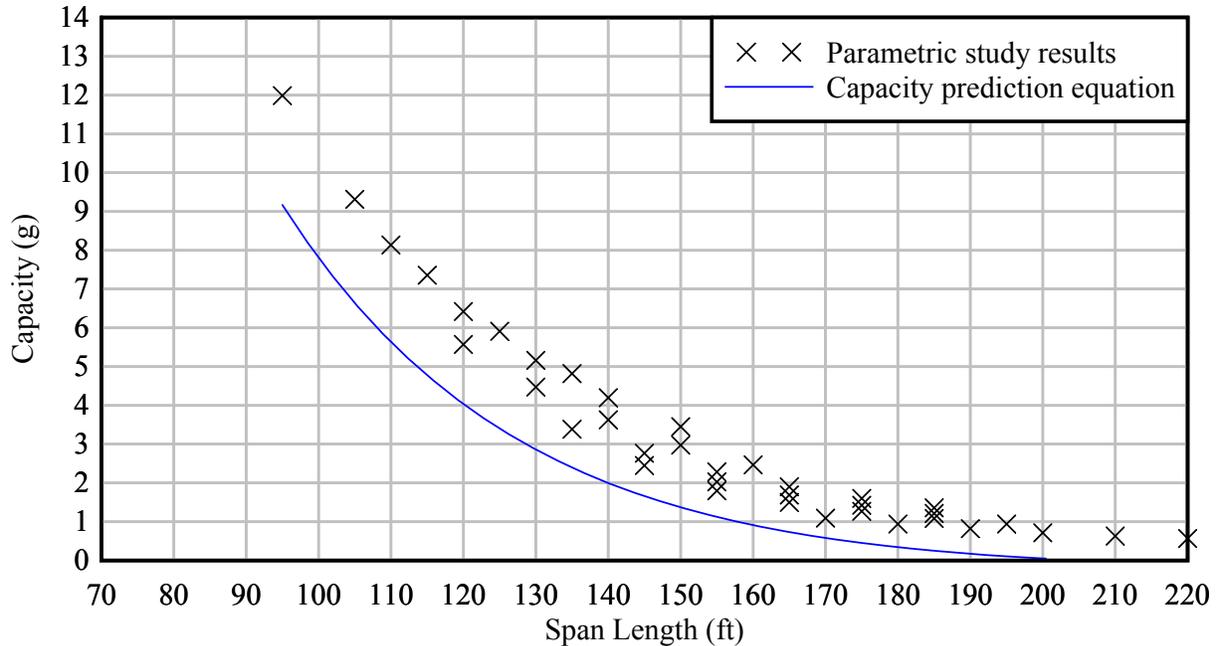
Figure E.17. Prediction of system capacity for systems with moment-resisting braces (k_{brace} = 200,000 kip-ft/rad) with 1 interior brace point in 120-psf wind (Equation 9.17)

Figure E.18. Prediction of system capacity for systems with moment-resisting braces (k_{brace} = 200,000 kip-ft/rad) with 1 interior brace point in 160-psf wind (Equation 9.17)

APPENDIX F
EXAMPLE CALCULATIONS:
GLOBAL PRESSURE COEFFICIENT FOR STRENGTH LIMIT STATE

      This appendix contains example calculations for computing the global pressure coefficient for a multi-girder system (discussed in Chapter 5). It should be noted that this analysis procedure is intended for global strength calculations only (as opposed to stability calculations).

Global pressure coefficient for strength design calculations
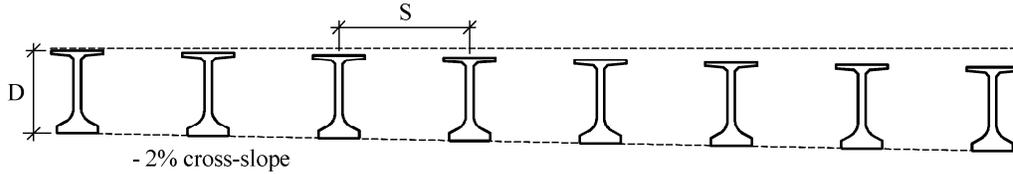
Section view

<u>System parameters...</u>

FIB78 ... Girder type

$n := 8$ ... Number of girders

$D := 78$ ... (in) Section depth

$S := 120$ ... (in) Girder spacing

$\theta_{cross\text{-}slope} := -2\%$ ... (%) Girder cross-slope

$\theta_{cross\text{-}slope} := atan\left(\theta_{cross\text{-}slope}\right) = -0.02$ ... Convert from % to rad

$\theta_{wind} := 2.5$ ... (deg) Assumed maximum wind angle

$\theta_{wind} := \theta_{wind} \cdot \dfrac{\pi}{180} = 0.044$ ... Convert from deg to rad

<u>Shielding model...</u>
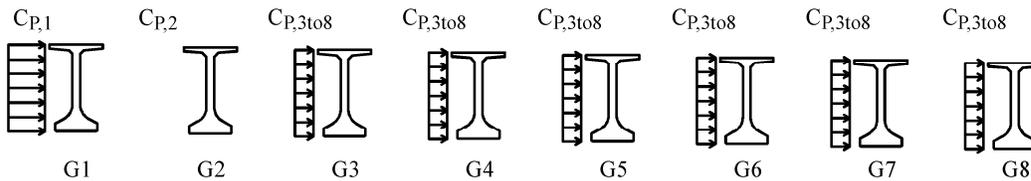
$C_{P,1} := 2.0$ ... Pressure coefficient of leading (windward) girder (G1)

$C_{P,2} := 0.0$ ... Pressure coefficient of 1st shielded girder (G2)

$C_{P,3to8} := 0.5 \cdot C_{P,1} = 1.0$ ... Pressure coefficient of subsequent shielded girders (G3 to G8)

$$C_P := \begin{pmatrix} C_{P,1} & C_{P,2} & C_{P,3to8} & C_{P,3to8} & C_{P,3to8} & C_{P,3to8} & C_{P,3to8} & C_{P,3to8} \end{pmatrix}$$
$$\quad\ \ G1 \quad\ \ G2 \quad\ \ G3 \quad\ \ G4 \quad\ \ G5 \quad\ \ G6 \quad\ \ G7 \quad\ \ G8$$

<u>Calculation of global pressure coefficient...</u>

$\theta_{max} := \left|\theta_{wind}\right| + \left|\theta_{cross\text{-}slope}\right| = 0.064$ ... (rad) Maximum angle between wind and cross-slope (Equation 5.20)

$D_{projected} := D + (n - 1) \cdot S \cdot tan\left(\theta_{max}\right) = 131.5$ ... (in) Projected depth of girder system (Equation 5.19)

$\alpha := 0.240 + 0.136\left(\dfrac{D_{projected}}{D}\right) = 0.469$ ... Reduction factor for global pressure coefficient (Equation 5.18)

$C_{P,global\text{-}strength} := \alpha \cdot \sum C_P = 3.75$ ... Global pressure coefficient for strength calculations (Equation 5.17)

200

APPENDIX G
EXAMPLE CALCULATIONS:
BEARING PAD STIFFNESS

This appendix contains example calculations for computing the stiffnesses of a rectangular steel-reinforced elastomeric bearing pad in all six (6) degrees of freedom, using the simplified procedures discussed in Chapter 6. All four deformation modes are included: shear, torsion, compression (axial) and rotation.

Stiffness analysis of rectangular steel-reinforced elastomeric bearing pad

Plan view

Side view
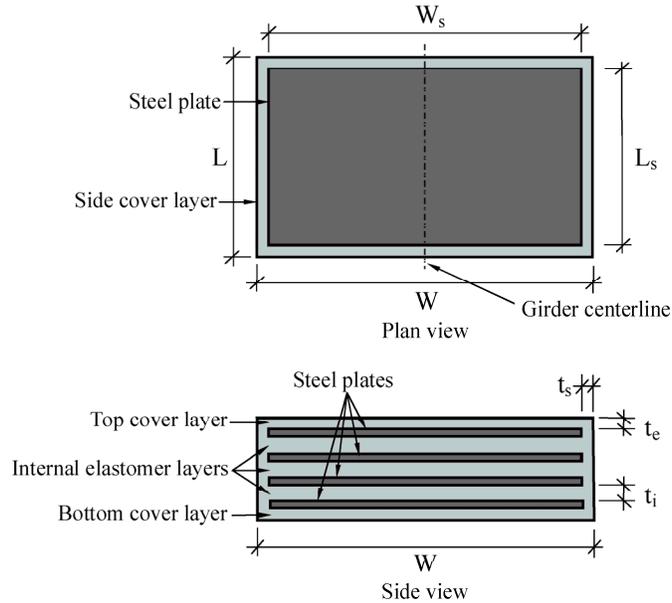
Pad dimensions...

Pad Type G   ... Bearing pad design (FDOT, 2012c)

$L := 10$ ... (in) Length of pad

$W := 32$ ... (in) Width of pad

$n := 3$ ... (in) Number of internal elastomer layers

$t_i := 0.5$ ... (in) Thickness of internal elastomer layers

$t_e := 0.25$ ... (in) Thickness of external (top and bottom) cover layers

$t_s := 0.25$ ... (in) Thickness of side cover layer

$L_s := L - 2t_s = 9.5$ ... (in) Length of steel plates

$W_s := W - 2t_s = 31.5$ ... (in) Width of steel plates

$T := n \cdot t_i + 2 \cdot t_e = 2$ ... (in) Total elastomer thickness

Elastomer material properties...

$G := 0.150$ ... (ksi) Elastomer shear modulus

$K := 200$ ... (ksi) Elastomer bulk modulus: default value

Bearing conditions...

$\phi := 0.023$ ... (rad) Slope angle between bottom of girder and top of pad

$F_{axial} := 75$ ... (kip) Axial load (reaction force from girder self-weight)

Shear stiffness...

$k_{shear} := \dfrac{L \cdot W \cdot G}{T} = 24.0$ ... (kip/in) Shear stiffness of pad, kip/in (Equation 6.3)

<u>Torsional stiffness...</u>

$$J_{pad} := \left(\frac{W \cdot L^3}{16}\right)\left[\frac{16}{3} - 3.36\left(\frac{L}{W}\right)\left(1 - \frac{L^4}{12W^4}\right)\right] = 8568 \qquad \text{... (in}^4\text{) Torsional constant of pad (Equation 6.5)}$$

$$k_{torsion} := \frac{J_{pad} \cdot G}{T} = 643 \qquad\qquad\qquad\qquad \text{... (kip-in/rad) Torsional stiffness of pad (Equation 6.4)}$$

<u>Axial stiffness of internal elastomer layer...</u>

$$S_i := \frac{L_s \cdot W_s}{2 \cdot t_i \cdot (L_s + W_s)} = 7.299 \qquad\qquad\qquad \text{... Shape factor of internal elastomer layer (Equation 6.9)}$$

$$\lambda_i := S_i \cdot \sqrt{\frac{3 \cdot G}{K}} = 0.346 \qquad\qquad\qquad \text{... Compressibility index of internal layer (Equation 6.12)}$$

$$B_{a,i} := \left(2.31 - 1.86 \cdot \lambda_i\right) + \left(-0.90 + 0.96\lambda_i\right)\left(1 - \min\left(\frac{L_s}{W_s}, \frac{W_s}{L_s}\right)\right)^2 = 1.389 \qquad \text{... Fitting parameter (Equation 6.13)}$$

$$k_{layer,i} := \frac{L_s \cdot W_s}{t_i} \cdot 3G \cdot \left(1 + B_{a,i} \cdot S_i^2\right) = 20200 \qquad \text{... (kip/in) Axial stiffness of internal layer (Equation 6.11)}$$

<u>Axial stiffness of external elastomer layer...</u>

$$S_e := \frac{L_s \cdot W_s}{2 \cdot t_e \cdot (L_s + W_s)} = 14.598 \qquad\qquad\qquad \text{... Shape factor of external layer (Equation 6.9)}$$

$$\lambda_e := S_e \cdot \sqrt{\frac{3 \cdot G}{K}} = 0.692 \qquad\qquad\qquad \text{... Compressibility index of external layer (Equation 6.12)}$$

$$B_{a,e} := \left(2.31 - 1.86 \cdot \lambda_e\right) + \left(-0.90 + 0.96\lambda_e\right)\left(1 - \min\left(\frac{L_s}{W_s}, \frac{W_s}{L_s}\right)\right)^2 = 0.907 \qquad \text{... Fitting parameter (Equation 6.13)}$$

$$k_{layer,e} := \frac{L_s \cdot W_s}{t_e} \cdot 3G \cdot \left(1 + B_{a,e} \cdot S_e^2\right) = 1 \times 10^5 \qquad \text{... (kip/in) Axial stiffness of external layer (Equation 6.11)}$$

<u>Combined axial stiffness...</u>

$$k_{axial} := \left[n \cdot \left(\frac{1}{k_{layer,i}}\right) + 2 \cdot \left(\frac{1}{k_{layer,e}}\right)\right]^{-1} = 5966 \qquad \text{... (kip/in) Axial stiffness of pad (Equation 6.12)}$$

<u>Bending roll stiffnesses of bearing pad...</u>

$$k_{roll,bending} := \frac{k_{axial} \cdot L^2}{45} = 13258 \qquad\qquad\qquad \text{... (kip-in/rad) Bending roll stiffness of pad (Equation 6.30)}$$

203

Overturning roll stiffnesses of bearing pad...

$$p := \sqrt{\frac{9 \cdot F_{axial}}{2 \cdot L \cdot \phi \cdot k_{axial}}} = 0.496$$

... Portion of pad area in contact with girder (Equation 6.29)

$$p := \begin{vmatrix} 1 & \text{if } p > 1 \\ p & \text{otherwise} \end{vmatrix} = 0.496$$

$$k_{roll,overturning} := p^2(3 - 2p) \frac{k_{axial} \cdot W^2}{45} = 67054$$

... (kip-in/rad) Bending roll stiffness of pad (Equation 6.29)

Unit conversions...

$$k_{shear} := k_{shear} \cdot 12 = 288$$

... (kip/ft) Shear stiffness of pad

$$k_{axial} := k_{axial} \cdot 12 = 71592$$

... (kip/ft) Axial stiffness of pad

$$k_{torsion} := k_{torsion} \div 12 = 53.6$$

... (kip-ft/rad) Torsional stiffness of pad

$$k_{roll,overturning} := k_{roll,overturning} \div 12 = 5588$$

... (kip-ft/rad) Overturning roll stiffness of pad

$$k_{roll,bending} := k_{roll,bending} \div 12 = 1105$$

... (kip-ft/rad) Bending roll stiffness of pad

204

APPENDIX H
EXAMPLE CALCULATIONS:
TEMPORARY BRACING ASSESSMENT FOR AN FIB BRIDGE

This appendix contains example calculations demonstrating the assessment of temporary bracing for a typical FIB bridge using the capacity equations described in Chapters 8 and 9. In addition to the wind capacity of a single girder during the initial construction stage, the capacity of the complete multi-girder system is evaluated using both strut braces and moment-resisting braces.

Design of temporary bracing for an FIB bridge

Plan view

- 2% cross-slope

Section view
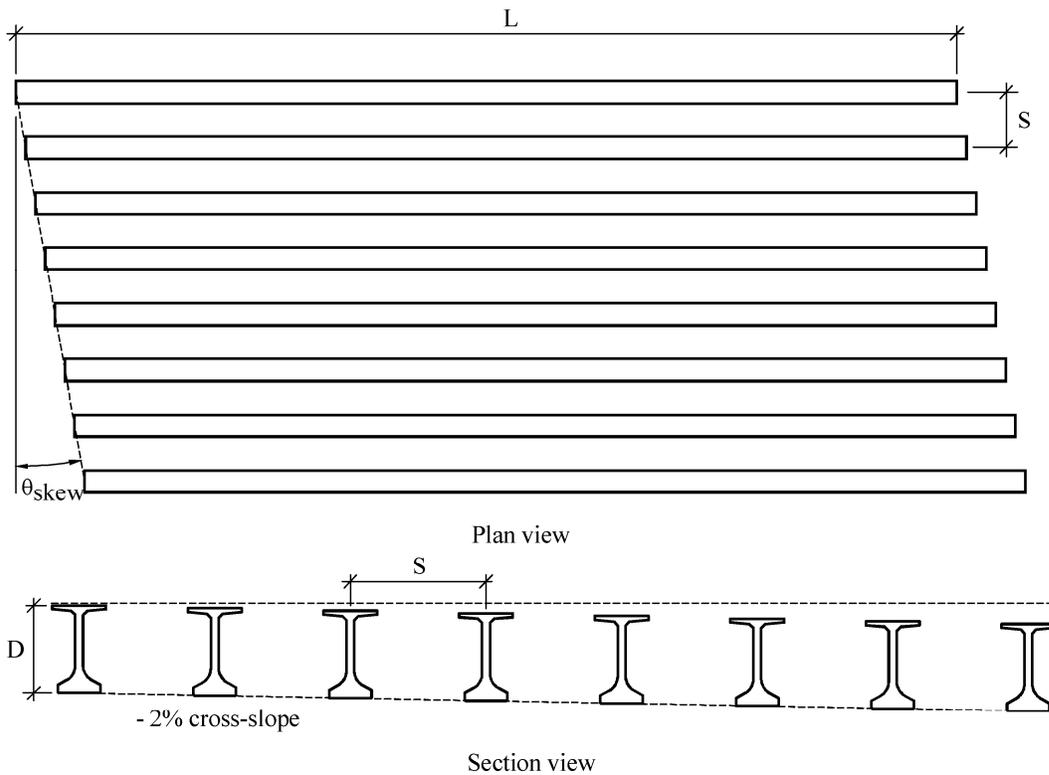
<u>System parameters...</u>

FIB78   ... Girder type

$D := 78$ ... (in) Section depth

$w_{sw} := 1146$ ... (lbf/ft) Girder self-weight

$L := 170$ ... (ft) Span length

$n := 8$ ... Number of girders

$S := 10$ ... (ft) Girder spacing

$\theta_{skew} := 10$ ... (deg) Skew angle

$\theta_{skew} := \theta_{skew} \cdot \dfrac{\pi}{180} = 0.175$ ... Convert from deg to rad

<u>Wind loads...</u>
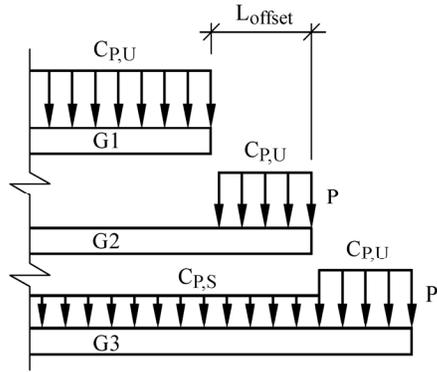
$V := 110$ ... (mph) Basic wind speed

$G := 0.85$ ... Gust effect factor (SDG §2.4.1E)

$z := 20$ ... (ft) Elevation of bridge girders

$K_z := 2.01 \cdot \left(\dfrac{z}{900} \right)^{0.2105} = 0.902$ ... Velocity pressure exposure coefficient (SDG §2.4.1D)

$C_{P,U} := 2.0$ ... Pressure coefficient for <u>unshielded</u> FIB (Girder G1) (Figure 5.17)

$C_{P,S} := 1.0$ ... Pressure coefficient for <u>shielded</u> FIB (girders G3, G4, etc) (Figure 5.17)

$P_U := 0.6 \left(2.56 \cdot 10^{-6} \cdot K_z \cdot V^2 \cdot G \cdot C_{P,U} \right) = 0.028$ ... (ksf) Design wind pressure for unshielded FIB (SDG §2.4.1D)

$P_U := P_U \cdot 1000 = 28.5$ ... Convert from ksf to psf

$P_S := 0.6 \left(2.56 \cdot 10^{-6} \cdot K_z \cdot V^2 \cdot G \cdot C_{P,S} \right) = 0.014$ ... (ksf) Design wind pressure for shielded FIB (SDG §2.4.1D)

$P_S := P_S \cdot 1000 = 14.2$ ... Convert from ksf to psf

$L_{offset} := S \cdot \tan \left(\theta_{skew} \right) = 1.8$ ... (ft) Skew offset length (see figure above)

$L_{shielded} := L - L_{offset}$ ... (ft) Shielded length
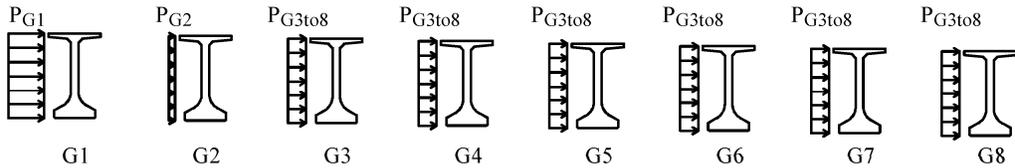
$P_{G1} := P_U = 28.5$ ... (psf) Average wind load on girder G1

$P_{G2} := \dfrac{0 \cdot L_{shielded} + P_U \cdot L_{offset}}{L} = 0.3$ ... (psf) Average wind load on girder G2

$P_{G3to8} := \dfrac{P_S \cdot L_{shielded} + P_U \cdot L_{offset}}{L} = 14.4$ ... (psf) Average wind load on girders G3, G4, etc.

$P_{bar} := \dfrac{P_{G1} + P_{G2} + P_{G3to8} \cdot (n - 2)}{n} = 14.4$ ... (psf) Average wind load per girder (Equation 9.7)

207

<u>Compute anchor roll stiffness...</u>
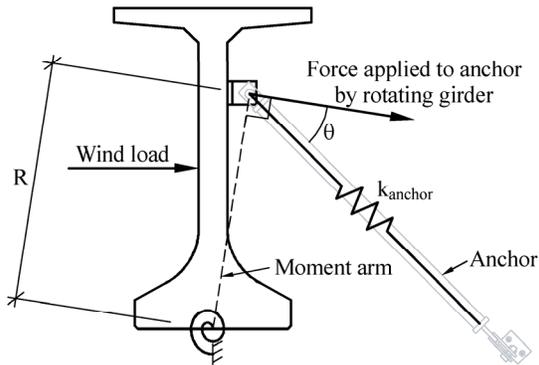
$k_{anchor} := 75$ ... (kip/in) Axial stiffness of anchor (Figure 7.6)

$R := 55$ ... (in) Anchor moment arm (Figure 7.6)

$\theta := 45$ ... (deg) Angle between anchor and girder force vector (Figure 7.6)

$\theta := \theta \cdot \dfrac{\pi}{180}$ ... Convert from deg to rad

$k_{roll,anchor} := k_{anchor} \cdot (\cos(\theta))^2 \cdot R^2 = 113438$ ... (kip-in/rad) Roll stiffness of anchor (Equation 7.4)

$k_{roll,anchor} := k_{roll,anchor} \div 12 = 9453$ ... Convert from kip-in/rad to kip-ft/rad

<u>Compute wind capacity of individual girder...</u>

$P_{max,0} := 123e^{\frac{-L}{100}}\left(1 + 15e^{\frac{-D}{22}}\right) - 750e^{\frac{-D}{16}} - 16 = 10.47$ ... (psf) Wind capacity of unanchored girder (Equation 8.2)

$P_{max} := P_{max,0} + 11e^{\frac{-L}{22}}\left(k_{roll,anchor}\right) = 56.29$ ... (psf) Final wind capacity of anchored girder (Equation 8.6)

$P_{G1} = 28.498$ $P_{max} > P_{G1}$ ... OK (Wind capacity exceeds design wind load)

<u>Compute capacity of multi-girder system (strut braces)...</u>

$C_0 := 39 \cdot e^{\frac{-L}{48}} + 0.5 = 1.63$ ... (g) Baseline system capacity (Equation 9.2)

$C := C_0 + \dfrac{k_{roll,anchor}}{n}\left(\dfrac{100 - D}{125000}\right) - \dfrac{\sqrt{P_{bar}}}{37000}\left(L^2 - 405L - 0.01L \cdot \dfrac{k_{roll,anchor}}{n} + 50000\right) - \dfrac{D \cdot P_U}{48w_{sw}} = 0.973$

            ... (g) Final system capacity (Equation 9.22)

$C < 1$ ... Not OK

K-Brace design

End moments released

Fixed

Rigid links

E = 29000 ksi
A = 2.86 in^2
I = 4.32 in^4

Pin

M
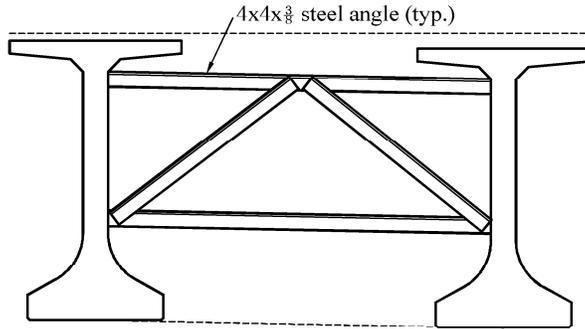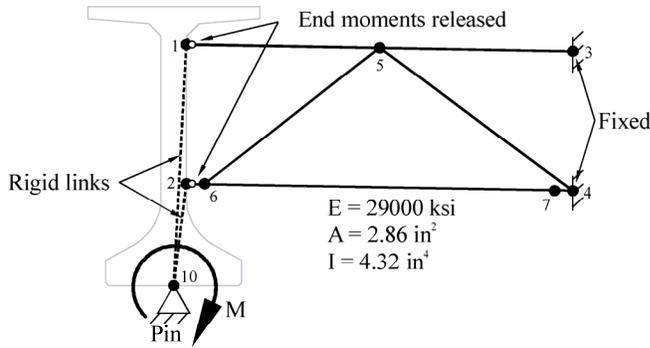
Node	X-Coordinate	Y-Coordinate
1	3.50	69.50
2	3.50	24.00
3	116.50	67.10
4	116.50	21.60
5	60.00	68.30
6	6.50	23.94
7	113.50	21.66
10	0.00	0.00

Structural model used for
determination of effective brace stiffness

$M := 1$ ... (kip-in) Unit moment load applied to structural model

$\theta_{10} := 2.26 \cdot 10^{-7}$ ... (rad) Angular displacement computed from model at node 10

$k_{brace} := \dfrac{M}{\theta_{10}} = 4.425 \times 10^6$ ... (kip-in/rad) Effective brace stiffness

$k_{brace} := k_{brace} \div 12 = 3.687 \times 10^5$ ... Convert from kip-in/rad to kip-ft/rad

209

<u>Compute capacity of multi-girder system (K-braces at girder ends)</u>

Table 9.4

n_i	Brace locations	ω
0	End bracing	1.0
1	Midpoint bracing	1.4
2	Third-point bracing	1.6
3	Quarter-point bracing	1.7

$n_i := 0$ ...Number of interior brace points

$\omega := 1$ ...Interior brace coefficient (Table 9.4, reproduced above)

$$C := C_0 + \omega \cdot \frac{620 \cdot k_{brace} \cdot e^{\frac{-L}{30}}}{k_{brace} + 1000000} - \frac{\sqrt{P_{bar}}}{1000000}\left(8 \cdot L^2 + 0.004 \cdot L \cdot k_{brace} - 5100 \cdot L - k_{brace} + 900000\right) - \frac{D \cdot P_U}{48 w_{sw}} = 1.612$$

... (g) Final system capacity (Equation 9.23)

$C > 1$ ... OK

210

APPENDIX I
DETAILED REPORTS FROM WIND TUNNEL TESTS

All wind tunnel testing, including model fabrication, wind load measurement, and data normalization, was performed by Boundary Layer Wind Tunnel Laboratory at the University of Western Ontario (UWO). This appendix consists of the full text of the final reports from UWO detailing the tests that were performed and the results that were obtained. There are two separate reports because testing was perform in two rounds, with the first round consisting of all 1-, 2-, and 5-girder tests and the second round consisting of all 10-girder tests.

Note that these reports are self-contained documents that use their own terminology and naming conventions. Even fundamental terms such as *drag* and *lift* do not have the same meaning in the UWO reports as they do in rest of this report. In particular, <u>do not use the raw data from the tables in the UWO reports</u> without reading them carefully to understand how the data should be interpreted. For a presentation of the UWO data that uses the terminology defined elsewhere in this report, see Appendix B.

Alan G. Davenport Wind Engineering Group

A Study of Wind Forces on
BRIDGE GIRDERS WHILE UNDER CONSTRUCTION
Section Model Investigation

L. KONG / J.P.C. KING

TABLE OF CONTENTS

LIST OF TABLES

LIST OF FIGURES

ACKNOWLEDGEMENTS

SUMMARY AND MAIN FINDINGS

This report on the stud y of wind forces o n bridge girders while un der construction provides information from the section model testing of multiple configurations of bridge girders typically used in the State of Florida. These are comprised of: 1) Wide Flange Plate Girders, 2) Narrow Flange plate Girders, 3) Box Girders, 4) 78-inch deep "Florida" I-Beams and 5) 45-inch deep "Florida" I-Beams.

The aim of this study was to evaluate:

1. the static force coefficients for five types of bridge girders

2. the effects of shielding on leeward girders by the windward girder for various girder arrangements

The section models of th ese five type s of b ridge girders have been constructed at two geometric scales relative to the prototypes to facilitate model construction and are as follows:

a) 1:25 scale for three girder types: 1) the wide flange plate girders; 2) the narrow flange plate girders; and 3) the Box Girders
b) 1:28 scale for two girde r types: 4) the 78-in ch "Florida" I-beams; and 5) the 45-inch "Florida" I-beams

All tests were performed in smooth flow with turbulence intensities less than 0.5%. The highlights and main findings of this study are as follows:

- A drag coefficient of 2.12 was obtained for the single Wide and Narrow Flange Plate Girders at an angle of attack of 0 degrees. This value is comparable to published data for similar sections.

- The drag coefficient for singl e 78-inch and 45-i nch "Florida" I-beams are 1.89 and 1.85 respectively for an angle of attack of 0 degrees. This is sig nificantly smaller than the drag coefficient for the single wide / narrow flange plate girder (with a Cd of 2.12). The reasons for the lower drag coefficient for the Florida I-beams cannot be ascertained without additional flow and / or pressure measurements, however it is suspected that it may be due to the wider top flange and the chamfered lower corners present in the Florida I-beams.

- The single box girder has a drag coeffi cient of 1.81 at an angle o f attack of 0 degrees, which is similar to a value of 1.7 which has appeared in other codes for similar sections.

- The analysis of the force data to estimate a "shiel ding coefficient" indicates that shielding results primarily from the wi ndward girder blocking the wind from fully impactin g <u>all</u> downwind girders. The addition of more girders upstream provides minimal additional shielding.

DETAILS OF THE STUDY

Project Name: Wind Forces on Bridge Girders While Under Construction.

Project Location: Florida.

Project Description: The project is a criti cal component of a larger p roject with the Florida Department of Transport ation (FDOT). The prop er bracing of bridge girders for e xtreme wind during the c onstruction process is the primary focus of this study. The critical component, as part of the FDOT Project, is an accurate quantification of wind loads on the girders during construction. This includes the windward girder, as well as an e stimation of the effects of shielding on the interior girde rs, including the influence of spaci ng and cross-slope on shielding. Five different girder types have been selected for study as well as two girder spacing and two cross slopes.

Test Dates: Static Section Model Tests – August 2011

Preliminary Reporting: Static Force Coefficients – August 2011

Report Scope: The report is organized as follows:

                              Section 1 – Introduction
                              Section 2 – Section Model Study - Static Tests

General Reference: Discussion and details of the general methodology used by the Alan G Davenport Wind Engineering Group can be found in "Wind Tunnel Testing – A General Outline" [Reference 1].

1 INTRODUCTION

1.1 General

The wind tunnel study of "Wind forces on b ridge girders while under construction" is a critical component of a larger project with the Florida Department of Transportation (FDOT). The proper bracing of bridge girders for extreme wind during the construction process is the primary focus of this investigation. As a critical component of the FDOT Project, a primary focus of the current wind stu dy is to have an accurate quantification of wind loa ds on typical types of gird ers during construction. This includes the windward girder, as well as an estimation of the effect s of shielding on the interio r girders, including the influence of spa cing and cross-slope on shielding. Five different girde r types have b een selected for investigation with two girder spacing and two cross slopes, as described in Table 1.1.

A comprehensive study of wind effects of these gi rder configurations has been undertaken and the results of these investigations are presented in this report. The test details, including the test number, test conditions, test sequences, location of the instru mented girder and their co rresponding file name s, are given sequentially for the five types of girders in Tables 1.2 to 1.6 as:

a) Wide Flange Plate Girders (Table 1.2): Comprised of 29 tests, up to five girders, spaci ng of 10ft and 14ft, two slopes of 2% and 8%, test angles of 0°, $\pm2.5^o$ and $\pm5^o$
b) Narrow Flange Plate Girder (Table 1.3) Comprised of 11 tests, up to five girders, spacing of 10ft and 14ft, one slope of 2%, test angles of 0°, $\pm2.5^o$ and $\pm5^o$
c) Box Girders (Table 1.4): Compri sed of 5 tests, up to two gird ers, spacing of 20ft and 22ft, one slope of 0%, test angles of 0°, $\pm5^o$ and $\pm10^o$
d) 78-inch "Florida" I-beam (Table 1.5): Compri sed of 11 tests, up to five I-beams, spacing of 10ft and 13ft, one slope of 2%, test angles of 0°, $\pm2.5^o$ and $\pm5^o$
e) 45-inch "Florida" I-Beam (Table 1.6): Compri sed of 11 tests, up to five I-beams, spa cing of 10ft and 13ft, one slope of 2%, test angles of 0°, $\pm2.5^o$ and $\pm5^o$

Rigid section models of the five girder cross se ctions (7ft in l ength) have been con structed at two geometric scales relative to the prototypes to facilitate model fabrication as follows:

a) 1:25 scale for three gird er types: 1) th e wide flange plate girde rs; 2) the na rrow flange plate girders; and 3) the Box Girders
b) 1:28 scale for two girder types: 4) the 78-inch "Florida" I-beams; and 5) the 45-inch "Florida" I-beams

The section model study was performed at the inlet of the High Speed Section of the Boundary Layer Wind Tunnel II. Tests of the section models were per formed in smooth, uniform flow condition s to evaluate the static forces on the section.

The 7 ft long section models correspond to 175ft a nd 196ft lon g sections of the prototype s at the geometric scales of 1 to 2 5 and 1 to 28, respectively. The length of model was chose n in order that the lateral correlation effects of the wind are modeled properly and not to reflect any specific prototype girder length. Configurations of the five girder types are given in Figures 1.1 to 1.5. Test configurations including girder arrangements, test number designations and test conditions are given schematically in Figures 1.6 to 1.10. A na ming convention "XMN" is use d in the fi gures and tables, where X is a girder type, spacing and cross-slope indicator (with letter de signations "A" through "M" and omitting "I"), and M is the number of girders in the test (1 through 5) and N is the gi rder number being tested (1 through 5 with 1 being the windward girder).

Views of the model s and wind tunn el set-up are giv en in Figure s 1.11 to 1.15 for the Wide Flange Girders, the Narro w Flange Girders, the Box Gird ers, the 78 -inch "Florida" I-beams and the 45-in ch "Florida" I-beams, respectively. Figure 1.11 (B) Te st A21 refers to the test of the wide flan ge girder with 10ft spacing, 2% slope co nfiguration, with 2 girders present and the 1st (i.e. upwind) girder being tested, while Test C51 in Figure 1.11 (D) refers to the te st of the wide flange girder with 10ft spacing, 8% slope configuration, with 5 girders present and the 1st (i.e. upwind) girder being tested.

2 SECTION MODEL STUDY - STATIC TESTS

2.1 General

The section models were mounted on the BLWTL Bridge 3-component balance, which is capable of measuring the total forces on the sections (X and Z body forces as well as the torque). The centers of measurement of the forces for the wide and narrow plate girders, as well as the deep and shallow Florida I-beams are at the mid-height of the sections (as opposed to the centroid of the section), while the center of measurement for the box girder is 2.46ft above the bottom plate.

Tests were performed adjusting the model inclination relative to the mean wind flow. The apparatus which rotates the test model also rotates the "dummy" model(s) situated either upwind or downwind of the instrumented model girder. Lift and Drag were calculated from the measured X and Z body force components. The sign conventions for the definition of the force coefficients for each of the five girder types are given in Figures 2.1 to 2.5 respectively.

A typical force coefficient is defined as follows:

$$C_{x,z,l,d} = \frac{F_{x,z,l,d}}{qD} \qquad (2.1)$$

in which: C is an aerodynamic coefficient,
   F is the mean aerodynamic force per unit length,
   $q = \frac{1}{2}\rho V^2$ is the mean wind velocity pressure,
   ρ is the density of air (taken as 0.00238 slug/ft^3),
   V is the mean wind velocity in ft/s, and
   D is the overall depth of the section, see Table 2.1.

The subscripts x,z,l,d refer to the X and Z body force components and lift and drag respectively. It is important to note that C_x, C_z and C_m are "Body-Force Coefficients" and not aligned with the axis of the wind (i.e as a "drag" coefficient) nor perpendicular to the wind (i.e. as a "lift" coefficient).

The torque coefficient is defined:

$$C_m = \frac{F_t}{qD^2} \qquad (2.2)$$

in which: F_t is the mean aerodynamic torque per unit length.

All tests were carried out for the section models in smooth flow (I_u< 0.5%) for angles of mean vertical inclination between -5 to +5 degrees, in increments of 2.5 degrees, except for the box girder models, which were performed for angles between -10 to +10 degrees in increments of 5 degrees.

2.2 Test Results

The static aerodynamic coefficients from the tests of the section models are summarized in the following tables: 1) Tables 2.2 to 2.5 for the Wide Flange Girders; 2) Tables 2.6 and 2.7 for the Narrow Flange Girders; 3) Table 2.8 for the Box Girders; 4) Tables 2.9 and 2.10 for the 78-inch "Florida" I-beams; and 5) Tables 2.11 and 2.12 for the 45-inch "Florida" I-beams. The corresponding summary curves of force coefficient vs. angle of attack are shown in the following figures: 1) Figures 2.6 to 2.13 for the Wide Flange Girders; 2) Figures 2.14 to 2.17 for the Narrow Flange Girders; 3) Figures 2.18 to 2.21 for the Box Girders; 4) Figures 2.22 to 2.25 for the 78-inch "Florida" I-beams; and 5) Figures 2.26 to 2.29 for the 45-inch "Florida" I-beam arrangements.

Note that the force coefficients are normalized by section depth in order to facilitate comparisons with published results of similar girder cross sections.

A simplified "Shielding Coefficient" is defined for the 0° tests in order to present some general conclusions regarding multiple girder arrangements. The drag coefficients which were obtained from the tests of multiple girder arrangements at 0 degrees are normalized by the drag coefficient for the single, isolated girder at 0 degrees as follows:

$$C_s = \frac{C_{d\,n,m}}{C_{d1}}$$
(2.3)

where: C_s = Shielding Coefficient

$C_{d_{m,n}}$ = Drag Coefficient for the "m" girder configuration, *for* girder number "n"

C_{d_1} = Drag Coefficient for the isolated girder

The results are plotted relative to girder position (1 or 2 for the two girder case and 1 through 5 for the 5 girder case). Figures 2.30 and 2.31 present the effective shielding coefficients for the Wide Flange Girders with 2% and 8% cross-slopes respectively. The shielding coefficients for the Narrow Flange Girders, the Box Girders, the 78-inch "Florida" I-beams, and the 45-inch "Florida" I-beams are given in Figures 2.32 to 2.35 respectively.

Typical Bridge Codes do not provide specific drag coefficients for specific girder types, so only general comparisons can be made. Several international design codes provide drag coefficients for plate and box girders which can be compared to those determined from the current study [2,3,4]. Unfortunately, the AASHTO LRFD Code [5] does not provide drag coefficients for different girder types, rather it prescribes a design pressure which is associated with a 100mph fastest-mile wind speed and cannot be compared directly to the results of the current study without some interpretation.

A summary of the observed behavior of the section models is as follows:

- A drag coefficient of 2.12 was obtained for both the single Wide and Narrow Flange Plate Girders at 0 degrees angle of attack. This value is comparable to published data for sections with similar flange width to depth ratios [2, 3]. The flange width to depth ratios of these two types of girders are 0.16 and 0.33 approximately.

- The drag coefficient for single 78-inch and 45-inch "Florida" I-beams are 1.89 and 1.85 respectively for an angle of attack of 0 degrees. This is significantly smaller than the drag coefficient of 2.12 for the single Wide or Narrow Flange Girder. The change in drag coefficient with aspect ratio has been shown for rectangular cylinders to exhibit a slight increase at an aspect ratio of 0.6 to 0.7 and then decrease with increasing afterbody length. The data from the current tests does not follow this trend as the drag coefficient decreases with increasing aspect ratio. The reasons for the lower drag coefficient for the Florida I-beams cannot be ascertained without additional flow and / or pressure measurements, however it is suspected that it may be due to the wider top flange and the chamfered lower corners present in the Florida I-beams.

- The single box girder has a drag coefficient of 1.81 at an angle of attack of 0 degrees, which is similar to a value of 1.7 which has appeared in other codes for similar sections [3].

- The analysis of the force data to estimate a "shielding coefficient" indicates that shielding results primarily from the windward girder blocking the wind from fully impacting <u>all</u> downwind girders. The addition of more girders upwind of the subject girder does not provide significant additional shielding.

- Since all sections tested have sharp edged corners, it is expected that the effects of Reynolds number on the force coefficients are minimal. The "Reynolds number" is the ratio of the inertial force to viscous force of the fluid (i.e. air) and is computed as $Re = VD/\gamma$, where V is the mean

wind speed in ft/s, D is the overall section depth in ft as given in Table 2.1 and γ is the kinematic viscosity of air (1.615×10^{-4} ft^2/s). Note also that all tests were performed in "smooth" flow.

- The test wind speeds and corresponding Reynolds numbers are listed in Table 2.13.

2.3 Translation of Force Coefficients to the Section Centroid

The static force coefficients given in Section 2.2, which are referenced to the mid-height of the sections for the box girder and the Florida I-beams can be transformed to their centroid locations through a simple transformation of coordinates.

Figure 2.36 shows an example of the sign convention used in the transformation. Note that o is the mid-height location of the section and o' is the centroid. Assuming h is the distance between the mid-height and the centroid of the section, the body force coefficients to the centroid can be obtained as:

$$C_X' = C_X$$
$$C_Z' = C_Z \qquad\qquad (2.4)$$
$$C_m' = C_m + C_X \times \frac{h}{D}$$

The drag and lift coefficients relative to the centroid of the section are calculated as:

$$C_D' = C_X' \cos\alpha + C_Z' \sin\alpha$$
$$C_L' = -C_X' \sin\alpha + C_Z' \cos\alpha \qquad\qquad (2.5)$$

REFERENCES

1. "Wind Tunnel Testing: A General Outline", The Boundary Layer Wind Tunnel Laboratory, The University of Western Ontario, May 2007.

2. "User's Guide – NBC 2005, Structural Commentaries", Canadian Commission on Building and Fire Codes, National Research Council Canada, 2005

3. "Design Manual for Roads and Bridges, BS 5400", BD 37/01, August 2001.

4. "Minimum Design Loads for Buildings and Other Structures", ASCE-7-10, American Society of Civil Engineering, Washington, 2010.

5. "AASHTO LRFD Design Specifications – Fifth Edition", American Association of State Highway and Transportation Officials, Washington, 2010.

TABLE 1.1   SUMMARY OF STATIC SECTION MODEL TESTS

A) WIDE FLANGE PLATE GIRDER		Spacing between Girders	Instrumented Girder	Cross-Slope	No. of Tests	Test Angles
Test A1	Single Girder	-	1	-	1	$0^o, \pm2.5^o, \pm5^o$
Test A2	Two Girders	10 ft	1,2	2%	2	$0^o, \pm2.5^o, \pm5^o$
Test B2	Two Girders	14 ft	1,2	2%	2	$0^o, \pm2.5^o, \pm5^o$
Test C2	Two Girders	10 ft	1,2	8%	2	$0^o, \pm2.5^o, \pm5^o$
Test D2	Two Girders	14 ft	1,2	8%	2	$0^o, \pm2.5^o, \pm5^o$
Test A5	Five Girders	10 ft	1,2,3,4,5	2%	5	$0^o, \pm2.5^o, \pm5^o$
Test B5	Five Girders	14 ft	1,2,3,4,5	2%	5	$0^o, \pm2.5^o, \pm5^o$
Test C5	Five Girders	10 ft	1,2,3,4,5	8%	5	$0^o, \pm2.5^o, \pm5^o$
Test D5	Five Girders	14 ft	1,2,3,4,5	8%	5	$0^o, \pm2.5^o, \pm5^o$

B) NARROW FLANGE PLATE GIRDER		Spacing between Girders	Instrumented Girder	Cross-Slope	No. of Tests	Test Angles
Test E1	Single Girder	-	1	-	1	$0^o, \pm2.5^o, \pm5^o$
Test E2	Two Girders	10 ft	1,2	2%	2	$0^o, \pm2.5^o, \pm5^o$
Test F2	Two Girders	14 ft	1,2	2%	2	$0^o, \pm2.5^o, \pm5^o$
Test E5	Five Girders	10 ft	1,2,3	2%	3	$0^o, \pm2.5^o, \pm5^o$
Test F5	Five Girders	14 ft	1,2,3	2%	3	$0^o, \pm2.5^o, \pm5^o$

C) BOX GIRDER		Spacing between Girders	Instrumented Girder	Cross-Slope	No. of Tests	Test Angles
Test G1	Single Girder	-	1	-	1	$0^o, \pm5^o, \pm10^o$
Test G2	Two Girders	20 ft	1,2	0 %	2	$0^o, \pm5^o, \pm10^o$
Test H2	Two Girders	22 ft	1,2	0 %	2	$0^o, \pm5^o, \pm10^o$

TABLE 1.1 (CONT.)   SUMMARY OF STATIC SECTION MODEL TEST

D) 78-INCH "FLORIDA" I-BEAM		Spacing between Girders	Instrumented Girder	Cross-Slope	No. of Tests	Test Angles
Test J1	Single Girder	-	1	-	1	0°, $\pm2.5^o$, $\pm5^o$
Test J2	Two Girders	10 ft	1,2	2%	2	0°, $\pm2.5^o$, $\pm5^o$
Test K2	Two Girders	13 ft	1,2	2%	2	0°, $\pm2.5^o$, $\pm5^o$
Test J5	Five Girders	10 ft	1,2,3	2%	3	0°, $\pm2.5^o$, $\pm5^o$
Test K5	Five Girders	13 ft	1,2,3	2%	3	0°, $\pm2.5^o$, $\pm5^o$

E) 45-INCH "FLORIDA" I-BEAM		Spacing between Girders	Instrumented Girder	Cross-Slope	No. of Tests	Test Angles
Test L1	Single Girder	-	1	-	1	0°, $\pm2.5^o$, $\pm5^o$
Test L2	Two Girders	10 ft	1,2	2%	2	0°, $\pm2.5^o$, $\pm5^o$
Test M2	Two Girders	13 ft	1,2	2%	2	0°, $\pm2.5^o$, $\pm5^o$
Test L5	Five Girders	10 ft	1,2,3	2%	3	0°, $\pm2.5^o$, $\pm5^o$
Test M5	Five Girders	13 ft	1,2,3	2%	3	0°, $\pm2.5^o$, $\pm5^o$

TABLE 1.2   WIDE FLANGE PLATE GIRDERS – TEST DETAILS AND CONDITIONS

A) WIDE FLANGE PLATE GIRDER		Spacing between Girders	Girder Tested	Cross-Slope	Test Sequence	File Name
Angles：0°, ±2.5°, ±5°: **Smooth Flow, 1:25 Scale**						
A11	Single Girder	-	1	-	12	B063A1E01R001
A21	Two Girders	10 ft	1	2%	13	B063A2E01R001
A22	Two Girders	10 ft	2	2%	14	B063A2E02R001
A51	Five Girders	10 ft	1	2%	16	B063A5E01R001
A52	Five Girders	10 ft	2	2%	15	B063A5E02R001
A53	Five Girders	10 ft	3	2%	19	B063A5E03R001
A54	Five Girders	10 ft	4	2%	18	B063A5E04R001
A55	Five Girders	10 ft	5	2%	17	B063A5E05R001
B21	Two Girders	14 ft	1	2%	20	B063B2E01R006
B22	Two Girders	14 ft	2	2%	21	B063B2E02R001
B51	Five Girders	14 ft	1	2%	23	B063B5E01R001
B52	Five Girders	14 ft	2	2%	22	B063B5E02R001
B53	Five Girders	14 ft	3	2%	26	B063B5E03R001
B54	Five Girders	14 ft	4	2%	25	B063B5E04R001
B55	Five Girders	14 ft	5	2%	24	B063B5E05R005
C21	Two Girders	10 ft	1	8%	27	B063C2E01R001
C22	Two Girders	10 ft	2	8%	28	B063C2E02R001
C51	Five Girders	10 ft	1	8%	30	B063C5E01R001
C52	Five Girders	10 ft	2	8%	29	B063C5E02R001
C53	Five Girders	10 ft	3	8%	33	B063C5E03R001
C54	Five Girders	10 ft	4	8%	32	B063C5E04R001
C55	Five Girders	10 ft	5	8%	31	B063C5E05R001

TABLE 1.2 (CONT.)   WIDE FLANGE PLATE GIRDERS – TEST DETAILS AND CONDITIONS

A) WIDE FLANGE PLATE GIRDER		Spacing between Girders	Girder Tested	Cross-Slope	Test Sequence	File Name
Angles：0°, ±2.5°, ±5°: Smooth Flow, 1:25 Scale						
D21	Two Girders	14 ft	1	8%	35	B063D2E01R001
D22	Two Girders	14 ft	2	8%	34	B063D2E02R001
D51	Five Girders	14 ft	1	8%	38	B063D5E01R001
D52	Five Girders	14 ft	2	8%	39	B063D5E02R001
D53	Five Girders	14 ft	3	8%	40	B063D5E03R001
D54	Five Girders	14 ft	4	8%	36	B063D5E04R001
D55	Five Girders	14 ft	5	8%	37	B063D5E05R001

TABLE 1.3   NARROW FLANGE PLATE GIRDERS – TEST DETAILS AND CONDITIONS

B) NARROW FLANGE PLATE GIRDER		Spacing between Girders	Girder Tested	Cross-Slope	Test Sequence	File Name
Angles：0°, ±2.5°, ±5°: Smooth Flow, 1:25 Scale						
E11	Single Girder	-	1	-	1	B063NFE99R001
E21	Two Girders	10 ft	1	2%	2	B063B2E01R001
E22	Two Girders	10 ft	2	2%	3	B063E2E02R001
E51	Five Girders	10 ft	1	2%	5	B063E5E01R001
E52	Five Girders	10 ft	2	2%	4	B063E5E02R001
E53	Five Girders	10 ft	3	2%	6	B063E5E03R001
F21	Two Girders	14 ft	1	2%	7	B063F2E01R001
F22	Two Girders	14 ft	2	2%	8	B063F2E02R001
F51	Five Girders	14 ft	1	2%	10	B063F5E01R001
F52	Five Girders	14 ft	2	2%	9	B063F5E02R001
F53	Five Girders	14 ft	3	2%	11	B063F5E03R001

TABLE 1.4   BOX GIRDERS – TEST DETAILS AND CONDITIONS

C) BOX GIRDER		Spacing between Girders	Girder Tested	Cross-Slope	Test Sequence	File Name
Angles: 0°, ±5°, ±10°: Smooth Flow, 1:25 Scale						
G11	Single Girder	-	1	-	52	B063G1E01R006
G21	Two Girders	20 ft	1	0 %	53	B063G2E01R001
G22	Two Girders	20 ft	2	0 %	56	B063G2E01R006
H21	Two Girders	22 ft	1	0 %	54	B063H2E01R001
H22	Two Girders	22 ft	2	0 %	55	B063H2E02R001

TABLE 1.5   78-INCH "FLORIDA" I-BEAM – TEST DETAILS AND CONDITIONS

D) 78-INCH "FLORIDA" I-BEAM		Spacing between Girders	Girder Tested	Cross-Slope	Test Sequence	File Name
Angles： 0°, ±2.5°, ±5°: **Smooth Flow, 1:28 Scale**						
J11	Single Girder	-	1	-	57	B063J1E01R006
J21	Two Girders	10 ft	1	2%	58	B063J2E01R001
J22	Two Girders	10 ft	2	2%	61	B063J2E02R001
J51	Five Girders	10 ft	1	2%	63	B063J5E01R001
J52	Five Girders	10 ft	2	2%	62	B063J5E02R001
J53	Five Girders	10 ft	3	2%	67	B063J5E03R001
K21	Two Girders	13 ft	1	2%	59	B063K2E01R001
K22	Two Girders	13 ft	2	2%	60	B063K2E02R001
K51	Five Girders	13 ft	1	2%	65	B063K5E01R001
K52	Five Girders	13 ft	2	2%	64	B063K5E02R001
K53	Five Girders	13 ft	3	2%	66	B063K5E03R001

TABLE 1.6   45-INCH "FLORIDA" I-BEAM – TEST DETAILS AND CONDITIONS

E) 45-INCH "FLORIDA" I-BEAM		Spacing between Girders	Girder Tested	Cross-Slope	Test Sequence	File Name
Angles：0°, ±2.5°, ±5°： Smooth Flow, 1:28 Scale						
L11	Single Girder	-	1	-	41	B063L1E01R001
L21	Two Girders	10 ft	1	2%	42	B063L2E01R001
L22	Two Girders	10 ft	2	2%	43	B063L2E02R001
L51	Five Girders	10 ft	1	2%	45	B063L5E01R001
L52	Five Girders	10 ft	2	2%	44	B063L5E02R001
L53	Five Girders	10 ft	3	2%	46	B063L5E03R001
M21	Two Girders	13 ft	1	2%	51	B063M2E01R001
M22	Two Girders	13 ft	2	2%	50	B063M2E02R001
M51	Five Girders	13 ft	1	2%	49	B063M5E01R001
M52	Five Girders	13 ft	2	2%	48	B063M5E02R001
M53	Five Girders	13 ft	3	2%	47	B063M5E03R001

TABLE 2.1 OVERALL DEPTHS OF PROTOTYPE GIRDERS

PROTOTYPE CONFIGURATION	PROTOTYPE OVERALL DEPTH* (ft)	MODEL SCALE
A) Wide Flange Plate Girder	8+1/12+1/12 = 8.167	1:25
B) Narrow Flange Plate Girder	8+1/12+1/12 = 8.167	1:25
C) Box Girder	6+(3/4)//12+(1/2)/12 = 6.104	1:25
D) 78-inch "Florida" I-Beam	6+6/12 = 6.5	1:28
E) 45-inch "Florida" I-Beam	3+9/12 = 3.75	1:28

* Note the overall depth was used for normalizing to obtain the force coefficients.

TABLE 2.2 STATIC FORCE COEFFICIENTS - WIDE FLANGE PLATE GIRDER, 2% SLOPE, 10FT SPACING, SMOOTH FLOW

		Angle of Attack (deg)	-5	-2.5	0	2.5	5
A11	Wide, single	Cx (X Body Force)	2.13	2.13	2.12	2.13	2.13
		Cz (Z Body Force)	0.00	0.00	-0.01	-0.01	-0.02
		Ct (Torque)	0.03	0.03	0.03	0.03	0.03
		Cd (Drag)	2.12	2.13	2.12	2.12	2.12
		Cl (Lift)	0.19	0.09	-0.01	-0.11	-0.21
A21	Wide, 2% slope, 2 girders, 10ft spacing, 1st	Cx (X Body Force)	2.23	2.25	2.26	2.25	2.24
		Cz (Z Body Force)	0.02	0.01	-0.01	-0.02	-0.03
		Ct (Torque)	0.03	0.03	0.03	0.03	0.03
		Cd (Drag)	2.22	2.24	2.26	2.25	2.23
		Cl (Lift)	0.21	0.11	-0.01	-0.12	-0.23
A22	Wide, 2% slope, 2 girders, 10ft spacing, 2nd	Cx (X Body Force)	-0.36	-0.37	-0.35	-0.36	-0.35
		Cz (Z Body Force)	-0.04	-0.02	0.00	0.01	0.03
		Ct (Torque)	0.00	0.00	-0.01	-0.01	-0.01
		Cd (Drag)	-0.36	-0.36	-0.35	-0.36	-0.35
		Cl (Lift)	-0.08	-0.04	0.00	0.02	0.06
A51	Wide, 2% slope, 5 girders, 10ft spacing, 1st	Cx (X Body Force)	1.99	2.05	2.08	2.06	2.00
		Cz (Z Body Force)	0.05	0.03	-0.01	-0.05	-0.07
		Ct (Torque)	0.03	0.03	0.03	0.03	0.03
		Cd (Drag)	1.97	2.04	2.08	2.06	1.99
		Cl (Lift)	0.22	0.12	-0.01	-0.14	-0.24
A52	Wide, 2% slope, 5 girders, 10ft spacing, 2nd	Cx (X Body Force)	-0.11	-0.09	-0.07	-0.08	-0.11
		Cz (Z Body Force)	-0.01	-0.01	0.00	-0.01	0.01
		Ct (Torque)	0.00	0.00	0.00	0.00	0.00
		Cd (Drag)	-0.11	-0.09	-0.07	-0.08	-0.11
		Cl (Lift)	-0.02	-0.01	0.00	0.00	0.02
A53	Wide, 2% slope, 5 girders, 10ft spacing, 3rd	Cx (X Body Force)	-0.24	-0.29	-0.44	-0.34	-0.26
		Cz (Z Body Force)	-0.05	-0.04	-0.01	0.03	0.05
		Ct (Torque)	0.00	0.00	-0.01	-0.01	-0.01
		Cd (Drag)	-0.23	-0.29	-0.44	-0.33	-0.25
		Cl (Lift)	-0.07	-0.05	-0.01	0.05	0.07
A54	Wide, 2% slope, 5 girders, 10ft spacing, 4th	Cx (X Body Force)	0.03	-0.15	-0.27	-0.24	-0.06
		Cz (Z Body Force)	-0.03	-0.07	-0.02	0.06	0.06
		Ct (Torque)	-0.01	-0.02	-0.01	0.01	0.02
		Cd (Drag)	0.04	-0.15	-0.27	-0.23	-0.06
		Cl (Lift)	-0.03	-0.07	-0.02	0.07	0.07
A55	Wide, 2% slope, 5 girders, 10ft spacing, 5th	Cx (X Body Force)	0.34	0.29	0.27	0.29	0.31
		Cz (Z Body Force)	-0.17	-0.11	-0.03	0.07	0.14
		Ct (Torque)	0.00	0.00	0.00	0.01	0.01
		Cd (Drag)	0.36	0.29	0.27	0.30	0.32
		Cl (Lift)	-0.14	-0.10	-0.03	0.06	0.11

TABLE 2.3   STATIC FORCE COEFFICIENTS - WIDE FLANGE PLATE GIRDER, 2% SLOPE, 14FT SPACING, SMOOTH FLOW

		Angle of Attack (deg)	-5	-2.5	0	2.5	5
B21	Wide, 2% slope, 2 girders, 14ft spa., 1st	Cx (X Body Force)	2.19	2.20	2.22	2.21	2.19
		Cz (Z Body Force)	0.02	0.01	-0.01	-0.02	-0.04
		Ct (Torque)	0.03	0.03	0.03	0.03	0.03
		Cd (Drag)	2.18	2.20	2.22	2.21	2.18
		Cl (Lift)	0.21	0.11	-0.01	-0.12	-0.23
B22	Wide, 2% slope, 2 girders, 14ft spa., 2nd	Cx (X Body Force)	-0.46	-0.48	-0.52	-0.51	-0.48
		Cz (Z Body Force)	-0.12	-0.07	-0.02	0.03	0.08
		Ct (Torque)	-0.01	-0.01	-0.01	-0.01	-0.01
		Cd (Drag)	-0.45	-0.48	-0.52	-0.51	-0.47
		Cl (Lift)	-0.16	-0.09	-0.02	0.06	0.12
B51	Wide, 2% slope, 5 girders, 14ft spa., 1st	Cx (X Body Force)	1.89	1.97	2.01	1.98	1.90
		Cz (Z Body Force)	0.04	0.03	-0.01	-0.04	-0.06
		Ct (Torque)	0.03	0.03	0.03	0.03	0.02
		Cd (Drag)	1.88	1.97	2.01	1.97	1.88
		Cl (Lift)	0.21	0.11	-0.01	-0.13	-0.22
B52	Wide, 2% slope, 5 girders, 14ft spa., 2nd	Cx (X Body Force)	-0.17	-0.16	-0.17	-0.16	-0.17
		Cz (Z Body Force)	-0.03	-0.01	0.00	0.01	0.02
		Ct (Torque)	0.00	0.00	0.00	0.00	-0.01
		Cd (Drag)	-0.17	-0.16	-0.17	-0.15	-0.17
		Cl (Lift)	-0.04	-0.02	0.00	0.01	0.03
B53	Wide, 2% slope, 5 girders, 14ft spa., 3rd	Cx (X Body Force)	-0.22	-0.39	-0.50	-0.46	-0.32
		Cz (Z Body Force)	-0.07	-0.08	-0.03	0.05	0.07
		Ct (Torque)	-0.01	-0.01	-0.01	0.00	0.00
		Cd (Drag)	-0.21	-0.39	-0.50	-0.46	-0.31
		Cl (Lift)	-0.09	-0.10	-0.03	0.07	0.10
B54	Wide, 2% slope, 5 girders, 14ft spa., 4th	Cx (X Body Force)	0.26	0.15	0.10	0.14	0.23
		Cz (Z Body Force)	-0.07	-0.07	-0.01	0.07	0.08
		Ct (Torque)	0.00	-0.01	0.00	0.01	0.01
		Cd (Drag)	0.27	0.15	0.10	0.14	0.23
		Cl (Lift)	-0.05	-0.06	-0.01	0.06	0.06
B55	Wide, 2% slope, 5 girders, 14ft spa., 5th	Cx (X Body Force)	0.63	0.63	0.57	0.64	0.71
		Cz (Z Body Force)	0.08	0.05	-0.01	-0.06	-0.08
		Ct (Torque)	-0.01	0.00	0.01	0.02	0.03
		Cd (Drag)	0.64	0.64	0.57	0.65	0.71
		Cl (Lift)	0.03	0.02	-0.01	-0.03	-0.02

TABLE 2.4 STATIC FORCE COEFFICIENTS - WIDE FLANGE PLATE GIRDER, 8% SLOPE, 10FT SPACING, SMOOTH FLOW

		Angle of Attack (deg)	-5	-2.5	0	2.5	5
A11	Wide, single	Cx (X Body Force)	2.13	2.13	2.12	2.13	2.13
		Cz (Z Body Force)	0.00	0.00	-0.01	-0.01	-0.02
		Ct (Torque)	0.03	0.03	0.03	0.03	0.03
		Cd (Drag)	2.12	2.13	2.12	2.12	2.12
		Cl (Lift)	0.19	0.09	-0.01	-0.11	-0.21
C21	Wide, 8% slope, 2 girders, 10ft spacing, 1st	Cx (X Body Force)	2.24	2.24	2.26	2.26	2.26
		Cz (Z Body Force)	0.03	0.02	0.01	-0.01	-0.02
		Ct (Torque)	0.03	0.03	0.03	0.03	0.03
		Cd (Drag)	2.23	2.24	2.26	2.25	2.25
		Cl (Lift)	0.23	0.12	0.01	-0.11	-0.22
C22	Wide, 8% slope, 2 girders, 10ft spacing, 2nd	Cx (X Body Force)	-0.36	-0.36	-0.39	-0.36	-0.36
		Cz (Z Body Force)	-0.09	-0.05	-0.03	-0.01	0.00
		Ct (Torque)	0.00	0.00	0.00	-0.01	-0.01
		Cd (Drag)	-0.35	-0.36	-0.39	-0.36	-0.36
		Cl (Lift)	-0.12	-0.07	-0.03	0.00	0.03
C51	Wide, 8% slope, 5 girders, 10ft spacing, 1st	Cx (X Body Force)	1.86	1.94	2.00	2.05	2.05
		Cz (Z Body Force)	0.06	0.06	0.04	0.01	-0.04
		Ct (Torque)	0.03	0.03	0.03	0.03	0.03
		Cd (Drag)	1.84	1.94	2.00	2.05	2.03
		Cl (Lift)	0.22	0.14	0.04	-0.08	-0.22
C52	Wide, 8% slope, 5 girders, 10ft spacing, 2nd	Cx (X Body Force)	-0.11	-0.12	-0.11	-0.08	-0.08
		Cz (Z Body Force)	-0.02	-0.02	-0.01	0.00	-0.01
		Ct (Torque)	0.00	0.00	0.00	0.00	0.00
		Cd (Drag)	-0.11	-0.12	-0.11	-0.08	-0.08
		Cl (Lift)	-0.03	-0.03	-0.01	0.00	0.00
C53	Wide, 8% slope, 5 girders, 10ft spacing, 3rd	Cx (X Body Force)	-0.10	-0.22	-0.29	-0.32	-0.32
		Cz (Z Body Force)	-0.03	-0.06	-0.06	-0.03	0.01
		Ct (Torque)	0.00	0.00	0.00	0.00	-0.01
		Cd (Drag)	-0.10	-0.22	-0.29	-0.32	-0.32
		Cl (Lift)	-0.03	-0.07	-0.06	-0.02	0.04
C54	Wide, 8% slope, 5 girders, 10ft spacing, 4th	Cx (X Body Force)	0.27	0.10	-0.15	-0.24	-0.26
		Cz (Z Body Force)	-0.01	-0.02	-0.05	-0.04	0.03
		Ct (Torque)	0.01	0.00	-0.01	-0.01	0.00
		Cd (Drag)	0.27	0.10	-0.15	-0.24	-0.25
		Cl (Lift)	0.02	-0.01	-0.05	-0.03	0.06
C55	Wide, 8% slope, 5 girders, 10ft spacing, 5th	Cx (X Body Force)	0.49	0.40	0.33	0.27	0.28
		Cz (Z Body Force)	-0.17	-0.11	-0.07	-0.03	0.07
		Ct (Torque)	0.02	0.02	0.01	0.01	0.01
		Cd (Drag)	0.50	0.40	0.33	0.27	0.28
		Cl (Lift)	-0.13	-0.09	-0.07	-0.04	0.04

TABLE 2.5 STATIC FORCE COEFFICIENTS - WIDE FLANGE PLATE GIRDERS
8% SLOPE, 14FT SPACING, SMOOTH FLOW

		Angle of Attack (deg)	-5	-2.5	0	2.5	5
D21	Wide, 8% slope, 2 girders, 14ft spa., 1st	Cx (X Body Force)	2.22	2.21	2.22	2.24	2.25
		Cz (Z Body Force)	0.04	0.03	0.01	-0.01	-0.02
		Ct (Torque)	0.03	0.03	0.03	0.03	0.03
		Cd (Drag)	2.21	2.21	2.22	2.24	2.24
		Cl (Lift)	0.24	0.12	0.01	-0.10	-0.22
D22	Wide, 8% slope, 2 girders, 14ft spa., 2nd	Cx (X Body Force)	-0.34	-0.47	-0.48	-0.52	-0.55
		Cz (Z Body Force)	-0.23	-0.15	-0.08	-0.04	0.02
		Ct (Torque)	-0.02	-0.01	-0.01	-0.01	-0.01
		Cd (Drag)	-0.32	-0.47	-0.48	-0.52	-0.54
		Cl (Lift)	-0.26	-0.17	-0.08	-0.01	0.06
D51	Wide, 8% slope, 5 girders, 14ft spa., 1st	Cx (X Body Force)	1.77	1.85	1.93	1.99	1.97
		Cz (Z Body Force)	0.04	0.04	0.03	-0.01	-0.04
		Ct (Torque)	0.03	0.03	0.03	0.03	0.03
		Cd (Drag)	1.76	1.85	1.93	1.99	1.95
		Cl (Lift)	0.19	0.12	0.03	-0.09	-0.22
D52	Wide, 8% slope, 5 girders, 14ft spa., 2nd	Cx (X Body Force)	-0.14	-0.18	-0.18	-0.18	-0.17
		Cz (Z Body Force)	-0.03	-0.04	-0.02	-0.01	0.00
		Ct (Torque)	0.00	0.00	0.00	0.00	0.00
		Cd (Drag)	-0.14	-0.18	-0.18	-0.18	-0.17
		Cl (Lift)	-0.05	-0.05	-0.02	0.00	0.02
D53	Wide, 8% slope, 5 girders, 14ft spa., 3rd	Cx (X Body Force)	-0.05	-0.18	-0.34	-0.48	-0.49
		Cz (Z Body Force)	-0.05	-0.06	-0.08	-0.05	0.03
		Ct (Torque)	0.00	-0.01	-0.01	-0.02	-0.01
		Cd (Drag)	-0.05	-0.17	-0.34	-0.48	-0.49
		Cl (Lift)	-0.05	-0.07	-0.08	-0.03	0.07
D54	Wide, 8% slope, 5 girders, 14ft spa., 4th	Cx (X Body Force)	0.47	0.27	0.22	0.24	0.19
		Cz (Z Body Force)	-0.03	-0.04	-0.05	-0.01	0.06
		Ct (Torque)	0.01	0.00	0.00	0.00	0.02
		Cd (Drag)	0.47	0.27	0.22	0.24	0.19
		Cl (Lift)	0.01	-0.03	-0.05	-0.02	0.04
D55	Wide, 8% slope, 5 girders, 14ft spa., 5th	Cx (X Body Force)	1.05	0.84	0.65	0.65	0.67
		Cz (Z Body Force)	-0.02	-0.03	-0.03	0.00	0.07
		Ct (Torque)	0.04	0.04	0.03	0.02	0.01
		Cd (Drag)	1.04	0.84	0.65	0.65	0.68
		Cl (Lift)	0.07	0.01	-0.03	-0.03	0.01

TABLE 2.6   STATIC FORCE COEFFICIENTS - NARROW FLANGE PLATE GIRDERS 2% SLOPE, 10FT SPACING, SMOOTH FLOW

		Angle of Attack (deg)	-5	-2.5	0	2.5	5
E11	Narrow, single	Cx (X Body Force)	2.13	2.12	2.12	2.13	2.12
		Cz (Z Body Force)	-0.04	-0.04	-0.04	-0.04	-0.05
		Ct (Torque)	0.01	0.01	0.00	0.00	0.00
		Cd (Drag)	2.12	2.12	2.12	2.12	2.11
		Cl (Lift)	0.15	0.05	-0.04	-0.14	-0.23
E21	Narrow, 2% slope, 2 girders, 10ft spacing, 1st	Cx (X Body Force)	2.22	2.23	2.25	2.24	2.23
		Cz (Z Body Force)	-0.03	-0.04	-0.04	-0.05	-0.05
		Ct (Torque)	0.01	0.01	0.01	0.00	0.00
		Cd (Drag)	2.22	2.23	2.25	2.24	2.22
		Cl (Lift)	0.16	0.06	-0.04	-0.15	-0.25
E22	Narrow, 2% slope, 2 girders, 10ft spacing, 2nd	Cx (X Body Force)	-0.24	-0.24	-0.26	-0.24	-0.24
		Cz (Z Body Force)	-0.01	0.00	0.00	0.00	0.00
		Ct (Torque)	0.00	0.00	-0.01	-0.01	-0.01
		Cd (Drag)	-0.24	-0.24	-0.26	-0.24	-0.24
		Cl (Lift)	-0.03	-0.01	0.00	0.01	0.02
E51	Narrow, 2% slope, 5 girders, 10ft spacing, 1st	Cx (X Body Force)	2.01	2.06	2.09	2.07	2.02
		Cz (Z Body Force)	-0.02	-0.02	-0.04	-0.05	-0.06
		Ct (Torque)	0.01	0.01	0.01	0.00	0.00
		Cd (Drag)	2.00	2.06	2.09	2.06	2.00
		Cl (Lift)	0.16	0.07	-0.04	-0.14	-0.24
E52	Narrow, 2% slope, 5 girders, 10ft spacing, 2nd	Cx (X Body Force)	-0.08	-0.07	-0.07	-0.07	-0.07
		Cz (Z Body Force)	-0.01	0.00	0.00	0.00	0.00
		Ct (Torque)	0.00	0.00	-0.01	-0.01	-0.01
		Cd (Drag)	-0.08	-0.07	-0.07	-0.07	-0.07
		Cl (Lift)	-0.02	0.00	0.00	0.00	0.01
E53	Narrow, 2% slope, 5 girders, 10ft spacing, 3rd	Cx (X Body Force)	-0.21	-0.28	-0.34	-0.33	-0.27
		Cz (Z Body Force)	-0.03	-0.02	-0.01	0.01	0.02
		Ct (Torque)	-0.01	0.00	-0.01	-0.01	-0.01
		Cd (Drag)	-0.21	-0.28	-0.34	-0.33	-0.26
		Cl (Lift)	-0.05	-0.03	-0.01	0.02	0.04

TABLE 2.7   STATIC FORCE COEFFICIENTS - NARROW FLANGE PLATE GIRDERS 2% SLOPE, 14FT SPACING, SMOOTH FLOW

		Angle of Attack (deg)	-5	-2.5	0	2.5	5
F21	Narrow, 2% slope, 2 girders, 14ft spa., 1st	Cx (X Body Force)	2.22	2.20	2.20	2.21	2.22
		Cz (Z Body Force)	-0.03	-0.03	-0.04	-0.05	-0.05
		Ct (Torque)	0.02	0.02	0.01	0.07	0.13
		Cd (Drag)	2.22	2.20	2.20	2.21	2.21
		Cl (Lift)	0.16	0.06	-0.04	-0.15	-0.25
F22	Narrow, 2% slope, 2 girders, 14ft spa., 2nd	Cx (X Body Force)	-0.44	-0.38	-0.36	-0.37	-0.41
		Cz (Z Body Force)	-0.06	-0.02	0.00	0.01	0.03
		Ct (Torque)	-0.03	-0.03	-0.02	-0.03	-0.03
		Cd (Drag)	-0.43	-0.38	-0.36	-0.37	-0.40
		Cl (Lift)	-0.09	-0.04	0.00	0.03	0.07
F51	Narrow, 2% slope, 5 girders, 14ft spa., 1st	Cx (X Body Force)	1.90	1.96	1.99	1.95	1.90
		Cz (Z Body Force)	-0.01	-0.02	-0.03	-0.05	-0.05
		Ct (Torque)	0.13	0.13	0.13	0.13	0.12
		Cd (Drag)	1.89	1.96	1.99	1.95	1.88
		Cl (Lift)	0.15	0.07	-0.03	-0.13	-0.22
F52	Narrow, 2% slope, 5 girders, 14ft spa., 2nd	Cx (X Body Force)	-0.13	-0.14	-0.16	-0.14	-0.13
		Cz (Z Body Force)	-0.01	0.00	0.00	0.00	0.01
		Ct (Torque)	-0.01	-0.01	-0.01	-0.01	-0.01
		Cd (Drag)	-0.13	-0.14	-0.16	-0.14	-0.13
		Cl (Lift)	-0.02	-0.01	0.00	0.01	0.02
F53	Narrow, 2% slope, 5 girders, 14ft spa., 3rd	Cx (X Body Force)	-0.36	-0.50	-0.09	-0.17	-0.43
		Cz (Z Body Force)	-0.06	-0.05	-0.01	0.04	0.06
		Ct (Torque)	-0.05	-0.06	-0.01	0.00	-0.01
		Cd (Drag)	-0.35	-0.49	-0.09	-0.17	-0.42
		Cl (Lift)	-0.09	-0.07	-0.01	0.04	0.10

TABLE 2.8 STATIC FORCE COEFFICIENTS - BOX GIRDERS, 0% SLOPE, SMOOTH FLOW

		Angle of Attack (deg)	-10	-5	0	5	10
G11	Single Box Girder	Cx (X Body Force)	1.74	1.68	1.81	1.93	1.87
		Cz (Z Body Force)	1.16	1.62	1.22	1.03	0.71
		Ct (Torque)	0.90	0.84	0.79	0.79	0.75
		Cd (Drag)	1.51	1.53	1.81	2.02	1.97
		Cl (Lift)	1.44	1.76	1.22	0.86	0.37
G21	0% slope, 2 box girders, 20ft spacing, 1st	Cx (X Body Force)	1.42	1.51	1.69	1.75	1.74
		Cz (Z Body Force)	1.32	1.63	0.87	0.59	0.26
		Ct (Torque)	0.77	0.78	0.72	0.71	0.67
		Cd (Drag)	1.17	1.37	1.69	1.80	1.76
		Cl (Lift)	1.54	1.75	0.87	0.43	-0.05
G22	0% slope, 2 box girders, 20ft spacing, 2nd	Cx (X Body Force)	0.65	0.34	-0.45	-0.36	0.17
		Cz (Z Body Force)	-1.07	-1.09	-0.39	0.67	0.94
		Ct (Torque)	0.04	-0.15	-0.16	-0.02	0.11
		Cd (Drag)	0.83	0.43	-0.45	-0.30	0.33
		Cl (Lift)	-0.94	-1.06	-0.39	0.69	0.90
		Angle of Attack (deg)	-10	-5	0	5	10
H21	0% slope, 2 box girders, 22ft spacing, 1st	Cx (X Body Force)	1.39	1.48	1.68	1.73	1.73
		Cz (Z Body Force)	1.37	1.65	0.85	0.61	0.22
		Ct (Torque)	0.76	0.76	0.71	0.69	0.67
		Cd (Drag)	1.13	1.33	1.68	1.77	1.74
		Cl (Lift)	1.60	1.78	0.85	0.45	-0.08
H22	0% slope, 2 box girders, 22ft spacing, 2nd	Cx (X Body Force)	0.76	0.45	-0.34	-0.26	0.30
		Cz (Z Body Force)	-0.98	-1.04	-0.54	0.72	1.01
		Ct (Torque)	0.12	-0.07	-0.19	0.02	0.15
		Cd (Drag)	0.92	0.53	-0.34	-0.19	0.47
		Cl (Lift)	-0.83	-1.00	-0.54	0.74	0.94

TABLE 2.9 STATIC FORCE COEFFICIENTS - 78-INCH "FLORIDA" I-BEAMS, 2% SLOPE, 10FT SPACING, SMOOTH FLOW

		Angle of Attack (deg)	-5	-2.5	0	2.5	5
J11	78" Florida I-beam, single I-beam	Cx (X Body Force)	1.90	1.89	1.89	1.90	1.91
		Cz (Z Body Force)	0.18	0.17	0.15	0.14	0.13
		Ct (Torque)	0.02	0.01	0.00	-0.01	-0.01
		Cd (Drag)	1.87	1.88	1.89	1.90	1.91
		Cl (Lift)	0.35	0.25	0.15	0.06	-0.03
J21	78" Florida I-beam, 2 I-beams, 2% slope, 10ft space, 1st I-beam	Cx (X Body Force)	1.95	1.97	1.97	1.98	2.00
		Cz (Z Body Force)	0.24	0.20	0.16	0.13	0.09
		Ct (Torque)	0.03	0.01	0.01	-0.01	0.01
		Cd (Drag)	1.92	1.96	1.97	1.99	2.00
		Cl (Lift)	0.41	0.29	0.16	0.04	-0.08
J22	78" Florida I-beam, 2 I-beams, 2% slope, 10ft space, 2nd I-beam	Cx (X Body Force)	-0.37	-0.50	-0.55	-0.56	-0.55
		Cz (Z Body Force)	-0.25	-0.16	-0.03	0.07	0.18
		Ct (Torque)	-0.03	-0.03	-0.02	-0.02	-0.01
		Cd (Drag)	-0.34	-0.49	-0.55	-0.55	-0.53
		Cl (Lift)	-0.28	-0.18	-0.03	0.09	0.23
J51	78" Florida I-beam, 5 I-beams, 2% slope, 10ft space, 1st I-beam	Cx (X Body Force)	1.57	1.65	1.71	1.70	1.66
		Cz (Z Body Force)	0.24	0.22	0.15	0.09	0.04
		Ct (Torque)	0.08	0.07	0.07	0.06	0.06
		Cd (Drag)	1.54	1.64	1.71	1.71	1.66
		Cl (Lift)	0.38	0.29	0.15	0.01	-0.10
J52	78" Florida I-beam, 5 I-beams, 2% slope, 10ft space, 2nd I-beam	Cx (X Body Force)	-0.17	-0.22	-0.30	-0.28	-0.20
		Cz (Z Body Force)	-0.02	-0.03	-0.01	0.02	0.03
		Ct (Torque)	0.00	0.00	-0.01	-0.02	-0.01
		Cd (Drag)	-0.17	-0.21	-0.30	-0.28	-0.20
		Cl (Lift)	-0.04	-0.04	-0.01	0.04	0.05
J53	78" Florida I-beam, 5 I-beams, 2% slope, 10ft space, 3rd I-beam	Cx (X Body Force)	-0.08	-0.27	-0.33	-0.35	-0.26
		Cz (Z Body Force)	-0.05	-0.10	-0.05	0.06	0.07
		Ct (Torque)	-0.01	-0.02	-0.02	0.00	0.01
		Cd (Drag)	-0.08	-0.27	-0.33	-0.34	-0.25
		Cl (Lift)	-0.06	-0.12	-0.05	0.08	0.10

TABLE 2.10 STATIC FORCE COEFFICIENTS- 78-INCH "FLORIDA" I-BEAMS, 2% SLOPE, 13FT SPACING, SMOOTH FLOW

		Angle of Attack (deg)	-5	-2.5	0	2.5	5
K21	78" Florida I-beam, 2 I-beams, 2% slope, 13ft space, 1st I-beam	Cx (X Body Force)	1.87	1.88	1.90	1.90	1.91
		Cz (Z Body Force)	0.24	0.20	0.17	0.14	0.10
		Ct (Torque)	0.07	0.06	0.05	0.04	0.06
		Cd (Drag)	1.84	1.87	1.90	1.91	1.91
		Cl (Lift)	0.40	0.28	0.17	0.05	-0.07
K22	78" Florida I-beam, 2 I-beams, 2% slope, 13ft space, 2nd I-beam	Cx (X Body Force)	-0.30	-0.49	-0.58	-0.61	-0.56
		Cz (Z Body Force)	-0.34	-0.24	-0.09	0.07	0.22
		Ct (Torque)	-0.04	-0.04	-0.03	-0.02	0.00
		Cd (Drag)	-0.27	-0.47	-0.58	-0.60	-0.54
		Cl (Lift)	-0.36	-0.27	-0.09	0.10	0.27
K51	78" Florida I-beam, 5 I-beams, 2% slope, 13ft space, 1st I-beam	Cx (X Body Force)	1.54	1.61	1.65	1.64	1.58
		Cz (Z Body Force)	0.21	0.19	0.14	0.09	0.05
		Ct (Torque)	0.08	0.07	0.07	0.06	0.06
		Cd (Drag)	1.52	1.60	1.65	1.64	1.58
		Cl (Lift)	0.35	0.26	0.14	0.02	-0.08
K52	78" Florida I-beam, 5 I-beams, 2% slope, 13ft space, 2nd I-beam	Cx (X Body Force)	-0.19	-0.23	-0.21	-0.20	-0.18
		Cz (Z Body Force)	-0.04	-0.05	-0.01	0.02	0.03
		Ct (Torque)	0.00	-0.01	-0.01	-0.01	-0.01
		Cd (Drag)	-0.19	-0.23	-0.21	-0.20	-0.18
		Cl (Lift)	-0.06	-0.06	-0.01	0.03	0.04
K53	78" Florida I-beam, 5 I-beams, 2% slope, 13ft space, 3rd I-beam	Cx (X Body Force)	-0.04	-0.24	-0.40	-0.39	-0.24
		Cz (Z Body Force)	-0.14	-0.14	-0.05	0.07	0.09
		Ct (Torque)	-0.02	-0.03	-0.02	0.00	0.01
		Cd (Drag)	-0.03	-0.23	-0.40	-0.39	-0.23
		Cl (Lift)	-0.14	-0.15	-0.05	0.08	0.11

TABLE 2.11 STATIC FORCE COEFFICIENTS- 45-INCH "FLORIDA" I-BEAMS, 2% SLOPE, 10FT SPACING, SMOOTH FLOW

		Angle of Attack (deg)	-5	-2.5	0	2.5	5
L11	45" Florida I-beam, single I-beam	Cx (X Body Force)	1.81	1.83	1.85	1.85	1.84
		Cz (Z Body Force)	0.48	0.42	0.37	0.30	0.24
		Ct (Torque)	-0.02	-0.03	-0.06	-0.07	-0.08
		Cd (Drag)	1.76	1.81	1.85	1.86	1.86
		Cl (Lift)	0.64	0.50	0.37	0.22	0.08
L21	45" Florida I-beam, 2 I-beams, 2% slope, 10ft space, 1st I-beam	Cx (X Body Force)	1.59	1.63	1.66	1.67	1.65
		Cz (Z Body Force)	0.41	0.38	0.32	0.23	0.15
		Ct (Torque)	-0.01	-0.01	-0.02	-0.05	-0.07
		Cd (Drag)	1.55	1.61	1.66	1.68	1.66
		Cl (Lift)	0.55	0.45	0.32	0.16	0.01
L22	45" Florida I-beam, 2 I-beams, 2% slope, 10ft space, 2nd I-beam	Cx (X Body Force)	-0.29	-0.44	-0.52	-0.42	-0.22
		Cz (Z Body Force)	-0.47	-0.25	0.04	0.29	0.47
		Ct (Torque)	-0.04	0.00	0.03	0.05	0.04
		Cd (Drag)	-0.24	-0.42	-0.52	-0.41	-0.18
		Cl (Lift)	-0.49	-0.27	0.04	0.31	0.48
L51	45" Florida I-beam, 5 I-beams, 2% slope, 10ft space, 1st I-beam	Cx (X Body Force)	1.38	1.44	1.48	1.48	1.43
		Cz (Z Body Force)	0.32	0.30	0.26	0.17	0.09
		Ct (Torque)	0.00	-0.02	-0.03	-0.05	-0.06
		Cd (Drag)	1.34	1.42	1.48	1.48	1.44
		Cl (Lift)	0.44	0.36	0.26	0.10	-0.03
L52	45" Florida I-beam, 5 I-beams, 2% slope, 10ft space, 2nd I-beam	Cx (X Body Force)	-0.29	-0.37	-0.42	-0.41	-0.26
		Cz (Z Body Force)	-0.16	-0.09	0.06	0.19	0.17
		Ct (Torque)	0.02	0.02	0.02	0.03	0.02
		Cd (Drag)	-0.28	-0.37	-0.42	-0.40	-0.24
		Cl (Lift)	-0.18	-0.11	0.06	0.21	0.19
L53	45" Florida I-beam, 5 I-beams, 2% slope, 10ft space, 3rd I-beam	Cx (X Body Force)	0.14	-0.02	-0.06	-0.01	0.16
		Cz (Z Body Force)	-0.25	-0.17	0.02	0.19	0.26
		Ct (Torque)	-0.02	-0.02	0.01	0.02	0.00
		Cd (Drag)	0.17	-0.01	-0.06	0.00	0.18
		Cl (Lift)	-0.24	-0.17	0.02	0.19	0.24

TABLE 2.12 STATIC FORCE COEFFICIENTS- 45-INCH "FLORIDA" I-BEAMS, 2% SLOPE, 13FT SPACING, SMOOTH FLOW

		Angle of Attack (deg)	-5	-2.5	0	2.5	5
M21	45" Florida I-beam, 2 I-beams, 2% slope, 13ft space, 1st I-beam	Cx (X Body Force)	1.54	1.58	1.60	1.60	1.60
		Cz (Z Body Force)	0.33	0.30	0.27	0.21	0.16
		Ct (Torque)	-0.01	-0.01	-0.04	-0.06	-0.07
		Cd (Drag)	1.50	1.57	1.60	1.61	1.60
		Cl (Lift)	0.46	0.37	0.27	0.14	0.02
M22	45" Florida I-beam, 2 I-beams, 2% slope, 13ft space, 2nd I-beam	Cx (X Body Force)	-0.02	0.04	-0.41	-0.14	-0.12
		Cz (Z Body Force)	-0.45	-0.16	-0.02	0.22	0.47
		Ct (Torque)	-0.06	-0.01	0.01	0.03	0.04
		Cd (Drag)	0.02	0.04	-0.41	-0.13	-0.08
		Cl (Lift)	-0.45	-0.16	-0.02	0.22	0.48
M51	45" Florida I-beam, 5 I-beams, 2% slope, 13ft space, 1st I-beam	Cx (X Body Force)	1.38	1.44	1.47	1.45	1.40
		Cz (Z Body Force)	0.28	0.27	0.24	0.17	0.12
		Ct (Torque)	-0.01	-0.02	-0.04	-0.06	-0.06
		Cd (Drag)	1.35	1.43	1.47	1.46	1.41
		Cl (Lift)	0.40	0.33	0.24	0.11	-0.01
M52	45" Florida I-beam, 5 I-beams, 2% slope, 13ft space, 2nd I-beam	Cx (X Body Force)	-0.33	-0.44	-0.49	-0.41	-0.25
		Cz (Z Body Force)	-0.28	-0.17	0.05	0.22	0.27
		Ct (Torque)	0.01	0.01	0.03	0.04	0.02
		Cd (Drag)	-0.30	-0.44	-0.49	-0.40	-0.23
		Cl (Lift)	-0.31	-0.19	0.05	0.24	0.29
M53	45" Florida I-beam, 5 I-beams, 2% slope, 13ft space, 3rd I-beam	Cx (X Body Force)	0.51	0.48	0.56	0.53	0.66
		Cz (Z Body Force)	-0.10	-0.01	0.09	0.11	0.11
		Ct (Torque)	0.02	0.01	-0.01	-0.03	-0.05
		Cd (Drag)	0.51	0.48	0.56	0.54	0.67
		Cl (Lift)	-0.05	0.02	0.09	0.09	0.05

TABLE 2.13 WIND TUNNEL TEST WIND SPEEDS AND CORRESPONDING REYNOLDS NUMBERS

PROTOTYPE CONFIGURATION	TEST WIND SPEED (ft/s)	REYNOLDS NUMBER
A) Wide Flange Plate Girder	37.3	77000
B) Narrow Flange Plate Girder	37.2	77000
C) Box Girder	38.1	59000
D) 78-inch "Florida" I-Beam	38.3	56000
E) 45-inch "Florida" I-Beam	39.3	33000

FIGURES
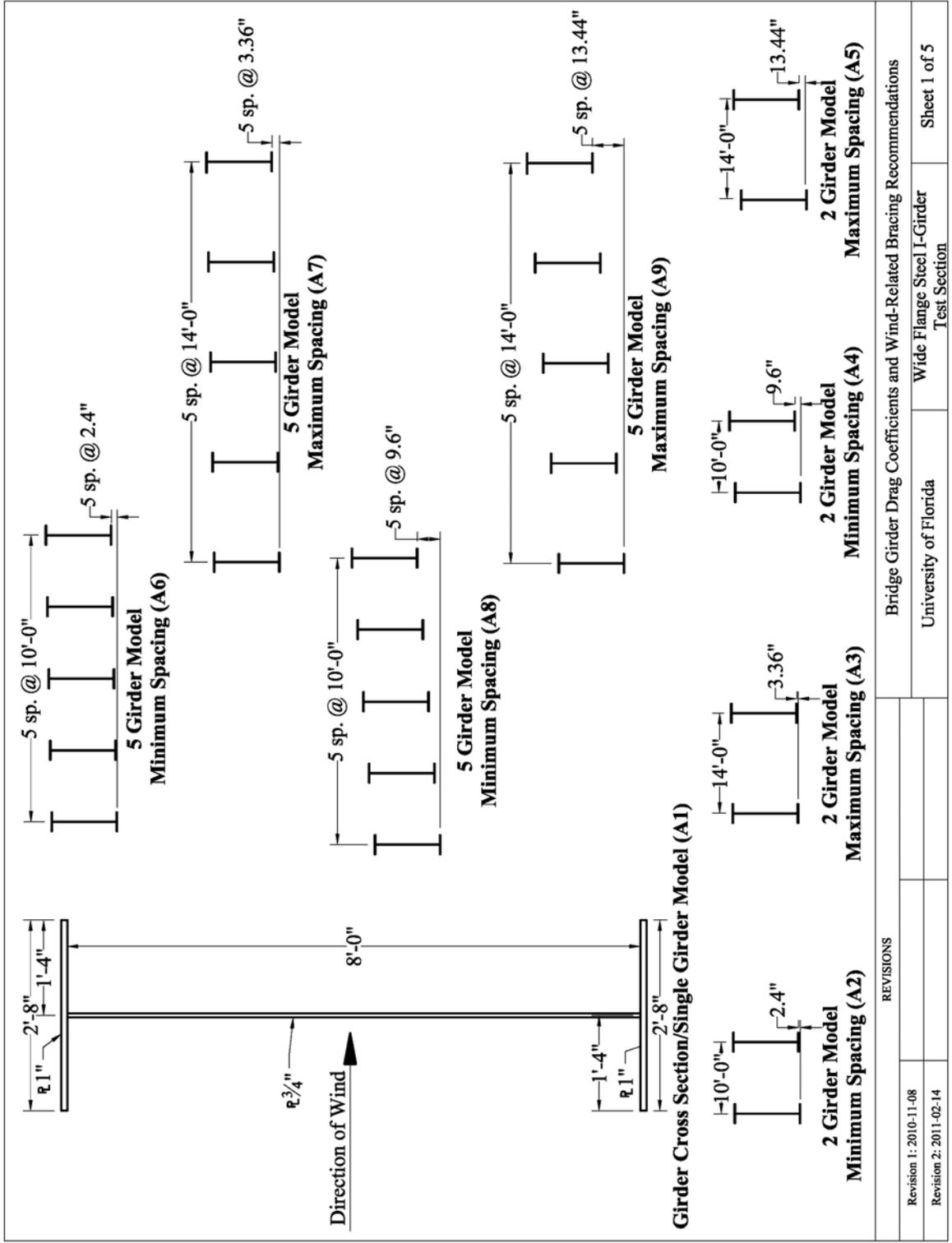
FIGURE 1.1 PROTOTYPE CONFIGURATION OF THE WIDE FLANGE PLATE GIRDERS

		Bridge Girder Drag Coefficients and Wind-Related Bracing Recommendations	
REVISIONS		University of Florida	Wide Flange Steel I-Girder Test Section
Revision 1: 2010-11-08			
Revision 2: 2011-02-14			Sheet 1 of 5
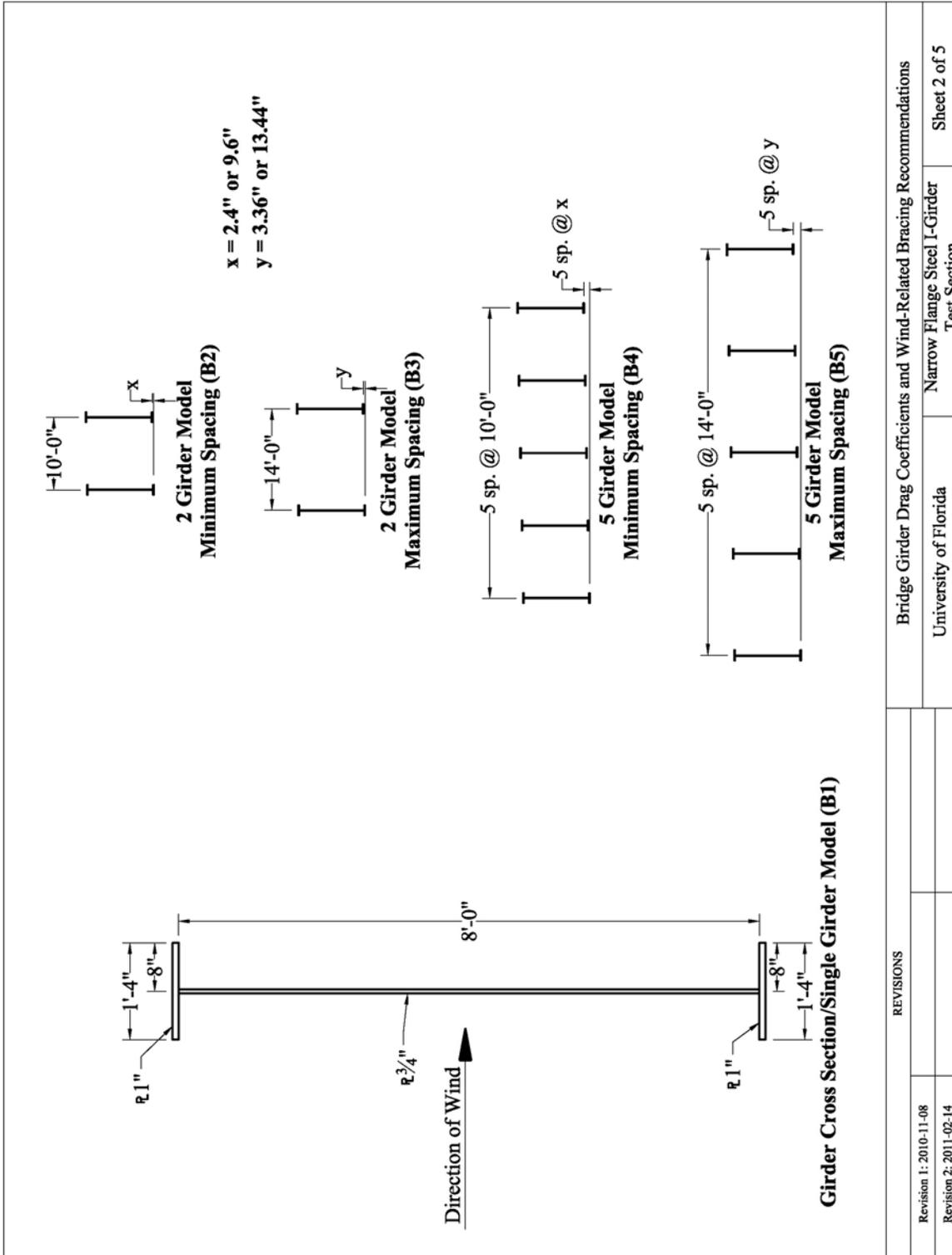
FIGURE 1.2   PROTOTYPE CONFIGURATION OF THE NARROW FLANGE PLATE GIRDERS

x = 2.4" or 9.6"
y = 3.36" or 13.44"

2 Girder Model
Minimum Spacing (B2)

2 Girder Model
Maximum Spacing (B3)

5 Girder Model
Minimum Spacing (B4)

5 Girder Model
Maximum Spacing (B5)

10'-0"

14'-0"

5 sp. @ 10'-0"

5 sp. @ x

5 sp. @ 14'-0"

5 sp. @ y

Girder Cross Section/Single Girder Model (B1)

8'-0"

1'-4"

8"

ℝ1"

ℝ 3/4"

Direction of Wind

REVISIONS

Bridge Girder Drag Coefficients and Wind-Related Bracing Recommendations

University of Florida

Narrow Flange Steel I-Girder
Test Section

Sheet 2 of 5

Revision 1: 2010-11-08

Revision 2: 2011-02-14

FIGURE 1.3   PROTOTYPE CONFIGURATION OF THE BOX GIRDERS

Symm. about ₵

Girder Cross Section/Single Girder Model (C1)

6'-0"

5'-0"

3'-6"

1"

R 9/16"

R 1/2"

R 3/4"

1'-4"

8"

1
4

Direction of Wind

2 Girder Model Maximum Spacing (C3)

22'-0"

2 Girder Model Minimum Spacing (C2)

20'-0"

Bridge Girder Drag Coefficients and Wind-Related Bracing Recommendations

| University of Florida | Steel Box Girder Test Section | Sheet 3 of 5 |

REVISIONS

Revision 1: 2010-11-08

Revision 2: 2011-02-14

FIGURE 1.4   PROTOTYPE CONFIGURATION OF THE 78-INCH "FLORIDA" I-BEAM

2 Girder Model
Minimum Spacing (D2)

2 Girder Model
Maximum Spacing (D3)

5 Girder Model
Minimum Spacing (D4)

5 Girder Model
Maximum Spacing (D5)

Girder Cross Section/Single Girder Model (D1)

Direction of Wind

Symm. about ₵

R1'-3"

¾" Chamfer

REVISIONS		Bridge Girder Drag Coefficients and Wind-Related Bracing Recommendations	
Revision 1: 2010-11-08		University of Florida	78" Florida I-Beam Test Section	Sheet 4 of 5
Revision 2: 2012-02-14			

FIGURE 1.5   PROTOTYPE CONFIGURATION OF T HE 45-INCH "FLORIDA" I-BEAM

Girder Cross Section/Single Girder Model (E1)

2 Girder Model Minimum Spacing (E2)

2 Girder Model Maximum Spacing (E3)

5 Girder Model Minimum Spacing (E4)

5 Girder Model Maximum Spacing (E5)

REVISIONS		Bridge Girder Drag Coefficients and Wind-Related Bracing Recommendations	
Revision 1: 2010-11-08		University of Florida	45" Florida I-Beam Test Section
Revision 2: 2011-02-14			Sheet 5 of 5

WIND

WIDE FLANGE
GIRDER

TEST

TEST "A"

4.8" spacing
2% Offset

A11
A21
A22
A52
A54
A51
A55
A53

TEST "B"

6.72" spacing
2% Offset

B21
B22
B52
B54
B51
B55
B53

TEST "C"

4.8" spacing
8% Offset

C21
C22
C52
C54
C51
C55
C53

TEST "D"

6.72" spacing
8% Offset

D21
D22
D52
D54
D51
D55
D53

**FIGURE 1.6   TEST CONFIGURATIONS AND DESIGNATIONS – WIDE FLANGE PLATE
GIRDERS (1:25 SCALE, RED – TESTED GIRDER)**

WIND

NARROW FLANGE
GIRDER

TEST "E"

4.8" spacing
2% Offset

NARROW FLANGE GIRDER

		TEST
	I I	E11
	I I	E21
	I I	E22
I I I I I		E52
I I I I I		E51
I I I I I		E53

TEST "F"

6.72" spacing
2% Offset

	I I	F21
I I		F22
I I I I I		F52
I I I I I		F51
I I I I I		E53

**FIGURE 1.7   TEST CONFIGURATIONS AND DESIGNATIONS – NARROW FLANGE PLATE
GIRDERS (1:25 SCALE, RED – TESTED GIRDER)**

WIND

BOX GIRDER

TEST "G"
9.6" spacing
0% Offset

TEST
G11
G21
G22

TEST "H"
10.56" spacing
0% Offset

H21
H22
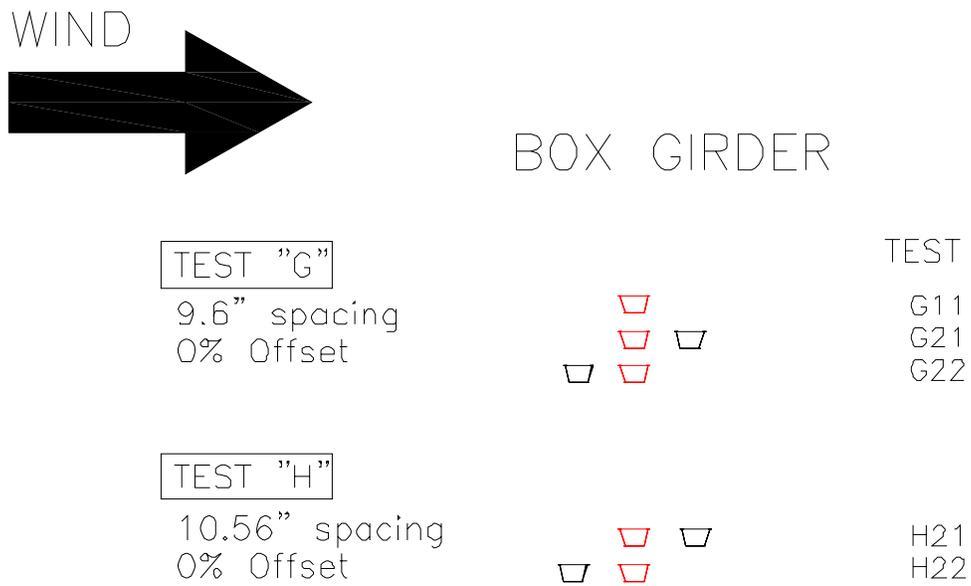
**FIGURE 1.8   TEST CONFIGURATIONS AND DESIGNATIONS – BOX GIRDERS
(1:25 SCALE, RED – TESTED GIRDER)**

WIND
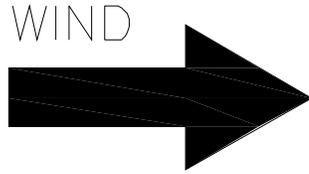
DEEP FLORIDA
I—BEAM

TEST "J"

4.286 spacing
2% Offset

	TEST
I	J11
I I	J21
I I	J22
I I I I	J52
I I I I	J51
I I I I I	J53

TEST "K"

5.571" spacing
2% Offset

I I	K21
I I	K22
I I I I I	K52
I I I I I	K51
I I I I I	K53

FIGURE 1.9   TEST CONFIGURATIONS AND DESIGNATIONS – 78-INCH "FLORIDA" I-BEAM (1:28 SCALE, RED – TESTED I-BEAM)

WIND
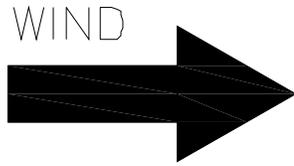
SHALLOW FLORIDA
I-BEAM

TEST

TEST "L"
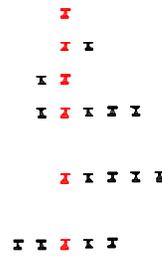
4.286 spacing
2% Offset

L11
L21
L22
L52

L51

L53

TEST "M"

5.571" spacing
2% Offset
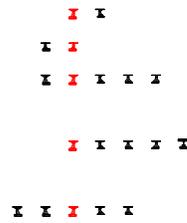
M21
M22
M52

M51

M53

FIGURE 1.10 TEST CONFIGURATIONS AND DESIGNATIONS – 45-INCH "FLORIDA" I-BEAM (1:28 SCALE, RED – TESTED I-BEAM)
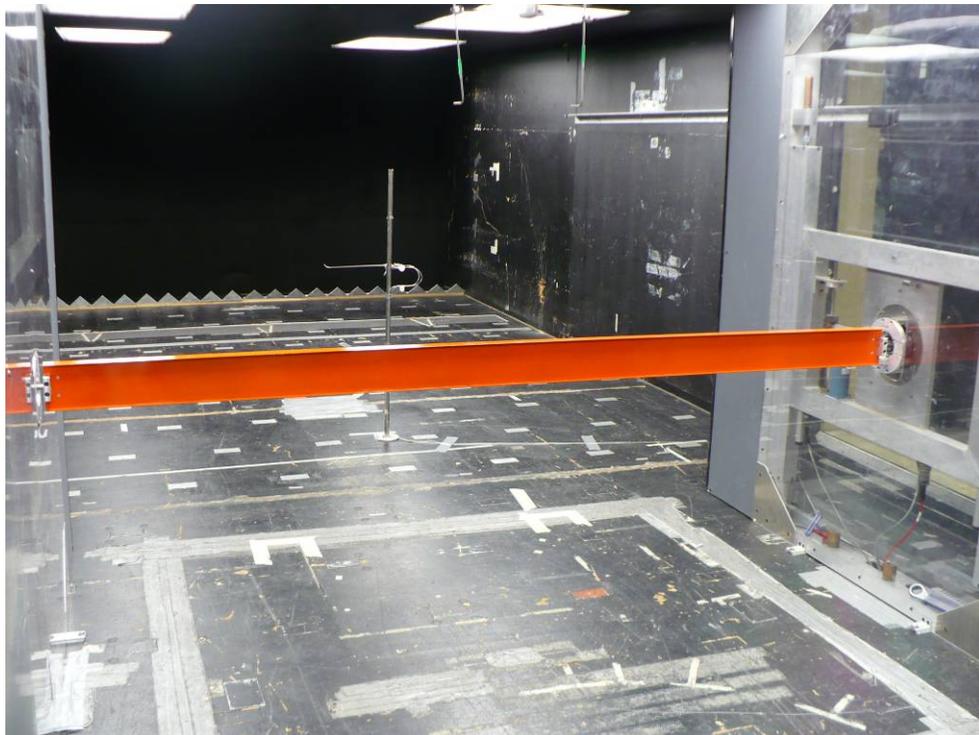
a) SINGLE GIRDER (TEST A11)
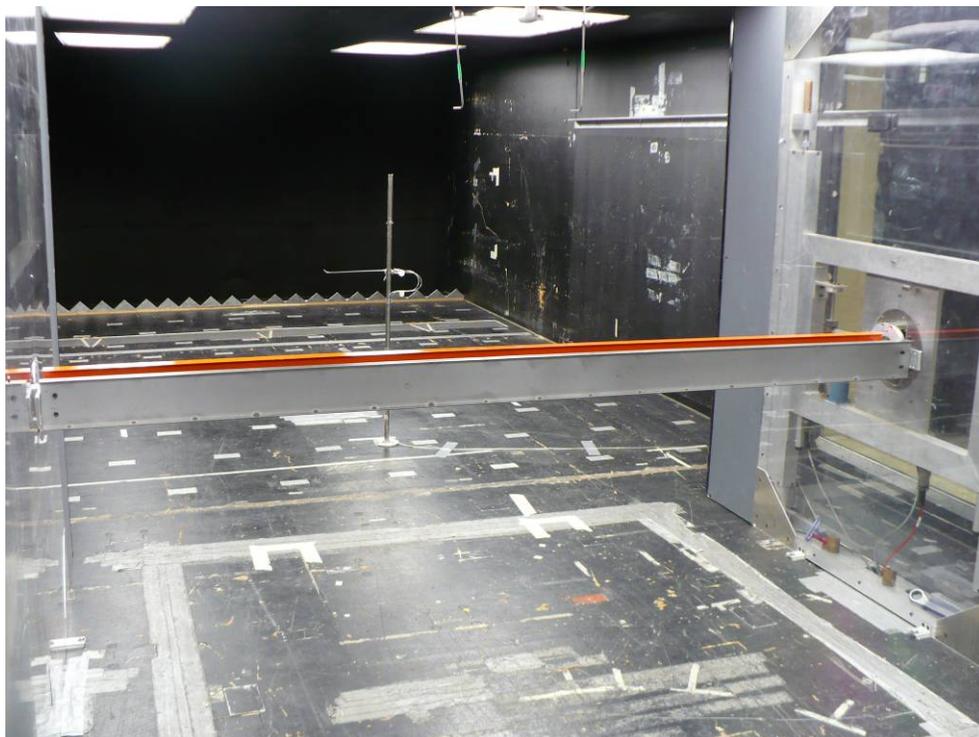
b) TWO GIRDERS (TEST A21)

FIGURE 1.11 SECTION MODEL TEST SET-UP – WIDE FLANGE PLATE GIRDER
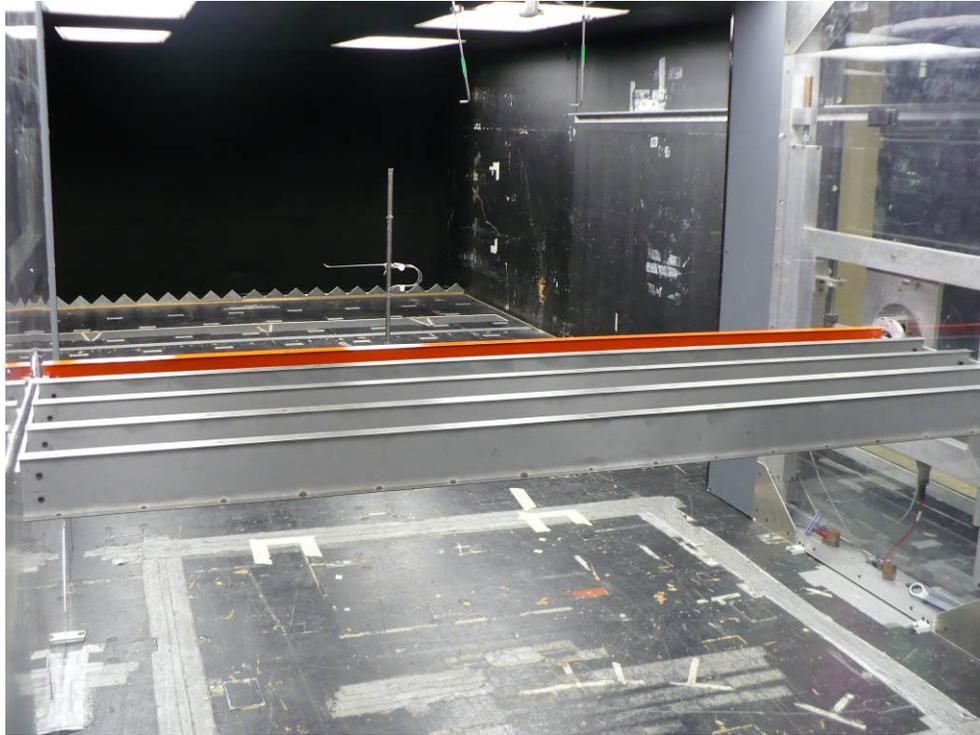
c) FIVE GIRDERS (TEST B51)
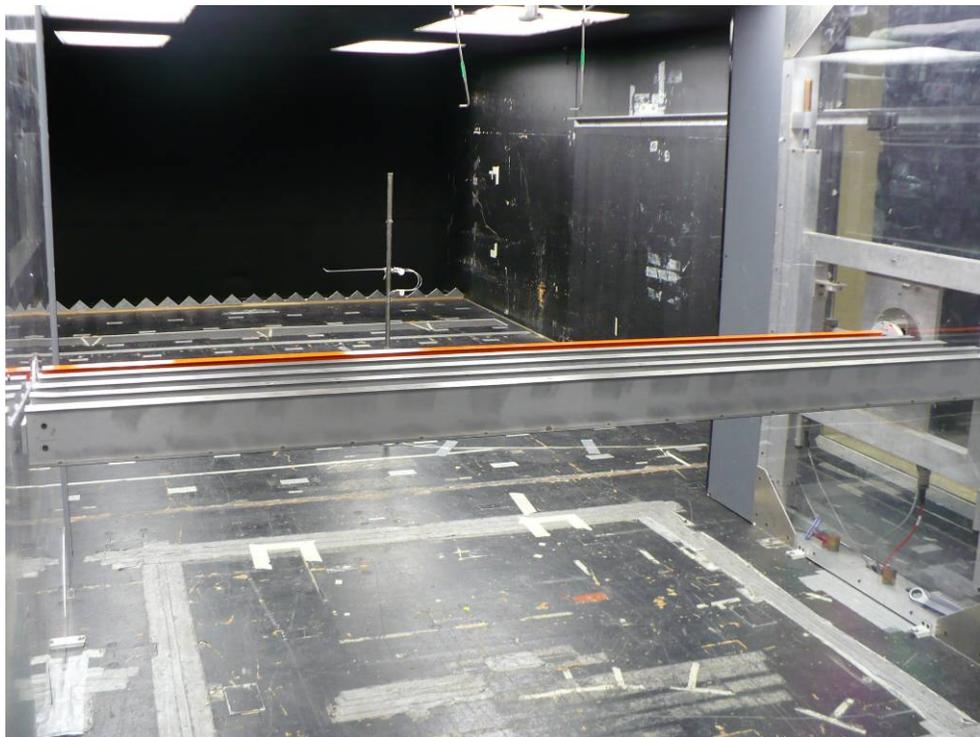
d) FIVE GIRDERS (TEST C51)

**FIGURE 1.11 (CONT.)   SECTION MODEL TEST SET-UP – WIDE FLANGE PLATE
GIRDER**

e) TWO GIRDERS (TEST D22)
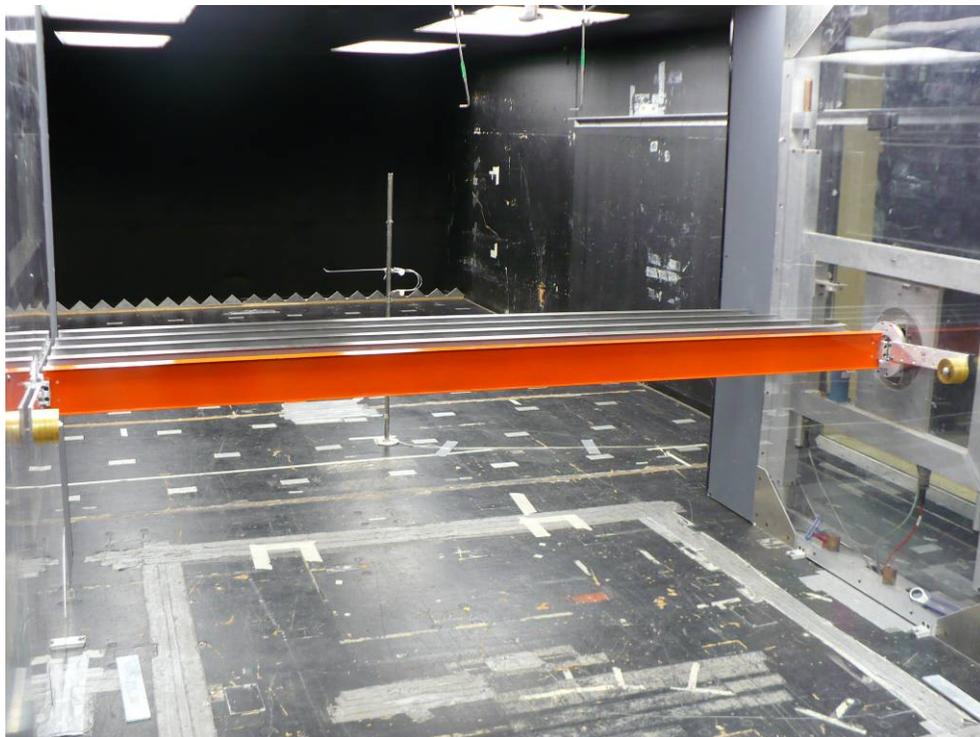
f) FIVE GIRDERS (TEST D55)

FIGURE 1.11 (CONT.)   SECTION MODEL TEST SET-UP – WIDE FLANGE PLATE GIRDER

a) SINGLE GIRDER (TEST E11)

b) TWO GIRDERS (TEST E21)

FIGURE 1.12 SECTION MODEL TEST SET-UP – NARROW FLANGE PLATE GIRDER

c) FIVE GIRDERS (TEST E52)
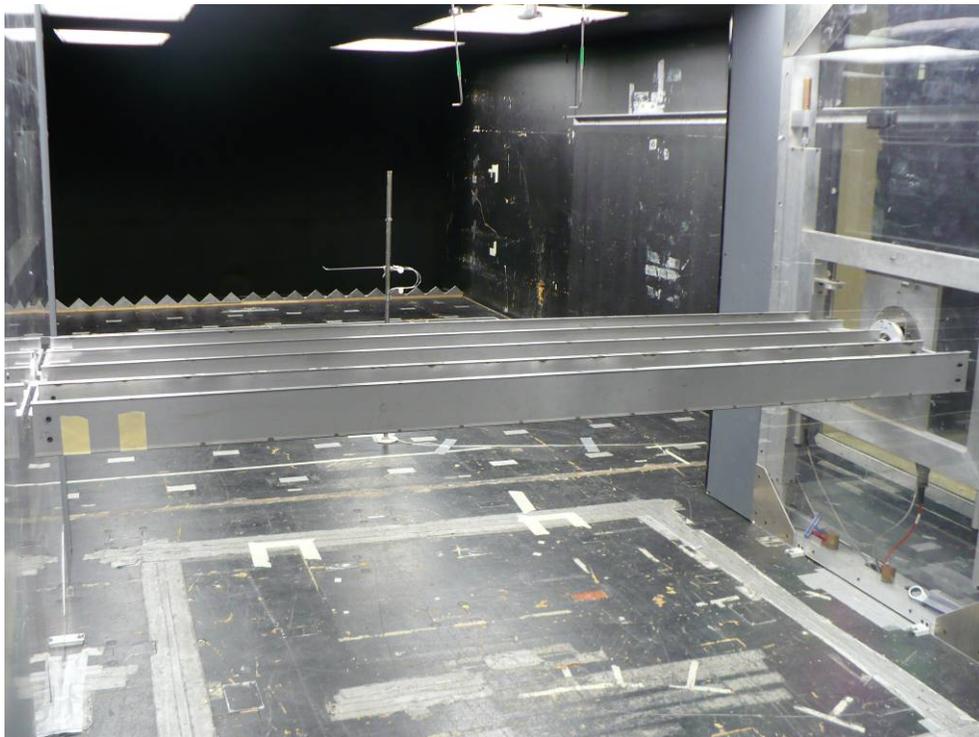
d) FIVE GIRDERS (TEST F53)

FIGURE 1.12 (CONT.)   SECTION MODEL TEST SET-UP – NARROW FLANGE PLATE GIRDER

a) SINGLE BOX (TEST G11)

b) TWO BOXES (TEST G22)

FIGURE 1.13 SECTION MODEL TEST SET-UP – BOX GIRDER

c) TWO BOXES (TEST G21)
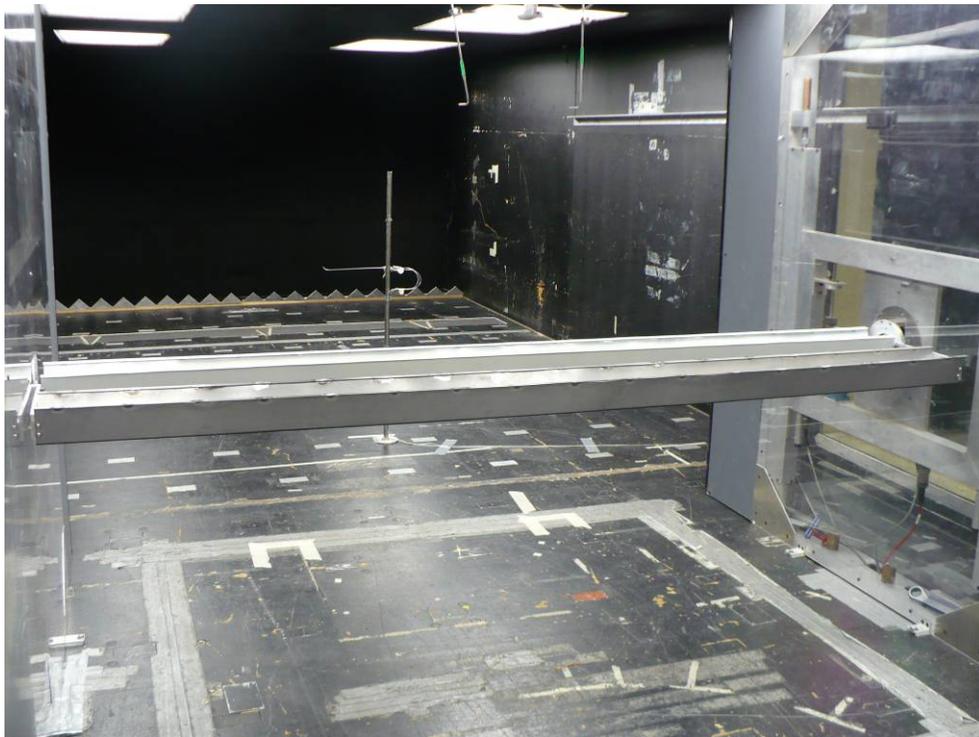
d) TWO BOXES (TEST H21)

FIGURE 1.13 (CONT.)   SECTION MODEL TEST SET-UP – BOX GIRDER

a) SINGLE I-BEAM (TEST J11)
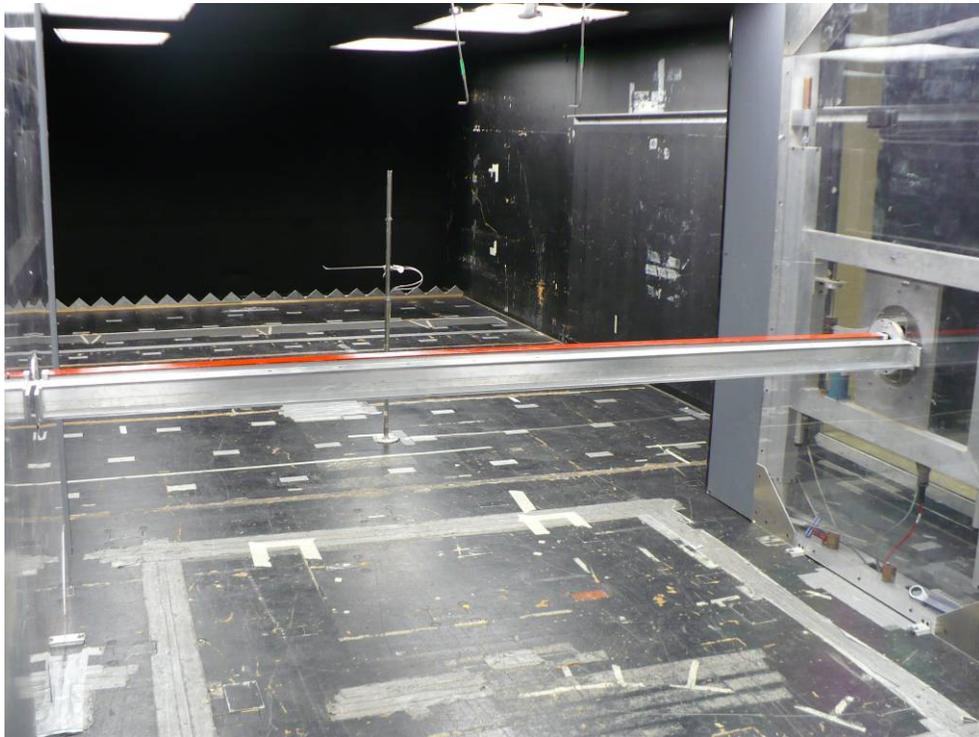
b) TWO I-BEAMS (TEST J21)

FIGURE 1.14 SECTION MODEL TEST SET-UP – 78-INCH "FLORIDA" I-BEAM
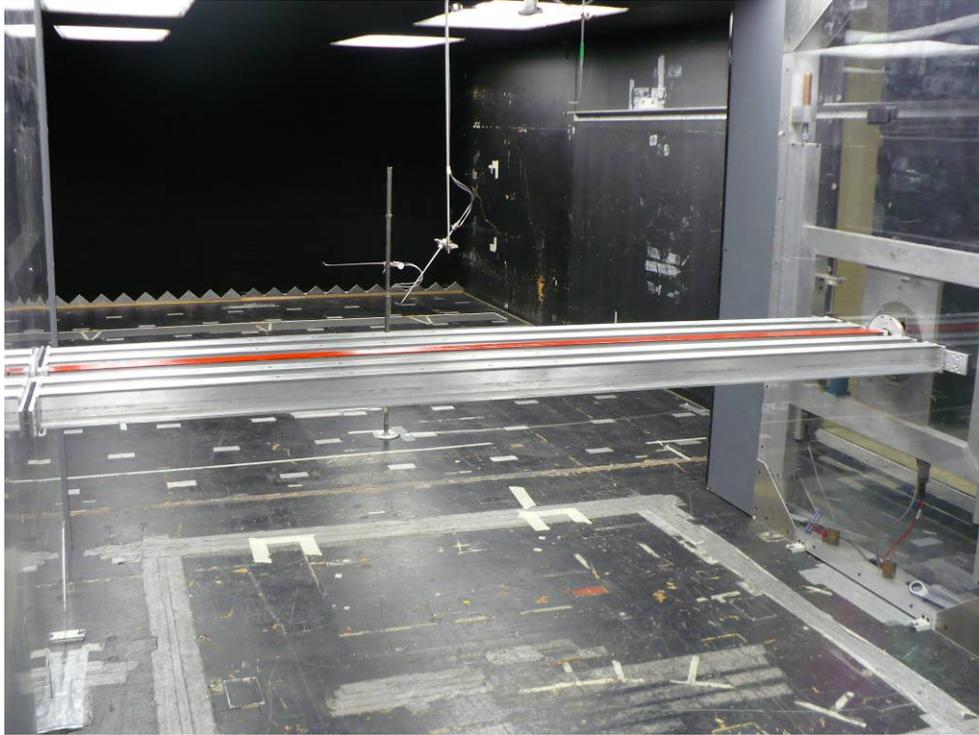
c) FIVE I-BEAMS (TEST J53)
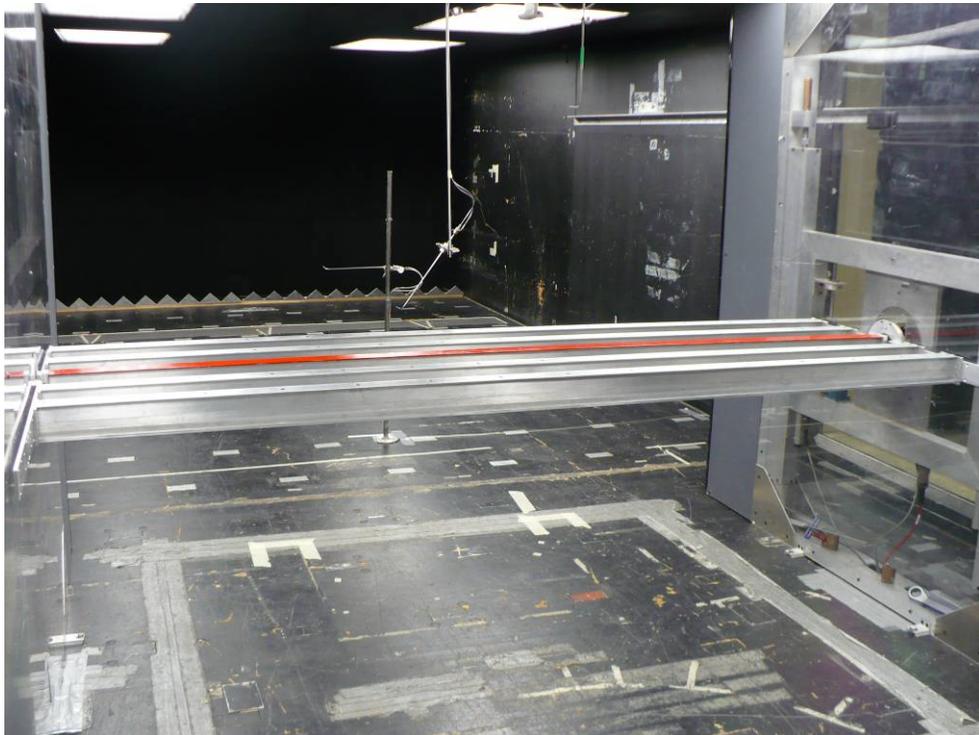
d) FIVE I-BEAMS (TEST K53)

FIGURE 1.14 (CONT.)   SECTION MODEL TEST SET-UP – 78-INCH "FLORIDA" I-BEAM

a) SINGLE I-BEAM (TEST L11)
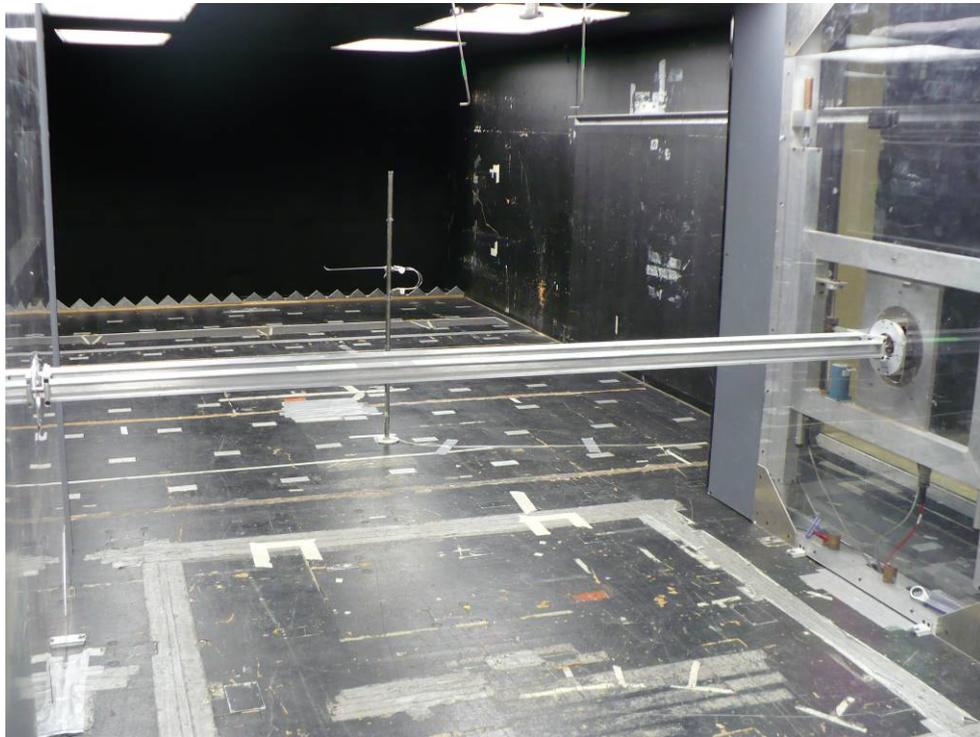
b) TWO I-BEAMS (TEST L22)

FIGURE 1.15 SECTION MODEL TEST SET-UP – 45-INCH "FLORIDA" I-BEAM

c) FIVE I-BEAMS (TEST M22)
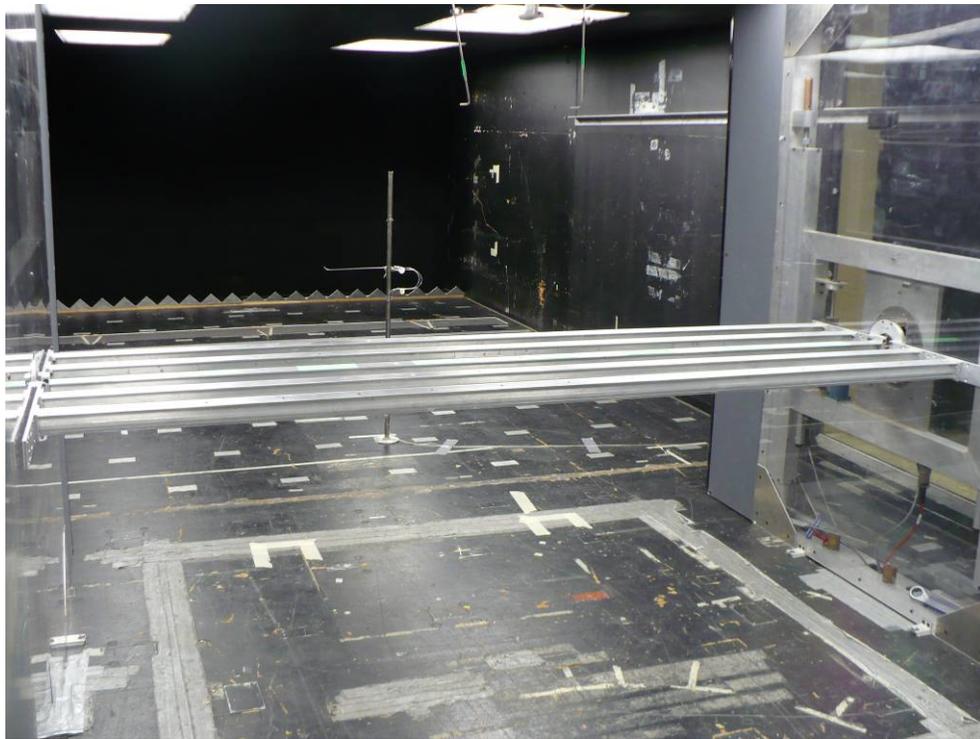
d) FIVE I-BEAMS (TEST M53)

FIGURE 1.15 (CONT.)   SECTION MODEL TEST SET-UP – 45-INCH "FLORIDA" I-BEAM
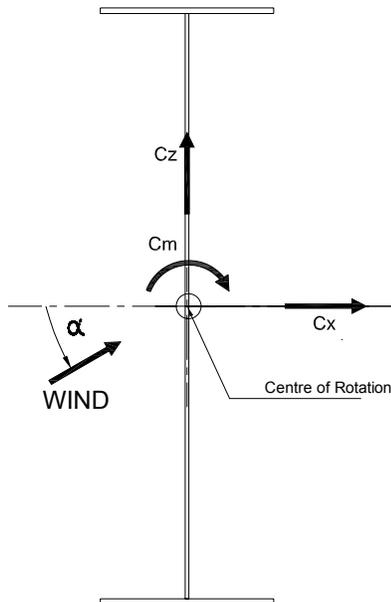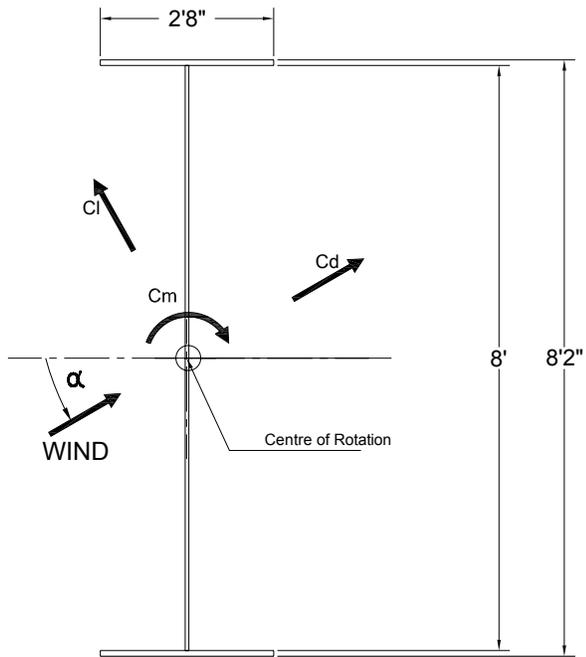
FIGURE 2.1   SIGN CONVENTION OF FORCES – WIDE FLANGE PLATE GIRDER
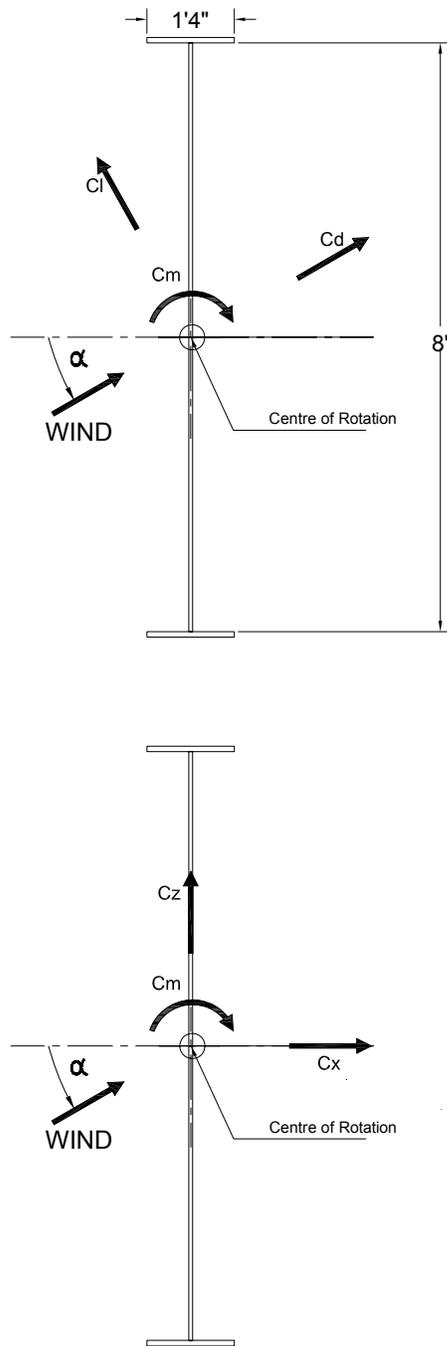
FIGURE 2.2   SIGN CONVENTION OF FORCES – NARROW FLANGE PLATE GIRDER
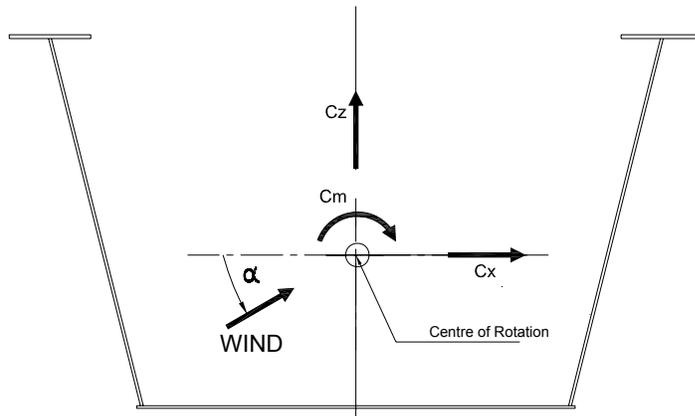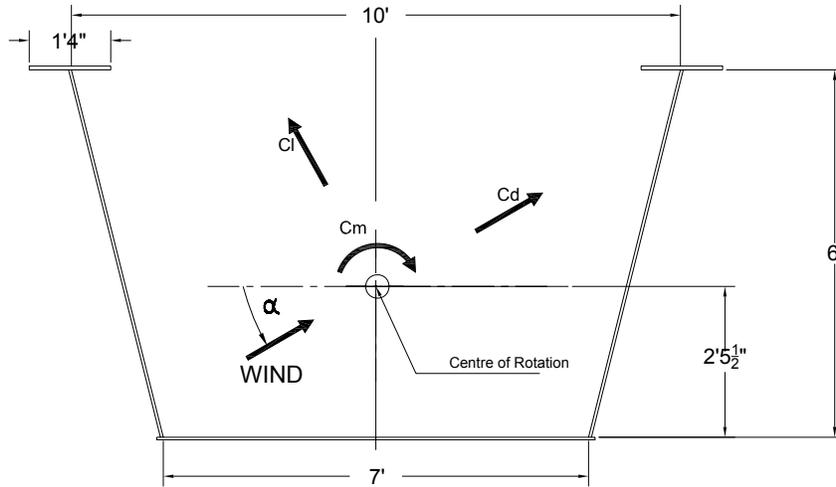
FIGURE 2.3   SIGN CONVENTION OF FORCES – BOX GIRDER
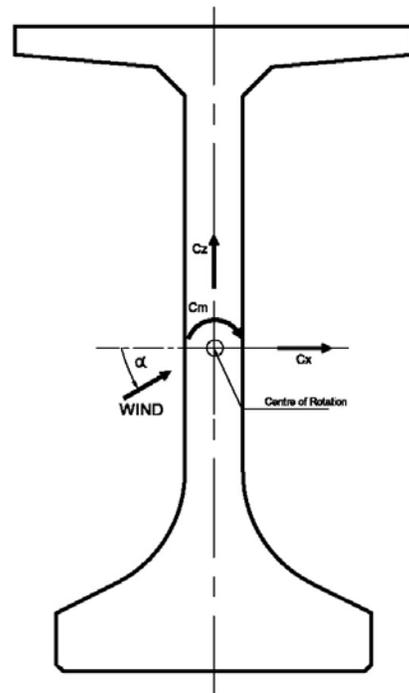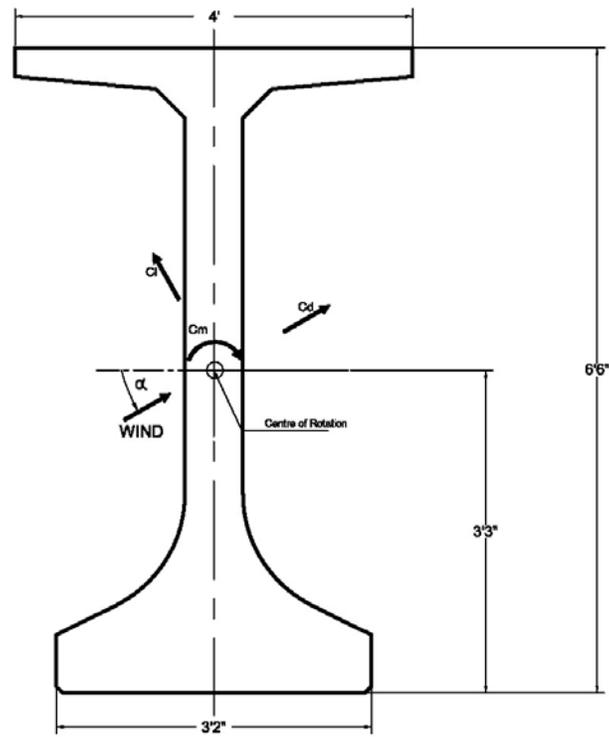
FIGURE 2.4 SIGN CONVENTION OF FORCES – 78-INCH "FLORIDA" I-BEAM
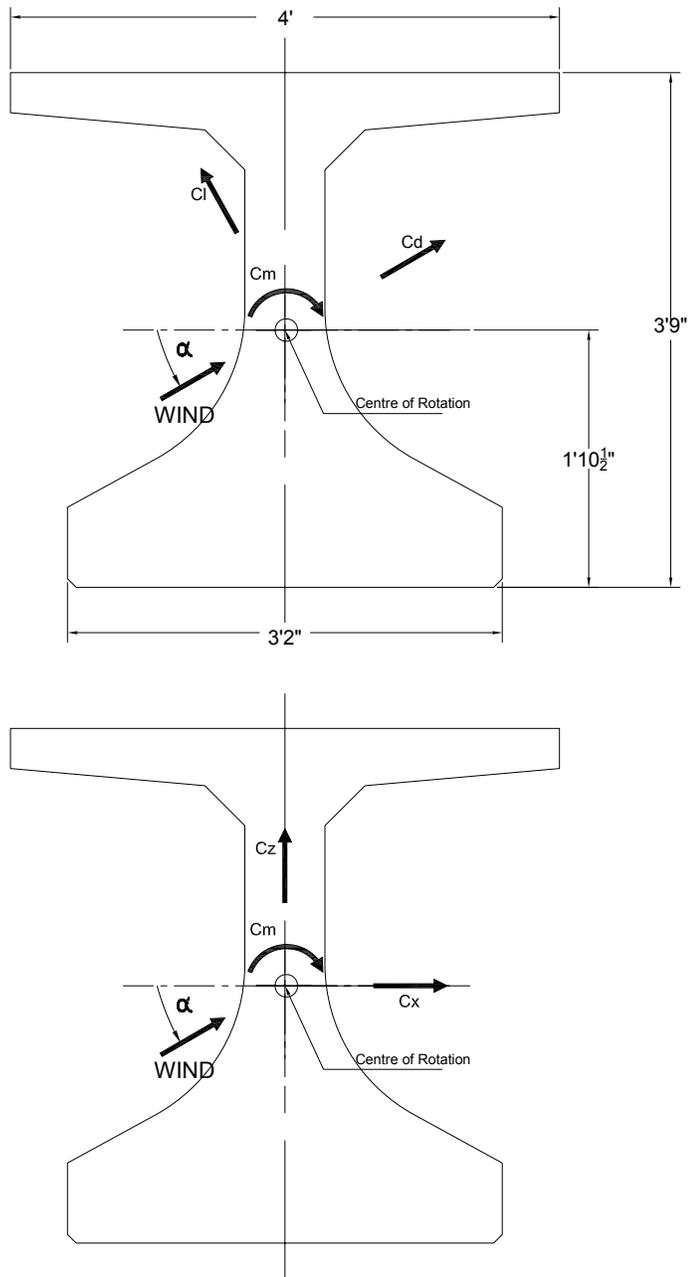
FIGURE 2.5   SIGN CONVENTION OF FORCES – 45-INCH "FLORIDA" I-BEAM

Wide Flange, 2% Slope, 10ft Spacing

Wide Flange, 2% Slope, 10ft Spacing

FIGURE 2.6   STATIC FORCE COEFFICIENTS (BODY FORCES) – WIDE FLANGE GIRDER, 2% SLOPE, 10FT SPACING

Wide Flange, 2% Slope, 10ft Spacing

Wide Flange, 2% Slope, 10ft Spacing

FIGURE 2.7   STATIC FORCE COEFFICIENTS (WIND AXIS FORCES) – WIDE FLANGE GIRDER, 2% SLOPE, 10FT SPACING

Wide Flange, 2% Slope, 14ft Spacing

Wide Flange, 2% Slope, 14ft Spacing

FIGURE 2.8   STATIC FORCE COEFFICIENTS (BODY FORCES) – WIDE FLANGE GIRDER, 2% SLOPE, 14FT SPACING

Wide Flange, 2% Slope, 14ft Spacing

♦ A11 ■ B21 ▲ B22 ● B51 □ B52 ○ B53 △ B54 ◇ B55

Wide Flange, 2% Slope, 14ft Spacing

♦ A11 ■ B21 ▲ B22 ● B51 □ B52 ○ B53 △ B54 ◇ B55

FIGURE 2.9   STATIC FORCE COEFFICIENTS (WIND AXIS FORCES) – WIDE FLANGE GIRDER, 2% SLOPE, 14FT SPACING

FIGURE 2.10 **STATIC FORCE COEFFICIENTS (BODY FORCES) – WIDE FLANGE GIRDER, 8% SLOPE, 10FT SPACING**

Wide Flange, 8% Slope, 10ft Spacing

Wide Flange, 8% Slope, 10ft Spacing

FIGURE 2.11   STATIC FORCE COEFFICIENTS (WIND AXIS FORCES) – WIDE FLANGE GIRDER, 8% SLOPE, 10FT SPACING

Wide Flange, 8% Slope, 14ft Spacing

Wide Flange, 8% Slope, 14ft Spacing

FIGURE 2.12   STATIC FORCE COEFFICIENTS (BODY FORCES) – WIDE FLANGE GIRDER, 8% SLOPE, 14FT SPACING

FIGURE 2.13 **STATIC FORCE COEFFICIENTS (WIND AXIS FORCES) – WIDE FLANGE GIRDER, 8% SLOPE, 14FT SPACING**

Narrow Flange, 2% Slope, 10ft Spacing

Narrow Flange, 2% Slope, 10ft Spacing

FIGURE 2.14   **STATIC FORCE COEFFICIENTS (BODY FORCES) – NARROW FLANGE GIRDER, 2% SLOPE, 10FT SPACING**
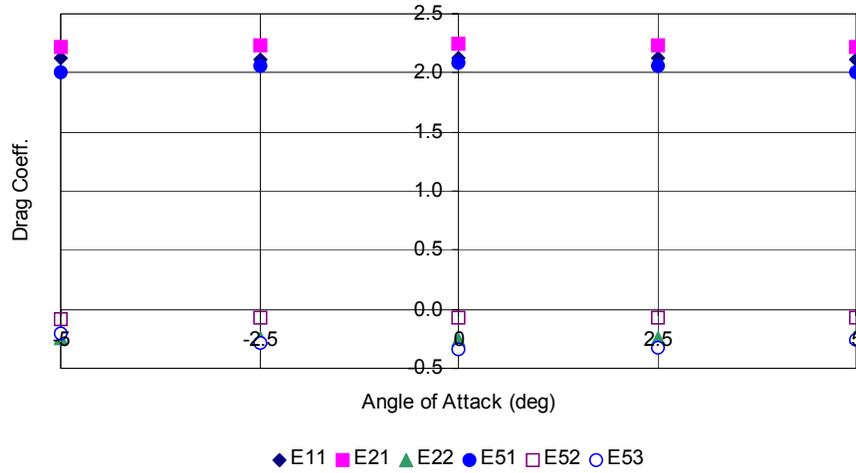
Narrow Flange, 2% Slope, 10ft Spacing
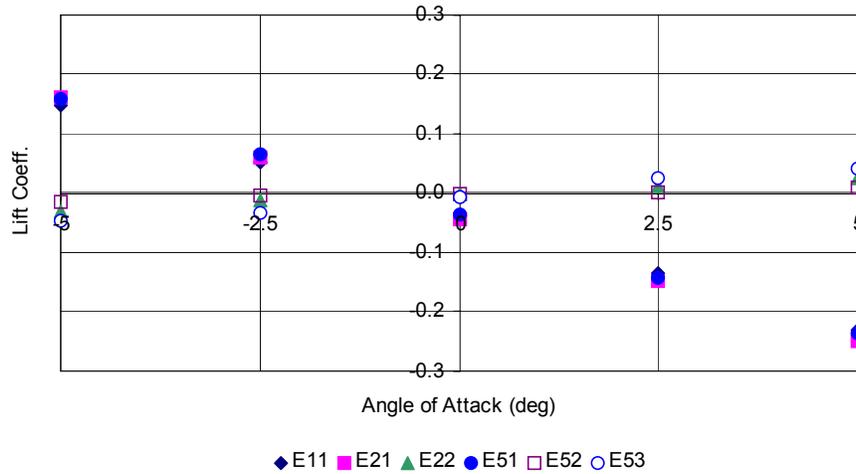
Narrow Flange, 2% Slope, 10ft Spacing
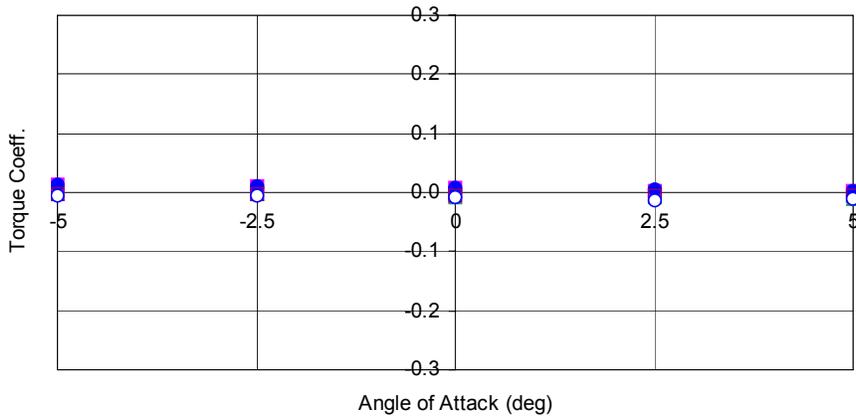
FIGURE 2.15   STATIC FORCE COEFFICIENTS (WIND AXIS FORCES) – NARROW FLANGE GIRDER, 2% SLOPE, 10FT SPACING

Narrow Flange, 2% Slope, 14ft Spacing

♦ E11 ■ F21 ▲ F22 ● F51 □ F52 ○ F53

Narrow Flange, 2% Slope, 14ft Spacing

♦ E11 ■ F21 ▲ F22 ● F51 □ F52 ○ F53
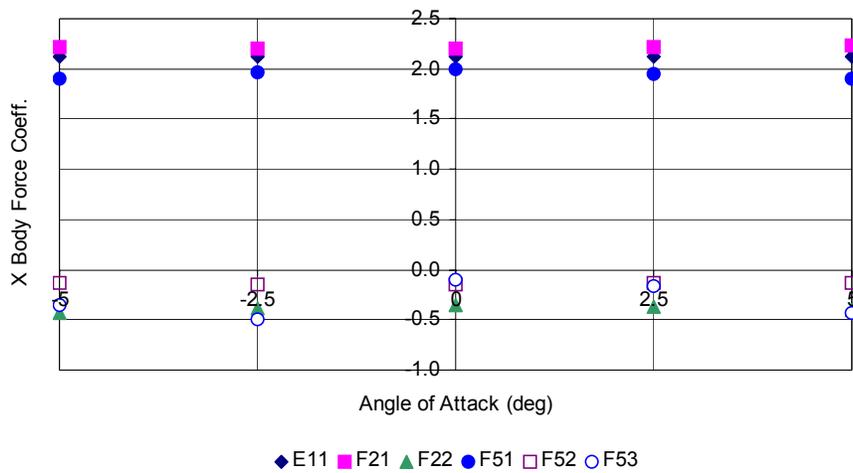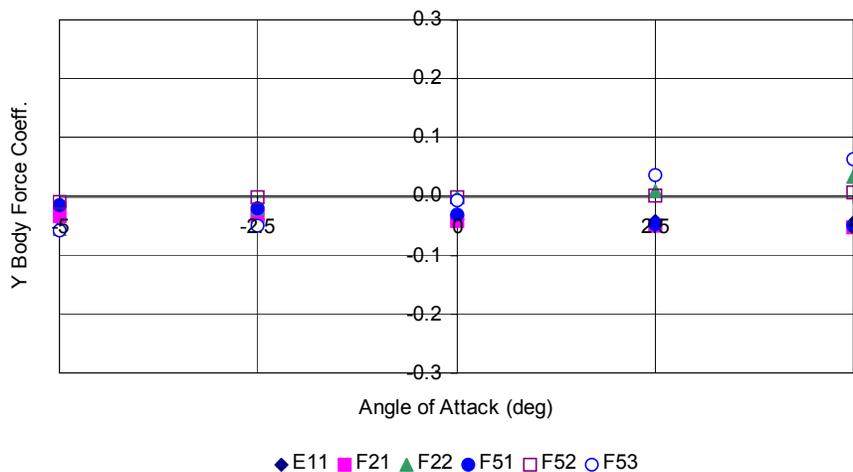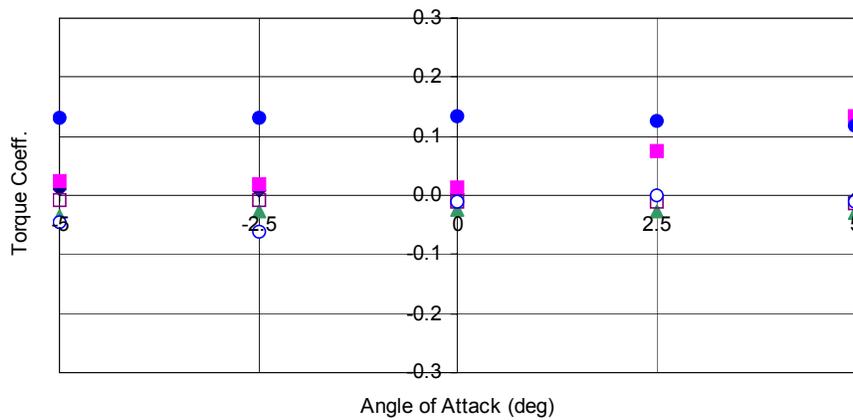
FIGURE 2.16   **STATIC FORCE COEFFICIENTS (BODY FORCES) – NARROW FLANGE GIRDER, 2% SLOPE, 14FT SPACING**
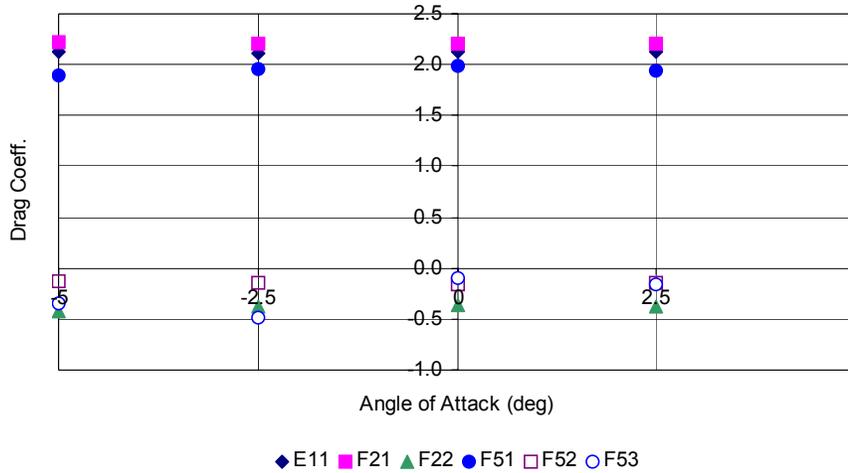
Narrow Flange, 2% Slope, 14ft Spacing
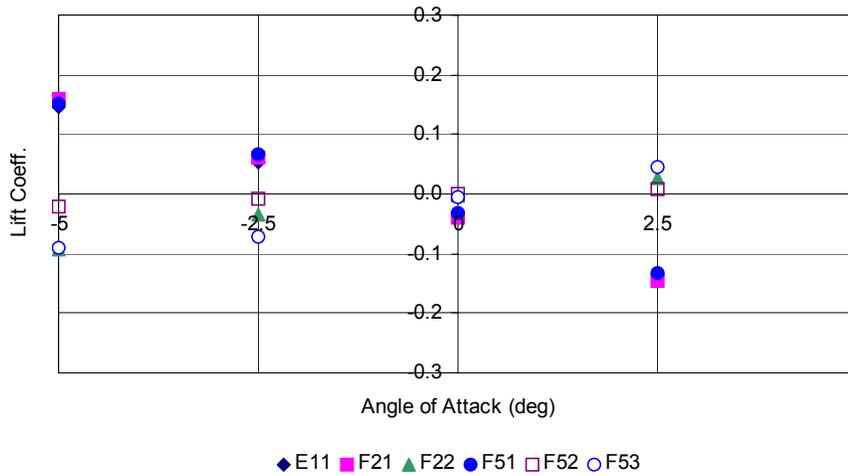
Narrow Flange, 2% Slope, 14ft Spacing
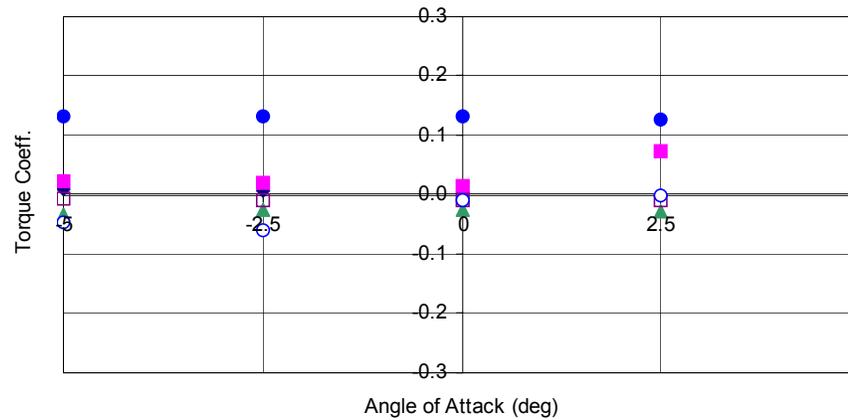
FIGURE 2.17   STATIC FORCE COEFFICIENTS (WIND AXIS FORCES) – NARROW FLANGE GIRDER, 2% SLOPE, 14FT SPACING

X Body Force Coeff.

Angle of Attack (deg)

◆ G11 ■ G21 ▲ G22

Box Girders, 0% Slope, 20ft Spacing

Y Body Force Coeff.

Angle of Attack (deg)

◆ G11 ■ G21 ▲ G22

Box Girders, 0% Slope, 20ft Spacing

Torque Coeff.
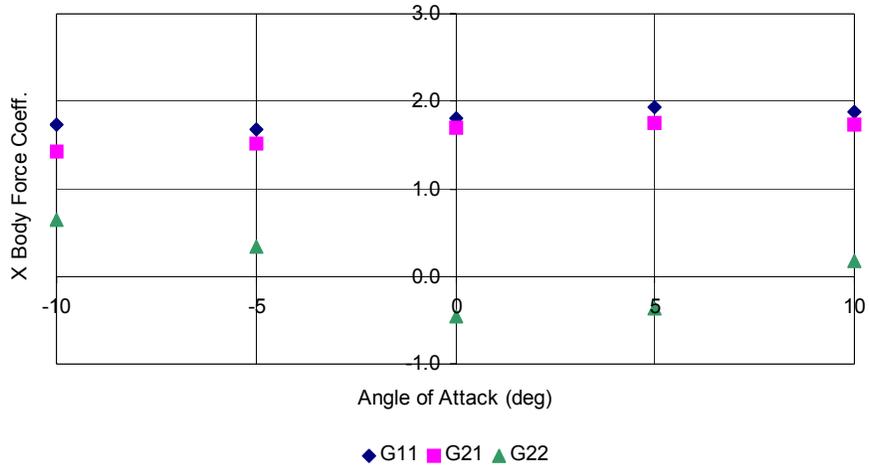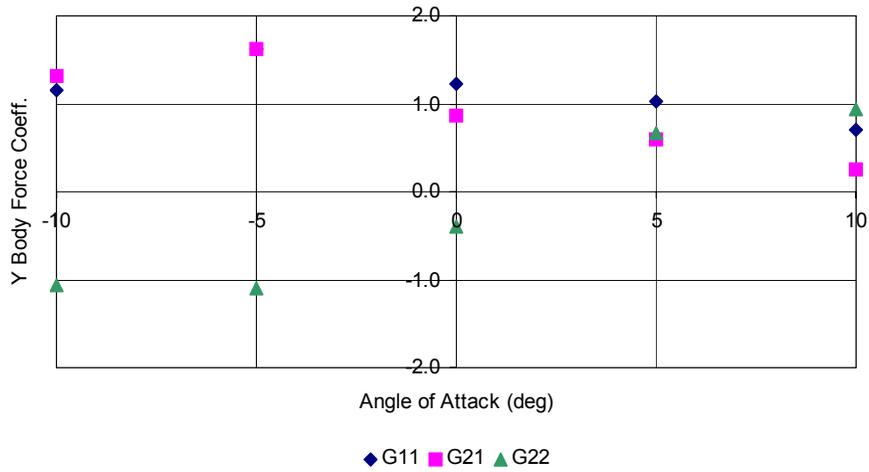
Angle of Attack (deg)
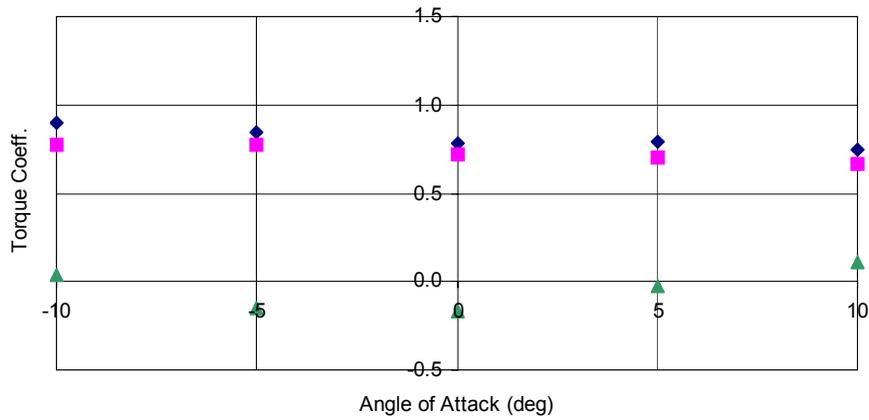
FIGURE 2.18   STATIC FORCE COEFFICIENTS (BODY FORCES) – BOX GIRDERS, 0% SLOPE, 20FT SPACING
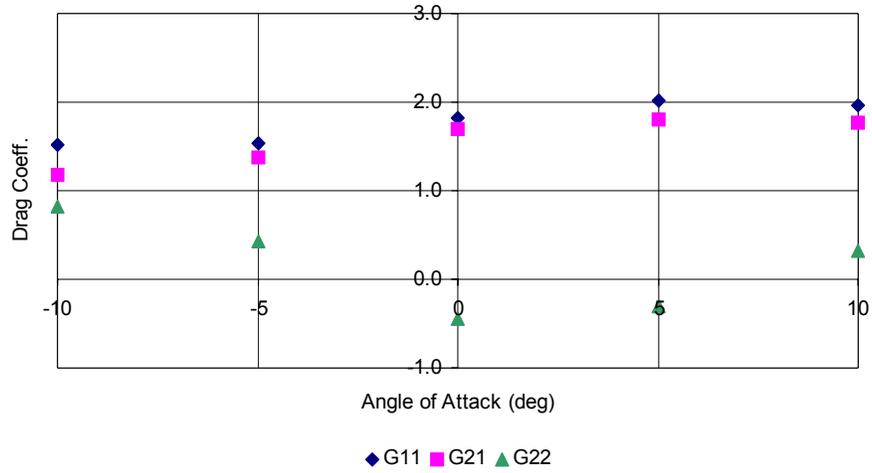
Box Girders, 0% Slope, 20ft Spacing
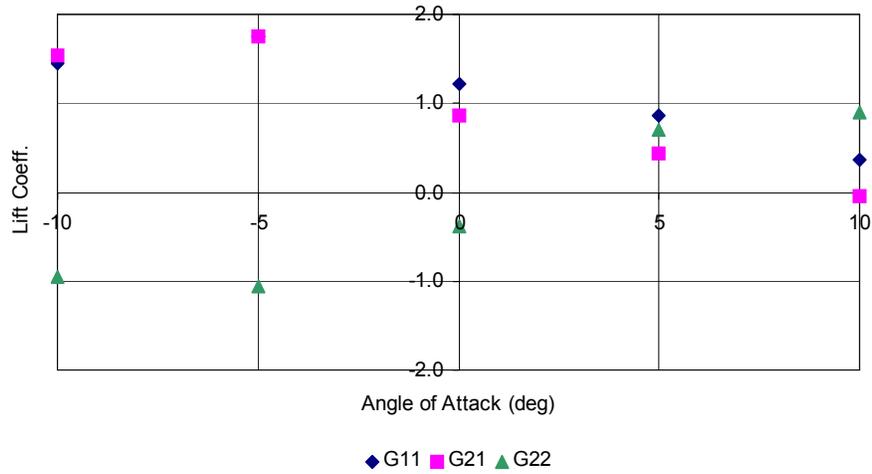
Box Girders, 0% Slope, 20ft Spacing
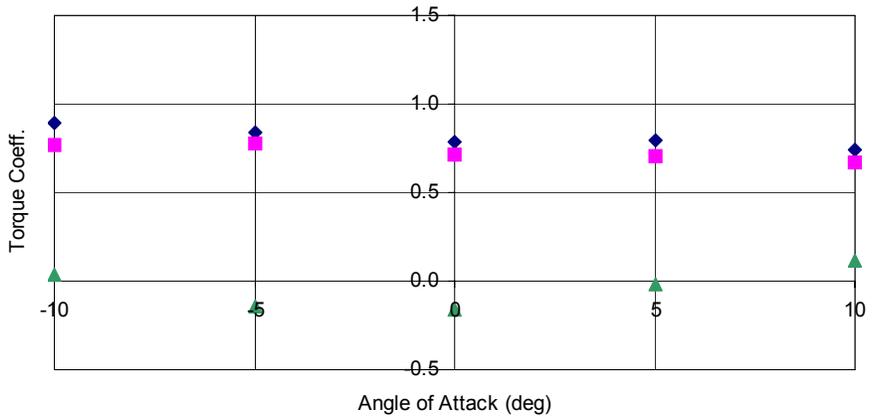
FIGURE 2.19   **STATIC FORCE COEFFICIENTS (WIND AXIS FORCES) – BOX GIRDERS, 0% SLOPE, 20FT SPACING**
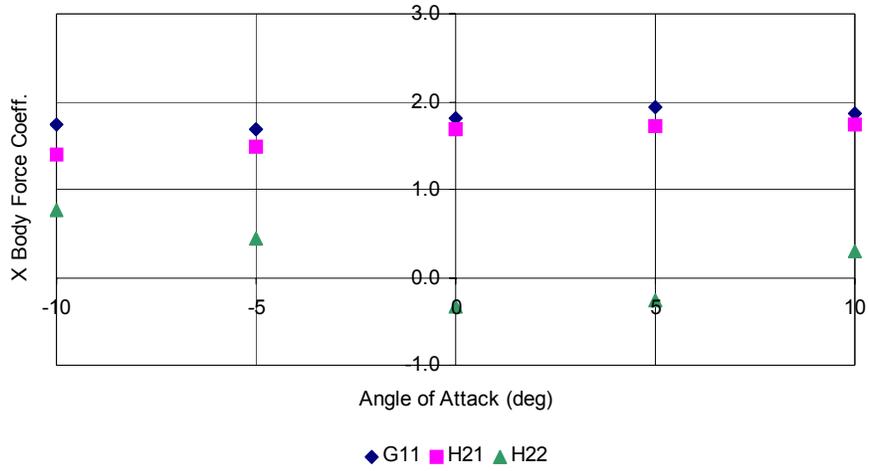
Box Girders, 0% Slope, 22ft Spacing
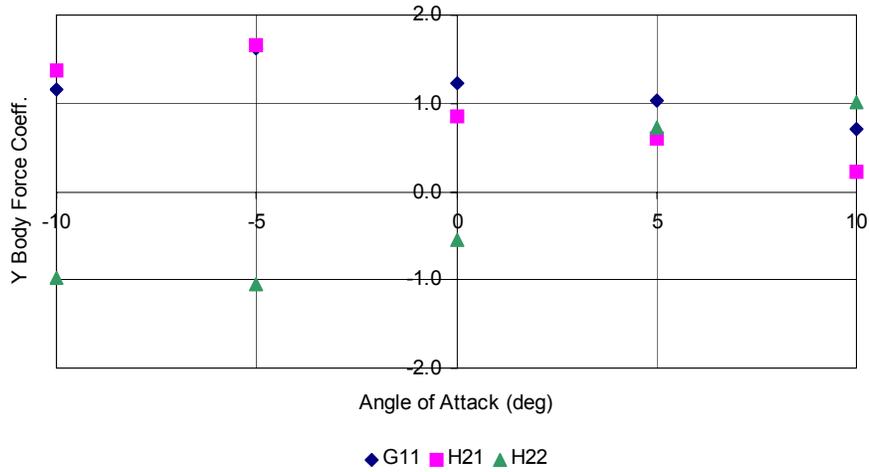
Box Girders, 0% Slope, 22ft Spacing
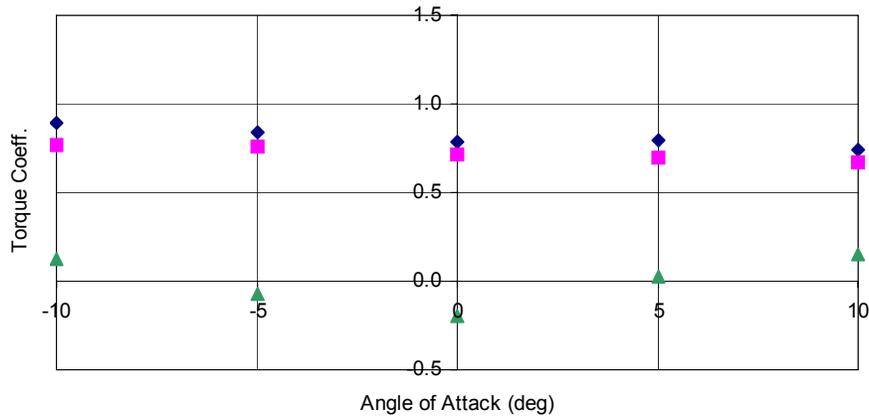
FIGURE 2.20   **STATIC FORCE COEFFICIENTS (BODY FORCES) – BOX GIRDERS, 0% SLOPE, 22FT SPACING**
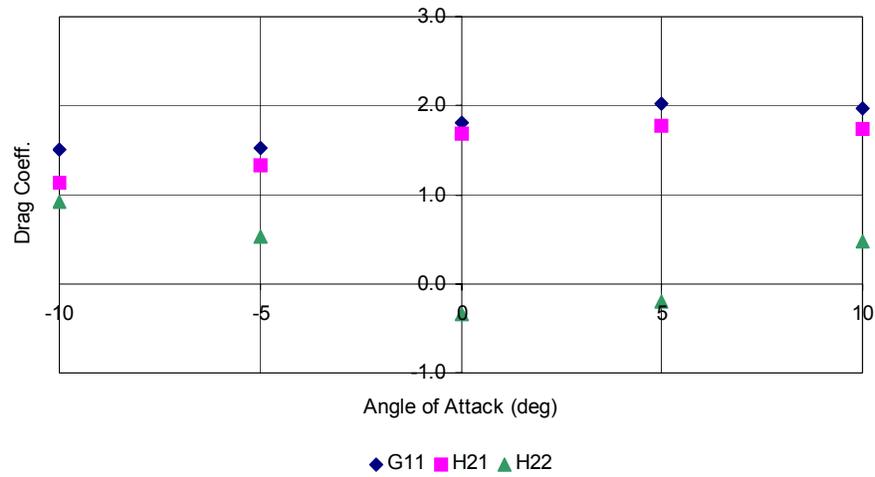
Box Girders, 0% Slope, 22ft Spacing
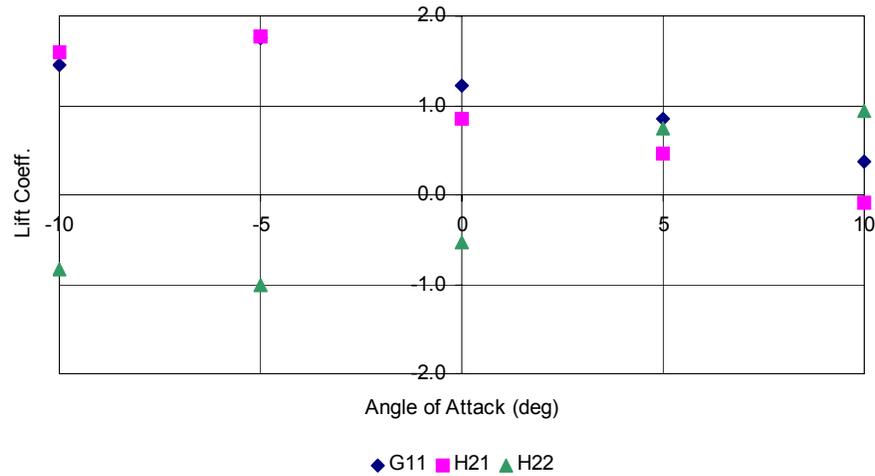
Box Girders, 0% Slope, 22ft Spacing
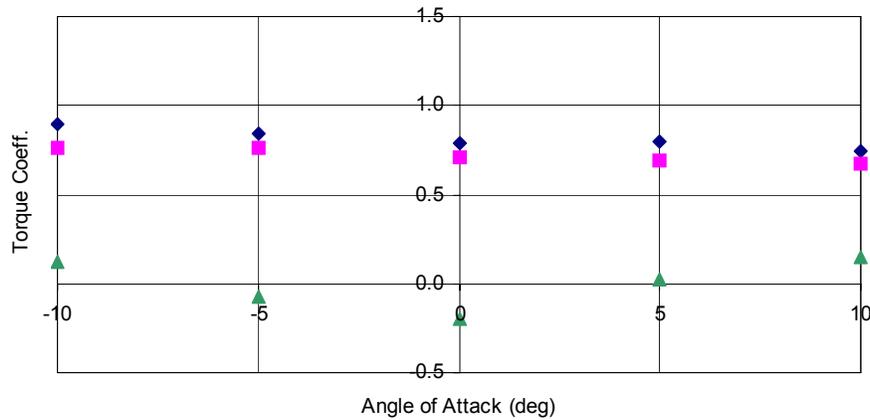
FIGURE 2.21   STATIC FORCE COEFFICIENTS (WIND AXIS FORCES) – BOX GIRDERS, 0% SLOPE, 22FT SPACING
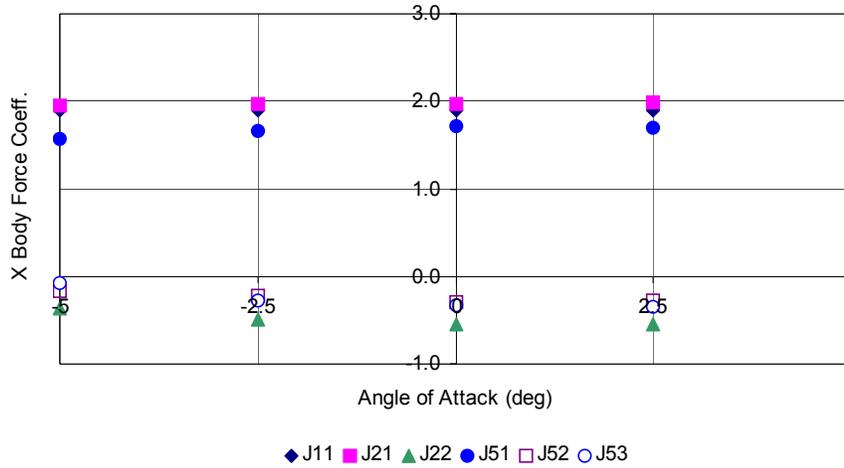
78" Florida I-Beam, 2% Slope, 10ft Spacing
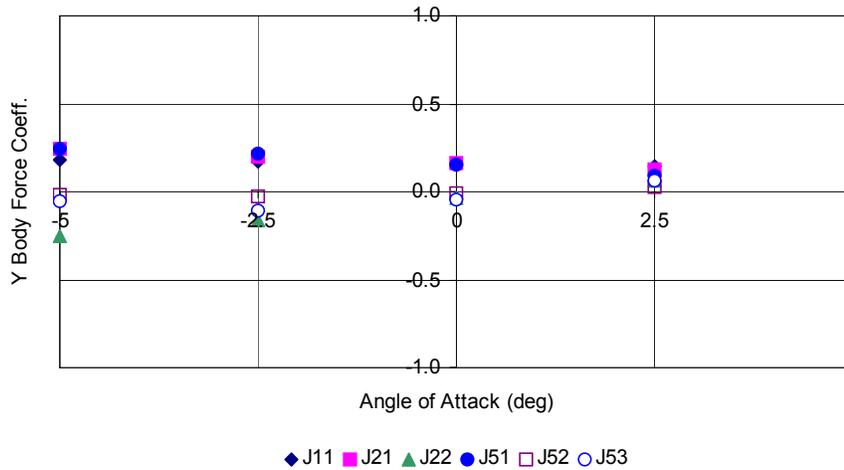
78" Florida I-Beam, 2% Slope, 10ft Spacing
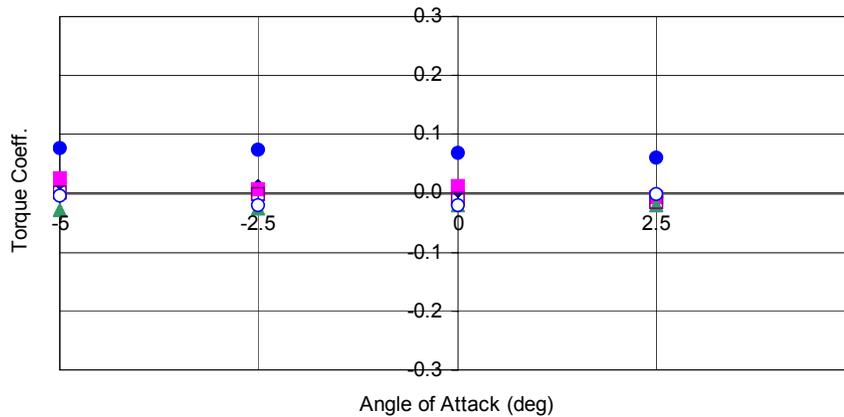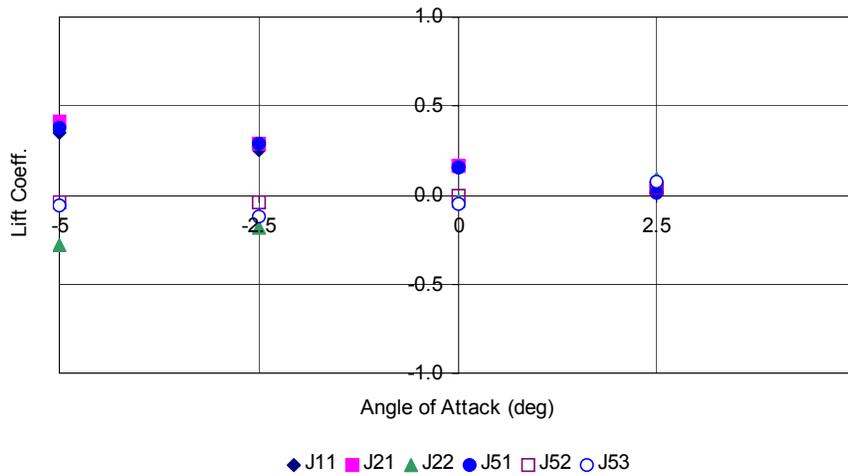
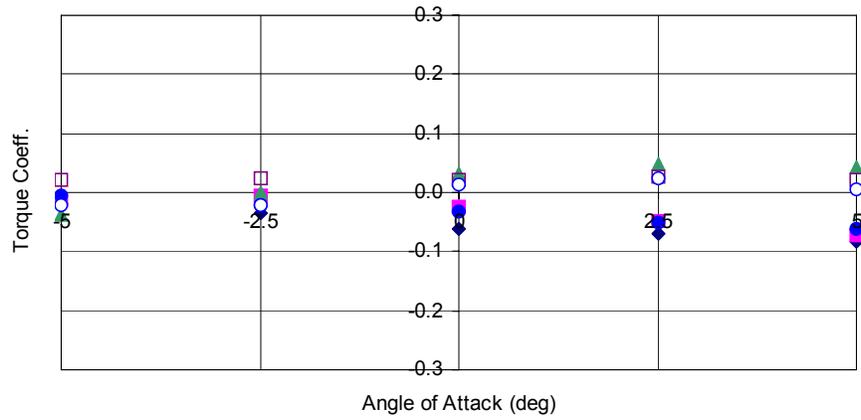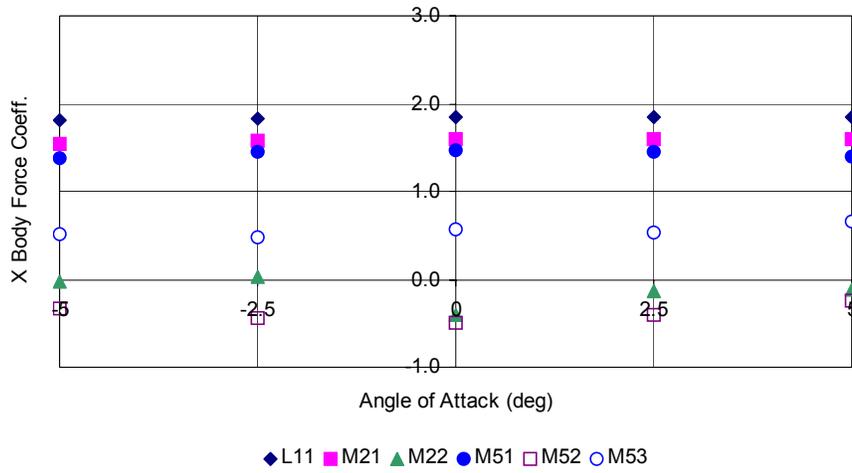**FIGURE 2.22   STATIC FORCE COEFFICIENTS (BODY FORCES) – 78-INCH "FLORIDA" I-BEAMS, 2% SLOPE, 10FT SPACING**
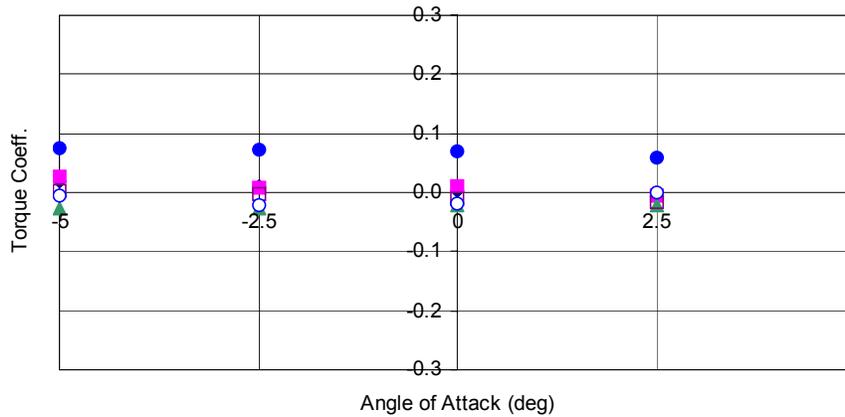
FIGURE 2.23   STATIC FORCE COEFFICIENTS (WIND AXIS FORCES) – 78-INCH "FLORIDA" I-BEAMS, 2% SLOPE, 10FT SPACING
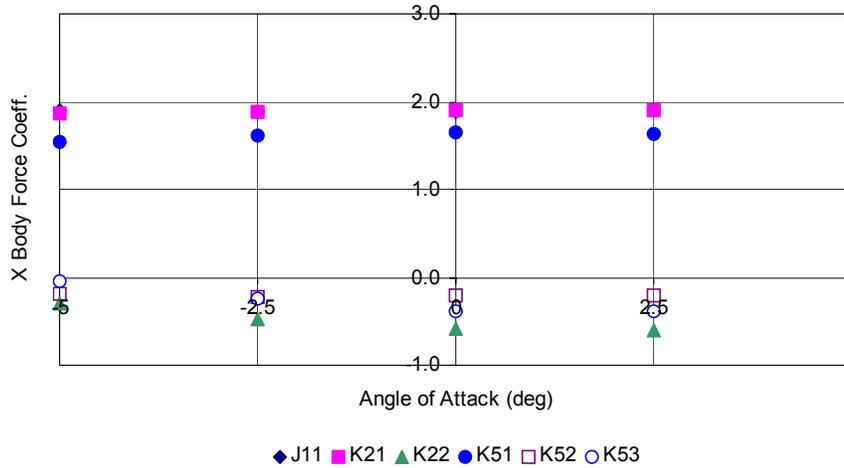
Chart 1: X Body Force Coeff. vs. Angle of Attack (deg)

Legend: ◆ J11　■ K21　▲ K22　● K51　□ K52　○ K53

78" Florida I-Beam, 2% Slope, 13ft Spacing

Chart 2: Y Body Force Coeff. vs. Angle of Attack (deg)

Legend: ◆ J11　■ K21　▲ K22　● K51　□ K52　○ K53

78" Florida I-Beam, 2% Slope, 13ft Spacing
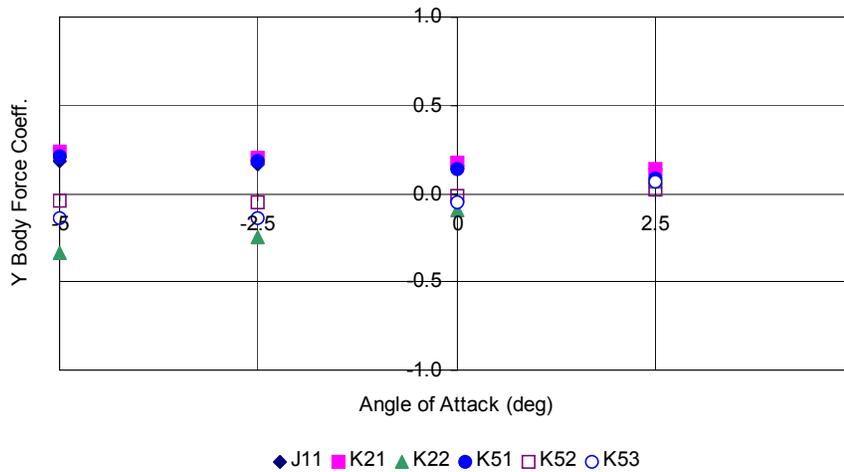
Chart 3: Torque Coeff. vs. Angle of Attack (deg)
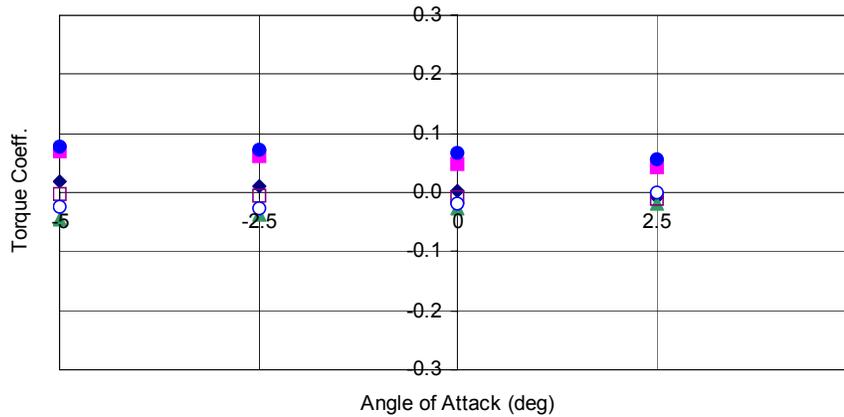
FIGURE 2.24   STATIC FORCE COEFFICIENTS (BODY FORCES) – 78-INCH "FLORIDA" I-BEAMS, 2% SLOPE, 13FT SPACING
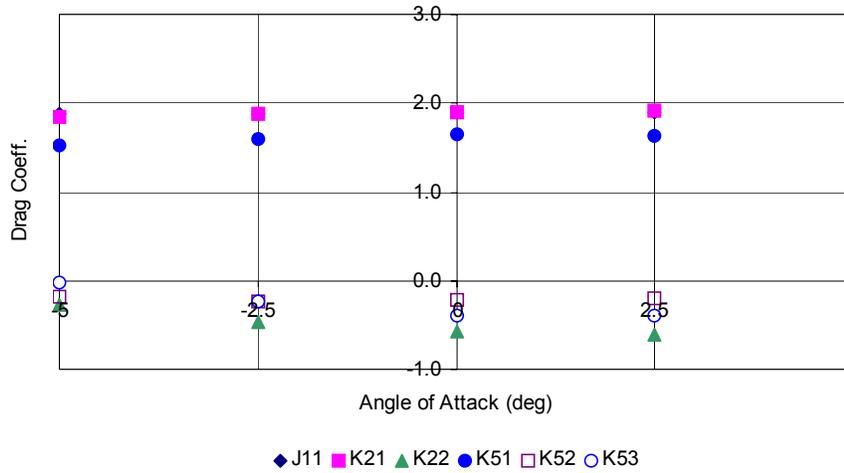
78" Florida I-Beam, 2% Slope, 13ft Spacing
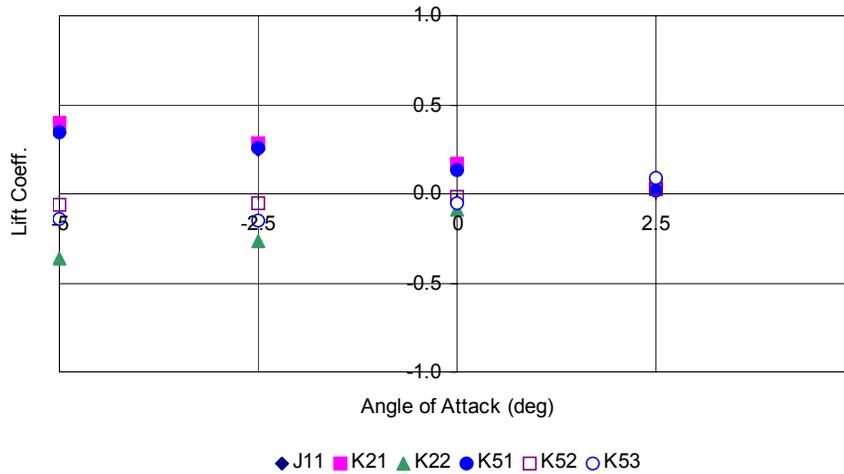
78" Florida I-Beam, 2% Slope, 13ft Spacing
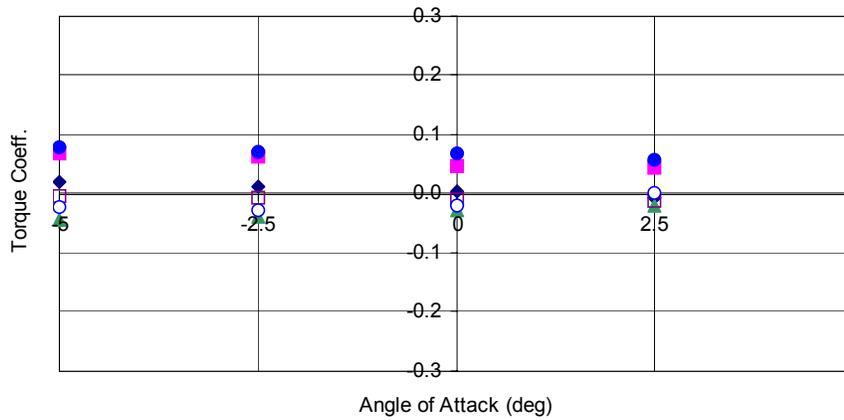
FIGURE 2.25   STATIC FORCE COEFFICIENTS (WIND AXIS FORCES) – 78-INCH "FLORIDA" I-BEAMS, 2% SLOPE, 13FT SPACING
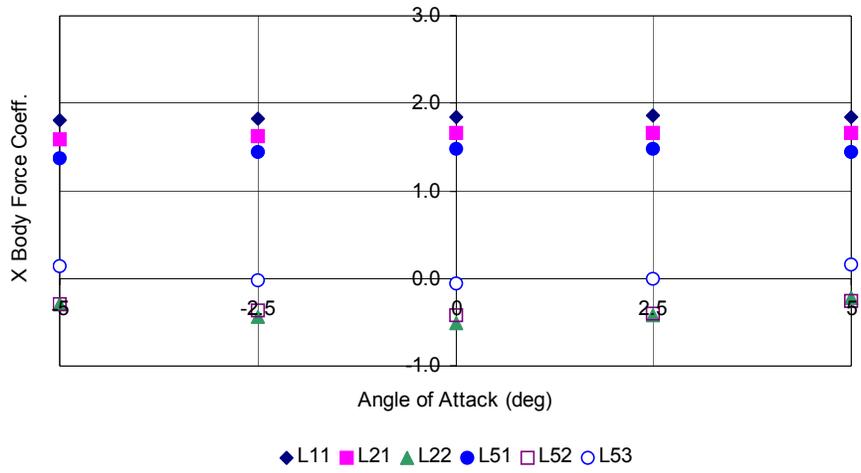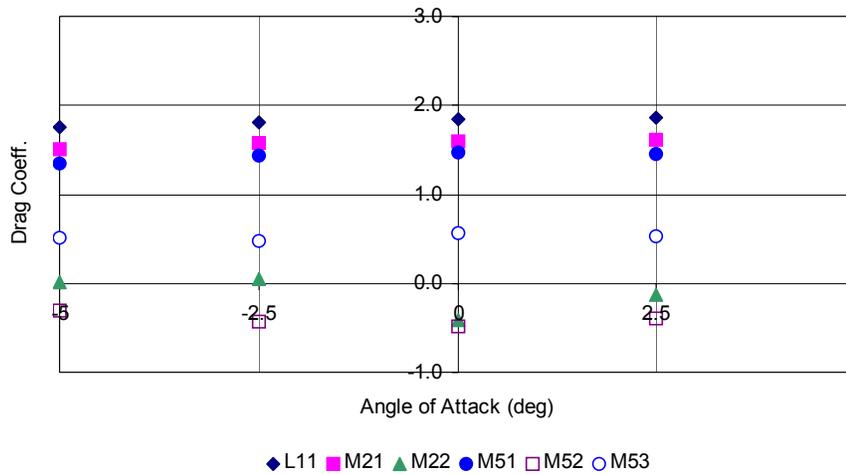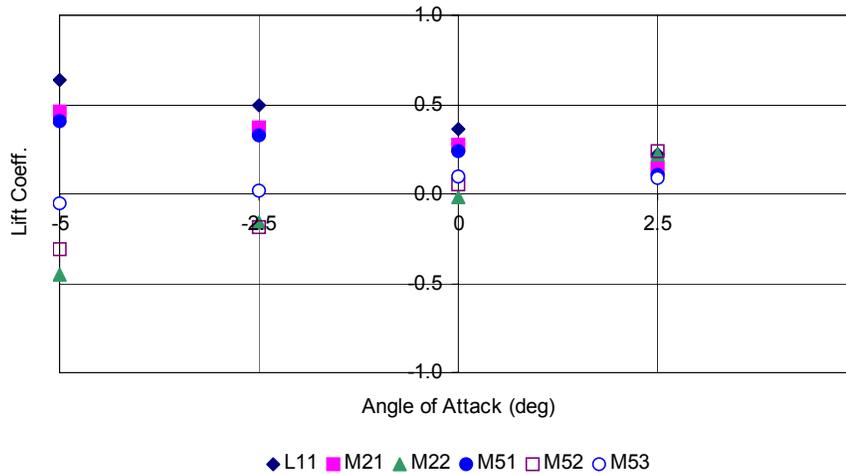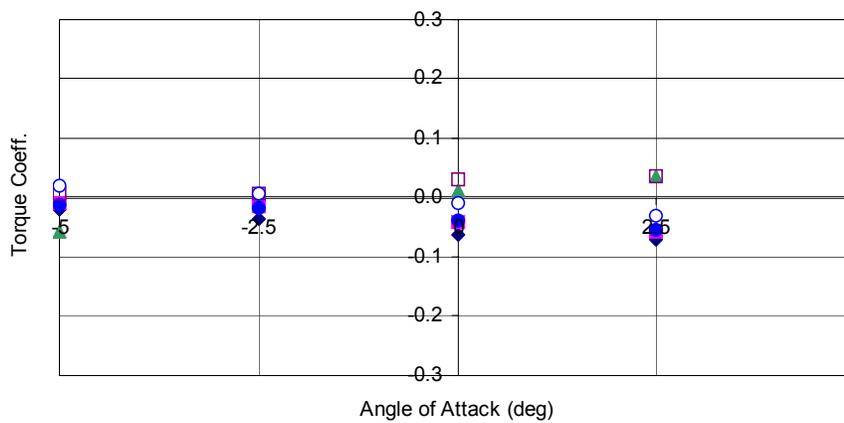
45" Florida I-Beam, 2% Slope, 10ft Spacing
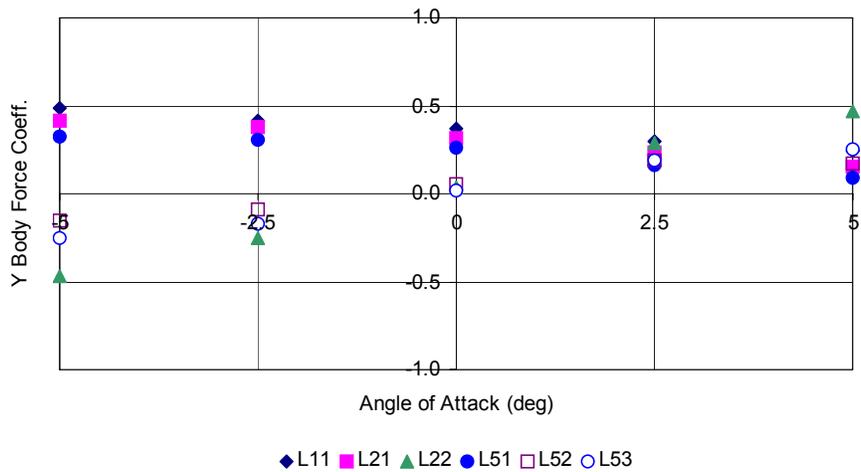
45" Florida I-Beam, 2% Slope, 10ft Spacing
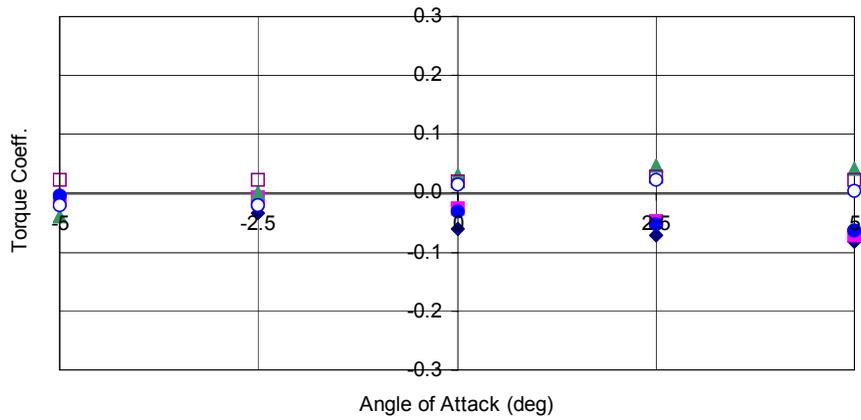
FIGURE 2.26   **STATIC FORCE COEFFICIENTS (BODY FORCES) – 45-INCH "FLORIDA" I-BEAMS, 2% SLOPE, 10FT SPACING**
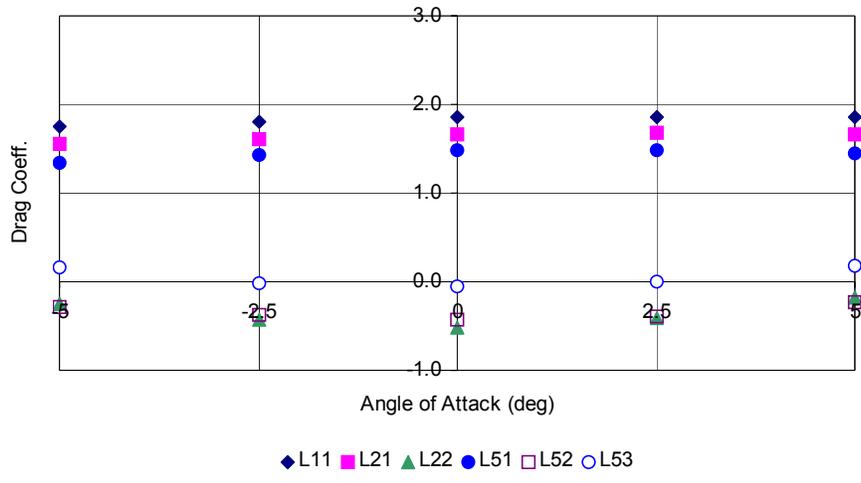
Drag Coeff.

Angle of Attack (deg)

♦ L11 ■ L21 ▲ L22 ● L51 □ L52 ○ L53

45" Florida I-Beam, 2% Slope, 10ft Spacing

Lift Coeff.

Angle of Attack (deg)

♦ L11 ■ L21 ▲ L22 ● L51 □ L52 ○ L53

45" Florida I-Beam, 2% Slope, 10ft Spacing

Torque Coeff.
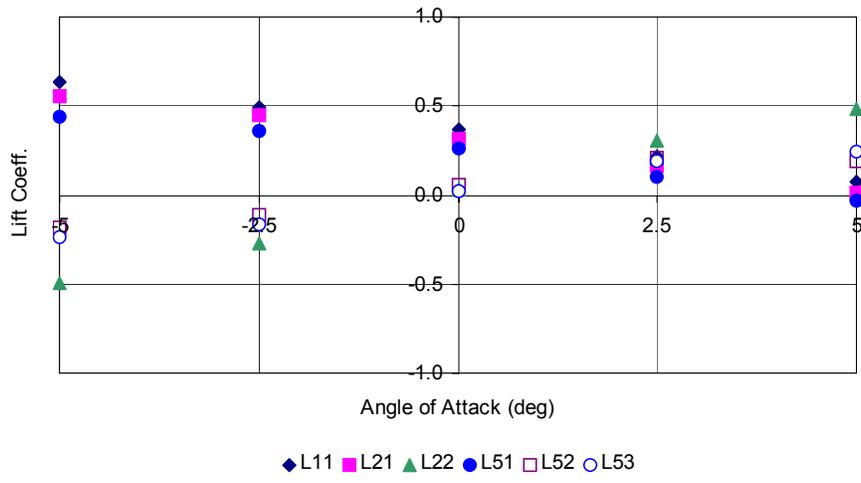
Angle of Attack (deg)

FIGURE 2.27   STATIC FORCE COEFFICIENTS (WIND AXIS FORCES) – 45-INCH "FLORIDA" I-BEAMS, 2% SLOPE, 10FT SPACING

45" Florida I-Beam, 2% Slope, 13ft Spacing
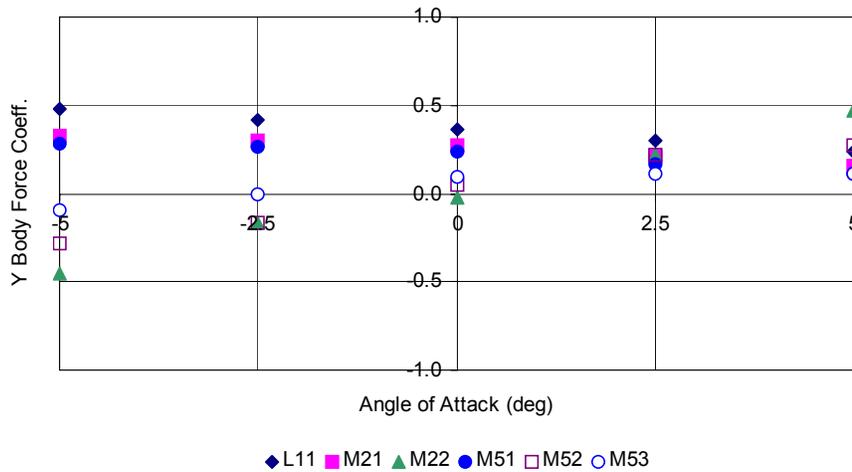
45" Florida I-Beam, 2% Slope, 13ft Spacing
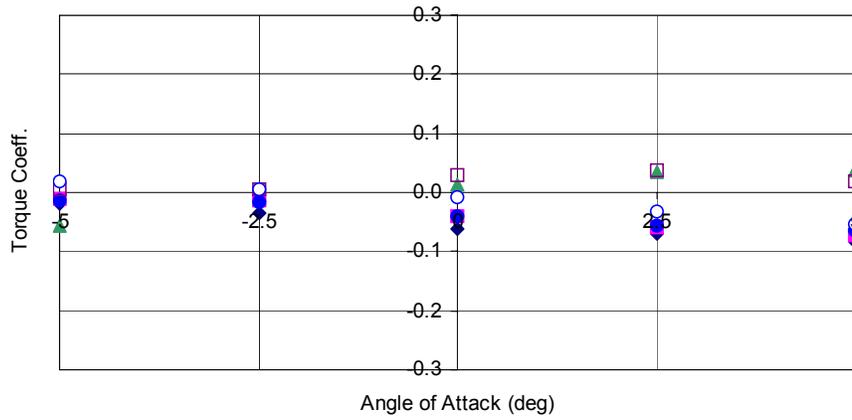
FIGURE 2.28   STATIC FORCE COEFFICIENTS (BODY FORCES) – 45-INCH "FLORIDA" I-BEAMS, 2% SLOPE, 13FT SPACING

45" Florida I-Beam, 2% Slope, 13ft Spacing

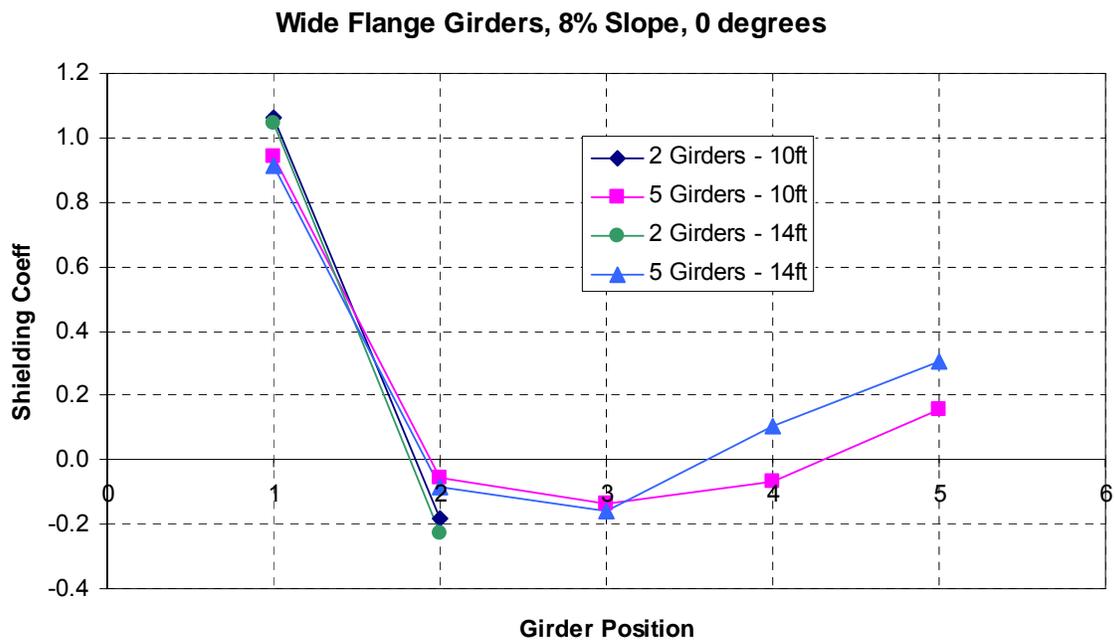45" Florida I-Beam, 2% Slope, 13ft Spacing

FIGURE 2.29   STATIC FORCE COEFFICIENTS (WIND AXIS FORCES) – 45-INCH "FLORIDA" I-BEAMS, 2% SLOPE, 13FT SPACING
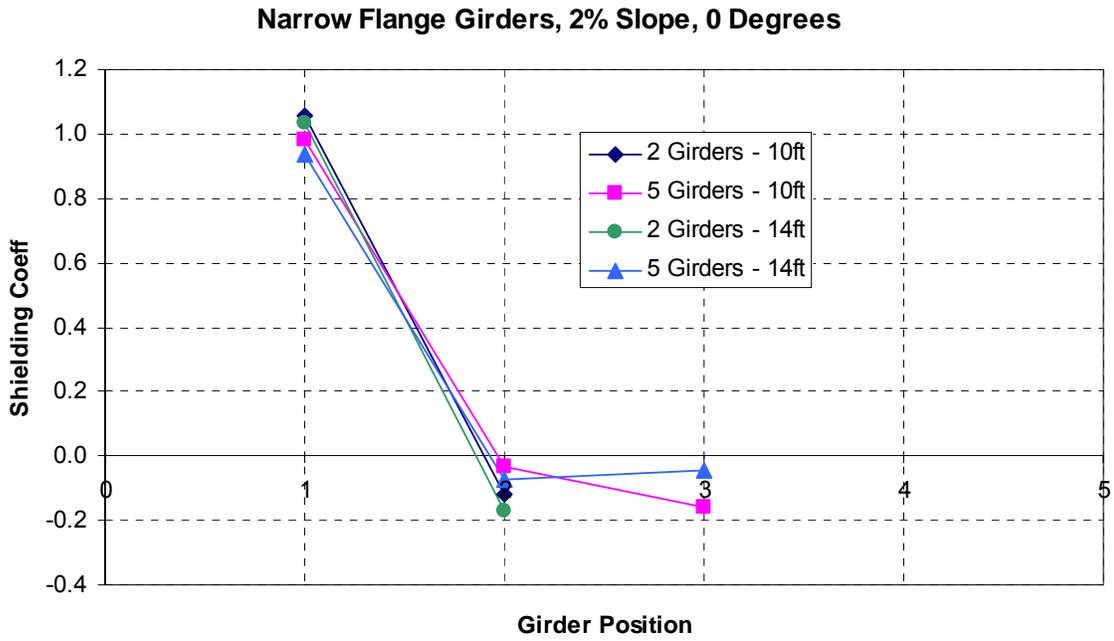
Wide Flange Girders, 2% Slope, 0 Degrees
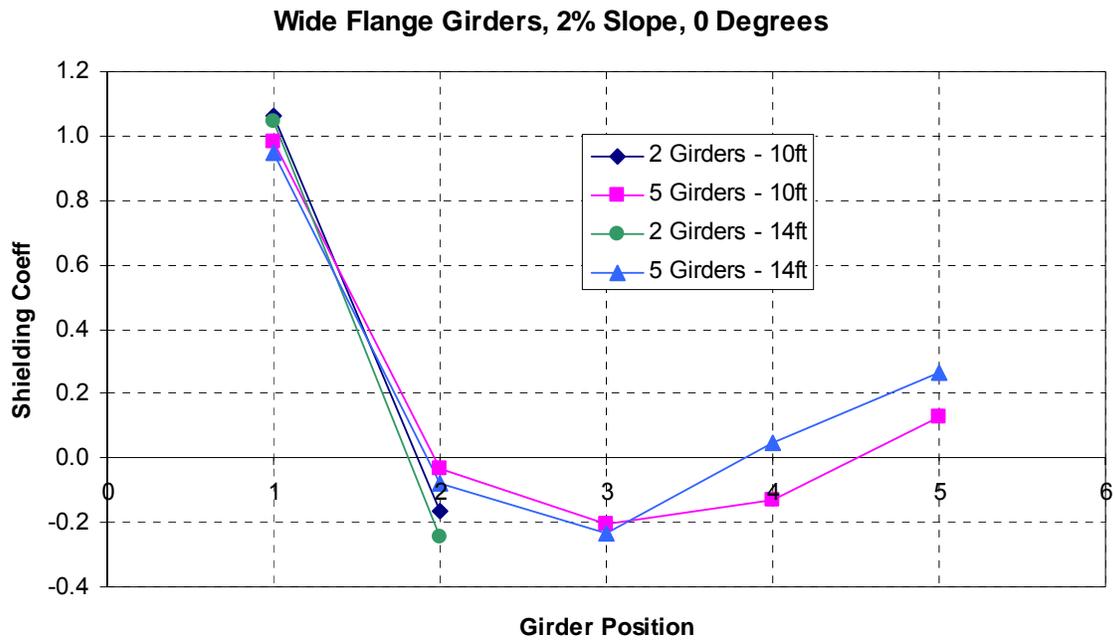
FIGURE 2.30   **SHIELDING COEFFICIENTS – WIDE FLANGE GIRDERS, 2% SLOPE, 0 DEGREES**

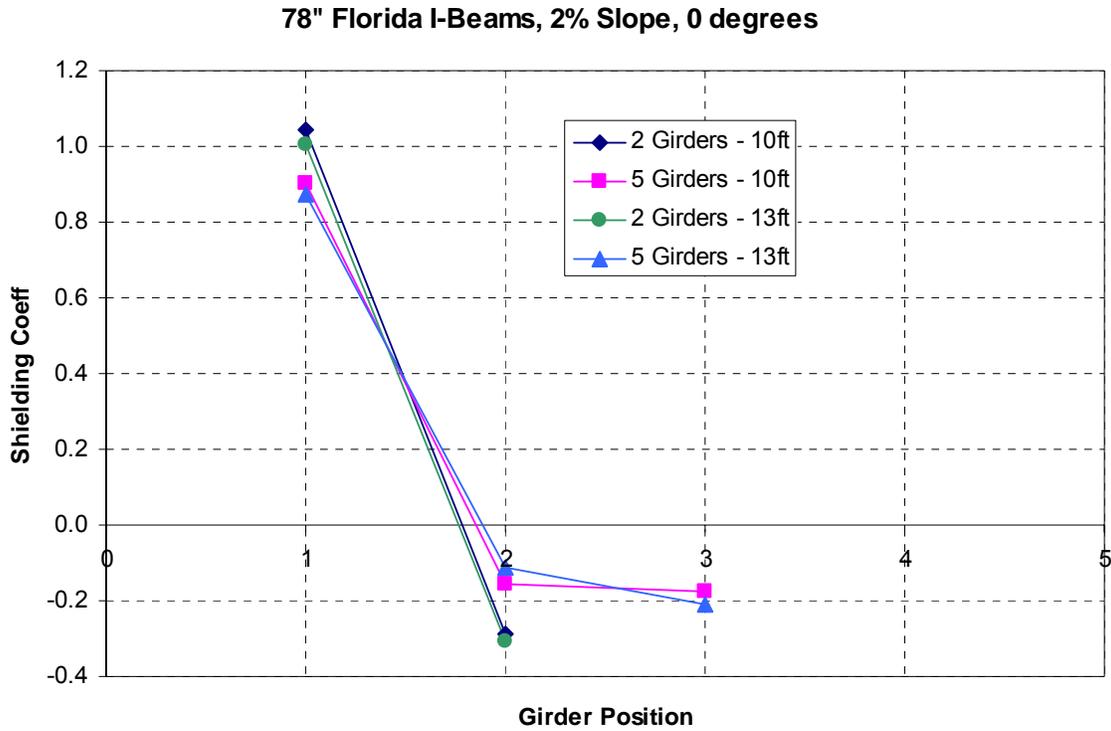Wide Flange Girders, 8% Slope, 0 degrees

FIGURE 2.31   **SHIELDING COEFFICIENTS – WIDE FLANGE GIRDERS, 8% SLOPE, 0 DEGREES**

Narrow Flange Girders, 2% Slope, 0 Degrees

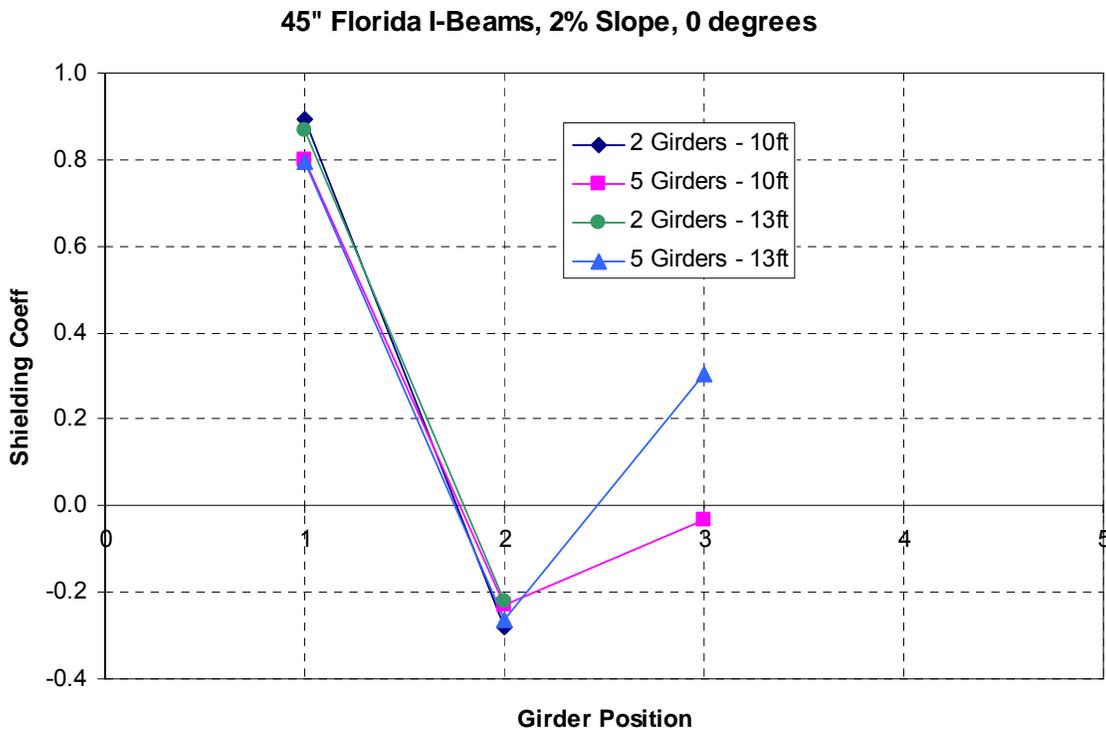FIGURE 2.32   SHIELDING COEFFICIENTS – NARROW FLANGE GIRDERS, 2% SLOPE, 0 DEGREES

Box Girders, 0% Slope, 0 Degrees
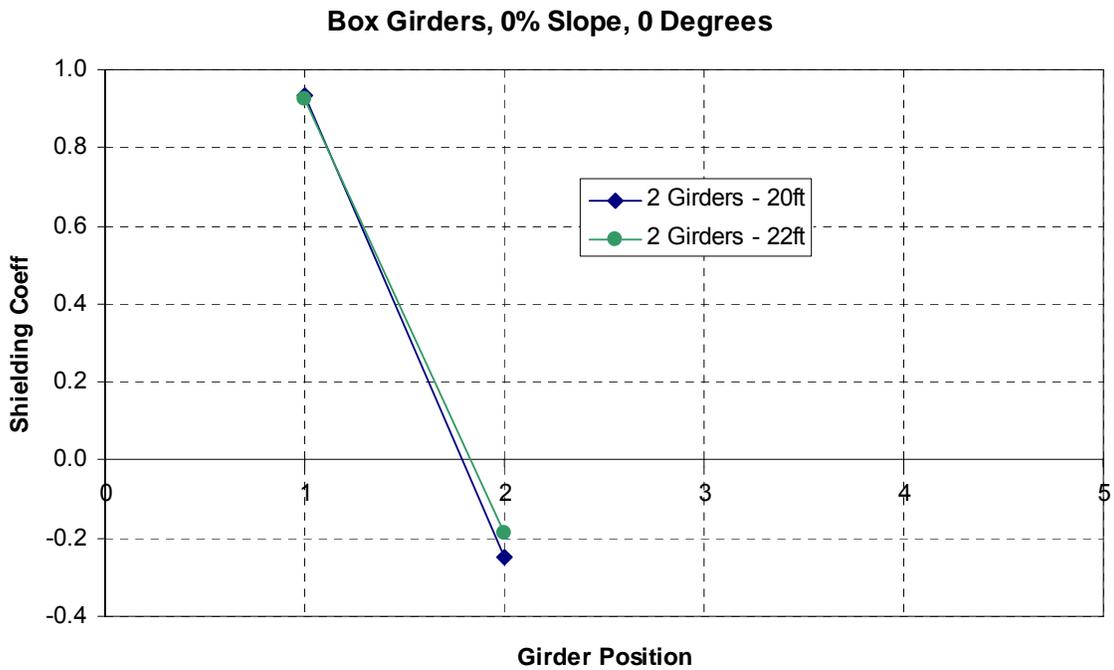
FIGURE 2.33   SHIELDING COEFFICIENTS – BOX GIRDERS, 0% SLOPE, 0 DEGREES

78" Florida I-Beams, 2% Slope, 0 degrees

FIGURE 2.34   **SHIELDING COEFFICIENTS – 78-INCH "FLORIDA" I-BEAMS, 2% SLOPE, 0 DEGREES**

45" Florida I-Beams, 2% Slope, 0 degrees

FIGURE 2.35   **SHIELDING COEFFICIENTS – 45-inch "Florida" I-BEAMS, 2% SLOPE, 0 DEGREES**
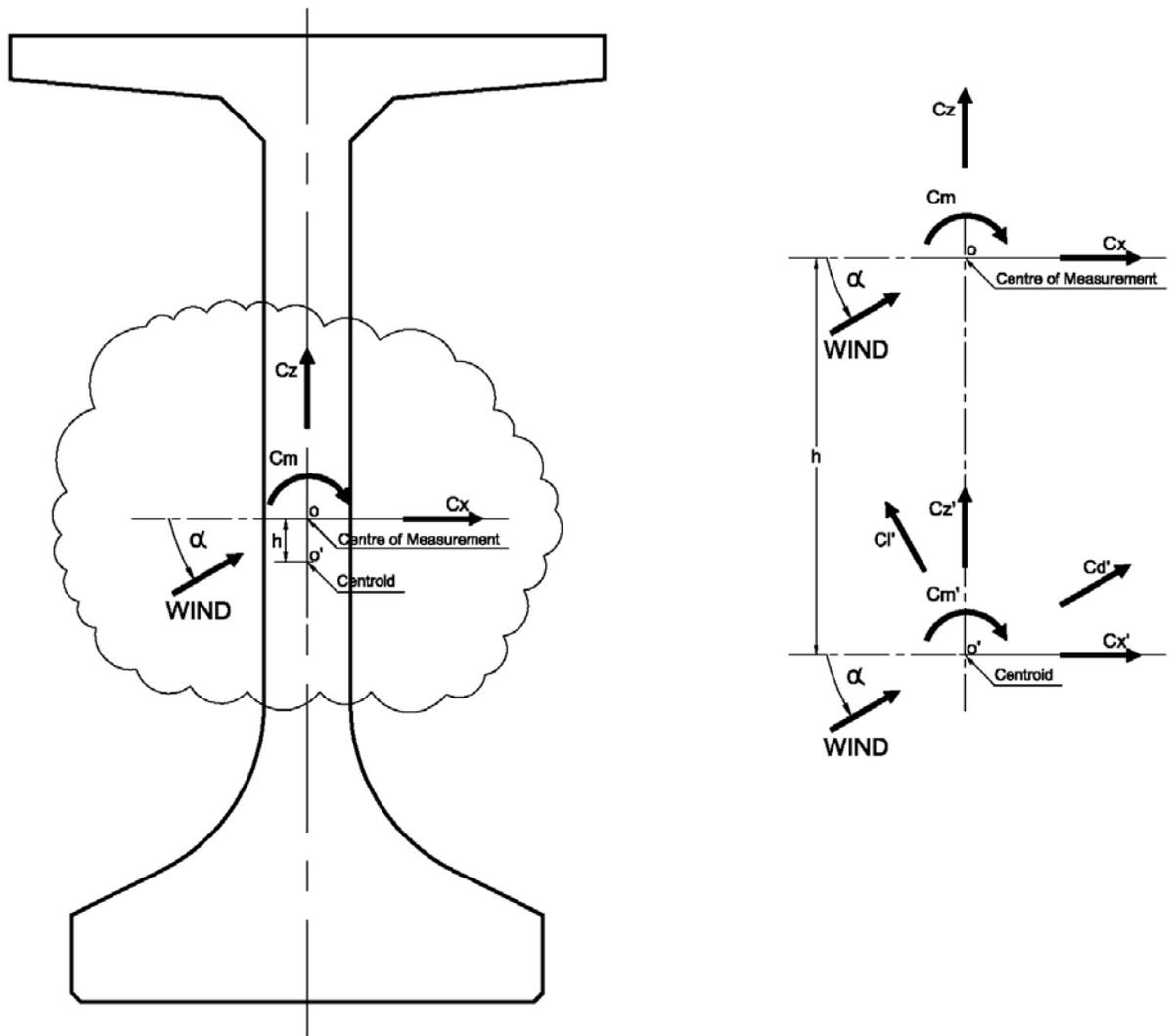
FIGURE 2.36 SIGN CONVENTION OF FORCES – CENTROID LOCATION

Alan G. Davenport Wind Engineering Group

A Study of Wind Forces on
BRIDGE GIRDERS WHILE UNDER CONSTRUCTION
Section Model Investigation

L. KONG / J.P.C. KING

303

TABLE OF CONTENTS

LIST OF TABLES

LIST OF FIGURES

ACKNOWLEDGEMENTS

SUMMARY AND MAIN FINDINGS

This report on the study of "Wind Forces on Bridge Girders While Under Construction" is an extension of the study performed for five similar types of bridge girders and reported in [1]. The five types of girders examined in the earlier study were based on bridge girder types commonly used in the State of Florida for short to medium span highway bridges. The girder types examined were comprised of: a) wide flange plate girders, b) narrow flange plate girders, c) box girders, d) 78-inch deep "Florida" I-beams and e) 45-inch deep "Florida" I-beams. The current study concerned the addition of five additional girders to three of the five types of girders examined in the earlier study. Both the previous and the current reports provide information from the section model testing of the bridge girders.

The current study concerns the static aerodynamic testing of: 1) Wide Flange Plate Girders, 2) 78-inch deep "Florida" I-Beams and 3) 4 5-inch deep "Florida" I-Beams. All girder arrangements have ten girders in a group with the instrumented girder at each of the ten available locations within the arrangement.

The aim of this study was to evaluate:

1. the static force coefficients for each girder within the configuration of ten for each of the three types of bridge girders;

2. the effects of shielding on leeward girder(s) by the windward girder(s) within the grouping of ten girders.

The section models of the bridge girders have been constructed at two geometric scales relative to the prototype dimensions in order to facilitate model construction and are as follows:

a) 1:25 scale for the wide flange plate girders;
b) 1:28 scale for the 78- and 45-inch "Florida" I-beams.

All tests were performed in smooth flow with turbulence intensities less than 0.5%. The highlights and main findings of this study are as follows:

- The drag coefficients of the 78" and 45" Florida I-beams for the instrumented girder at 1st position (i.e. windward location) at 0° angle of attack are essentially the same for each of the cross-bridge slopes examined (+2% and -2%). The 78" Florida I-beam has a drag coefficient of about 1.55, while the 45" Florida I-beam has a drag coefficient of 1.52, with the normalizing dimension based on the nominal girder height.

- The variation of the drag coefficient at 0° angle of attack between girder position changes is quite significant for the first to third interior position behind the windward girder. After this, the position change of the instrumented girder is observed to have only a small effect on the drag coefficient.

- The "shielding coefficient" indicates that shielding results primarily from the windward girder blocking the wind from fully impacting all downwind girders. The addition of more girders upwind of the subject girder does not provide significant additional shielding.

DETAILS OF THE STUDY

Project Name: Wind Forces on Bridge Girders While Under Construction.

Project Location: Florida.

Project Description: The project is an extension of a previous project performed by the Laboratory and reported in [1]. This study is a critical component of a larger project with the Florida De partment of Tran sportation (FDOT). The proper bracing of bridge gi rders for extreme win d during the con struction process is the primary focus of this study. The critical compo nent, as part of the FDOT Project, is a n accurate quantification of wind load s on the girders during construction. This inclu des the wind ward girder, as well as an estimation of the effects of shiel ding on the interi or girders, in cluding the influence of cross-slo pe on shielding. Three di fferent girder types, identical to those studied in [1], have been selected for this investigation in an arrangement as a group of ten girders with two different cross slopes.

Test Dates: Static Section Model Tests – March and May 2012

Preliminary Reporting: Static Force Coefficients – March and May 2012

Report Scope: The report is organized as follows:

Section 1 – Introduction
Section 2 – Section Model Study - Static Tests

General Reference: Discussion and details of the general methodology used by the Alan G Davenport Wind Engineering Group can be found in "Wind Tunnel Testing – A General Outline" [Reference 2].

1 INTRODUCTION

1.1 General

The wind tunnel study of "Wind Forces on Bridge Girders While Under Construction" is an extension of a previous project performed at the Boundary Layer Wind Tunnel Laboratory and reported in [1]. This study is a cri tical component of a larger project with the Florida Department of Transportation (FDOT). The proper bracing of bridge girders for extreme wind during the construction process is the primary focus of the inve stigation. As a critical component of th e FDOT Project, a prima ry focus of th e current wi nd study is to h ave an accurate quantification of wind l oads on typical types of girde rs during construction. This includes the wind ward girder, as well as an e stimation of the effects of shielding on the interio r girders, including the influen ce of cro ss-slope on shielding. Three different girder types, which are identical to those studied in [1], have been selected for further investigation, as described in Table 1.1.

All tests in this stu dy were performed on gro upings of ten gird ers with one instrumented girder sequentially placed at each po sition and nine non- instrumented dummy girde rs at th e remaining positions. The test details, includin g the test numb er, test co nditions, test se quences, location of the instrumented girder and their corresponding file names, are given in Tables 1.2 to 1.4:

   a) Wide Flange Plate Girders (Table 1.2): Comprised of 10 tests, ten girders with the instrumented girder at ten different positions from windward to the leeward position; girders spacing 14ft; cross slope 8%, test angles 0°, $\pm2.5^o$ and $\pm5^o$
   b) 78-inch "Florida" I-beam (Table 1.3): Comprised of 20 tests, ten girders with the in strumented girder at ten different pos itions from windward to the leeward pos ition; girders spaced 13ft; cross slopes $\pm2\%$; test angles 0°, $\pm2.5^o$ and $\pm5^o$
   c) 45-inch "Florida" I-beam (Table 1.4): Comprised of 20 tests, ten girders with the in strumented girder at ten different pos itions from windward to the leeward pos ition; girders spaced 13ft; cross slopes $\pm2\%$; test angles 0°, $\pm2.5^o$ and $\pm5^o$

Rigid section models of the three gi rder cross sections (7ft in length) have b een constructed at two geometric scales relative to the prototypes to facilitate model fabrication:

   a) 1:25 scale for the wide flange plate girders
   b) 1:28 scale for the 78-inch and 45-inch "Florida" I-beams

The section model study was performed at the inlet of the High Speed Section of the Boundary Layer Wind Tunnel II. Tests of the section models were per formed in smooth, uniform flow condition s to evaluate the static forces on the section.

The 7 ft long section models correspond to 175ft a nd 196ft lon g sections of the prototype s at the geometric scales of 1 to 2 5 and 1 to 28, respectively. The length of model was chose n in order that the lateral correlation effects of the wind are modeled properly and not to reflect any specific prototype girder length. Cross section details of the th ree girder types are given in Figures 1.1 to 1.3. Test configuration s including girder arrangements, test num ber designations and test conditions are given sch ematically in Figures 1.4 to 1.6.

Figure 1.7 shows a sample set-up of the section model in the wind tunnel, while Figure 1.8 presents a close-up view of the static section model test rig.

Views of the model arrangements and corresponding wind tunnel set-up are given in Figures 1.9 to 1.13 for th e Wide Flange Girders with a cro ss slope of 8%, th e 78-inch "Florida" I-beams with cross slopes of $\pm2\%$, and the 45-inch "Florida" I-beams with cross slopes of $\pm2\%$, respectively.

2 SECTION MODEL STUDY - STATIC TESTS

2.1 General

The section models were mounted on the BLWTL Bridge 3-component section model force balance, which is cap able of measuring the tot al forces on the sections (X and Z bo dy forces as well as the torque). The cente rs of measure ment of the fo rces for the wide plate girders and both the deep and shallow Florida I-beams are all at the mid-height of the sections (as opposed to the centroid of the section).

Tests were performed adjusting the model inclination relative to the mean wind flow. The apparatus which rotates the test model also rotates the "dummy" model(s) situated either upwind or downwind of the instrumented model girder. Lift and Drag were calculated from the mea sured X an d Z body force components. The sign conventions for the definition of the force coeffici ents for each of the three girder types are given in Figures 2.1 to 2.3 respectively.

A typical force coefficient is defined as follows:

$$C_{x,z,l,d} = \frac{F_{x,z,l,d}}{qD} \qquad (2.1)$$

in which: C is an aerodynamic coefficient,
F is the mean aerodynamic force per unit length,
$q = \frac{1}{2}\rho V^2$ is the mean wind velocity pressure,
ρ is the density of air (taken as 0.00238 slug/ft^3),
V is the mean wind velocity in ft/s, and
D is the overall depth of the section, see Table 2.1.

The subscripts x,z,l,d refer to the X an d Z body force components and lift and drag respectively. It is important to note that C_x, C_z and C_m are "Body-Force Co efficients" and not aligned with the axis of the wind (i.e as a "drag" coefficient) nor perpendicular to the wind (i.e. as a "lift" coefficient).

The torque coefficient is defined:

$$C_m = \frac{F_t}{qD^2} \qquad (2.2)$$

in which: F_t is the mean aerodynamic torque per unit length.

All tests were carried out for the section models in smooth flow (I_u< 0.5%) for angles of mean vertical inclination between -5 to +5 degrees, in increments of 2.5 degrees.

2.2 Test Results

The static a erodynamic coefficients from the te sts of the section model s are summ arized in the following tables:

1) Table 2.2 for the Wide Flange Girders with a cross slope of +8%;

2) Table 2.3 for the 78-inch "Florida" I-beams with a cross slope of +2%;

3) Table 2.4 for the 78-inch "Florida" I-beams with a cross slope of -2%;

4) Table 2.5 for the 45-inch "Florida" I-beams with a cross slope of +2%: and

5) Table 2.6 for the 45-inch "Florida" I-beams with a cross slope of -2%.

The corresponding summary curves of force coefficient vs. angle of attack are shown in the following figures:

1) Figures 2.4 and 2.5 for the Wide Flange Girders;

2) Figures 2.6 and 2.7 for the 78-inch "Florida" I-beams with a cross slope of +2%;

3) Figures 2.8 and 2.9 for the 78-inch "Florida" I-beams with a cross slope of -2%;

4) Figures 2.10 and 2.11 for the 45-inch "Florida" I-beams with a cross slope of +2%; and

5) Figures 2.12 and 2.13 for the 45-inch "Florida" I-beams with a cross slope of -2%.

Note that the force coefficients are normalized by section depth in order to facilitate comparisons with published results of similar girder cross sections.

The wind tunnel test wind speeds and corresponding Reynolds numbers for the three girder types tested are summarized in Table 2.7. Reynolds number is calculated based upon the test wind speed at girder height and the girder model section depth.

A simplified "Shielding Coefficient" is defined for the 0° tests in order to present some general conclusions regarding multiple girder arrangements. The drag coefficients obtained from the current study of ten girder arrangements at 0 degrees are normalized by the drag coefficient for the single, isolated girder at 0 degrees (obtained in the earlier study and reported in [1]) as follows:

$$C_s = \frac{C_{dn}}{C_{d1}}$$
(2.3)

where: C_s = Shielding Coefficient

C_{dn} = Drag Coefficient for girder number "n" of the ten girders arrangements

C_{d1} = Drag Coefficient for the isolated girder from [1]

The results are plotted relative to girder position. Figure 2.14 presents the effective shielding coefficients for the Wide Flange Girders with a cross-slope of 8%. The shielding coefficients for the 78-inch "Florida" I-beams with cross slopes of ±2% and the 45-inch "Florida" I-beams with cross slopes of ±2% are given in Figures 2.15 to 2.18 respectively. Results from previous tests [1] are also plotted in the figures for the same girder spacing and slope for comparative purposes.

A summary of the main results of the current section model tests are as follows:

- The drag coefficients for the 78" and 45" Florida I-beams for the instrumented girder at 1st position (i.e. windward position) at 0° angle of attack are essentially the same with slopes at +2% and -2%. The 78" Florida I-beam has a drag coefficient of about 1.55, while the 45" Florida I-beam has a drag coefficient of 1.52.

- It is noted that there is significant variation of the drag coefficient at 0° angle of attack for girder position within the 10-girder arrangement for the instrumented girder in the 2nd to 4th position. Minimal variation was observed in the drag coefficients for the instrumented girder in the 5th to the 10th position.

- As discussed in [1], the "shielding coefficient" as defined in Equation (2.3) indicates that shielding results primarily from the windward girder blocking the wind from fully impacting all downwind

girders. The addition of additional girders upwind of the subject girder does not provide significant additional shielding.

- Since all sections tested have sharp edged corners, it is expected that the effects of Reynolds number on the force coefficients are minimal. The "Reynolds number" is the ratio of the inertial force to viscous force of the fluid (i.e. air) and is computed as $Re = VD/\gamma$, where V is the mean wind speed in ft/s, D is the overall section depth in ft as given in Table 2.1 and γ is the kinematic viscosity of air (1.615×10^{-4} ft^2/s). The test wind speeds and corresponding Reynolds numbers are listed in Table 2.7.

2.3   Translation of Force Coefficients to the Section Centroid

The static force coefficients given in Section 2.2, which are referenced to the mid-height of the sections for the Florida I-beams, can be transformed to their centroid locations through a simple transformation of coordinates.

Figure 2.19 shows an example of the sign convention used in the transformation. Note that o is the mid-height location of the section and o' is the centroid. Assuming h is the distance between the mid-height and the centroid of the section, the body force coefficients to the centroid can be obtained as:

$$C'_X = C_X$$

$$C'_Z = C_Z \tag{2.4}$$

$$C'_m = C_m + C_X \times \frac{h}{D}$$

The drag and lift coefficients relative to the centroid of the section are calculated as:

$$C'_D = C'_X \cos\alpha + C'_Z \sin\alpha$$

$$C'_L = -C'_X \sin\alpha + C'_Z \cos\alpha \tag{2.5}$$

REFERENCES

1. Kong, L. and King, J.P.C., "A Study of Wind Forces on Bridge Girders While Under Construction – Section Model Investig ation", The University of Weste rn Ontario, Faculty of Engineerin g Research Report, BLWT-SS29-2011, London, Ontario, Canada 2011.

2. "Wind Tunnel Testing: A General Outline", The Boundary Laye r Wind Tun nel Laboratory, The University of Western Ontario, May 2007.

TABLE 1.1   SUMMARY OF STATIC SECTION MODEL TESTS

GIRDER TYPE AND CONFIGURATION		Spacing between Girders	Instrumented Girder Position	Cross-Slope	No. of Tests	Test Angles
A) Wide Flange Plate Girder	Ten Girders	14 ft	1,2,3,4,5, 6,7,8,9,10	8%	10	$0^o, \pm2.5^o, \pm5^o$
B) 78 in "Florida" I-Beam	Ten Girders	13 ft	1,2,3,4,5, 6,7,8,9,10	2%	10	$0^o, \pm2.5^o, \pm5^o$
C) 78in "Florida" I-Beam	Ten Girders	13 ft	1,2,3,4,5, 6,7,8,9,10	-2%	10	$0^o, \pm2.5^o, \pm5^o$
D) 45in "Florida" I-Beam	Ten Girders	13 ft	1,2,3,4,5, 6,7,8,9,10	2%	10	$0^o, \pm2.5^o, \pm5^o$
E) 45in "Florida" I-Beam	Ten Girders	13 ft	1,2,3,4,5, 6,7,8,9,10	-2%	10	$0^o, \pm2.5^o, \pm5^o$

TABLE 1.2   WIDE FLANGE PLATE GIRDERS – TEST DETAILS AND CONDITIONS

A) WIDE FLANGE PLATE GIRDER		Spacing between Girders	Girder Tested	Cross-Slope	Test Sequence	File Name
Angles：0°, ±2.5°, ±5°: Smooth Flow, 1:25 Scale						
W9	Ten Girders	14 ft	10	8%	1	F051W9E01R001
W8	Ten Girders	14 ft	9	8%	2	F051W8E01R001
W7	Ten Girders	14 ft	8	8%	3	F051W7E01R001
W6	Ten Girders	14 ft	7	8%	4	F051W6E01R001
W5	Ten Girders	14 ft	6	8%	5	F051W5E01R001
W4	Ten Girders	14 ft	5	8%	6	F051W4E01R001
W3	Ten Girders	14 ft	4	8%	7	F051W3E01R001
W2	Ten Girders	14 ft	3	8%	8	F051W2E01R001
W1	Ten Girders	14 ft	2	8%	9	F051W1E01R001
W0	Ten Girders	14 ft	1	8%	10	F051W0E01R001

TABLE 1.3   78-INCH "FLORIDA" I-BEAM – TEST DETAILS AND CONDITIONS

B) and C) 78-INCH "FLORIDA" I-BEAM	Spacing between Girders	Girder Tested	Cross-Slope	Test Sequence	File Name
Angles：0°, ±2.5°, ±5°: Smooth Flow, 1:28 Scale					
D9	Ten Girders	10	2%	11	F051D9E01R001
D8	Ten Girders	9	2%	12	F051D8E01R001
D7	Ten Girders	8	2%	13	F051D7E01R001
D6	Ten Girders	7	2%	14	F051D6E01R001
D5	Ten Girders	6	2%	15	F051D5E01R001
D4	Ten Girders	5	2%	16	F051D4E01R001
D3	Ten Girders	4	2%	17	F051D3E01R001
D2	Ten Girders	3	2%	18	F051D2E01R001
D1	Ten Girders	2	2%	19	F051D1E01R001
D0	Ten Girders	1	2%	20	F051D0E01R001
T9	Ten Girders	10	-2%	21	F051T9E01R001
T8	Ten Girders	9	-2%	22	F051T8E01R001
T7	Ten Girders	8	-2%	23	F051T7E01R001
T6	Ten Girders	7	-2%	24	F051T6E01R001
T5	Ten Girders	6	-2%	25	F051T5E01R001
T4	Ten Girders	5	-2%	26	F051T4E01R001
T3	Ten Girders	4	-2%	27	F051T3E01R001
T2	Ten Girders	3	-2%	28	F051T2E01R001
T1	Ten Girders	2	-2%	29	F051T1E01R001
T0	Ten Girders	1	-2%	30	F051T0E01R001

TABLE 1.4   45-INCH "FLORIDA" I-BEAM – TEST DETAILS AND CONDITIONS

D) and E) 45-INCH "FLORIDA" I-BEAM		Spacing between Girders	Girder Tested	Cross-Slope	Test Sequence	File Name
Angles：0°, ±2.5°, ±5°: Smooth Flow, 1:28 Scale						
S9	Ten Girders	13 ft	10	2%	31	F051S9E01R001
S8	Ten Girders	13 ft	9	2%	32	F051S8E01R001
S7	Ten Girders	13 ft	8	2%	33	F051S7E01R001
S6	Ten Girders	13 ft	7	2%	34	F051S6E01R001
S5	Ten Girders	13 ft	6	2%	35	F051S5E01R001
S4	Ten Girders	13 ft	5	2%	36	F051S4E01R001
S3	Ten Girders	13 ft	4	2%	37	F051S3E01R001
S2	Ten Girders	13 ft	3	2%	38	F051S2E01R001
S1	Ten Girders	13 ft	2	2%	39	F051S1E01R001
S0	Ten Girders	13 ft	1	2%	40	F051S0E01R001
L9	Ten Girders	13 ft	10	-2%	41	F051L9E01R001
L8	Ten Girders	13 ft	9	-2%	42	F051L8E01R001
L7	Ten Girders	13 ft	8	-2%	43	F051L7E01R001
L6	Ten Girders	13 ft	7	-2%	44	F051L6E01R001
L5	Ten Girders	13 ft	6	-2%	45	F051L5E01R001
L4	Ten Girders	13 ft	5	-2%	46	F051L4E01R001
L3	Ten Girders	13 ft	4	-2%	47	F051L3E01R001
L2	Ten Girders	13 ft	3	-2%	48	F051L2E01R001
L1	Ten Girders	13 ft	2	-2%	49	F051L1E01R001
L0	Ten Girders	13 ft	1	-2%	50	F051L0E01R001

TABLE 2.1   OVERALL DEPTHS OF PROTOTYPE GIRDERS

PROTOTYPE CONFIGURATION	PROTOTYPE OVERALL DEPTH* (ft)	MODEL SCALE
A) Wide Flange Plate Girder	8.167	1:25
B) and C) 78-inch "Florida" I-Beam	6.5	1:28
D) and E) 45-inch "Florida" I-Beam	3.75	1:28

* Note the overall depth was used for normalizing to obtain the force coefficients.

TABLE 2.2 STATIC FORCE COEFFICIENTS - WIDE FLANGE PLATE GIRDER, 14FT SPACING, 8% CROSS SLOPE, SMOOTH FLOW

		Angle of Attack (deg)	-5	-2.5	0	2.5	5
W9	Wide, 8% slope, 10 girders, 14ft spacing, 10th (leeward)	Cx (X Body Force)	1.23	1.00	0.70	0.56	0.52
		Cz (Z Body Force)	-0.02	-0.03	-0.04	-0.02	0.03
		Ct (Torque)	-0.03	-0.03	-0.01	-0.01	-0.01
		Cd (Drag)	1.23	1.00	0.70	0.56	0.52
		Cl (Lift)	0.09	0.01	-0.04	-0.04	-0.02
W8	Wide, 8% slope, 10 girders, 14ft spacing, 9th	Cx (X Body Force)	1.31	0.96	0.60	0.47	0.44
		Cz (Z Body Force)	0.01	0.02	0.02	0.00	0.02
		Ct (Torque)	-0.02	-0.02	-0.01	0.00	-0.01
		Cd (Drag)	1.30	0.95	0.60	0.47	0.44
		Cl (Lift)	0.13	0.07	0.02	-0.02	-0.02
W7	Wide, 8% slope, 10 girders, 14ft spacing, 8th	Cx (X Body Force)	1.15	0.80	0.53	0.44	0.42
		Cz (Z Body Force)	0.04	0.05	0.03	0.00	0.02
		Ct (Torque)	-0.02	-0.01	0.00	0.00	-0.01
		Cd (Drag)	1.14	0.80	0.53	0.44	0.42
		Cl (Lift)	0.14	0.08	0.03	-0.02	-0.02
W6	Wide, 8% slope, 10 girders, 14ft spacing, 7th	Cx (X Body Force)	0.99	0.63	0.42	0.38	0.38
		Cz (Z Body Force)	0.06	0.05	0.02	0.00	0.03
		Ct (Torque)	-0.02	-0.01	-0.01	0.00	-0.01
		Cd (Drag)	0.98	0.63	0.42	0.38	0.38
		Cl (Lift)	0.14	0.08	0.02	-0.02	-0.01
W5	Wide, 8% slope, 10 girders, 14ft spacing, 6th	Cx (X Body Force)	0.75	0.49	0.38	0.37	0.38
		Cz (Z Body Force)	0.06	0.05	0.02	0.00	0.03
		Ct (Torque)	-0.02	-0.01	-0.01	-0.01	-0.01
		Cd (Drag)	0.74	0.49	0.38	0.37	0.38
		Cl (Lift)	0.13	0.07	0.02	-0.02	-0.01
W4	Wide, 8% slope, 10 girders, 14ft spacing, 5th	Cx (X Body Force)	0.51	0.35	0.34	0.34	0.34
		Cz (Z Body Force)	0.04	0.02	0.01	0.00	0.03
		Ct (Torque)	-0.01	0.00	0.00	0.00	-0.01
		Cd (Drag)	0.50	0.34	0.34	0.34	0.34
		Cl (Lift)	0.08	0.04	0.01	-0.02	0.00
W3	Wide, 8% slope, 10 girders, 14ft spacing, 4th	Cx (X Body Force)	0.15	0.04	0.05	0.04	0.04
		Cz (Z Body Force)	-0.01	-0.03	-0.03	-0.02	0.04
		Ct (Torque)	0.00	0.01	0.00	0.00	-0.01
		Cd (Drag)	0.15	0.04	0.05	0.04	0.04
		Cl (Lift)	0.00	-0.03	-0.03	-0.02	0.03
W2	Wide, 8% slope, 10 girders, 14ft spacing, 3rd	Cx (X Body Force)	-0.16	-0.25	-0.34	-0.43	-0.42
		Cz (Z Body Force)	-0.05	-0.06	-0.06	-0.03	0.04
		Ct (Torque)	0.00	0.01	0.00	0.01	0.01
		Cd (Drag)	-0.15	-0.25	-0.34	-0.43	-0.41
		Cl (Lift)	-0.06	-0.07	-0.06	-0.01	0.07
W1	Wide, 8% slope, 10 girders, 14ft spacing, 2nd	Cx (X Body Force)	-0.13	-0.15	-0.15	-0.13	-0.12
		Cz (Z Body Force)	-0.02	-0.02	-0.01	0.00	0.00
		Ct (Torque)	0.00	0.00	0.00	0.00	0.00
		Cd (Drag)	-0.13	-0.15	-0.15	-0.13	-0.12
		Cl (Lift)	-0.03	-0.03	-0.01	0.00	0.01
W0	Wide, 8% slope, 10 girders, 14ft spacing, 1st (windward)	Cx (X Body Force)	1.54	1.65	1.77	1.80	1.79
		Cz (Z Body Force)	0.00	-0.01	-0.02	-0.06	-0.10
		Ct (Torque)	0.00	0.00	0.00	0.01	0.01
		Cd (Drag)	1.53	1.65	1.77	1.80	1.77
		Cl (Lift)	0.13	0.06	-0.02	-0.13	-0.25

TABLE 2.3 STATIC FORCE COEFFICIENTS - 78-INCH "FLORIDA" I-BEAMS, 13FT SPACING, 2% CROSS SLOPE, SMOOTH FLOW

		Angle of Attack (deg)	-5	-2.5	0	2.5	5
D9	78" Florida girders, +2% slope, 10 girders, 13ft spacing, 10th	Cx (X Body Force)	0.75	0.46	0.35	0.31	0.58
		Cz (Z Body Force)	-0.11	-0.09	0.00	0.12	0.22
		Ct (Torque)	-0.04	-0.03	-0.01	0.00	0.00
		Cd (Drag)	0.76	0.46	0.35	0.31	0.60
		Cl (Lift)	-0.05	-0.07	0.00	0.11	0.17
D8	78" Florida girders, +2% slope, 10 girders, 13ft spacing, 9th	Cx (X Body Force)	0.74	0.40	0.31	0.27	0.57
		Cz (Z Body Force)	-0.04	-0.03	0.02	0.09	0.11
		Ct (Torque)	-0.03	-0.02	-0.01	0.00	-0.01
		Cd (Drag)	0.74	0.40	0.31	0.28	0.58
		Cl (Lift)	0.02	-0.01	0.02	0.07	0.06
D7	78" Florida girders, +2% slope, 10 girders, 13ft spacing, 8th	Cx (X Body Force)	0.63	0.35	0.29	0.26	0.47
		Cz (Z Body Force)	0.00	-0.01	0.02	0.08	0.07
		Ct (Torque)	-0.03	-0.02	-0.01	-0.01	-0.01
		Cd (Drag)	0.63	0.35	0.29	0.26	0.47
		Cl (Lift)	0.05	0.00	0.02	0.07	0.02
D6	78" Florida girders, +2% slope, 10 girders, 13ft spacing, 7th	Cx (X Body Force)	0.55	0.33	0.29	0.26	0.36
		Cz (Z Body Force)	0.02	-0.01	0.02	0.08	0.06
		Ct (Torque)	-0.02	-0.02	-0.01	-0.01	-0.01
		Cd (Drag)	0.54	0.33	0.29	0.26	0.37
		Cl (Lift)	0.07	0.01	0.02	0.06	0.03
D5	78" Florida girders, +2% slope, 10 girders, 13ft spacing, 6th	Cx (X Body Force)	0.45	0.31	0.28	0.27	0.31
		Cz (Z Body Force)	0.02	0.00	0.02	0.07	0.06
		Ct (Torque)	-0.02	-0.02	-0.01	0.00	-0.01
		Cd (Drag)	0.45	0.31	0.28	0.27	0.31
		Cl (Lift)	0.06	0.01	0.02	0.06	0.03
D4	78" Florida girders, +2% slope, 10 girders, 13ft spacing, 5th	Cx (X Body Force)	0.39	0.27	0.26	0.35	0.33
		Cz (Z Body Force)	0.01	-0.02	0.02	0.04	0.05
		Ct (Torque)	-0.01	-0.01	-0.01	-0.01	-0.01
		Cd (Drag)	0.39	0.27	0.26	0.35	0.33
		Cl (Lift)	0.05	0.00	0.02	0.03	0.02
D3	78" Florida girders, +2% slope, 10 girders, 13ft spacing, 4th	Cx (X Body Force)	0.18	0.10	0.04	0.05	0.07
		Cz (Z Body Force)	-0.05	-0.06	-0.01	0.07	0.09
		Ct (Torque)	0.00	0.00	0.00	-0.01	-0.01
		Cd (Drag)	0.18	0.11	0.04	0.06	0.07
		Cl (Lift)	-0.03	-0.06	-0.01	0.07	0.08
D2	78" Florida girders, +2% slope, 10 girders, 13ft spacing, 3rd	Cx (X Body Force)	-0.14	-0.27	-0.23	-0.26	-0.25
		Cz (Z Body Force)	-0.07	-0.10	-0.02	0.09	0.09
		Ct (Torque)	0.01	0.01	0.01	-0.02	-0.01
		Cd (Drag)	-0.13	-0.26	-0.23	-0.25	-0.24
		Cl (Lift)	-0.09	-0.11	-0.02	0.10	0.11
D1	78" Florida girders, +2% slope, 10 girders, 13ft spacing, 2nd	Cx (X Body Force)	-0.19	-0.20	-0.19	-0.17	-0.16
		Cz (Z Body Force)	-0.03	-0.03	0.00	0.02	0.03
		Ct (Torque)	0.00	0.00	0.00	0.00	0.01
		Cd (Drag)	-0.18	-0.20	-0.19	-0.17	-0.16
		Cl (Lift)	-0.05	-0.04	0.00	0.03	0.04
D0	78" Florida girders, +2% slope, 10 girders, 13ft spacing, 1st	Cx (X Body Force)	1.41	1.52	1.57	1.56	1.48
		Cz (Z Body Force)	0.16	0.15	0.10	0.05	0.02
		Ct (Torque)	-0.02	-0.02	-0.01	-0.01	0.00
		Cd (Drag)	1.39	1.51	1.57	1.56	1.47
		Cl (Lift)	0.28	0.21	0.10	-0.02	-0.11

TABLE 2.4 STATIC FORCE COEFFICIENTS- 78-INCH "FLORIDA" I-BEAMS, -13FT SPACING, -2% CROSS SLOPE, SMOOTH FLOW

		Angle of Attack (deg)	-5	-2.5	0	2.5	5
T9	78" Florida girders, -2% slope, 10 girders, 13ft spacing, 10th	Cx (X Body Force)	0.42	0.32	0.33	0.60	0.94
		Cz (Z Body Force)	-0.16	-0.05	0.08	0.16	0.15
		Ct (Torque)	-0.02	-0.01	0.00	0.01	0.02
		Cd (Drag)	0.43	0.32	0.33	0.60	0.95
		Cl (Lift)	-0.12	-0.03	0.08	0.14	0.07
T8	78" Florida girders, -2% slope, 10 girders, 13ft spacing, 9th	Cx (X Body Force)	0.36	0.29	0.30	0.57	1.02
		Cz (Z Body Force)	-0.09	-0.02	0.05	0.04	0.06
		Ct (Torque)	-0.01	0.00	0.00	0.00	0.01
		Cd (Drag)	0.37	0.29	0.30	0.58	1.02
		Cl (Lift)	-0.06	-0.01	0.05	0.01	-0.02
T7	78" Florida girders, -2% slope, 10 girders, 13ft spacing, 8th	Cx (X Body Force)	0.32	0.27	0.28	0.47	0.89
		Cz (Z Body Force)	-0.07	-0.02	0.05	0.01	0.02
		Ct (Torque)	-0.01	0.00	0.00	0.00	0.01
		Cd (Drag)	0.32	0.27	0.28	0.47	0.89
		Cl (Lift)	-0.04	0.00	0.05	-0.01	-0.06
T6	78" Florida girders, -2% slope, 10 girders, 13ft spacing, 7th	Cx (X Body Force)	0.29	0.27	0.28	0.38	0.68
		Cz (Z Body Force)	-0.06	-0.01	0.05	0.02	-0.01
		Ct (Torque)	-0.01	-0.01	0.00	0.00	0.01
		Cd (Drag)	0.29	0.27	0.28	0.38	0.68
		Cl (Lift)	-0.04	0.00	0.05	0.00	-0.07
T5	78" Florida girders, -2% slope, 10 girders, 13ft spacing, 6th	Cx (X Body Force)	0.32	0.31	0.33	0.37	0.53
		Cz (Z Body Force)	-0.03	0.01	0.04	0.02	0.00
		Ct (Torque)	0.00	0.00	0.00	0.00	0.00
		Cd (Drag)	0.32	0.31	0.33	0.37	0.53
		Cl (Lift)	0.00	0.02	0.04	0.01	-0.05
T4	78" Florida girders, -2% slope, 10 girders, 13ft spacing, 5th	Cx (X Body Force)	0.28	0.27	0.30	0.36	0.41
		Cz (Z Body Force)	-0.05	-0.01	0.04	0.01	0.01
		Ct (Torque)	-0.01	0.00	-0.01	-0.01	0.00
		Cd (Drag)	0.28	0.27	0.30	0.36	0.41
		Cl (Lift)	-0.03	0.01	0.04	0.00	-0.03
T3	78" Florida girders, -2% slope, 10 girders, 13ft spacing, 4th	Cx (X Body Force)	0.13	0.05	0.05	0.07	0.13
		Cz (Z Body Force)	-0.09	-0.04	0.05	0.07	0.04
		Ct (Torque)	0.00	0.00	-0.01	-0.01	-0.01
		Cd (Drag)	0.14	0.06	0.05	0.07	0.14
		Cl (Lift)	-0.08	-0.03	0.05	0.07	0.03
T2	78" Florida girders, -2% slope, 10 girders, 13ft spacing, 3rd	Cx (X Body Force)	-0.24	-0.36	-0.38	-0.28	-0.16
		Cz (Z Body Force)	-0.11	-0.05	0.06	0.09	0.08
		Ct (Torque)	0.01	0.01	-0.01	-0.01	-0.01
		Cd (Drag)	-0.23	-0.36	-0.38	-0.27	-0.15
		Cl (Lift)	-0.13	-0.06	0.06	0.10	0.09
T1	78" Florida girders, -2% slope, 10 girders, 13ft spacing, 2nd	Cx (X Body Force)	-0.21	-0.20	-0.18	-0.17	-0.15
		Cz (Z Body Force)	-0.02	0.00	0.03	0.04	0.04
		Ct (Torque)	0.00	0.00	0.01	0.01	0.00
		Cd (Drag)	-0.20	-0.20	-0.18	-0.16	-0.15
		Cl (Lift)	-0.04	0.00	0.03	0.05	0.05
T0	78" Florida girders, -2% slope, 10 girders, 13ft spacing, 1st	Cx (X Body Force)	1.52	1.57	1.55	1.46	1.37
		Cz (Z Body Force)	0.14	0.09	0.04	0.01	-0.01
		Ct (Torque)	-0.02	-0.02	-0.01	0.00	0.00
		Cd (Drag)	1.51	1.57	1.55	1.46	1.36
		Cl (Lift)	0.27	0.16	0.04	-0.06	-0.13

TABLE 2.5   STATIC FORCE COEFFICIENTS- 45-INCH "FLORIDA" I-BEAMS, 13FT SPACING, 2% CROSS SLOPE, SMOOTH FLOW

		Angle of Attack (deg)	-5	-2.5	0	2.5	5
S9	45" Florida girders, +2% slope, 10 girders, 13ft spacing, 10th	Cx (X Body Force)	0.67	0.41	0.32	0.33	0.52
		Cz (Z Body Force)	-0.11	-0.09	0.01	0.16	0.28
		Ct (Torque)	0.15	0.08	0.05	0.03	0.03
		Cd (Drag)	0.68	0.42	0.32	0.33	0.54
		Cl (Lift)	-0.05	-0.07	0.01	0.14	0.23
S8	45" Florida girders, +2% slope, 10 girders, 13ft spacing, 9th	Cx (X Body Force)	0.57	0.36	0.28	0.29	0.45
		Cz (Z Body Force)	-0.08	-0.06	0.02	0.14	0.22
		Ct (Torque)	0.13	0.07	0.03	0.03	0.03
		Cd (Drag)	0.58	0.36	0.28	0.30	0.47
		Cl (Lift)	-0.03	-0.04	0.02	0.12	0.18
S7	45" Florida girders, +2% slope, 10 girders, 13ft spacing, 8th	Cx (X Body Force)	0.51	0.33	0.26	0.28	0.38
		Cz (Z Body Force)	-0.07	-0.04	0.02	0.12	0.18
		Ct (Torque)	0.12	0.07	0.04	0.04	0.04
		Cd (Drag)	0.52	0.33	0.26	0.28	0.40
		Cl (Lift)	-0.02	-0.03	0.02	0.11	0.14
S6	45" Florida girders, +2% slope, 10 girders, 13ft spacing, 7th	Cx (X Body Force)	0.46	0.31	0.26	0.27	0.34
		Cz (Z Body Force)	-0.06	-0.04	0.01	0.11	0.17
		Ct (Torque)	0.10	0.06	0.04	0.03	0.03
		Cd (Drag)	0.46	0.31	0.26	0.27	0.35
		Cl (Lift)	-0.02	-0.03	0.01	0.10	0.14
S5	45" Florida girders, +2% slope, 10 girders, 13ft spacing, 6th	Cx (X Body Force)	0.44	0.33	0.29	0.27	0.34
		Cz (Z Body Force)	-0.05	-0.04	0.02	0.11	0.17
		Ct (Torque)	0.09	0.06	0.04	0.03	0.04
		Cd (Drag)	0.45	0.33	0.29	0.28	0.35
		Cl (Lift)	-0.01	-0.02	0.02	0.09	0.14
S4	45" Florida girders, +2% slope, 10 girders, 13ft spacing, 5th	Cx (X Body Force)	0.44	0.36	0.35	0.32	0.36
		Cz (Z Body Force)	-0.06	-0.03	0.04	0.10	0.16
		Ct (Torque)	0.09	0.06	0.05	0.04	0.05
		Cd (Drag)	0.44	0.36	0.35	0.32	0.37
		Cl (Lift)	-0.02	-0.01	0.04	0.08	0.13
S3	45" Florida girders, +2% slope, 10 girders, 13ft spacing, 4th	Cx (X Body Force)	0.55	0.52	0.47	0.44	0.46
		Cz (Z Body Force)	0.04	0.11	0.09	0.09	0.13
		Ct (Torque)	0.11	0.08	0.06	0.05	0.06
		Cd (Drag)	0.54	0.51	0.47	0.44	0.47
		Cl (Lift)	0.08	0.13	0.09	0.07	0.09
S2	45" Florida girders, +2% slope, 10 girders, 13ft spacing, 3rd	Cx (X Body Force)	0.48	0.63	0.72	0.69	0.61
		Cz (Z Body Force)	-0.03	0.15	0.18	0.08	0.06
		Ct (Torque)	0.05	0.11	0.12	0.07	0.06
		Cd (Drag)	0.48	0.63	0.72	0.69	0.62
		Cl (Lift)	0.01	0.17	0.18	0.05	0.00
S1	45" Florida girders, +2% slope, 10 girders, 13ft spacing, 2nd	Cx (X Body Force)	-0.22	-0.38	-0.48	-0.49	-0.38
		Cz (Z Body Force)	-0.29	-0.28	-0.12	0.11	0.22
		Ct (Torque)	-0.10	-0.05	-0.04	-0.01	-0.01
		Cd (Drag)	-0.19	-0.36	-0.48	-0.49	-0.36
		Cl (Lift)	-0.31	-0.30	-0.12	0.13	0.25
S0	45" Florida girders, +2% slope, 10 girders, 13ft spacing, 1st	Cx (X Body Force)	1.38	1.49	1.52	1.51	1.38
		Cz (Z Body Force)	0.26	0.23	0.18	0.12	0.08
		Ct (Torque)	0.13	0.13	0.11	0.11	0.09
		Cd (Drag)	1.35	1.48	1.52	1.51	1.39
		Cl (Lift)	0.38	0.30	0.18	0.06	-0.05

TABLE 2.6   STATIC FORCE COEFFICIENTS- 45-INCH "FLORIDA" I-BEAMS, 13FT SPACING, -2% CROSS SLOPE, SMOOTH FLOW

		Angle of Attack (deg)	-5	-2.5	0	2.5	5
L9	45" Florida girders, -2% slope, 10 girders, 13ft spacing, 10th	Cx (X Body Force)	0.43	0.31	0.30	0.49	0.89
		Cz (Z Body Force)	-0.18	-0.07	0.09	0.22	0.24
		Ct (Torque)	0.08	0.04	0.02	0.02	0.02
		Cd (Drag)	0.45	0.31	0.30	0.50	0.91
		Cl (Lift)	-0.14	-0.05	0.09	0.19	0.16
L8	45" Florida girders, -2% slope, 10 girders, 13ft spacing, 9th	Cx (X Body Force)	0.39	0.28	0.28	0.39	0.74
		Cz (Z Body Force)	-0.15	-0.05	0.08	0.15	0.17
		Ct (Torque)	0.07	0.03	0.02	0.03	0.02
		Cd (Drag)	0.40	0.28	0.28	0.40	0.75
		Cl (Lift)	-0.11	-0.04	0.08	0.14	0.10
L7	45" Florida girders, -2% slope, 10 girders, 13ft spacing, 8th	Cx (X Body Force)	0.35	0.27	0.27	0.37	0.72
		Cz (Z Body Force)	-0.14	-0.04	0.08	0.14	0.16
		Ct (Torque)	0.06	0.03	0.03	0.02	0.02
		Cd (Drag)	0.36	0.27	0.27	0.37	0.73
		Cl (Lift)	-0.11	-0.03	0.08	0.12	0.09
L6	45" Florida girders, -2% slope, 10 girders, 13ft spacing, 7th	Cx (X Body Force)	0.33	0.27	0.27	0.33	0.58
		Cz (Z Body Force)	-0.12	-0.04	0.07	0.13	0.13
		Ct (Torque)	0.06	0.04	0.03	0.02	0.02
		Cd (Drag)	0.34	0.27	0.27	0.34	0.59
		Cl (Lift)	-0.09	-0.03	0.07	0.12	0.08
L5	45" Florida girders, -2% slope, 10 girders, 13ft spacing, 6th	Cx (X Body Force)	0.34	0.28	0.27	0.32	0.48
		Cz (Z Body Force)	-0.11	-0.03	0.06	0.13	0.13
		Ct (Torque)	0.05	0.03	0.02	0.02	0.02
		Cd (Drag)	0.35	0.28	0.27	0.33	0.49
		Cl (Lift)	-0.08	-0.02	0.06	0.11	0.09
L4	45" Florida girders, -2% slope, 10 girders, 13ft spacing, 5th	Cx (X Body Force)	0.38	0.35	0.32	0.34	0.50
		Cz (Z Body Force)	-0.10	-0.02	0.06	0.13	0.13
		Ct (Torque)	0.06	0.04	0.03	0.02	0.02
		Cd (Drag)	0.39	0.35	0.32	0.35	0.51
		Cl (Lift)	-0.07	0.00	0.06	0.12	0.09
L3	45" Florida girders, -2% slope, 10 girders, 13ft spacing, 4th	Cx (X Body Force)	0.52	0.48	0.42	0.44	0.51
		Cz (Z Body Force)	0.01	0.05	0.05	0.09	0.12
		Ct (Torque)	0.09	0.05	0.03	0.03	0.02
		Cd (Drag)	0.51	0.47	0.42	0.44	0.52
		Cl (Lift)	0.06	0.07	0.05	0.07	0.08
L2	45" Florida girders, -2% slope, 10 girders, 13ft spacing, 3rd	Cx (X Body Force)	0.65	0.69	0.62	0.58	0.27
		Cz (Z Body Force)	0.08	0.13	0.05	0.04	0.21
		Ct (Torque)	0.11	0.08	0.05	0.03	0.03
		Cd (Drag)	0.64	0.68	0.62	0.58	0.29
		Cl (Lift)	0.13	0.16	0.05	0.01	0.18
L1	45" Florida girders, -2% slope, 10 girders, 13ft spacing, 2nd	Cx (X Body Force)	-0.30	-0.42	-0.47	-0.46	-0.24
		Cz (Z Body Force)	-0.37	-0.19	0.00	0.23	0.14
		Ct (Torque)	-0.07	-0.06	-0.02	-0.01	-0.01
		Cd (Drag)	-0.27	-0.41	-0.47	-0.45	-0.23
		Cl (Lift)	-0.39	-0.21	0.00	0.25	0.16
L0	45" Florida girders, -2% slope, 10 girders, 13ft spacing, 1st	Cx (X Body Force)	1.47	1.53	1.52	1.42	1.29
		Cz (Z Body Force)	0.29	0.24	0.18	0.12	0.08
		Ct (Torque)	0.14	0.13	0.12	0.10	0.08
		Cd (Drag)	1.44	1.51	1.52	1.42	1.30
		Cl (Lift)	0.42	0.31	0.18	0.06	-0.03

TABLE 2.7   WIND TUNNEL TEST WIND SPEEDS AND CORRESPONDING REYNOLDS NUMBERS

PROTOTYPE CONFIGURATION	TEST WIND SPEED (ft/s)	REYNOLDS NUMBER
A) Wide Flange Plate Girder	36.1	76000
B) 78-inch "Florida" I-Beam	37.4	56000
C) 45-inch "Florida" I-Beam	37.1	32000

FIGURES
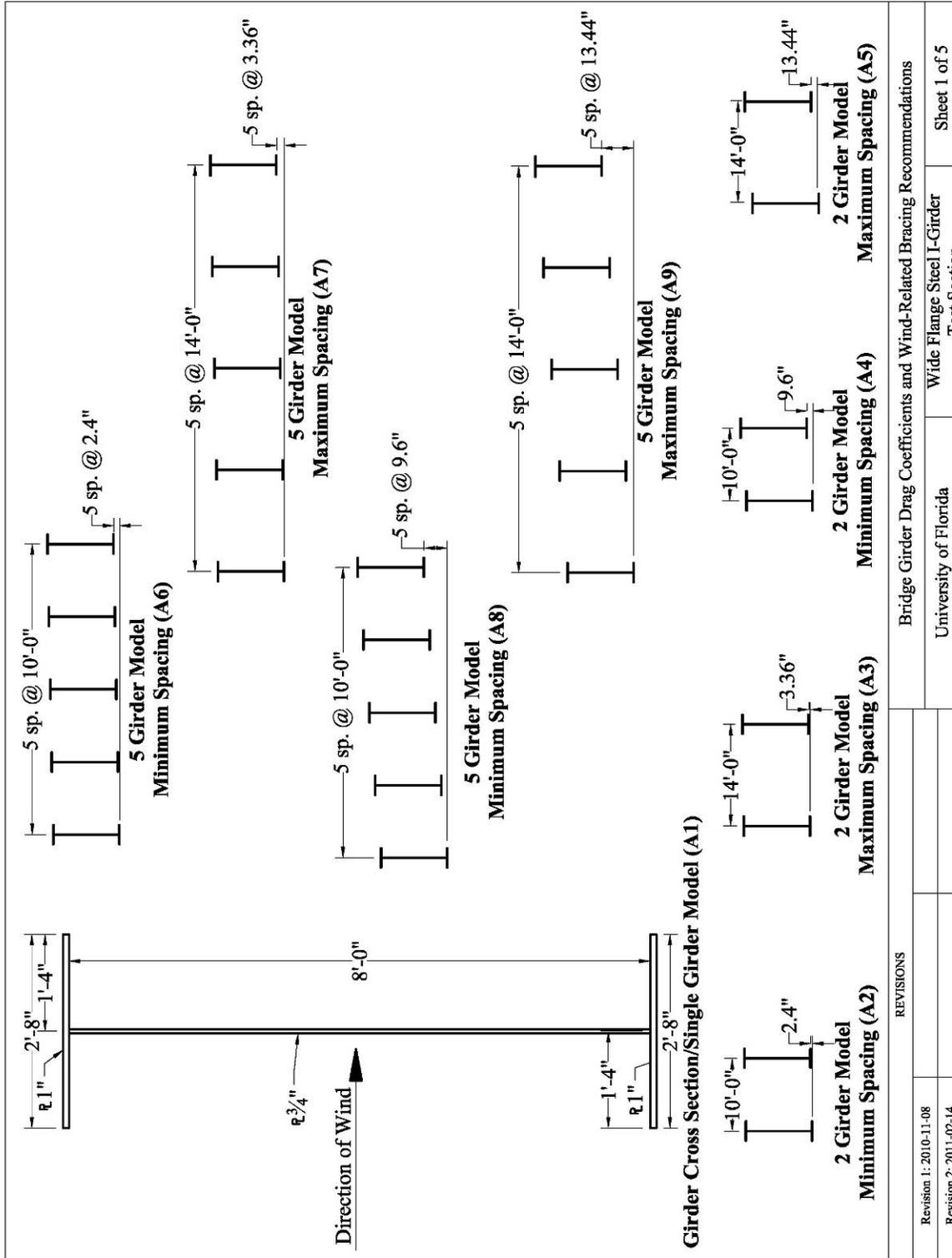
FIGURE 1.1   PROTOTYPE DIMENSIONS OF WIDE FLANGE PLATE GIRDERS

Girder Cross Section/Single Girder Model (A1)

Direction of Wind

8'-0"

2'-8"   1'-4"   R 1"   R 3/4"

2 Girder Model
Minimum Spacing (A2)
10'-0"   2.4"

2 Girder Model
Maximum Spacing (A3)
14'-0"   3.36"

2 Girder Model
Minimum Spacing (A4)
10'-0"   9.6"

2 Girder Model
Maximum Spacing (A5)
14'-0"   13.44"

5 Girder Model
Minimum Spacing (A6)
5 sp. @ 10'-0"   5 sp. @ 2.4"

5 Girder Model
Maximum Spacing (A7)
5 sp. @ 14'-0"   5 sp. @ 3.36"

5 Girder Model
Minimum Spacing (A8)
5 sp. @ 10'-0"   5 sp. @ 9.6"

5 Girder Model
Maximum Spacing (A9)
5 sp. @ 14'-0"   5 sp. @ 13.44"

REVISIONS	Bridge Girder Drag Coefficients and Wind-Related Bracing Recommendations		
Revision 1: 2010-11-08	University of Florida	Wide Flange Steel I-Girder Test Section	Sheet 1 of 5
Revision 2: 2011-02-14			

FIGURE 1.2   PROTOTYPE DIMENSIONS OF 78-INCH "FLORIDA" I-BEAM

Girder Cross Section/Single Girder Model (D1)

2 Girder Model
Minimum Spacing (D2)

2 Girder Model
Maximum Spacing (D3)

5 Girder Model
Minimum Spacing (D4)

5 Girder Model
Maximum Spacing (D5)

Direction of Wind

Symm. about ₵

R1'-3"

¾" Chamfer

Bridge Girder Drag Coefficients and Wind-Related Bracing Recommendations

| University of Florida | 78" Florida I-Beam Test Section | Sheet 4 of 5 |

REVISIONS

Revision 1: 2010-11-08

Revision 2: 2012-02-14

FIGURE 1.3   PROTOTYPE DIMENSIONS OF 45-INCH "FLORIDA" I-BEAM

Bridge Girder Drag Coefficients and Wind-Related Bracing Recommendations

| University of Florida | 45" Florida I-Beam Test Section | Sheet 5 of 5 |

REVISIONS

Revision 1: 2010-11-08
Revision 2: 2011-02-14
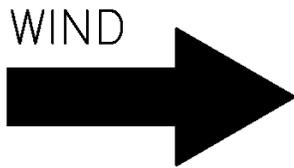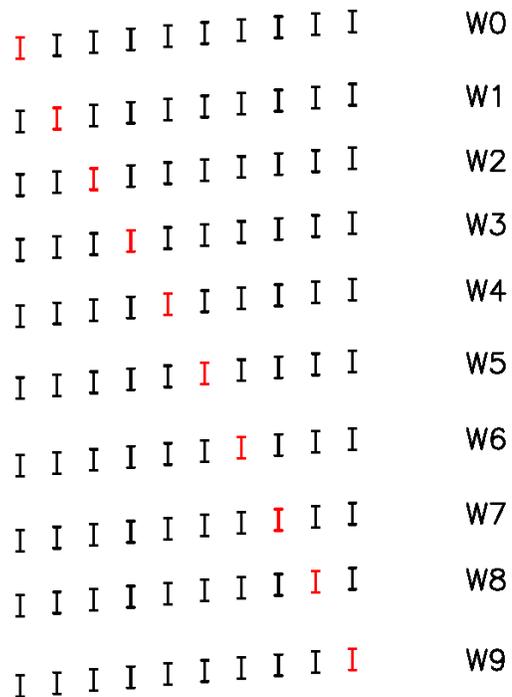
FIGURE 1.4   TEST CONFIGURATIONS AND DESIGNATIONS – WIDE FLANGE PLATE GIRDERS (1:25 SCALE, RED – INSTRUMENTED GIRDER)

WIND →

DEEP FLORIDA
I-BEAM

TEST "D"
5.571" spacing
+2% Cross Slope

TEST

I I I I I I I I I I   D0

I I I I I I I I I I   D1

I I I I I I I I I I   D2

I I I I I I I I I I   D3

I I I I I I I I I I   D4

I I I I I I I I I I   D5

I I I I I I I I I I   D6

I I I I I I I I I I   D7
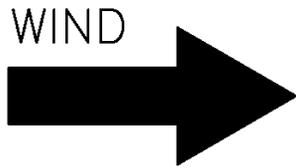
I I I I I I I I I I   D8
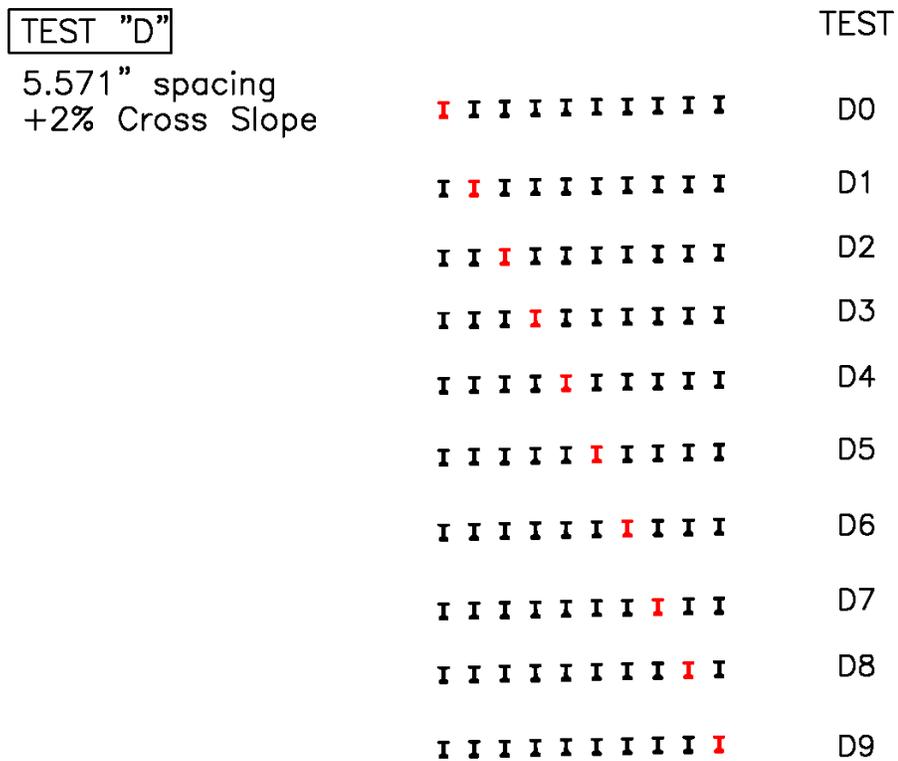
I I I I I I I I I I   D9

FIGURE 1.5   TEST CONFIGURATIONS AND DESIGNATIONS – 78-INCH "FLORIDA" I-BEAM (1:28 SCALE, RED – INSTRUMENTED I-BEAM)

FIGURE 1.5 (CONT.) TEST CONFIGURATIONS AND DESIGNATIONS – 78-INCH "FLORIDA" I-BEAM (1:28 SCALE, RED – INSTRUMENTED I-BEAM)

WIND →

SHALLOW FLORIDA
I-BEAM

TEST

TEST "S"
5.571" spacing
+2% Cross Slope
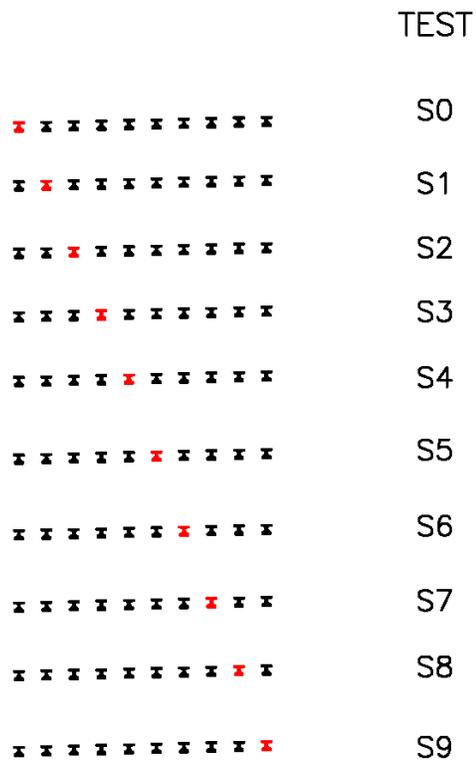
ɪ ɪ ɪ ɪ ɪ ɪ ɪ ɪ ɪ ɪ   S0

ɪ ɪ ɪ ɪ ɪ ɪ ɪ ɪ ɪ ɪ   S1

ɪ ɪ ɪ ɪ ɪ ɪ ɪ ɪ ɪ ɪ   S2

ɪ ɪ ɪ ɪ ɪ ɪ ɪ ɪ ɪ ɪ   S3

ɪ ɪ ɪ ɪ ɪ ɪ ɪ ɪ ɪ ɪ   S4

ɪ ɪ ɪ ɪ ɪ ɪ ɪ ɪ ɪ ɪ   S5

ɪ ɪ ɪ ɪ ɪ ɪ ɪ ɪ ɪ ɪ   S6

ɪ ɪ ɪ ɪ ɪ ɪ ɪ ɪ ɪ ɪ   S7

ɪ ɪ ɪ ɪ ɪ ɪ ɪ ɪ ɪ ɪ   S8

ɪ ɪ ɪ ɪ ɪ ɪ ɪ ɪ ɪ ɪ   S9

FIGURE 1.6   TEST CONFIGURATIONS AND DESIGNATIONS – 45-INCH "FLORIDA"
I-BEAM (1:28 SCALE, RED – INSTRUMENTED I-BEAM)

WIND ➡
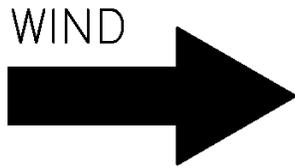
SHALLOW FLORIDA
I—BEAM

TEST

TEST "L"

5.571" spacing
−2% Cross Slope

ꟷꟷꟷꟷꟷꟷꟷꟷꟷꟷ   L0

ꟷꟷꟷꟷꟷꟷꟷꟷꟷꟷ   L1

ꟷꟷꟷꟷꟷꟷꟷꟷꟷꟷ   L2

ꟷꟷꟷꟷꟷꟷꟷꟷꟷꟷ   L3

ꟷꟷꟷꟷꟷꟷꟷꟷꟷꟷ   L4

ꟷꟷꟷꟷꟷꟷꟷꟷꟷꟷ   L5

ꟷꟷꟷꟷꟷꟷꟷꟷꟷꟷ   L6

ꟷꟷꟷꟷꟷꟷꟷꟷꟷꟷ   L7

ꟷꟷꟷꟷꟷꟷꟷꟷꟷꟷ   L8

ꟷꟷꟷꟷꟷꟷꟷꟷꟷꟷ   L9

**FIGURE 1.6 (CONT.) TEST CONFIGURATIONS AND DESIGNATIONS – 45-INCH
"FLORIDA" I-BEAM (1:28 SCALE, RED – INSTRUMENTED I-BEAM)**
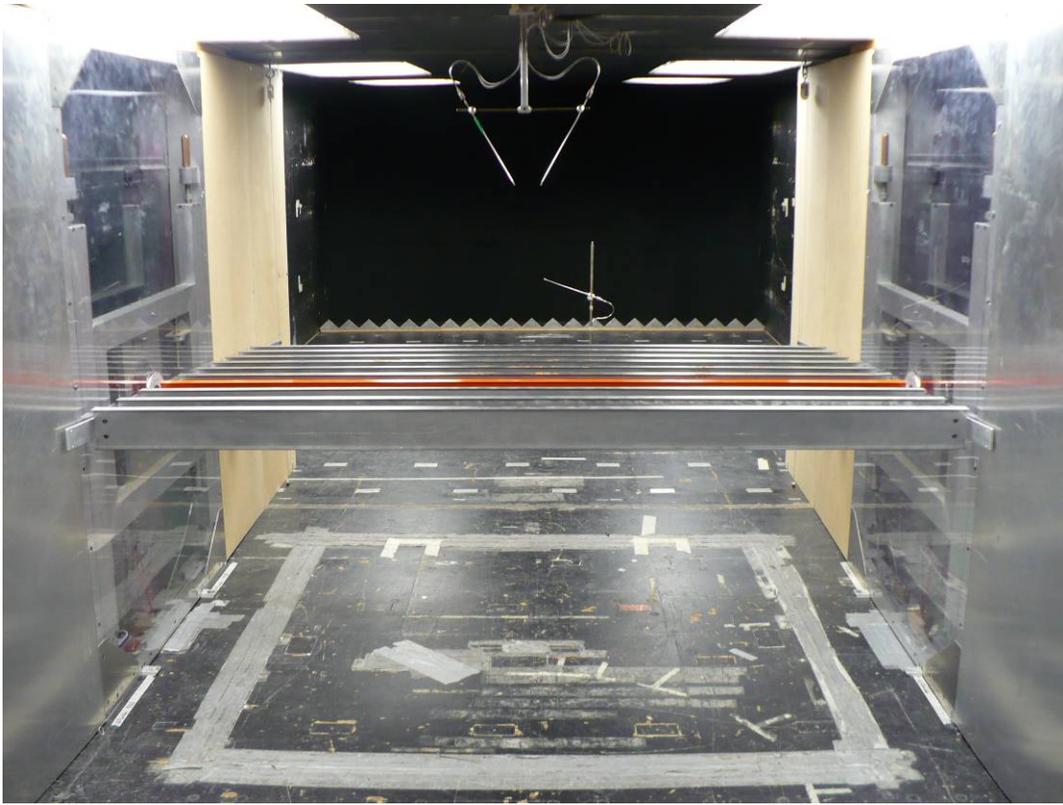
FIGURE 1.7   STATIC SECTION MODEL TEST SET-UP
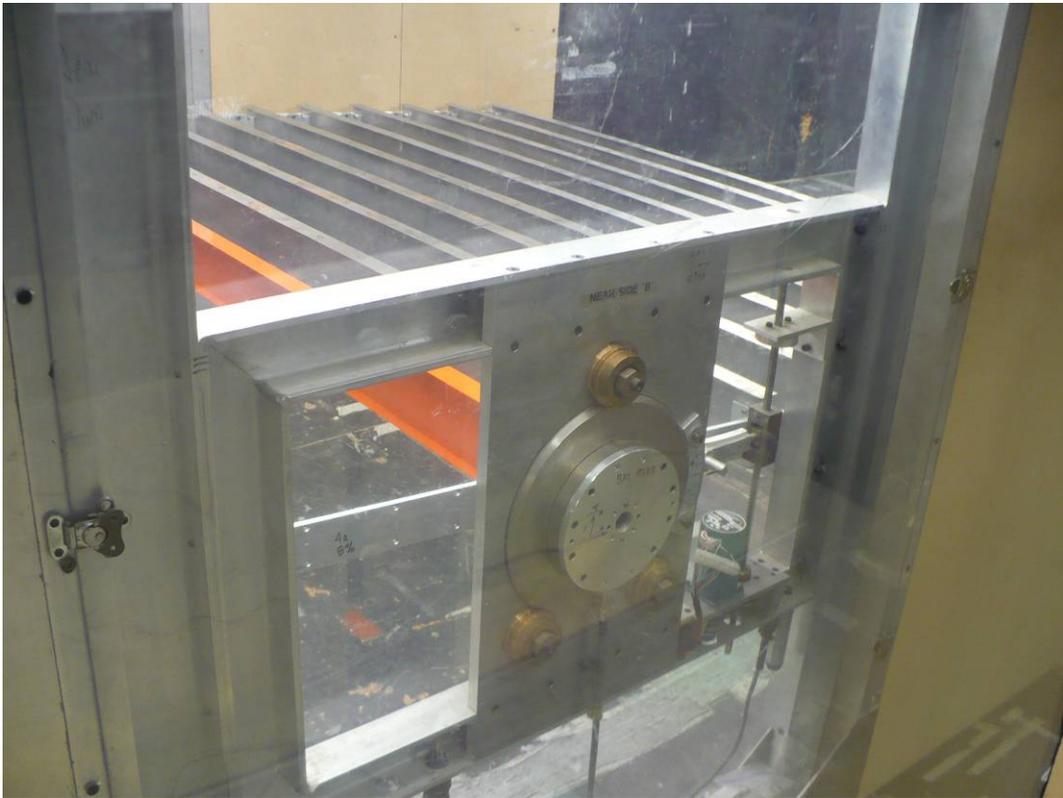
FIGURE 1.8   STATIC SECTION MODEL TEST RIG

a) TEST W9, INSTRUMENTED GIRDER LEEWARD (10TH POSITION)
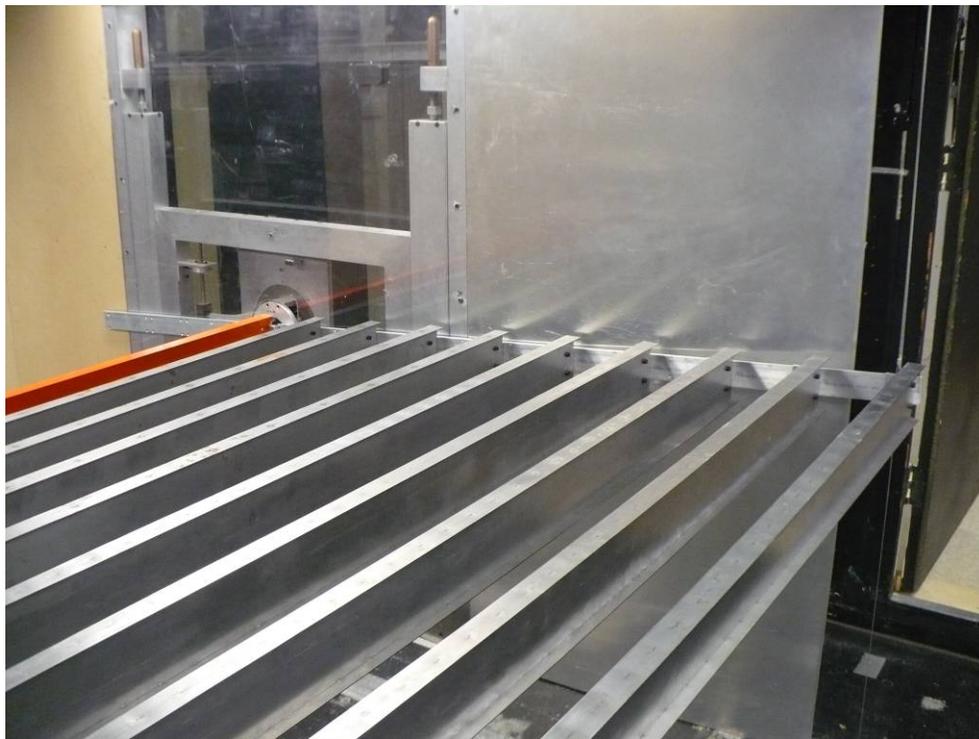
b) TEST W0, INSTRUMENTED GIRDER WINDWARD (1st POSITION)

FIGURE 1.9   SECTION MODEL TEST SET-UP – WIDE FLANGE PLATE GIRDER, 8% CROSS SLOPE

c) TEST W6, INSTRUMENTED GIRDER AT 7TH POSITION

FIGURE 1.9 (CONT.) SECTION MODEL TEST SET-UP – WIDE FLANGE PLATE GIRDER, 8% CROSS SLOPE
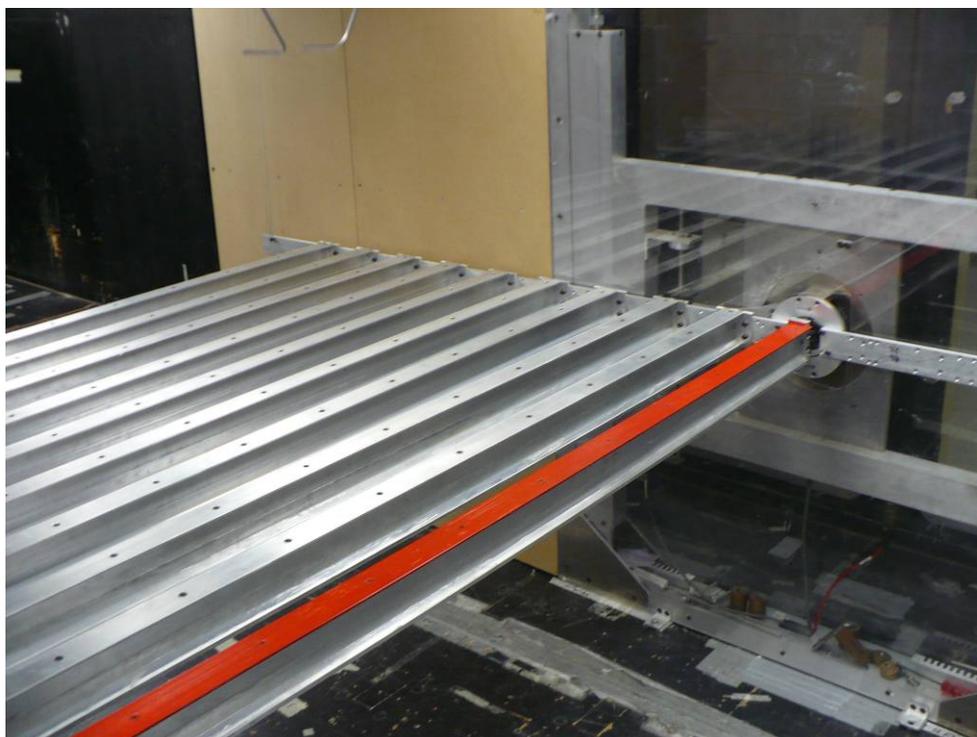
a) TEST D9, INSTRUMENTED I-BEAM LEEWARD (10TH POSITION)

b) TEST D0, INSTRUMENTED I-BEAM WINDWARD (1st POSITION)

FIGURE 1.10 SECTION MODEL TEST SET-UP – 78-INCH "FLORIDA" I-BEAM, 2% CROSS SLOPE

c) TEST D5, INSTRUMENTED GIRDER AT 6TH POSITION

FIGURE 1.10 (CONT.)   SECTION MODEL TEST SET-UP – 78-INCH "FLORIDA" I-BEAM, 2% CROSS SLOPE

a) TEST T9, INSTRUMENTED I-BEAM LEEWARD (10TH POSITION)
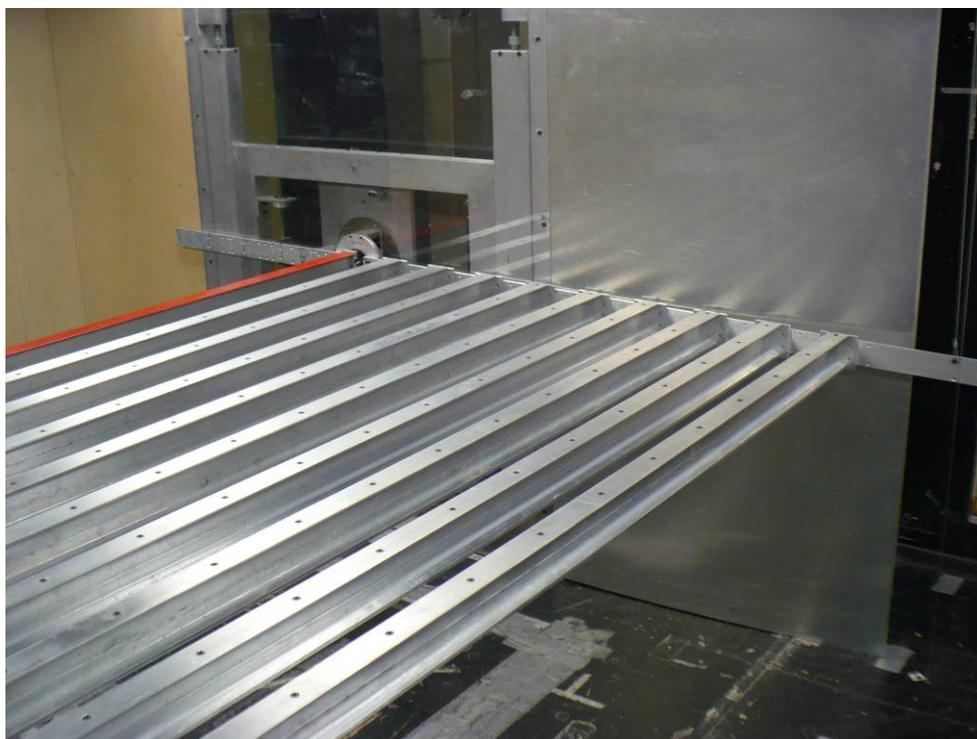
b) TEST T0, TESTED I-BEAM AT WINDWARD (1st POSITION)

FIGURE 1.11 SECTION MODEL TEST SET-UP – 78-INCH "FLORIDA" I-BEAM, -2% CROSS SLOPE

c) TEST T4, INSTRUMENTED GIRDER AT 5TH POSITION

FIGURE 1.11 (CONT.)   **SECTION MODEL TEST SET-UP – 78-INCH "FLORIDA" I-BEAM, -2% CROSS SLOPE**
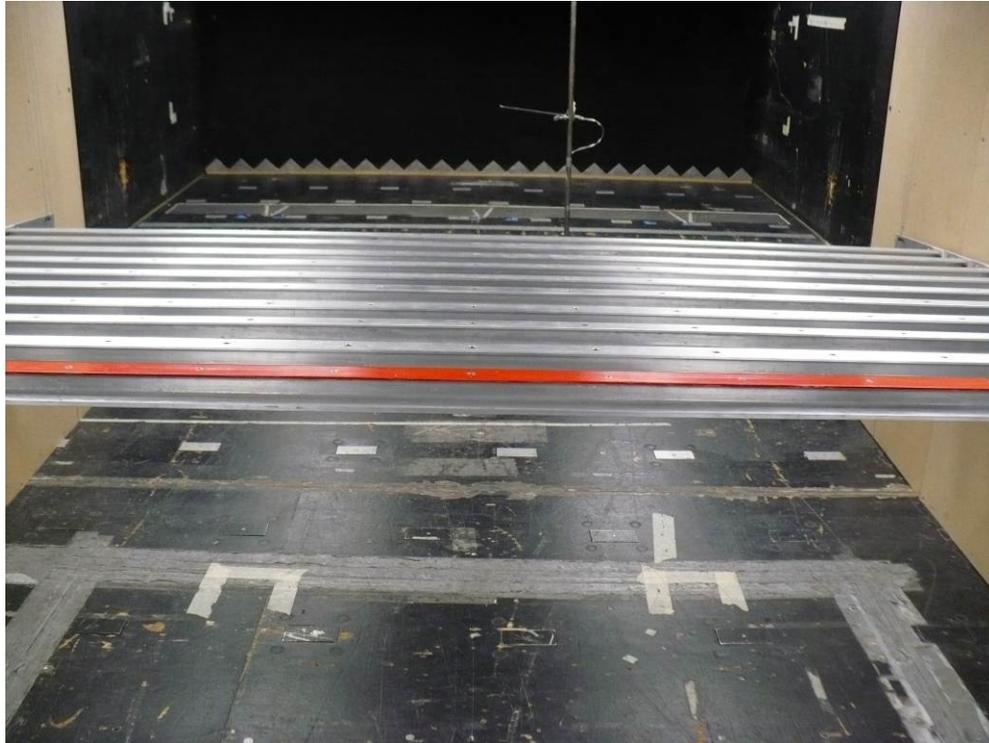
a) TEST S9, TESTED I-BEAM LEEWARD (10TH POSITION)
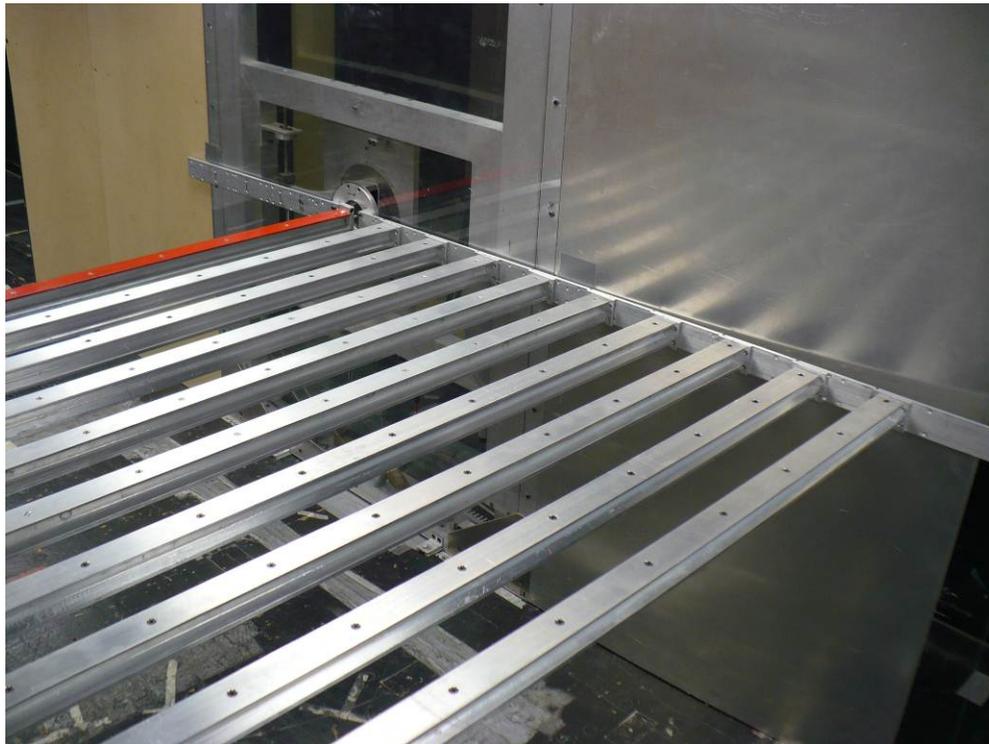
b) TEST S0, TESTED I-BEAM WINDWARD (1st POSITION)

**FIGURE 1.12 SECTION MODEL TEST SET-UP – 45-INCH "FLORIDA" I-BEAM,
2% CROSS SLOPE**

c) TEST S5, INSTRUMENTED GIRDER AT 6TH POSITION

FIGURE 1.12 (CONT.)   SECTION MODEL TEST SET-UP – 45-INCH "FLORIDA" I-BEAM, 2% CROSS SLOPE

a) TEST L9, TESTED I-BEAM LEEWARD (10TH POSITION)

b) TEST L0, TESTED I-BEAM WINDWARD (1st POSITION)

FIGURE 1.13 SECTION MODEL TEST SET-UP – 45-INCH "FLORIDA" I-BEAM, -2% CROSS SLOPE

c) TEST L5, INSTRUMENTED GIRDER AT 6TH POSITION

FIGURE 1.13 (CONT.)   **SECTION MODEL TEST SET-UP – 45-INCH "FLORIDA" I-BEAM, -2% CROSS SLOPE**
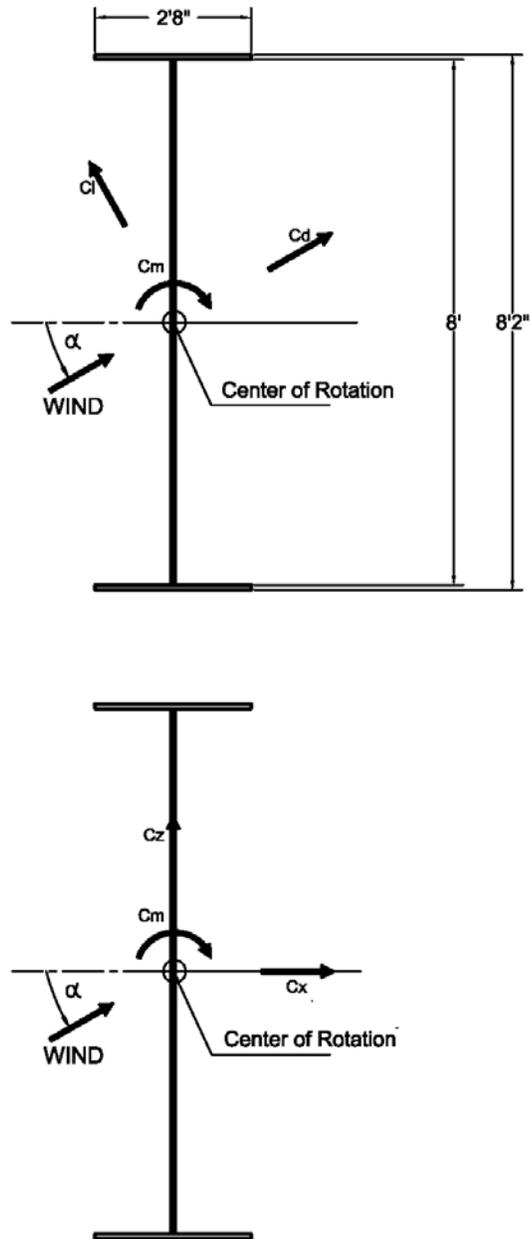
FIGURE 2.1   SIGN CONVENTION OF FORCES – WIDE FLANGE PLATE GIRDER
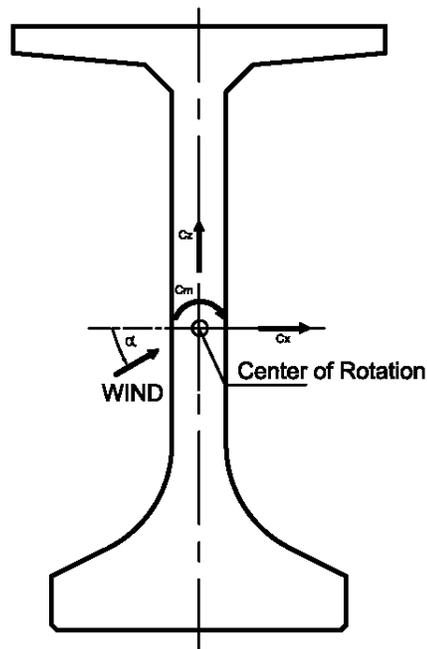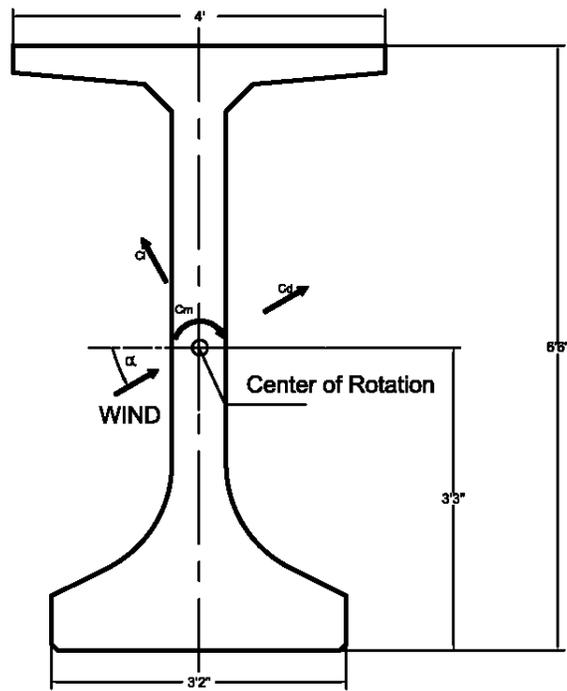
FIGURE 2.2   SIGN CONVENTION OF FORCES – 78-INCH "FLORIDA" I-BEAM

FIGURE 2.3   SIGN CONVENTION OF FORCES – 45-INCH "FLORIDA" I-BEAM

FIGURE 2.4   **STATIC FORCE COEFFICIENTS (BODY FORCES) – WIDE FLANGE GIRDER, 8% CROSS SLOPE, 14FT SPACING**
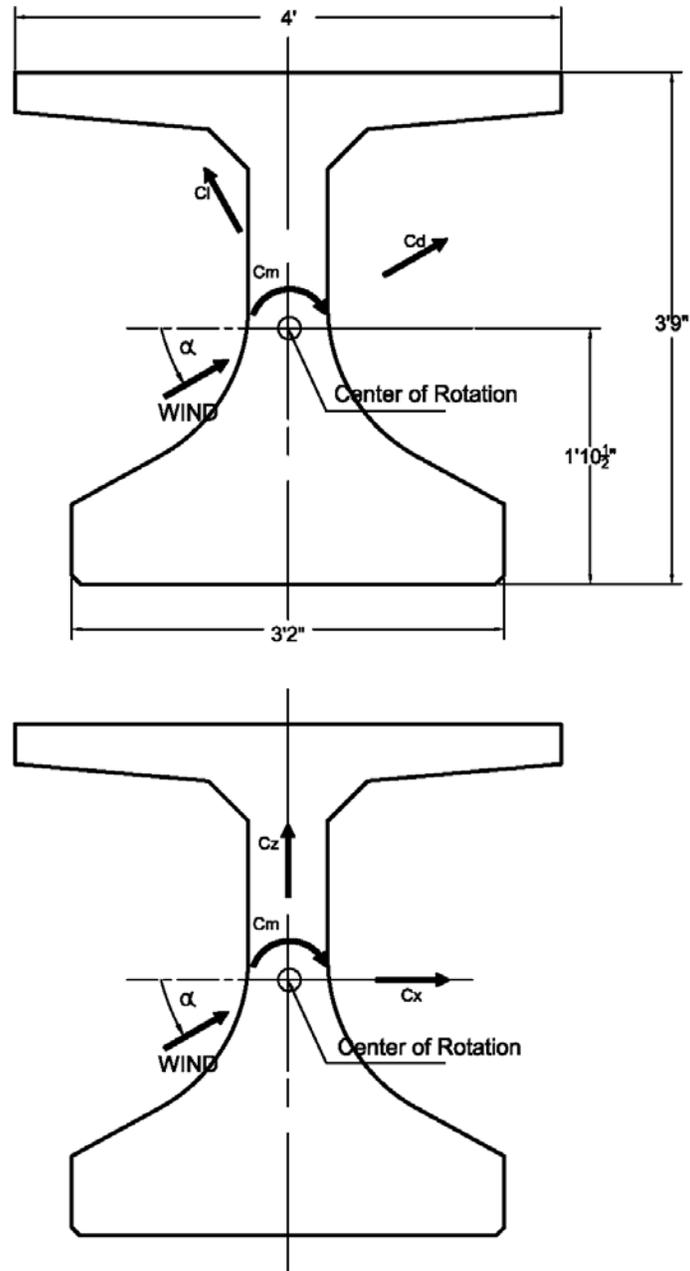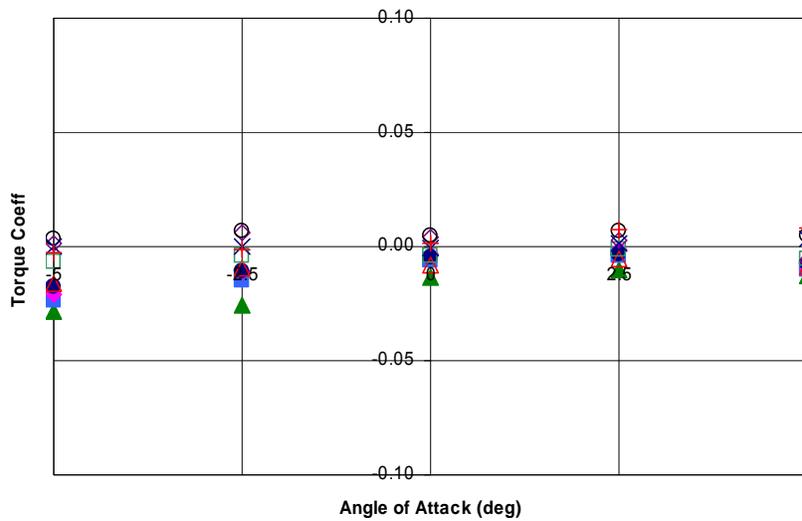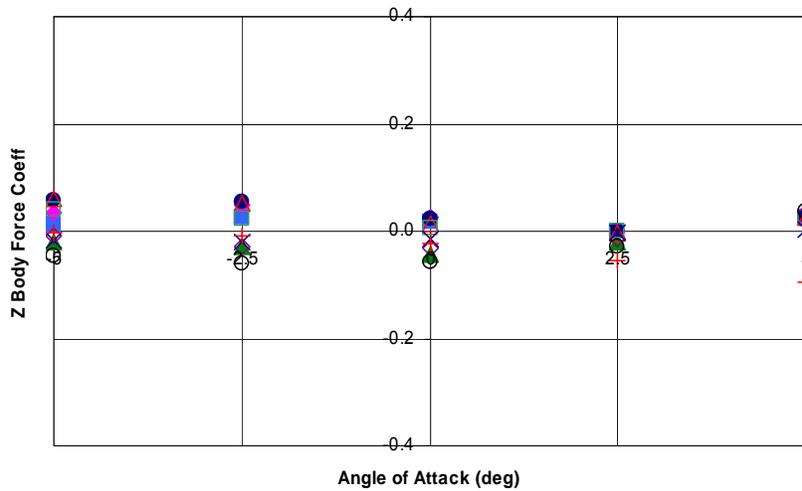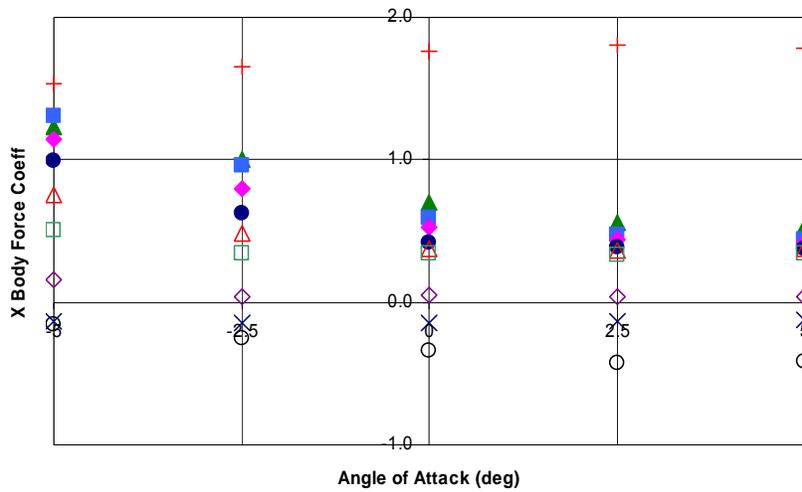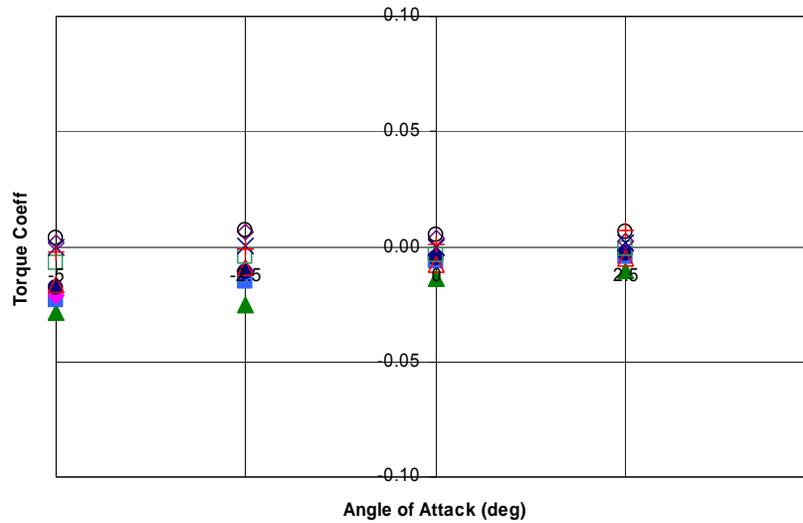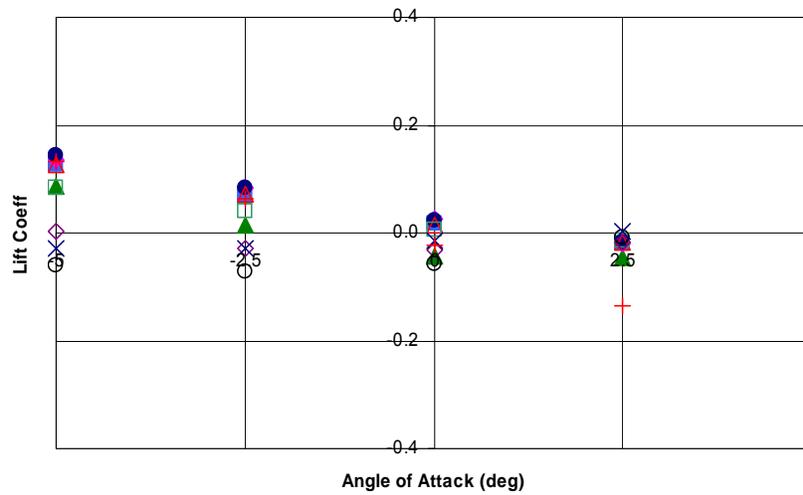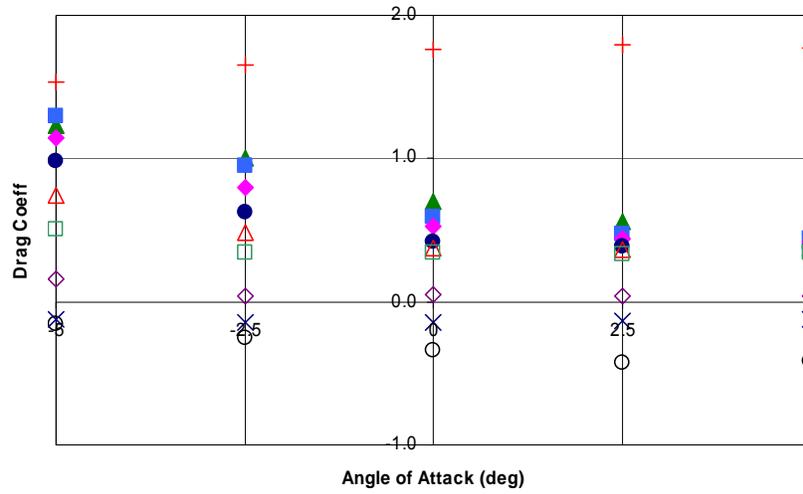
Legend: ▲ W9 ■ W8 ◆ W7 ● W6 △ W5 □ W4 ◇ W3 ○ W2 ✕ W1 + W0

FIGURE 2.5   STATIC FORCE COEFFICIENTS (WIND AXIS FORCES) – WIDE FLANGE GIRDER, 8% CROSS SLOPE, 14FT SPACING

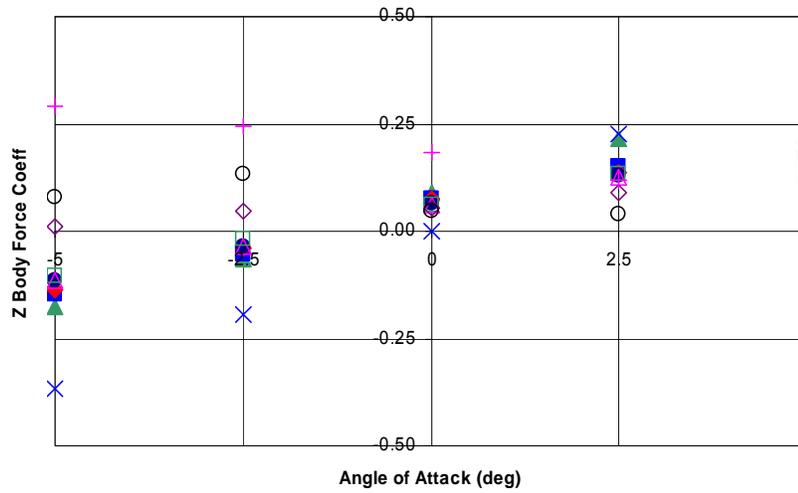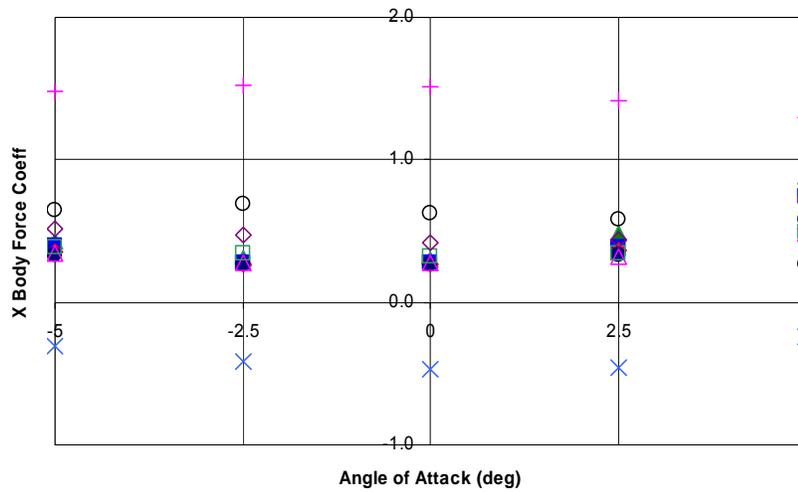**FIGURE 2.6** **STATIC FORCE COEFFICIENTS (BODY FORCES) – 78-INCH "FLORIDA" I-BEAMS, 2% CROSS SLOPE, 13FT SPACING**

FIGURE 2.7 STATIC FORCE COEFFICIENTS (WIND AXIS FORCES) – 78-INCH "FLORIDA" I-BEAMS, 2% CROSS SLOPE, 13FT SPACING

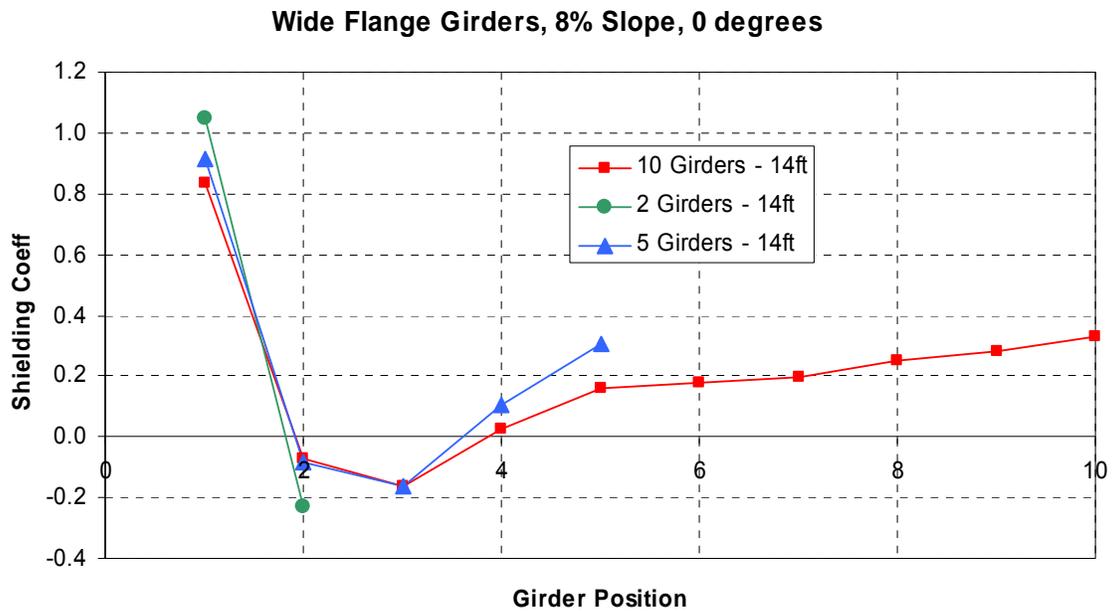**FIGURE 2.8**   **STATIC FORCE COEFFICIENTS (BODY FORCES) – 78-INCH "FLORIDA" I-BEAMS, -2% CROSS SLOPE, 13FT SPACING**

FIGURE 2.9   STATIC FORCE COEFFICIENTS (WIND AXIS FORCES) – 78-INCH "FLORIDA" I-BEAMS, -2% CROSS SLOPE, 13FT SPACING

**FIGURE 2.10** **STATIC FORCE COEFFICIENTS (BODY FORCES) – 45-INCH "FLORIDA" I-BEAMS, 2% CROSS SLOPE, 13FT SPACING**

FIGURE 2.11   STATIC FORCE COEFFICIENTS (WIND AXIS FORCES) – 45-INCH "FLORIDA" I-BEAMS, 2% CROSS SLOPE, 13FT SPACING

FIGURE 2.12   STATIC FORCE COEFFICIENTS (BODY FORCES) – 45-INCH "FLORIDA" I-BEAMS, -2% CROSS SLOPE, 13FT SPACING

FIGURE 2.13 **STATIC FORCE COEFFICIENTS (WIND AXIS FORCES) – 45-INCH "FLORIDA" I-BEAMS, -2% CROSS SLOPE, 13FT SPACING**

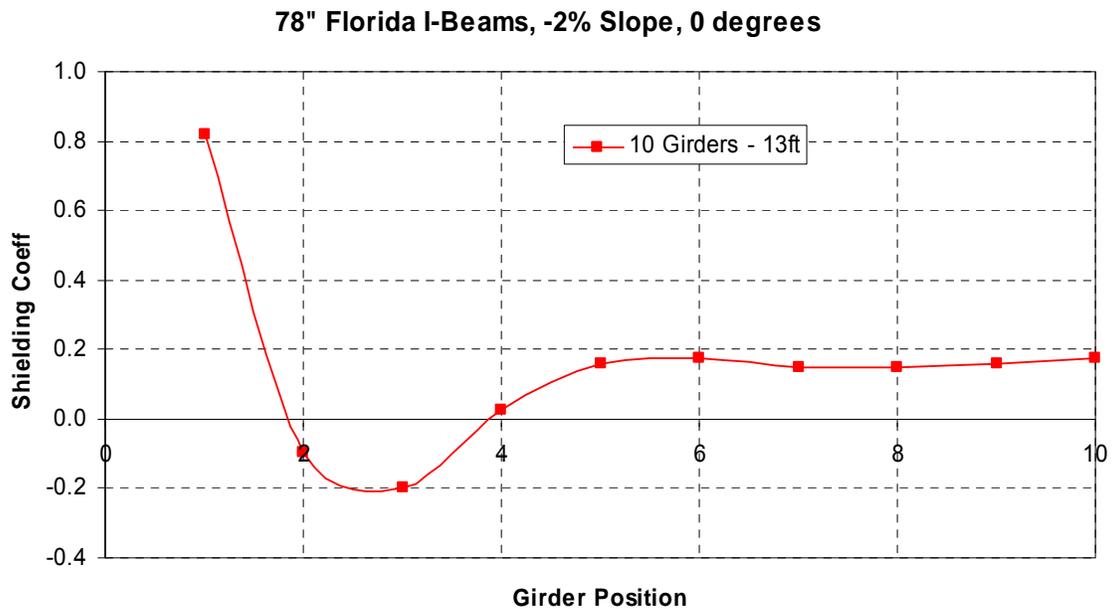**Wide Flange Girders, 8% Slope, 0 degrees**

NOTE:- Test results for 2 girders and 5 girders are from the tests reported in [1].

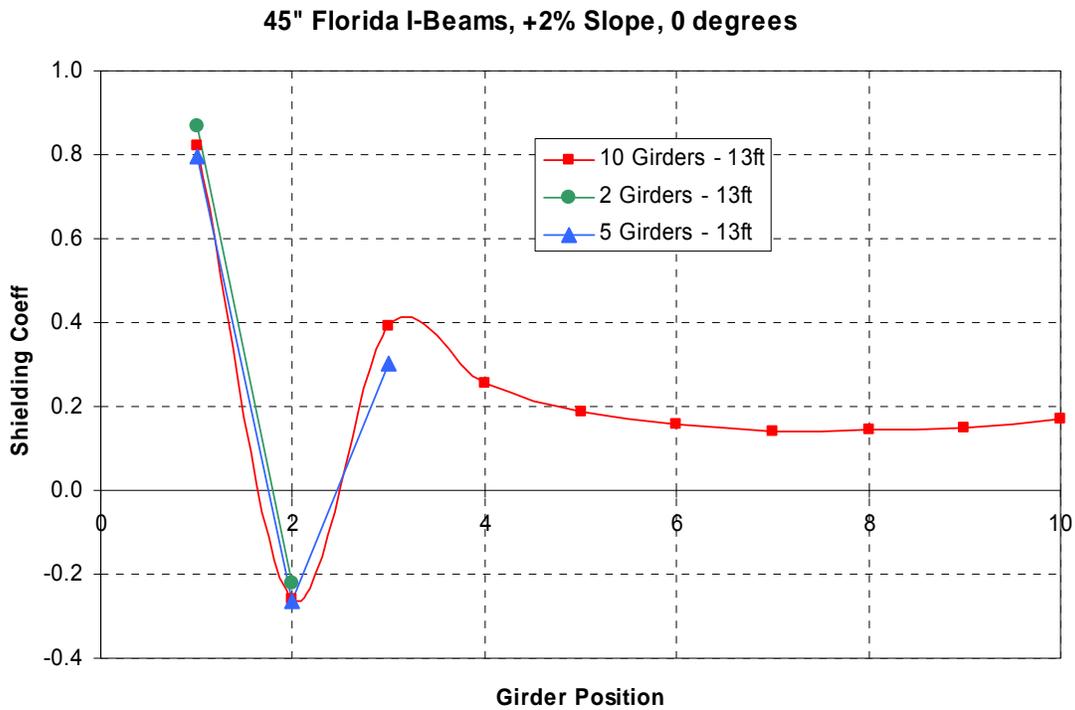**FIGURE 2.14**   **SHIELDING COEFFICIENTS – WIDE FLANGE GIRDERS, 8% CROSS SLOPE, 0 DEGREES**

78" Florida I-Beams, +2% Slope, 0 degrees
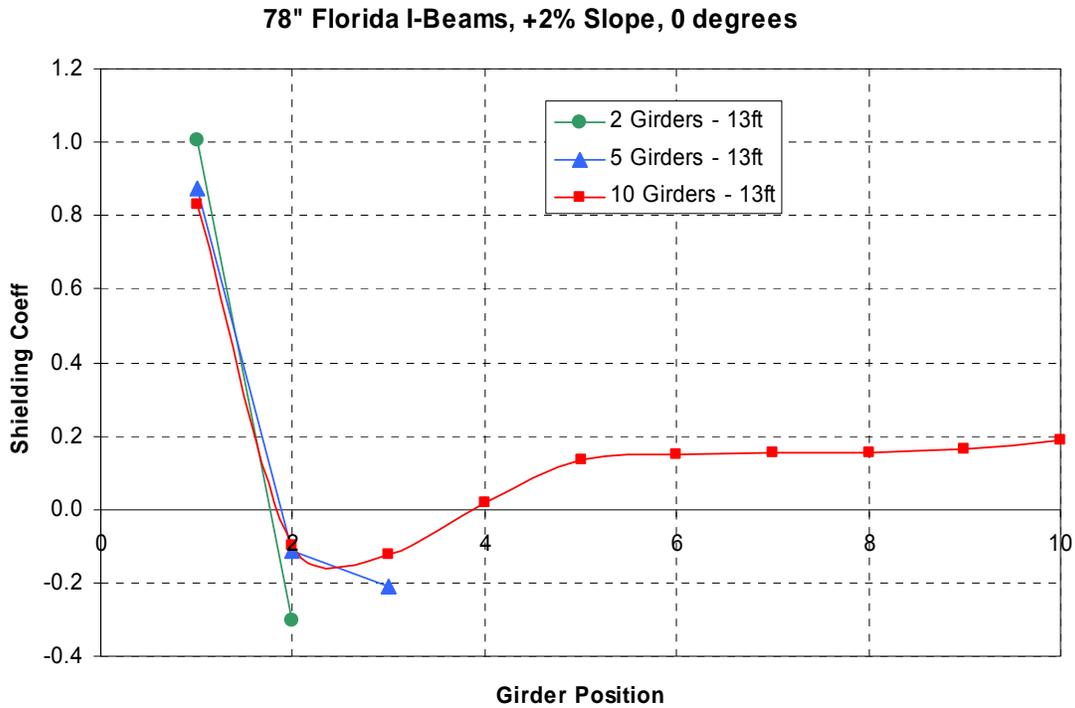
Note that results for the 2 girders and 5 girders are from the tests reported in [1].

FIGURE 2.15   **SHIELDING COEFFICIENTS – 78-INCH "FLORIDA" I-BEAMS, 2% CROSS SLOPE, 0 DEGREES**
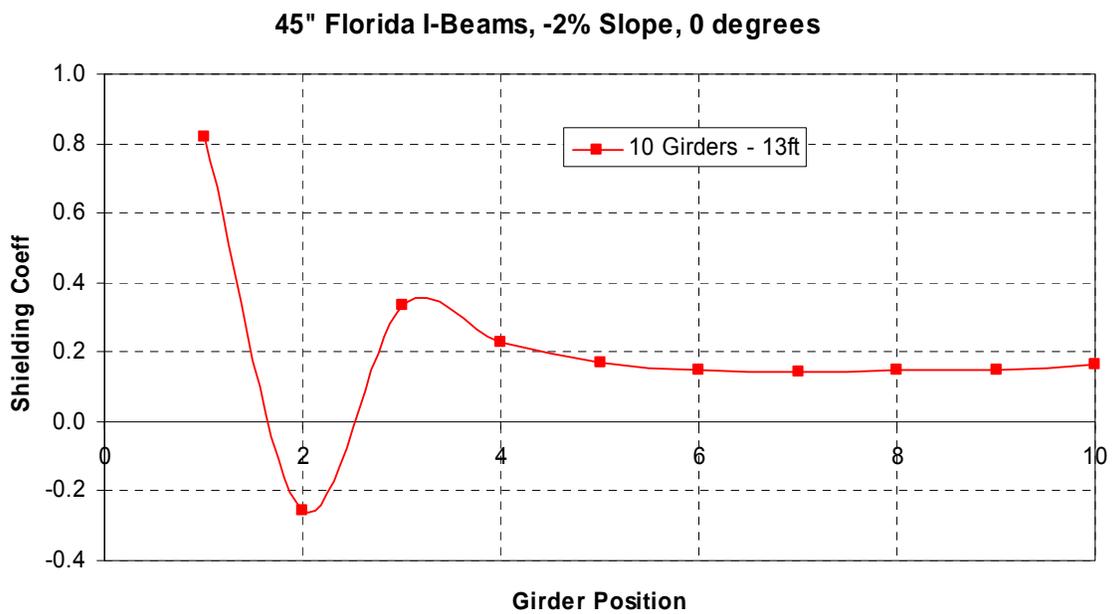
78" Florida I-Beams, -2% Slope, 0 degrees

FIGURE 2.16   **SHIELDING COEFFICIENTS – 78-INCH "FLORIDA" I-BEAMS, -2% CROSS SLOPE, 0 DEGREES**
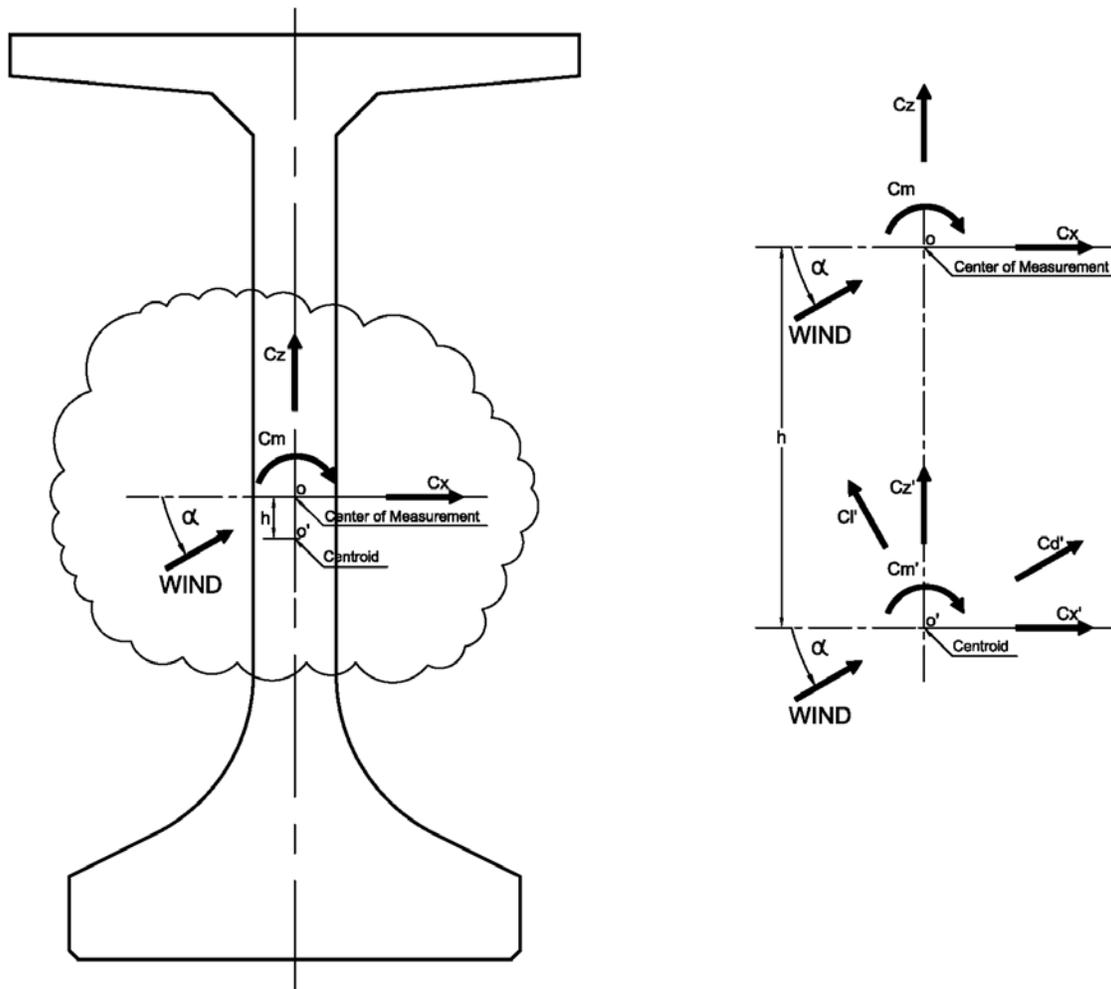
45" Florida I-Beams, +2% Slope, 0 degrees

Note that results for the 2 girders and 5 girders are from the tests reported in [1].

FIGURE 2.17 **SHIELDING COEFFICIENTS – 45-INCH "FLORIDA" I-BEAMS, 2% CROSS SLOPE, 0 DEGREES**

45" Florida I-Beams, -2% Slope, 0 degrees

FIGURE 2.18 **SHIELDING COEFFICIENTS – 45-INCH "FLORIDA" I-BEAMS, -2% CROSS SLOPE, 0 DEGREES**

FIGURE 2.19 SIGN CONVENTION OF FORCES – CENTROID LOCATION